Water Science and Technology Library

Ramakar Jha · Vijay P. Singh ·
Vivekanand Singh · L. B. Roy ·
Roshni Thendiyath *Editors*

Groundwater and Water Quality

Hydraulics, Water Resources and Coastal Engineering

Springer

Water Science and Technology Library

Volume 119

The aim of the *Water Science and Technology Library* is to provide a forum for dissemination of the state-of-the-art of topics of current interest in the area of water science and technology. This is accomplished through publication of reference books and monographs, authored or edited. Occasionally also proceedings volumes are accepted for publication in the series. *Water Science and Technology Library* encompasses a wide range of topics dealing with science as well as socio-economic aspects of water, environment, and ecology. Both the water quantity and quality issues are relevant and are embraced by *Water Science and Technology Library*. The emphasis may be on either the scientific content, or techniques of solution, or both. There is increasing emphasis these days on processes and *Water Science and Technology Library* is committed to promoting this emphasis by publishing books emphasizing scientific discussions of physical, chemical, and/or biological aspects of water resources. Likewise, current or emerging solution techniques receive high priority. Interdisciplinary coverage is encouraged. Case studies contributing to our knowledge of water science and technology are also embraced by the series. Innovative ideas and novel techniques are of particular interest.

Comments or suggestions for future volumes are welcomed.

Vijay P. Singh, Department of Biological and Agricultural Engineering & Zachry Department of Civil and Environment Engineering, Texas A&M University, USA
Email: vsingh@tamu.edu

All contributions to an edited volume should undergo standard peer review to ensure high scientific quality, while monographs should also be reviewed by at least two experts in the field.

Manuscripts that have undergone successful review should then be prepared according to the Publisher's guidelines manuscripts: https://www.springer.com/gp/authors-editors/book-authors-editors/book-manuscript-guidelines

Ramakar Jha · Vijay P. Singh · Vivekanand Singh ·
L. B. Roy · Roshni Thendiyath
Editors

Groundwater and Water Quality

Hydraulics, Water Resources and Coastal Engineering

Springer

Editors
Ramakar Jha
Department of Civil Engineering
National Institute of Technology Patna
Patna, India

Vivekanand Singh
Department of Civil Engineering
National Institute of Technology Patna
Patna, India

Roshni Thendiyath
Department of Civil Engineering
National Institute of Technology Patna
Patna, India

Vijay P. Singh
Department of Biological and Agricultural Engineering
Texas A&M University
College Station, TX, USA

L. B. Roy
Department of Civil Engineering
National Institute of Technology Patna
Patna, India

ISSN 0921-092X ISSN 1872-4663 (electronic)
Water Science and Technology Library
ISBN 978-3-031-09550-4 ISBN 978-3-031-09551-1 (eBook)
https://doi.org/10.1007/978-3-031-09551-1

This Springer imprint is published by the registered company Springer Nature Switzerland AG
The registered company address is: Gewerbestrasse 11, 6330 Cham, Switzerland

Contents

About the Editors

Ramakar Jha is a chair professor at the Department of Civil Engineering and has 30 years of experience in the field of Hydrology and water resources engineering. Dr Jha is presently working as Chair Professor in the Department of Civil Engineering, National Institute of Technology (NIT) Patna-INDIA, which is a Premier Institute in India under the Ministry of Human Resource Development, Government of India. Dr. Jha has served at various levels from Scientist-B to Scientist-E1 at National Institute of Hydrology (NIH), Roorkee, India and as Professor in the Department of Civil Engineering, NIT Rourkela. He has worked and working as Country Co-ordinator of UNESCO- GWADI and Principal Investigator for many International (EU-FP7, DAAD, ADB, AUS-Aid) and National research and consultancy projects (ISRO, DST, MoWR, MHRD). Moreover, he served as Chair for many administrative positions and received a coupel of international and national awards for research papers. Presently, he is working as Dr Rajendra Prasad Chair for Water resources under the Ministry of Water Resources, Government of India in the Department of Civil Engineering, NIT Patna, Bihar.

V. P. Singh A Texas A&M professor of Indian origin is receiving a prestigious award for his world-renowned work on water. Vijay P. Singh is receiving the 2013 Lifetime Achievement Award from the American Society of Civil Engineers-Environmental and Water Resources Institute, otherwise known as the ASCE-EWRI. The award is in recognition of Singh's work in the field of hydrology, which is the study of water in all aspects, such as quality, distribution, preservation, transportation, etc. Some of the work he has done has even created an entire new branch of hydrology – called entropic hydrology – that is connected to the study of entropy, which means essentially the study of order and disorder as it relates to the physical universe. His work is considered fundamental for flood planning and water modeling around the world. Since earning his doctorate degree, Singh has held teaching positions in some of the most well-known universities in the US. He was an Associate Research Professor of Civil Engineering at George Washington University from 1977-78, an Associate Professor of Civil Engineering at Mississippi University from 1978-81, and an adjunct professor as well as the coordinator of the Environmental and Water

Resources Systems Engineering Program at Louisiana State University from 1999-2006 and 2001-2006, respectively. Singh joined Texas A&M University in 2006, where he currently wears a number of different hats. He is a professor of biological and agricultural engineering, a professor of civil and environment engineering, and a Caroline and William N. Lehrer Distinguished Chair in Water Engineering (Hydrology). He has authored or edited around 10 published works in the fields of engineering and hydrology.

Chapter 1
Identification of the Parameters to Estimate the Capillary Rise from Shallow Groundwater Table Using Field Crop Experiments

Arunava Poddar, Navsal Kumar, and Vijay Shankar

Abstract Capillary rise from groundwater is known as the upward flow of moisture in the soil and is a significant component of soil water balance, specifically in the occurrence of a shallow groundwater table (SGT). Extraction of moisture from the SGT needs a proper understanding of the capillary rise. Various soil, crop, and environmental parameters possess a significant effect on the capillary rise. The objective of the study is to identify the impact of crop parameters on the capillary rise by performing field crop experiments on crops i.e., Wheat, Maize, Indian mustard, and Pea. Experiments are conducted using a Lysimetric setup on an agricultural farm at Hamirpur, Himachal Pradesh, India. Various models are considered to investigate the influencing parameters for capillary rise due to the crops for local climatic conditions. Regression analysis and performance indicators are used to perform analysis for the present study. Crop parameters (root depth, plant height, leaf area index), crop evapotranspiration, and soil moisture variation are found to affect capillary rise from the SGT. The proper understanding and estimation of capillary rise will supplement in optimized usage of moisture for irrigation purposes in areas with a SGT.

Keywords Capillary rise · Water table · Crop evapotranspiration · Plant transpiration · Soil moisture

1.1 Introduction

The irrigation system used effectively contributes to intelligent water use. Numerous aspects were developed which have altered the thinking regarding the irrigation systems management (Sharma and Kumar, 2021; Poddar et al. 2017; Kumar et al.

A. Poddar (✉)
Civil Engineering Department, Shoolini University, Solan, Himachal Pradesh 173229, India
e-mail: arunava.nithrs@gmail.com

N. Kumar · V. Shankar
Civil Engineering Department, National Institute of Technology Hamirpur, Hamirpur, Himachal Pradesh 177005, India

R. Jha et al. (eds.), *Groundwater and Water Quality*, Water Science and Technology Library 119, https://doi.org/10.1007/978-3-031-09551-1_1

2019b). Whenever water supplies are found to be limited, all available sources of moisture are assessed as potential sources of irrigation water.

Approximately 40% of world food requirement is fulfilled by irrigated agriculture and it is expected to keep playing an important role in fulfilling the expected world's demand for food (Poddar et al. 2021a). Nowadays, SGT can be considered as an alternative source for meeting crop-water requirements. Root water uptake (RWU) is a dynamic component of the water balance system required to manage the irrigation system efficiently (Kumar et al. 2019a, 2020). Various models for RWU have been evaluated to have optimized irrigation schedules for various crops (Ojha et al. 2009; Poddar et al. 2020, 2021b). The upward movement of water from the SGT is termed "capillary rise". Understanding and proper prediction of capillary rise can be an advantage for scheduling irrigation for different crops.

Numerous researchers have provided models to predict the capillary rise that occurs in the unsaturated zone (Prathapar et al. 1992; Zammouri 2001; Raes et al. 2003; Yang et al. 2011; Liu et al. 2014; Wang et al. 2016; Poddar et al. 2018). Since the parameters for each model varies, it is assumed that the parameters required to predict capillary rise are influenced by local conditions. Based on extensive literature review, it has been observed that capillary rise studies in hilly terrains are lacking. Hence, a study of the capillary rise occurring from SGT during RWU for the hilly region is required.

Hence, the present work aims to identify the parameters to predict capillary rise from the SGT.

1.2 Models Used for the Investigation

After an extensive literature review, six models are used for the comparative study. The models are Quasi-steady state analytical model (QSSAM) (Prathapar et al. 1992), Averianov formula (AF) (Schoeller 1961), Modified Transient state analytical model (MTSAM) (Jorenush and Sepaskhah 2003), Modified Averianov formula (MAF) (Yang et al. 2011), Quick capillary rise height estimation (QCRHE) (Liu et al. 2014) and groundwater uptake estimation method (GUEM) referred from (Wang et al. 2016). For details of the models, refer to the references given above.

1.3 Study Area

The site selected for study is an agricultural farm in Hamirpur, Himachal Pradesh, India which is situated in the mid-hills of the north-western Himalayas. The site is located at 31°42′40.824" N (latitude) and 76°31′33.384" E (longitude), and the elevation is 895 m (2,936 ft) above mean sea level. The average temperature of January (coldest) and June (hottest) is 8 °C and 34.3 °C respectively. Meteorological parameters were determined based on daily values of climatic variables obtained

from All Weather Station (AWS) located at National Institute of Technology (NIT) Hamirpur.

1.4 Field Crop Experiments

A setup of two Lysimeters (1.5 × 1.5 × 2 m) was installed in the center of the experimental field at NIT, Hamirpur. Lysimeters were filled with sandy loam soil. Soil properties were examined experimentally in the Geotechnical Laboratory of Civil Engineering Department, NIT Hamirpur. Drainage from one of the Lysimeters is restricted to form water table conditions. A water table variation from 1.3–2.2 m is maintained with the help of piezometers. The other lysimeter is provided with free drainage. For the lysimeters, the daily soil moisture variation at an interval of 0.1 m is measured by the soil moisture profile probe (Diviner 2000 probe, M/S Sentek Sensor Technologies, Stepney, SA, Australia). The difference in moisture depletion between the two lysimeters represents the quantity of moisture contributed by the shallow GWT through the capillary rise. Table 1.1 shows the depth-wise mean textural fractions distribution (Trout et al. 1982), particle density, field capacity, permanent wilting point, and available water which were performed in a Geotechnical laboratory.

Field crop experiments were performed on wheat, maize, Indian mustard, and pea with details been given in Table 1.2. In Fig. 1.1, wheat, maize, peas, and Indian mustard can be seen in their crop development stage. Figure 1.2 shows the variation of crop parameters (root depth, plant height, and leaf area index (LAI)) observed at regular intervals during the crop period. Reference evapotranspiration (ET_0) is obtained using the FAO-56 Penman–Monteith equation.

1.5 Performance Evaluation Indicator for Models

The Coefficient of determination (R^2) (Luo and Marios, 2010) and Nash–Sutcliffe efficiency (NSE) (Legates and McCabe, 1999) are utilized to assess the execution of the models compared to observed values of capillary rise. R^2 indicates the degree of linear dependency and NSE validates the reliability of models and the maximum value for both evaluation indices is 1. The performance of a model is considered better when R^2 and NSE are higher and MBE is lower. The equations are

$$R^2 = \frac{\sum_{cr=1}^{n} \left(Ob_{cr} - \overline{Ob_{cr}}\right)\left(Es_{cr} - \overline{Es_{cr}}\right)}{\sqrt{\sum_{cr=1}^{n} \left(Ob_{cr} - \overline{Ob_{cr}}\right)^2} \sqrt{\sum_{cr=1}^{n} \left(Es_{cr} - \overline{Es_{cr}}\right)^2}} \tag{1.1}$$

$$NSE = 1 - \frac{\sum_{cr=1}^{n} \left(Ob_{cr} - Es_{cr}\right)^2}{\sum_{cr=1}^{n} \left(Ob_{cr} - \overline{Ob_{cr}}\right)^2} \tag{1.2}$$

Table 1.1 Soil properties for the study area

Soil depth (m)	Bulk density (g/c.c)	Gravel (%)	Sand (%)	Silt (%)	Clay (%)	Particle density (g/c.c)	Field capacity (F_c) (cm^3/cm^3)	Permanent wilting point (PWP) (cm^3/cm^3)	Available water (cm^3/cm^3)
0.0–0.2	1.51	27.0	54.98	23.83	21.19	2.54	0.22	0.07	0.15
0.2–0.4	1.56	32.40	57.48	24.41	18.11	2.59	0.212	0.072	0.14
0.4–0.6	1.63	24.70	59.24	24.27	16.49	2.61	0.208	0.058	0.15
0.6–0.8	1.67	26.03	55.07	29.62	15.31	2.63	0.206	0.066	0.14
0.8–1.0	1.72	25.10	51.6	34.4	14.0	2.58	0.205	0.057	0.15

Table 1.2 Details of crops

Crop	Date of sowing	Date of harvesting	Duration (days)	Growth stages (days)				Irrigation provided (DAS)	Spacing (cm)
				I	II	III	IV		
Wheat (*Triticumaestivum*)	1st January 2015	4th May 2015	124	24	33	42	25	22nd, 39th, 50th, 71st, 90th, 118th	20 × 5
Maize (*Zea mays*)	11th May 2015	9th September 2015	120	22	36	40	22	20th, 44th, 64th, 89th	50 × 20
Pea (*Pisumsativum*)	18th September 2015	16th December 2015	90	18	30	25	17	10th, 22nd, 36th, 56th, 70th	40 × 15
Indian mustard (*Brassica Juncea*)	22nd January 2016	14th May 2016	114	19	32	38	25	11th, 25th, 37th, 59th, 91st	40 × 15

Fig. 1.1 Experimental view of wheat, maize, peas, and Indian mustard in the crop development stage

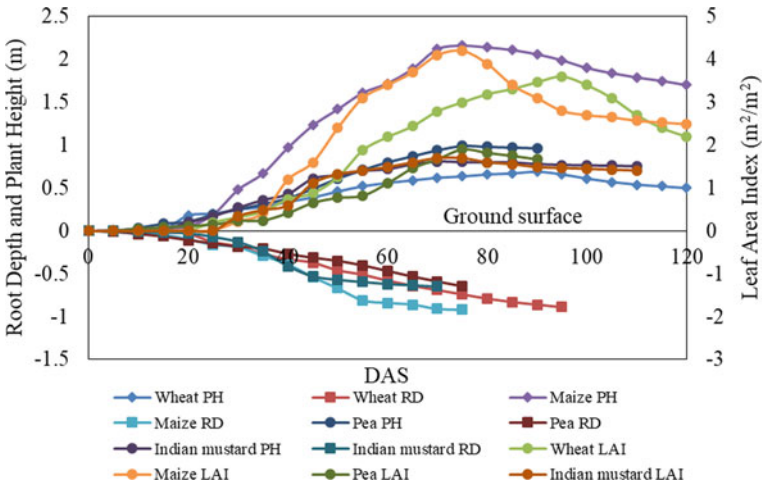

Fig. 1.2 Variation of root depth, plant height, and leaf area index for wheat, maize, and pea

where n = number of observations, Es_{cr} Ob_{cr}, = estimated and observed values. $\overline{Ob_{cr}}$ $\overline{Es_{cr}}$ = observed and estimated average values.

1.6 Results and Discussions

Performance evaluation of Models

Error statistics, i.e., R^2 and NSE values for the models are given in Table 1.3. R^2 and NSE values obtained from the models, i.e., QSSAM, AF, MTSAM, QCRH, and GUEM are lesser than 0.61 which indicates the poor performance of the models. Hence it is predicted that these models possess inadequate applicability for capillary rise estimation which is mostly due to inappropriate and tediously accessible input parameter requirement.

This necessitates the investigation of few easily accessible parameters which can be utilized to formulate a model to determine the capillary rise from the SGT.

Relation between the capillary rise and few easily accessible parameters

The SGT depth was fluctuated from 1.3 to 2.2 m to observe, variation of the capillary rise for wheat, maize, pea, and Indian mustard but brevity Fig. 1.3 shows the variation of capillary rise with days after sowing for wheat, maize, pea, and Indian mustard at 1.5 m depth. Figure 1.3 also shows the seasonal variations of each crop. It was observed that in the summer months, the values of the capillary rise were higher for the crops as compared to the winter months.

The relationship of capillary rise with root depth, plant height, LAI, ET_0, soil moisture, and groundwater table are investigated.

A linear relationship as specified by Table 1.4 ($p < 0.01$) exists between root depth, plant height, and LAI with high determination coefficients (r^2). These parameters are important in understanding plant growth, determining RWU, and irrigation scheduling (Stenitzer et al. 2007). Root depth, plant height, and LAI are easily

Table 1.3 Error statistics of estimated values in comparison with observed values

Crops	Evaluation indicators	Models					
		QSSAM	AF	MTSAM	MAF	QCRH	GUEM
Wheat	R^2	0.42	0.57	0.56	0.66	0.55	0.58
	NSE	0.48	0.55	0.58	0.71	0.59	0.52
Maize	R^2	0.52	0.54	0.59	0.68	0.51	0.58
	NSE	0.45	0.50	0.56	0.71	0.54	0.56
Peas	R^2	0.53	0.58	0.54	0.65	0.55	0.59
	NSE	0.46	0.54	0.59	0.69	0.59	0.54
Indian mustard	R^2	0.47	0.51	0.53	0.67	0.55	0.57
	NSE	0.49	0.53	0.55	0.73	0.58	0.59

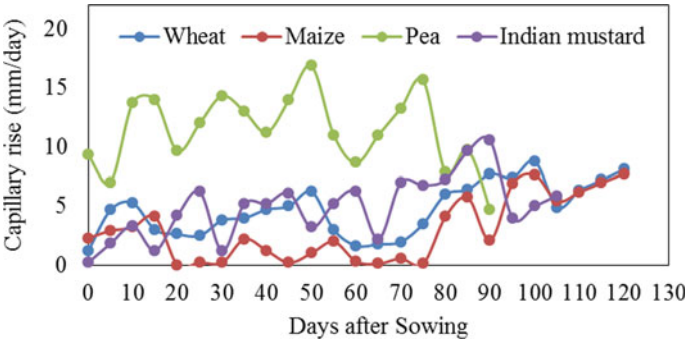

Fig. 1.3 Variation of the capillary rise for wheat, maize, pea, and Indian mustard at 1.5 m depth

accessible crop parameters and must be considered to predict capillary rise from the SGT.

The results of the experiments specify that a good correlation exists between the capillary rise and ET_0 at various depths of the water table. Determination coefficients between capillary rise and ET_0 at 1.3, 1.5, 1.7, 2.0 and 2.2 m SGT depths are 0.71, 0.77, 0.73, 0.68, and 0.61 respectively. Yang et al. (2011) also found capillary rise to have a considerable correlation with pan evaporation when the water table is at 1.5 m.

Table 1.5 shows an inverse correlation between capillary rise (at 1.3, 1.5, and 1.7 m depths) with soil moisture variation and available moisture in soil layers at 10–50 cm depths. Results from the study of Prathapar et al. (1992) were found consistent with the present study.

Table 1.4 Regression models of capillary rise with root depth, plant height, and leaf area index

Water table (m)	Root depth		Plant height		Leaf area index	
	Regression model	r^2	Regression model	r^2	Regression model	r^2
1.3	$Y = 1.917x + 1.0237$	0.63	$Y = 2.017x + 1.0237$	0.65	$Y = 2.512x + 1.0237$	0.64
1.5	$Y = 3.634x + 1.352$	0.74	$Y = 3.371x + 1.352$	0.76	$Y = 3.987x + 1.352$	0.77
1.7	$Y = 8.543x + 1.354$	0.67	$Y = 9.026x + 1.686$	0.67	$Y = 9.926x + 1.121$	0.67

Table 1.5 Regression model of capillary rise with root depth, plant height, and leaf area index

	Water level (m)	Soil moisture at various depths (cm)					
		0–20	20–40	40–60	60–80	80–100	100–120
Capillary rise	1.3	−0.487	−0.521	−0.549	−0.587	−0.545	−0.521
	1.5	−0.687	−0.723	−0.754	−0.766	−0.754	−0.742
	1.7	−0.552	−0.652	−0.642	−0.682	−0.647	−0.684

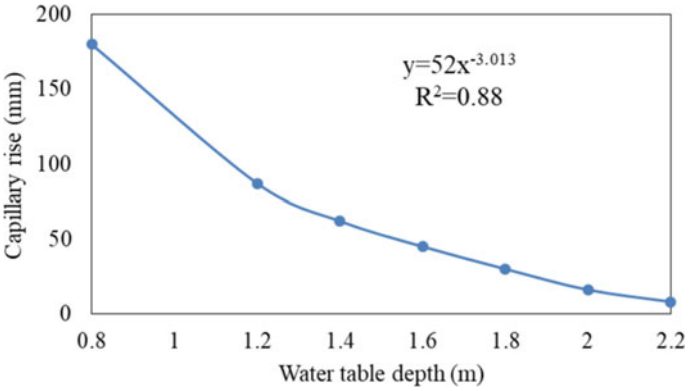

Fig. 1.4 Correlation between the capillary rise and water table depth

A power of exponential function with a high correlation coefficient was observed between the capillary rise and groundwater table depth as shown in Fig. 1.4 Similar results were found in the study of Warrick (1988) and Yang et al. (2011) which shows maximum capillary rise is directly proportional to water table depth.

From the above results and field crop experiments, it is found that root depth, plant height, LAI, ET_0, soil moisture, and groundwater table have good relationship with the capillary rise from SGT at depth 1.5 m. Hence an empirical relation can be formulated incorporating the above parameters.

1.7 Conclusion

The objective of the present study is to recognize and determine easily accessible parameters that affect the capillary rise in a cropped soil. Wheat, maize, pea, and Indian mustard were planted to examine the variation of capillary rise based on crops with fluctuation in the water table and to identify the major parameters that influence the capillary rise. It was observed that crop parameters (root depth, plant height, leaf area index), reference evapotranspiration, soil moisture, and groundwater table affected capillary rise. A linear relationship exists between the crop parameters (root depth, plant height, and leaf area index) with high determination coefficients. A close correlation exists between the capillary rise and reference evapotranspiration at various depths of the water table. Inverse correlation between capillary rise (at 1.3, 1.5, 1.7, 2.0, and 2.2 m depths) with soil moisture variation exists. As depth of the water table was increased, capillary rise obtained from the water table was observed to decrease. Hence root depth, plant height, leaf area index, reference evapotranspiration, soil moisture, and groundwater table can be used as variables to determine the capillary rise from the SGT in cropped soil. The work will further help in optimized irrigation scheduling for the regions having SGT.

Acknowledgements The authors gratefully acknowledge the Department of Civil Engineering, National Institute of Technology Hamirpur for providing necessary facilities related to the study. The financial support was received through DBT-NERC sponsored project titled "Social-economic-environmental tradeoffs in managing Land-river interface (2019–2021)".

References

Fu QP, Zhang JH, Wang QJ (2008) Adaptability study on empirical formulae of frequent phreatic evaporation in Xinjiang. Agric Res Arid Areas 26:182–188

Jorenush MH, Sepaskhah AR (2003) Modelling capillary rise and soil salinity for shallow saline water table under irrigated and non-irrigated conditions. Agric Water Manag 61(2):125–141

Kumar N, Poddar A, Dobhal A, Shankar V (2019a) Performance assessment of PSO and GA in estimating soil hydraulic properties using near-surface soil moisture observations. Compusoft 8(8):3294–3301

Kumar N, Poddar A, Shankar V (2019b) Optimizing irrigation through environmental canopy sensing–a proposed automated approach. In AIP conference proceedings, vol 2134, no. 1. AIP Publishing LLC, p 060003. https://doi.org/10.1063/1.5120228

Kumar N, Shankar V, Poddar A (2020) Agro-hydrologic modelling for simulating soil moisture dynamics in the root zone of Potato based on crop coefficient approach under limited climatic data. ISH J Hydraul Eng 1–17

Legates DR, McCabe GJ (1999) Evaluating the use of "goodness-of-fit" measures in hydrologic and hydroclimatic model validation. Water Resour Res 35(1):233–241

Liu Q, Yasufuku N, Miao J, Ren J (2014) An approach for quick estimation of maximum height of capillary rise. Soils Found 54(6):1241–1245

Luo Y, Marios S (2010) Seasonal groundwater contribution to crop-water use assessed with lysimeter observations and model simulations. J Hydrol 389:325–335

Ojha CSP, Hari Prasad KS, Shankar V, Madramootoo CA (2009) Evaluation of a nonlinear root water uptake model. J Irrig Drain Eng (ASCE) 35(3):303–312

Poddar A, Kumar N, Kumar R, Shankar V, Jat MK (2020) Evaluation of non-linear root water uptake model under different agro-climates. Curr Sci 119(3):485

Poddar A, Sharma A, Shankar V (2017) Irrigation scheduling for potato (solanum tuberosum l.) based on daily crop coefficient approach in a sub-humid sub-tropical region. In Proceedings of hydro-2017 international, L. D. College of Engineering Ahmedabad, India

Poddar A, Kumar N, Shankar V (2018) Effect of capillary rise on irrigation requirements for wheat. In: Proceedings of international conference on sustainable technologies for intelligent water management (STIWM-2018), IIT Roorkee, India

Poddar A, Kumar N, Shankar V (2021a) Performance evaluation of four models for estimating the capillary rise in wheat crop root zone considering shallow water table. In: Pandey A, Mishra S, Kansal M, Singh R, Singh VP (eds) Hydrological extremes. Water science and technology library, vol 97. Springer, Cham. https://doi.org/10.1007/978-3-030-59148-9_29

Poddar A, Kumar N, Shankar V (2021b) Evaluation of two irrigation scheduling methodologies for potato (Solanum tuberosum L.) in north-western mid-hills of India. ISH J Hydraul Eng 27(1):90–99. https://doi.org/10.1080/09715010.2018.1518733

Prathapar SA, Robbins CW, Meyer WS, Jayawardane NS (1992) Models for estimating capillary rise in a heavy clay soil with a saline shallow water table. Irrig Sci 13(1):1–7

Raes D, Deproost P (2003) Model to assess water movement from a shallow water table to the root zone. Agric Water Manag 62(2):79–91

Schoeller H (1961) Les eauxsouterraines. Masson etCieEditeurs, Paris

Sharma BB, Kumar N (2021) IoT-based intelligent irrigation system for paddy crop using an internet-controlled water pump. Int J Agric Environ Inf Syst (IJAEIS) 12(1):21–36. https://doi.org/10.4018/IJAEIS.20210101.oa2

Stenitzer E, Diestel H, Zenker T, Schwartengräber R (2007) Assessment of capillary rise from shallow groundwater by the simulation model SIMWASER using either estimated pedotransfer functions or measured hydraulic parameters. Water Resour Manage 21(9):1567–1584

Trout TJ, Garcia-Castillas IG, Hart WE (1982) Soil water engineering: field and laboratory manual. Academic Publishers, Jaipur, India

Wang X, Huo Z, Feng S, Guo P, Guan H (2016) Estimating groundwater evapotranspiration from irrigated cropland incorporating root zone soil texture and moisture dynamics. J Hydrol 543:501–509

Yang J, Li B, Shiping L (2000) A large weighing lysimeter for evapotranspiration and soil water–groundwater exchange studies. Hydrol Process 14(10):1887–1897

Yang F, Zhang G, Yin X, Liu Z, Huang Z (2011) Study on capillary rise from shallow groundwater and critical water table depth of a saline-sodic soil in western Songnen plain of China. Environ Earth Sci 64(8):2119–2126

Zammouri M (2001) Case study of water table evaporation at Ichkeul Marshes (Tunisia). J Irrig Drain Eng 127(5):265–271

Chapter 2
Study of Groundwater Table Fluctuations in the Command Area of Bhagwanpur Distributary of the Eastern Gandak Project

Mani Bhushan, Souvik Mukherjee, Ashutosh Upadhyaya, and Lal Bahadur Roy

Abstract Study of groundwater fluctuation and estimation of groundwater recharge is an important aspect of water resource investigation, management, and development. In this paper, groundwater fluctuation has been analyzed and groundwater recharge has been estimated by water table fluctuation method as a case study for the data of the year from 1996 to 2003 for the command area of Bhagwanpur Distributary in Eastern Gandak Project in Bihar, India. Relation between rainfall and groundwater recharge has been estimated for the periods pre-monsoon to post-monsoon Kharif. During the observation period, groundwater level mostly remained within the top 6 m of subsurface soil at each of the three locations. Highest water table has been found at 0.27 m below the ground surface at Goraul-2 site in August 1999 during the monsoon period and the lowest water table of 6.35 m below ground surface was found at Bhagwanpur-1 location in 1996 during the month of May in pre-monsoon period. Average annual groundwater fluctuation for the period from May to May at Bhagwanpur-1, Saraiya-1, and Goraul-2 were +0.48 m, +0.0025 m and +0.18 m, respectively. The results of the yearly groundwater fluctuation indicate the rising trend of groundwater table. Average monsoon groundwater recharge at Bhagwanpur-1, Saraiya-1, and Goraul-2 during were 24.78%, 21.09%, and 30.27% of rainfall, respectively. Average monsoon rainfall during 1996–2003 was 1158.15 mm and average depth of groundwater recharge at Bhagwanpur-1, Saraiya-1, and Goraul-2 were 273 mm, 248 mm, and 334 mm. respectively.

Keywords Groundwater fluctuation · Groundwater recharge · Water Table Fluctuation Method (WTF)

M. Bhushan · L. B. Roy (✉)
Civil Engineering Department, NIT Patna, Ashok Rajpath, Mahendru, Patna 800005, India
e-mail: lbroy@nitp.ac.in

S. Mukherjee
NIT Patna, Ashok Rajpath, Mahendru, Patna 800005, India

A. Upadhyaya
Division of Land and Water Management, ICAR Research Complex for Eastern Region, ICAR, Patna, India

R. Jha et al. (eds.), *Groundwater and Water Quality*, Water Science and Technology Library 119, https://doi.org/10.1007/978-3-031-09551-1_2

2.1 Introduction

Water sustains plants and plants sustain life, i.e., it has been rightly said that water is life. The primary source of water on the earth is precipitation. Most of the part of rainfall goes as runoff during monsoon season. Some quantity of water percolates the soil surface and joins the groundwater with a very slow rate of recharge. Study of groundwater level data is significant in evaluation, development, and management of groundwater (Nayak et al. 2003).

Groundwater recharge is defined as its entry into the saturated zone of water made available at the water table surface (Freeze and Cherry 1979). Accurate estimation of recharge is difficult because the process is complex and depends on numerous local factors, including precipitation amount, intensity and duration, evapotranspiration rate, runoff, geology, soil characteristics, topography, vegetation, and land use (Memon 1995).

Study of groundwater also provides information about crop growth. As all crops need good root aeration in order to produce optimum yield. Waterlogging of the entire root zone for a period of two or three days is likely to be fatal if it occurs at the crop germination stage but is not so serious during the active growing stage for irrigated dry crops (Smedema and Rycroft 1983).

According to USGS groundwater information, selected methods for estimating the groundwater recharge in humid regions are broadly classified into five types. These are water budget method, unsaturated zone method, groundwater method, stream flow method, and tracer method. For the present study, water table fluctuation (WTF) method which comes under Groundwater methods has been used for recharge calculation. As per Healy and Cook (2002), WTF method is applicable to unconfined aquifers and the aquifer in the study area is an unconfined aquifer.

2.2 The Study Area

Bihar is an eastern state in India. About 40% of the total cropped area in Bihar is flood affected. The temperature during summer is nearly 35–40 and 18–29 °C during winters. Heavy rainfall is witnessed during monsoon seasons. Sometimes little amount of rains is also observed during summers and winters. Also there is not much scope for improvement in the yield of crops due to waterlogging, poor drainage, and ill water management.

The command area of Bhagwanpur Distributary of the Eastern Gandak Project in Bihar lies in between 26° 01′ 21 ′N and 25° 52′ N and the longitude of 85° 09′ E to 85° 14′ E under the eastern Gandak Project, Bihar. Bhagwanpur distributary is a tail end distributary of the eastern Gandak Canal system. It is part of Vaishali Branch Canal which offtakes from Tirhut Main Canal. It has two sub-distributaries, i.e., Patehra sub-distributary and Rikhar sub-distributary. Bhagwanpur distributary starts near the village Manikpur, southeast to Saraiya and flows up to the villages Lalpura in Lalganj

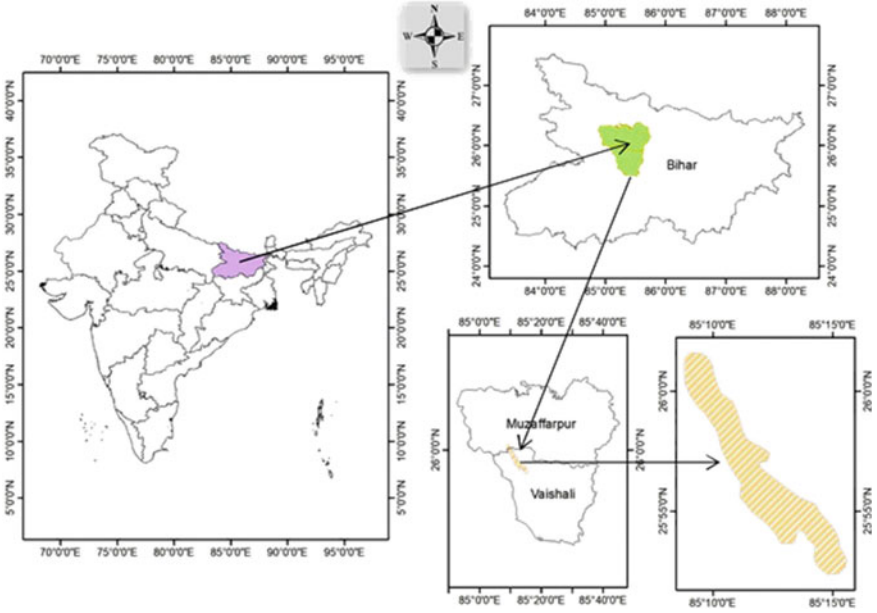

Fig. 2.1 Location map of the study area

block. Irrigation area covered by Bhagwanpur Distributary is almost around 4500 ha, which includes many villages in Saraiya block in Muzaffarpur district and Vaishali and Lalganj blocks in Vaishali district in the state of Bihar in India.

The study area lies under the agro-climatic zone I. Texture of the soil is mainly sandy loam and loam and the soil is young alluvial calcareous. Average slope of the land is varying between 0 and 10% and elevation is varying roughly between 50 and 60 m above from mean sea level. Average annual rainfall in the area is 1171.5 mm for the period 1981–2016. For the present study, three observation sites of Central Ground Water Board have been selected. These are Bhagwanpur-1 (Latitude 25.854 N, Longitude 85.320 E), Saraiya-1 (Latitude 26.016 N, Longitude 85.166 E), and Goraul-2 (Latitude 25.941 N, Longitude 85.325 E). All the three groundwater sites are very close to the study area. As there was no observation site available within the study area, analysis of data from these three sites have been done in the present study (Fig. 2.1).

2.3 Methodology

The groundwater levels are analyzed for the duration of 8 years between 1996 and 2003, for all the three observation sites. Data have been collected from Central Ground Water Board, India. Data are available for four different periods. These are

Table 2.1 Approximate percentage of deep percolation loss from rainfall (Source: USBR Drainage Manual 1993)

Texture of soil	Deep percolation (%)	Texture of soil	Deep percolation (%)
Loamy sand	30	Clay loam	10
Sandy loam	26	Silt clay loam	6
Loam	22	Sandy clay	6
Silt loam	18	Clay	6
Sandy clay loam	14		

Pre-Monsoon (observed between 20 and 30th May), Monsoon (observed between 20st and 30th August), Post-Monsoon Kharif (observed between 01 and 10th November), and Post-Monsoon Rabi (observed between 1st and 10th January). Trend of groundwater rise and range of groundwater fluctuation was determined by graphical approach.

The Water Table Fluctuation (WTF) Method is very simple and easy to apply as per Delin et al. (2007). Recharge by the WTF is estimated from the following equation by Healy and Cook (2002). To apply the WTF method Sy should be known or estimated and it is assumed that it remains constant over the time period of water table fluctuation.

$$R(tj) = Sy * \Delta H(tj) \tag{2.1}$$

where R(tj) is the recharge occurring in cm between time t0 and tj,

Sy is specific yield (dimensionless) and

ΔH (tj) is the water table rise in cm attributed to the recharge period.

Main challenge of WTF method is to estimate the value of specific yield. From the "Report of the Groundwater Resource Estimation Committee" by the Ministry of Water Resources Govt. of India (2009), it has been noted that for sandy alluvial soil in India, specific yield value varies between 12 and 18%. Therefore for this study, specific yield value has been assumed to be 15%, i.e., average of the two values as given in Table 2.2.

For the estimation of groundwater rise or build up during pre-monsoon to post-monsoon Kharif, deep percolation from rainfall is very important. Therefore, based on deep percolation loss as given in Table 2.1 and specific value as given in Table 2.2, groundwater rise can be estimated.

2.4 Results and Discussion

It is observed from Figs. 2.2, 2.3, and 2.4, which during each year for the period between 1996 and 2003, groundwater level in post-monsoon Kharif was always

Table 2.2 Specific yield for different kind of geological formation in the zone of water table fluctuation (*Source* Ministry of Water Resource, Government of India, 2009)

Soil formation	Range of specific yield in percentage
Sandy alluvial area	12–18
Valley fills	10–14
Silty/clayey alluvial area	5–12
Granites	2–4
Basalts	1–3
Laterite	2–4
Weathered phyllites, shales, schist and associated rocks	1–3
Sandstone	1–8
Limestone	3
Highly karstified limestone	7

higher than that of pre-monsoon. It indicates that significant amount of recharge takes place every year during monsoon.

Groundwater zoning is done from waterlogging point of view. Higher the groundwater level, more likely that affects the optimum growth of crops because subsurface waterlogging within the root zone creates the aeration problem. Groundwater level below 3 m does not affect the crop growth. Therefore, it is a safe zone for crops. Most of the crops have root zone less than 2 m. Therefore below this depth, groundwater zone varies from worst to bad. Beyond 2 m of depth alarming zone starts. Based on this concept groundwater zoning has been done and shown in Table 2.3.

It is observed from Fig. 2.2 that during Monsoon in 2004, the groundwater table reached within the top 1 m soil depth. For crops with root zone depth within top 1 m or less than 1 m, this depth of water table is not desirable. Even in the post-monsoon

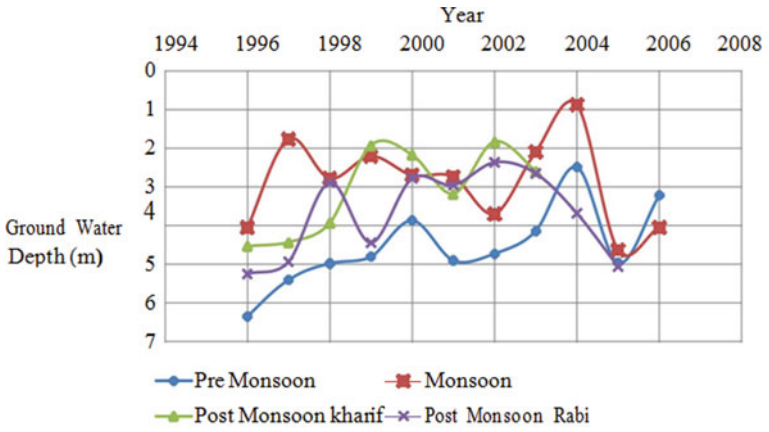

Fig. 2.2 Fluctuation of groundwater table at Bhagwanpur-1

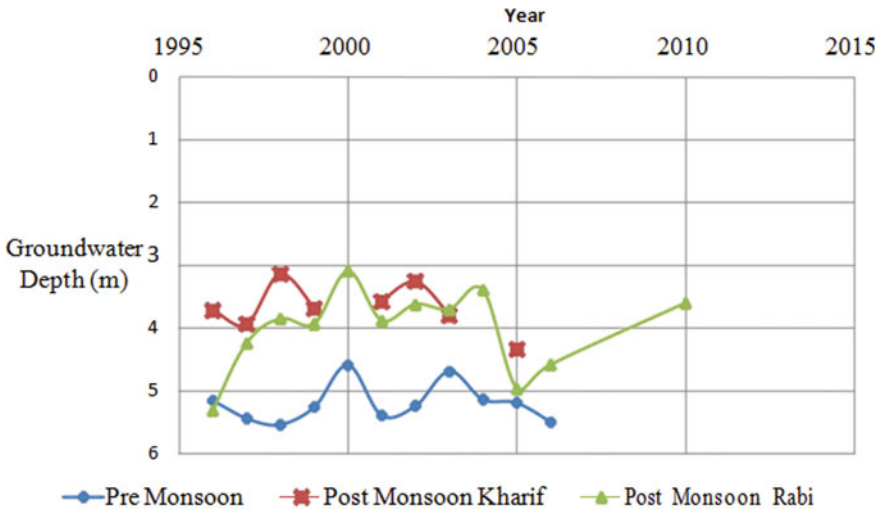

Fig. 2.3 Fluctuation of groundwater table at Saraiya-1

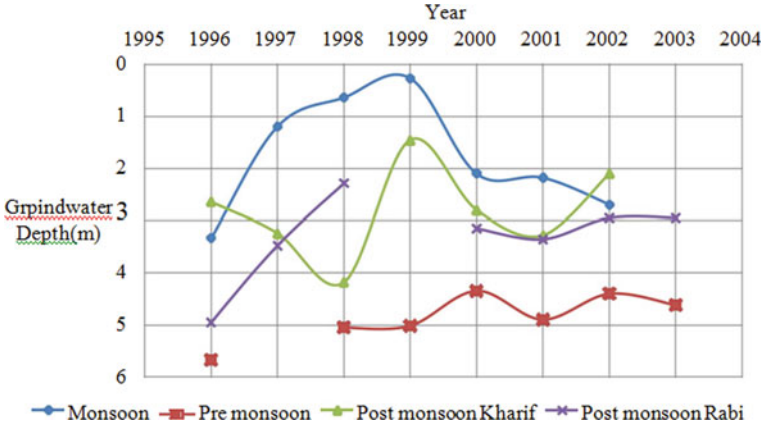

Fig. 2.4 Fluctuation of groundwater table at Goraul-2

season in 1999 and 2002 the water table is within 2 m from soil surface. Therefore, the crops with high root zone depth may suffer from subsurface waterlogging.

For the year from 1997 to 1999, there is a tendency of rising water table during monsoon season as shown in Fig. 2.4. Particularly in the year 1999, the groundwater table during monsoon and post-monsoon Kharif varied within 1.5 m, which will be harmful for most of the cereal crops. The monsoon groundwater table depths in 1998 and 1999 are 0.64 m and 0.27 m respectively, which are deeply encroach the root zone depth causing high damage to crops during this period. At Goraul-2 the pre-monsoon groundwater table remains well below ground level varying between 4 to

Table 2.3 Groundwater depth at Bhagwanpur-1 in Vaishali district during 1996–2006

Year of observation	Pre-monsoon (m)	Monsoon (m)	Post-monsoon Kharif (m)	Post-monsoon Rabi (m)	Maximum fluctuation (m)	Remarks
1996	6.35	4.05	4.53	5.25	2.3	Safe
1997	5.4	1.77	4.43	4.93	3.63	Bad
1998	4.98	2.78	3.93	2.89	2.2	Alarming
1999	4.8	2.21	1.93	4.44	2.87	Bad
2000	3.87	2.7	2.17	2.78	1.7	Alarming
2001	4.9	2.74	3.18	2.96	2.16	Alarming
2002	4.73	3.7	1.83	2.37	2.9	Bad
2003	4.14	2.1	2.6	2.65	2.04	Alarming
2004	2.49	0.88	NA	3.68	2.8	Worst
2005	4.96	4.63	NA	5.06	0.43	Safe
2006	3.22	4.05	NA	NA	NA	Incorrect

6 m. But, in the monsoon it remains within top 3 m and in post-monsoon Kharif, the groundwater table remains between 1 and 4 m of soil depth, which indicates that the recharge rate at Goraul-2 is higher than that at Bhagwanpur-1 and Saraiya-1 stations.

For the site Saraiya-1, as shown in Fig. 2.3 and Table 2.4, data for monsoon period were unavailable. The reason behind unavailability of data is that due to flood during monsoon the observation well could be submerged. But, observing the data of the other sites, it can be interpreted that groundwater table during monsoon may vary between 2 and 3 m or even higher during the observation period.

Table 2.4 Groundwater depth at Saraiya-1 in Muzaffarpur District from 1996 to 2006

Year of observation	Pre-monsoon (m)	Post-monsoon Kharif (m)	Post-monsoon Rabi (m)	Maximum fluctuation (m)	Remarks
1996	5.16	3.72	5.31	1.44	Safe
1997	5.44	3.94	4.24	1.5	Safe
1998	5.54	3.14	3.85	2.4	Safe
1999	5.26	3.69	3.93	1.57	Safe
2000	4.59	NA	3.09	1.5	Safe
2001	5.39	3.58	3.88	1.81	Safe
2002	5.24	3.26	3.62	1.98	Safe
2003	4.69	3.8	3.7	0.99	Safe
2004	5.14	NA	3.39	1.75	Safe
2005	5.19	4.34	4.96	0.85	Safe
2006	5.5	NA	4.58	0.92	Safe

From Tables 2.6, 2.7, and 2.8, it is observed that the average groundwater fluctuation between pre-monsoon and post-monsoon rabi is the highest at Goraul-2, i.e., 1.63 m and the lowest at Saraiya-1, i.e., 1.21 m. At Bhagwanpur-1, average groundwater fluctuation between the same period for a year is 1.36 m. On yearly basis comparison between May and May, at Saraiya-1 groundwater level remained almost constant with an average rise of 0.0025 m per year. But Bhagwanpur-1 site shows a tendency of rising water table with an rate of 0.48 m per year, whereas for Goraul-2 average groundwater rise is moderate, i.e., 0.18 m per year. During post-monsoon rabi, Goraul-2 shows a high rise at an average of 1.03 m per year. At the other two sites, the increments are 0.37 m and 0.23 m per year respectively. At Bhagwanpur-1 average pre-monsoon groundwater rise, i.e., 0.48 m is higher than the average post-monsoon rabi groundwater rise, i.e., 0.37 m. At Goraul-2 and Saraiya-1, the average groundwater rise between post-monsoon rabi is higher than that of pre-monsoon. Observing all the fluctuation data, it is clearly seen that at all the three locations groundwater level is rising (Table 2.5).

Table 2.5 Groundwater depth at Goraul-2 in Vaishali District from 1996 to 2003

Year of observation	Pre-monsoon (m)	Monsoon (m)	Post-monsoon Kharif (m)	Post-monsoon Rabi (m)	Maximum fluctuation (m)	Remarks
1996	5.67	3.33	2.64	4.95	3.03	Alarming
1997	NA	1.2	3.24	3.48	NA	Bad
1998	5.5	0.64	4.18	2.29	4.86	Worst
1999	5.02	0.27	1.46	NA	NA	Worst
2000	4.35	2.1	2.8	3.15	2.25	Alarming
2001	4.9	2.18	3.28	3.36	2.72	Alarming
2002	4.4	2.7	2.1	2.95	2.3	Alarming
2003	4.62	NA	NA	2.95	NA	Alarming

Table 2.6 Comparison of groundwater fluctuation during different periods at Bhagwanpur-1

Season	Fluctuation (May–Jan) (m)	Fluctuation (May–May) (m)	Fluctuation (Jan–Jan) (m)
1996–97	+1.1	+0.95	–
1997–98	+0.47	+0.42	+0.32
1998–99	+2.09	+0.18	+2.04
1999–2000	+0.36	+0.93	−1.55
2000–2001	+1.09	−1.03	+1.66
2001–2002	+1.94	+0.17	−0.18
2002–2003	+2.36	+0.59	+0.59
2003–2004	+1.49	+1.65	−0.28
Average	+1.36	+0.48	+0.37

Table 2.7 Comparison of groundwater fluctuation during different periods at Saraiya-1

Season	Fluctuation (May–Jan) (m)	Fluctuation (May–May) (m)	Fluctuation (Jan–Jan) (m)
1996–97	−0.15	−0.28	–
1997–98	+1.2	−0.10	+1.07
1998–99	+1.69	+0.28	+0.39
1999–2000	+1.33	+0.67	−0.08
2000–2001	+1.5	−0.80	+0.84
2001–2002	+1.51	+0.15	−0.79
2002–2003	+1.62	+0.55	+0.26
2003–2004	+0.99	−0.45	−0.08
Average	+1.21	+0.0025	+0.23

Table 2.8 Comparison of groundwater fluctuation during different periods at Goraul-2

Season	Fluctuation (May–Jan) (m)	Fluctuation (May–May) (m)	Fluctuation (Jan–Jan) (m)
1996–97	+0.72	–	–
1997–98	–	–	+1.47
1998–99	+3.21	+0.48	+1.19
1999–2000	–	+0.67	+2.29
2000–2001	+1.2	−0.55	–
2001–2002	+1.54	+0.5	−0.21
2002–2003	+1.45	−0.22	+0.41
2003–2004	+1.67	–	–
Average	+1.63	+ 0.18	+1.03

Analyzing Fig. 2.5a–c the above statement is justified, because the trend lines show that the groundwater level was rising during the observation period between 1996 and 2003. But, the rate of groundwater level rise is not the same for all the three locations. The slope of trend line in Fig. 2.5a, for Bhagwanpur-1 is the highest among all the three. Whereas, in Fig. 2.5c, the slope of trend line is very small, which indicates that at Goraul-2, groundwater table was very close to dynamic equilibrium condition during the observation period of 1996–2003. At Saraiya-1 the rate of rise of groundwater level remains between the other two sites.

Based on the water table build up during pre-monsoon to post-monsoon Kharif as given in Table 2.10, groundwater recharge has been calculated by WTF method. Average rainfall during June to October from 1996 to 2003 is 1158.15 mm. The average recharge at Bhagwanpur-1, Saraiya-1, and Goraul-2 are 273 mm, 248 mm, and 334 mm, respectively, as shown in Fig. 2.9 and average groundwater table rises are 1.82 m, 1.66 m, and 2.23 m respectively. Average groundwater recharge at

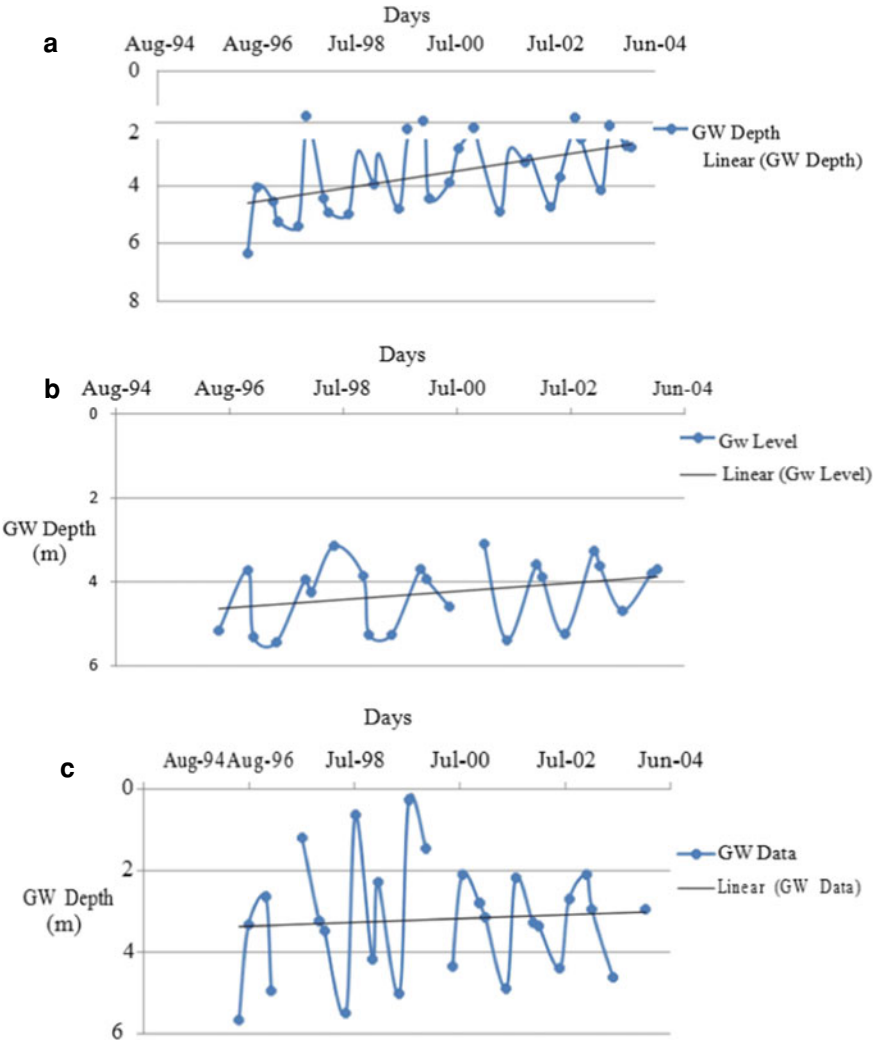

Fig. 2.5 **a** Trend of fluctuation of groundwater table at Bhagwanpur-1 from 1996 to 2003 **b** Trend of fluctuation of groundwater table at Saraiya-1 from 1996 to 2003; **c** Trend of fluctuation of groundwater table at Goraul-2 from 1996 to 2003

Bhagwanpur-1, Saraiya-1, and Goraul-2 are 24.78%, 21.09%, and 30.27%, respectively, of the monsoon rainfall. Therefore it is observed that groundwater recharge is maximum at Goraul-2 site in spite of the fact that trend of groundwater rise is lesser than that at the other two sites (Table 2.9).

Recharge as a percentage of rainfall is not constant during all the years of observations. For Bhagwanpur-1, Saraiya-1, and Goraul-2, it is varying between 10.22% to 40.67%, 14.27% to 27.76%, and 12.85% to 50.83% respectively. In the year 1998,

Table 2.9 Fluctuation between the beginning and ending of observation period

Location	Period	Groundwater rise or fall (m)
Bhagwanpur-1	May 1996–May 2006	+3.13
Goraul-2	May 1996–May 2003	+1.05
Saraiya-1	May 1996–May 2006	−0.34

the monsoon rainfall was the highest, but recharge as a percentage of rainfall is not the maximum. Therefore, it can be interpreted that percentage of recharge does not always depend on the amount and intensity of rainfall but also on other factors like soil type and texture, specific yield, etc. In Figs. 2.6, 2.7, and 2.8 comparison of rainfall and recharge has been presented graphically at Bhagwanpur-1, Saraiya-1, and Goraul-2 station, respectively. At Bhagwanpur highest monsoon recharge took place in the year 2002 and lowest recharge took place in 1997 as shown in Fig. 2.6. At Saraiya the highest monsoon recharge took place in 1998 and lowest in 2003 as shown in Fig. 2.7. At Goraul station, in the year 1998 the lowest groundwater recharge took place, whereas in 1999 the highest recharge occurred as shown in Fig. 2.8.

In Fig. 2.9, comparison of recharge at the three places has been shown by bar graph. During 1996–2003, among these three locations the highest monsoon recharge took place in 1999 at Goraul-2 and lowest at Saraiya-1 in 2003. Recharge at Bhagwanpur-1 was varying between 145 and 435 mm with an average of 273 mm per year. During the observation period recharge at Saraiya-1 was varying between 133 and 360 mm with an average of 248 mm per year. Recharge at Goraul-2 was varying between 198 and 534 mm with an average of 334 mm per year. Therefore, it is seen that the average groundwater recharge was maximum at Goraul-2 and minimum at Saraiya-1.

As calculated in Table 2.11 the average of the estimated groundwater build up from pre-monsoon to post-monsoon Kharif is 2.00 m. Observed values at Bhagwanpur-1, Saraiya-1 and Goraul-2 are deviating by −9, −17, and +11.5% .

Table 2.10 Calculation for groundwater recharge by Water Table Fluctuation (WTF) method during monsoon

Year	Rainfall during June–October (mm)	Bhagwanpur-1			Saraiya-1			Goraul-2		
		ΔH (m)	R (m)	% of rainfall	ΔH (m)	R (m)	% of rainfall	ΔH (m)	R(m)	% of rainfall
1996	894	1.82	0.273	30.53	1.44	0.216	24.16	3.03	0.4545	50.83
1997	1187.7	0.97	0.1455	12.25	1.5	0.225	18.94	–	–	–
1998	1540.3	1.05	0.1575	10.22	2.4	0.36	23.37	1.32	0.198	12.85
1999	1146	2.87	0.4305	37.56	1.57	0.2355	20.54	3.56	0.534	46.59
2000	1032.5	1.7	0.255	24.69	–	–	–	1.55	0.2325	22.51
2001	1460	1.72	0.258	17.67	1.81	0.2715	18.59	1.62	0.243	16.64
2002	1069.5	2.9	0.435	40.67	1.98	0.297	27.76	2.3	0.345	32.25
2003	935.2	1.54	0.231	24.70	0.89	0.1335	14.27	–	–	–
Average	1158.15	1.82	0.273	24.78	1.66	0.248	21.09	2.23	0.334	30.27

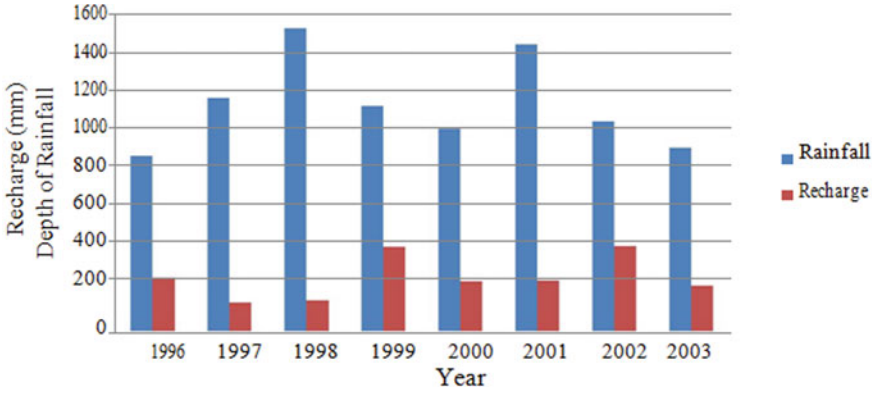

Fig. 2.6 Comparison of rainfall and recharge at Bhagwanpur-1

Table 2.11 Comparison between estimated and observed groundwater rise during pre-monsoon to post-monsoon Kharif

Year	Rainfall during June–October (mm)	Deep percolation @ 26% (mm)	Estimated	ΔH (m)		
				Bhagwanpur observed	Saraiya observed	Goraul observed
1996	894	232.44	1.55	1.82	1.44	3.03
1997	1187.7	308.8	2.06	0.97	1.5	
1998	1540.3	400.48	2.67	1.05	2.4	1.32
1999	1146	297.96	1.98	2.87	1.57	3.56
2000	1032.5	268.45	1.79	1.7		1.55
2001	1460	379.6	2.53	1.72	1.81	1.62
2002	1069.5	278.07	1.85	2.9	1.98	2.3
2003	935.2	243.15	1.62	1.54	0.89	
Average	1158.15	301.12	2.00	1.82	1.66	2.23

2.5 Conclusions

From the above analysis of groundwater fluctuation, the following conclusions are drawn,

1. Maximum average fluctuation occurred between pre-monsoon and post-monsoon Kharif and the least fluctuation occurred between two successive pre-monsoon groundwater depths.
2. From 1996 to 2003, at Bhagwanpur-1, groundwater fluctuated mostly within a range of 2–5 m below ground surface, which is in alarming to safe zone from subsurface waterlogging point of view, i.e., it will not cause any severe damage to crops.

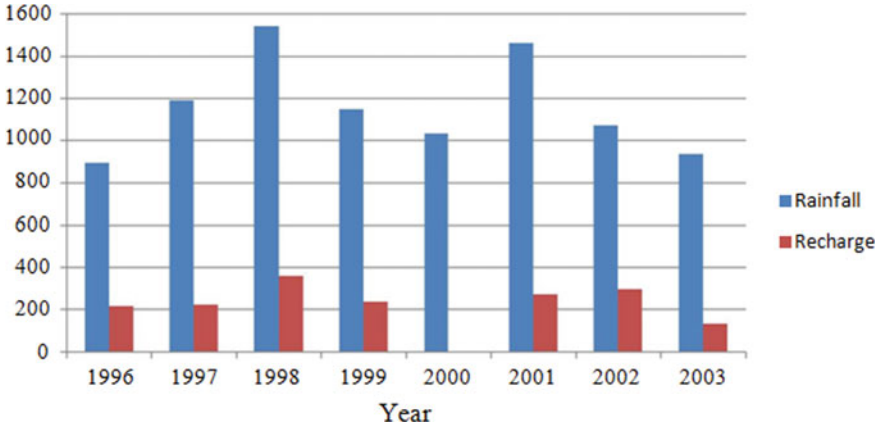

Fig. 2.7 Comparison of rainfall and recharge at Saraiya-1

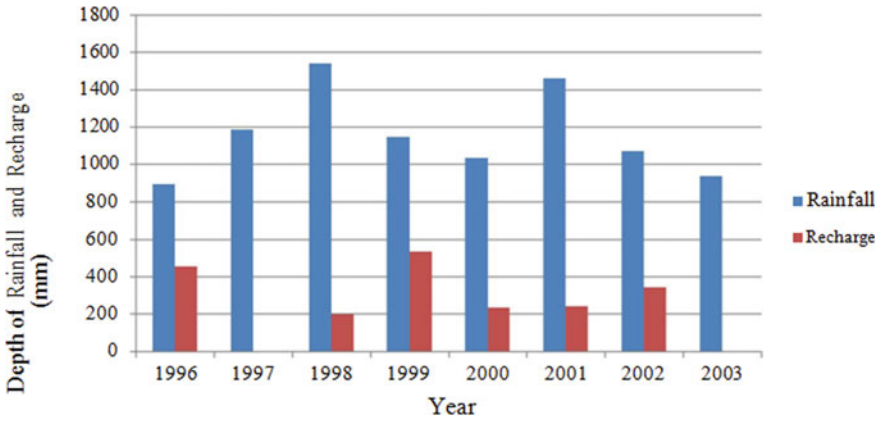

Fig. 2.8 Comparison of rainfall and recharge at Goraul-2

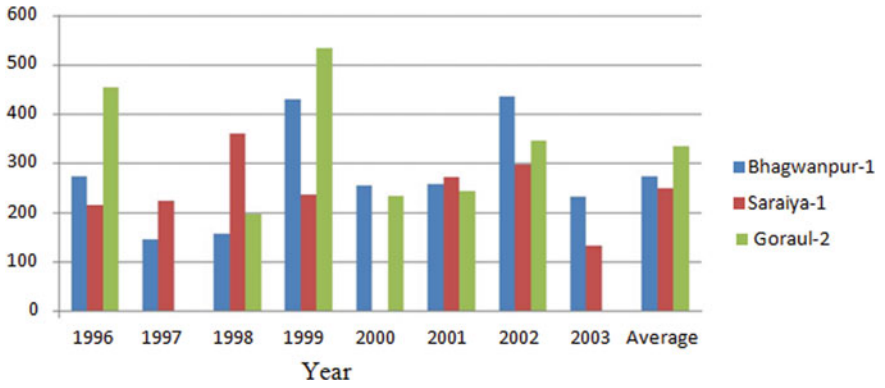

Fig. 2.9 Comparison of groundwater recharge at three locations

Table 2.12 Zone of groundwater level

Depth of groundwater level (m)	Zone
0–1	Worst
1–2	Bad
2–3	Alarming
Below 3	Safe

3. At Goraul-2 fluctuation occurred in a range of 0–6 m below ground level including high water table within 1 m below the ground level several times. Water table reaching top 1 m indicates the worst condition for any crop production except rice.
4. At Saraiya-1, water table remains consistently below 3 m from ground surface creating safe condition from drainage point of view.
5. Average of recharge percentage of the three locations is 25.38%.

Acknowledgements The authors are thankful to the agro-meteorological department of Indian Agricultural Research Institute (IARI), Pusa and Central Ground Water Board (CGWB), India for providing the necessary data for the above analysis.

Appendices

Status of groundwater level from a drainage point of view is determined as per Roy and Kumar (1996) given in Table 2.12. Based on this Table, remarks have been provided on the status of groundwater depth at three different locations as mentioned in Tables 2.3, 2.4, and 2.5.

References

Delin GN, Healy RW, Lorenz DL, Nimmo JR (2007) Comparison of local to regional scale estimates of groundwater recharge in Minnesota, USA. J Hydrol 334:231–249

Freeze RA, Cherry JA (1979) Groundwater Prentice-Hall Inc. Englewood Cliffs, NJ

Healy RW, Cook PG (2002) Using ground water level to estimate recharge. Hydrol J 10:91–109

Memon BA (1995) Quantitative analysis of springs. Environ Geol 26:111–120

Nayak TR, Bhar AK (2003) Monitoring groundwater fluctuation in a part of Bundelkhand. Hydrol J 26(1–2):45–53

Roy LB, Kumar S (1996) Concept of critical water table depth for optimum crop production. In: Sixth ICID drainage workshop on 'drainage and environment'. Slovania

Smedema LK, Rycroft DW (1983) Land drainage: planning and design of agricultural drainage system. Cornell University Press, Ithaca, New York

U. S Department of the Interior Bureau of Reclamation (1993) Drainage manual, a water resources technical publication

Chapter 3
Assessment of Heavy Metals in Sediments from Exploratory Wells for Riverbank Filtration Sites Impacted by Extreme Environmental Conditions Using Principal Component Analysis

G. Krishan, C. Sandhu, T. Grischek, N. C. Ghosh, S. Singh, H. Ganapathi, and N. Arora

Abstract Heavy metal contamination of sediments is often observed as a result of the expansion of industrial sectors and agro-economic systems, especially in developing regions. The high pollution of the river Yamuna in India, especially the substantial heavy metal contamination not only to the river but also increasingly to groundwater in Mathura and Agra regions is of concern for the production of drinking water. Consequently, this study focused on a prognosis of the risk of heavy metal contamination during the investigations for a new riverbank filtration (RBF) site in the cities of Mathura and Agra. Twenty sediment samples were taken at each site during the drilling of an exploratory well for RBF up to a depth of 30 m. The heavy metals As, Cd, Cr, Cu, Fe, Mn, Ni, Pb and Zn were analysed in soil and aquifer sediments and water from the exploratory wells. Principal component analysis (PCA) was subsequently performed for the heavy metal concentrations in the soil and sediment samples. In general, the heavy metal concentrations found in the aquifer sediments were significantly lower compared to concentrations in riverbed

Former affiliation of the Author N. C. Ghosh—Groundwater Hydrology Division, National Institute of Hydrology, Roorkee, Uttarakhand, India.

G. Krishan (✉) · N. C. Ghosh · S. Singh
Groundwater Hydrology Division, National Institute of Hydrology, Roorkee, Uttarakhand, India
e-mail: drgopal.krishan@gmail.com; drgopal.krishan.nihr@gov.in

C. Sandhu · T. Grischek
Division of Water Sciences, Faculty of Civil Engineering, University of Applied Sciences Dresden, Dresden, Germany

N. C. Ghosh
Bengal Institute of Technology, Kolkata, West Bengal, India

H. Ganapathi
Department of Regional Water Studies, TERI School of Advanced Studies, New Delhi, India

N. Arora
Department of Soil and Crop Management, Central Soil Salinity Research Institute, Karnal, Haryana, India

R. Jha et al. (eds.), *Groundwater and Water Quality*, Water Science and Technology Library 119, https://doi.org/10.1007/978-3-031-09551-1_3

material reported in literature, lower than WHO limits for agricultural soils (except Cd and Pb in Agra) and lower than values in other literature sources. While the heavy metal concentrations found in the exploratory well water in Mathura were generally found to be within the WHO drinking water guideline limits, the mean concentrations of Cd and Pb in the exploratory well in Agra significantly exceeded the WHO guideline values. The study concluded that the risk of leaching of heavy metals and consequent contamination to groundwater by the vertical movement of irrigation water is expected to be significantly greater compared to the movement of infiltrated river water through the riverbed during the RBF. Consequently, caution should be exercised when selecting flood-plain areas for new RBF sites that have been irrigated in the past with surface water impacted by heavy metals. The major sources of heavy metals identified by PCA were mainly natural and to a certain extent anthropogenic, especially in the upper layers of the soil/aquifer and is also indicative of a lesser risk of heavy metal contamination during RBF. Nevertheless, for RBF to be effective at new sites impacted by extreme environmental conditions, well-head and source-protection zones have to be implemented to avoid contamination of the aquifer from above ground anthropogenic activities. Furthermore, frequent water quality monitoring for not only heavy metals, but also other parameters in the RBF well(s), river and ambient (landward side) groundwater is important.

Keywords Heavy metals · Sediments · Riverbank filtration · Principal component analysis · Drinking water

3.1 Introduction

Soil, aquifer sediments and groundwater and surface water are crucial components of rural and urban environments that are vulnerable to heavy metal contamination from natural and anthropogenic sources such as mining activities, electronics manufacturing, the use of synthetic products including but not limited to pesticides, paints, batteries, the discharge of industrial wastes including from refineries and land application of industrial or domestic sludge (United States Department of Agriculture 2000; Omwene et al. 2018; Chukwujindu et al. 2018; Wu et al. 2018; Mondal et al. 2010). The vertical distribution of heavy metals in soil and sediment profiles can show large variations (Brümmer et al. 1986; Reiners et al. 1975) and is strongly affected by land use (Jansson 1987). Not only is the excess heavy metal accumulation in upper soils (unsaturated zone) toxic to humans, fauna and flora, but also in the dissolved ionic form in water (Chaturvedi et al. 2018). The most common problematic cationic metals (metallic elements whose forms in soil are positively charged cations, e.g. Pb^{2+}) are mercury, cadmium, lead, nickel, copper, zinc, chromium and manganese, whereas common problematic anionic compounds (elements whose forms in soil are combined with oxygen and are negatively charged, e.g. MoO_4^{2-}) are arsenic, molybdenum, selenium and boron.

The approx. 200 km long stretch of the river Yamuna between the National Capital Region Delhi and the downstream cities of Mathura and Agra in India is amongst the most severely polluted rivers worldwide due to the discharge of partially to untreated municipal and industrial wastewater, accompanied with the disposal of solid waste along the riverbanks (Bhargava 2006). Other than from an ecological perspective, the Yamuna's pollution is of concern for the conventional drinking water production plants in Mathura and Agra, because of the removal of the high concentrations of pathogens, suspended solids, dissolved organic carbon (DOC) and turbidity from the river water is problematic (Singh et al. 2010; Kumar et al. 2012). Moreover, studies during the last four decades confirm that wastewater discharged into the Yamuna and Ganga rivers is attributed as a key source of heavy metal toxicity to the river ecosystem (Chakarvorty et al. 2015; Subramanian and Sitasawad 1984; Singh et al. 2014; Pal et al. 2017; Paul 2017), with up to 292 tons in total for Ni, Cr, Pb, Fe and Zn derived from industrial effluents and municipal wastes disposed annually into the Yamuna river in the vicinity of Delhi alone in/before 1984 (Subramanian and Sitasawad 1984). More recently, the concentrations of certain heavy metals in groundwater in the Mathura region, such as Ni, Fe, Pb, Cr, Cd and Mn, were reported to exceed the Indian Standard drinking water limits (Ahmed et al. 2018). Ahmed et al. (2018) attribute this exceedance to agricultural activities and the upstream discharge of wastewater from paint production, refineries and industries.

On the other hand, water quality investigations at an existing horizontal collector well in the Yamuna riverbed at Gokul barrage in Mathura and riverbank-side vertical wells in Agra found that the natural water treatment technique of riverbank filtration (RBF) can serve at least as a pre-treatment for drinking water production by partial removal of pathogens, turbidity, suspended solids, dissolved organic carbon (DOC) and organic micropollutants (OMPs) (Singh et al. 2010; Krishan et al. 2016; Glorian et al. 2018; Sandhu et al. 2019). In situations of high organic content in surface waters such as in Mathura and where pre-chlorination during conventional treatment is practised, RBF can result in lower doses of chlorine before flocculation (Singh et al. 2010; Kumar et al. 2012).

The regions of Mathura and Agra belong to the most populated regions in the state of Uttar Pradesh. Furthermore, both cities have a high floating population from tourism. A large number of pilgrims visit the banks of the Yamuna in Mathura as it is one of the seven sacred places in Hinduism (Bhargava 2006; Ahmed et al. 2018). Agra is famous worldwide for its historical monuments. Both regions are heavily reliant on groundwater abstractions to meet domestic and irrigational water demand, with Mathura region having 164,294 private tube wells (Ahmed et al. 2018; Khan 2016–2017). These factors and the water quality issues in the two regions have driven the need for sustainable and robust water treatment and management solutions. One such potential solution is RBF, which is an element of integrated water resources management, conjunctive surface and groundwater use and a component of managed aquifer recharge (Grischek and Ray 2009; Dillon et al. 2019). This served as a motivation for the commencement of RBF investigations by drilling one exploratory vertical well each in Mathura and in Agra during 2017/2018.

Although heavy metals have been included in a risk-based assessment of the RBF site in Haridwar by the river Ganga (Bartak et al. 2015), neither river nor groundwater is contaminated by them at this specific site. Nevertheless, the investigation of heavy metals during RBF is recommended, especially if a risk from them is perceived (Bartak et al. 2015). Consequently, as there is scant literature on the presence of heavy metals in aquifer sediments during the exploration phases for new RBF sites, this study focuses on a prognosis of the risk of heavy metal contamination at new RBF sites that are influenced by extreme environmental conditions like those prevailing along the Yamuna.

3.2 Materials and Methods

3.2.1 Study Area

The cities of Mathura and Agra are located in the state of Uttar Pradesh, North India, 150 and 200 km, respectively, to the South of the capital New Delhi (Fig. 3.1). Mathura and Agra, with a metropolitan population of nearly 455,000 and 1.8 million inhabitants respectively (Census of India 2011), rank amongst the larger cities on the banks of the Yamuna in the alluvial Indo-Gangetic Plain.

The region has thick unconsolidated alluvial sediments and high-yield groundwater wells, however groundwater in the Agra-Mathura areas is characterised by high salinity (Misra and Mishra 2006). The salinity (in terms of electrical conductivity) of river and bankside groundwater in these areas was found to be relatively high (~1700 and ~2000–3400 μS/cm, respectively) (Krishan et al. 2016).

Silty, sandy and loamy soils are commonly found in the Agra-Mathura region (Khan 2016–2017). As reported by the Central Groundwater Board (CGWB) (Khan 2016–2017), the depth to groundwater is generally shallow at 2.65–14.34 m below ground level (BGL) during the pre-monsoon and 1.33–14.0 m BGL during post-monsoon. The region is underlain by younger and older alluvium of quaternary age. The alluvial deposits include silt, sand, clay, kankar and gravels, and occasionally thick bands of clays. Mathura is reported to have a relatively extensive network of 103,770 irrigation canals (Khan 2016–2017).

3.2.2 Soil and Sediment Sampling and Analysis

Soil and sediment samples were collected during rotary drilling of exploratory boreholes of 550 mm diameter (150 mm diameter for casing and filter screen pipes) in Mathura and Agra. The boreholes were drilled up to a depth of 30 m in Mathura and 43 m in Agra. 20 samples were collected from each borehole. Soil texture was determined using dry sieving analysis at Soil Water Laboratory of National Institute

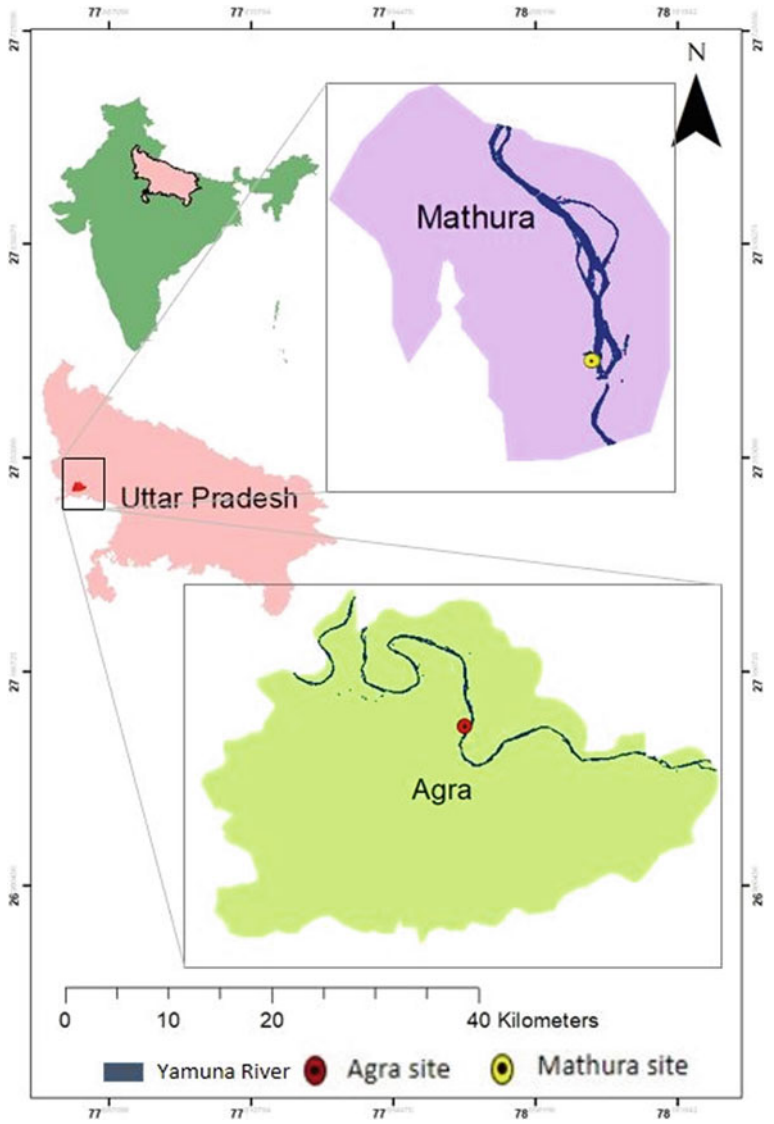

Fig. 3.1 Study area

of Hydrology, Roorkee. Soil texture classification was done using the soil texture classification triangle (Fig. 3.2).

It is observed that the sediments at Mathura range between poorly graded sandy loam to loamy sand at all depths except silty loam in patches from 8 to 20 m depth. In Agra, sediments at almost all depths range from poorly graded sandy loam in

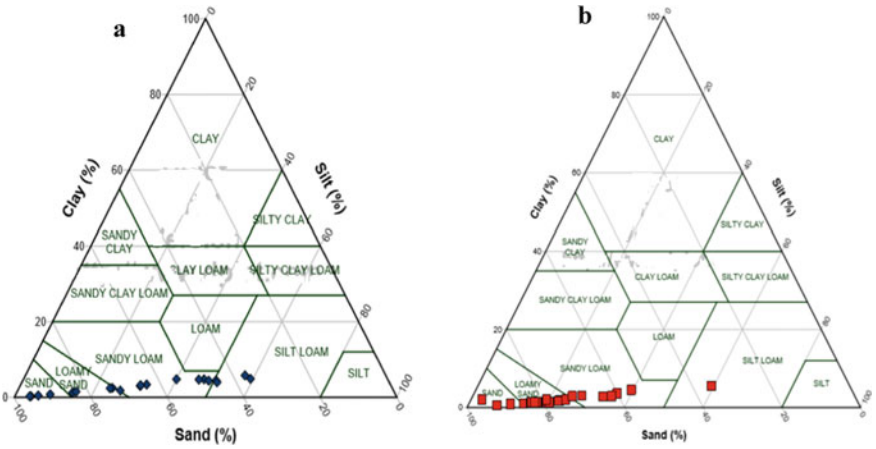

Fig. 3.2 Soil texture classification **a** Mathura, **b** Agra

the upper layer up to 2 m to loamy (silty) sand at greater depth up to 43 m. These observations conform to those reported by CGWB (Khan 2016–2017).

The grain size fraction of <1 mm of all sediment samples was extracted for analysis of Cd, Cr, Ni and Pb using 0.5 M Ethylenediaminetetraacetic acid (EDTA) and As, Fe, Mn, Zn and Cu using 0.005 M Diethylenetriamine pentaacetate (DTPA) (Lindsay and Norwell 1978). The extracts were analysed for As, Cd, Cr, Cu, Fe, Mn, Ni, Pb and Zn using a inductively coupled plasma emission spectrometer (ICPE 9000 series, Shimadzu) at the Central Analytical Facility, CSSRI (ICAR), Karnal.

3.2.3 Water Sampling and Analysis

Five water samples were collected for the analysis of heavy metals from each exploratory well in Mathura and Agra at 12-h intervals during their 60-h development after drilling was completed. All samples were filtered with 0.45-μm syringe filters. Subsequently, the samples were conserved with nitric acid. The analyses for heavy metals were conducted using a inductively coupled plasma emission spectrometer (ICPE 9000 series, Shimadzu) at the Central Analytical Facility, CSSRI (ICAR), Karnal.

3.2.4 Principal Component Analysis

Principal component analysis (PCA) was subsequently performed for the heavy metal concentrations in the soil and sediment samples according to Everitt and Dunn

(1992). The objective of applying PCA was to identify the major causes of variance of heavy metal concentrations in the soil and aquifer sediment at the sites of the RBF exploratory wells. PCA is a statistical tool to determine the key variables in a large set of data, to examine multivariate relationships and explain data variance by reducing the number of variables (Everitt and Dunn 1992). It has been used to estimate spatial and temporal patterns of heavy metal contamination (Shine et al. 1995; Krishan et al. 2018), performance evaluation of agricultural drainage water (Nasr and Zahran 2016), multivariate assessment of water quality (Jankowska et al. 2017) and an evaluation of water quality of the Yamuna river (Jaiswal et al. 2019). Correlations between OMP removals and hydrogeochemical conditions during RBF have also been investigated using PCA (Maeng 2010).

3.3 Results and Discussion

3.3.1 Heavy Metal Concentrations in Soil and Aquifer Sediments of Exploratory Well Mathura

The sediment composition and heavy metal concentrations found in the sediments of the exploratory well in Mathura are compared to the WHO limits for agricultural soils (Kinuthia et al. 2020; WHO 1993, 2011), to the limits for pollution of well-head protection zones defined by the senate-department for urban development of Berlin (SVfS 2005) (which are widely applied in Germany) and to data from an aquifer sediment study at the RBF site Torgau by the river Elbe, Germany (Grischek et al. 1993) (Table 3.1). Further, Table 3.1 also includes a comparison of these concentrations to heavy metal concentrations determined for the Yamuna riverbed/bank sediments up to depths of 35–50 cm as reported in Ajmal et al. (1985) and Jha et al. (1990). A perusal of data in Table 3.1 indicates that the heavy metal concentrations in the sediments from the exploratory well are substantially lower compared to corresponding metal concentrations in the riverbed/bank sediment reported in previous studies (Ajmal et al. 1985; Jha et al. 1990). The upper 0–5 cm of sediment is relatively more abundant in heavy metal concentrations compared to the deeper sediment, with a general decrease of concentrations observed with increasing depth (Jha et al. 1990).

It is not possible to observe a natural cycle of sedimentation because of cultivation within the dry river bed and excavation of riverbed sediments for construction in the non-monsoon season and redistribution of reworked sediments during monsoon floods (Jha et al. 1990). Furthermore, with the mean grain size of suspended sediments (constituted of 40–50% clay minerals) in the range of 14–20 μm and grain size of bed and core sediments 10-times greater (Jha 1986), suspended sediment-particles are therefore enriched in metals compared with core sediments (Jha et al. 1990). This implies that heavy metals in the river water are effectively adsorbed onto the riverbed sediments.

Table 3.1 Statistical summary of sediment composition and heavy metal concentration at Mathura ($n = 20$)

Parameter	Sediment (%)				Concentration (μg/kg)								
	Gravel	Sand	Silt	Clay	As	Cd	Cr	Cu	Fe	Mn	Ni	Pb	Zn
Minimum	0.03	35.8	3.8	0.3	23	48	26	2	192	147	33	18	8
Maximum	6.6	95.8	54.8	5.8	66	114	40	101	1180	2560	59	277	102
Average	1.96	65.87	29.52	2.95	46	90	32	27.0	498	541	42	78	40
Stdev	2.26	19.99	17.17	1.76	13	18	3	27	256	533	5.8	568	21
Yamuna riverbed/bank[a]	n.a.	n.a.	n.a.	n.a.	n.d.	310–660	8.6–200k	8.8–19.8k	4,600–6,500k	193–558k	5.2–32k	1–9.3k	198–292k
WHO limits for agricultural soil (WHO 1993, 2011)	–	–	–	–	n.s.	3	100	n.s.	n.s.	n.s.	50	100	n.s.
Well-head protection zone limits (SVfS 2005)					40k	3k	200k	120k	n.s.	n.s.	140k	200k	400k
RBF, Torgau, Germany (Grischek et al. 1993)					<1k	<1k	<5k	3k	1000k	<10k	<10k	<10k	<10k

[a] Ajmal et al. (1985), concentrations reported in μg/g, here converted to μg/kg; k: '000; n.a.: not applicable; n.d.: not determined; n.s.: not specified

3.3.2 PCA of Heavy Metals in Soil and Aquifer Sediments of Exploratory Well Mathura

Table 3.2 shows the correlation matrix for PCA of As, Cd, Cr, Cu, Fe, Mn, Ni, Pb and Zn. Only few parameters exhibited significant correlation relationships. Moderate and positive correlation of Cd can be observed with Cr, Cu, Ni and Zn ($r = 0.472$–0.635); and Cu with Ni, Pb and Zn ($r = 0.52$–0.748) while high and positive correlation of Cr can be observed with Cu, Ni and Zn ($r = 0.713$–0.949). The variation in correlation may be due to the contribution of these metals from different sources. This observation conforms to a previous study by Ahmed et al. (2018), who did not observe a significant correlation among evaluated heavy metals in groundwater in Mathura. Ahmed et al. (2018) also suggested that these heavy metals are not associated with each other and stated that the heavy metals originate from different anthropogenic and natural sources in groundwater.

To reduce data but simultaneously maximise information from original data, the observations are rotated into orthogonally correlated variables or principal components (PCs) (Jankowska et al. 2017; Jaiswal et al. 2019), where the new axes represent the directions of maximum variances (see also Fig. 3.3). Table 3.3 represents the determined initial PC and their eigenvalue and variance contributed in each PC. The table shows eigenvalues for each component in which two PCs were obtained with eigenvalues >1 and thereby accounting for almost 74.3% of the total variance in the heavy metal dataset. This in turn implies that the first four PCs are the most significant component which represent 74.3% of the variance in heavy metal concentrations (39.5% by PC1, 19.0% by PC2, 9.5% by PC3 and 6.3% by PC4).

It is observed that only 2 factors are present with an eigenvalue greater than 1. Here, factor 1 explains 55% of variance in the data, whereas factor 2 explains 18.9% variance in the data. Correlation of the factorial component and heavy metal concentration is given in Table 3.4 which shows that there is a moderate positive

Table 3.2 PCA correlation matrix of heavy metal concentrations in soil and sediment samples from exploratory well in Mathura

	As	Cd	Cr	Cu	Fe	Mn	Ni	Pb	Zn
As	1								
Cd	**−0.449**	1							
Cr	−0.419	**0.574**	1						
Cu	−0.414	**0.472**	**0.949**	1					
Fe	**−0.504**	0.307	0.294	0.356	1				
Mn	−0.288	0.106	−0.170	−0.079	**0.560**	1			
Ni	**−0.596**	**0.579**	**0.713**	**0.748**	**0.557**	0.223	1		
Pb	**−0.610**	0.146	0.439	**0.520**	**0.795**	0.260	**0.530**	1	
Zn	**−0.609**	**0.635**	**0.721**	**0.685**	**0.592**	−0.060	**0.801**	**0.610**	1

Bold represents good correlation—moderate to high

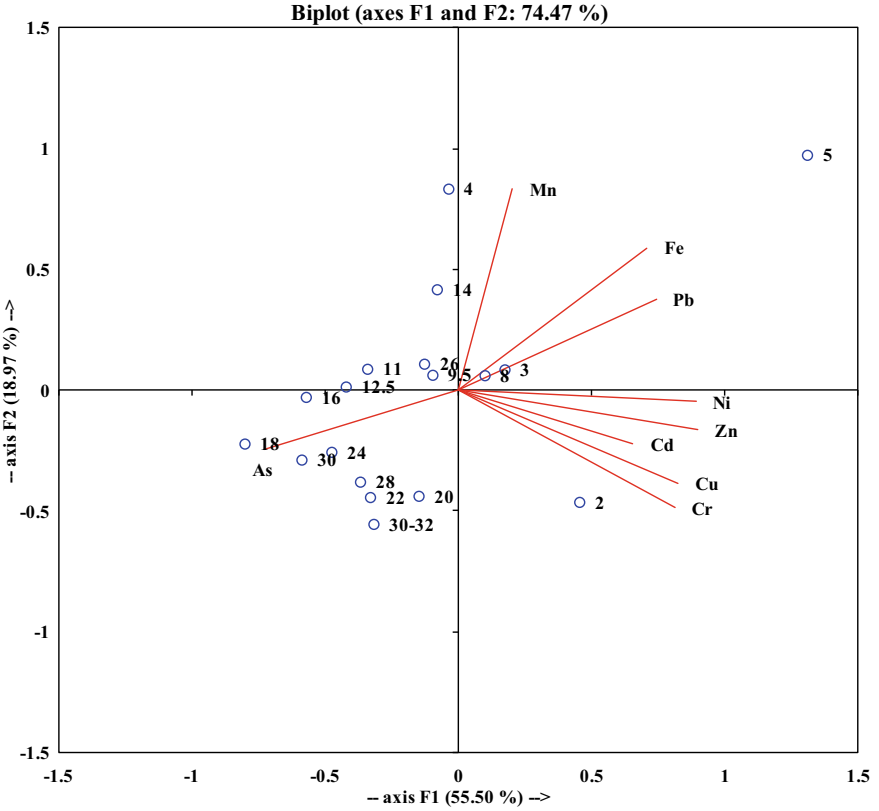

Fig. 3.3 Coordinates of principal component axis based on heavy metals concentrations and sampling depths (Dots—1 to 32 m) at Mathura

Table 3.3 Total variance (Mathura)

	F1	F2
Eigenvalue	4.99	1.71
% variance	55.5	18.9
Cumulative %	55.5	74.5

correlation of Cd, Cr, Ni, Fe, Pb and Zn with factor 1 while there is a negative correlation of As with factor 1. On the other hand factor 2 is negative correlated with most of the metals except Fe, Mn and Pb.

Table 3.4 Factorial component versus heavy metal concentrations (Mathura)

	F1	F2
As	−0.327	−0.190
Cd	0.293	−0.170
Cr	0.363	−0.373
Cu	0.368	−0.295
Fe	0.317	0.452
Mn	0.091	0.637
Ni	0.399	−0.037
Pb	0.332	0.287
Zn	0.401	−0.125

3.3.3 Heavy Metal Concentrations in Water Samples from Exploratory Well Mathura

The mean values of heavy metal concentrations from 5 water samples (1 sample per 12 h over 60 h pumping period) from the exploratory well are compared to Yamuna water and other groundwater samples collected in the vicinity of the exploratory well (Table 3.5). The exploratory well water samples generally do not indicate a health risk when compared to the WHO (2017) guideline values (Table 3.5). For heavy metals posing a health risk (As, Cd, Cr, Cu, Ni), the observed mean concentrations in the RBF exploratory well water were below the guideline values. However, the mean concentration of Pb (0.02 mg/L; Table 3.5) marginally exceeds the guideline value (0.01 mg/L). This could be attributed to the new well casing pipes, because elevated lead concentrations can be found in such manufactured components (WHO 2017). Marginally elevated concentrations of Cu and Ni in exploratory well water compared to Yamuna river and groundwater may also originate from the fluids used for well drilling and if so, then regular well operation is expected to flush these out. The observed concentrations in the exploratory well water (Table 3.5) are also significantly lower compared to those found in a recent study (Ahmed et al. 2018) in groundwater in the Mathura region. Consequently, the risk of heavy metal contamination in the RBF exploratory well water in Mathura is expected to be low.

3.3.4 Heavy Metal Concentrations in Soil and Aquifer Sediments of Exploratory Well Agra

The sediment composition and heavy metal concentrations found in the sediments of the exploratory well in Agra are presented and compared similar to Mathura. As for Mathura, the heavy metal concentrations in the RBF exploratory well sediments are compared to heavy metal concentrations determined for the Yamuna riverbed/bank

Table 3.5 Heavy metal concentrations in RBF exploratory well water compared to Yamuna river and groundwater in Mathura and WHO (2017) guideline values

Sample	As	Cd	Cr	Cu	Fe	Mn	Ni	Pb	Zn
RBF exploratory well (mean value; $n = 5$)	≤0.01	≤0.001	≤0.002	0.8	0.2	0.3	0.01	0.02	<0.3
Yamuna water	0.01[e]	<0.001[d]	<0.002–0.03[d]	<0.015[d]	≤1.4[d,e]	≤0.2[d,e]	≤0.006[d]	≤0.005[d]	≤0.1[d]
Groundwater[e]	0.02–0.03[d,e]	<0.001[d]	<0.002[d]	<0.015[d]	0.2[e]	0.3–0.4[d,e]	<0.004[d]	<0.004[d]	n.d.
Groundwater in Mathura region[f]	n.d.	1.8 (0.9–3.6)	1.9 (0.4–3.8)	0.04 (b.d.l.–0.4)	2.6 (0.9–4.8)	0.1 (b.d.l.–0.7)	3.4 (1.5–5.1)	2.3 (0.6–5.9)	0.5 (0.2–0.8)
WHO guideline value (2017)	0.01	0.003	0.05	2.0	0.3	0.4[a]	0.07	0.01[b]	3.0[c]

All concentrations in mg/L

b.d.l.: below detection limit; n.d.: not determined; [a] Health limit, acceptability limit is 0.1 mg/L; [b] Provisional WHO (2017) value; [c] Acceptability limit only; [d] Data from Ajmal et al. (1985) and/or Sandhu et al. (2019); [e] Data from Glorian et al. (2018); [f] Mean (min.–max.) values from Ahmed et al. (2018)

sediments up to depths of 35–50 cm as reported in Ajmal et al. (1985) and Jha et al. (1990) (Table 3.6). Similar to Mathura, the heavy metal concentrations in the sediments from the exploratory well in Agra are substantially lower compared to corresponding metal concentrations in the riverbed/bank sediment reported in other studies (Ajmal et al. 1985; Jha et al. 1990). However, it is observed that the concentrations of Cd and Pb in the exploratory well sediments significantly exceed the WHO limits for agricultural soils (WHO 1993, 2011).

3.3.5 PCA of Heavy Metals in Soil and Aquifer Sediments of Exploratory Well in Agra

Table 3.7 shows the correlation matrix for PCA of As, Cd, Cr, Cu, Fe, Mn, Ni, Pb and Zn obtained in Agra RBF exploratory well sediment samples. High and positive correlation can be observed between As, Cd, Co, Cr and Ni ($r = 0.924$ to 0.941); and Cu with Pb and Zn ($r = 0.914$ to 0.951) while moderate and positive correlation of Cu can be observed with Fe and Mn ($r = 0.567$ to 0.596). The high correlation may be due to the contribution of these metals from same source. Table 3.8 represents the determined initial Principal Component (PC) and its eigenvalue and per cent of variance contributed in each PC. Table 3.8 shows the eigenvalue for each component in which four PCs were obtained with eigenvalues >1 summing almost 95% of the total variance in the heavy metal dataset. Eigenvalues show that the first 3 PCs are the most significant components which represent more than 99% of the variance in heavy metal concentration (total 49.7% by PC1, 33.7% by PC2 and 11.7% by PC3). Correlation of the factorial component and heavy metal concentration is given in Table 3.9 which shows that in factor 1 almost all metals have positive correlation, while in factor 2 Fe, Cu, Mn, Zn have positive correlation and in factor 3 Fe and Mn have good correlation.

3.3.6 Heavy Metal Concentrations in Water Samples from Exploratory Well Agra

As for Mathura, the mean values of heavy metal concentrations from 5 water samples (1 sample per 12 h over 60 h pumping period) from the exploratory well in Agra are compared to Yamuna water and other groundwater samples collected in the vicinity of the exploratory well (Table 3.10). But contrary to Mathura, the mean concentrations of Cd and Pb significantly exceed the WHO guideline value (2017) of 0.003 and 0.01 mg/L, respectively. As their concentrations in the sediment samples are also high (Table 3.6), their leaching and mobilisation from the sediments into groundwater cannot be ruled out. However, based on studies by Sehgal et al. (2012) and Ahmed et al. (2020) that address impacts of irrigation by directly abstracted Yamuna water

Table 3.6 Statistical summary of sediment and heavy metal concentration at Agra ($n = 20$)

Parameter	Sediment (%)				Concentration (μg/kg)								
	Gravel	Sand	Silt	Clay	As	Cd	Cr	Cu	Fe	Mn	Ni	Pb	Zn
Minimum	0.02	35.1	4.4	0.6	33.3	36.3	24.5	36.0	71.8	14.7	9.8	134.0	12.3
Maximum	2.02	95.2	59.4	5.5	159	159	161	1192	25,500	5275	132	3875	4100
Average	0.39	75.31	22.44	2.1	63.9	72.6	56.6	236	4152	826	37.6	571	488
Stdev	0.63	13.2	11.99	1.2	29.9	32.2	33.2	271	6457	1248	31.5	824	958
Yamuna riverbed/bank[a]	n.a.	n.a.	n.a.	n.a.	n.d.	500–1400	40–110k	5500–90k	1900–9600k	330–700k	9.5–40k	9.9–14.4k	60–130k
WHO limits for agricultural soil (WHO 1993, 2011)	–	–	–	–	n.s.	3	100	n.s.	n.s.	n.s.	50	100	n.s.
Well-head protection zone limits (SVfS 2005)					40k	3k	200k	120k	n.s.	n.s.	140k	200k	400k

[a] Ajmal et al. (1985) and Jha et al. (1990), concentrations reported in μg/g, here converted to μg/kg; k: '000; n.a.: not applicable; n.d.: not determined; n.s.: not specified

Table 3.7 Correlation matrix (Agra)

	As	Cd	Co	Cr	Cu	Fe	Mn	Ni	Pb	Zn
As	1									
Cd	**0.941**	1								
Co	**0.924**	**0.797**	1							
Cr	**0.939**	**0.840**	**0.916**	1						
Cu	0.224	**0.528**	−0.009	0.052	1					
Fe	0.081	0.310	0.029	0.172	**0.567**	1				
Mn	0.167	0.376	0.213	0.076	**0.596**	**0.696**	1			
Ni	**0.929**	**0.836**	**0.989**	**0.921**	0.077	0.134	0.290	1		
Pb	0.171	**0.445**	−0.097	−0.029	**0.951**	0.334	0.386	−0.037	1	
Zn	0.163	0.431	−0.145	−0.020	**0.914**	0.353	0.323	−0.086	**0.972**	1

Bold represents good correlation—moderate to high

Table 3.8 Total variance (Agra)

	F1	F2	F3
Eigenvalue	4.969	3.374	1.167
% variance	49.689	33.738	11.675
Cumulative %	49.689	83.427	95.102

Table 3.9 Factorial component versus heavy metal concentrations (Agra)

	F1	F2	F3
As	0.414	−0.176	−0.176
Cd	0.441	0.000	−0.125
Co	0.371	−0.291	0.030
Cr	0.380	−0.251	−0.041
Cu	0.236	0.456	−0.070
Fe	0.178	0.273	0.608
Mn	0.214	0.253	0.596
Ni	0.391	−0.250	0.081
Pb	0.187	0.454	−0.316
Zn	0.174	0.454	−0.339

on heavy metal uptake by vegetables/crops grown in the Yamuna basin, the risk of leaching of heavy metals and consequent contamination to groundwater by the vertical movement of irrigation water is expected to be significantly greater compared to the movement of infiltrated river water through the riverbed during the RBF process because of the significantly high sorption capacity of the riverbed sediments (Ajmal et al. 1985; Jha et al. 1990). Furthermore, the provisional WHO guideline value for Pb (Table 3.10) means that the calculated guideline value is below the level that can

be achieved through practical treatment methods and source control (WHO 2017). The concentrations of the other heavy metals are below the WHO guideline value and are uncritical.

3.3.7 *Synthesis of PCA and Vertical Distribution of Heavy Metals in Exploratory Well Sediments*

Figure 3.3 shows that the first two principal components provide a general view on the temporal and spatial variations of metal concentrations in the sediments in Mathura. In Mathura, samples from depth of 1 to 5 m BGL were positively and largely affected by trace metals Cr, Cu, Zn, Cd, Ni, Mn, Fe and Pb. The concordance of such parameters and samples near to ground surface may be specifically associated with impacts from anthropogenic activities like sewage sludge, domestic wastes (Bhargava 2006) and irrigation (Sehgal et al. 2012; Ahmed et al. 2020) in the area around the exploratory wells.

PC1 was also negatively affected by As, which was closely related to the samples from greater depths of 16–18 m BGL. Therefore, this component seems to measure the preponderance of other heavy metals over As. In Mathura, second principle component (PC2) explained 19% of the total variance on parameters and Pb, Zn and Mn (3–5 m BGL) were positively and largely influential. It was also negatively and largely affected by Cr, Cu, Zn, Cd and Ni (1–2 m BGL). PC2 underlined that the importance of the contamination through anthropogenic origin is more prominent which has leached down to a depth of 5 m BGL as the soil is poorly graded sandy loam.

Similar component loading patterns were obtained for PC1 at Agra (Fig. 3.4). It was positively and largely influenced by heavy metal contamination to a depth of 2–11 m BGL and at a depth of 23 and 27 m. While, with 33.7% of the total variance, PC2 was positively influenced by Fe, Mn, Zn, Cu and Pb (at a depth of 8–11, 23 and 27 m) and negatively affected by Co, Cr, Ni, As (at a depth of 2–5 m). The contamination by Cd was close to the axis origins of factor 2, implying that its contribution to the total variation was less affected by factor 2.

Vertical variations of heavy metals can also be seen in Figs. 3.5 and 3.6 for Mathura and Agra, respectively. The concentrations of all the metals in the soil and sediments except Cd were found within the specified range (Kinuthia et al. 2020; WHO 2017). Moreover, the comparison of the metal concentrations in soil and sediments from the RBF exploratory wells in Mathura and Agra (Figs. 3.5 and 3.6) to the European Commission's directive EEC/86/278 (1986), shows that all metal concentrations including Cd are well below the limits mentioned in the directive. By comparison, concentrations of these metals in the soil of agricultural fields from at least nine locations along the Yamuna in Delhi within a distance of 250 m from the bank at a depth of 15 cm are significantly higher (Sehgal et al. 2012). However, after Fe and

Table 3.10 Heavy metal concentrations in RBF exploratory well water compared to Yamuna river and groundwater in Agra and WHO (2017) guideline values

Sample	As	Cd	Cr	Cu	Fe	Mn	Ni	Pb	Zn
RBF exploratory well (mean value; $n = 5$)	≤0.01	0.05	0.03	0.002	0.11	0.08	0.04	0.05	0.01
Yamuna water	0.01[e]	<0.001[d]	≤0.01[d]	0.006–0.03[d]	0.17–0.75[d]	0.06–0.12[d]	≤0.009[d]	≤0.002[d]	0.07–0.10[d]
Groundwater	0.03[e]	<0.001[d]	<0.002[d]	<0.015[d]	0.75	0.58	<0.004[d]	<0.004[d]	n.d.
WHO guideline value (2017)	0.01	0.003	0.05	2.0	0.3	0.4[a]	0.07	0.01[b]	3.0[c]

All concentrations in mg/L

b.d.l.: below detection limit; n.d.: not determined; [a] Health limit, acceptability limit is 0.1 mg/L; [b] Provisional WHO (2017) value; [c] Acceptability limit only (WHO 2017); [d] Data from Ajmal et al. (1985) and/or Sandhu et al. (2019); [e] Data from Glorian et al. (2018)

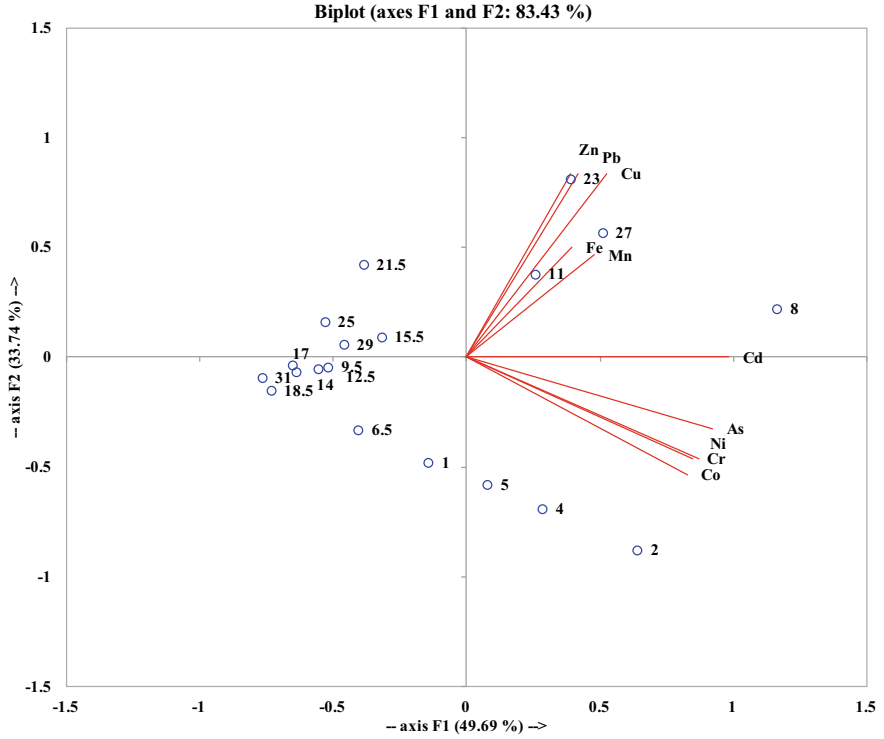

Fig. 3.4 Coordinates of principal component axis based on heavy metals concentrations and sampling depths (Dots—1 to 32 m) at Agra

Mn that occur naturally in relatively higher concentrations compared to other metals, Pb is found to be high (Figs. 3.5 and 3.6).

In this context, heavy metal concentrations, including for Pb, were found in higher concentrations in unwashed vegetables (compared to washed) grown and sold in/around Agra in areas with busy traffic or industry (Kumar 2013). As inferred from Kumar (2013), a possible source of Pb in the upper soil samples could also be from atmospheric pollution. Consequently, this reaffirms the statement that the risk from heavy metal concentrations found in the sediments is expected to be lower during RBF as compared to contamination from direct above ground Yamuna river irrigation water application.

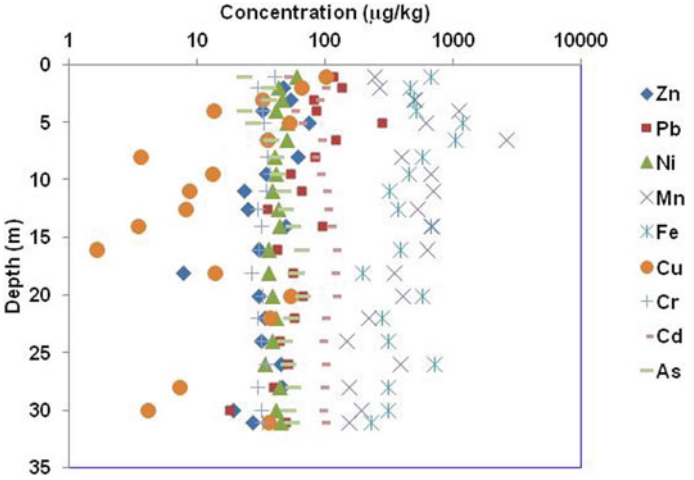

Fig. 3.5 Vertical distribution of heavy metal concentrations in sediment profile at Mathura

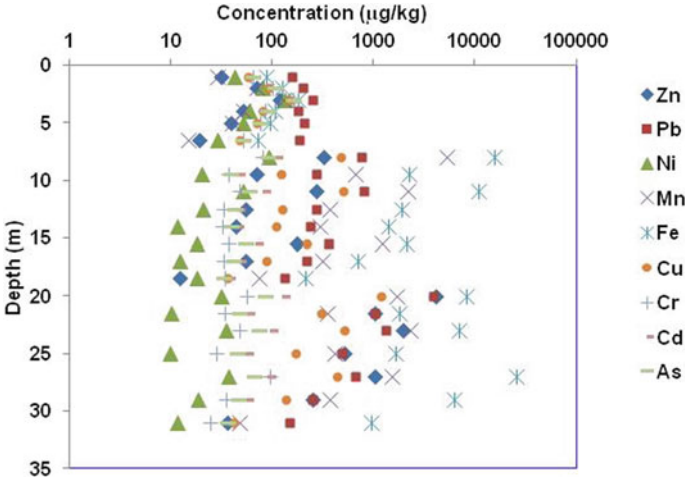

Fig. 3.6 Vertical distribution of heavy metal concentrations in sediment profile at Agra

3.4 Summary and Conclusions

The high microbiological, organic and inorganic pollution of the river Yamuna, especially the substantial heavy metal contamination not only to the river but also increasingly to groundwater in the highly populated Mathura and Agra regions in India is a motivation to enhance the use of the natural water treatment technique of RBF for the production of drinking water. This study focuses on a prognosis of the risk of heavy metal contamination at new RBF sites that are influenced by extreme environmental

conditions like those prevailing along the Yamuna. The heavy metals As, Cd, Cr, Cu, Fe, Mn, Ni, Pb and Zn were analysed in soil and aquifer sediments and water from an exploratory well for RBF in Mathura and Agra.

In general, the heavy metal concentrations found in the aquifer sediments were significantly lower compared to concentrations in riverbed material reported in literature, lower than WHO limits for agricultural soils (except Cd and Pb in Agra) and to limits specified for well-head protection zones in Berlin as well as to concentrations found in sediments at a RBF site by the river Elbe in Germany. While the heavy metal concentrations in the exploratory well water in Mathura over a 60-h pumping duration were generally found to be within the WHO drinking water guideline limits, the mean concentrations of Cd and Pb in the exploratory well in Agra significantly exceeded the WHO guideline values during the same pumping period. As the concentrations of Cd and Pb in the sediment samples are also high, their leaching and mobilisation from the sediments into groundwater cannot be ruled out. However, the risk of leaching of heavy metals and consequent contamination to groundwater by the vertical movement of irrigation water is expected to be significantly greater compared to the movement of infiltrated river water through the riverbed during the RBF process because of the significantly high sorption capacity of the riverbed sediments. This is concluded from the substantial removal of heavy metals within the first 0.5 m depth of the riverbed material, as observed in other studies on the investigation of heavy metals in the Yamuna riverbed. Nevertheless, in densely populated river basins impacted by heavy metal containing wastewaters and where the riverside flood-plain is sought-after for growing vegetables (agriculture), top-soil and eventual aquifer sediment contamination by heavy metals should be expected from directly abstracted river water used for irrigation. Consequently, caution should be exercised when selecting flood-plain areas for new RBF sites that have been irrigated in the past directly with surface waters impacted by heavy metals.

Using PCA, the major sources of heavy metals were identified to be mainly natural and to a certain extent anthropogenic, especially in the upper layers that may have undergone seasonal re-working due to flood-plain erosion during monsoon and subsequent deposition. This also indicates a lesser risk of heavy metal contamination to the wells from subsurface processes during RBF. This study observed that Cd, Ni, Cr and Pb are suitable parameters for assessing anthropogenic impacts on sediments at new RBF sites exposed to extreme environmental conditions. However, As, Fe, Mn are more representative parameters for the impact of natural dissolution and precipitation processes and should also be taken into account.

For RBF to be effective at new sites impacted by extreme environmental conditions, well-head and source-protection zones have to be implemented to avoid contamination to the aquifer from above ground anthropogenic activities, including small-scale agriculture within the well catchment areas (often a common practise in the absence of well-head/source-protection zones). Furthermore, this study highlights the importance of frequent water quality monitoring for not only heavy metals, but also microbiological and organic parameters including for emerging pollutants in the RBF well(s), river and ambient (landward side) groundwater.

Acknowledgements The presented work was carried out under the Project "Peyjal Suraksha" funded by Ministry of Water Resources, River Development and Ganga Rejuvenation, Government of India, and the project "CCRBF—Expansion of the Indo-German Competence Centre for Riverbank Filtration" (2020–2023) funded by the Federal Ministry of Education and Research of Germany (BMBF; grant no. 01DU20003A), within the programme CONNECT.

References

Ahmed S, Khurshid S, Qureshi F, Hussain A, Bhattacharya A (2018) Heavy metals and geo-accumulation index development for groundwater of Mathura city, Uttar Pradesh. Desalination Water Treat 138:291–300

Ahmed S, Khurshid S, Madan R, Abu Amarah BA, Naushad M (2020) Water quality assessment of shallow aquifer based on Canadian Council of Ministers of the environment index and its impact on irrigation of Mathura District, Uttar Pradesh. J King Saud Univ Sci 32:1218–1225

Ajmal M, Khan MA, Nomani AA (1985) Distribution of heavy metals in water and sediments of selected sites of Yamuna river (India). Environ Monit Assess 5(2):205–2014

Bartak R, Page D, Sandhu C, Grischek T, Saini B, Mehrotra I, Jain CK, Ghosh NC (2015) Application of risk-based assessment and management to riverbank filtration sites in India. J Water Health 13(1):174–189

Bhargava DS (2006) Revival of Mathura's ailing Yamuna river. Environmentalist 26:111–122

Brümmer GW, Gerth J, Herms U (1986) Heavy metal species, mobility and availability in soils. Z Pflanzenernährung Bodenkunde 149:382–398

Census of India (2011) City census. Office of the registrar general and census commissioner, India, Ministry of Home Affairs, Government of India. https://www.census2011.co.in/city.php. Accessed 2 Mar 2021

Chakarvorty M, Dwivedi AK, Shukla AD, Kumar S, Niyogi A, Usmani M, Pati JK (2015) Geochemistry and magnetic measurements of suspended sediment in urban sewage water vis-à-vis quantification of heavy metal pollution in Ganga and Yamuna Rivers, India. Environ Monit Assess 187:604–621

Chaturvedi A, Bhattacharjee S, Singha AK, Kumar V (2018) A new approach for indexing groundwater heavy metal pollution. Ecol Indic 87:323–331

Chukwujindu I, Lari B, Osakwe SA, Tesi GO, Nwajei GE, Martincigh BS (2018) Distribution, sources and ecological risks of metals in surficial sediments of the Forcados River and its Estuary, Niger Delta, Nigeria. Environ Earth Sci 77:227

Dillon P, Stuyfzand P, Grischek T et al (2019) Sixty years of global progress in managed aquifer recharge. Hydrogeol J 27(1):1–30

EEC/86/278 (1986) Council directive on the protection of the environment, and in particular of the soil, when sewage sludge is used in agriculture. Off J Eur Communities L 181(6):6–12

Everitt BS, Dunn G (1992) Applied multivariate data analysis. Oxford University Press, New York, p 304

Glorian H, Börnick H, Sandhu C, Grischek T (2018) Water quality monitoring in Northern India for an evaluation of the efficiency of bank filtration sites. Water 10:1804

Grischek T, Dehnert J, Nestler W, Treutler HC, Freyer K (1993) Description of system conditions during bank filtration based on investigation of bore cores. In: Proceedings of the 2nd Dresdner Grundwasserforschungstage. Dresden, pp 207–220 (in German)

Grischek T, Ray C (2009) Bank filtration as managed surface—groundwater interaction. Int J Water 5(2):125–139

Jaiswal M, Hussain J, Gupta SK, Nasr M, Nema AK (2019) Comprehensive evaluation of water quality status for entire stretch of Yamuna River, India. Environ Monit Assess 191:208–224

Jankowska J, Radzka E, Rymuza K (2017) Principal component analysis and cluster analysis in multivariate assessment of water quality. J Ecol Eng 18(2):92–96
Jansson P-E (1987) Simulated soil temperature and moisture at a clearcutting in central Sweden. Scand J For Res 2:127–140
Jha PK (1986) Nature of chemical and sediment load in the Yamuna River Basin. Ph.D thesis, Jawaharlal Nehru University, New Delhi, 207 pp
Jha PK, Subramanian V, Sitasawad R, Van Grieken R (1990) Heavy metals in sediments of the Yamuna river (A tributary of the Ganges), India. Sci Tot Environ 95:7–27
Khan S (2016–2017) Hydrogeology of Uttar Pradesh. Report, Central Ground Water Board, Northern Region, Lucknow, India
Kinuthia GK, Ngure V, Beti D et al (2020) Levels of heavy metals in wastewater and soil samples from open drainage channels in Nairobi, Kenya: community health implication. Sci Rep 10:8434. https://doi.org/10.1038/s41598-020-65359-5
Krishan G, Singh S, Sharma A, Sandhu C, Grischek T, Ghosh NC, Gurjar S, Kumar S, Singh RP, Glorian H, Börnick H (2016) Assessment of water quality for river bank filtration along Yamuna River in Agra and Mathura. Int J Environ Sci 7(1):56–67
Krishan G, Chandniha SK, Lohani AK, Yadav BK, Arora NK, Singh S, Kumar CP, Sharma LM, Bhardwaj AK (2018) Assessment of heavy metals in relation to soil pollution at Mewat, Haryana, India. Curr World Environ 13(3):299–306
Kumar S (2013) Appraisal of heavy metal concentration in selected vegetables exposed to different degrees of pollution in Agra, India. Environ Monit Assess 185:2683–2690
Kumar P, Mehrotra I, Börnick H, Schmalz V, Worch E, Schmidt W, Grischek T (2012) Riverbank filtration: an alternative to pre-chlorination. J Indian Water Works Assoc Spec Issue 50–58
Lindsay WL, Norwell WA (1978) Development of DTPA of soil test for Zn, Fe, Mn and Cu. J Am Soil Sci 42:421–428
Maeng SK (2010) Multiple objective treatment aspects of bank filtration. PhD dissertation, Delft University of Technology and UNESCO-IHE Institute for Water Education, Delft, The Netherlands. CRC Press/Balkema, The Netherlands, 196 pp
Misra AK, Mishra A (2006) Groundwater quality monitoring in shallow and deep aquifers in Saidabad Tahsil area, Mathura district, India. Environ Monit Assess 117:345–355
Mondal NC, Singh VS, Puranik SC, Singh VP (2010) Trace element concentration in groundwater of Pesarlanka Island, Krishna Delta, India. Environ Monit Assess 163:215–227
Nasr M, Zahran H (2016) Performance evaluation of agricultural drainage water using modeling and statistical approaches. Egypt J Aquat Res 42(2):141–148
Omwene PI, Öncel MS, Çelen M, Kobya M (2018) Heavy metal pollution and spatial distribution in surface sediments of Mustafakemalpaşa stream located in the world's largest borate basin (Turkey). Chemosphere 208:782–792
Pal R, Dubey RK, Dubey SK, Singh AK (2017) Assessment of heavy metal pollution through index analysis for Yamuna water in Agra Region, India. Int J Curr Microbiol Appl Sci 6(12):1491–1498
Paul D (2017) Research on heavy metal pollution of river Ganga: a review. Ann Agrar Sci 15:278–286
Reiners WA, Marks RH, Vitousek PM (1975) Heavy metals in subalpine and alpine soils of New Hampshire. Oikos 26:264–275
Sandhu C, Grischek T, Börnick H, Feller J, Sharma SK (2019) A water quality appraisal of some existing and potential riverbank filtration sites in India. Water 11:215
Sehgal M, Garg A, Suresh R, Dagar P (2012) Heavy metal contamination in the Delhi segment of Yamuna basin. Environ Monit Assess 184:1181–1196
Shine JP, Ika RV, Ford TE (1995) Multivariate statistical examination of spatial and temporal patterns of heavy metal contamination in New Bedford Harbor marine sediments. Environ Sci Technol 29(7):1781–1788
Singh P, Kumar P, Mehrotra I, Grischek T (2010) Impact of riverbank filtration on treatment of polluted river water. J Environ Manag 91(5):1055–1062

Singh AK, Srivastava SC, Verma P, Ansari A, Verma A (2014) Hazard assessment of metals in invasive fish species of the Yamuna River, India in relation to bioaccumulation factor and exposure concentration for human health implications. Environ Monit Assess 186:3823–3836

Subramanian V, Sitasawad R (1984) A study on water quality in the River Yamuna around Delhi, India. Water Qual Bull 9:219–222

SVfS (2005) Evaluation criteria for the assessment of groundwater pollution in Berlin (Berliner Liste 2005). Senatsverwaltung für Stadtentwicklung Berlin, ABl. Nr. 35/22.07.2005, Germany (in German)

United States Department of Agriculture (2000) Natural resources conservation service. Soil Quality Institute 411 S. Donahue Dr. Auburn, AL 36832 334-844-4741 X-177 Urban technical note No. 3, September, 2000

WHO (1993) Standard maxima for metals in Agricultural soils. WHO Press, Geneva, Switzerland

WHO (2011) Adverse health effects of heavy metals in children. Children's Health and the Environment; WHO Training Package for the Health Sector

WHO (2017) Guidelines for drinking-water quality: fourth edition incorporating the first addendum. WHO Press, Geneva, Switzerland

Wu W, Wu P, Yang F, Sun D-L, Zhang D-X, Zhou Y-K (2018) Assessment of heavy metal pollution and human health risks in urban soils around an electronics manufacturing facility. Sci Tot Environ 630:53–61

Chapter 4
Simulation of Re-Aeration Coefficient Using Anfis and Arima Models

Sameer Arora and Ashok K. Keshari

Abstract Identification of the assimilative capacity of the river becomes point of interest now a days, as the rivers are receiving a significant amount of wastewater load from urban agglomerations. Re-aeration represents the process of interaction among the air–water interface to absorb the oxygen from the atmosphere and indicates the capacity of the water to hold the pollutant without affecting the state of the river. The soft computing technique, adaptive neuro-fuzzy inference system (ANFIS) is applied to identify the re-aeration coefficient of Yamuna River, Delhi. The hybrid model is developed using ANFIS and autoregressive integrated moving average (ARIMA). The results obtained from the ANFIS are combined with the time series modeling technique ARIMA model. Combination of various hydraulic and water quality parameters were used to design the input for models. Takagi–Sugeno (TS) technique was used to design the ANFIS models and autocorrelation (ACF) and partial autocorrelation (PACF) functions were used for ARIMA model. Performance of the ANFIS models was measured using coefficient of determination (R^2), root mean square error (RMSE), and coefficient of correlation (R). Several ANFIS models were designed and results of best model with least RMSE and highest R^2 are used as input to ARIMA model to obtain the re-aeration coefficient for each sampling location. Results indicate that ANFIS model with combination of hydraulic and water quality parameter provides the best fit model with both the spatial and temporal variations.

Keywords Re-aeration coefficient · Yamuna river · Wastewater · ANFIS · ARIMA

4.1 Introduction

Stream water quality is greatly influenced by the dissolved oxygen (DO) concentration present in water. DO concentration up to the saturation limit of the river represents the no organic impurities in the water body (Hanbay et al. 2009). Treated/untreated

S. Arora (✉) · A. K. Keshari
Department of Civil Engineering, Indian Institute of Technology, Delhi (IITD), New Delhi 110016, India
e-mail: sameer_arora01@yahoo.co.in

R. Jha et al. (eds.), *Groundwater and Water Quality*, Water Science and Technology Library 119, https://doi.org/10.1007/978-3-031-09551-1_4

wastewater from open drains joins the water body and deteriorates the water quality and ground water either through percolation via bed or hyporheic zone (Parmar and Bhardwaj 2013). Concentration of chemicals in wastewater discharge and initial flow available in river defines the quality of the river water after mixing (Mimikou et al. 2000). Dissolved oxygen followed by biochemical oxygen demand (BOD), ammonia, and chloride are the major parameters that influences the water quality significantly on the reduction in peak flow of the river (Senhorst and Zwolsman 2005). DO concentration replenishes majorly by atmospheric re-aeration process and oxygen generation through photosynthesis. Whereas decomposition of organic matter, sediment oxygen demand, and oxygen consumption by aquatic plants are the sinks of oxygen. Overall water quality is simulated by both the hydrological as well as physio-chemical parameters, which necessitates the collection of real-time data for the design the modern water resource management programs to the prediction of water quality along with the growth in population, increased industrial demand, and irrigation requirements (Arora and Keshari 2017). Location of sparsely located hydrological and metrological stations, reliability of data, and concurrency of hydrological and water quality data are the major limitations that urge the requirement of improved models for the prediction of river water quality.

Several studies were carried out to identify the relation between water quality and hydrological parameters (Prathumratana et al. 2008; Hanh et al. 2010; Wang et al. 2015; Ghane et al. 2016; Zounemat-Kermani et al. 2016; Al-Aboodi et al. 2017; Bou-Fakhreddine et al. 2018). Although dynamics of various parameters such as dissolved oxygen, biochemical oxygen demand, chemical oxygen demand, and nonlinear behavior in riverine ecosystem make it difficult to apply statistical models for prediction of water quality (Loperfido et al. 2009; Ranković et al. 2010) as these models require accurate and tremendous information on processes and coefficients of various physio-chemical processes varies along with the spatial and temporal variation (Basant et al. 2010). Soft computing techniques (data-driven models) have been applied by various researchers to water resource applications effectively to demonstrate the complex nonlinear systems (Singh et al. 2004; Bhardwaj and Parmar 2014; Emamgholizadeh et al. 2014; Zounemat-Kermani et al. 2016; Katimon et al. 2017) such as adaptive neuro-fuzzy inference system (ANFIS), autoregressive integrated moving average (ARIMA), etc. within their ability to model nonlinear system.

ANFIS is a growing AI technique widely being used in the water resource applications. ANFIS requires less time to train and to define the problem due to the lesser dimensions of parameters and initialization of parameters (Bou-Fakhreddine et al. 2018). Combination of fuzzy logic and neural network generates the model with higher accuracy than the fuzzy reasoning system of parameters (Aquil et al. 2006; Mayilvaganan et al. 2011). It also helps in the removal of fuzzy logic drawbacks to generate the systematic control system and provides the better adaptation and design of well-organized input–output structure using neural network learning ability (Chang and Chang 2006; Rankovic et al. 2012) designed models to predict the stream flow using ANFIS and RBF. Results indicate that ANFIS performs better as compared to RBF and produces model of higher accuracy (Wang et al. 2009) utilized ANN, ANFIS, ARMA, and SVM to quantify the river discharge and quantified that

ANFIS is able to design models with greater accuracy than other techniques (Ebtehaj et al. 2017) determined the discharge coefficient of the weir using ANFIS and for the identification of input parameters for ANFIS model, genetic algorithm (GA) is used. Out of the two different methods of ANFIS, subtractive clustering (SC) performs with better accuracy over fuzzy C means (FCM) (Galavi et al. 2013; Tiwari et al. 2018; Yaseen et al. 2017) forecasted the stream flow using ANFIS and the hybrid model of ANFIS-FFA and found that the hybrid model performs better than ANFIS (Al-Aboodi et al. 2017) compared the ANN, ANFIS, and ARIMA for the prediction of river flow. Results indicate that ANFIS has better performance over the other two techniques due to the greater rule base and ability of ANFIS to perform the clustering of the database. Accuracy of the models can be further improved with the selection of an appropriate model or hybrid model for the prediction of various parameters.

ARIMA is another growing soft computing technique able to predict the time series data. ARIMA is the combination of autoregressive (AR), integrated (I), and moving average (MA) that have been applied successfully in water resource applications (Hanh et al. 2010; Ullah and Choudhury 2013; Katimon et al. 2017). Hanh et al. (2010) identified the combined impact of hydrology and climate on the water quality of Mekong River using ARIMA models and produced consistent positive results. Ömer-Faruk (2010) predicted the water quality parameters such as temperature, DO, and boron using a combination of ARIMA features and neural network to handle both the linear and nonlinear data. Irvine et al. (2011) predicted the water quality parameter such as temperature, DO, turbidity, conductivity, and water level in Mekong river using ARIMA. Results obtained from ARIMA model found successful in predicting the trend and used for one month ahead prediction. Valipour et al. (2012) compared ARIMA and ARMA to forecast the water in the reservoir and found that ARIMA produces a better model than ARMA for time series data analysis. ARIMA can generate a new set of time series data from the input data with the similar statistical parameters.

In the present study, ANFIS and ARIMA were used to model the re-aeration of Yamuna River through five-year data sets of different locations in study area and to identify the critical parameters causing the maximum variation in the re-aeration coefficient of Yamuna River. Mohd Ekhwan et al. (2012) conducted a study including both the water quality and hydrological variables and found that hydraulic characteristics of the river are considerably affected by the water quality parameters and vice versa. Accuracy of the model is tested out using root mean square error (RMSE), coefficient of correlation (R), and coefficient of determination (R^2). Best model identified through various ANFIS models is used as an input to the ARIMA to generate the re-aeration coefficient. As the sampling sites vary significantly at shorter distances, ARIMA is used to obtain the coefficient specific for each location and standard errors have been identified with the observed coefficient.

4.2 Study Area and Database

4.2.1 Study Area

River Yamuna is influenced by the problems imparted by industrialization, urbanization, and rapid agricultural developments similar to other riverine systems. Yamuna River originates from Yamunotri, India located at 31° 01′ N and 78° 46′ E, and joins the Ganga River in Allahabad in the Uttar Pradesh state of India. River travels around 1376 km before its confluence into the Ganga. After traveling around 348 km crossing Uttarakhand and Haryana, enters Delhi at Palla village. The most threatened part of the river starts at Delhi when it enters through the Wazirabad barrage and leaves Okhla Barrage followed by the stretch up to Agra. At Wazirabad the river is trapped through a barrage and around 950 MLD of water is abstracted for drinking water supply to urban agglomeration at Delhi (CPCB 2006). At the Wazirabad barrage, most of the river fresh water is diverted to meet the demand of the water supply of Delhi and barely any water is left in the downstream conditions during summer, as only wastewater discharged from the several drains flows into the channel as shown in Fig. 4.1. Najafgarh drain discharges about three times the flow available in the river and deteriorates the water quality significantly as shown in Fig. 4.1. After traveling about 22 km downstream of Wazirabad barrage and receiving effluent from 17 major drains and 4 drains that fall into Agra and Gurgaon canal (CPCB 2006) containing domestic and industrial wastewater, river water is again diverted at Okhla barrage. From this barrage, water is being diverted for irrigation purposes in the state of Haryana. Similarly as to downstream of Wazirabad, at the downstream Okhla barrage, the water flows in the river is the drain water of domestic and industrial origin contributed mainly by the Shahdara drain as shown in Fig. 4.1.

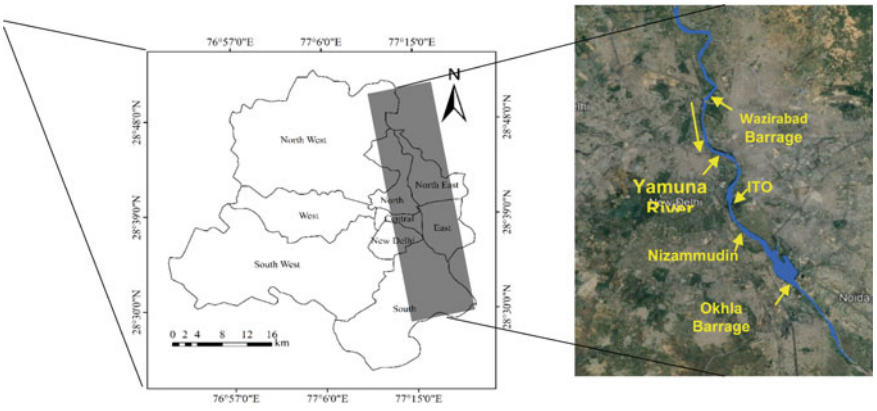

Fig. 4.1 Inset map of India, indicating the location of Yamuna river in the Delhi stretch in between Wazirabad Barrage and Okhla Barrage, Delhi India

Delhi falls into the subtropical with greater variation in summer and winter temperature. Average temperature of Delhi in summers is near 32 ˚C and maximum temperature in summers is about 45 ˚C. Whereas, average winter temperature is between 12 and 13 ˚C. Monsoon starts in Delhi in the late June and last till mid of September. Amount of average annual precipitation received in Delhi is about 790 mm with the maximum in the month of July and August, i.e., around 470 mm followed by a minimum of 190 mm in the month of June and September. All four months define the monsoon season of Delhi. Hence there are greater chances of dilution of water quality of Yamuna River due to the direct flow and runoff received by the river.

4.2.2 Data Collection and Analysis

The study was conducted for a period of 60 months over the 4 monitoring stations. First sampling location was just 0.3 km downstream of Wazirabad barrage contains only the river water. At the downstream of barrage, Najafgarh drain joins the river at merely 0.5 km and discharges about four times the flow available in the river (CPCB 2006) as shown in Fig. 4.1. ITO Bridge, Nizammudin, and Okhla Barrage are other monitoring stations as shown in Fig. 4.1. After wazirabad, two major drains (Najafgarh drain and Supplementary drain) and eight minor drains join before the ITO. At the downstream of ITO, wastewater from the power plant and domestic drains joins the river at the right bank. Nizammudin reflects the characteristics of wastewater received from the drains carrying the domestic and industrial discharge, whereas water quality at the Okhla Barrage sampling location get diluted due to the confluence of the Hindon cut canal into the river. ITO is approximately 12 km downstream of Wazirabad, Nizammuddin is 16 km downstream, and Okhla is 21 km downstream of Wazirabad.

Some of the parameters are tested out at the sampling site after collection and parameters that are required to be tested out in the laboratory are preserved with appropriate reagents to maintain the characteristics of the sample collected (APHA 2005). Most of the hydraulic and physio-chemical parameters were tested out including depth (m), velocity (m/s), discharge (m^3/s), slope (1/S), width (m), pH, temperature (°C), dissolved oxygen (mg/l), biochemical oxygen demand (mg/l), chemical oxygen demand (mg/l), ammonia (μS/cm), total kjheldal nitrogen (μS/cm), conductivity, fecal coliform (MPN/100 ml), and total coliform (MPN/100 ml). All the parameters were analyzed using standard and recommended methods (APHA 2005).

4.3 Methodology

4.3.1 Adaptive Neuro-Fuzzy Inference System

The ANFIS is the combination of feed-forward neural network and fuzzy inference system able to model the system with the arrangement of neurons using a neural network and fuzzy logic. ANFIS organizes the input–output data selection based on learning techniques and constructs the mapping of input–output using the fuzzy rules. For the application of fuzzy rules, two commonly used fuzzy inference systems (FIS) are Mamdani fuzzy inference system (M-FIS) and Takagi–Sugeno fuzzy inference system (TS-FIS). Both the FIS have different fuzzification and defuzzification procedures, however, TS-FIS produces more compact and accurate results as compared to M-FIS (Takagi and Sugeno 1985; El-Shafie et al. 2007). For ANFIS structure minimum of two input x_1 and x_2 and two fuzzy if–then rules for output, y are required as shown in Fig. 4.2. The feed-forward equations of ANFIS are presented by the rule base containing two Takagi–Sugeno if-then rules as follows:

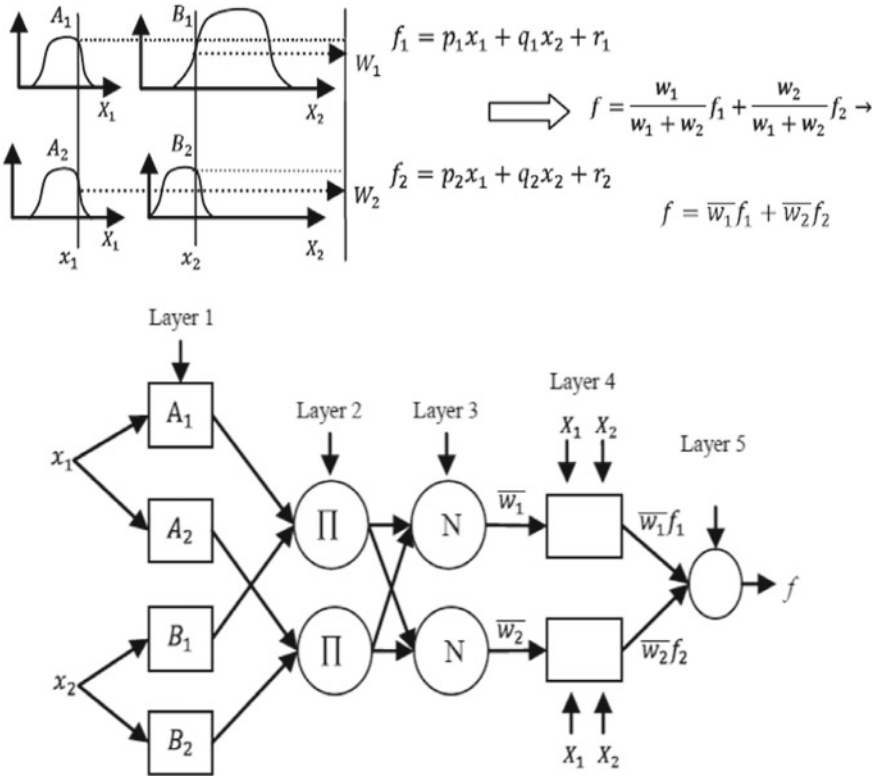

Fig. 4.2 Rule formation of ANFIS and division of different layers in ANFIS function

If x is A_1 and y is B_1, then $f_1 = p_1x + q_1y + r_1$ Rule 1.

If x is A_2 and y is B_2, then $f_2 = p_2x + q_2y + r_2$ Rule 2.

ANFIS structure is described in five layers excluding the input layer (Toprak 2009) can be described as a multi-layered neural network:

Layer 0: Define the input layer with n no. of nodes.

Layer 1: It provides the membership function of each node through the fuzzification of Gaussian rules as

$$\mu_{Ai}(x) = \exp\left\{-\left[\left(\frac{x - c_i}{a_i}\right)^2\right]^{b_i}\right\}$$

where a_i, b_i and c_i are the adaptive parameter functions. Values of these functions are assigned on the basis of the algorithm selected during the training of the program. These parameters are known as premise parameters after assigning the values to the adaptive parameters. Each input node is trained against the different membership functions to obtain the value of premise parameters.

Layer 2: Each fuzzified node is multiplied by the AND operator to provide the strength to each node. The membership values $\mu_{Ai}(x)$ and $\mu_{Bi}(y)$ are multiplied to gain the strength, where x and y are the linguistic values of A_i and B_i and w_i is the antecedent function of rule 1.

$$w_i = \mu_{Ai}(x) \cdot \mu_{Bi}(y)$$

Layer 3: All the nodes are normalized with the provided strength as

$$\overline{w_i} = \frac{w_i}{\sum_{j=1}^{R} w_j}$$

where $\overline{w_i}$ is the sum of the strength of ith operators computed in layer 2.

Layer 4: Each node computes the linear function where coefficient of functions is calculated using the error of backpropagation neural network.

$$\overline{w_i} f_i = \overline{w_i}(p_0x_0 + p_1x_1 + p_2)$$

where p_i is the parameter for I input values and $\overline{w_i}$ is the output of layer 3. For the training of parameters in this layer least square approximation method is used.

Layer 5: This represents the summation of outputs of every node obtained from the Layer 4 computed as follows and the detailed architecture of ANFIS is shown in Fig. 4.2:

$$\sum_i \overline{w_i} f_i = \frac{\sum_i w_i f_i}{\sum_i w_i}$$

To design the complex nonlinear models, input in ANFIS is divided into different parts to create local spaces which further employs the local model that is linear in nature for each partitioned input space. For splitting ANFIS input function, model uses fuzzy MFs which covers the input space and activate several local regions simultaneously using single input by overlapping (Zounemat-Kermani and Teshnehlab 2008). Number of membership function plays an important role as the MFs controls the resolution of the partitioned input functions and approximation of ANFIS model. Grid partitioning and sub-clustering are commonly used method for the generation of FIS with varying number of MFs used on the basis of input data. Triangular and Gaussian are the commonly used MFs with linear system. Optimization methods available for the training of MFs are the backpropagation algorithm and hybrid-learning algorithm (Firat and Güngör 2007). Inference operations are identified through fuzzy if–then rules and MFs used to define the rules. Each fuzzy unit converts the received input to the fuzzy set. FIS receives either fuzzy sets or crisp input for modeling of MFs and delivers the fuzzy sets information to the output layer. The defuzzification interface again converts the fuzzy set into a crisp output (Nayak et al. 2005). Out of two commonly available FIS for ANFIS modeling, TS-FIS produces more accurate and simplified results. TS-FIS derives the linear output function using a first-order polynomial of the input variables and is known as first-order TS-FIS function, whereas with constant output function, it is known as zero-order TS-FIS (Takagi and Sugeno 1985; Shu and Ouarda 2007). Selection of a particular MF and number of rules plays an important part in the designing of ANFIS architecture. Researchers have concluded that Gaussian MF delivers improved results over triangular MF in practice (Aquil et al. 2006; Tiwari et al. 2018) and produces the minimum mean square error using a combination of different input–output pairs.

4.3.2 Autoregressive Integrated Moving Average

Autoregressive Integrated Moving Average (ARIMA) is a time series model that represents the data with different stochastic processes. ARIMA implements the linear model in the time series and follows the statistical distribution, such as the normal distribution (Parmar and Bhardwaj 2015). ARIMA is flexible to build the optimal model with numerous time series variations using Box-Jenkins methodology.

An ARIMA (n, m) model is the hybrid model of two generalized forms of model Autoregressive AR(n) and Moving Average MA(m) models and is commonly used for univariate non-stationary time series modeling. AR and MAR are the generic models and combination of them is used to develop the time series model known as the autoregressive moving average (ARMA) model (Alsudani and Liu 2017). ARMA (n, m) can be represented using mathematical functions as

$$y_t = c + \in_t + \sum_{i=1}^{n} \emptyset_i y_{t-i} + \sum_{j=1}^{m} \emptyset_j y_{t-j}$$

$$y_t = c + \emptyset_1 y_{t-1} + \emptyset_2 y_{t-2} + \ldots + \emptyset_n y_{t-n} + \in_t$$

where n and m represent the autoregressive and moving average terms, respectively. To identify the optimal model for the time series data, autocorrelation function (ACF) and partial autocorrelation function (PACF) analysis are carried out. These are the two statistical measures identifies the inter-relation between the observations (Parmar and Bhardwaj 2015). To develop the model and predict the variables, ACF and PACF are plotted against the time lag generated from the manipulation of lag operator. Ranking of the AR and MA models are identified using the plots of ACF and PACF.

Backshift in the observations are generated in ARMA using the lag function. The lag function in the model is estimated as

$$L(y_t) = y_t$$

where as ARIMA model is the advanced version of ARMA model, also able to handle the non-stationarity of data. Mathematically ARIMA (n,d,m) models are represented with the inclusion of lag function as

$$\emptyset(L)(1-L)^d y_t = \theta(L)\varepsilon_t$$

$$\left(1 - \sum_{i=1}^{n} \emptyset_i L_i\right)(1-L)^d y_t = \left(1 - \sum_{j=1}^{m} \emptyset_j L_j\right)\varepsilon_t$$

where n, d, and m represent the order of autoregressive, integrated, and moving average functions respectively. The value of these functions can be zero or greater than zero. The integer d is the important function between the ARIMA and ARMA models because as and when the value of d becomes zero, ARIMA model reduces to ARMA. For most of the ARIMA models, the preferred value of d is equal to one.

4.3.3 Evaluation of ANFIS and ARIMA Models

Water quality and hydraulic parameters were combined to design the various models using ANFIS and ARIMA models for the identification and prediction of the re-aeration coefficient for the Yamuna River. Five different combinations of parameters were formulated to identify the best combination of the parameter that defines the variation in re-aeration coefficient with the least deviation from the observed values of coefficient. Predictor variables considered in the study for designing the models include both the hydraulic and water quality parameters as shown in Table 4.1, whereas the re-aeration coefficient is considered as a response variable for

Table 4.1 ANN and ANFIS models designed with combinations of different parameters

ANFIS models	Parameters
ANFIS-1	Velocity and Depth
ANFIS-2	Velocity, Depth, and Discharge
ANFIS-3	Velocity, Depth, Discharge, and DO
ANFIS-4	Velocity, Depth, Discharge, DO, and BOD
ANFIS-5	Velocity, Depth, Discharge, DO, BOD, and Conductivity

model design. The performance of all the developed models was tested out using the statistical measures R, R^2, and $RMSE$.

$$R = \frac{\sum_{i-1}^{n} \left\{ (y_{pi} - \overline{y}_p)(y_{mi} - \overline{y}_m) \right\}}{\sqrt{\sum_{i-1}^{n} (y_{pi} - \overline{y}_p)^2 \sum_{i=1}^{m} (y_{mi} - \overline{y}_m)^2}}$$

$$R^2 = 1 - \frac{\sum_{i=1}^{n} (y_{pi} - y_{mi})^2}{\sum_{i=1}^{n} (y_{pi} - \overline{y}_p)^2}$$

$$RMSE = \sqrt{\frac{\sum_{i=1}^{n} (y_{pi} - y_{mi})^2}{n}}$$

where y_p (1/day) and y_m are the predicted and observed re-aeration coefficients, respectively, for n number of observations. $\overline{y}_p$ and $\overline{y}_m$ are the mean of re-aeration coefficient for both the predicted and observed values. The coefficient of determination is commonly known as the coefficient of efficiency which may be written in a number of ways and provides the percentage of variance in the observed variable in the model. This method is the standard measure of accuracy that generates the result in the range of 0–1, where 0 represents the lowest and a value approaching 1 indicates the optimal relationship with the measured values of the target parameter. The correlation coefficient represents the degree of correlation between the observed and estimated values. The coefficient of efficiency compares the residual and initial variance and could vary depending upon the initial variance of observed data.

4.4 Results and Discussion

4.4.1 Model Input

To identify the optimal model, hydraulic and water quality data of Yamuna River is divided into three parts for training, testing, and validation. Data set selected for the training purpose is 60% of the total data of 180 samples and to obtain the error

from the trained datasets. 20% of the data is used for the testing of the model on the basis of observed errors. Another 20% of the data is used for the validation purpose to compare the model with the trained model and to improve the results on the basis of model performance. For ANFIS Takagi–Sugeno fuzzy inference system (TS-FIS) is used to study the variation and prediction of re-aeration coefficient. Gaussian membership functions have been used with three functions for each input. Inputs are varied according to the models designed with a different set of combinations of parameters. Grid partition is used for the development of if–then fuzzy rules for the models with less input variables and sub-clustering is used for the large input variable models. The gaussian membership function is used in grid partitioning which is connected with each data point to form the clusters. Multidimensional data space is converted into specified numbers of clusters and fuzzy logic identifies the center of each cluster with multiple iterations to minimize the center, whereas sub-clustering works on numbers of clusters at the same time and operates the iterations for the optimization of model using subtractive clustering. Sub-clustering works on one algorithm and produces faster results as compared to grid partitioning.

Out of the various combinations of input parameters, model with lowest RMSE and highest R^2 is selected as an input to the ARIMA model. As ARIMA is univariate and predicts one parameter at a time, output from ANFIS is taken as input to the ARIMA model for the estimation of re-aeration coefficient of the river and plotted with the observed values of the coefficient. Gaussian distribution function is used to define the ARIMA model on the one order of differencing, autoregressive, and moving average.

4.4.2 Selection of Best ANFIS Model

Five combinations were designed using various parameters (depth, velocity, discharge, dissolved oxygen, biochemical oxygen demand, and conductivity) in ANFIS to predict the impact of parameters on the variation of re-aeration coefficient of the river as shown in Table 4.1. Models were tested on the Gaussian function through grid partitioning using up to 20 epochs in each run. ANFIS consumes the operation time on the basis of input parameters and the membership function defined for each input. In the designed model ANFIS-1, ANFIS-2, and ANFIS-3, input parameters were 2, 3, and 4, respectively, and 3 membership functions were used for each input parameter. Whereas ANFIS-4 contains the five input parameters and ANFIS-5 models contain six input parameter and 2 membership functions were used for each input to reduce the operation time as well as the assignment of the rule base of every membership function.

First three fuzzy models were tested with the grid partitioning method and the last two models were applied on the subtractive fuzzy clustering. Datasets for each model are distributed into three parts as training, testing, and validation and further compared with the observed variables to test the performance of tested dataset as

Table 4.2 Training and testing results of different ANFIS models

Models	Training			Testing		
	R	R^2	RMSE	R	R^2	RMSE
ANFIS-1	0.854	0.729	0.1031	0.843	0.710	0.1108
ANFIS-2	0.879	0.772	0.0927	0.872	0.760	0.0928
ANFIS-3	0.887	0.790	0.0801	0.881	0.776	0.0802
ANFIS-4	0.938	0.879	0.0323	0.927	0.859	0.0324
ANFIS-5	0.966	**0.933**	0.0185	0.959	**0.919**	0.0291

shown in Table 4.2. Model with R^2 between 0.50 and 0.75 is considered as satisfactory model whereas models with R^2 greater than 0.75 is considered as good model. Out of all the five models, ANFIS-5 comes out with minimum RMSE and maximum R^2. Robustness of the ANFIS is based on the generation of rule base with the contribution of membership function for each input combination (Arora and Keshari 2017). Better performances by the model containing hydraulic and water quality including organic parameter can be attributed to the fact that the re-aeration coefficient is affected by all the physical, chemical, and biological operations that occur in the riverine system significantly. Physical processes dominate with high flow and velocity, whereas chemical and biological processes dominated in the conditions where the water quality falls in the category of class C or below containing high organic load. The study validates that the ANFIS model can be successfully used to predict the re-aeration coefficient of the river using a combination of hydraulic and water quality parameters.

4.4.3 Hybrid ANFIS-ARIMA

In order to reduce the error involved in ANFIS, results obtained from ANFIS-5 are taken as input to the ARIMA model to generate the hybrid model for the identification of re-aeration coefficient. Optimal ANFIS model obtained from the best input combinations is shown in Fig. 4.3. Performance of ARIMA is evaluated on the statistical error as shown in Table 4.3. ARIMA is generated separately for each sampling location to calculate the re-aeration coefficient for each location due to significant variation in the water quality. ARIMA (1,2,1) models were generated using Gaussian distribution method, where, 1, 2, and 1 are integers that indicates the order of autoregressive, integrated, and moving average functions of ARIMA, respectively. Time series modeling of Kr developed using ARIMA model is as follows:

$$(1 - \emptyset_1 L)(1 - L)^2 y_t = (1 + \theta_1 L)\varepsilon_t + c$$

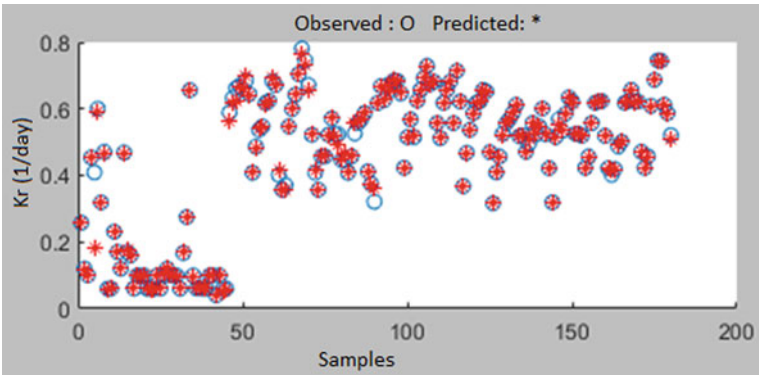

Fig. 4.3 Re-aeration coefficient obtained from observed coefficient and predicted values from ANFIS-5 model

Table 4.3 Statistical evaluation of ARIMA results for each sampling location Training and testing results of different ANFIS models

Location	Parameter	Value	Standard error	T statistic	P-value
Wazirabad barrage	Constant	0.0019	0.0028	0.6687	0.5037
	AR{1}	−0.3084	0.0978	−3.1544	0.0016
	MA{1}	−0.9419	0.0560	−16.8089	2.0989e-63
	Variance	0.0282	0.0040	7.1417	9.2179e-13
ITO bridge	Constant	−0.0012	0.0021	−0.5887	0.5561
	AR{1}	0.0086	0.2183	0.0396	0.9684
	MA{1}	−0.9989	0.0817	−12.2416	1.8635e-34
	Variance	0.0313	0.0036	8.6256	6.3736e-18
Nizammudin bridge	Constant	−0.0013	0.0024	−0.5285	0.5969
	AR{1}	0.0164	0.2193	0.0749	0.9403
	MA{1}	−1.004	0.0785	−12.7396	3.5622e-37
	Variance	0.0409	0.0058	7.0469	1.8288e-12
Okhla barrage	Constant	−0.0006	0.0017	−0.3375	0.7357
	AR{1}	0.0103	0.3721	0.0277	0.9778
	MA{1}	−1.0011	0.1284	−7.7884	6.7887e-15
	Variance	0.0349	0.0056	6.2704	3.6012e-10

where L is the lag operator, y_t is the actual error, ε_t is the random error, $\emptyset$ and θ are the model parameters and c is a constant. Best model using the above equation is obtained at a lag of 1 and 2 degrees of integration. Table 4.3 contains the statistical results of ARIMA model and it was found that minimum error found at Okhla barrage was 0.0017 which accounts for the 99.6% of confidence limit in the results of model. From the results, it was found that ARIMA can be used to forecast the

re-aeration coefficient. Combination of ANFIS results with ARIMA comes out to be a desirable feature that can be used as a potential tool for the identification of re-aeration coefficient for each specific location and can be tested over other water quality parameters (Fig. 4.4).

4.5 Conclusion

Study was conducted using a combination of data-driven models to improve the performance of the designed system, considering the rapidly changing properties of river water along with the stream flow. In this paper, ANFIS is used to design the five different models with the various combination of input parameters to identify the contribution of each parameter in the variation of re-aeration coefficient of Yamuna River, India. TS-FIS is used to model the parameters using different membership functions for each input variable. Models obtained from the ANFIS are tested out on the basis of RMSE, R, and R^2 to the identification of accuracy with respect to the observed results. Optimal model with a value of RMSE and the highest R^2 is selected for designing of hybrid model. In this paper, ANFIS is integrated with the ARIMA to form the hybrid ANFIS-ARIMA model, utilizing the time series forecasting of the ARIMA with the if–then rule base analysis of ANFIS. Hybrid model was applied to the Yamuna River, India to identify the re-aeration coefficient. The results show that the ANFIS-ARIMA model reduces the errors obtained from the ANFIS model alone. ARIMA performs the difference operation for a non-stationary time series data and the combined model utilizes the logic function along with the difference operation to increase the accuracy of the model. Results reflect that hybrid model can be successfully utilized in the identification and prediction of re-aeration coefficient and can also be used for various application pertaining to water resource management and water quality prediction.

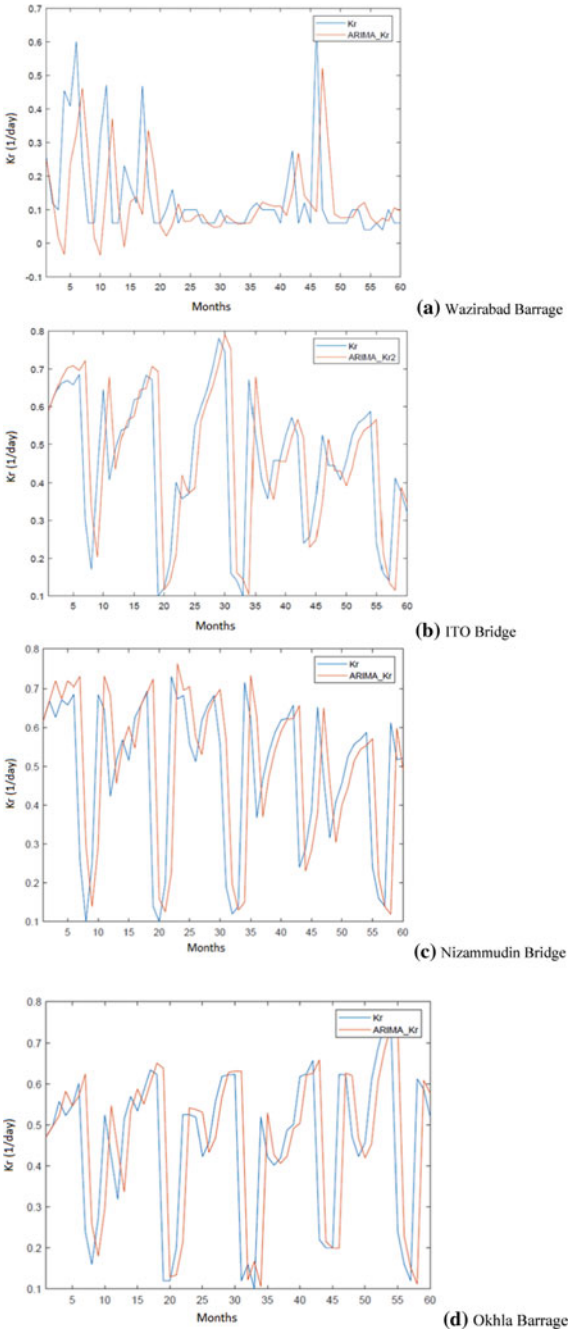

Fig. 4.4 Observed and predicted re-aeration coefficient obtained from ARIMA at (**a**) Wazirabad Barrage, (**b**) ITO Bridge, (**c**) Nizammudin Bridge and (**d**) Okhla barrage

References

Al-Aboodi AH, Dakheel AA, Ibrahim HT (2017) Comparison of data-driven modelling techniques for predicting river flow in an arid region. Int J Appl Eng Res 12(11):2647–2655

Alsudani RSA, Liu JC (2017) The use of some of the information criterion in determining the best model for forecasting of thalassemia cases depending on iraqi patient data using ARIMA model. J Appl Math Phys 5:667–679

APHA (2005) Standard method to the examination of water and wastewater, 21st edn. American Public Health Association, American Water-Works Association, Water Environment Federation, Washington, DC

Aquil M, Kita I, Yano A, Nishiyama S (2006) A Takagi-Sugeno fuzzy system for the prediction of river stage dynamics. JARQ 40(4):369–378

Arora S, Keshari AK (2017) Estimation of re-aeration coefficient using MLR for modelling water quality of rivers in urban environment. Groundw Sustain Dev

Basant N, Gupta S, Malik A, Singh KP (2010) Linear and nonlinear modelling for simultaneous prediction of dissolved oxygen and biochemical oxygen demand of the surface water—a case study. Chemom Intell Lab Syst 104:172–180

Bhardwaj R, Parmar KS (2014) Water quality management using statistical analysis and time-series prediction model. Appl Water Sci. https://doi.org/10.1007/s13201-014-0159-9

Bou-Fakhreddine B, Mougharbel I, Faye A, Chakra SA, Pollet Y (2018) Daily river flow prediction based on two-phase constructive fuzzy systems modeling: a case of hydrological—meteorological measurements asymmetry. J Hydrol 558(2018):255–265

Chang F, Chang Y (2006) Adaptive neuro-fuzzy inference system for prediction of water level in reservoir. Adv Water Resour 29(1):1–10

CPCB (2006) Water quality status of Yamuna river (1999–2005). Central Pollution Control Board, Ministry of Environment & Forests, Assessment and Development of River Basin Series: ADSORBS/41/2006-07

Ebtehaj I, Bonakdari H, Shamshirband S, Ismail Z, Hashim R (2017) New approach to estimate velocity at limit of deposition in storm sewers using vector machine coupled with firefly algorithm. J Pipeline Syst Eng Pract 8

El-Shafie A, Taha MR, Noureldin A (2007) A neuro-fuzzy model for inflow forecasting of the Nile River at Aswan high dam. Water Resour Manag 21:533–556

Emamgholizadeh S, Kashi H, Marofpoor I, Zalaghi E (2014) Prediction of water quality parameters of Karoon river (Iran) by artificial intelligence-based models. Int J Environ Sci Technol 11(3):645–656

Firat M, Güngör M (2007) River flow estimation using adaptive neuro fuzzy inference system. Math Comput Simul 75(3–4):87–96

Galavi H, Mirzaei M, Shui LT, Valizadeh N (2013) Klang river-level forecasting using ARIMA and ANFIS models. Am Water Works Assoc 105(9):E496–E506

Ghane E, Ranaivoson AZ, Feyereisen GW, Rosen CJ, Moncrief JF (2016) Comparison of contaminant transport in agricultural drainage water and urban stormwater runoff. PLoS ONE 11(12):e0167834

Hanbay D, Baylar A, Batan M (2009) Prediction of aeration efficiency on stepped cascades by using least square support vector machines. Expert Syst Appl 36:4248–4252

Hanh PTM, Anh NV, Ba DT, Sthiannopkao S, Kim KW (2010) Analysis of variation and relation of climate, hydrology and water quality in the lower Mekong River. Water Sci Technol 62(7):1587

Irvine KN, Richey JE, Holtgrieve GW, Sarkkula J, Sampson M (2011) Spatial and temporal variability of turbidity, dissolved oxygen, conductivity, temperature, and fluorescence in the lower Mekong River-Tonle Sap system identified using continuous monitoring. Int J River Basin Manag 9(2):151–168

Katimon A, Shahid S, Mohsenipour M (2017) Modeling water quality and hydrological variables using ARIMA: a case study of Johor river, Malaysia. Sustain Water Resour Manag. https://doi.org/10.1007/s40899-017-0202-8

Loperfido JV, Just CL, Schnoor JL (2009) High-frequency diel dissolved oxygen stream data modeled for variable temperature and scale. J Environ Eng 135(12):1250–1256
Mayilvaganan M, Naidu K (2011) Comparison of membership functions in adaptive-network based fuzzy inference system (ANFIS) for the prediction of groundwater level of a watershed. J Comput Appl Res Dev 1:35–42
Mimikou MA, Baltas E, Varanou E, Pantazis K (2000) Regional impacts of climate change on water resources quantity and quality indicators. J Hydrol 234(1–2):95–109
Mohd Ekhwan T, Mohd Khairul Amri K, Muhammad Barzani G, Mokhtar J, Nor Azlina AA, Pan IL (2012) Water quality status and hydrological analysis in upper tropical river, Malaysia. Int J Agric Crop Sci 4(2):33–39
Nayak PC, Sudheer KP, Rangan DM, Ramasastri KS (2005) Short-term flood forecasting with a neuro-fuzzy model. Water Resour Res 41(4) (Art no W04004)
Ömer-Faruk D (2010) A hybrid neural network and ARIMA model for water quality time series prediction. Eng Appl Artif Intell 23(4):586–594
Parmar KS, Bhadwaj R (2013) Wavelet and statistical analysis of river water quality parameters. Appl Math Comput 219:10172–10182
Parmar KS, Bhardwaj R (2015) Statistical, time series, and fractal analysis of full stretch of river Yamuna (India) for water quality management. Environ Sci Pollut Res 22(1):397–414
Prathumratana L, Sthiannopkao S, Kim KW (2008) The relationship of climatic and hydrological parameters to surface water quality in the lower Mekong river. Environ Int 34(6):860–866
Ranković V, Radulović J, Radojević I, Ostojić A, Čomić L (2010) Neural network modeling of dissolved oxygen in the Gruža reservoir Serbia. Ecolog Model 221(8):1239–1244
Ranković V, Radulović J, Radojević I, Ostojić A, Čomić L (2012) Prediction of dissolved oxygen in reservoirs using adaptive network-based fuzzy inference system. J Hydroinf 14(1):167–179
Senhorst HAJ, Zwolsman JJG (2005) Climate change and effects on water quality: a first impression. Water Sci Technol 51(5):53–59
Shu C, Ouarda TBMJ (2007) Flood frequency analysis at ungauged sites using artificial neural networks in canonical correlation analysis physiographic space. Water Resour Res 43:W07438
Singh KP, Malik A, Mohan D, Sinha S (2004) Multivariate statistical techniques for the evaluation of spatial and temporal variations in water quality of Gomti river (India)—a case study. Water Res 38(18):3980–3992
Takagi T, Sugeno M (1985) Fuzzy identification of systems and its applications to modeling and control. IEEE Trans Syst Man Cybern 15(1):116–132
Tiwari S, Babbar R, Kaur G (2018) Performance evaluation of two ANFIS models for predicting water quality index of River Satluj (India). Adv Civil Eng 2018:1–10
Toprak ZF (2009) Flow discharge modeling in open canals using a new fuzzy modeling technique (SMRGT). CLEAN-Soil Air Water 37(9):742–752
Ullah N, Choudhury P (2013) Flood flow modeling in a river system using adaptive neuro-fuzzy inference system. Environ Manag Sustain Dev 2(2):54–68
Valipour M, Banihabib ME, Behbahani SR (2012) Parameters estimate of autoregressive moving average and auto-regressive integrated moving average models and compare their ability for inflow forecasting. J Math Stat 8(3):330–338
Wang W, Chau K, Xu D, Chen XY (2015) Improving forecasting accuracy of annual runoff time series using ARIMA based on EEMD decomposition. Water Resour Manag 29:2655–2675
Wang W, Chau KW, Chang CT, Qui L (2009) A comparison of performance of several artificial intelligence methods for forecasting monthly discharge time series. J Hydrol 374(3–4):294–306
Yaseen ZM, Ebtehaj I, Bonakdari H, Deo RC, Danandeh Mehr A, Mohtar WHM, Diop L, El-shafie A, Singh VP (2017) Novel approach for streamflow forecasting using a hybrid ANFIS-FFA model. J Hydrol. https://doi.org/10.1016/j.jhydrol.2017.09.007
Zounemat-Kermani M, Teshnehlab M (2008) Using adaptive neuro-fuzzy inference system for hydrological time series prediction. Appl Soft Comput 8(2):928–936
Zounemat-Kermani M, Kisi Ö, Adamowski J, Ramezani-Charmahineh A (2016) Evaluation of data driven models for river suspended sediment concentration modeling. J Hydrol 535:457–472

Chapter 5
Identification of Unknown Number of Clandestine Groundwater Contamination Source Locations and Their Release Flux History

Anirban Chakraborty and Om Prakash

Abstract As a method of disposal, large amounts of untreated toxic waste are frequently buried underground. The extensive contamination of groundwater has arisen from such indiscrete methods of clandestine disposal. This means of disposal is often used to escape the expense of adequate waste management and the untraceability of such unauthorized disposals. However, the effect of such disposals manifests in form of groundwater contamination, which if left unchecked would potentially pollute the entire aquifer. Such contaminated aquifers must be recovered using the appropriate remediation method. Effective remediation strategy only depends on the exact estimation of contamination source characteristics, i.e., number of sources, locations, and release histories of such pollutant sources. In case of groundwater contamination, the number and location of the sources cannot be deciphered. Thus the challenge is to identify the number of contamination sources, their locations, and their flux release history from sparsely available contamination measurement concentration data. Methodologies developed so far rely on prior information about the number of contaminant sources present in the study area or the potential source locations that are known with certainty. However, such assumptions seldom hold true in real-world scenarios of groundwater contamination originating from clandestine sources. In this study, a noble technique for simultaneously estimating the unknown number of clandestine contamination sources, locations along, and release flux history is demonstrated. Simulated Annealing (SA) is used as the optimization algorithm in a linked simulation optimization (LSO)-based framework. Number of contaminant sources and locations are considered as unknown decision variables in the proposed method. The developed methodology is applied to a hypothetical study area. The results demonstrate the applicability of the methodology in estimating the number of groundwater contamination sources, locations, and release history, even

A. Chakraborty (✉) · O. Prakash (✉)
Department of Civil and Environmental Engineering, Indian Institute of Technology Patna, Bihta, Bihar 801106, India
e-mail: anirban.pce15@iitp.ac.in

O. Prakash
e-mail: om.prakash@iitp.ac.in

R. Jha et al. (eds.), *Groundwater and Water Quality*, Water Science and Technology Library 119, https://doi.org/10.1007/978-3-031-09551-1_5

though there is no prior information about the number of clandestine contamination sources and locations available.

Keywords Groundwater contamination · Source identification · Clandestine sources · Linked simulation–optimization · Simulated Annealing

5.1 Introduction

Groundwater is one of the world's most important sources of drinking water. The need for freshwater grows in parallel with the global population. Global water use is estimated to have tripled in the last 50 years (Water 2014). The long-term stability of these resources is jeopardized due to extensive anthropogenic pollution of groundwater aquifers (Dey and Prakash 2020a, b) Toxic chemicals which are derivatives of industrial activities, are responsible for groundwater aquifer contamination. Industries that produce hazardous chemicals also use ineffective waste management practices. Clandestine deposits of contaminated wastes are often espoused by industries to minimize the cost of waste management prior to disposal. Eventually, these contaminated substances leach into the groundwater with precipitation and spread along with groundwater flow, thus contaminating the entire aquifer. A contaminated aquifer needs to be reclaimed by adopting a suitable remediation technique. Effective remediation strategy only depends on the exact estimation of contamination source characteristics, i.e., the number of sources, locations, and release histories of such pollutant sources.

When contamination in groundwater is initially discovered, generally very little information is known about the number and locations of the contamination sources. Thus, estimation of a number of clandestine contamination source locations and release flux history from sparse contamination concentration measurement data is a challenging task and it is considered as an inverse ill-posed problem (Yeh 1986).

Several methodologies like least square based (Gorelick et al. 1983), neural network-based techniques, (Singh et al. 2004) surrogate model-based approach (Keshari and Datta 2001) are used for the characterization of groundwater contamination sources. For estimating the unknown source characteristics linked simulation–optimization method (Datta et al. 2013, Chakraboty and Prakash (2020, 2021a, b) holds good as it can efficiently perform with a limited number of concentration measurement data. Mahar and Datta (1997) identified the location and release histories of contaminant sources using optimal monitoring network assuming explicitly known potential contamination source locations. Prakash and Datta (2014) gave a SA-based LSO technique for determining activity initiation time for contamination sources. Jha and Datta (2015) recovered release flux histories using similar LSO methods for a distributed source.

LSO-based techniques are effective in reconstructing the source flux release histories only when the number of sources and their locations is well known or the potential source locations are known with a fair degree of certainty (Guneshwor et al. 2018).

This knowledge about the number of sources, and their actual/potential locations (Ghafouri et al. 2017) are implicitly assumed to be known in the existing methods of source identification, which is seldom true in real-life scenarios of groundwater contamination from clandestine sources. To fill up this critical gap, a new approach is proposed that can simultaneously characterize the number of clandestine sources of pollution, locations and release in the study region, even though the number of sources and their locations remain unknown.

5.2 Methodology Development

In this study, we use an LSO approach. The LSO approach incorporates the flow and contamination transport simulation model in the groundwater system as a set of binding constraints in the optimization framework, which is solved iteratively. Therefore, any possible solution to the optimization model needs to satisfy the flow and transport simulation models. A three-dimensional (3D) numerical groundwater flow model, MODFLOW (Harbaugh and McDonald 1996), and the 3D modular pollutant transport model MT3D (Zheng 1990) incorporating the governing Eqs. (5.1) and (5.2) are used for simulation of groundwater flow and pollutant transport, respectively.

$$\frac{\partial}{\partial x}K_{xx}\frac{\partial h}{dx}\frac{\partial}{\partial y}+K_{yy}\frac{\partial h}{\partial y}+\frac{\partial}{\partial z}K_{zz}\frac{\partial h}{\partial z}\pm W=S_s\frac{\partial h}{\partial t} \tag{5.1}$$

where

K_{xx}, K_{yy}, and K_{zz} are the hydraulic conductivity along the x, y, and z coordinate (LT^{-1}), h is the head difference between the entry and exit point of the aquifer (L), W is the volumetric flux per unit volume where positive sign (+) means sources and negative sign (−) means sinks (T^{-1}), S_s is the specific storage of the porous material (L^{-1}), t is time (T), x, y and z are the Cartesian co-ordinates (L).

$$\frac{\partial C}{\partial t}=\frac{\partial}{\partial x_j}(D_{ij}\frac{\partial c}{\partial x_j})-\frac{\partial}{\partial x_i}(v_iC)\frac{q_s}{\theta}C_s+\sum_{K=1}^{N}R_k \tag{5.2}$$

where C is the concentration of conservative contaminants dissolved in groundwater (ML^{-3}), t is time (T), x_i is the distance along the respective cartesian coordinate axis (L), D_{ij} is the hydrodynamic dispersion coefficient tensor (L^2T^{-1}), v_i is the seepage or linear pore water velocity (LT^{-1}) and is related to the specific discharge or Darcy flux through the relationship, $v_i = q_i/\theta$, q_s is the volumetric flux of water per unit volume of aquifer representing fluid sources (positive) and sinks (negative) (T^{-1}), C_s is the concentration of the sources or sinks (ML^{-3}), θ is the effective porosity of the porous medium (dimension less), $\sum_{k=1}^{N} R_k$ is chemical reaction term for each of the N species considered ($ML^{-3}\ T^{-1}$).

Simulated Annealing (SA) is used as the algorithm for solving the optimization problem with an objective of minimizing the difference between the simulated and measured pollutant concentrations at the observed locations. The basic concept of SA is derived from thermodynamics (Kirkpatrick et al. 1983). Each iteration of the optimization model decrease the residual error given in Eq. (5.3), by suitably adjusting the values of the explicit decision variables based on the algorithm control parameters (initial temperature, temperature reduction factor, etc.). The decision variables constitute the unknown source characteristics, i.e., number of contamination sources, their locations, and flux release history such that the optimal values of these decision variables give the best estimate of the unknown source characteristics. In this study MATLAB (2017a) toolbox "simulannealbnd" for SA is used as an optimization algorithm. The binding constraints in Eqs. (5.4) and (5.5) essentially show the linking of the simulation model to the optimization model.

$$Minimize\ F = \sum_{k=1}^{nk} \sum_{iob=1}^{nob} Abs(cest_{iob}^{k} - cobs_{iob}^{k}) \tag{5.3}$$

Subject to

$$cest_{iob}^{k} = \sum_{i=1}^{n} f(C_{si}, x_i, y_i, z_i, t) \tag{5.4}$$

$$x_{\min} < x_i < x_{\max};\ y_{\min} < y_i < y_{\max};\ z_{\min} < z_i < z_{\max} \tag{5.5}$$

Abs is the absolute difference;

$cest_{iob}^{k}$ is the data which is simulated by the transport model at iob site, and kth time, nob is the available sites, where concentration can be measured, $cobs_{iob}^{k}$ is the field data at iob site and at the end of monitoring time step k, x_i, y_i, z_i represents the grid location of the ith source of contamination such that the source is confined within the actual study area by choosing the values of x_{max}, y_{max}, z_{max} to be the boundary values. The contaminant sources number is denoted by n. The basic flow chart of SA-based linked simulation optimization is presented in Fig. 5.1.

5.2.1 Illustration of the Study Area

The boundary condition of hypothetical study area is illustrated in Fig. 5.2. The hypothetical area is made of single layer, homogeneous, anisotropic unconfined aquifer of area 1 km × 1 km. In Table 5.1, the detailed hydrogeological parameters are mentioned. The area is divided into 400 (20 × 20) grids, having two clandestine sources of contamination denoted by red triangle. For three sampling well sites denoted by blue circles, reported pollutant concentration measurements at 100, 200,

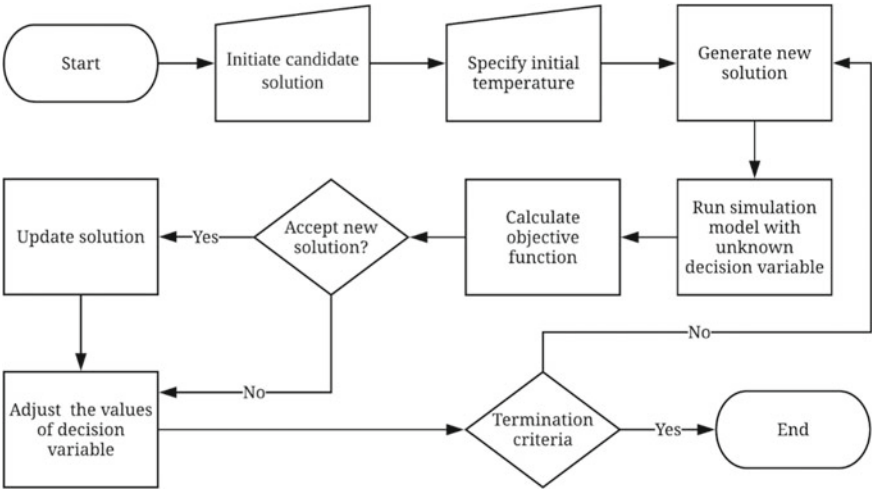

Fig. 5.1 Schematic diagram of SA-based linked simulation optimization

300, 400, and 500 days are simulated using GMS 10.1. The sources' entire contamination duration is split into five cycles, each of hundred days. To validate the technique, four separate scenarios are solved in which the upper limit (n) on the number of possible sources (P) present in the research area is defined, with $n = 2, 3, 4$, and 5 for defining actual source characteristics, respectively (S). All the four hundred grids are considered as a plausible location for the sources in the four scenarios. It should be noted that the technique relies on the optimal value of the decision variables to estimate the number of contamination sources present in the region, their position, and source flux release for each stress period given by SIJ, where I represent the source number and J represents the stress period number for the actual source. PIJ, on the other hand, represents.

In order to reflect real-life conditions, where the concentration measurements are erroneous, the numerically simulated observed concentrations were perturbed to incorporate measurement errors. The numerically simulated observed pollutant concentration data is perturbed with a random measurement error with a maximum deviation of 10 percent of the measured concentration value as shown in Eqs. (5.6) and (5.7).

$$cobs_{iob}^{k}(1 + err) = {}^{pert}cobs_{iob}^{k} \tag{5.6}$$

$$err = \mu per \times rand \tag{5.7}$$

${}^{pert}cobs_{iob}^{k}$ is the perturbed observed concentration measurement at location *iob* at monitoring time step *k,*

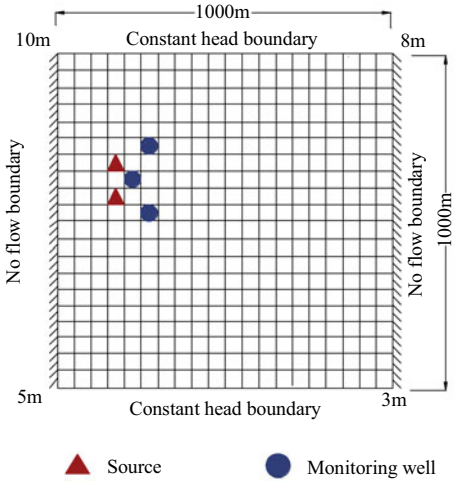

Fig. 5.2 Plan view of study area

Table 5.1 Hydrological parameter of study area

Parameters	Value
Total domain length	1 km
Total domain width	1 km
Thickness	10 m
Unit grid length	50 m
Unit grid width	50 m
K_{xx} (hydraulic conductivity)	20
K_{yy}/K_{xx} (horizontal anisotropy)	1.29
Porosity	0.3
Longitudinal dispersivity of the domain throughout	25 m/d
Transverse dispersivity of the domain throughout	10 m/d
Source location grid (actual)	(9,4,1), (7,4,1)

err is error term,

μper is maximum deviation expressed as percentage,

rand is a random fraction between −1.0 and +1.0 generated using a uniform distribution.

In order to test the performance evaluation of the SA-based linked simulation–optimization methodology four scenarios have been formulated based on the number of maximum potential sources. The four scenarios are described in Table 5.2.

Table 5.2 Description of scenario for performance evaluation

Scenario	Description
1	$n = 2$
2	$n = 3$
3	$n = 4$
4	$n = 5$

5.3 Results and Discussion

The performance evaluation results of the developed methodology for finding the unknown number of clandestine sources, their locations, and the flux history are presented in Fig. 5.3a, b for scenario one. The actual number of sources present in the study area is estimated based on the grid locations of the potential sources. Figure 5.3a shows the x- and y- co-ordinates of grid containing the sources. The result shows that the method is able to find the two actual sources and their respective grid locations precisely, both in case of erroneous and error-free observation data.

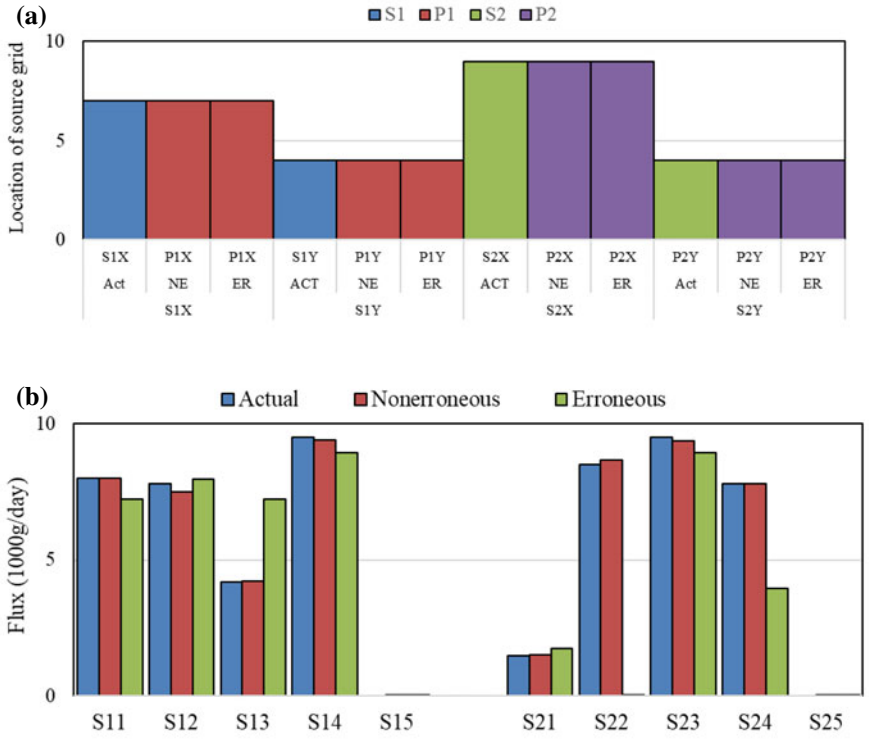

Fig. 5.3 **a** Location of source grid for scenario 1. **b** Flux values of identified source for scenario 1

Figure 5.3b shows the unknown source flux variables for every identified clandestine source for each stress period (S11, S12, S13, S14, S15, S21, S22, S23, S24, and S25) marked on the x-axis. The estimated source flux for both the identified sources matches closely with the actual flux value when tested with error-free data. There is a significantly larger deviation of identified flux from the actual flux value in the case of S13, S22, and S24 in case of erroneous observation data. Early convergence of objective function values due to unadjusted SA parameters could be the reason for the deviation in the estimated flux values.

Results of source location identification for scenario two are presented in Fig. 5.4a. In this scenario, the maximum number of potential sources is kept at three which is more than the actual number of sources present. The methodology is able to find the co-ordinates of all the three potential source locations for both erroneous and non- erroneous observation data. On careful examination of the grid co-ordinates it is seen that potential source P1 and P3 occupy the same grid location and therefore represent one actual source S1.

Since P1 and P3 represent one source together, hence the equivalent source flux will be the summation of the source fluxes for both the potential sources for every stress period. Figure 5.4b shows the unknown source flux variables for every identified clandestine source for each stress period (P1J + P3J = S1J, J represent stress

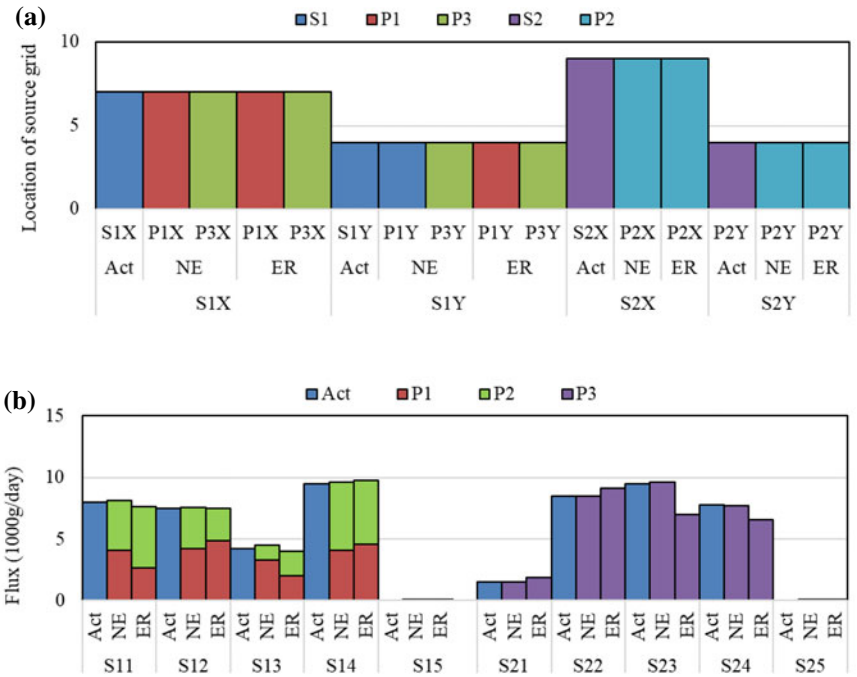

Fig. 5.4 **a** Location of source grid for scenario 2. **b** Flux values of identified source for scenario 2

period) marked on the x-axis. The summation of the estimated source flux for P1 and P3 matches closely with the actual flux value when tested with error-free data.

Results of source location identification for scenario three are presented in Fig. 5.5a. In this scenario, the maximum number of potential sources is kept at four which is more than the actual number of sources present.

The methodology is able to find the co-ordinates of all the four potential source locations. On careful examination of the grid co-ordinates it is seen that potential source P1 and P2 are in the same grid location as actual source S1 and potential source P3 and P4 occupy the same grid location as the actual source S2 while using non-erroneous data. Thus, all the four potential sources effectively represent only two actual sources. The results of source location identification using perturbed observation data are slightly deviated by one grid location for potential source P4 from the actual source location. This might be due to the error, which is incorporated in the observation data used in the linked simulation optimization-based source identification model.

Figure 5.5b shows the unknown source flux variables for every identified clandestine source for each stress period (S11, S12, S13, S14, S15, S21, S22, S23, S24, and S25) marked on the x-axis. Since P1 and P2 represent one actual source (S1)

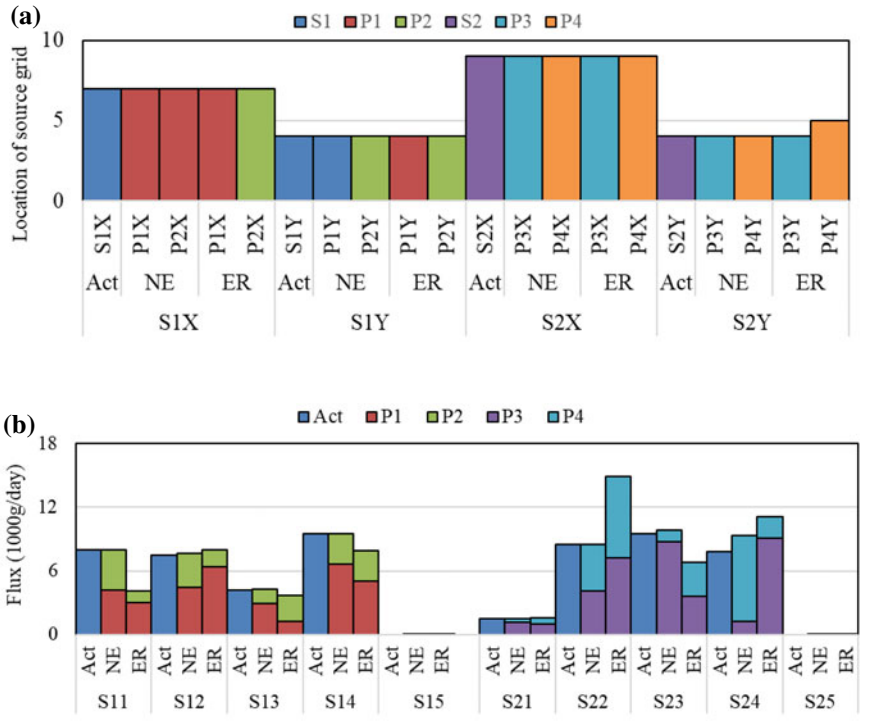

Fig. 5.5 **a** Location of source grid for scenario 3. **b** Flux values of identified source for scenario 3

together, and P3 and P4 together represent the other actual source (S2). Hence, the equivalent source flux will be the summation of the source fluxes for both the sources for every stress period (P1J + P2J = S1J, and P3J + P4J = S2J, J represents stress period). The estimated source flux for both the identified sources matches closely with the actual flux value when tested with error-free data. There is a deviation from the actual flux value in case of erroneous observation data for S22. This deviation of estimated flux can be eliminated by altering of SA parameter for which the objective function attained its early convergence.

Results of source location identification for scenario four are presented in Fig. 5.6a. In this scenario, the maximum number of potential sources is kept at five which is more than the actual number of sources present. The methodology is able to estimate the co-ordinates of all the five potential source locations. Careful examination of the estimated grid co-ordinates shows that potential source P1, P2, and P3 occupy the same grid location as actual source S1, for non-erroneous data. The other source is not clearly identified even in case of non-erroneous data. The location of P5Y is shifted from its original position for non-erroneous observation data. The perturbed data which is used to identify the location of sources is shifted for potential source 2, 4, and 5 from actual source position. However, the deviation is of only one grid cell in all the cases except P5. The accuracy efficiency of the result decreases with the increase of the decision variables to be identified. In this scenario, the method is sensitive to the erroneous observation data. This deviation can be further reduced by the altering the SA parameter for a rigorous search for optimal solution.

Figure 5.6b shows the unknown source flux variables for every identified clandestine source for each stress period (S11, S12, S13, S14, S15, S21, S22, S23, S24, and S25) marked on the x-axis. P1, P2, and P3 together represent one actual source, and P4 and P5 together represent the other source. Therefore, equivalent source flux will be the summation of the source fluxes of potential sources P1, P2, and P3 for actual source S1, and P4 and P5 for actual source S2 for every stress period (P1J + P2J + P3J = S1J and P4J + P5J = S2J, J represents stress period). The estimated source flux for both the identified sources matches closely with the actual flux value when tested with error-free data. There is significantly larger deviation in identifying the release histories with erroneous data for S11, S12, and S14. The deviation of estimated flux is due to the large number of unknown variables to be identified. It is required to regulate the SA parameters for getting better convergence of objective function value.

5.4 Conclusions

The newly established LSO-based method for estimating the number of groundwater contamination sources, locations, and release history is implemented successfully. The method is able to successfully estimate the unknown number of sources and their locations for the non-erroneous observation data even when there is no prior

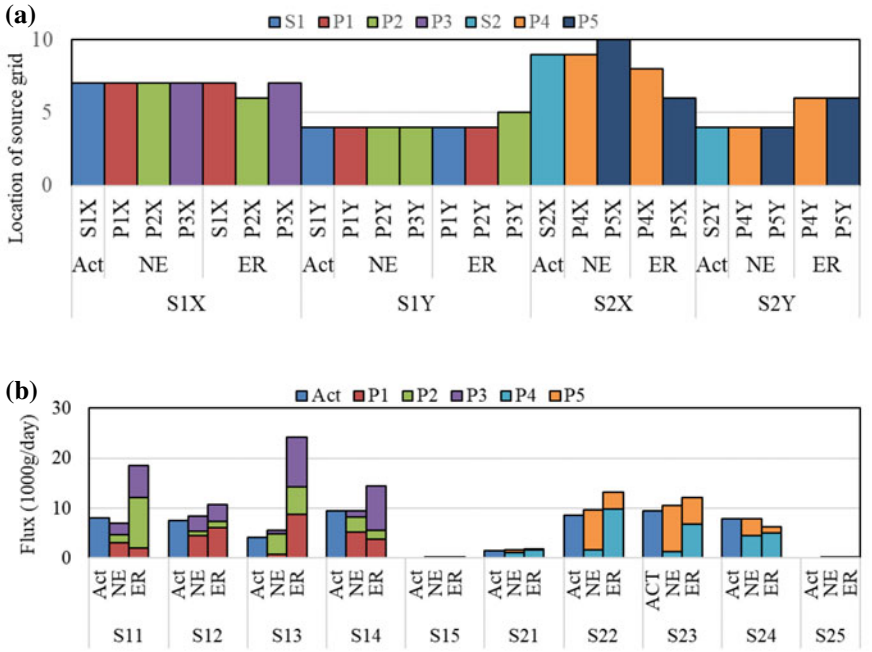

Fig. 5.6 **a** Location of source grid for scenario 4. **b** Flux values of identified source for scenario 4

information about the same. For successful identification of groundwater contamination sources, this approach overcomes one of the essential shortcomings of previous methodologies, which involved prior knowledge about the total number of sources present in the study area, or the exact possible source locations. In its present form, the approach only applies where the total number of presumed plausible sources in the study area exceeds or equals the real number of sources. The restricted evaluations performed in this study demonstrate the method's applicability to real-world problems of finding unknown groundwater contamination sources where no prior knowledge about the number of sources or their positions is available.

References

Chakraborty A, Prakash O (2020) Identification of clandestine groundwater contamination sources using heuristics optimization algorithms: a comparison between simulated annealing and particle swarm optimization. Environ Monit Assess 192(12):1–19

Chakraborty A, Prakash O (2021a) Identification of clandestine groundwater contamination source locations and their release flux history. In: IOP conference series: earth and environmental science, vol 626, no. 1. IOP Publishing, p 012003

Chakraborty A, Prakash O (2021b) Characterization of groundwater contamination sources by kriging based linked simulation optimization. Int J Geomate 20(81):79–850

Datta B, Prakash O, Campbell S, Escalada G (2013) Efficient identification of unknown groundwater contamination sources using linked simulation-optimization incorporating monitoring location impact factor and frequency factor. Water Resour Manage 27(14):4959–4976
Dey S, Prakash O (2020a) Management of saltwater intrusion in coastal aquifers: an overview of recent advances. Environ Process Manage 321–344
Dey S, Prakash O (2020b) Managing saltwater intrusion using conjugate sharp interface and density dependent models linked with pumping optimization. Groundw Sustain Dev 11:100446
Ghafouri H, Mosharaf-Dehkordi M, Afzalan B (2017) Identification of immiscible NAPL contaminant sources in aquifers by a modified two-level saturation based imperialist competitive algorithm. J Contam Hydrol 202:33–46
Gorelick SM, Evans B, Remson I (1983) Identifying sources of groundwater contamination: an optimization approach. Water Resour Res 19(3):779–790
Guneshwor L, Eldho T, Kumar AV (2018) Identification of groundwater contamination sources using meshfree RPCM simulation and particle swarm optimization. Water Resour Manage 32(4):1517–1538
Harbaugh AW, McDonald MG (1996) Programmer's documentation for MODFLOW-96, an update to the US Geological Survey modular finite-difference ground-water flow model. US Geological Survey; Branch of Information Services [distributor]
Jha M, Datta B (2015) Application of unknown groundwater contamination source release history estimation methodology to distributed sources incorporating surface-groundwater interactions. Environ Forensics 16(2):143–162
Keshari AK, Datta B (2001) A combined use of direct search algorithms and exterior penalty function method for groundwater contamination management. J Porous Media 4(3)
Kirkpatrick S, Gelatt CD, Vecchi MP (1983) Optimization by simulated annealing. Science 220(4598):671–680
Mahar PS, Datta B (1997) Optimal monitoring network and ground-water–contamination source identification. J Water Resour Plan Manag 123(4):199–207
Prakash O, Datta B (2014) Characterization of groundwater contamination sources with unknown release time history. J Water Resour Prot 6:337–350
Singh RM, Datta B, Jain A (2004) Identification of unknown groundwater contamination sources using artificial neural networks. J Water Resour Plan Manag 130(6):506–514
Water U (2014) The United Nations world water development report 2014: water and energy. United Nations, Paris
Yeh WWG (1986) Review of parameter identification procedures in groundwater hydrology: the inverse problem. Water Resour Res 22(2):95–108
Zheng C (1990) {MT3D} A modular three-dimensional transport model

Dr. Anirban Chakraborty has completed his Doctoral degree from the Department of Civil and Environmental Engineering, Indian Institute of Technology Patna. His area of expertise is in groundwater management.

Dr.Om Prakash is the Assistant Professor in the Department of Civil and Environmental Engineering, Indian Institute of Technology Patna. He has pursued his Ph.D. from James Cook University, Australia. His area of expertise is in numerical modelling of groundwater flow and contaminant transport in groundwater system.

Chapter 6
Development of Multiple Linear Regression Model for Heavy Metal Prediction Around Eklahare Thermal Power Plant, Nashik, Maharashtra

Vrushali V. Sasane and Alka S. Kote

Abstract The present paper is aimed to develop a Cadmium (Cd) prediction model using multiple linear regression (MLR) by taking major primary parameters viz. pH, temperature (T), electrical conductivity (EC), total dissolved solids (TDS), total hardness (TH), alkalinity $(HCO)_3$, nitrate $(NO_{3)}$, sulfate (SO_4) and fluoride (Fl) in the groundwater of Eklahare village, Nashik, Maharashtra (India). For this purpose, four sources are identified and monitored during the pre-monsoon and post-monsoon seasons by collecting the samples. The correlation coefficient among the selected parameters and their association with Cd is identified. A good correlation among Cd, EC, TDS, TH, NO_3, SO_4 and Fl has been observed. The more or less same trend is observed during both the seasons. The MLR model is developed and then tested for new inputs of a predictor. For the pre-monsoon season, the model predicted Cd, with an R^2 value of 0.607 and MSE 0.000037, whereas R^2 of 0.767 with MSE 0.000001 is observed for the post-monsoon model.

Keywords Groundwater · Thermal power plant · Fly ash · Cadmium · Multiple linear regression

6.1 Introduction

Industrialization and urbanization have increased energy demand leading to a global energy crisis. In the context of India, this demand is mainly met by the coal-based thermal power plant with its share of 58.40% of total electricity generation. This conventional fossil fuel-based energy generation results in serious implication for surrounding water resources and the ecosystem.

A. S. Kote (✉)
Dr. D. Y. Patil Institute of Technology, SPPU, Pimpri, Pune, India
e-mail: alkakote26@gmail.com

V. V. Sasane
SRES Sanjivani College of Engineering, SPPU, KopargaonAhmednagar, India
e-mail: sasanevrushalicivil@sanjivani.org.in

R. Jha et al. (eds.), *Groundwater and Water Quality*, Water Science and Technology Library 119, https://doi.org/10.1007/978-3-031-09551-1_6

Effluents from thermal power plants mainly include ash disposal, thermal discharges, wastewater effluents and coal storage runoff. The coal ash has varying compositions and volumes. Ash is rich in the major constituents, namely CaO, MgO, Na_2O, K_2O, SiO_2, Fe_2O_3, MnO, TiO_2 and P_2O_5 (Deshmukh et al. 1994). Besides, ash is also rich in trace elements such as Cd, Pb, Ni, Cu and Cr (Singh et al. 2010). The disposal of ash is carried out by the wet method, where ash-loaded water slurry is carried to the ash pond (Khati Varada et al. 2014). In most of the ash ponds, the leaching of heavy metals is due to the unlined construction of the ash ponds (Singh et al. 2010).

Heavy metal-enriched leachate from ash pond penetrates the groundwater and increases the turbidity of water due to the release of ash in surrounding water bodies. Looking at the serious effects of heavy metal, monitoring and early estimation of it become important. Futuristic estimation of heavy metal concentration in groundwater is only possible with an effective prediction tool. MLR is a statistical technique, which provides a user-friendly approach to getting the prediction model in the form of mathematical expression.

Thus, the objective of this study is to assess the heavy metal contamination in groundwater and to develop a cadmium (Cd) prediction model using multiple linear regression (MLR) for Eklahare village.

6.2 Study Area

Eklahare village is located in Nashik district of Maharashtra (India), and it has a total geographical area of 9.15 km^2. It houses Nashik Thermal Power Station (NTPS). It commenced in the year 1970 and is situated on the left bank of the Godavari River. The thermal power station has a rated capacity of 630 MW and has 3 units of 210 MW each. It uses a coal-fired boiler to produce steam for power generation. The location of Eklahare village and the thermal power plant is shown in Fig. 6.1.

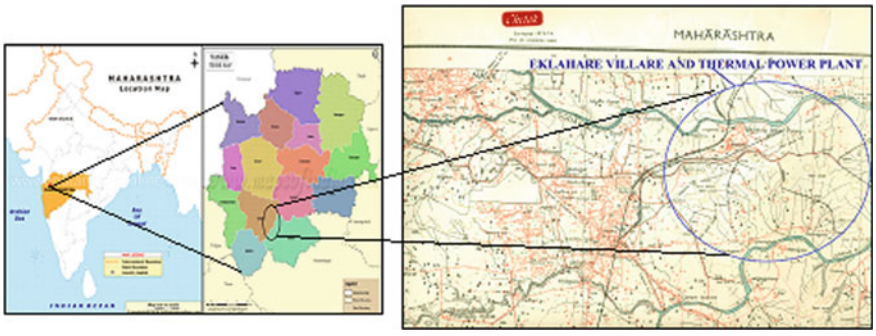

Fig. 6.1 Location map of study area

The field survey and interview with the residents of Eklahare village suggest that the residents are facing many health issues and a decline in agricultural yield. Groundwater quality in Eklahare village is not addressed and monitored for heavy metal contamination due to effluent discharge. Therefore, it is imperative to predict heavy metals for initiating preventive measures.

6.3 Materials and Methods

The groundwater quality in Eklahare village is assessed by collecting total four samples during the pre-monsoon season, i.e. March 2018–May 2018, and the postmonsoon season, i.e. October 2017–December 2017 period. The samples are collected in sterilized polyethylene bottles and analyzed for physical–chemical parameters and heavy metals. The procedure for analysis is adopted as prescribed by the APHA manual. Prior to water quality analysis, the coal and fly ash samples are analyzed to select the heavy metals for prediction modeling.

6.3.1 Data Analysis and Model Development

This section describes association of groundwater quality parameters by correlation analysis, model development using MLR and, its testing and criteria for prediction perfromance evaluation.

6.3.1.1 Pearson Correlation Coefficient

The degree of linear association between any two water quality variables is measured by a simple correlation coefficient named as Pearson correlation coefficient (R). It is a single summary number, which shows the relationship that exists between two variables and the strength of the linear relation between them in terms of positive and negative values. And it has great significance in regression analysis. The Pearson correlation coefficient is computed by using the formula given below in Eq. (6.1).

$$R = \left[\frac{\sum (x_i - \overline{x_i})(y_i - \overline{y_i})}{\sqrt{\sum (x_i - \overline{x_i})^2 (y_i - \overline{y_i})^2}} \right] \tag{6.1}$$

where the variables x and y represent two different water quality parameters; $n =$ number of data points/number of groundwater samples. R is always between -1 and $+1$. The R value closer to ± 1 implies that the association is closer to a perfect linear relation (Bhor et al. 2013).

6.3.1.2 Multiple Linear Regression (MLR)

A MLR is a statistical approach, which provides the relationship between two or more independent/predictor variables (x_i) and dependant/predictand variable (y_i) in the form of a mathematical expression. The selection of predictors and predictand is mainly based on the R value between them. The multiple linear regression model is expressed as below

$$y_i = \beta_0 + \beta_i x_{i,1} + \beta_2 x_{i,2} + ... + \beta_n x_{i,n} + e_i \tag{6.2}$$

where $x_{i,n}$ = value of nth predictor, ß = regression constant, ß = coefficient on nth predictor, n = total number of predictors, y_i = predictand and e_i = error term (Mokkaram 2016).

6.3.1.3 Model Development

During model development, a data set is divided into two groups: 75% observations for training/developing the model and 25% observations for testing the models. Two separate models are built for pre-monsoon and post-monsoon seasons.

The model building is carried out using MINITAB 17 statistical software. The stepwise regression (backward elimination) method is used. The alpha value to remove the significance level is set to 0.15. Therefore, the predictor, which has a t-test P value less than 0.15 will enter the model, indicating its capability in prediction.

6.3.1.4 Performance Criteria

The criterion adopted in assessing the model performance includes coefficient of determination (R^2) and mean square error (MSE) between the actual and predicted values. R^2 defines the degree of correlation between the observed and predicted values, whereas MSE measures the average of the square of the error. The smaller values of MSE ensure the best performance (Ahmed et al. 2014).

$$R^2 = \frac{\left[\sum (x_i - \overline{x_i})(y_i - \overline{y_i})\right]^2}{\sum (x_i - \overline{x_i})^2 (y_i - \overline{y_i})^2} \tag{6.3}$$

$$MSE = \frac{1}{n} \sum [x_{Observed} - x_{\mathrm{Pr}edicted}]^2 \tag{6.4}$$

6.4 Results and Discussion

The physico-chemical analysis of groundwater samples in pre- and post-monsoon seasons revealed the groundwater quality scenario in Eklahare village. The result presented in Table 6.1 shows that the concentration level gets lowered in the pre-monsoon season, and its minimum concentration is 0.00069 mg/l and maximum 0.0068 mg/l. This decreasing trend may be due to a lack of water to take away the leachate from the ash pond to groundwater.

The result presented in Table 6.2 shows that during the post-monsoon, the concentration level of Cd rose gradually, having a lower concentration in October and higher in December. All the samples showed a concentration above permissible levels ranging 0.00095–0.017 mg/l, indicating the alarming situation in the study area. The increased Cd may cause tubular dysfunction, kidney stones and osteomalacia.

6.4.1 Correlation Analysis

Correlation analysis is carried out for the parameter to determine the association of Cd with other parameters. It is carried out to find the predictor of Cd. The detailed analysis is discussed below, and it is represented in Tables 6.3 and 6.4, for pre- and post-monsoon seasons, respectively.

Table 6.1 Groundwater quality in Eklahare during pre-monsoon season

Station	pH	T	EC	TDS	TH	HCO_3	NO_3	SO_4	Fl	Cd
BIS	6.5–8.5	NG	NG	500	200	NG	45	200	1.5	0.003
March 2018										
S1	7.87	28	212.0	1580	1293.6	304.5	47.87	327.5	0.74	0.0068
S2	7.56	27.7	87.9	694	480.2	491.4	5.4	62.5	0.48	0.00015
S3	8.47	29.3	68.8	521	411.6	226.8	48.16	50	0.71	0.00088
S4	7.92	28.10	61.3	396	362.6	329.7	5.32	27.5	0.52	0.00069
April 2018										
S1	7.16	27.8	208.0	1590	1276.8	336.6	42.28	390	0.84	0.0041
S2	7.29	28	95.2	714	446.4	536.8	1.68	62.5	0.65	0.00081
S3	8.56	27.7	65.7	462	336	217.8	40.04	86.25	0.50	0.00091
S4	7.61	27.7	46.8	356	324.48	338.8	36.18	35	0.30	0.0036
May 2018										
S1	7.56	29.3	274.0	1650	1234.8	312.4	45.92	175	0.40	0.0011
S2	8.19	28.3	98.9	608	419.4	552.2	1.12	67.5	0.70	0.00097
S3	7.94	28.3	87.9	533	427.28	288.2	40.88	60	0.90	0.0034
S4	8.04	28.10	521	368	329.2	349.8	31.92	32.5	0.60	0.0023

Table 6.2 Groundwater quality in Eklahare during post-monsoon season

Station	pH	T	EC	TDS	TH	HCO_3	NO_3	SO_4	Fl	Cd
BIS	6.5–8.5	NG	NG	500	200	NG	45	200	1.5	0.003
October 2017										
S1	7.79	27.8	127.6	855	1207.36	238.02	42.5	340.2	1.28	0.0049
S2	7.84	28	109.7	735	621.32	562.4	32.02	272.8	0.68	0.0001
S3	8.76	27.7	98.95	663	495.88	254.82	32.38	124.12	1.08	0.0001
S4	7.92	27.7	97	650	417.48	338.59	29.72	193.5	0.46	0.0026
November 2017										
S1	7.54	29.3	193.98	1295.1	1293.43	247.32	45.12	367.5	1.35	0.0067
S2	7.64	28.3	124.94	837.12	601.24	521.89	35.42	281.38	0.97	0.0012
S3	7.81	28.3	91.83	615.32	475.31	293.31	48.59	183.02	1.14	0.00095
S4	7.71	28.1	83.52	559.59	419.7	314.74	31.32	216.4	0.85	0.0043
December 2017										
S1	7.36	28	306.7	1748	1308.3	270.26	56.1	397.12	1.42	0.017
S2	7.62	27.7	156.4	894.39	568.4	490.12	28.4	304.26	1.28	0.0045
S3	8.62	29.3	67.8	594.74	480.2	348.08	58.6	297.41	1.12	0.011
S4	7.73	28.1	46.2	413.78	426.3	290.79	30.42	242.67	1.04	0.006

Table 6.3 Correlation analysis for pre-monsoon season

Parameter	pH	T	EC	TDS	TH	HCO_3	NO_3	SO_4	Fl	Cd
pH	1									
T	0.252	1								
EC	−0.107	0.128	1							
TDS	−0.498	0.209	0.275	1						
TH	−0.472	0.186	0.304	0.990	1					
HCO_3	−0.437	−0.265	−0.059	−0.061	−0.145	1				
NO_3	0.182	0.327	0.261	0.394	0.459	−0.837	1			
SO_4	−0.420	−0.080	0.228	0.893	0.920	−0.165	0.453	1		
Fl	0.031	0.069	0.059	0.209	0.223	−0.019	0.142	0.390	1	
Cd	−0.212	−0.244	0.234	**0.469**	**0.554**	−0.296	**0.557**	**0.664**	0.368	1

Pre-monsoon season: The correlation shown in Table 6.3 represents that Cd has a significant relation with the parameters in the order of TDS (0.469) < TH(0.554) < NO_3 (0.557) < SO_4 (0.664), hence for the development of cadmium prediction model TDS, TH, NO_3 and SO_4 are selected.

Post-monsoon season: Table 6.4 illustrates the chemical association of Cd and it depicts that it has good relation with EC, TDS, TH, NO_3 and SO_4. It is in the order of

Table 6.4 Correlation analysis for post-monsoon season

Parameter	pH	T	EC	TDS	TH	HCO_3	NO_3	SO_4	Fl	Cd
pH	1									
T	0.100	1								
EC	−0.539	−0.003	1							
TDS	−0.512	0.118	0.989	1						
TH	−0.464	0.198	0.800	0.851	1					
HCO_3	−0.129	−0.133	−0.113	−0.151	−0.354	1				
NO_3	0.059	0.613	0.405	0.472	0.482	−0.378	1			
SO_4	−0.571	0.359	0.697	0.746	0.804	0.024	0.489	1		
Fl	−0.198	0.288	0.553	0.577	0.644	−0.397	0.558	0.578	1	
Cd	−0.234	0.333	**0.608**	**0.635**	**0.531**	−0.358	**0.686**	**0.694**	**0.545**	1

TH (0.531) < Fl (0.545) < EC (0.608) < TDS (0.635) < NO_3 (0.686) < SO_4 (0.694). So TH, Fl, EC, TDS, NO_3 and SO_4 are selected as predictors for cadmium prediction.

6.4.2 MLR Model

The MLR model development is carried out by providing the input parameters obtained in correlation analysis. For the pre-monsoon season, TDS, TH, NO_3 and SO_4 are provided for model development, whereas EC, TDS, TH, NO_3, SO_4 and Fl are provided for the post-monsoon model.

Pre-monsoon season: The pre-monsoon model is developed using TDS, TH, NO_3 and SO_4. During model development, NO_3 and SO_4 get eliminated. In the training phase, the model has proposed the prediction accuracy (R^2) of 0.666 with an MSE of 0.000002.

$$Cadmium_{\mathrm{Pre-monsoon}} = 0.000438 - 0.000016 \times TDS + 0.000023 \times TH \quad (6.5)$$

Testing of Cd $_{\text{Pre-monsoon}}$ Model: The obtained model is tested for 3 new sample inputs of TH and TDS. And the model predicted the values with R^2, 0.607 accuracy with MSE of 0.000001. So the model performed satisfactorily during the testing phase.

Post-monsoon season: The Cd model is developed using TH, Fl, EC, TDS, NO_3 and SO_4 as a predictor and stepwise regression is done. During backward elimination, Fl, TDS, TH and SO_4 were eliminated from the model due to a *t*-test *P* value being greater than 0.15. It indicates that these parameters have the less predicting ability. In training, the model has projected R^2, 0.828 with MSE, 0.000007. The model is given as follows:

Table 6.5 Performance comparison in training and testing phases

Sr. no	Season	Training		Testing	
		R^2	MSE	R^2	MSE
1	Pre-monsoon	0.666	0.000002	0.607	0.000001
2	Post-monsoon	0.828	0.000007	0.767	0.000037

$$Cadmuim_{Post-monsoon} = -0.0145 + 0.000042 \times EC + 0.00032 \times NO_3 \quad (6.6)$$

Testing of Cd $_{\text{Post-monsoon}}$ Model: The above model is tested for 3 new sample values of EC and NO_3. The prediction accuracy is checked by plotting the observed versus predicted values and the R^2 value obtained is 0.767 with an MSE of 0.000037.

Summary

Overall performance of both MLR models during the training and testing phases with respect to statistical performance parameters, i.e. R^2 and MSE is presented in Table 6.5.

6.5 Conclusion

The overall MLR model is found quite effective in predicting the Cd in groundwater of Eklahare. The model predicted the Cd with R^2 value 0.607 and 0.767 in the post-monsoon and pre-monsoon periods, respectively. If we compare it with training performance, both models performed reasonably well during testing also. So the proposed MLR models could be effectively used to predict the concentration of Cd in the groundwater of Eklahare. Hence, MLR provides us the conventional statistical user-friendly approach for the development of the prediction model.

Acknowledgements The author is thankful to Principal and H.O.D. of SRES's Sanjivani College of Engineering, Department of Civil Engineering Kopargaon, Ahmednagar, Maharashtra (India), for institutional facility and cooperation.

References

Ahmed AAM (2014) Prediction of dissolved oxygen in Surma River by biochemical oxygen demand and chemical oxygen demand using artificial neural networks. J King Saudi Univ 29(2):151–158

Bhor M, Kadave P, Bhor A, Bhor S, Bhosale M, Bholay AD (2013) Water quality assessment of the river Godavari, at Ramkund, Nashik, (Maharashtra), India. Int J Eng Sci 2(2):64–68

Deshmukh AN, Shah KC, Srivastava BN (1994) Impact of rainy season (monsoon) on fly ash dispersal—a case study of Koradi thermal power plant, Maharashtra. Gondwana Geol Mag 8(1):17

Khati Varada V, Gulwade Deepali P, Deo SS (2014) Quality assessment of surface and ground water around thermal power plants at Warora district, Chandrapur (MS). J Chem Pharm Res 6(7):1856–1860

Mokarram M (2016) Modeling of multiple regression and multiple linear regressions for prediction of groundwater quality (case study: north of Shiraz). Model Earth Syst Environ 2:3

Singh R, Singh RK, Gupta NC, Guha BK (2010) Assessment of heavy metals in fly ash and groundwater—a case study of NTPC Badarpur Thermal Power Plant, Delhi. Pollut Res 29:685–689

Chapter 7
Integrated Approach for Groundwater Recharge Assessment—A Review

Venkanagouda B. B. Patil and K. N. Lokesh

Abstract In the present century, groundwater recharge is a major issue since there is scarcity of freshwater availability. The excess utilization of groundwater is a hazard to the water quality as well as for water table and makes hydrological imbalance which includes both quality and quantity of the groundwater. Artificial groundwater recharge becomes very essential to enhance the hydrodynamic condition of groundwater. Recharging methods are several, and it depends on the need, possibilities and several factors which will influence the recharging. Geologically, one has to study very systematically to locate groundwater recharge potential zones (GWRPZ). The literature review highlights the various criteria which are considered for GWRPZ. Remote Sensing (RS) and Geographic Information System (GIS) tools have made it easier to find the best locations for groundwater recharge. The RS and GIS techniques commonly consider the various thematic maps like slope, lithology, geomorphology, land use land cover, soil, drainage and lineament maps for integrated overlay analysis. These layers will be integrated in GIS environment, and knowledge-based rankings will be assigned to each part of individual thematic layer based on its significance to derive the GWRPZ. The present paper insights into the review on locating potential groundwater recharge zones by various methods and parameters which are already considered and the new parameters which can be considered to enhance the accuracy level to locate the potential groundwater recharge zones. The importance of vertical electrical sounding (VES) is also highlighted.

Keywords Groundwater recharge · Remote sensing · Overlay analysis · VES · GIS · Decision support system

7.1 Introduction

For nourishment of any lifecycle and for any developing activity, groundwater acts as the world's utmost precious and important natural resource (Hutti and Nijagunappa

V. B. B. Patil (✉) · K. N. Lokesh
Department of Civil Engineering, National Institute of Technology Karnataka (NITK), Srinivasnagar Post, Surathkal 575025, Karnataka, India
e-mail: venkzpatil@gmail.com

R. Jha et al. (eds.), *Groundwater and Water Quality*, Water Science and Technology Library 119, https://doi.org/10.1007/978-3-031-09551-1_7

2011; Ghosh et al. 2016). One of the most important and depleting resources in both rural and urban areas is water. In densely populated countries, the demand for water is high, hence the groundwater demand increases. Variation in the climatic conditions are badly affecting the monsoon seasons, and the over-exploitation of groundwater to meet the requirements leads to depletion in groundwater level which will further affect investment and operational cost. Percolation of the rainwater into the subsurface has diminished significantly, because of developmental activities in urban areas which results in the reduction of availability of groundwater tremendously.

Evaluating, handling and development of this resource for sustainable usage grow into a vital problem in human life, particularly the areas with low and erratic rainfall and deeper level of groundwater occurrence (Jasrotia et al. 2009). Effective planning of consumption of groundwater is of extreme importance (Kumar et al. 2008). In defining groundwater recharging potential zones (GWRPZ) in regions of hard rock, some very extensive research on hydrogeology have been done by a number of scholars and academics. Especially in countries like India, areas which are semi-arid and hard rock regions are facing regular water inadequacy events generally in summer months and also in drought years.

In India, the rainfall is extremely variable due to the different rainy season pattern and diverse topographical conditions like plane land, mountain, valley, etc. Spatially, rainfall is 100 mm which is very low in Rajasthan and 11,000 mm in Mausingram, Meghalaya (Sharma and Paul 1998). Even in national agricultural and water policy of Government of India, the prerequisite of water recharge and water conservation has been stressed. Various structures for groundwater recharge, like check dams, nalla bunds, percolation tanks, harvesting bunds, farm bunds, etc. are built at suitable sites that check water flow, flood, and afford agriculture to downstream areas and also influence groundwater recharge (Singh et al. 2009).

Groundwater recharge occurs naturally and artificially. But to meet the human requirements, there is a need of artificial groundwater recharge, to enhance the quantity as well as quality. Infiltration is the process through which natural groundwater recharge takes place by percolating from earth's surface to subsurface and which reaches either to the confined aquifer or unconfined aquifer. Aquifers will form based on these two kinds of recharge processes, whereas decrease in the infiltration or groundwater recharge will make the subsurface dry and aquifers become empty. Groundwater recharge structure is a significant mechanism of watershed improvement. Since the amount of normal precipitation is totally insufficient, enhancement of aquifers by artificial groundwater recharge, especially in the arid and semi-arid areas of India, is crucial, as the intensity of normal rainfall is totally insufficient to produce any moisture surplus under normal infiltration conditions (Mukherje 2016).

Selection of any specific method for artificial groundwater recharge depends on the various criteria like topography of the area, lithological variations, geomorphological observations, rainfall trend and many more. Remote sensing and geographic information system (RS and GIS) are the modern practices becoming significant in the present days. Geoinformatics tools perform a vital part in the development in the field of hydrology (Krishna 1996, 2005; Durga Rao et al. 2001; Anbazhagan and Ramasamy 2001; Kumari and Krishna 2013). They play a crucial role for successful

analysis of any hydrological investigations to collect information, especially in spatial and temporal domains, which is the greatest advantage of using both RS and GIS.

Yadav et al. (2012) and Mukherje (2016), have discussed various methods for artificial groundwater recharge some of which are commonly adopted methods and are classified as direct surface methods, direct subsurface methods and indirect methods. Direct surface methods include flooding, surface spreading, percolation tanks, stream augmentation, over-irrigation, ditch and furrow method, bench terracing, gully plugs, contour bunds, contour trenches and stream channel modification. Direct subsurface approaches comprise injection wells, recharge pits and shafts, gravity-head and recharge wells and connector wells, and indirect methods include induced recharge, bore blasting, hydro fracturing, groundwater dams, etc. (Yadav et al. 2012; Mukherje 2016).

This paper mainly deliberates on the methodology to locate suitable site selection for artificial groundwater recharge. This paper also presents identification of most favorable locations for groundwater recharge (GWR) and suggests suitable structures using decision support system (DSS) which is based on GIS that uses remotely sensed data and limited field survey. These methods have enough potential of enhancing the water resources by integral approach by using the recent developments. Hence, location of groundwater recharge sites and construction of suitable structures are very much needed since the majority of areas in the hard rock areas of India are semi-arid and rain-fed because of erratic precipitation. Available excess runoff due to rainfall needs to be collected in respective structures for better use of it for agricultural, domestic and industrial requirements (Kadam et al. 2012).

7.2 Materials and Methodology

In order to identify the most appropriate locations for artificial groundwater recharge, many factors were considered in various literatures by various authors. RS and GIS tools are the essential techniques to prepare several thematic layers. The most common thematic layers which were considered in previous work include Geomorphology, Lithology/Geology, Slope, Contour, Land use/Land Cover (Lu/Lc), depth to groundwater level, drainage, rainfall, soil, lineament and drainage density map.

7.3 Factors Influencing Groundwater Recharge

Identification and location of GWRPZ especially depends on direct analysis of some observed topographical features like geological and geomorphic and their hydrologic characters. It is necessary to know the depth of the bedrock and the permeability and porosity of the area to increase the accuracy level considering the subsurface layer using vertical electrical sounding approach.

7.3.1 Lithology/Geology

Regarding recharge areas, type of lithology which is exposed in the area and its character are most important since other factors are greatly dependent on it (Ghosh et al. 2016). Edet et al. (1998), explained that some hydrogeologists neglected this factor since they were considering drainage and lineaments as a part of lithology. Later, other researchers (Magesh et al. 2012; Acharya and Nag 2013) incorporated this geology feature since it strongly influences infiltration. With this reason, it is essential to incorporate this factor for groundwater recharge studies. Lithology/Geology maps are published maps from government organizations and which are in a regional scale. To prepare those maps, we need to digitize them and bring them to our required area of interest. Since the geology maps with high resolution with scale 1:50,000, 1: 25,000 are expensive; maximum researchers have preferred the small-scale maps which are available at a very low price.

7.3.2 Slope

In locating the groundwater recharge zones, slope plays a significant role since it is an important factor which plays different roles with respect to different angles of slopes. Slope with high steep angle indicates greater velocity so it causes very less recharge due to quick runoff in the course of rainfall, letting deficient time to penetrate the surface and recharge the saturated zone (Rokade et al. 2007; Gumma and Pavelic 2012; Selvam et al. 2014). On the contrary, surface with comparatively moderate sloping terrains influences more recharge, so lower the slope, the better the recharge (Döll et al. 2002). Thematic maps such as contour and slope maps will be prepared from freely available data by different government organizations of various countries and which can be accessed by people from other countries too. Usually, slope map will be prepared from Digital Elevation Model (DEM) and from the same data, even contour map may be extracted. The most preferable resolution for DEM is 1 Arc second (30 m) resolution. DEM is offered by ASTER and SRTM.

7.3.3 Geomorphology

Geomorphology factor of an area is analyzed based on the type of landforms, associated vegetation, areal extent, etc. (Dinesh Kumar et al. 2007). Field survey is very essential to classify the various landforms. Geomorphology maps are available since they are published from government organizations and which are in a regional scale. Preparation of this map also requires the geology map along with field visits and ground truth data.

7.3.4 Land Use/land Cover

Generally, Lu/Lc means the surface features and alteration by structures built on it in later cases and the changes observed on periodical bases. Artificial structures like buildings, roads, embankments and other developmental activities built by human beings are reducing the rate of infiltration by acting as an impermeable layer on the surface. But with respect to groundwater recharge consideration, areas with vegetation and agricultural activities are treated as the effective places to enhance the recharge rate. In the present days, RS and GIS tools offer realistic basic data on Lu/Lc (Ghosh et al. 2016).

For Lu/Lc maps, there is a need of cloud-free satellite data and it also depends on which organization we order the data for a specific area. The major organizations are like NRSC, NASA, BHUVAN websites and many more. In the Indian scenario, according to available literature, the most preferred data set is linear imaging self-scanning scanner (LISS) data with various resolutions like 72.5, 36, 23.6 and 5.8 m from IRS, CARTOSAT and RESOURCESAT satellites. To enhance the resolution, in some literature, they have merged the panchromatic (PAN) data with LISS-III and LISS-IV. Since the Landsat data with 30 m resolution is freely available, this is also considered by some authors and also merged with PAN data in some cases. Landsat offers PAN data at 15 m resolution. The usage of LISS-IV data is started since last few years and is found very less in the available literature since the data is not freely available.

7.3.5 Groundwater Contour

It can be also called as depth to groundwater. Due to the monsoonal variations, diversified rainfall and exploitation of groundwater for various purposes create imbalance in the groundwater level. The groundwater level fluctuates highly especially in non-rainy seasons since the only process of exploitation will be active instead of recharge. We can expect the highest level of groundwater during monsoon season as compared to the other seasons. It is essential to know the depth of groundwater table to think of groundwater recharge. Depth to groundwater map was prepared by the observation of well data by drawing the contours for different depths of groundwater. For accurate measurement, it is essential for the researchers to carry out field observations for at least one year, from which one can understand the fluctuation of the groundwater level on monthly and yearly basis. From various authors, the data need to be compared with the existing data for at least 10–15 years to draw the inference.

7.3.6 Soil Type

The permeability of any area almost depends on the topmost layer of the surface which is the soil layer. Transmission and infiltration of runoff or surface water from surface into an aquifer system is mainly dependent on soil type and its texture (Anbazhagan et al. 2005). Various types of soils can be expected in the world and even within small diameter areas. Formation of any soil type depends on the topography, parent rock, climate and numerous geological agents which act as key factors in runoff and groundwater recharge (Rashid et al. 2012). Soil and soil depth components show a significant part in the recharge course. As per the various research, this data was used from NBSS LUP in Indian literature. The maps produced from this board are freely available, and are helpful for the researchers to use them for various applications.

7.3.7 Drainage

This factor is primarily dependent on the underlying lithology, so it is a key indicator for identification of water infiltration (Shaban et al. 2006). As Ghosh et al. (2016), clearly said, the higher the density of drainage, the lesser the recharge rate and vice versa. With concern to extraction of more appropriate drainage pattern, manual extraction is more preferable by many researchers rather than one which is created from the satellite imageries (Tribe 1991; Ichoku et al. 1996; Martinez-Casasnovas and Stuiver 1998). Extraction and examination of drainage pattern can be done in several ways like it can be prepared from toposheets, aerial photos, and field data and also from DEM or satellite data. Drainage density maps can be prepared by using drainage map.

7.3.8 Lineaments

Lineaments are hydrogeologically more significant factors since they offer the paths for groundwater drive. Shaban et al. (2006) said for groundwater flow the connected lineaments create subsurface path. The higher the number of lineaments, the more the paths for groundwater flow and we can expect more infiltration which improves the recharge capacity. In many of the landscapes especially in hard rock terrains, lineaments are a key factor in groundwater recharge studies (Rashid et al. 2012). Groundwater potential zones are associated with lineament zones as suggested by Srivastava and Bhattacharya (2006). So based on groundwater potential zones, we can identify the recharge zones. Lineaments are associated with fractures and faults which causes secondary porosity and permeability which are an indicator of the suitable recharge zones (Kumar et al. 2007). Lineament maps can be derived from geomorphology maps.

7.3.9 Rainfall

The amount of runoff will be determined based on the rainfall and number of annual rainy days in any specific areas under study, which makes sense to think of the suitable area for recharge. The more rainfall will create more runoff which makes the availability of higher amount of water for infiltration. Based on the various amounts of rainfall, we can create isohyetal map.

7.3.10 Iso Resistivity

One has to carry out the geophysical field survey with the VES approach using Schlumberger configuration to understand the subsurface layers and to know the depth of bedrock and groundwater table. From the obtained apparent resistivity data, we can create an iso resistivity map for different resistivities for various layers that can be identified easily, and later it is overlayed on the other layers. So it necessary to carry out this survey to get the complete picture of the subsurface with regards to recharge studies.

7.4 Suitability Map for Groundwater Recharge and Discussion

All the prepared thematic maps viz. lithology/geology, slope, geomorphology, Lu/Lc, lineaments, drainage, groundwater contour, soil type, rainfall and apparent resistivity need to be converted into raster format, subsequently respective theme weight to be assigned based on the field knowledge and various classes and ranks to be given. So here the first step will be the weighted overlay analysis (Oikonomidis et al. 2015) which has been carried out in ArcGIS of various versions like 9.3.1, 9.3.2, 10.3, etc. in the present day.

Lithology/geology + Slope + Geomorphology + lineament + landuse/landcover + Soil type + slope + drainage + Rainfall + Apparent resistivity + Groundwater contour.

7.4.1 Decision Support System

After creating various thematic layers, these layers have to undergo processing for various considerations. For locating potential sites for groundwater recharge (GWR) technologies, decision support system (DSS) is the common most method which will be implemented using ArcGIS software. The concept of workflow is shown with a

flowchart in Fig. 7.1. DSS has mainly three key processes which include data input and preprocessing, main processing and lastly outputs of potential sites for different types of groundwater recharge structures (Mbilinyi et al. 2007).

To achieve high accuracy, many authors have conducted ground truth survey to identify the existing structures and later compared it with the potential rainwater harvesting map by overlaying on it. This kind of investigation shows 75–100% accuracy which directs us for field application (Kadam et al. 2012).

Once we created all these thematic layers, these will be treated with different weightage based on their importance in the field. The weightage will be assigned differently for each layer like 1 to 5 with ranking or weightage in such a way that 1 is less important and 5 is highly favorable and later all these weightages will be added and based on that the areas with high weightage will be treated as suitable sites for groundwater recharge.

With some surface factors, it is essential to add a few subsurfaces or indirect factors like subsurface lithology, subsurface layers, fracture zones, depth to water table and depth to bedrock data to make the work more accurate. The area which will get more score after all weightage assessment will be treated as more preferable. Finally, after all this analysis and overlay, we can obtain an output map showing a suitable site for groundwater recharge with the classifications like from poor to excellent. For artificial groundwater recharge for the Indian scenario, the list of thematic layers and the source for it have been given in Table 7.1. Based on the observation in the literature, the list contains most preferable layers and the source which was commonly used by the maximum number of authors in the previous studies.

The significant input of this paper is to recommend the consideration of a new layer which is the depth to bedrock map, which can be obtained by conducting Vertical Electrical Sounding (VES) with the Schlumberger configuration method.

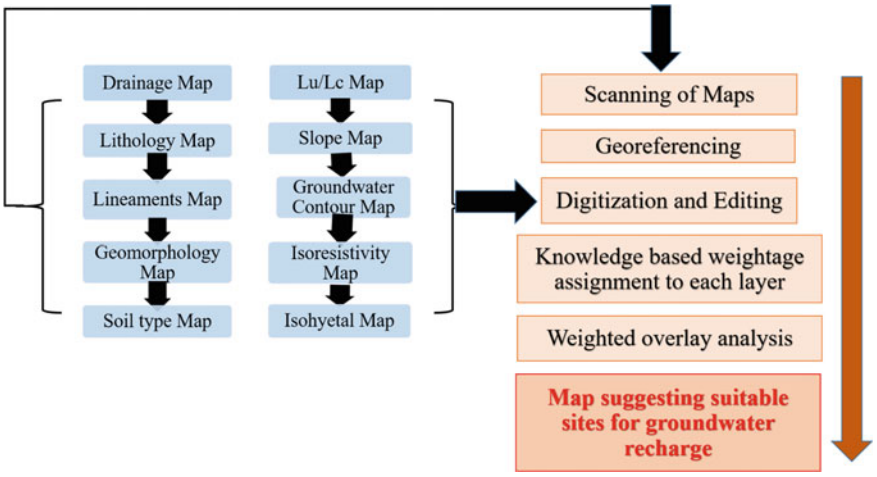

Fig. 7.1 Flowchart for Groundwater recharge Potential Map

Table 7.1 Source for thematic layers

Contour map	SOI toposheets (1:50,000) and SRTM DEM (l Arc Second)
Slope map	Will be extracted from DEM
Land use land cover map	RESOURCESAT-I LISS IV (Resolution 5.3 m)
Soil type map	Will be prepared from the maps published by NBSS/LUP or KRSAC
Drainage and water bodies map	SOI toposheets (1:50,000) and SRTM DEM (l Arc Second)
Geomorphology map	Maps published by GSI and KRSAC
Lineaments map	Can be extracted from land use land cover map
Lithology map	GSI and KSRSAC (scale 1:250,000, 1:50,000)
Soil depth map	Geophysical field survey
DEM	Bhuvan website
Depth to bed rock map	Geophysical field survey
Ground water level map	CGWB, MGD and also field survey
Groundwater quality suitability map for agriculture	Field survey
Map showing the suitable sites for groundwater recharging structures	Field survey and all other thematic layers

Apart from that, it is also useful to know the subsurface details like fractured zone, jointed zone faulted zone, soil depth and many more aspects. So to make recharge effectively and to increase the groundwater level effectively, one must have to carry out the VES of that particular area.

7.5 Conclusion

The foremost objective is to discuss the assessment of site suitability conditions for artificial groundwater recharge which is a significant step toward maximizing water availability particularly in arid and semi-arid areas.

Many authors have considered RS and GIS approaches with common factors like geology map, geomorphology map, LU /LC map, drainage map, soil map, rainfall map and slope map to suggest suitable sites for groundwater recharge. There is a need of upgradation in various aspects like resolution, number of factors for recharge and the integrative study. For artificial groundwater recharge sites, there is a necessity to know the subsurface, which can be carried out by conducting VES without affecting the ground and by which we can understand the subsurface layers in detail. From VES, we can prepare iso resistivity maps and also soil depth map by which we can suggest suitable sites for recharge along with the RS and GIS approaches. The

higher the resolution, the more the accuracy and things can be identified and can be differentiated easily.

For better water management, one has to look into three additional factors which are soil depth, depth to bedrock and high-resolution data along with the various factors which are considered in the earlier studies by various authors. GIS environment has made work much easier to create various thematic maps. Later, those can be integrated to generate the most suitable groundwater recharge sites. For development of watershed in remote areas, various factors are to be assessed which can be derived based on the RS data in which GIS plays a significant role to locate the suitable sites based on the final output by considering various factors. This work can be practiced in all kinds of terrains irrespective of lithology, soil, area, country with little care, modifications and alterations. In spite of all these studies, one has to incorporate the criteria like environmental concern, socioeconomic factors, wildlife protection and agricultural conditions to develop the model effectively. Therefore, this review work recommends ore research to be carried out by an integrated approach of field work, VES survey and RS and GIS in water resource enhancement. The work can be utilized effectively if we consider more number of factors.

Acknowledgements The authors are thankful to NITK authorities for extending facilities to carry out the research work. We are also grateful to the NIT Patna and coordinators of HYDRO 2018, for organizing the conference.

References

Acharya T, Nag SK (2013) Study of groundwater prospects of the crystalline rocks in Purulia District, West Bengal, India using remote sensing data. Earth Resour 1(2):54–59

Anbazhagan S, Ramasamy SM (2001) Remote sensing based artificial recharge studies—a case study from Precambrian Terrain, India. In: Dillon PJ (ed) Management of aquifer recharge for sustainability, pp 553–556

Anbazhagan S, Ramasamy SM, Gupta SD (2005) Remote sensing and GIS for artificial recharge study, runoff estimation and planning in Ayyar basin, Tamil Nadu, India. Environ Geol 48(2):158–170

Anonymous (2002) World Bank report on water resources

Dinesh Kumar PK, Gopinath G, Seralathan P (2007) Application of remote sensing and GIS for the demarcation of groundwater potential zones of a river basin in Kerala, southwest coast of India. Int J Remote Sens 28(24):5583–5601

Döll P, Lehner B, Kaspar F (2002) Global modeling of groundwater recharge. In: Proceedings of third international conference on water resources and the environment research. Technical University of Dresden, Germany. ISBN 3-934253

Durga Rao KHV, Hariprasad V, Roy PS (2001) A suitable site. Making water everybody's business, vol 20. Centre for Science and Environment, New Delhi, pp 243–245

Ghosh PK, Bandyopadhyay S, Jana NC (2016) Mapping of groundwater potential zones in hard rock terrain using geoinformatics: a case of Kumari watershed in western part of West Bengal. Model Earth Syst Environ 2(1):1

Gumma MK, Pavelic P (2012) Mapping of groundwater potential zones across Ghana using remote sensing, geographic information systems, and spatial modeling. Environ Monit Assess. https://doi.org/10.1007/s10661-012-2810-y

Hutti B, Nijagunappa R (2011) Identification of groundwater potential zone using geoinformatics in Ghataprabha basin, North Karnataka, India. Int J Geomat Geosci 2(1):91–109

Ichoku A, Meisels A, Chorowicz J (1996) Detection of drainage channel networks on digital satellite images. Int J Remote Sens 17(9):1659–1678

Jasrotia AS, Majhi A, Singh S (2009) Water balance approach for rainwater harvesting using remote sensing and GIS techniques, Jammu Himalaya, India. Water Resour Manag 23(14):3035–3055

Kadam AK, Kale SS, Pande NN, Pawar NJ, Sankhua RN (2012) Identifying potential rainwater harvesting sites of a semi-arid, basaltic region of Western India, using SCS-CN method. Water Resour Manag 26(9):2537–2554

Krishna AP (1996) Remote sensing approach for watershed based resources management in the Sikkim Himalaya: a case study. J Indian Soc Remote Sens 24(2):71–83

Krishna AP (2005) Snow and glacier cover assessment in the high mountains of Sikkim Himalaya. Hydrol Process 19(12):2375–2383

Kumar MG, Agarwal AK, Bali R (2008) Delineation of potential sites for water harvesting structures using remote sensing and GIS. J Indian Soc Remote Sens 36(4):323–334

Kumari N, Krishna AP (2013) Geospatial techniques based assessment of groundwater recharge site suitability. Int J Adv Remote Sens GIS 2(1):96

Magesh NS, Chandrasekar N, Soundranayagam JP (2012) Delineation of groundwater potential zones in Theni district, Tamil Nadu, using remote sensing, GIS and MIF techniques. Geosci Front 3(2):189–196

Martinez-Casasnovas JA, Stuiver HJ (1998) Automatic delineation of drainage networks and elementary catchments from digital elevation models. Int J Aerosp Surv Earth Sci (ITC J) 1998(3/4):198–208

Mbilinyi BP, Tumbo SD, Mahoo H, Mkiramwinyi FO (2007) GIS-based decision support system for identifying potential sites for rainwater harvesting. Phys Chem Earth Parts A/B/C 32(15–18):1074–1081

Mukherje D (2016) A review on artificial groundwater recharge in India. SSRG Int J Civ Eng (SSRG-IJCE) 3(1)

Oikonomidis D, Dimogianni S, Kazakis N, Voudouris K (2015) A GIS/remote sensing-based methodology for groundwater potentiality assessment in Tirnavos area, Greece. J Hydrol 525:197–208

Rashid M, Lone MA, Ahmed S (2012) Integrating geospatial and ground geophysical information as guidelines for groundwater potential zones in hard rock terrains of south India. Environ Monit Assess 184(8):4829–4839

Rokade VM, Kundal P, Joshi AK (2007) Groundwater potential modeling through remote sensing and GIS: a case study of Rajura Taluka, Chandrapur District, Maharashtra. J Geol Soc India 69(5):943–948

Selvam S, Magesh NS, Sivasubramanian P, Soundranayagam JP, Manimaran G, Seshunarayana T (2014) Deciphering of groundwater potential zones in Tuticorin, Tamil Nadu, using remote sensing and GIS techniques. J Geol Soc India 84:597–608

Shaban A, Khawlie M, Abdallah C (2006) Use of remote sensing and GIS to determine recharge potential zone: the case of Occidental Lebanon. Hydrogeol J 14(4):433–443

Sharma BR, Paul DK (1998) Water resources of India. In: Singh GB, Sharma BR (eds) 50 years of natural resources management research. Division of Natural Resources Management, Krishi Bhavan, ICAR, New Delhi, pp 31–48

Singh JP, Singh D, Litoria PK (2009) Selection of suitable sites for water harvesting structures in Soankhad watershed, Punjab using remote sensing and geographical information system (RS&GIS) approach—a case study. J Indian Soc Remote Sens 37(1):21–35

Tribe A (1991) Automated recognition of valley heads from digital elevation models. Earth Surf Process Landf 16(1):33–49

Yadav A, Sonje A, Mathur P, Jain DA (2012) A review on artificial groundwater recharge. Int J Pharm Biosci 3(3):304–311

Chapter 8
Effect of Indira Sagar Dam on the Health Assessment of Narmada River

B. S. Gopikrishna and Pranab K. Mohapatra

Abstract River health is defined as the condition of a river (Xu and Liu in Water Resour 41(2):218–224, 2014). It depends on hydrology, water quality, river biota and social functions. This chapter deals only with the river health aspects based on hydrologic parameters. This is achieved by analysing different time series of flows for the same river. Different indices are analysed in the present study to understand the present condition of the Narmada river. These indices are selected based on their suitability for Indian rivers and data availability for the river. The present study uses different software such as SAAS, IHA, Flow Health and RAP to analyse the data. Monthly and daily discharge data are used for this purpose. The values of the indices are verified for high-flow and low-flow seasons of the river. In this paper, river health is compared between two time periods before and after the impact of the Indira Sagar dam. It is observed that river health has declined during the post-impact period.

Keywords River health index · Narmada river · Predictability · Seasonality flow shift · Base flow index

8.1 Introduction

River health index is used to understand the condition of a river with respect to a past or a reference state. Two locations, Handia and Mandleshwar, on the upstream and downstream of the Indira Sagar dam, respectively, are considered to find the effect of a dam on river health. Handia is located 141 km downstream of the Tawa dam, which has a power station operational since 1997. Tawa dam is inside the watershed of both Handia and Mandleshwar. Both the sites are on the bank of Narmada River and are in Madhya Pradesh, India. The area of the watershed for Handia is 52520.11 km^2 and for Mandleshwar it is 72342.83 km^2 (Fig. 8.1). In this analysis, daily discharge data obtained from WRIS (2018) have been used. The missing data are filled by the linear interpolation method. In the present study, the years 1978–2005 are the pre-impact

B. S. Gopikrishna · P. K. Mohapatra (✉)
Discipline of Civil Engineering, IIT Gandhinagar, Gandhinagar 382355, India
e-mail: pranabm@iitgn.ac.in

R. Jha et al. (eds.), *Groundwater and Water Quality*, Water Science and Technology Library 119, https://doi.org/10.1007/978-3-031-09551-1_8

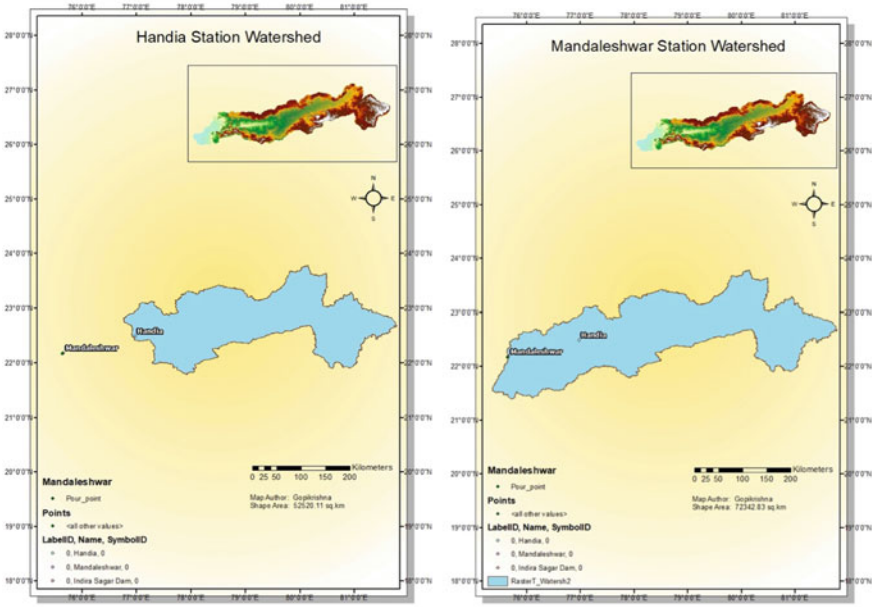

Fig. 8.1 Watershed delineation of Handia and Mandleshwar

period and the years 2006–2015 are the post-impact period. Note that the dam was built in the year 2006.

First, the water year is determined. The water year may be different from the calendar year. The aim of the water year is to have an entire high-flow season in the same year during the time period. From the daily discharge data, the total volume of water for a six-month period starting from every month is determined for the pre-impact period. The period which has maximum volume is taken as the start of the water year and high-flow season. The impact of water regulation due to the operation of the Indira Sagar dam is analysed from these data.

8.2 Methodology

Though several river health indices (RHI) are reported in the literature, the present study is based on 11 RHIs. The methodology for each index is discussed below.

8.2.1 Flood Frequency Analysis

Outliers in the data are computed (Pilon and Harvey 1994) and are eliminated from the data. For determining outliers, a significance value of $\alpha = 10\%$ has been used. Discharge data for annual maxima is converted to logarithmic values. The frequency factor of log Pearson distribution depends on return period and skewness coefficient.

For High Outliers:

$$Y(\mathrm{T}) = \mathrm{avg}(Y) + KT(\sigma(\mathrm{Y})) \tag{8.1}$$

For Low Outliers:

$$Y(\mathrm{T}) = \mathrm{avg}(Y) - KT(\sigma(\mathrm{Y})) \tag{8.2}$$

Y(T)—Logarithmic Discharge values.
σ(Y)—Standard deviation of logarithmic discharge values.
KT—Frequency Factor.

8.2.2 Base Flow Separation

Base flow is computed by Digital Recursive Method (Nathan and MacMahon 1990). The general equation is given as

$$f_k = \alpha f_{k-1} + \frac{(1+\alpha)}{2}(y_k - y_{k-1}) \tag{8.3}$$

Filter parameter (α) = 0.925.
y_k = Original stream flow.
f_k = Filtered quick response at kth sampling.
$y_\mathrm{k} - f_\mathrm{k}$ = Filtered base flow.
After separating base flow, the Base Flow Index (BFI) is calculated as

$$\mathrm{BFI} = \frac{\text{Volume of Base Flow}}{\text{Total flow Volume}} \tag{8.4}$$

8.2.3 Median Flow Duration Curve

Individual Flow Duration Curve for both seasons of every year is plotted for pre-impact and post-impact periods. For every percentile exceedance, a single median discharge value is computed. Now, these median discharge values are plotted against

their corresponding exceedance values to generate a new Flow Duration Curve. Then flow duration curves of pre-impact and post-impact periods are compared.

8.2.4 Colwell Indices

Predictability is determined. Predictability is the converse of uncertainty (Colwell 1974). Predictability is the summation of two different components, Constancy (C) and Contingency (M). Contingency is the degree to which time of occurrence of a phenomenon determines the state of the river. Constancy defines how unaltered is the state of discharge through different time periods. These parameters are computed as per mathematics of Information theory as specified by (Colwell 1974). Before computing the values, the data is converted to logarithmic values with the base 2. To eliminate the linear approximate correlation between standard deviation (SD) and mean (μ) of discharge data, logarithmic distribution is taken. The data is divided into 12 states to identify the changes clearly while analysing the effect.

8.2.5 Timing of Annual Extreme Water Conditions

Julian's date of every annual 1-day maximum and 1-day minimum is determined. Julian dates are the representation of each water year date by an integer value from 1 to 366. For non-leap years, the Julian date of 60 is skipped. These extreme flows are crucial for accessing special habitats during reproduction and to avoid predation for aquatic organisms and also providing food for birds and other animals. Thus, they play a vital role in evolution strategies (Nature Conservancy 2007).

8.2.6 Persistently Higher Flow (PH)

While computing PH, monthly discharge $Q_{(mo)}$ data is used. So, $Q_{(mo)}$ is computed from daily discharge data. PH means that flow is constantly higher than the expected discharge value $Q_{(ex)}$ during the low-flow season of a post-impact water year. This phenomenon is not a problem in the high-flow season. Here, $Q_{(ex)}$ is taken as the 75th percentile of discharge value in the low-flow season of the pre-impact period. If $Q_{(mo)} > Q_{(ex)}$ a value of (+1) is given, else zero. A summation of all the consecutive values of (+1) is done. PH score is determined as follows:

$$\text{Annual maximum cumulative total} = 6$$

$$\text{Score} = 0 \tag{8.5}$$

$$\text{Annual maximum cumulative total} \leq 1$$

$$\text{Score} = 1 \tag{8.6}$$

$$\text{Annual maximum cumulative total} > 1$$

$$\text{Score} = 1.2 - 0.2(\text{Max.cumulative total}) \tag{8.7}$$

8.3 Persistently Lower Flow (PL)

When $Q_{(mo)}$ of a post-impact water year is constantly less than $Q_{(ex)}$ for the same month during the pre-impact period, $Q_{(ex)}$ is taken as the 25th percentile of $Q_{(mo)}$ of the pre-impact period. If $Q_{(mo)}$ is less than $Q_{(ex)}$ a value of (-1) is given, else zero. Consecutive values of (-1) are added. This process can continue into the next water year until a zero is encountered. The score for PL is given as follows.

$$\text{Annual minimum cumulative total} \leq -12$$

$$\text{Score} = 0 \tag{8.8}$$

$$\text{Annual minimum cumulative total} \geq -1$$

$$\text{Score} = 1 \tag{8.9}$$

$$-12 < \text{Annual minimum cumulative total} < -1$$

$$\text{Score} = 1.0909 + 0.0909(\text{min.cumulative total}) \tag{8.10}$$

8.3.1 Persistently Very Low Flow (PVL)

The flow is considered to be persistently very low flow (PVL), when $Q_{(mo)}$ in the post-impact period is less than the 1st percentile $Q_{(mo)}$ for all the months and years combined in the pre-impact period. This indicates cease flow or zero flow condition. If $Q_{(mo)}$ is less than $Q_{(ex)}$, a value of (+1) is assigned. All the consecutive values of

(+1) are summed. The score for PVL is given as follows.

$$\text{Annual maximum cumulative total} > 6$$

$$\text{Score} = 0 \tag{8.11}$$

$$\text{Annual maximum cumulative total} = 0$$

$$\text{Score} = 1 \tag{8.12}$$

$$\text{Annual maximum cumulative total} > 0$$

$$\text{Score} = \frac{\text{Cumulative Total}}{6} \tag{8.13}$$

8.3.2 Seasonality Flow Shift (SFS)

It indicates shift of seasons in the post-impact period. The rank of $Q_{(mo)}$ is defined for each water year in the pre-impact period. The median monthly flow for the entire pre-impact period is calculated and ranked. The absolute difference in rank of $Q_{(mo)}$ for every pre-impact water year to the median monthly flow is determined. The mean deviation of the difference in ranks is computed which is in the range 1–6. Similarly, ranking is done for every water year of the post-impact period, then the absolute difference in ranks with respect to median monthly flows of the pre-impact period is determined. Now mean deviation in ranks of the post-impact period is computed. The annual mean distribution of the post-impact period is compared with the pre-impact period deviation. The score for SFS is given as follows.

$$\text{Percentile distribution of test year in the range} < \text{75th percentile of post-impact period}$$

$$\text{Score} = 1 \tag{8.14}$$

$$\text{Percentile distribution of test year in the range} > \text{75th percentile of post-impact period}$$

$$\text{Score} = 4 - 4\frac{\text{(Percentile in parameter pre-impact distributon)}}{100} \tag{8.15}$$

8.3.3 Small Floods

In this analysis, small flood is defined as an event which has an initial high flow value greater than or equal to the peak discharge value of a two-year return interval and less than an eight-year return interval. Peak flow and timing of floods are important aspects of small floods. Small floods cover all river rises that overtop the main channel but not extreme floods. Small floods are important for fish migration and maintaining ecological balance. Since the post-impact data is not sufficient, large floods are not studied in this paper.

8.3.4 Rate of Water Condition Change

It has two different aspects.

Rise Rate: It corresponds to the period in which daily changes in flow are positive: Median of all positive differences in consecutive daily values.

Fall Rate: It corresponds to the period in which daily changes in flow are negative. Median of all negative differences in consecutive daily values.

8.4 Results and Discussion

8.4.1 Effect of Water Regulation in Low-Flow Season

It is observed that in the low-flow season, for both the locations, discharge values have increased for the post-impact period compared to that of the pre-impact period (Figs. 8.2–8.3). In this season, the difference in pre-impact and post-impact period discharge is higher in Mandleshwar than in Handia. Ideally, there should not be any change in the flow value of Handia. The attributes observed may be due to the Tawa dam upstream at Handia. However, the pre-impact period peak value (1007 cumec) in the low-flow season at Handia is higher than the corresponding value (505 cumec) of the post-impact period.

These variations in discharge values may be associated with water supply for irrigation, power generation and other purposes, subsequently affecting the riparian environment which suffers due to lack of nourishment.

8.5 Effect of Flood Control

It is observed that the magnitude of small floods dropped significantly during post-impact periods at both locations. The effect at Mandleshwar is due to Flood control

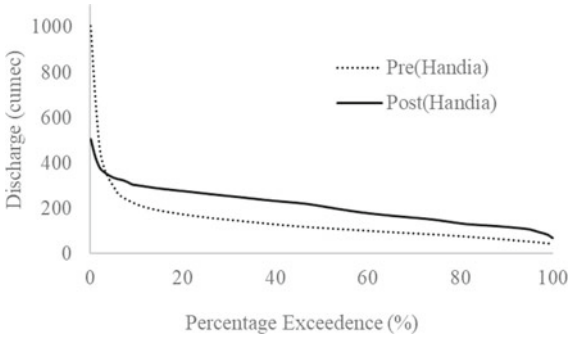

Fig. 8.2 Median FDC, low-flow season at Handia

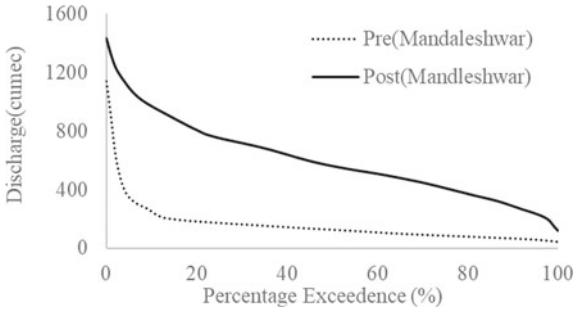

Fig. 8.3 Median FDC, low-flow season at Mandleshwar

Table 8.1 Flood frequency analysis

	Mandleshwar (Downstream of Dam)		Handia (Upstream of Dam)	
Recurrence interval	Discharge pre-impact (cumec)	Discharge post-impact (cumec)	Discharge pre-impact (cumec)	Discharge post-impact (cumec)
1.5	16,590	8004	13,323	8087
2	20,928	12,769	15,847	10,809
4	29,361	24,242	20,025	17,388
6	21,874	21,554	33,702	31,0060

operations of the Indira Sagar dam. For Handia, it can be due to the Tawa dam for the same reason. Floods play a vital role in recharging flood plain water tables and provide nutrients to riparian ecology (Conservancy, Nature 2007) (Table 8.1).

8.5.1 Predictability of Flow

The median seasonal predictability value has increased from 0.52 to 0.67 at Handia and 0.58–0.72 at Mandleshwar even though there is a small drop in the predictability

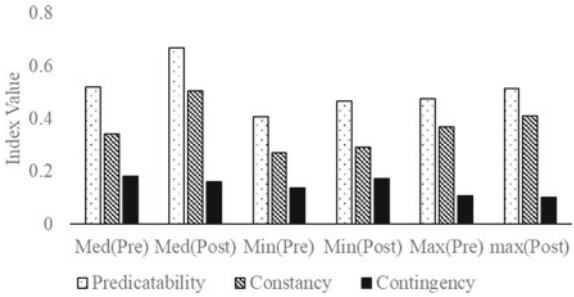

Fig. 8.4 Colwell seasonal predictability at Handia

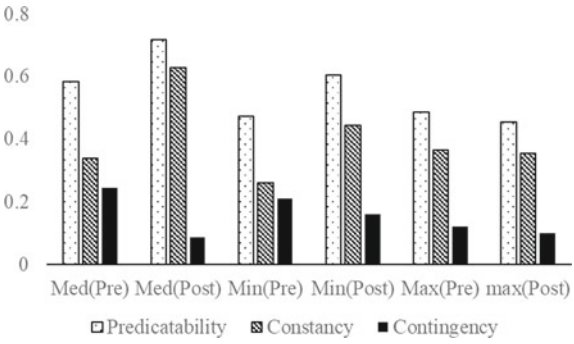

Fig. 8.5 Colwell seasonal predictability at Mandleshwar

of maximum values from 0.49 to 0.45 at Mandleshwar (Figs. 8.4 and8.5). This shows that discharge values during the post-impact period are tending towards constant values since the predictability is dominated by constancy, which may be interpreted as the result of water regulation and storage.

8.5.2 Storage Affecting Base Flow

In Figs. 8.6 and 8.7, sustained increase in base flow during the entire post-impact period at both locations can be observed. This shows the negative impact of dam storage on the river. Storage of water during floods and high flows and releasing water during low-flow season could be the main reason for this observation. Low flows are very important for a river ecosystem as it determines the amount of aquatic life available. It also gives a chance for various plant species to grow when the land is dry (Conservancy 2007).

It is observed that discharge values are high beyond the limit during a low-flow period for the prolonged duration at both locations (Table 8.2). The PH scores are found to be zero for every year (except for 2007) in the post-impact period at Mandleshwar. It indicates a very large deviation (except for 2007). PH values at Handia are observed to have moderate to large deviations. Since Mandleshwar is

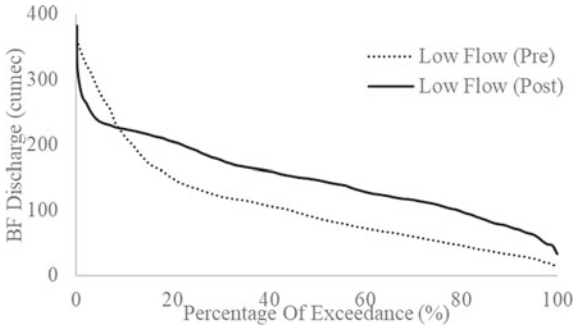

Fig. 8.6 Base flow index during low-flow season at Handia

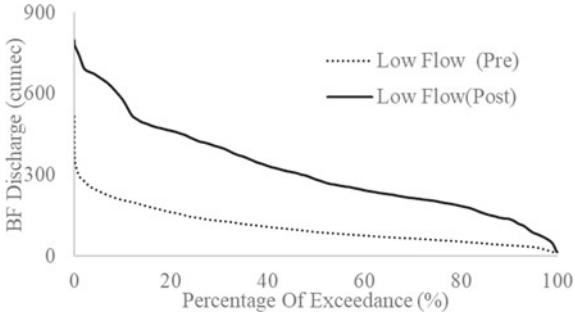

Fig. 8.7 Base flow index during low-flow season at Mandleshwar

downstream of the dam, river health has declined to a greater extent. From Table 8.2, it can be observed that PL values show very small deviations during the post-impact period when compared to the pre-impact period. However, no deviation is observed in PVL. Therefore, there is no case of cease flow in the post-pandemic period compared to the pre-impact period (Table 8.3).

Table 8.2 PH, PL and PVL scores at Handia and Mandleshwar

Year	PH Handia	PH Mandleshwar	PL Handia	PL Mandleshwar	PVL Handia	PVL Mandleshwar
2006	0.2	0	1	1	1	1
2007	0.8	0.6	1	0.91	1	1
2008	0.4	0	0.91	0.91	1	1
2009	0.4	0	1	0.91	1	1
2010	1	0	1	1	1	1
2011	0	0	1	1	1	1
2012	0.4	0	1	1	1	1
2013	0.6	0	1	1	1	1
2014	0.2	0	1	0.91	1	1
2015	0.2	0	0.73	0.91	1	1

Table 8.3 Deviation level of PH, PL, PVL and SFS based on score

0–0.2	Very large
0.21–0.4	Large
0.41–0.6	Moderate
0.61–0.8	Small
0.81–1	Very small

From the results, it can be inferred that mean discharge values are sufficient during the high-flow season. It is exceeding the limit during the low-flow season due to untimely water releases for irrigation, power generation and other purposes. This is detrimental to the ecosystem of the river. Deviation levels are considered as per Flow Health software guidelines (Gippel et al. 2012).

8.5.3 Persistent Change in River Condition

8.5.4 Seasonality of Water Flow Conditions

From Table 8.4, it can be observed that the seasonality of discharge is declined by a very large value (marked in red) during the post-impact period at Mandleshwar. Restricted flows, flood control actions and untimely water releases lead to changes in seasonality downstream of the river. No particular trend in seasonality shift is observed at Handia, since it is upstream of the Indira Sagar dam and far downstream of Tawa dam to have any significant changes. As shown in Figs. 8.8 and 8.9, the Julian dates of maximum discharges have not undergone considerable change. In the case of median Julian date for minimum, it is analysed as 228.5 cumec for the pre-impact period and 238.5 cumec for the post-impact period at Mandleshwar. It is not a considerable difference, however, the coefficient of dispersion of the values changed from 0.05 during pre-impact to 0.23 in the post-impact period. This shows that the low-flow period is most affected by the dam.

8.5.5 Rate of Water Change Condition

It may be observed in Table 8.5 that there is a change in rise and fall rates of daily discharge at both locations, but the effect is very large at Mandleshwar. Since it is located downstream of the dam, the rate of change is high. Due to dam operations, discharge values are altered artificially so the rate of change is large. The rate of change has also increased at Handia, but the change is small and relatively smaller since it is far downstream of the Tawa dam.

Table 8.4 SFS scores at Handia and Mandleshwar

Year	SFS (Handia)	SFS (Mandleshwar)
2006	0.44	0.15
2007	1	0
2008	1	0
2009	0	0.15
2010	1	0
2011	1	0
2012	0	0
2013	1	0
2014	0.4	0
2015	0	0

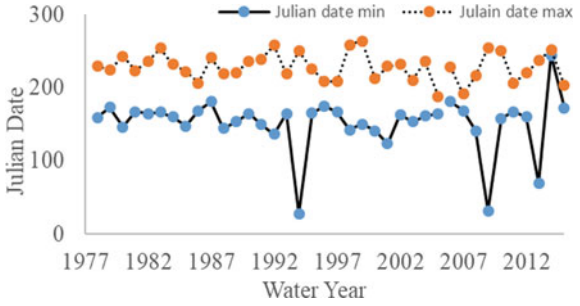

Fig. 8.8 Maximum and minimum discharges at Handia

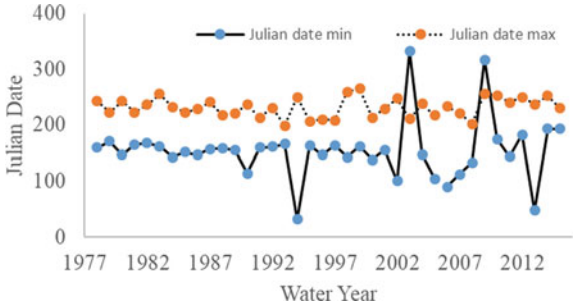

Fig. 8.9 Maximum and minimum discharges at Mandleshwar

Table 8.5 Rise rate and Fall rate at Handia and Mandleshwar

	Handia		Mandleshwar	
	Median (Pre-impact)	Median (Post-impact)	Median (Pre-impact)	Median (Post-impact)
Rise rate	10.75	17.08	14.45	126.7
Fall rate	−9.525	−17.24	−14	−118.5

8.6 Conclusion

The findings of the present study suggest that the health of the Narmada river has declined at Handia and Mandleshwar. The decline is more at Mandleshwar since it is located downstream of the dam. Handia, though located upstream of the dam exhibits symptoms of health deterioration during the post-impact period. This effect may be attributed to another dam (Tawa dam) upstream of Handia, which has a power station operational since 1996, upstream of Handia. The major changes in river health have occurred during low-flow season and flood periods. Important findings from the present study are.

- Results indicate a sharp decline in the rate of discharge during small floods.
- Rise and fall rates of discharge values increased by large values, especially at Mandleshwar.
- Base Flow values have increased during low-flow seasons. No cease flow condition is observed.
- The seasonality of the river flow has been altered significantly at both locations, during the post-impact period. Dispersion of Julian dates for extreme flows has been considerable in post-impact period.
- All the above results show obvious alterations during the post-impact period like high flows during low-flow season and reduced magnitude of floods.
- These changes to the flow regime are threatening the riparian environment. This may disturb the ecological balance.

Acknowledgements The authors are thankful to IIT Gandhinagar for funding this work.

References

Colwell RK (1974) Predictability, constancy, and contingency of periodic phenomena. Ecology 55(5):1148–1153

Conservancy N (2007) Indicators of hydrologic alteration. Version 7 User's manual. Nat Conserv

Gippel CJ, Marsh N, Grice T (2012) Flow health-software to assess the deviation of river flows from reference and to design a monthly environmental flow regime. Tech Manual User Guide, Version 2.0

Nathan RJ, McMahon TA (1990) Evaluation of automated techniques for base flow and recession analyses. Water Resour Res 26(7):1465–1473

Pilon PJ, Harvey KD (1994) Consolidated frequency analysis. Reference manual, Environment Canada, Ottawa, Canada

WRIS. http://www.india-wris.nrsc.gov.in/. Narmada basin data acquired on 07 May 2018

Xu S, Liu Y (2014) Assessment for river health based on variable fuzzy set theory. Water Resour 41(2):218–224

B. S. Gopikrishna earned his B Tech from IIT Gandhinagar and is currently pursuing M Tech at IIT Guwahati. He worked in a project for a short tenure at IIT Gandhinagar. This study part of his work in the project.

Pranab K. Mohapatra is a professor at IIT Gandhinagar. His research area includes transients in pipes and in open channels. He uses both experiments and numerical modeling to conduct his studies. He is associated with several projects on river health, integrated urban water management etc.

Chapter 9
Study and Modelling of Trace Contaminant Transport Under Drowned Condition

A. R. Laiju, Muskan Mayank, S. Sarkar, and P. K. Sharma

Abstract This study is focused on the trace removal of hexavalent chromium [Cr(VI)] using a weak base anion exchanger, Amberlite IRA 96, in the presence of competing anions such as sulphate, chloride and bicarbonate in natural water conditions. Batch equilibrium studies such as isotherm study, kinetic study and fixed bed sorption study revealed the transport of toxic Cr(VI) from aqueous solution to the exchanger surface, uptake capacity and overall rate-controlling step. Anion exchanger showed selectivity towards the toxic Cr(VI) with a high sorption capacity found fitted by the Freundlich model. Mobile region transport is described by the convection–dispersion model equation, and the choice for Cr(VI) transfer between liquid and solid phases can be done by considering the non-equilibrium MIM (mobile–immobile) model. Fixed bed column confirmed feed water containing 200 μg/L of Cr(VI) with competing anion could treat up to 628 Bed Volumes (BVs) before exhaustion, and the possibility of regeneration proves the real-life application of the ion exchange process in trace contaminant removal from drowned ground conditions.

Keywords Tracer transport · Fixed bed sorption · Isotherm modelling · MIM model · Drowned condition

9.1 Introduction

Groundwater resources serve as a major source of drinking water. The surface water, which contains undesirable substances from natural or anthropogenic sources, reaches groundwater under the force of gravity after passing through the subsurface

A. R. Laiju · M. Mayank (✉)
Department of Civil Engineering, NIT Uttarakhand, Srinagar, Garhwal 246174, India
e-mail: muskan.mayank@nituk.ac.in

A. R. Laiju
e-mail: laijuar739@nituk.ac.in

S. Sarkar · P. K. Sharma
Department of Civil Engineering, IIT Roorkee, Roorkee 247667, India

R. Jha et al. (eds.), *Groundwater and Water Quality*, Water Science and Technology Library 119, https://doi.org/10.1007/978-3-031-09551-1_9

zone. For shallow depth of the water table, the groundwater can rise upward to the root zone by vapour diffusion and capillary rise. The subsurface zone is often regarded as filter media for removing undesirable substances and is the main stratum controlling water movement from land surface to aquifer. This zone is rich in clay or organic matter and promotes sorption, biological degradation and transformation of contaminants. The hydrogeological properties of the subsurface zone are responsible for maintaining the quality of groundwater resources (McCord and Selker 2009).

The transport of contaminants through the subsurface zone is complex and unpredictable. Various anthropogenic activities such as untreated wastewater disposal, leakage in sewers and leachate from landfill are responsible for contaminant transport to the subsurface ultimately leading to groundwater quality deterioration. Different types of contaminants, which are reactive and non-reactive in nature, can interact with soils, sediments and other geologic materials. These contaminants move along different flow paths with variable velocities, and ultimately reach groundwater. The major processes responsible for determining the quality of groundwater are mainly advection, diffusion, dispersion and adsorption. Therefore, a complete understanding of the transport process and flow mechanism is required to control and reduce the effect of contaminant concentration in groundwater conditions. Table 9.1 shows the mechanism and governing equation of contaminant transport through porous media.

Chromium is unique among heavy metals because the toxicity of other heavy metals is regulated based on their total concentration but for chromium, based on its oxidation state. Two forms of chromium are usually present in the drinking water conditions, trivalent chromium [Cr(III)], and hexavalent chromium [Cr(VI)] (McNeill et al. 2012). Among the two, Cr(III) is an essential micronutrient, but based on the chemical, toxicological and epidemiological evidence, Cr(VI) can be considered as a confirmed human carcinogen (Höll et al. 2004). As per the latest guidelines of WHO (World Health Organization), the regulatory limit of total chromium (sum of Cr(III) and Cr(VI)) is 50 μg/L (Seidel and Corwin 2013). The movement of Cr(VI) is associated with the movement of water fluxes in soils; the need for detailed analysis of transport mechanism and contaminant behaviour with respect to time needs to be considered and evaluated with the water fluxes through the subsurface zone. The rate of removal of toxic Cr(VI) depends on the phenomenon of advection, diffusion, dispersion and adsorption. Adsorption and ion exchange can be considered as economical and feasible techniques for the trace removal of Cr(VI) from contaminated groundwater conditions (Korngold et al. 2003; Sharma et al. 2008).

9.2 Objectives

The problem of groundwater contamination is a major concern alarming millions of people around the world. Hexavalent Chromium [Cr(VI)] is one of the emerging inorganic contaminants in groundwater resources due to natural and anthropogenic activities. In this study, a weak base anion exchanger, Amberlite IRA 96 (denoted as IRA 96), was used for the trace removal of toxic Cr(VI) in presence of competing

Table 9.1 Mechanism and governing equation of contaminant transport through porous media

Zone	Process/Parameter	Governing equation	Physical significance	SI units
Unsaturated (Ref. Šimůnek and Genuchten 2008)	Advection	$\theta \frac{\partial c}{\partial t} = -q \frac{\partial c}{\partial x}$	c = Cr(VI) concentration q = Advective flux θ = porosity of medium $\frac{\partial c}{\partial t}$ = Rate of change of contaminant $\frac{\partial c}{\partial x}$ = Concentration gradient	c = mg/m^3 q = m/s θ = m^3 of water/m^3 of soil or media
	Diffusion	$\frac{\partial c}{\partial t} = D \frac{\partial^2 c}{\partial x^2}$	c = Cr(VI) concentration D = Diffusivity $\frac{\partial^2 c}{\partial x^2}$ = Concentration gradient	c = mg/m^3 D = m^2/s
	Dispersion	$D_h = \alpha_s V + D^*$	D_h = Hydrodynamic dispersion α_s = Dispersivity (medium characteristics) D^* = Molecular diffusion	D_h = m^2/s α_s = m D^* = m^2/s
	Retardation	$R = 1 + \frac{\rho K_d}{\theta}$	R = Retardation coefficient ρ = Bulk density of the material of medium	ρ = g/cm^3
Saturated (Ref. Alabi et al. 2016)	Velocity flux of Cr(VI)	$Q = KA(h_1 - h_2)/L$ $K = QL/Ah$ $V = Ki$ $i = \Delta h/L$	V = Darcy's velocity K = Hydraulic conductivity i = Hydraulic gradient Δh = Head difference	V = m/s K = m/s Δh = m

(continued)

Table 9.1 (continued)

Zone	Process/Parameter	Governing equation	Physical significance	SI units
	Hydraulic conductivity	$K = \frac{g}{\nu} \cdot c \cdot f(n) \cdot d_e^2$ $n = 0.255(1 + 0.83^U)$	K = Hydraulic conductivity g = Acceleration due to gravity v = Kinematic viscosity C = Sorting coefficient f(n) = Porosity function d_e = Effective grain diameter n = Porosity of medium U = Uniformity coefficient	g = m^2/s c = mg/m^3 d_e = mm

anions such as sulphate, chloride and bicarbonate in saturated conditions for identifying the sorption behaviour. Some discussion on the physical non-equilibrium MIM model is also done to understand the flow process and transport mechanism of Cr(VI) between mobile and immobile pore domains.

9.3 Description on MIM Model of Cr(VI) Transport

Mobile–Immobile Model: In the soil matrix's micropore area, the water remains immobile and only dissolved Cr(VI) is transferred by the process of molecular diffusion.

Flow Model: This model has two different regions which are given by Van Genuchten, 1976, which divides the liquid phase into mobile (movable, inter-aggregate) that corresponds to the dissolved solute transport and immobile (static, intra-aggregate) regions.

$$\theta = \theta_{mo} + \theta_{im} \tag{9.1}$$

$$\frac{\partial \theta_{mo}(h_{mo})}{\partial t} = \frac{\partial}{\partial z}(K(h_{mo})[\frac{\partial h_{mo}}{\partial z} + 1]) - S_{mo}(h_{mo}) - \Gamma_w \tag{9.2}$$

$$\frac{\partial \theta_{im}(h_{im})}{\partial t} = -S_{im}(h_{im}) + \Gamma_w \tag{9.3}$$

where K represents hydraulic conductivity, [LT^{-1}], h represents pressure head, [L], θ_{mo}, θ_{im} represents moisture contents in mobile and immobile regions [L^3 L^{-3}], S represents the source/sink term [T^{-1}] and Γ_w represents water transfer rate between inter- and intra-aggregate pore domains.

Transport Model: The linear form of the adsorption equation is considered in which the sorbed concentration of solute is distributed proportionally to the solute concentration (Šimůnek and Genuchten 2008).

$$s = K_d c \tag{9.4}$$

where s is the sorbed concentration [M M^{-1}], c is the solute concentration [ML^{-3}] and K_d is the distribution coefficient [L^3M^{-1}].

The governing equation for physical non-equilibrium transport for the MIM model is given by Šimůnek and Genuchten (2008);

$$\frac{\partial \theta_{mo}(c_{mo})}{\partial t} + f_{mo}\rho\frac{\partial s_{mo}}{\partial t} = \frac{\partial}{\partial z}(\theta_{mo}D_{mo}\frac{\partial c_{mo}}{\partial z}) - \frac{\partial q_{mo}c_{mo}}{\partial z} - \varphi_{mo} - \Gamma_s \tag{9.5}$$

$$\frac{\partial \theta_{im}(c_{im})}{\partial t} + (1 - f_{mo})\rho \frac{\partial s_{im}}{\partial t} = \Gamma_s - \varphi_{im} \tag{9.6}$$

$$\Gamma_s = \omega(c_{mo} - c_{im}) + \Gamma_w c^* \tag{9.7}$$

$c^* = c_{mo}$, if $\Gamma_w > 0$ otherwise it equals c_{im} for $\Gamma_w < 0$ (for MIM Model)

where c_{mo}, c_{im} represent solute concentrations in mobile/immobile regions, [ML^{-3}], φ_{mo}, φ_{im} represents source or sink term, [ML^{-3} T^{-1}] and Γ_s represents solute mass transfer rate between inter- and intra-aggregate pore domains [ML^{-3} T^{-1}].

The advection–dispersion type equation helps to describe the solute transfer process (Šimůnek and Genuchten 2008);

$$\frac{\partial \theta_c}{\partial t} + \rho \frac{\partial s}{\partial t} = \frac{\partial}{\partial z}(\theta D \frac{\partial c}{\partial z}) - \frac{\partial qc}{\partial z} - \varphi \tag{9.8}$$

where ρ is the bulk density of soil [ML^{-3}], D is the dispersion coefficient [L^2T^{-1}] and q is the volumetric flux density [LT^{-1}].

9.4 Experimental Methodology

Commercially available weak base anion exchanger was selected for the removal of Cr(VI). All the chemicals used were of AR grade and purchased from Merck. Cr(VI) standard of 200 mg/L was prepared by diluting $K_2Cr_2O_7$ in ultrapure deionized water (prepared from Ultrapure water purification system). Preconditioning of IRA 96 was done with 1 N HCl for removing impurities present during the manufacturing process.

Batch equilibrium adsorption studies were performed in a shaking incubator at temperatures 25 ± 0.5 °C and 100 rpm with 250 mL solution containing Cr(VI) and kept in contact with the IRA 96 for 24 h. Adsorption experiments were performed to investigate the adsorption capacity of IRA 96, the effect of pH and adsorbent dosage. The effect of dosage was determined by varying the dosage of IRA 96 between 0.2 and 1.2 g/L with an initial Cr(VI) concentration of 2 mg/L at pH 7. For the effect of pH, the pH of the Cr(VI) solution has been varied from 4 to 8.5 at a constant 0.8 g/L dosage. Adsorption isotherm studies were conducted in batch mode in a shaking incubator at 25 ± 0.5 °C, 100 rpm, dosage of 0.2 g, 100 mg/L of sulphate, chloride and bicarbonate concentration at pH 7 and 250 mL solution of initial Cr(VI) concentration varying in the range of 1–30 mg/L and were equilibrated for 48 h. After 48 h, the equilibrium concentration of Cr(VI) is determined and Langmuir and Freundlich isotherm modelling is performed. For the kinetic study, a volume of 1 L solution containing 2 mg/L of Cr(VI), 100 mg/L of competing anions concentration and IRA 96 dosage of 0.2 g/L at pH 7 were stirred at 300 rpm using the

Jar test apparatus, and samples were collected at definite intervals until equilibrium is attained.

Cr(VI) concentration was determined by the colorimetric method at 540 nm using split double beam UV—Visible spectrophotometer (T60 UV, PG instruments, UK). Cr(VI) sorption capacity and Cr(VI) removal efficiency (η %) can be calculated by Eqs. 9.9 and 9.10.

$$q_e = \frac{V(C_0 - C_f)}{m} \tag{9.9}$$

$$\eta(\%) = \frac{C_0 - C_f}{C_0} \times 100 \tag{9.10}$$

where q_e is the Cr(VI) intake capacity (mg/g), m is the mass of adsorbent (g) added, V is the volume of solution (L) and C_0 and C_f represent the initial and final concentrations (mg/L), respectively.

9.4.1 Fixed Bed Column Study

Fixed bed column studies were performed in a column of 11 mm internal diameter and 300 mm height. For evaluating the selectivity of IRA 96, the influent water containing 200 µg/L of Cr(VI) and 100 mg/L of sulphate, chloride and bicarbonate at pH 7.1 ± 0.1 were stored and fed to the column bed with the help of a microprocessor-based peristaltic pump (Ravel instruments, India). Flow rate during the service run and regeneration was controlled at a constant rate throughout the column study. Samples were collected at definite bed volumes (BVs, volume of water treated per volume of resin) and Cr(VI) concentration was determined. Cr(VI) sorption (C_s, mg/L) during the column run and maximum sorption capacity (q_{ec}, mg/g) can be determined using Eqs. 9.11 and 9.12 from the breakthrough curve.

$$C_s = C_o - C_b \tag{9.11}$$

$$q_{ec} = \frac{V_r}{1000\,m} \int_{BV=0}^{BVexh} (C_o - C_b) \times d(BV) \tag{9.12}$$

where C_0 and C_b are initial Cr(VI) concentration and Cr(VI) sorbed at definite bed volume, respectively (mg/L), V_r is volume of resin (cc), BV_{exh} is bed volume at sorbent exhaustion and m is dry mass of sorbent in column (g).

9.5 Results and Discussion

9.5.1 Effect of Resin Dosage

The effect of IRA 96 dosage on Cr(VI) removal was studied by varying the amount of resin in the solution while keeping the initial Cr(VI) concentration constant as 2 mg/L at pH 7. Increase in IRA 96 dosage increased the Cr(VI) removal efficiency from 16.9 to 32% by increasing the dosage from 0.2 to 1.2 g/L as shown in Fig. 9.1. The increase in removal efficiency is due to an increase in the number of sites containing Cl^- counterion increases for exchange of Cr(VI) between the liquid phase and the exchanger phase (Bahowick et al. 1993). After 0.8 g/L, the increment increase in Cr(VI) removal was not increased as significantly; this is due to the fact that some of the adsorption sites become unsaturated during the process (Shi et al. 2009). If the dosage is increased by keeping the initial concentration constant, the amount of Cr(VI) sorbed per unit mass showed a decrease due to the unavailability of Cr(VI) ions for the adsorption sites (Babu and Gupta 2008; Pehlivan and Cetin 2009).

9.5.2 Effect of Solution pH

From the predominance diagram, predominant Cr(VI) species, $HCrO_4^-$ and CrO_4^{2-} exist in natural water conditions, $HCrO_4^-$ for a pH between 1 and 6.5 and divalent CrO_4^{2-} for a pH above 6.5. Dimerization of $HCrO_4^-$ ions ($Cr_2O_7^{2-}$) is possible if the concentration is higher than 1 g/L (Sharma, Petrusevski and Amy 2008). From Fig. 9.2, the maximum Cr(VI) removal efficiency obtained was 48.3% at pH 4. As the pH increased, IRA 96 showed a decrease in removal efficiency. The increased

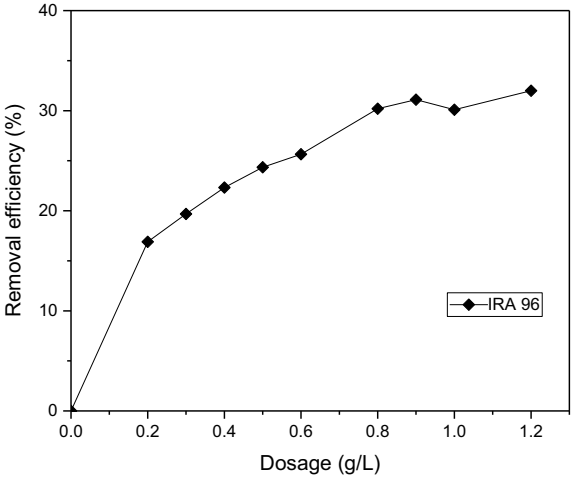

Fig. 9.1 Effect of IRA 96 dosage on Cr(VI) removal efficiency. Condition: Cr(VI) concentration = 2 mg/L, contact time = 24 h, pH = 7, RPM = 100, Temperature = 25 ± 0.5 °C and volume of solution = 250 mL

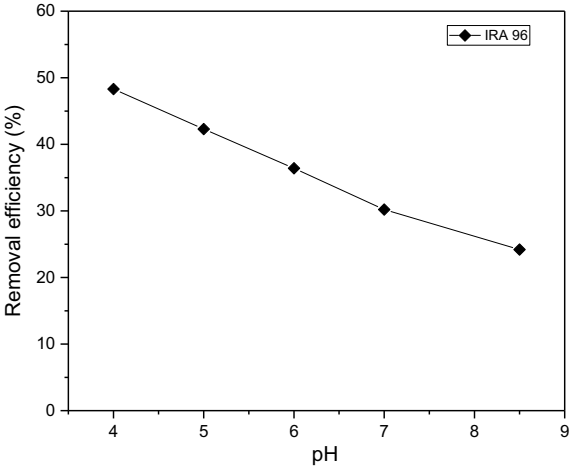

Fig. 9.2 Effect of pH on Cr(VI) removal efficiency for IRA 96. Conditions: Cr(VI) concentration = 2 mg/L, dosage = 0.8 g/L, contact time = 24 h, RPM = 100 and Temperature = 25 ± 0.5 °C

Cr(VI) removal efficiency at an acidic pH is mainly due to the fact that $HCrO_4^-$, being monovalent, can attach to a single adsorption site, and CrO_4^{2-}, a divalent, needs to bind to two sites (A K. Sengupta and Clifford 1986; Pehlivan and Cetin 2009). At an alkaline pH, the adsorption trend is likely decreased due to the competition between CrO_4^{2-} and OH^- for the adsorption sites on the adsorbent, which results in lower uptake.

9.5.3 Isotherm Study

To evaluate the mechanistic parameter associated with the adsorption of Cr(VI) by IRA 96, the results of the isotherm experiments were analysed with Langmuir and Freundlich isotherm models. The obtained isotherm model parameters are given in Table 9.2. From Table 9.2 R^2 (correlation coefficient) indicates that the adsorption data for Cr(VI) by IRA 96 were well fitted by both Langmuir and Freundlich isotherms. Separation factor or equilibrium factor (R_L) of the Langmuir model was computed and it is observed that values are in the range of 0–1, indicating that the Cr(VI) adsorption on IRA 96 is favourable. The R^2 values of both Langmuir and Freundlich models are close to 1, but the Langmuir model shows a better R^2 value for Cr(VI) adsorption than the Freundlich model. This result demonstrates that the adsorption is a monolayer coverage onto a surface containing a finite number of adsorption sites for Cr(VI). Based on Langmuir isotherm, the maximum sorption capacity is obtained as 1.68 mg/g. The Freundlich constant 'n' ranges from 1 to 10, which also indicates that the adsorption is favourable.

Table 9.2 Parameters of Langmuir and Freundlich isotherm models

Adsorbent	Langmuir isotherm				Freundlich isotherm		
	Q_{max} (mg/g)	b (L/mg)	R_L	R^2	n	k_f (mg/g)	R^2
IRA 96	1.68	0.60	0.10	0.998	2.69	0.62	0.925

9.5.4 Kinetic Study

Figure 9.3 shows the effect of contact time on the removal of Cr(VI) by IRA 96. The removal efficiency increases with time and equilibrium in 400 min is attained. It is clear from Fig. 9.3 that initially the Cr(VI) sorption is rapid up to 150 min, afterwards it showed a gradual removal rate, and remained in equilibrium after 300 min from the start of the experiment. Cr(VI) sorption with respect to the time curve is smooth and continuous leading to saturation showing homogeneous coverage of Cr(VI) species on the surface of the adsorbent. Initially, the faster kinetics may be due to the greater number of active adsorption sites available for Cr(VI) and the electrostatic force of interaction between the liquid phase and exchanger phase. Slower kinetics afterwards is due to saturation of active adsorption sites for further sorption of $HCrO_4^-$ or CrO_4^{2-}.

Understanding the sorption mechanism further focused on the determination of kinetics parameters based on the pseudo-first-order kinetic and pseudo-second-order kinetics (Weber and Chakravorti 1974; Barassi et al. 2009; Wu et al. 2009; Hu et al. 2011). Kinetics parameters were determined according to Eqs. 9.13 and 9.14 and presented in Table 9.3, where k_1 and k_2 are pseudo-first-order and pseudo-second-order rate constants, and q_e and q_t represent the adsorption capacity at equilibrium and at time 't'.

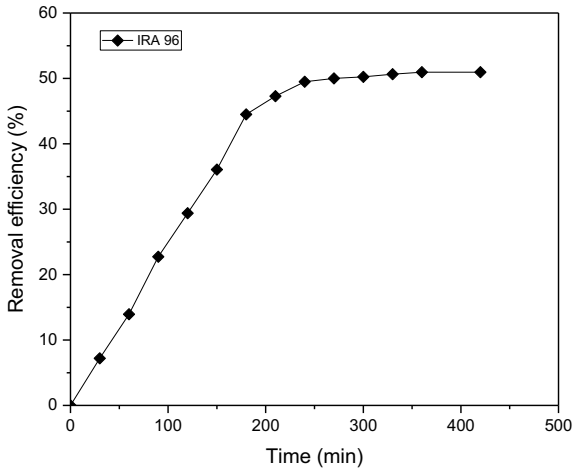

Fig. 9.3 Variation of Cr(VI) with respect to time. Conditions: Cr(VI) concentration = 2 mg/L, competing anion concentration = 100 mg/L, pH = 7, dosage = 0.2 g/L, RPM = 300 and volume of solution = 1000 mL

Table 9.3 Parameters of kinetic study

Adsorbent	Removal efficiency (%)	q_e, exp (mg/g)	Pseudo-first-order kinetic model				Pseudo-second-order kinetic model			
			q_e, cal (mg/g)	k_1 (1/h)	R^2	Δq_e (%)	q_e, cal (mg/g)	k_2 (g/mg h)	R^2	Δq_e (%)
IRA 96	50.95	5.09	5.86	0.38	0.98	16.96	8.30	0.04	0.96	19.57

$$\log(q_e - q_t) = \log q_e - \frac{k_1 t}{2.303} \tag{9.13}$$

$$\frac{t}{q_t} = \frac{1}{k_2 q_e^2} + \frac{1}{q_e} t \tag{9.14}$$

For pseudo-second-order kinetics, the experimental q_e values did not agree with the calculated q_e values obtained from the linearized equation. This shows that the adsorption of Cr(VI) on IRA 96 is not a second-order reaction. Pseudo-first-order kinetics shows a good agreement between the experimental q_e and calculated q_e values (Table 9.3), and it can be seen that the R^2 for pseudo-first-order kinetics and pseudo-second-order kinetic models are very close to 1. Based on the comparison, it is found that the pseudo-first-order model fitted better than pseudo-second-order kinetics. This confirms that the adsorption capacity between the experimental Cr(VI) uptake capacity ($q_{e,cal}$, (mg/g)) and theoretically calculated Cr(VI) sorption capacity ($q_{e,exp,}$ (mg/g)) values are well represented by the pseudo-first-order kinetics for the Cr(VI) adsorption.

The applicability of the kinetic model to describe the adsorption behaviour was further evaluated by the normalized standard deviation, Δq_e (%), Eq. 9.15. Based on the highest R^2 value and the lowest Δq_e value (Table 9.3), the pseudo-first-order kinetics was the most suitable equation to describe the adsorption kinetics of Cr(VI) on IRA 96.

$$\Delta q_e(\%) = 100\sqrt{\frac{\sum\left[\left(q_{e,exp} - q_{e,cal}\right)/q_{e,exp}\right]^2}{N-1}} \tag{9.15}$$

9.5.5 Fixed Bed Column Study

Fixed bed adsorption studies were performed to understand the applicability of IRA 96 for the trace removal of Cr(VI) from contaminated water. When feed water containing Cr(VI) is introduced through the inlet of a column, rapid and effective Cr(VI) adsorption occurs during the initial stage of column operations. Upper layers of sorbent are continuously in contact with the highest Cr(VI) concentration and a small amount of Cr(VI) may escape from the first layer of adsorbent that are removed from the lower layer of the adsorbent bed. As the feed continues to the column, the top layer becomes saturated with the incoming Cr(VI) and becomes less effective for further adsorption. Thus, the adsorption zone moves further downward to the next fresh adsorbent sites in the column (Knox et al. 2016). As the adsorption zone moves further downward, more Cr(VI) tends to escape to the effluent, and the adsorbent gets saturated when the influent Cr(VI) concentration equals the effluent Cr(VI). The effectiveness of the fixed bed column study can be explained in terms of the breakthrough curve. Breakthrough appearance and shape are very important in fixed

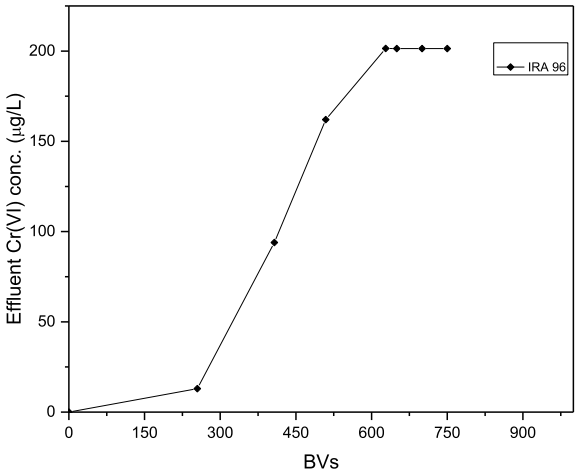

Fig. 9.4 Breakthrough curve during fixed bed column study. Conditions: Cr(VI) concentration = 2 mg/L, SO_4^{2-}, Cl^- and HCO_3^- concentration = 100 mg/L, Flow rate = 1.5 mL/min, EBCT = 3.9 min and pH 7.1 ± 0.1

bed sorption study for evaluating the loading behaviour of Cr(VI) adsorption from solution, the smooth operation of column run and response of adsorbent during fixed bed adsorption (Lim and Aris 2014). Figure 9.4 shows the breakthrough histories of Cr(VI) by IRA 96. Total BVs of Cr(VI) removed by IRA 96 is 628 BVs during the service run, and the amount of Cr(VI) removed was calculated from the breakthrough curve and is approximately 0.19 mg/g.

9.6 Conclusion

The result of this investigation contributed to the knowledge of adsorption interaction with trace Cr(VI) species in contaminated groundwater conditions. The flow process and transport of tracer are described by using the MIM model. Weak base anion exchange resin was used to remove trace concentration of Cr(VI), and showed selectivity towards the target Cr(VI) species. The batch isotherm study was well fitted by Freundlich isotherm and based on Langmuir isotherm, the maximum sorption capacity of IRA 96 was obtained as 1.68 mg/g. The kinetic study revealed that the sorption process is rapid and the very effective in removing low concentrations of Cr(VI). During fixed bed column study, IRA 96 was able to treat 200 µg/L of Cr(VI) concentration up to 628 BVs and was able to remove 0.19 mg/g of Cr(VI) before exhaustion.

References

Alabi OO, Ajah DT, Abidoye LK (2016) Mathematical modeling of hydraulic conductivity in homogeneous porous media: influence of porosity and implications in subsurface transport of contaminants

Babu BV, Gupta S (2008) Adsorption of Cr(VI) using activated neem leaves: kinetic studies. Adsorption 14(1):85–92. https://doi.org/10.1007/s10450-007-9057-x

Bahowick S, Dobie D, Kumamoto G (1993) Ion exchange resin for removing hexavalent chromium from ground water at treatment facility c: data on removal capacity, regeneration efficiency, and operation (Freon 113)

Barassi G et al (2009) Cr(VI) sorption behavior from aqueous solutions onto polymeric microcapsules containing a long-chain quaternary ammonium salt: kinetics and thermodynamics analysis. J Hazard Mater 172(1):262–268. https://doi.org/10.1016/j.jhazmat.2009.06.167

Höll WH, Xuan Z, Hagen K (2004) Forschungszentrum Karlsruhe in der Helmholtz-Gemeinschaft Wissenschaftliche Berichte FZKA 6994. Elimination of health-relevant heavy metals from raw waters of the drinking water supply in the PR China by means of weakly basic anion exchange resins

Hu X et al (2011) Adsorption of chromium (VI) by ethylenediamine-modified cross-linked magnetic chitosan resin: isotherms, kinetics and thermodynamics. J Hazard Mater. Elsevier B.V. 185(1):306–314. https://doi.org/10.1016/j.jhazmat.2010.09.034

Knox JC et al (2016) Limitations of breakthrough curve analysis in fixed-bed adsorption. Ind Eng Chem Res 55(16):4734–4748. https://doi.org/10.1021/acs.iecr.6b00516

Korngold E, Belayev N, Aronov L (2003) Removal of chromates from drinking water by anion exchangers. Sep Purif Technol 33(2):179–187. https://doi.org/10.1016/S1383-5866(03)00006-6

Lim AP, Aris AZ (2014) Continuous fixed-bed column study and adsorption modeling: removal of cadmium (II) and lead (II) ions in aqueous solution by dead calcareous skeletons. Biochem Eng J. Elsevier B.V. 87:50–61. https://doi.org/10.1016/j.bej.2014.03.019

McCord JT, Selker JS (2009) Transport phenomena and vulnerability of the unsaturated zone. Groundwater-Volume II 165

McNeill L et al (2012) State of the science of hexavalent chromium in drinking water. Water Res Found (May) 36. www.waterrf.org

Pehlivan E, Cetin S (2009) Sorption of Cr(VI) ions on two Lewatit-anion exchange resins and their quantitative determination using UV-visible spectrophotometer. J Hazard Mater 163(1):448–453. https://doi.org/10.1016/j.jhazmat.2008.06.115

Seidel CJ, Corwin CJ (2013) Total chromium and hexavalent chromium occurrence analysis. J Am Water Works Assoc 105(6). https://doi.org/10.5942/jawwa.2013.105.0050

Sengupta AK, Clifford D (1986) Important process variables in chromate ion exchange. Environ Sci Technol 20(2):149–155. https://doi.org/10.1021/es00144a006

Sharma SK, Petrusevski B, Amy G (2008) Chromium removal from water: a review. J Water Supply Res Technol AQUA 57(8):541–553. https://doi.org/10.2166/aqua.2008.080

Shi T et al (2009) Removal of hexavalent chromium from aqueous solutions by D301, D314 and D354 anion-exchange resins. J Hazard Mater 161(2–3):900–906. https://doi.org/10.1016/j.jhazmat.2008.04.041

Šimůnek J, van Genuchten MT (2008) Modeling nonequilibrium flow and transport processes using HYDRUS. Vadose Zone J 7(2):782–797

Weber W, Chakravorti RK (1974) Pore and solid diffusion models for fixed bed adsorbers. Am Inst Chem Eng J 20(2):229–238

Wu FC, Tseng RL, Juang RS (2009) Initial behavior of intraparticle diffusion model used in the description of adsorption kinetics. Chem Eng J 153(1–3):1–8. https://doi.org/10.1016/j.cej.2009.04.042

Chapter 10
ANN Modeling of Groundwater Development for Irrigation

Pritam Malakar and Susmita Ghosh

Abstract The groundwater level is required to keep within the permissible limit for sustainable groundwater development in any area. In the present study, an Artificial Neural Network (ANN) model has been developed for groundwater development with respect to state variables of a groundwater system, i.e., a maximum depth to water table for agricultural purposes. The zonal cropping areas are considered as inputs to the ANN model. The methodology has been illustrated in the Yamuna-Hindon Inter basin, India. The ANN model is performed for two different training algorithms like (i) Levenberg–Marquardt (LM) and (ii) Bayesian regularization (BR) and their performance was compared with the backpropagation (BP) algorithm. The prediction accuracy of both algorithms was tested using performance indices viz. mean square error (MSE), root mean square error (RMSE), and correlation coefficient (R^2). The performance of both the ANN training algorithms in predicting maximum depth to water table over the study area was found to be almost similarly good. However, the performance of the LM algorithm was found slightly superior to that of the BR algorithm as well as the BP algorithm.

Keywords Artificial Neural Network (ANN) · Feedforward Multilayer Neural Network (FNN) · Levenberg–Marquardt algorithm (LM) · Bayesian regularization algorithm (BR) · Groundwater modeling

10.1 Introduction

Groundwater is a very precisely available and dependable natural resource all over the world among various users to meet several needs (Firouzkouhi 2011). This resource should be utilized judiciously to maintain sustainability. But the lowering trend of

P. Malakar
NIT Silchar, Silchar, India

NIT Agartala, Agartala, India

S. Ghosh (✉)
Civil Engineering Department, NIT Silchar, Silchar, India
e-mail: susmita@civil.nits.ac.in

R. Jha et al. (eds.), *Groundwater and Water Quality*, Water Science and Technology Library 119, https://doi.org/10.1007/978-3-031-09551-1_10

groundwater level and aquifer depletion due to indiscriminate groundwater development and also increasing trend of groundwater/subsurface pollution are threatening the sustainability of water resources. Unsustainable groundwater usage leads to several socio/technical consequences, and these issues are increasing day by day throughout the world, especially in developing countries. In the present scenario, it is the first priority or utmost concern of a planner/manager, or user to maintain the yield from aquifers in a sustainable manner for long period (Sophocleous 2005; Todd and Mays 2005; Gorelick and Zheng 2015). Therefore, appropriate sustainable management/planning of surface water and groundwater usage conjunctively is the most important concern. Planning of groundwater development is carried out at two stages viz. (i) feasibility—ensuring acceptability/appropriateness of the groundwater development without affecting the social/technical restrictions and (ii) optimality—choose the best among all feasible alternatives. Feasibility means to check the desired level of various groundwater state variables like groundwater table depth, stream–aquifer inter-flow, seawater intrusion, etc. within a certain specified limit by considering relevant socio/technical issues. The next stage toward the planning is to pick up the most rewarding (kashyap and Chandra 1982) or least penalizing (Emch and Yeh 1998) optimal pattern from the array of the evolved feasible pattern.

The groundwater management problems have been addressed by forming an optimization problem. The optimization problem mainly comprises an array of decision variables, one or more than one objective function as per manager requirement, and an array of relevant constraints. The constraints and objective functions are explicit or implicit functions of the decision variables and state variables (Deininger 1970; Maddock 1972). The numerous significant constraints of groundwater management are limitations on the state variables such as maximum/minimum groundwater table depth (Ghosh and Kashyap 2012a, b), stream–aquifer interactions (Young and Bredehoeft 1972; Pulido-Velazquez et al. 2007), and seawater intrusion (Werner and Simmons 2009). The state variables are generally computed by physically based simulation models (Bredehoeft and Young 1970; Kashyap and Chandra 1982; Kumar 2013). Therefore, said models are numerical solutions of the selected governing differential equations using the finite difference/element method. And it becomes computationally quite expensive in planning programs due to the sequential calling of simulation models. The computational cost of planning problems has been reduced considerably in case of some planning practices like the kernel function-based approach (Maddock 1972; Ghosh and Kashyap 2012a, b), embedded technique (Gorelick and Remson 1982), and the physically based modeling techniques are also very much data-intensive. Thus, the use of a physically based model is being restricted due to the scarcity of required data which is a common problem in several parts of developing countries. Therefore, the computationally expensive and data-intensive physically based simulation models can be replaced by approximate/black-box models (Lefkoff and Gorelick 1990; Bhattacharya and Datta 2005, ASCE 2000, Mohanty et al. 2013) using relatively less computational time and data. The current study invokes artificial neural network (ANN) models as a simulation model. The ANN models are being used to simulate the aquifer response by considering several

sets of inputs like pumping patterns, weather parameters, and aquifer characteristics/conditions (Morshed and Kaluarachchi 1998; and Safavi et al. 2010). The outputs from the ANN models are aquifer parameters (Rizzo and Dougherty 1994), and water table/piezometric heads (Coulibaly et al. 2001; Daliakopoulos et al. 2005; Uddameri 2007; Trichakis et al. 2011). The input–output data sets for training and testing of the ANN models are generated from simulation models (Singh and Datta 2006; Safavi et al. 2010) or from field data (Coppola et al. 2005; Feng et al. 2008).

10.2 Present Study

The water requirement/demand for agricultural purposes is generally met by groundwater water entirely or in conjunction with surface water in canal command areas. As a result, the water table level declined excessively due to the unplanned withdrawal of groundwater resources. Effective modeling is essential to achieve sustainable agricultural groundwater development to restrict the lowering trend of water table depth. The ANN model has been developed considering crop areas and maximum water table depth as input and output, respectively, and illustrated at Yamuna-Hindon inter basin (Ghosh and Kashyap 2012a). The area falls under the command area of the Eastern Yamuna Canal system that starts from Yamuna river at Tajewala and also has abundant groundwater. In spite of that, the sustained lowering trend of water table level is observed in the several past reported studies (Kashyap and Chandra 1982; Mishra 1987; Rathi 1997; Ghosh 2011; Ghosh and Kashyap 2012a, b). Therefore, the ANN-based technique is utilized to simulate the groundwater levels for agricultural purposes considering the relevant groundwater state variable, i.e., a maximum depth to the water table. The zone-wise cropping pattern is a decision variable to quantify the requirement of groundwater for irrigation. In this study, the array of input–output data sets is used from the preceding studies (Ghosh and kashyap 2012a). Training of the ANN model has been done using two algorithms, i.e., Levenberg–Marquardt (LM) and Bayesian regularization (BR) and ANN architecture as feedforward multilayer neural network (FNN), and the developed ANN model performance with the previous study where training has been done using backpropagation is compared (Ghosh and Kashyap 2012a). The limitation of the backpropagation training algorithm is that it is an inefficient algorithm because of its slow convergence (Wilamowski and YuHao 2010). Therefore, in the present study, ANN models have been developed using Levenberg–Marquardt (LM) and Bayesian regularization (BR) training algorithms and with ANN architecture as a feedforward multilayer neural network (FNN).

10.3 Zonal Cropping Pattern

The study area is divided into two zones of uniform cropping pattern having alike hydrogeological characteristics, namely (I) centralized zone and (II) outer zone with

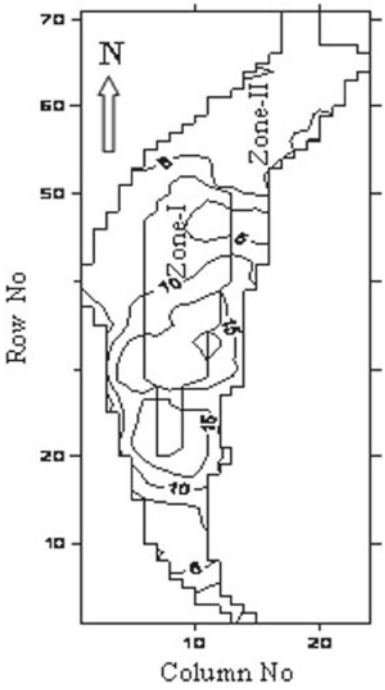

Fig. 10.1 Study area (Ghosh and Kashyap 2012a)

five different major crops, (a) paddy, (b) other kharif, (c) sugarcane, (d) wheat, and (e) other rabi.

10.4 Study Area

The study area is an agricultural area viz. the Hindon-Yamuna inter basin under the Eastern Yamuna canal system (India), area of 0.6 million hectares, from latitude 29° 18′–30° 25’ N and longitude 77° 1′ 30″–77° 40′ 45″ E (Fig. 10.1). The Yamuna and Hindon rivers are in the west and east directions, respectively, of the area. The two rivers meet at the southern end. The Siwalik Mountains are on the north side of the area.

10.5 Data

The major crops in this area are (a) paddy, (b) other kharif, (c) sugarcane, (d) wheat, and (e) other rabi. The area is separated in two zones (0.14 and 0.46 million ha) based on uniform cropping patter (Fig. 10.1). The tens crop-area matrix are as follows:

Table 10.1 Typical sample input and output data sets (Ghosh 2011)

Zone	a_1	a_2	a_3	a_4	a_5	D_{max}
1	12.9692	8.24774	9.82509	17.3934	0.386502	24.1229
2	14.9072	1.18408	9.33594	14.8987	10.1094	24.8448
1	0.859897	2.83655	11.894	1.14095	3.97282	26.3508
2	4.08903	1.98249	26.9565	4.75386	6.94958	25.7999
1	15.4811	7.16388	2.83331	23.1313	22.1833	26.1485
2	13.834	2.28658	14.4762	4.35599	0.75820	17.5441
1	5.57739	2.05444	9.34082	13.8232	1.18652	26.2885
2	4.67789	12.5568	3.16156	13.9262	2.27144	24.6855
1	12.9414	10.5560	5.89602	15.7663	8.2802	26.1040
2	19.4572	9.78525	1.28113	5.17804	17.9679	25.4882

[{(ajl), j = 1, 2, 3, 4, 5}, l = 1, 2]. The generated zonal crop areas of each crop are used from previous studies (Ghosh 2011).

The cropping areas and corresponding maximum groundwater table depth (D) are calculated using the ground elevations and model computed groundwater table elevations by Eq. (10.1) in previous studies (Ghosh 2011) and these data sets are used in this study.

$$D = \underset{i,k}{\text{Max}}\left[G_i - h^*_{ik}\right] \tag{10.1}$$

D Maximum groundwater table depth
G_i The ground elevations
h^*_{ik} Head under dynamic equilibrium.

There are shown some of the typical samples of data sets of input and output (Table 10.1), whereas inputs are that of zones 1 and 2, crop areas (% of geographical area) of a_1, a_2, a_3, a_4, a_5, and D_{max} is the output that is the maximum depth of the groundwater in meter sample in Table 10.1.

10.6 Artificial Neural Network

Artificial Neural Network (ANN) is an artificial intelligence method motivated by the working of the human brain. The human brain is possibly the most powerful information processing tool. ANN is a dominant huge data-driven, flexible computational tool having the ability to capture the physical behavior of any nonlinear and complex physical process with an acceptable accuracy level. An ANN comprises input, hidden, and output layers. The input layer represents input variables that are connected to the hidden layer and output layer simultaneously. The nodal output

values of the hidden layer are computed through specified activation functions and it computes the weights of the variables to search for the effects of predictors upon the target (dependent) variables. In the output layer, the computation process is ended and the results, i.e., output variables are achieved with a minor estimation error.

In this study, regarding the ANN model, ANN architecture as a feedforward neural network (FNN) is used. In the previous studies (Ghosh and kashyap 2012a), a backpropagation training algorithm had been used for ANN model. The limitation of the backpropagation training algorithm is that it converges slowly (Wilamowski and Hao 2010). Therefore, in the present study, ANN models have been developed using Levenberg–Marquardt (LM) and Bayesian regularization (BR) training algorithms.

10.7 Development of ANN Models

Generally, the large input–output data sets for the training and testing of the ANN networks are essential for ANN model development. In this study, 750 sets of uniform cropping patterns and the corresponding maximum depth of the groundwater tables are used to train and test an artificial neural network (Ghosh and Kashyap 2012a). 675 data sets are used for ANN training and the remaining 75 data sets are used for validation. The ANN models have been developed using Levenberg–Marquardt (LM) and Bayesian regularization (BR) training algorithms and with ANN architecture as feedforward multilayer neural network (FNN) using the MATLAB R2014a Neural Network Toolbox. In the training phase, the number of hidden layers and number of neurons at each hidden layer is increased one by one starting from the bare minimum model. The parameters like epoch and maximum fail also change to achieve the desired accuracy of the ANN model. The ANN architecture, i.e., the number of hidden layers and number of neurons at every layer is finalized by the trial-and-error method keeping performance indices of the trained ANN model in an acceptable range. Inputs and outputs of the ANN model have been normalized in the range of (0–1, 0.1–0.9), and to observe the effect of normalization. The adaption learning function is LEARGDM, the performance function is MSE, and the transfer function is LOGSIG. After the successful training of the ANN model, the ANN architecture is fixed and then tested with the remaining data sets. The mean squared error (MSE) and correlation coefficient (R^2) are computed for the training and testing phases, respectively (Tables 10.3 and 10.4) and considered as performance evaluation criteria in training and testing phases of the developed ANN model. The efficiency of the ANN model is measured by minimizing the MSE and maximizing the R^2 value.

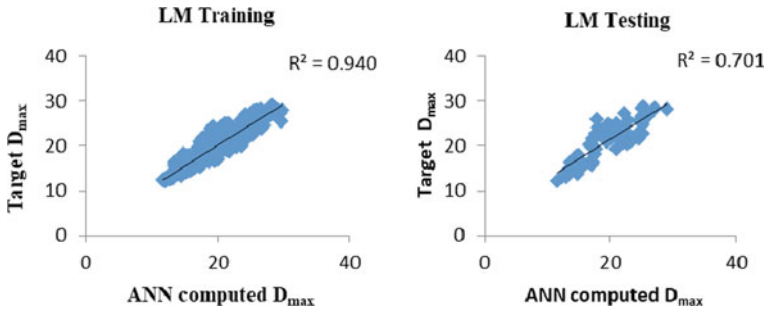

Fig. 10.2 Target and ANN computed D_{max} Levenberg–Marquardt training and testing (0–1)

10.8 Results and Discussion

After several trial runs with different combinations of epochs and maximum fails, the optimal ANN architecture is chosen for minimum MSE, i.e., 0.0044, and maximum R^2, i.e., 0.940.

An optimal design is completed for one hidden layer (10-10-1) with a feedforward multilayer neural network (FNN), and corresponding R^2 and MSE are given in Table 10.3 (normalized range: 0–1) and Table 10.4 (normalized range: 0.1–0.9). The two training algorithms such as Levenberg–Marquardt (LM) and Bayesian regularization (BR) are used for ANN training and their efficiency is computed. The target values and corresponding ANN computed values (Table 10.2) show good match for LM training and testing (Fig. 10.2) and BR training and testing (Fig. 10.3) in the (0–1) normalized range. In Figs. 10.4 and 10.5, it is observed that the target and ANN computed maximum groundwater table depth is also quite a good match using BR training for the (0.1–0.9) normalized range. Therefore, it may be concluded from Tables 10.3 and 10.4 that there is as such no more effect on the ANN model efficiency considering two separate normalized ranges viz. (0–1) and (0.1–0.9). And the application of an ANN has been successfully demonstrated using FNN architecture to compute maximum groundwater table depth for an agricultural area

.

10.9 Conclusion

ANN models have been developed in the case of groundwater development for irrigation considering the relevant groundwater state variable, i.e., Maximum depth of the groundwater table. The cropping pattern is a decision variable to quantify the requirement of groundwater for irrigation. An optimal design is completed for one hidden layer with ANN architecture as a feedforward multilayer neural network (FNN). The two training algorithms viz. LM and BR are used and their performance is assessed.

Table 10.2 Sample values Target and ANN computed D_{max} of data sets

Levenberg–Marquardt		Bayesian regularization	
Target value	ANN computed value	Target value	ANN computed value
20.6536	21.4354	12.4354	14.9065
22.5432	23.1886	25.2328	24.9856
26.3541	26.2355	22.9265	23.7649
14.9889	12.3245	13.4354	15.4354
25.6739	24.8971	23.5647	23.8795
13.4354	14.8985	19.4354	16.7853
15.9265	15.9281	23.7694	24.8793
26.0292	22.9098	16.8749	15.7832
13.9043	16.9087	21.9265	20.1236
15.4354	13.9807	19.4351	19.2138

Table 10.3 Performance index for normalized range (0–1)

Training algorithm	Epoch	ANN architecture	R^2		MSE	
			Training	Testing	Training	Testing
LMA	200	10-10-1	0.940	0.701	0.0044	0.027
BRA	200	10-10-1	0.905	0.700	0.0065	0.029
BPA	6000	10-7-1	0.922	0.813	0.0053	0.006

Table 10.4 Performance index for normalized range (0.1–0.9)

Training algorithm	Epoch	ANN architecture	R^2		MSE	
			Training	Testing	Training	Testing
LMA	200	10-10-1	0.911	0.700	0.0080	0.0209
BRA	200	10-10-1	0.906	0.710	0.0089	0.0222

The application of an ANN has been successfully demonstrated using FNN architecture to predict maximum groundwater table depth in the agricultural area. The prediction accuracy of both the ANN training algorithms has been tested using two performance indices like mean square error (MSE) and efficiency criterion (R^2).

LM and BR training achieved the desired accuracy level faster than BP. From Tables 10.3 and 10.4, it is clearly evident that the performance of both the ANN training algorithms to predict groundwater levels in this area is shown to be almost equally good, though the performance of the LM training algorithm shows slightly superior to that of the BR as well as the BP training algorithm. The normalized data set was done from the range 0.1–0.9 to avoid the extreme limits of the transfer function. But still, there is no effect after normalizing the range 0.1–0.9 and the same LM training algorithm was found slightly improved than that of the BR training

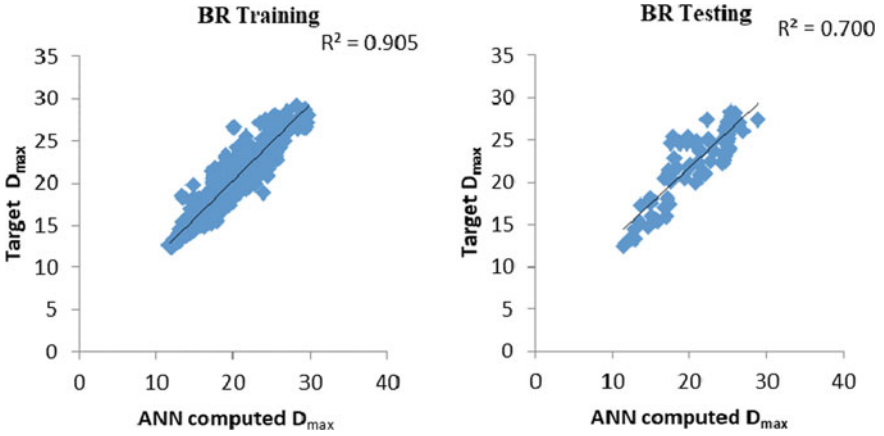

Fig. 10.3 Target and ANN computed D_{max} Bayesian regularization training and testing (0–1)

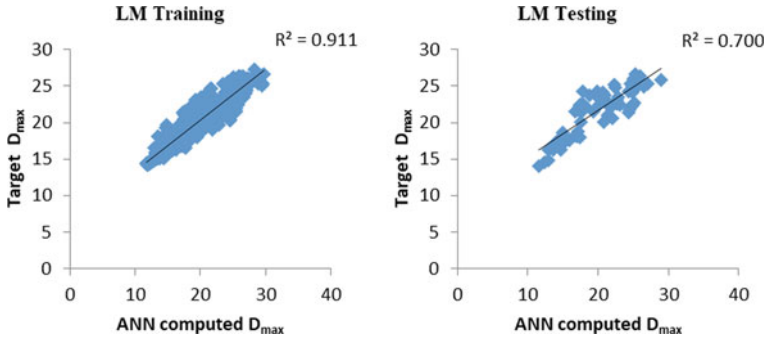

Fig. 10.4 Target and ANN computed D_{max} Levenberg–Marquardt training and testing (0.1–0.9)

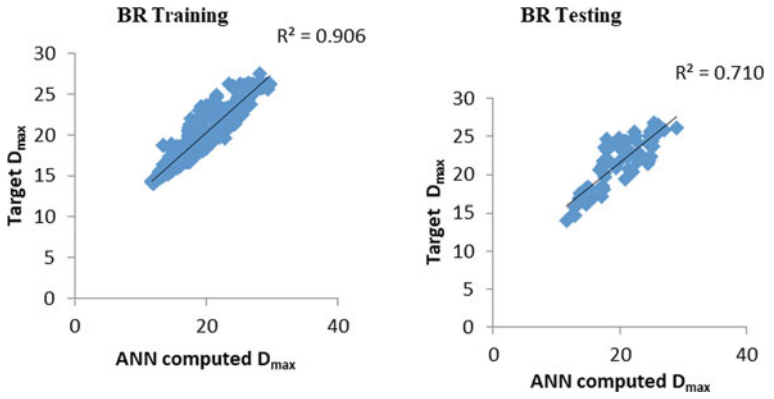

Fig. 10.5 Target and ANN computed D_{max} Bayesian regularization training and testing (0.1–0.9)

algorithms. The ANN model with respect to cropping pattern-maximum groundwater depth to the water table is more relevant for groundwater development for canal command area for irrigation than pumping-groundwater level done in the previous study.

References

ASCE (2000) Task committee on applications of artificial neural networks in hydrology. Artificial neural networks in hydrology. I: preliminary concepts. Hydrol Eng 5(2):115–123

Bhattacharya R, Datta B (2005) Optimal management of coastal aquifers using linked simulation optimization approach. Water Resour Manage 19:295–320

Bredehoeft JD, Young RA (1970) The temporal allocation of groundwater-a simulation approach. Water Resour Res 6(1):3–21

Coppola E, Rana A, Poulton M, Szidarovszky F, Uhl V (2005) A neural network model for predicting water table elevations. J. Ground Water 43(2):231–241

Coulibaly P, Anctil Ramon F, Bernard Bobee A (2001) Artificial neural network modeling of water table depth fluctuations. Water Resour Res 37(4):885–896

Daliakopoulos IN, Coulibaly P, Tsanis IK (2005) Groundwater level forecasting using artificial neural network. J Hydrol 309:229–240

Deininger RA (1970) System analysis of water supply systems. Water Resour Bull 6(4):573–580

Emch PG, Yeh WW (1998) Management model for conjunctive use of coastal surface water and ground water. J Water Resour Plan Manag 124(3):129–139

Feng S, Kang S, Huo Z, Li W, Chen S, Mao X (2008) Using neural network to simulate regional ground water affected human activities. J Ground Water 46(1):80–90

Firouzkouhi R (2011) Simulating groundwater resources of Aghili-Gotvand plain by using mathematical model of finite differences. MSD (Doctoral dissertation, Thesis, Shahid Chamran University of Ahwaz, Iran)

Ghosh S (2011) Kernel function and ANN based planning of groundwater development for irrigation. Doctoral thesis, Indian Institute of Technology, Roorkee, India

Ghosh S, Kashyap D (2012a) ANNbased model for planning of groundwater development for agricultural usage. Irrig Drain 61(4):555–564

Ghosh S, Kashyap D (2012b) Kernel function model for planning of agricultural groundwater development. J Water Resour Plan Manage, ASCE (published online). https://doi.org/10.1061/(ASCE)WR.1943-5452.0000178

Gorelick SM, Remson I (1982) Optimal location and management of waste disposal facilities affecting groundwater quality. Water Resour Bull 18:43–51

Gorelick SM, Zheng C (2015) Global change and the groundwater management challenge. Water Resour Res 51(5):3031–3051

Jeff Lefkoff L, Gorelick SM (1990) Simulating physical processes and economic behavior in saline, irrigated agriculture: model development. 26(7):1359–1369

Kashyap D, Chandra S (1982) A distributed conjunctive use model for optimal cropping pattern. In: Proceedings of the Exeter symposium, July, IAHS Publication 135, 377–384

Kumar CP (2013) Numerical modelling of ground water flow using MODFLOW. Ind J Sci 2(4):86–92

Maddock T III (1972) Algebric technological function from a simulation model. Water Resour Res 8(1):129–134

Mishra R (1987) Distributed aquifer response modeling in Yamuna-Hindon Doab. MTech dissertation, Indian Institute of Technology Roorkee, India

Mohanty S, Madan KJ, Kumar A, Panda DK (2013) Comparative evaluation of numerical model and artificial neural network for simulating groundwater flow in Kathajodi-Surua Inter-basin of Odisha. India J Hydrol 495:38–51

Morshed and Kaluarachchi (1998) Application of artificial neural network and genetic algorithm in flow and transport simulations. Adv Water Resour 22(2):145–158

Pulido-Velazquez D, Sahuquillo A, Andreu J (2007) An efficient conceptual model to simulate surface water body–aquifer interaction in conjunctive use management models. Water Resour Res 43:1–15

Rathi S (1997) Numerical modeling of aquifer response in Yamuna-Hindon doab. MTech dissertation, Indian Institute of Technology, Roorkee, India

Rizzo DM, Dougherty DE (1994) Characteristics of aquifer parameters using artificial neural networks: neural kriging. Water Resour Res 30(2):483–497

Safavi HR, Darzi F, Marino MA (2010) Simulation-optimization modelling of conjunctive use of surface and groundwater. Water Resour Manage 24(10):1965–1988

Singh RM, Datta B (2006) Identification of groundwater pollution sources using GA-based linked simulation optimization model. J Hydrol Eng ASCE 11(2):101–109

Sophocleous MA (2005) Groundwater recharge and sustainability in the high plains aquifer in Kansas, USA. Hydrogeol J 13:351–365

Trichakis JC, Nikolos IK, Karatzas GP (2011) Artificial neural network (ANN) based modelling for karstic groundwater level simulation. Water Resour Manage 25(4):1143–1152

Todd DK, Mays LW (2005) Groundwater hydrology. Wiley, Hoboken, N.J

Uddameri V (2007) Using statistical and artificial neural network models to forecast potentiometric levels at a deep well in South Texas. Environ Geol 51:885–895

Werner AD, Simmons CT (2009) Impact of sea-level rise on seawater intrusion in coastal aquifers. Ground Water 47(2):197–204

Wilamowski BM, Yu Hao (2010) Improved computation for Levenberg–Marquardt training. IEEE Trans Neural Netw 21(6):930–937

Young RA, Bredehoeft JD (1972) Digital computer simulation for solving management problems of conjunctive groundwater and surface water systems. Water Resour Res 8(3):533–556

Chapter 11
Assessment of Groundwater Quality with Special Reference to Arsenic in Ballia District, Uttar Pradesh, India

Sumant Kumar, Narayan C. Ghosh, Vinod Kumar, Ravi K. Saini, Rajesh Singh, Anju Chaudhary, and R. P. Singh

Abstract The groundwater resources are being utilized for drinking, irrigation and industrial purposes. There is a growing concern about the deterioration of groundwater quality due to geogenic and anthropogenic activities. Arsenic (As) contamination of groundwater is one of the major threats to human health especially in the Ganges River basin (GRB) and has attracted national and international attention. In the present study, the hydro-chemical characteristics of groundwater and its suitability for drinking and irrigation purposes were investigated in Ballia District, Uttar Pradesh. Groundwater samples were collected during the pre-monsoon season (May 2015) from the India-mark-hand pump (110–140 feet depth) from four As-affected blocks (Sohaon, Hanuman-Ganj, Belhari and Dubhad) of Ballia district. The water quality assessment for drinking and irrigation purposes has been carried out by evaluating the physico-chemical parameters of groundwater. The chemical analysis results revealed that calcium is found to be the dominant cation followed by Mg^{2+}, Na^{+} and K^{+}. HCO_3^{-} is found to be a major anion followed by Cl^{-} and SO_4^{2-}. The scatter diagram between ($Ca^{2+} + Mg^{2+}$) versus Tz^{+} for groundwater shows a strong positive correlation ($R^2 = 0.71$), and it reflects the high abundance of calcium and magnesium in the groundwater. The Piper diagram suggested that major hydro-geochemical facies is of Ca–Mg-HCO_3 type. The chemical results showed that approximately 70% of samples were enriched with As concentrations >10 μg/L (10 μg/L is the acceptable limit for drinking water; BIS, Indian Standard for drinking water-specification (IS 10500:2012). Arsenic concentration in the monitored water samples ranges from below detectable limit (BDL) to 461 μg/L. The concentration of Ca^{2+}, Mg^{2+} and HCO_3^{-} ions exceeded the acceptable limit of drinking water in many of groundwater samples. Groundwater falls under the good to a suitable category for irrigation purposes based on SAR value.

S. Kumar (✉) · N. C. Ghosh · V. Kumar · R. K. Saini · R. Singh · A. Chaudhary · R. P. Singh
National Institute of Hydrology, Roorkee, India
e-mail: sumantks@gmail.com

N. C. Ghosh
Bengal Institute of Technology, Kolkata, India

R. Jha et al. (eds.), *Groundwater and Water Quality*, Water Science and Technology Library 119, https://doi.org/10.1007/978-3-031-09551-1_11

Keywords Arsenic · Groundwater quality · Sodium adsorption ratio · Ballia district · Central Ganges Basin

11.1 Introduction

Safe drinking water is not accessible to almost 30% of urban and 90% of the rural inhabitants (Kumar et al. 2010) of India. Many researchers (Choubisa et al. 2001; Subramanian 2000; Singh et al. 2012) have identified a major crisis in the country in the form of declining quality of the available water resources and availability of potable water in many parts of India. The enriched concentration of arsenic in groundwater has also become a global concern and has been reported by many researchers worldwide especially in Cambodia (Nicholas et al. 2008), China (Smedley and Kinniburgh 2002), Nepal (Tandulkar et al. 2001), Bangladesh (Berg et al. 2001) and India (Chakraborti et al. 2003). There are a huge number of hydro-geological studies performed to delineate the source of the contamination and understand the cause in order to discover an arsenic-free aquifer and to find preventive and remedial measures (Van Geen et al. 2003). In the Indian subcontinent, the elevated concentration of As was firstly reported in Chandigarh area (Capital of states Haryana and Punjab) (Datta and Kaul 1976) followed by in a few districts of West Bengal (CGWB 1997; Chakraborti et al. 2003; McArthur et al. 2004; Mukherjee et al. 2006). In India, most of the studies are limited to Ganga–Brahmaputra–Meghna and lower Gangetic basins and a few studies have been carried out in the central Gangetic basin. The central Ganges basin comprises mainly the two states, Uttar Pradesh and Bihar, which is one of the largest fluvio-deltaic system, and these states consist of the most populous regions. In recent few decades, the increasing demand for groundwater for domestic, irrigation and industrial purposed with the growing population rate led to the extensive exploitations of fresh and potable groundwater. Nowadays, there is the problem of safe and potable groundwater in these regions as most of the areas are contaminated by As. Since Uttar Pradesh is the most heavily populated state of the central Gangetic basin, deterioration of health conditions in this study is a matter of chief concern. The problem of arsenic in Uttar Pradesh was first recognized in the year 2003 in district Ballia, and it is one of the severely affected districts by arsenic. Hence, in the present study, an attempt was made to understand the hydrochemistry of the study area. The arsenic distribution map for the four different blocks of Ballia would be an interesting scientific output along with its societal importance, and environmental implications and would provide the baseline data. The suitability of groundwater for drinking and irrigation purposes were also assessed.

11.2 Materials and Methodology

Study area

Ballia is the easternmost district of Uttar Pradesh, covering an area of 2981 km^2, and lies between 25° 33′ and 26° 11′ N latitudes and 83° 38′ and 84° 39′ E longitudes. The district is bounded on the north by Ghaghara River and on the south by Choti Saryu and Ganga Rivers. In the present study, we have focused mainly on four different blocks, i.e., Sohaon, Hanuman-Ganj, Belhari and Dubhad of Ballia district (Fig. 11.1). The study area has an average rainfall of 983 mm with a mean annual temperature of 27 °C, which varies from 5.4 to 41.5 ºC. Ballia is an agricultural dominant district. The district has two sources of irrigation: (a) Dharighat lift irrigation canal and (b) tube wells (groundwater) with a share of 72.61% for groundwater and 27.39% for surface water. The entire area forms an interfluve zone of Ghaghara and Ganga Rivers and possesses a plain flat topography.

Sampling approach and chemical analyses

Thirty-one groundwater samples from India-mark-hand pumps (110–140 feet depth) during pre-monsoon (May) of the year 2015. The sampling location of groundwater covers the 4 administrative blocks of Ballia district situated along the Ganga river bank. The details of the sampling location have been provided in Fig. 11.1. The samples were acquired for major solute analysis after filtering through a 0.45 μm membrane filter paper and collected in HDPE bottles after 20 min of purging of wells and after stabilization of in-field parameter (conductivity, pH) for consecutive measurements using a Hach EC-pH meter (HQ30d). Two sets of samples were collected as unpreserved and preserved from each location. The preserved samples were used for heavy/trace metal ions analysis while the unpreserved sample was used for major ion analysis. The concentration of arsenic was analysed by an inductively coupled plasma-mass spectrometer (ICP-MS, Model no: ELAN DRC-e, Perkin Elmer Inc). Na^+ and K^+ were determined by flame-photometer; Ca^{2+}, Mg^{2+} and HCO_3^- were determined by titration; and Cl^-, NO_3^- and SO_4^{2-} were determined by UV–visible spectrophotometer (Model no: DR-6000™, Hach Inc.). All the parameters were analysed as per Standard Methods (APHA, AWWA, WEF 2012).

11.3 Results and Discussion

11.3.1 Groundwater Chemistry

The statistical summary of various physico-chemical parameters is presented in Table 11.1. The pH ranged 6.54–8.56 (with median 7.25) indicating that most of the groundwater samples are mildly acidic to marginally alkaline in nature, while EC values ranged from 479 to 1047 μS/cm (with median 681 μS/cm). There was no apparent

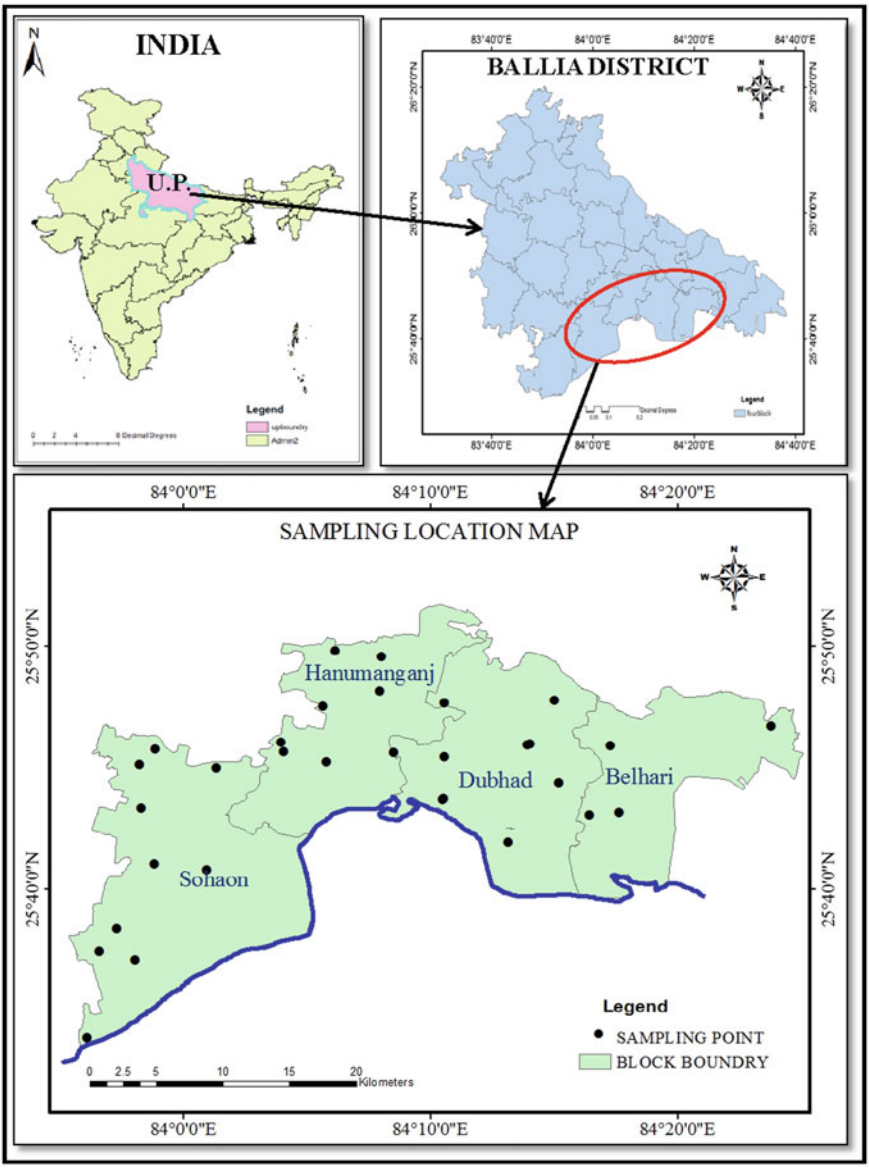

Fig. 11.1 Study area showing sampling location in four blocks of Ballia district (Uttar Pradesh)

Table 11.1 Statistical summary of physico-chemical parameters and compared with BIS (2012) standards for drinking water

Parameters	pH	EC	TDS	Cl^-	HCO_3^-	SO_4^{2-}	NO_3^-	Ca^{2+}	Mg^{2+}	Na^+	K^+	As (ppb)
Minimum	6.54	479	305	ND	195	ND	ND	26.7	10.4	13.7	1.4	3.22
Maximum	8.56	1047	744	213	547	45	2.9	110	57.5	100	10.5	461
Average	7.19	707	488	37	368	9.7	0.5	74	35	37.4	4.65	73
Acceptable limit (BIS 2012)	6.5–8.5	–	500	250	200	200	45	75	30	200	–	10
Permissible limit (BIS 2012)	No relaxation	–	2000	1000	600	400	100	200	100	–	–	50
% of sample exceeded acceptable limit	Nil	–	39	Nil	93	Nil	Nil	45	67	Nil	–	70

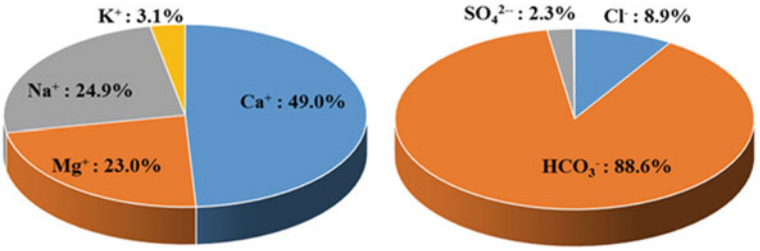

Fig. 11.2 Pie chart showing relative abundance of major ions in water samples

trend established between EC and PH values for the analysed samples in this study. The total dissolved solid (TDS) ranged from 306.0 to 745.0 mg/l with a median of 464.5 mg/l. Calcium (Ca^{2+}) is found to be the dominant cation in groundwater samples followed by Mg^{2+}, Na^{+} and K^{+}, whereas anion chemistry shows that HCO_3^{-} and Cl^{-} are the dominant anions followed by SO_4^{-} and NO_3^{-}. Figure 11.2 shows that Ca^{2+} is contributing on an average ~49.0% of the total cation charge (TZ^{+}), followed by Na^{+} (24.9%), Mg^{2+} (23.0%) and K^{+} (3.1%). The analysed results reveal that the overall alkaline earth ($Ca^{2+} + Mg^{2+}$) dominates the alkalis ($Na^{+} + K^{+}$). Similarly, among the anions, HCO_3^{-} contributes on an average ~88.6% of total anion charge (TZ^{+}) followed by Cl^{-} (8.9%), SO_4^{2-} (2.3%) and NO_3^{-} (0.2%). Chakrapani et al. (2009) reported that the major source of calcium and magnesium might be carbonate rocks containing calcite ($CaCO_3$) and dolomite $CaMg(CO_3)_2$, whereas a slight portion contributed by Ca-silicate minerals, i.e., Ca-plagioclase, gypsum and feldspar. The correlation between TDS and HCO_3^{-}, Ca^{2+}, Mg^{2+} and Na^{+} showed a good correlation (Table 11.2) suggesting that carbonate weathering is playing a major role in controlling the geochemistry of the groundwater in the study area.

11.3.2 Water Type and Hydro-chemical Facies

The Piper diagram is a useful plot classifying the types of water on the basis of their chemical characteristic. The triangular cationic field of the Piper diagram reveals that groundwater samples fall into the Ca^{2+} type, whereas in the anionic triangle majority of the samples fall into the bicarbonate type (Fig. 11.3). The diamond-shaped central field of the Piper diagram shows the major water types/facies as Ca–Mg-HCO_3^{-} and minor water types as Mg–Na-HCO_3^{-}. In the majority of the groundwater samples, alkaline earth metals ($Ca^{2+} + Mg^{2+}$) exceed alkali metal cations ($Na^{+} + K^{+}$). The abundance of these ($Ca^{2+} + Mg^{2+}$) in groundwater is endorsed by carbonate mineral weathering which is confirmed through the ($Ca^{2+} + Mg^{2+}$)/TZ^{+} ratio. In our study, groundwater of the area exhibited the dominance of weak acid ($HCO^{-}{}_3$) over strong acid ($SO_4^{2-} + Cl^{-}$).

Table 11.2 Correlation matrix of various analysed ions ($n = 31$)

	pH	EC	TDS	Cl^-	HCO_3^-	SO_4^{2-}	NO_3^-	Ca^{2+}	Mg^{2+}	Na^+	K^+	As
pH	1.00											
EC	−0.34	1.00										
TDS	−0.32	0.96	1.00									
Cl^-	−0.05	0.43	0.42	1.00								
HCO_3^-	−0.21	0.50	**0.49**	−0.41	1.00							
SO_4^{2-}	0.17	0.13	0.14	0.18	−0.25	1.00						
NO_3^-	−0.07	−0.11	−0.09	−0.08	0.09	−0.30	1.00					
Ca^{2+}	−0.15	0.66	**0.66**	0.34	0.48	−0.02	0.01	1.00				
Mg^{2+}	−0.17	0.56	**0.52**	0.20	0.49	0.02	0.04	0.59	1.00			
Na^+	−0.06	0.58	**0.55**	0.32	0.29	−0.10	−0.07	0.06	0.03	1.00		
K^+	0.15	0.13	0.13	0.49	−0.20	0.01	−0.07	0.43	0.41	−0.17	1.00	
As	−0.19	0.34	0.35	−0.10	0.43	−0.19	−0.09	0.35	−0.08	0.33	−0.10	1.00

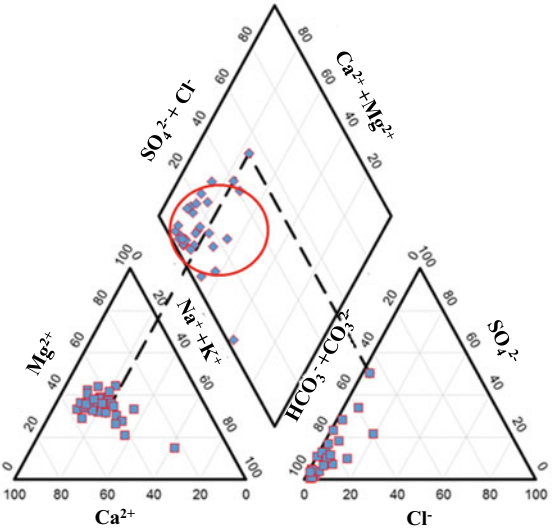

Fig. 11.3 Piper plots for the analysed samples of study area

Groundwater chemical compositions are controlled by a number of factors including geological structure, composition of infiltrating rainwater and mineralogical composition of rocks and anthropogenic activities in the area (Singh et al. 2008; Andre et al. 2005). The geochemical data was plotted on Gibbs's diagram (Gibbs 1970) and showed the ratio of $Na^+/(Na^+ + K^+)$ and $Cl^-/(Cl^- + HCO_3^-)$ versus TDS indicates the dominance of rock weathering in controlling the groundwater chemistry of the study area (Fig. 11.4).

11.3.3 Suitability of Groundwater for Drinking Purposes

The data obtained by hydro-geochemical analyses were evaluated in terms of their suitability for drinking and irrigation uses. The analysed parameters were compared with the standard guideline values recommended by the Bureau of Indian Standards (BIS 2012) for drinking and public health purposes (Table 11.1). The pH of groundwater samples is well within the safe limit of 6.5–8.5 except for one sample, prescribed for drinking water. The values of TDS exceeded the acceptable limit of 500 mg/L in 39% of samples, and none of the samples exceeds the permissible limit of 2,000 mg/L. Out of the 31 samples, 93.50% samples exceeded the acceptable limit for HCO_3^-. None of the samples for Cl^-, SO_4^{2-} and NO_3 showed the exceedance of the acceptable limit of 250 mg/L, 200 mg/L and 45 mg/L, respectively.

The acceptable limit for sodium concentration in drinking water is 200 mg/L (BIS 2012). A higher sodium intake may cause hypertension, congenital heart diseases, nervous disorder and kidney problems. Concentrations of Na^+ are within the acceptable limit of 200 mg/L in all the analysed groundwater samples. The concentration

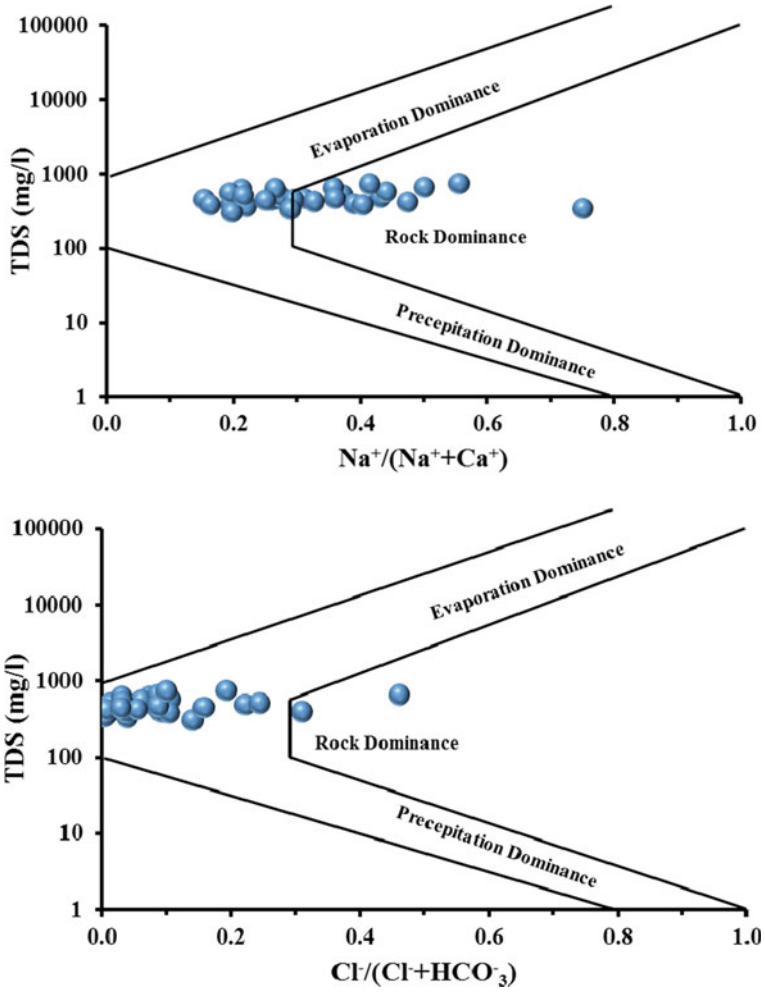

Fig. 11.4 Gibbs's diagram showing groundwater chemical composition

of Ca^{2+} and Mg^{2+} exceeded the acceptable limit of 75 and 30 mg/L in 45.20% and 67.70% of the groundwater samples, respectively. Calcium and magnesium are essential elements for the bone, nervous system and cell development. One possible adverse effect of ingesting a high concentration of Ca^{2+} for long periods may be an increased risk of kidney stones (Maragella et al. 1996).

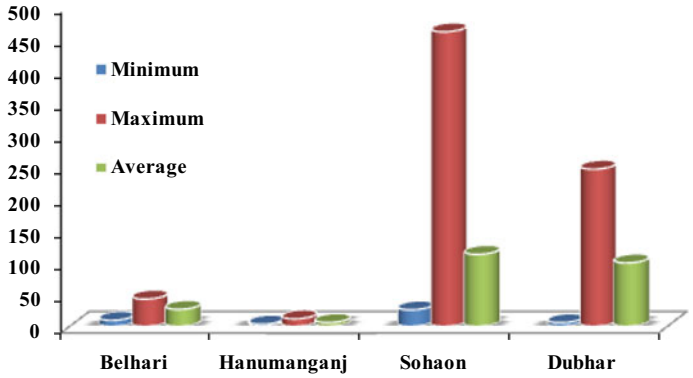

Fig. 11.5 Bar plots indicating blockwise **c**oncentrations of arsenic (ppb), in the study area

11.3.4 Arsenic Occurrence and Its Suitability for Drinking Purposes

The range of As concentrations varied from not detected to 461.10 ppb (average: 73.6 ppb). The acceptable and permissible limit for As is 10 and 50 ppb as per BIS, 2012. 70% of the analysed samples were found to exceed the acceptable limit. The bar chart of arsenic concentration (Fig. 11.5) showed that Sohaon and Dubhad blocks are the main hot spots for elevated Arsenic with concentrations varying from 25.7 to 461.1 and 5.6 to 246.0 ppb, respectively. On the other hand, the groundwater samples from Hanuman-Ganj and Belhari blocks showed less concentration of arsenic. High arsenic content in the groundwater samples of the Ballia district has also been reported by other researchers (Kumar et al. 2010; Chauhan et al. 2009). Ghosh and Singh (2009) reported that many people are affected by skin lesions in the district.

Spatial heterogeneity of As concentration in groundwater was observed in the study area as can be observed in Fig. 11.6. Hydrological, hydro-geological and hydro-geochemical characteristics of aquifers should be studied to understand the rampant occurrence of As in alluvial formation. The non-uniformity of As occurrence for the aquifers present in the alluvial flood plains has been reported by different investigators (Chauhan et al. 2009).

11.3.5 Suitability for Irrigation Uses

Total salt concentration (EC), sodium adsorption ratio (SAR), sodium percentage (Na%) and magnesium hazard (MH) are the important parameters which are widely used in assessing the suitability of water for irrigation uses (Ayers and Westcot 1985). Electrical conductivity (EC) and sodium concentration are very important in classifying irrigation water. Excess concentration of sodium in water affects soil properties

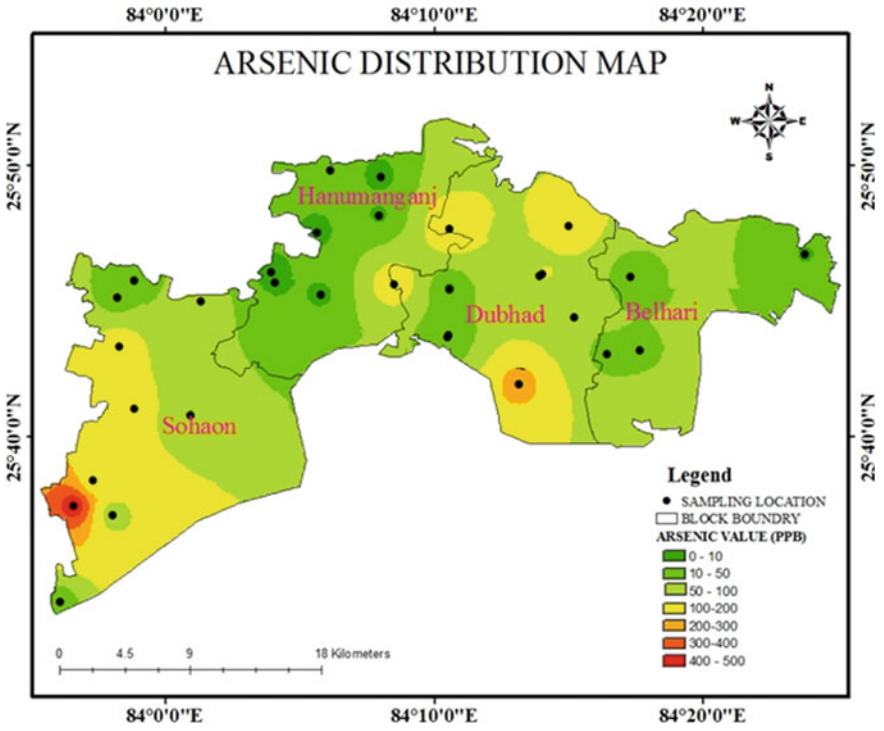

Fig. 11.6 Spatial distribution map of As concentration (ppb) in the groundwater samples of the study area

by replacing cations in soil and hence it is an important criterion in irrigation water classification. The extent of this replacement is estimated by sodium percentage (Na%) and sodium adsorption ratio (SAR) (Purushothaman et al. 2013; Singh et al. 2012).

Sodium Per Cent (Na%)

The Na% in the water samples is calculated by the equation:

$$\text{Na\%} = (\text{Na} + \text{K})/(\text{Ca} + \text{Mg} + \text{Na} + \text{K}) \times 100$$

The sodium percentage in the study area ranges from 14.6 to 68.85% (Avg: 27.41%). High Na% causes deflocculating and impairment of the tilth and permeability of soils. In general, as per the BIS guidelines for the quality of irrigation water, maximum sodium of 60% is recommended for irrigation water. The plot of analytical data on the Wilcox diagram (Wilcox 1955) relating electrical conductivity (EC) to Na% shows that Na% is well within the recommended values, and in general groundwater is excellent in quality for irrigation purposes (Fig. 11.7).

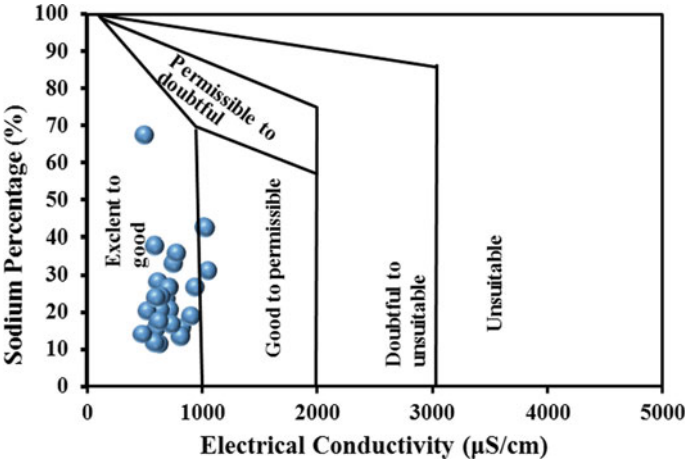

Fig. 11.7 Rating of groundwater samples on the basis of electrical conductivity and per cent of sodium (after Wilcox 1948)

11.3.6 Sodium Adsorption Ratio (SAR)

The suitability of groundwater for irrigation purposes is also studied based on USSL classification (plot between electrical conductivity and sodium adsorption ratio (USSL 1954)). In this diagram, irrigation water is classified as low (EC = <250 µS cm^{-1}), medium (250–750 µS cm^{-1}), high (750–2,250 µS cm^{-1}) and very high (2,250–5,000 µS cm^{-1}) salinity classes. The salinity hazard, a measure of TDS expressed in terms of EC, reduces the osmotic activity of plants and thus interferes with the adsorption of water and nutrient from the soil (Saleh and Du 2004). It is considered that high EC in water leads to the formation of saline soil and similarly; a high sodium concentration leads to the formation of alkaline soil. Salinity problem is generally encountered in irrigated agriculture where drainage is poor. Due to poor drainage, the water table rises close to the root zone of plants, causing the accumulation of sodium salts in the soil solution through capillary rise following surface evaporation of water. The sodium or alkali hazard in the water for irrigation is determined by calculating SAR which is expressed below

$$\mathrm{SAR} = \mathrm{Na}/\left[(\mathrm{Ca} + \mathrm{Mg})/2\right]0.5$$

The calculated value of SAR in the study area ranged 0.34–3.34 meq/l (Avg: 0.94). The plot of data on the US salinity diagram, in which the EC is taken as salinity hazard and SAR as alkalinity hazard, shows that majority of the water samples fall in the categories C2S1 and C3S1 indicating medium to high salinity and low medium alkali water (Fig. 11.8). Thus, it can be concluded that this water can be used for plants with good salt tolerance (Table 11.3).

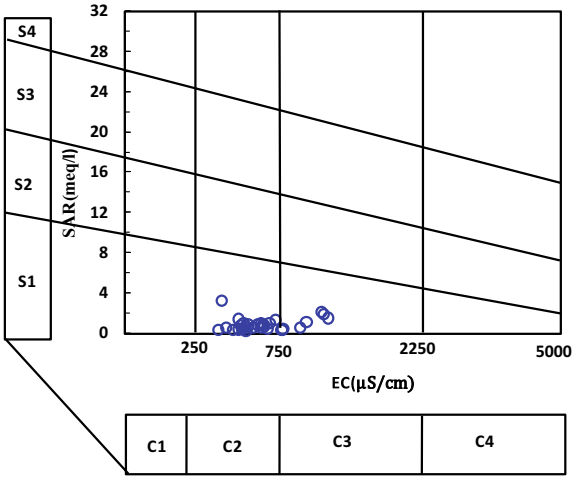

Fig. 11.8 Irrigation water classification based on sodium adsorption ratio (SAR) and EC

Table 11.3 Irrigation waters classified into four categories on the basis of SAR and EC

SAR	Water category	% sample	EC µS/cm	Water category	% sample
0–10	Excellent (S-1)	100	<250	Low (C-1)	0.0
10–18	Good (S-II)	–	250–750	Medium (C-II)	70.9
18–26	Fair (S-3)	–	750–2250	High (C-3)	29.1
>26	Poor (S-4)	–	>2250	Very High (C-4)	0.0

11.4 Conclusion

The groundwater chemistry of the study area showed the dominance of cations in the order $Ca^{2+} > Mg^{2+} > Na^{+} > K^{+}$. Alkaline earths ($Ca^{2+}$ and Mg^{2+}) account for 72.0% of the total cation concentrations (TZ^{+}). The anion chemistry of the analysed samples follows the abundance order of $HCO_3^{-} > Cl^{-} > SO_4^{-} > NO_3^{-}$. The Piper plot of chemical data revealed that the major water type is Ca^{2+}-Mg^{2+}-HCO_3^{-} as the dominant hydro-geochemical facies. Water chemistry of the study area strongly reflects the dominance of weathering of rock-forming minerals with secondary inputs from anthropogenic and atmospheric sources. Wilcox plot indicates that groundwater of these four blocks of Ballia is excellent to permissible quality for irrigation purposes. Based on the US salinity diagram, it can be concluded that the majority of the water samples fall in the categories C2S1 and C3S1 indicating medium to high salinity and low alkalinity. High arsenic concentrations were observed in the Sohaon and Dubhad block area in comparison to Hanuman-Ganj and Belhari blocks. In current study, results reveal that about 70.9% of analysed sample exceeded the acceptable limit >10 ppb (according to BIS standards, 2012) of the arsenic in drinking water.

References

Andre L, Franceschi M, Pouchan P, Atteia O (2005) Using geochemical data and modelling to enhance the understanding of groundwater flow in a regional deep aquifer, Aquitaine Basin, south-west of France. J Hydrol 305:40–62

APHA, AWWA, WEF (2012) Standard methods for the examination of water and wastewater, 22nd edn. American Public Health Association, Washington, DC

Ayers RS, Westcot DW (1985) Water quality for agriculture. Food and Agriculture Organization of the United Nations, Rome 29:174

Berg M, Tran HC, Nguyen TC, Pham HV, Schertenleib R, Giger W (2001) Arsenic contamination of groundwater and drinking water in Vietnam: a human health threat. Environ Sci Technol 35:2621–2626

BIS (2012) Draft Indian Standard drinking water-specification (Second Revision of IS 10500) ICS No. 13.060.20

CGWB (1997) High arsenic ground water in West Bengal. Technical report, series D, Central Ground Water Board (CGWB), Eastern Region, Calcutta, Government of India

Choubisa SL, Choubisam L, Choubisa DK (2001) Endemic fluorosis in Rajasthan. Indian J Environ Health 43:177–189

Chakraborti D, Mukherjee SC, Pati S, Sengupta MK, Rahman MM, Chowdhury UK, Lodh D, Chanda CR, Chakraborti AK, Basu GK (2003) Arsenic groundwater contamination in middle Ganga plain, Bihar, India: a future danger. Environ Health Prospect 111:1194–2120

Chakrapani GJ, Saini RK, Yadav SK (2009) Chemical weathering rates in the Alaknanda–Bhagirathi river basins in Himalayas, India. J Asian Earth Sci 34(3):347–362

Chauhan VS, Nickson RT, Chauhan D, Iyengar L, Sankararamakrishnan N (2009) Groundwater geochemistry of Ballia district, Uttar Pradesh, India and mechanism of arsenic release. Chemosphere 75:83–91

Datta DV, Kaul MK (1976) Arsenic content of tube well water I villages in northern India. A concept of arsenicosis. J Assoc Physicians India 24:599–604

Ghosh NC, Singh RD (2009) Groundwater arsenic contamination in India: vulnerability and scope for remedy

Gibbs RJ (1970) Mechanism controlling world water chemistry. Science 17:1088–1090

Kumar P, Kumar M, Ramanathan AL, Tsujimura M (2010) Tracing the factors responsible for arsenic enrichment in groundwater of the middle Gangetic Plain, India: a source identification perspective. Environ Geochem Health 32:129–146

Maragella M, Vitale C, Petrarulo M, Rovera L, Dutto F (1996) Effects of mineral composition of drinking water on risk for stone formation and bone metabolism in idiopathic calcium nephrolithiasis. Ciln Sci 91:313–318

McArthur JM, Banerjee DM, Hudson-Edwards KA, Mishra R, Purohit R, Ravenscroft P, Cronine A, Howartha RJ, Chatterjee A, Talukder T, Lowry D, Houghton S, Chadha DK (2004) Natural organic matter in sedimentary basins and its relation to arsenic in anoxic ground water: the example of West Bengal and its worldwide implications. Appl Geochem 19:1255–1293

Mukherjee A, Sengupta MK, Hossain MA, Ahamed S, Das B, Nayak B, Lodh D, Rahman MM, Chakraborti D (2006) Arsenic contamination in groundwater: a global perspective with emphasis on the Asian scenario. J Health Popul Nutr 24:142–163

Nicholas CP, Benjamin CB, Andrew NQ, Joshua DL, Michael S (2008) Geomorphic controls on groundwater arsenic distribution in the Mekong River Delta, Cambodia. Geology 36:891–894

Purushothaman P, Rao MS, Rawat YS, Kumar CP, Krishna G, Parveen T (2013) Evaluation of hydrogeochemistry and water quality in Bist-Doab region, Punjab, India. Environ Earth Sci 72(3):693–706

Saleh A, Du B (2004) Evaluation of SWAT and HSPF within BASINS program for the upper North Bosque River watershed in central Texas. Trans ASAE 47(4):1039

Singh AK, Mondal GC, Kumar S, Singh TB, Tewary BK, Sinha A (2008) Major ion chemistry, weathering processes and water quality assessment in upper catchment of Damodar River basin, India. Environ Geol 54:745–758

Singh AK, Raj B, Tiwari AK, Mahato MK (2012) Evaluation of hydrogeochemical processes and groundwater quality in the Jhansi district of Bundelkhand region, India. Environ Earth Sci 70(3):1225–1247

Smedley PL, Kinniburgh DG (2002) A review of the source, behaviour and distribution of arsenic in natural waters. Appl Geochem 17:517–568

Subramanian V (2000) Water: quantity-quality perspectives in South Asia. Kingston International Publishers Ltd., Surrey

Tandulkar N, Bhattacharya P, Mukherjee AB (2001) Managing arsenic for our future. In: Proceedings of the international conference on arsenic in the Asia-Pacific region, Adelaide, South Australia, 21–23 November, pp 103–105

USSL (US Salinity Laboratory) (1954) Diagnosis and improvement of saline and alkali soils. US Department of Agriculture Hand Book, No. 60

Van Geen A, Zheng Y, Versteeg R, Stute M, Horneman A, Dhar R, Steckler M, Gelman A, Small C, Ahsan H, Graziano JH, Hussain I, Ahmed KM (2003) Spatial variability of arsenic in 6000 tube wells in a 25 km^2 area of Bangladesh. Water Resour Res 39:1140

Wilcox LV (1955) Classification and use of irrigation waters. US Department of Agriculture, Circular 969, Washington, DC, USA

Chapter 12
Assessment of Hydraulic and Geoelectric Parameters of the Aquifers and Their Relationship Using Vertical Electrical Sounding in Gurpur Watershed, West Coast of India

H. S. Virupaksha

Abstract The investigation of the nature of subsurface formations by studying the variations in their electrical properties is the electrical resistivity method. 35 Vertical Electrical Soundings (VES) are conducted using a four-electrode Schlumberger array (1-D arrangement) with an electrode spacing (AB/2) separation up to 200 m. The Inverse Slope Method (ISM) is used for data interpretation. The computer iterative java supported software ATS 3.0 is used to process the data. Based on the obtained results, the hydraulic and geoelectric parameters are inferred. The overall layer resistivity values of all the layers are found to be in the range of 14 Ωm (VES 3)–7958 Ωm (VES 31). The overall thicknesses of the geoelectrical layers are found to be in the range of 1.3 m (VES 23)–76.2 m (VES 11). The depth to bedrock varies in the range of 3.7 m (VES 2)–44.4 m (VES 10). The aquifer thickness (h) varies from 19.5 m (VES 19) to 149.5 m (VES 15). The average values of Porosity, Hydraulic Conductivity, and Transmissivity are 28.4%, 0.23 m/day, and 15.9 m^2/day, respectively. The correlation of hydraulic conductivity (K) with the porosity (Ø), transmissivity (T), longitudinal unit conductance (S), and aquifer anisotropy (λ) shows a positive correlation (>0.7). The correlation of K to layer resistivity (ρ_0) and transverse unit resistance (TR) shows a good but negative correlation (< −0.7). The T shows a good correlation with S, λ, and K but a moderate correlation with Ø and Formation factor.

Keywords Electrical resistivity · Hydraulic conductivity · Transmissivity · Porosity · Gurpur

H. S. Virupaksha (✉)
Civil Engineering Department, National Institute of Technology Karnataka, Srinivasnagar 575025, Karnataka, India
e-mail: virupaksha.773@gmail.com

R. Jha et al. (eds.), *Groundwater and Water Quality*, Water Science and Technology Library 119, https://doi.org/10.1007/978-3-031-09551-1_12

12.1 Introduction

Groundwater is the most important and abundant source of freshwater available for drinking, domestic, irrigation, and industrial purposes. Even though groundwater is a naturally occurring renewable resource, still it is a very rare commodity in certain parts of the world. Therefore, there is a need for groundwater studies, and the understanding of the complexity of subsurface formation is of major concern. The nature of subsurface formations can be understood, by studying the variations in their electrical properties, by a Geophysical method known as the electrical resistivity method. Though 2D imaging and 3D tomography provide better results (Loke 2001; Kirsch 2006), they also have their disadvantages. The vertical electrical sounding (four-electrode arrangement) is still the important method in subsurface exploration (depth probing) because of good resistivity contrasts among the various lithological units, controlled depth of investigation, ease of operation, and inexpensive tools (Ali et al. 2015; Selvam 2016). Application of Geophysical, Remote Sensing (RS), and Geographical Information System (GIS) is highly helpful in the exploration of groundwater and subsurface formations (Anbazhagan et al. 2015; Selvarani et al. 2016).

During field investigations, the resistance (R) and thickness (h) are measured directly from the field data using computer iterative modeling techniques (Mahala et al. 2013; Eke et al. 2015). The most widely used configuration in electrical prospecting is the Schlumberger array, which assumes the subsurface formations to be horizontal.

This is the disadvantage in the case of non-horizontal formations, which yields distorted results (Loke 2001; Woobaidullah et al. 2008; Gupta et al. 2014, 2015; Majumdar et al. 2016). Delineation of Groundwater Potential Zones (GWPZ) can be done using VES data (Sreedevi et al. 2005; Shantharam and Elangovan 2018). Other than groundwater exploration and understanding subsurface lithology, studies can also be carried out on aquifer geoelectric parameters (Porosity and Formation Factor) and hydraulic parameters (Transmissivity and Hydraulic Conductivity) using VES data (Usman et al. 2015; Singh and Singh 2016; Thomas et al. 2018). As suggested by Maillet (1947), the average geoelectrical properties of the subsurface formations can be outlined by parameters known as Dar-Zarrouk (D-Z) Parameters. The thickness and the resistivity of the different geoelectrical layers help obtain these parameters. The D-Z parameters coupled with pumping test results help establish empirical relationships and the hydraulic behavior of the aquifers (Vereecken et al. 2006, Aretouyap et al. 2018).

There are several techniques available for interpretation based on different methodologies. However, the present study utilizes the Inverse Slope Method (ISM) and its contribution for understanding groundwater exploration, hydraulic and geoelectric parameters and their relationship.

12.2 Study Area

The Gurpur watershed comes on the southwest coast of peninsular India. The study area covers Dakshina Kannada district and parts of Udupi district (Karkala and Moodbidri taluk) in Karnataka state. The catchment is divided into high land/ghats, midland/hinterland, and low land/coastal regions based on terrain features and altitude (Neilson, 1972).

The study area (Fig. 12.1) is bound by Longitude 74° 47′ 31″ E to 75° 17′ 28″ E and 12° 50′ 02″ N to 13° 11′ 21″ N Latitudes, and the total area of the catchment is 877 km^2. There are majorly three types of soils found in the study area like alluvium, red loamy, and laterites. The weathered zone thickness including topsoil ranges between 20 and 40 m (Reghunath 1999). The Gurpur River, when reaches the lower coastal region, will traverse in perpendicular (South) direction to its earlier flow and confluence with Nethravathi River and flows into the Arabian Sea.

The climate of the Dakshina Kannada district is similar to other parts of the west coast of India. The Gurpur watershed experiences heavy rainfall and most of it is due to Orographic and Convective precipitation and high humidity (>78%). The average temperature throughout the year is around 30 °C ± 5. The average runoff for the past 16 years is found to be 3500 mm for the Gurpur-Nethravathi River basin, and the potential evapotranspiration is estimated as 1400 mm along the coast and average rainfall of about 3789.9 mm, which is the average of 30 years from 1971 to 2000 (Central Groundwater Board 2012).

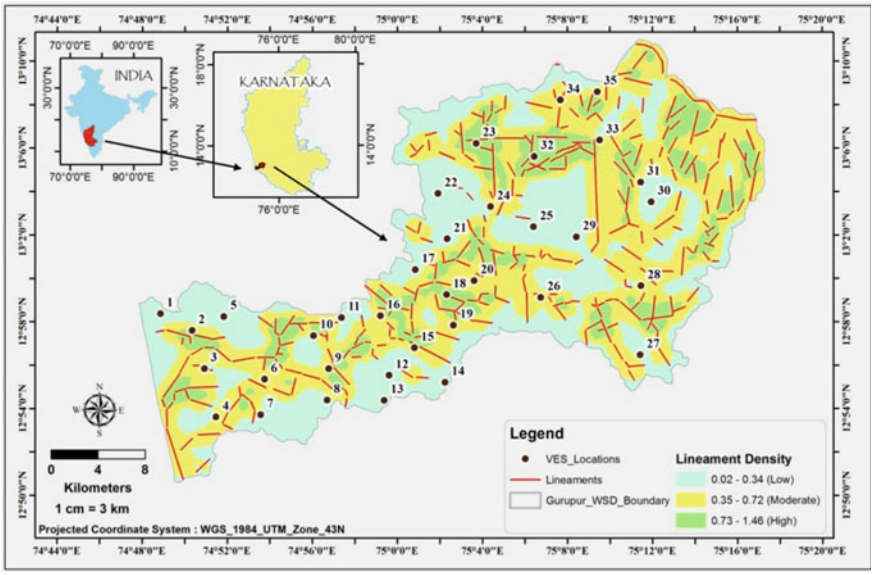

Fig. 12.1 Lineaments, lineament density, VES locations, and base map of Gurpur watershed

12.2.1 Geology

The Laterite capping can be seen as isolated patches on the west coast of India. The composition of laterite varies with the composition of the bedrock and the chemical decay (Ushie and Anike 2011). A significant proportion of laterite will be clay material. The major litho-unit is Peninsular Gneiss and minor litho-units like laterite and amphibolite (Gurumurthy 2013). The general litho-stratigraphic sequence of the Dakshina Kannada district is given by Balasubrahmanyan (1978).

Recent	Gravel and sand deposits (marine and fluvial)
Tertiary	Laterites
Proterozoic	Dolerite dykes Younger green stones (metasediments and metavolcanics)
Archaean	Granitoids, Charnockites, and other metamorphic rocks

12.3 Materials and Methods

12.3.1 Data Acquisition

The state-of-the-art microprocessor-based data acquisition system, Model SSR-MP-ATS signal stacking-based Signal Enhancement Resistivity meter possesses innovative features and advanced digital circuitry. This instrument gives the apparent resistivity (ρ_a) directly along with its corresponding depth values. 35 Vertical Electrical Soundings (VES) are carried out with current electrode spacing $\left(\frac{AB}{2}\right)$ up to 200 m.

The Schlumberger configuration is a four-electrode arrangement (A, M, O, N, and B) placed along a straight line with center 'O', respectively, in the same order. The outer terminals are current electrodes (AB) whereas the inner terminals are potential electrodes (MN). The electrode separation between AB and MN will be more for greater distances (Ramanuja Chary 2012; Poongothai and Sridhar 2017). The formula for calculating Apparent resistivity (ρ_a) can be seen in Eq. (12.1).

$$\rho_a = \left[\frac{\pi\left[\left(\frac{AB}{2}\right)^2 - \left(\frac{MN}{2}\right)^2\right]}{2\left(\frac{MN}{2}\right)}\right] * (R) \tag{12.1}$$

where R is the resistance offered by the material.

12.3.2 Interpretation of Resistivity Sounding Data

There are different methods of analyzing the resistivity sounding data like Qualitative and Quantitative methods. Again, there are several methods in the quantitative interpretation method. In the present study, the Inverse Slope Method (ISM) that is a direct method suggested by Narayan and Ramanujachary (1974) is used. For Schlumberger configuration, the plotting of ISM is done for $\left(\frac{AB}{2}\right)/\rho_a$ in Y-axis against $\left(\frac{AB}{2}\right)$ in X-axis. Similar to Curve Matching Technique (CMT), this method also utilizes best fitting straight-line segments, but when compared to conventional methods here the negative slope indicates the greater resistance. The exact thickness and depth of each layer are indicated with a sharp boundary. Once the profile line is ready, the slope for each segment is calculated and the true resistivity is obtained.

In the present study, the ISM Java-based software ATS-3.0 is used, in which the graph can either be obtained automatically with tolerance percentage or by manually joining the segments.

The layer resistivity (ρ) and layer thickness (h) are the important components of geoelectric layers. Utilizing these components, we can find out Dar Zarrouk (D-Z) parameters (Maillet 1947) which are,

A. Longitudinal Unit Conductance (S)
B. Transverse Unit Resistance (TR)
C. Aquifer Anisotropy (λ).

The S can be determined using the equation,

$$\mathrm{S} = \sum_{i=1}^{n} \frac{h_i}{\rho_i} \tag{12.2}$$

where h is layer thickness and

ρ is layer resistivity for 'n' number of layers.

The variation of the S value of each layer can be utilized qualitatively to identify the low resistivity materials and their thickness (Zohdy 1969). The high thickness of the layers is interpreted by large values whereas the lesser thickness of the shallow basement can be interpreted by smaller values of S.

The equation for TR is,

$$\mathrm{TR} = \sum_{i=1}^{n} h_i * \rho_i \tag{12.3}$$

where h is layer thickness, ρ is layer resistivity.

The λ can be determined using the equation,

$$\lambda = \sqrt{\mathrm{TR}} * \left(\frac{\mathrm{S}}{H}\right) \tag{12.4}$$

where H is the total thickness

Usually, λ will be near to unity and exceeds for the rocks having high resistivity indicating that the lesser the λ, the greater will be the Porosity and permeability (Keller and Frischknecht 1966).

The three factors useful in determining the amount of groundwater recharging in an unconfined aquifer are,

A. The amount of precipitation available for recharge (after evapotranspiration and runoff).
B. Vertical hydraulic conductivity of the formations within the recharge area will provide the volume of downward movement of recharged water to the aquifer.
C. Transmissivity of the aquifer and potentiometric gradient, indicating the Nett amount of water moving from recharge area.

The hydraulic and geoelectric parameters of an aquifer and their relationship are controlled by the composition and subsurface lithology of the aquifers (Niwas et al. 2003). If the aquifers transmit the maximum amount of water, indicates the possibility for recharge potential especially in humid regions. Lessor no transmissivity of the aquifers below the groundwater table indicates either the poor hydraulic conductivity or the lack of a potential recharge zone. The highly resistive subsurface medium shows an inverse relationship with the hydraulic flow (K) and electric current (ρ) passing horizontally in a typical unit column of an aquifer. The electric current in the highly conductive medium will exhibit vertical flow but hydraulic conductivity exhibits horizontal flow, indicating the direct relationship between ρ and K.

The hydraulic conductivity (K) can be expressed as

$$K = [(8 * 10^{-6}) * (e^{-0.0013\rho})] \tag{12.5}$$

Consider the unit cross-section of an aquifer medium from top to bottom in the vertical prism form; the K obeys Darcy's law and ρ in the aquifer medium obeys Ohm's law. These two laws are combined using prism form (Niwas and Singhal 1981). Therefore, for the K and ρ in a horizontal direction, the equation for the T of the aquifer medium is given by

$$T = [(8 * 10^{-6}) * (e^{-0.0013\rho})] * h \tag{12.6}$$

where ρ is bulk resistivity and

h is the thickness of the aquifer medium.

The aquifer medium with uniform resistivity and saturated with water will be constant for either TR or S. Therefore,

$$T = S \tag{12.7}$$

From Eq. (12.7), it is evident that for the highly resistive aquifer medium, the transmissivity will be proportional to longitudinal unit conductance. Also for a highly

conductive medium, the transmissivity is proportional to the transverse unit resistance (Niwas et al. 2011).

All the minerals and rocks have high resistivity except a few. Therefore, the electric current passing through water-saturated pore spaces will exhibit less resistivity. From Archie's law (Archie 1942), the resistivity of the saturated clay-free material can be expressed as

$$F = \left(\frac{\rho_0}{\rho_w}\right) \tag{12.8}$$

where ρ_0 is the resistivity of water-saturated sand.

ρ_w is the resistivity of pore space water.

F is intrinsic formation factor that includes all the properties of the material influencing electrical current flow.

The relationship between F and $\emptyset$ was first postulated by Humble oil company. The constants a and m are empirical with values 1 and 2, respectively, for a general average of typical reservoir rocks (Winsauer et al. 1952). The ρ_w can be measured using the equation

$$\rho_w = \left(\frac{10{,}000}{EC}\right) \tag{12.9}$$

where EC is the electrical conductivity (μS/cm) of the water sample of the aquifer.

Where the porosity ($\emptyset$) can be obtained through the equation

$$\emptyset = \left(\frac{a}{F}\right)^{\frac{1}{m}} \tag{12.10}$$

where m is the material constant.

a is an empirical constant.

12.4 Results and Discussion

12.4.1 Qualitative and Quantitative VES Analysis

35 soundings are interpreted using the direct method, which is a quantitative interpretation method, and the statistics of which are shown in Table 12.1. The graphs and geoelectric section of the soundings are prepared and interpreted using ISM (Fig. 12.3a, b). The top layer resistivity is found to be in the range of 74 Ωm (VES 5) to 5458 Ωm (VES 33), and the thickness is from 1.3 m (VES 7) to 21.6 m (VES 19). The selected graphs VES-18 and VE-20 are shown here for representation purposes

Table 12.1 Quantitative analysis of the VES data interpreted using inverse slope method

VES number	VES location	Number of layers	R1	R2	R3	R4	R5	T1	T2	T3	T4	Depth to bedrock	Aquifer thickness (h)
1	Kulai	2	1776	2156	∞			4.9	5.5			4.9	67.8
2	Tokuru 62	4	110	∞	17.5	182		3.7	8.1	29.2		3.7	125.7
3	Kunjathbailu	3	144	14	36			3.3	11.8			15	61.7
4	Bondel	4	296	552	396	3168		2.4	4.6	13.8		20.8	64.2
5	Bajpegrama	4	74	∞	379	238		5.1	15.6	24.1		5.1	94.3
6	Moodushedde	4	1235	2222	∞	6461		3.9	1.4	33		5.3	101.4
7	Paldaane/Kudupu	5	820	319	841	4211	∞	1.3	5.6	16.1	9.8	41.8	102.3
8	Fermai	4	1397	2159	531	207		5.9	27.5	27.9		33.5	108.1
9	Addoor	5	1375	734	1212	∞	6531	4.4	11.3	27.1	21.3	42.7	38.4
10	Gurpura	4	3277	901	2192	572		8.4	11.9	24.1		44.4	85.6
11	Ganjimatha	4	2514	1321	5650	∞		6.8	24.2	76.2		31	100.4
12	Kaavagudde	4	431	331	2335	500		2.8	12.1	54.6		32.9	72.1
13	Benjanapadavu	5	1544	2786	1899	∞	7197	8	4.1	3.1	22.8	12.1	95
14	Loretto	4	558	77	759	∞	∞	2.7	5.2	8	27.7	15.9	116.4
15	Varmala	5	234	478	4571	1600	∞	4.3	6.4	29.7	23.9	40.5	149.5
16	Kuppepadavu	4	1195	252	565	157		17.1	59.9	29.3		17.1	112.9
17	Iruvailu	4	1112	398	117	∞		16.2	25.4	24.3		16.2	49.7
18	Konnepadavu	5	1846	370	∞	50	∞	8.7	14.3	19.9	22.3	23	22.3
19	Malanturuguttu	4	639	1099	20	∞		21.6	42.2	19.5		21.6	19.5
20	siddakatte	5	523	∞	2284	859	∞	8.1	8.3	26.2	43	16.4	69.2
21	Pucchamogaru	4	1135	923	111	∞	∞	1.9	21.3	1.5	21.3	42.7	53.1

(continued)

Table 12.1 (continued)

VES number	VES location	Number of layers	R1	R2	R3	R4	R5	T1	T2	T3	T4	Depth to bedrock	Aquifer thickness (h)
22	Kallabettu	3	2060	5000	∞	∞	∞	5.6	1.5	27	2.2	16.1	96.7
23	Maarnad	5	1250	502	5000	405	∞	1.3	3.9	2.3	3.6	7.6	30.6
24	Maroor	5	984	2044	80	29	∞	9.6	6.6	5.2	21.3	16.2	26.5
25	Padanthadka	4	1348	816	∞	1761		21.6	2.6	23.3		42.1	94.6
26	Vamanapadavu	5	462	761	∞	1893	∞	11	32.1	21	21.3	43.0	21.3
27	Nadubottu	5	3360	221	586	3678	∞	8.9	23.2	1.6	21.3	8.9	56.1
28	Gardady	4	1238	183	418	∞		1.7	8.2	65.9		10.7	75.6
29	Moodukodi	4	5163	1573	562	∞		16.5	15.3	53.9		16.5	69.2
30	Pillya	4	296	132	∞	∞	101	3.3	7.6	21	21.3	11	41.7
31	Sulkeri	5	330	1864	3587	∞	7958	2	6.9	23.3	22.5	8.9	60.2
32	Kashipatna	3	1111	1047	2033			8.2	9.1			17.3	47.4
33	Naravi	4	5458	7287	2623	1014		4.1	28.8	22		4.1	82.1
34	Hosmar	4	837	3275	∞	5105		7.4	8.5	2.2		15.9	61.9
35	Eedu	5	583	136	288	514	∞	7.8	11.6	22.3	31.8	7.8	66.7

of the ISM data interpretation. The overall resistivity values are in the range of 14 Ωm (VES 3) to 7958 Ωm (VES 31). The thicknesses of the geoelectrical layers are found to be in the range of 1.3 m (VES 23)–76.2 m (VES 11). The depth to bedrock varies in the range of 3.7 m (VES 2) to 44.4 m (VES 10). The overall aquifer thickness (h) varies from 19.5 m (VES 19) to 149.5 m (VES 15).

The spatial distribution of depth to bedrock (Fig. 12.2) is prepared using the VES data. The depth to bedrock ranging from 9.2 to 25.5 m covers a maximum study area of more than 70% (622.46 km^2). The shallow basement covers 6% (57.01 km^2) of the study area. The deeper basement covers 4% (32.33 km^2). Shallow depth to bedrock can be seen in and around ghats, which extends to midland and also in parts of low lands. The deeper basements are interpreted in the midlands of the study area.

The single-layer sandwiched between two highly resistive rocks is indicated by the single resistivity value (Fig. 12.3a), and the multi-layered (Fig. 12.3b) aquifer formation shows several layers sandwiched between hard rock layers. In such cases, the average resistivity and total thickness of all layers of the aquifer are considered. Likewise, the aquifer resistivity and thickness for the 35 VES locations are considered and utilized for the analysis of the hydraulic and geoelectric parameters. In the present study, only confined aquifers are considered.

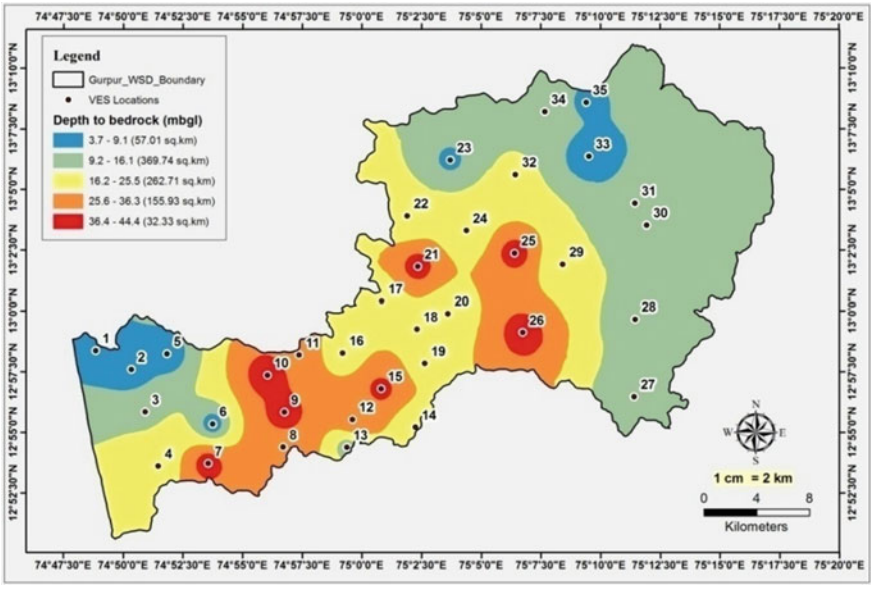

Fig. 12.2 Spatial distribution of depth to bedrock

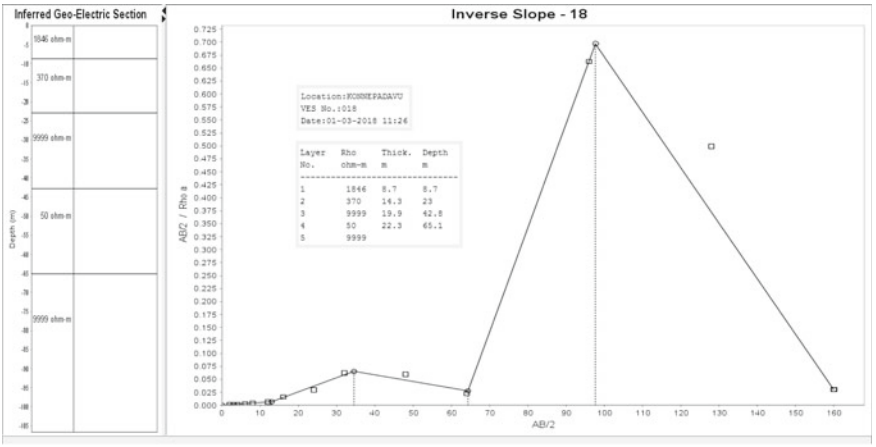

(a)

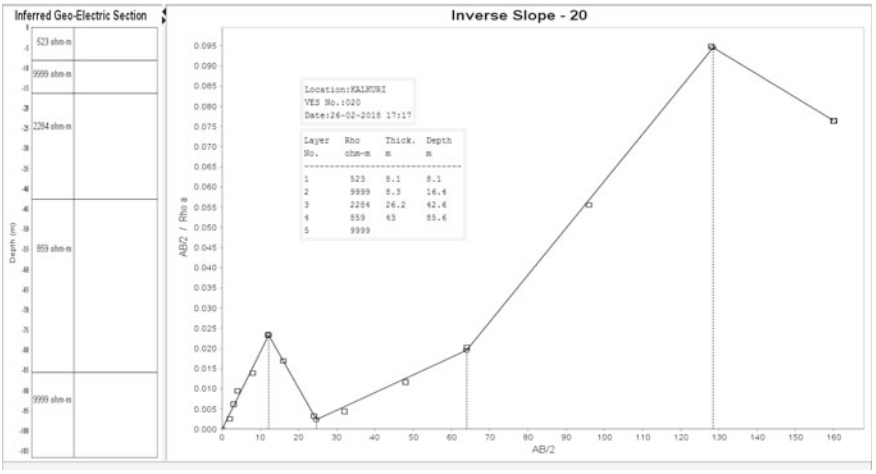

(b)

Fig. 12.3 **a** Selected graph for ISM interpretation (VES-18). **b** Selected graph for ISM interpretation (VES-20)

12.4.2 Hydraulic and Geoelectric Parameters

The aquifer parameters (Table 12.2) are inferred using the aquifer layer resistivity (ρ_0) and thickness (h). The K is in the range of 0.001 m/day (VES 22) to 0.64 m/day (VES 24) with an average of 0.23 m/day. The T is in the range of 0.10 m^2/day (VES 22) to 64.85 m^2/day (VES 24) with an average of 15.92 m^2/day.

The D-Z parameter (Table 12.2) like S is found to be in the range of 0.01 Ω^{-1} (VES 26) to 0.56 Ω^{-1} (VES 02) with an average of 0.13 Ω^{-1}. The TR is in the range

Table 12.2 Aquifer hydraulic and geoelectric parameters for 35 VES locations

VES number	VES location	ρ_0 (ohm-m)	ρ_w (ohm-m)	S (Ohm^{-1})	TR (Ohm m^2)	λ	F	K (m/day)	T (m^2/day)	Φ (%)
1	Kulai	1776	16.8	0.038	120412.8	0.2	105.5	0.069	4.7	9.7
2	Tokuru 62	225	20.7	0.559	28282.5	0.7	10.9	0.516	64.8	30.3
3	Kunjathbailu	144	39.1	0.428	8884.8	0.7	3.7	0.573	35.4	52.1
4	Bondel	3163	44.4	0.020	203064.6	0.1	71.2	0.011	0.7	11.9
5	Bajpegrama	617	49.0	0.153	58183.1	0.4	12.6	0.310	29.2	28.2
6	Moodushedde	3021.5	74.1	0.034	306380.1	0.2	40.8	0.014	1.4	15.7
7	Paldaane/Kudupu	4211	99.0	0.024	430785.3	0.2	42.5	0.003	0.3	15.3
8	Fermai	369	91.7	0.293	39888.9	0.5	4.0	0.428	46.2	49.9
9	Addoor	973	38.3	0.039	37363.2	0.2	25.4	0.195	7.5	19.8
10	Gurpura	572	38.2	0.150	48,963.2	0.4	15.0	0.329	28.1	25.8
11	Ganjimatha	3485.5	42.6	0.029	349944.2	0.2	81.9	0.007	0.7	11.0
12	Kaavagudde	500	153.8	0.144	36,050.0	0.4	3.3	0.361	26.0	55.5
13	Benjanapadavu	4548	142.9	0.021	432060.0	0.1	31.8	0.002	0.2	17.7
14	Loretto	759	40.0	0.153	88347.6	0.4	19.0	0.258	30.0	23.0
15	Varmala	1600	131.6	0.093	239200.0	0.3	12.2	0.086	12.9	28.7
16	Kuppepadavu	324.6	35.5	0.348	36647.3	0.6	9.2	0.453	51.2	33.1
17	Iruvailu	257.5	43.3	0.193	12797.8	0.4	5.9	0.495	24.6	41.0
18	Konnepadavu	210	48.3	0.106	4683.0	0.3	4.3	0.526	11.7	48.0
19	Malanturuguttu	586	35.8	0.033	11427.0	0.2	16.3	0.323	6.3	24.7
20	Siddakatte	1571.5	60.2	0.044	108747.8	0.2	26.1	0.090	6.2	19.6
21	Pucchamogaru	517	138.9	0.103	27452.7	0.3	3.7	0.353	18.7	51.8

(continued)

Table 12.2 (continued)

VES number	VES location	ρ_0 (ohm-m)	ρ_w (ohm-m)	S (Ohm^{-1})	TR (Ohm m^2)	λ	F	K (m/day)	T (m^2/day)	Φ (%)
22	Kallabettu	5000	52.1	0.019	483500.0	0.1	96.0	0.001	0.1	10.2
23	Maarnad	2702.5	48.1	0.011	82696.5	0.1	56.2	0.021	0.6	13.3
24	Maroor	54.5	17.0	0.486	1444.3	0.7	3.2	0.644	17.1	55.9
25	Padanthadka	1288.5	32.1	0.073	121892.1	0.3	40.2	0.129	12.2	15.8
26	Vamanapadavu	1893	91.7	0.011	40320.9	0.1	20.6	0.059	1.3	22.0
27	Nadubottu	1495	87.0	0.038	83869.5	0.2	17.2	0.099	5.6	24.1
28	Gardady	300.5	32.4	0.252	22717.8	0.5	9.3	0.468	35.4	32.8
29	Moodukodi	1067.5	55.9	0.065	73871.0	0.3	19.1	0.173	11.9	22.9
30	Pillya	101	26.7	0.413	4211.7	0.6	3.8	0.606	25.3	51.5
31	Sulkeri	4469.6	243.9	0.013	269069.9	0.1	18.3	0.002	0.1	23.4
32	Kashipatna	1540	75.8	0.031	72996.0	0.2	20.3	0.093	4.4	22.2
33	Naravi	1818.5	42.9	0.045	149298.9	0.2	42.4	0.065	5.3	15.4
34	Hosmar	4190	263.2	0.015	259361.0	0.1	15.9	0.003	0.2	25.1
35	Eedu	312.6	64.1	0.213	20850.4	0.5	4.9	0.460	30.7	45.3
Average		**1590.39**	**71.91**	**0.13**	**123304.74**	**0.32**	**26.08**	**0.23**	**15.92**	**28.36**

of 1444.25 Ω m^2 (VES 24) to 483500 Ω m^2 (VES 22). The aquifer anisotropy (λ) is ranging from 0.11(VES 26) to 0.75(VES 02) with an average of 0.32.

The geoelectric parameter (Table 12.2) like the Porosity (Ø) is ranging from 9.74% (VES 01) to 75.57% (VES 35) with an average of 28.36% for the coastal shallow aquifer having lithology of gneiss and charnockites. Also, the lineaments observed are fracture-controlled. The formation factor (F) is ranging from 1.75 (VES 35) to 105.49 (VES 01) with an average of 26.08.

The correlation matrix (Table 12.3) is prepared for the aquifer parameters. It is observed that the correlation for K concerning Ø, T, S, and λ shows a positive and good correlation (>0.7). The correlation for K to ρ_0 and TR shows a good but negative correlation indicating their inverse relationship. The F shows moderate correlation with all the parameters except for Ø. The logarithmic regression equation (Fig. 12.4) for K to Ø shows good correlation with $R^2 = 0.73$ (Eq. 12.11) and for K to F the $R^2 = 0.73$ (Eq. 12.12). The regression equations for T show moderate correlation of $R^2 = 0.5$ for Ø (Eq. 12.14) and the $R^2 = 0.5$ for F (Eq. 12.13). The correlation equations are as follows (Fig. 12.5),

$$K = 0.318 \ln(\text{Ø}) - 0.799 \tag{12.11}$$

$$K = -0.15 \ln(F) + 0.665 \tag{12.12}$$

$$T = -7.25 \ln(F) + 32.45 \tag{12.13}$$

$$T = 15.94 \ln(\text{Ø}) - 38.29 \tag{12.14}$$

Table 12.3 Correlation matrix of hydraulic and geoelectric parameters for 35 VES locations

	ρ_0	h	ρw	S	TR	λ	F	K	T	Φ
ρ_0	1									
h	0.17	1								
ρw	0.50	0.04	1							
S	-0.64	0.12	-0.36	1						
TR	0.92	0.43	0.38	-0.51	1					
λ	**-0.74**	0.16	-0.39	0.98	-0.57	1				
F	0.63	0.14	-0.19	-0.50	0.61	-0.56	1			
K	**-0.84**	-0.17	-0.39	0.86	**-0.73**	0.91	-0.66	1		
T	**-0.70**	0.35	-0.30	0.84	-0.56	0.89	-0.54	0.77	1	
Φ	-0.68	-0.23	0.04	0.68	-0.61	0.74	**-0.76**	0.85	0.58	1

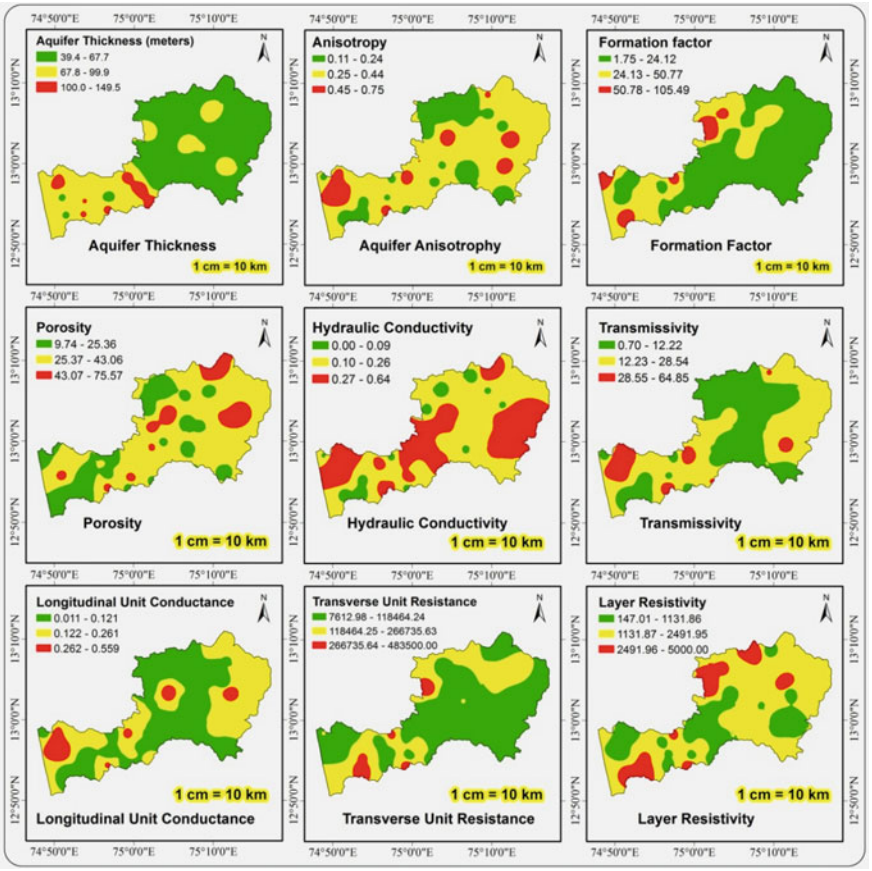

Fig. 12.4 Spatial distribution maps of the aquifer parameters

12.5 Conclusion

The present study is a watershed level study for hydraulic and geoelectric parameters for shallow coastal aquifers. Probing for greater depths was not possible in some VES locations because of the nonavailability of the open space on the surface. Therefore, in such locations, maximum depth of investigation is considered as the lower basement of the aquifer. Unlike the curve matching technique, the Inverse Slope Method gives a sharp boundary for different layers. In the study area, up to 5-layered formations can be observed. The correlation for hydraulic and geoelectric parameters shows a weak to good correlation. This method of calculating hydraulic parameters can be economic, time-saving, and alternative for pumping tests.

In this study, the electrical resistivity method (VES) is used in the exploration and estimation of groundwater. The study also provides a database for assessment,

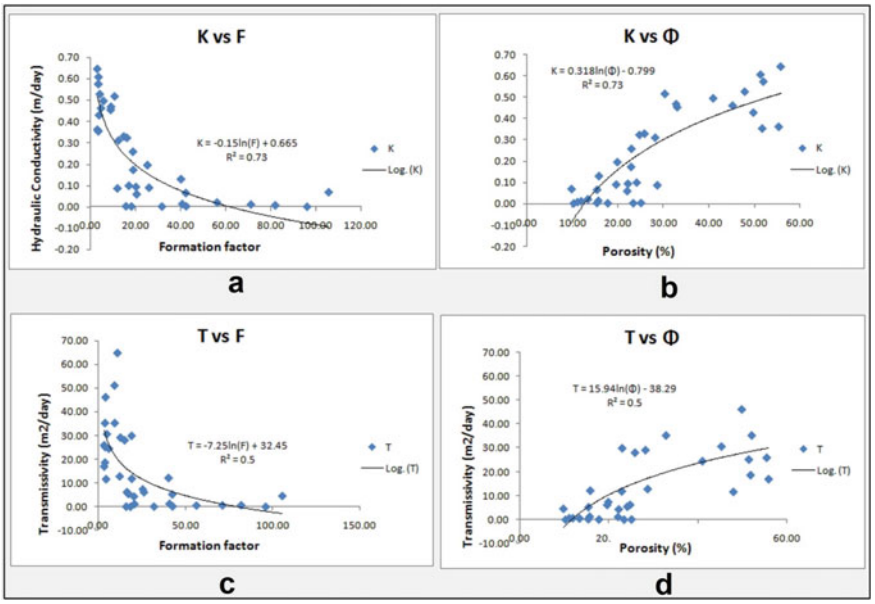

Fig. 12.5 Regression equations for hydraulic and geoelectric parameters

management, and drilling locations of boreholes within the Gurpur watershed. This study can be implemented for other coastal shallow aquifers.

Acknowledgements The author would like to thank the National Institute of Technology Karnataka, Surathkal for providing an Institute Fellowship and facilitating full-time research. Also, the authors like to thank Vignesh Bhat, Venkanagouda B. B. Patil, Kiran, K. O., Shannon M. Pinto, Sowmya, K. O., Thejashree, G., and Krishnamurthy, M. P. for their constant support and for assistance in the field for seeing this work through.

References

Ali YH, Priju CP, Prasad NBN (2015) Delineation of groundwater potential zones in deep midland aquifers along Bharathapuzha river basin, Kerala using geophysical methods. Aquatic Procedia 4:1039–1046

Anbazhagan S, Indhirajith R, Uma Maheshwaran S, Jothibasu A, Venkatesan A, Ramesh V (2015) Electrical resistivity survey and shallow subsurface geological study in hard rock terrain, Southern India. J Geol Soc India 85:305–312

Archie GE (1942) The electrical resistivity log as an aid in determining some reservoir characteristic. Trans Am Inst Min Eng 146:54–62

Aretouyap Z, Bisso D, Njandjock Nouck P, Amougou Menkpa LE, Asfahani J (2018) Hydrogeophysical characteristics of Pan-African aquifer specified through an alternative approach based on the interpretation of vertical electrical sounding data in the Adamawa region, Central Africa. Nat Res Res. https://doi.org/10.1007/s11053-018-9373-8

Balasubrahmanyan MN (1978) Geochronology and geochemistry of Archaean tonalitic gneisses and granites of South Kanara district, Karnataka state, India. In: Windley BN, Naqvi SM (eds) Archaean geochemistry. Elsevier, pp 59–78

Central Groundwater Board (2012) Groundwater information booklet of Dakshina Kannada district, Karnataka, pp 04–11

Eke DR, Opara AI, Inyang GE, Emberga TT, Echetama HN, Ugwuegbu CA, Onwe RM, Onyema JC, Chinaka JC (2015) Hydrogeophysical evaluation and vulnerability assessment of shallow aquifers of the Upper Imo river basin, Southeastern Nigeria. Am J Environ Prot 3(4):125–136

Gupta G, Maiti S, Erram VC (2014) Analysis of electrical resistivity data in resolving the saline and fresh water aquifers in West coast Maharashtra. J Geol Soc India 84:555–568

Gupta G, Patil SN, Padmane ST, Erram CV, Mahajan SH (2015) Geoelectric investigation to delineate groundwater potential and recharge zones in Suki river basin, north Maharashtra. J Earth Syst Sci 124(7):1487–1501

Gurumurthy GP (2013) Major ion, trace element and organic carbon geochemistry of river Nethravati, Southwest Coast of India. Thesis, pp 14–15

Keller GV, Frischknecht FC (1966) Electrical methods in geophysical prospecting. Peramon Press, London, 517 pp

Kirsch R (2006) Groundwater geophysics—a tool for hydrogeology. Springer, Berlin, Heidelberg, New York, p 87

Loke MH (2001) Tutorial: 2-D and 3-D electrical imaging surveys. Published at www.geoelectrical.comp, p 07

Mahala SC, Naik PC, Samal AK, Mohanty S (2013) Integrated geophysical investigation for selection of bore well sites near Rabana village, Jaipur district, Odisha, India. Int J Earth Sci Eng 06(5–1):1236–1242

Maillet R (1947) The fundamental equations of electrical prospecting. Geophysics 12(4):529–556. https://doi.org/10.1190/1.1437342

Majumdar RK, Kar S, Panda A, Samanta SK (2016) Hydrological characterization of budge budge and dum dum areas of South and North 24 Parganas districts, West Bengal using geoelectrical and geochemical methods. J Geol Soc India 88:330–338

Narayan SPV, Ramanujachary KR (1974) An inverse slope method of determining absolute resistivity. Geophysics 32:1036–1040

Neilson E (1972) The philosophy and pedagogy of inter-disciplinary coastal studies and research with particular reference to sedimentary process and morphological and evolutionary features of the Southwest coast of India. Kobenhavn, Denmark

Niwas S, Singhal DC (1981) Estimation of aquifer transmissivity from Dar Zarrouk parameters in porous media. J Hydrol 50:393–399

Niwas S, Olivar AL de Lima (2003) Aquifer parameter estimation from surface resistivity data. Ground Water 41(1):95–99

Niwas S, Tezkan B, Israil M (2011) Aquifer hydraulic conductivity estimation from surface geoelectrical measurements for Krauthausen test site, Germany. Hydrogeol J 19:307–315

Poongothai S, Sridhar N (2017) Application of geoelectrical resistivity technique for groundwater exploration in lower Ponnaiyar sub-watershed, Tamilnadu, India. IOP Conf Ser Earth Environ Sci 80:012071

Reghunath R (1999) Hydrogeological studies of Nethravati River basin, Karnataka State, India. PhD thesis

Ramanuja Chary KR (2012) Geophysical techniques for groundwater exploration (with special reference to resistivity techniques). Professional Books Publisher, Hyderabad, 1st Print, pp 14–15

Selvam S (2016) 1D geoelectrical resistivity survey for groundwater studies in coastal area: a case study from Pearl City, Tamil Nadu. J Geol Soc India 87:169–178

Selvarani GA, Elangovan K, Kumar CS (2016) Evaluation of groundwater potential zones using electrical resistivity and GIS in Noyyal river basin, Tamil Nadu. J Geol Soc India 87:573–582

Shantharam Y, Elangovan K (2018) Groundwater potential zones delineation using geoelectrical resistivity method and GIS for Coimbatore, India. Indian J Geo-Mar Sci 47(05):1088–1095

Singh S, Singh VS (2016) Estimation of hydraulic characteristics from electrical resistivity data in Coastal aquifers of South India. J Geol Soc India 88:77–86

Sreedevi PD, Subrahmanyam K, Ahmed S (2005) Integrated approach for delineating potential zones to explore for groundwater in the Pageru river basin, Cuddapah District, Andhra Pradesh, India. Hydrogeol J 13:534–543

Thomas AH, Fidelis A, Ushie, Okechukwu EA (2018) Hydraulic and geoelectric relationships of aquifers using Vertical Electrical Sounding (VES) in parts of Obudu, Southern Nigeria. World Sci News 94(2):261–275

Ushie FA, Anike OL (2011) Lateritic weathering of granite-gneisis in Obudu Plateau, South Eastern Nigeria. Global J Geol Sci 9(1):75–83

Usman AO, Omada JI, Omali AO, Akakuru OC (2015) Evaluation of the aquifer characteristics of Nteje and Environs, Anambra Basin, South Eastern, Nigeria. J Nat Sci Res 5(14):99

Vereecken H, Binley A, Cassiani G, Revil A, Titov K (2006) Applied hydrogeophysics. ISO Press, Amsterdam and Springer in conjunction with NATO, p 376

Winsauer WO, Shearin HM, Masson PH, Williams M (1952) Resistivity of brine-saturated sands in relation to pore geometry. AAPG Bull 36:253–277

Woobaidullah AS, Chowdhury SH, Ahmed KM, Rahman MW, Arafin KS, Al-Ejaz O (2008) Geo-electrical resistivity survey in the evaluation of hydrogeological condition in Haziganj Upazila, Chandpur District, Bangladesh. J Geol Soc India 72:753–762

Zohdy AAR (1969) The use of Schlumberger and equatorial soundings in groundwater investigations near El Paso, Texas. Geophysics 34(5):713–728

Chapter 13
Performance Monitoring and Re-design of a Traditional Household Filter Unit for Simultaneous Removal of Iron and Fluoride from Groundwater of Assam

Rajyalakshmi Garaga, Sri Harsha Kota, and Mohammad Jawed

Abstract The groundwater of Assam contains excessive amounts of dissolved iron [Fe(II)] and fluoride (F^-). The rural and semi-urban population uses variants of traditional household filter units, developed over past generations to remove Fe(II) from the groundwater. These filter units use river sand, wooden charcoal and gravel. However, the filter unit has neither been evaluated to assess its effectiveness in removing Fe(II) and F^-, if present in the groundwater nor the potential of filtering media been evaluated for its adsorptive capacity. Therefore, there is a need to carry out performance monitoring of a working filter unit in the field and to work out modification in the design if performance is not up to the mark. The field performance monitoring is carried out for a RCC pipe filter unit for 105 days. The Fe(II) in the groundwater varies in the range of 4.0–12.7 mg/L while the filtered water contains Fe(II) in the range of 0.11–0.15 mg/L. However, the F^- in the groundwater varies in the range of 0.5–2.5 mg/L while filtered water contains F^- in the range of 0.8–2.4 mg/L (much above the permissible limit of 1.0 mg/L). The filter unit is effective in removing Fe(II) but it fails to remove F^-. The batch adsorption studies are carried out to assess the adsorptive capacity of processed wooden charcoal (PWC) and processed sand (PS) from mono- and binary-ion systems of Fe(II) and F^-. The batch studies with binary-ion system [comprising of Fe(II) + F^-] indicate only Fe(II) adsorption by PWC while Fe(II) as well as F^- adsorption by PS but with a lesser extend compared to Fe(II) adsorption with PWC. Hence, the logical design approach for simultaneous removal of Fe(II) and F^- from groundwater is to use PWC bed followed by PS bed instead of sand bed followed by wooden charcoal as adopted in the RCC pipe field filter unit. The thickness of PWC and PS beds is estimated based on design parameters obtained for binary-ion system. The re-designed filter is yet to be tested in the field for its effectiveness in simultaneous removal of Fe(II) and F^-.

R. Garaga · S. H. Kota · M. Jawed (✉)
Department of Civil Engineering, Indian Institute of Technology Guwahati, Guwahati 781039, India
e-mail: jawed@iitg.ac.in

R. Jha et al. (eds.), *Groundwater and Water Quality*, Water Science and Technology Library 119, https://doi.org/10.1007/978-3-031-09551-1_13

Keywords Groundwater · Iron · Fluoride · Traditional household filter unit · Adsorption · Potable water

13.1 Introduction

Groundwater—the natural potable water resource is becoming an extremely finite reserve all over the world. The groundwater of Assam—a north-eastern province of India, is contaminated with high concentrations of iron [Fe(II)] and fluoride (F^-) in the range of 1–25 mg/L and 5–23 mg/L, respectively (Ahamad 2005). Severe contamination of groundwater with fluoride has led to fluorosis in consumers (Das et al. 2003). The World Health Organization (WHO) has set a guideline value of 0.3 mg/L and 1.5 mg/L for iron and fluoride, respectively, in drinking water (WHO 1993). Intensive research of the last few decades has led to the development of numerous methods/techniques and solutions to remove these contaminants from groundwater in developing countries including India (Ahamad and Jawed 2010; Suhag 2016). Still, none of these methods/techniques has found application in rural and semi-urban populations of Assam (Ahamad 2010). Rather, traditional indigenous household water filter units (fabricated with filtering medium of wooden charcoal, river sand and gravel) are being used by rural and semi-urban populations for the removal of iron (Das et al. 2007). However, the indigenous household filter units have neither been assessed for its effectiveness in removing iron and fluoride, if present in the groundwater nor the potential of media (wooden charcoal and river sand) been evaluated for its adsorptive capacity for iron and fluoride. Therefore, there is a need to carry out performance monitoring of a working filter unit and to work out modification(s) in the design if performance is not up to the mark for making the groundwater suitable for potable purposes. The present work is an effort in this direction.

13.2 Material and Methods

13.2.1 Monitoring of a Traditional Indigenous Household Filter Unit

A traditional indigenous household filter unit located at N 26°12′09.9″ and E 91°42′01.3″ in Abhoypur, Kamrup district—very close to IIT Guwahati campus is selected for its performance monitoring (Fig. 13.1a). This unit has been fabricated using one circular reinforced cement concrete (RCC) pipe having 0.60 m internal diameter and 1.15 m total height. The RCC pipe has two compartments—top compartment of height 0.80–0.90 m holds the filter media (namely wooden charcoal, river sand and gravel) while the bottom compartment of height 0.25–0.35 m stores the filtered water. The filtering medium is placed in layers: river sand (on top), wooden

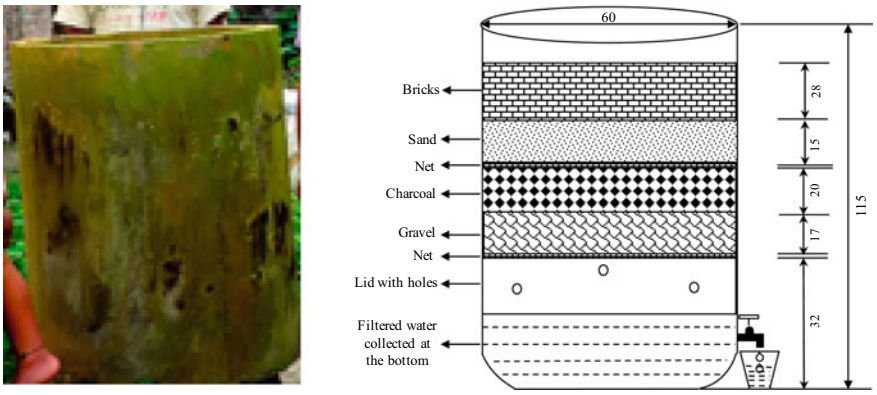

Fig. 13.1 Traditional indigenous household water filter unit: **a** existing field unit and **b** schematic diagram of the unit (All dimensions in cm)

charcoal (in middle) and gravel (at bottom). Bricks are also placed on top of the sand bed to protect it from getting disturbed when the groundwater is poured into the unit. At the interface of sand and charcoal layer as well as below the gravel bed, nylon nets with fine openings are provided to protect sand from getting washed into charcoal medium and into the filtered water respectively. A schematic diagram of the unit is shown in Fig. 13.1b. No specific sizes of sand and gravels are used in the filter while wooden charcoal is used as procured from the local market. Once the filter bed gets clogged, sand and gravel layers are removed from the filter, washed, dried and used again while wooden charcoals are replaced with a new stock as it gets disintegrated over a period of usage. The cost of the filter unit varies in the range of INR 350–500. In order to observe the performance of the selected field filter unit, the inlet and outlet concentrations of Fe(II) and F^- are monitored for 105 days. The samples are withdrawn twice in a week.

13.2.2 Wooden Charcoal

The wooden charcoal for the study (Fig. 13.2a) is obtained from Maligaon—situated at a distance of 13 km from IIT Guwahati campus on the Northern bank of River Brahmaputra. Upon enquiry with local vendors, it was informed that the wooden charcoal is generally prepared from woods obtained from hilltops situated all around Maligaon area. The size of procured wooden charcoal pieces varies in the range of 2.5 cm × 1.5 cm × 1.5 cm to 4.0 cm × 2.5 cm × 1.5 cm. The procured wooden charcoal is washed with de-mineralized water (Model: ELIX-A 10, M/S Millipore

Fig. 13.2 Filtering medium **a** wooden charcoal pieces as procured and **b** river sand procured from the filter site

Table 13.1 Estimated properties of PWC and PS

Properties	PWC	PS
Ash (inert) content (%)	5.5	99
Bulk density (kg/m^3)	290	1706
Moisture content (%)	12	0.5
Particle size range (μm)	425–300	300–150

SAS, France), dried at 105 °C in a drying hot air oven (Model: ICT, M/S International Commercial Trading, Kolkata, India) and then crushed to smaller particle sizes (Ahamad and Jawed 2007). The crushed charcoal particles are sieved as per IS 2720 (1975) and particles passing through 425 μm sieve openings but retaining on 300 μm sieve openings is selected for adsorptive capacity studies and termed as processed wooden charcoal (PWC). The characteristics of PWC are presented in Table 13.1.

13.2.3 River Sand

River sand—a local construction material is procured from the filter site (Fig. 13.2b). The sand is mined from the bottom of River Bharalu—meeting river Brahmaputra upstream approximately 19 km from IIT Guwahati campus. The semi-urban and rural populations generally use this sand in the traditional filter units in addition to wooden charcoal. The procured river sand is washed with de-mineralized water to separate foreign materials like floating debris, dirt, clay and dried at 105 °C in drying hot air oven. The dried sand particles are sieved as per IS 2720 (1975) and particles passing through 300 μm sieve openings but retaining on 150 μm sieve openings is selected for adsorptive capacity studies and termed as processed sand (PS). The characteristics of PS are presented in Table 13.1.

13.2.4 Adsorption Kinetic and Equilibrium Studies of Fe(II) and F^- Uptake from Mono- and Binary-Ion Systems Using Groundwater Samples

The required amounts of adsorbent doses are added in different sets of specimen tubes of 100 mL capacity with 50 mL of groundwater containing desired initial Fe(II) and F^- concentrations [i.e. 2 mg/L for F^- and 3 mg/L for Fe(II)]. A dilution factor of 4 has been used for Fe(II) in order to get the desired initial concentration near to 3 mg/L. In the case of binary-ion system, when the groundwater sample is diluted by 4 times to bring the initial Fe(II) concentration near to 3 mg/L, the F^- concentration is likely to be less than 2 mg/L and hence appropriate quantity of NaF is added to bring the concentration close to 2 mg/L. The specimen tubes with mixture are capped tightly so as to block entry of the air from outside, mounted on an end-over-end shaker (Model: ICT, M/S International Commercial Trading, Kolkata, India) and thoroughly mixed at a speed of 60 rpm. Specimen tubes are taken out one by one at pre-determined time intervals for kinetic studies. For equilibrium studies, the mixing is carried out for the fixed equilibrium time. The solid and liquid phases are separated immediately using a 0.40 μm Whatman filter paper and the residual ion concentrations in the liquid portion are estimated. All the experiments are conducted in duplicate. Experimental conditions used for kinetic and equilibrium studies are tabulated in Table 13.2.

13.2.5 Analytical Methods Used

All the chemicals used in the study are of analytical reagent grade (procured from M/S Merck Ltd., Mumbai, India). The residual concentrations of Fe(II) and F^- are, respectively, estimated by phenanthroline and SPADNS methods (APHA 2005) using a digital spectrophotometer (Model: 166, M/S Systronics India Ltd., India). pH is

Table 13.2 Experimental conditions for adsorption kinetic and equilibrium studies of Fe(II) and F^- uptakes using groundwater samples

Ion system	Adsorbate	Initial adsorbate conc. (mg/L)	Adsorbent	Kinetic studies	Equilibrium studies	
				Adsorbent dose (g per 50 mL)	Adsorbent dose (g per 50 mL)	Equilibrium time (min)
Mono	Fe(II)	3	PS	5.0	3.0–6.0	180
			PWC	1.5	0.5–2.0	
	F^-	2	PS	5.0	3.0–6.0	240
Binary	Fe(II) + F^-	3 [Fe(II)] + 2 (F^-)	PS	5.0	3.0–6.0	180
			PWC	1.5	0.5–2.0	

estimated using a digital pH meter (Model: μpH System 361, M/S Systronics India Ltd., India). Alkalinity and MPN are estimated as per APHA (2005).

13.3 Results and Discussion

13.3.1 Performance of a Traditional Indigenous Household Filter Unit

The samples from the filter unit and the groundwater source are collected twice in a week during the monitoring period. The collected samples are analyzed for pH, alkalinity and concentrations of Fe(II) and F^-. The variation in concentrations of Fe(II) and F^- in groundwater as well as filtered water are presented in Fig. 13.3. The groundwater Fe(II) concentration varies in the range of 4.0–12.7 mg/L whereas the filtered water sample Fe(II) concentrations vary in the range of 0.11–0.15 mg/L which is well below the permissible limit of 0.3 mg/L for Fe(II) in drinking water (IS 10500, 2012). The variation in F^- concentrations in the groundwater samples is in the range of 0.5–2.5 mg/L while the filtered water sample F^- concentration varies in the range of 0.8–2.4 mg/L. It appears that the filter unit is not effective in reducing the concentration of F^- from the groundwater and its concentration exceeds the permissible limit of 1.5 mg/L in drinking water (IS 10500, 2012). The variations in groundwater Fe(II) and F^- concentrations may be attributed to the heavy rainfalls during the monitoring period as the groundwater source is located in a low-lying area thereby receiving heavy percolation as well as seepage affecting the groundwater table at the source. Moreover, the filter unit is also installed very close to a piggery unit and hence chances of pathogenic contamination of groundwater as well as filtered water could not be ruled out. To check pathogenic contamination, MPN test is also carried out twice during the monitoring period. However, the MPN test results are negative, and the filtered water is found to be safe from the point of view of pathogenic contamination. The pH of both filtered and groundwater samples varies in the range of 6–7 while alkalinity for groundwater samples varies in the range of 146–246 mg/L as $CaCO_3$ and the filtered water in the range of 145–183 mg/L as $CaCO_3$ (Garaga 2015).

13.3.2 Adsorption Kinetic and Equilibrium Studies of Fe(II) and F^- Uptake from Mono- and Binary-Ion Systems Using Groundwater Samples

Batch kinetic and equilibrium adsorption studies are carried out with mono-ion system [monitoring either Fe(II) or F^- alone] and binary-ion system [comprising of Fe(II) + F^-] to investigate the potential of PWC and PS for removal of ion(s)

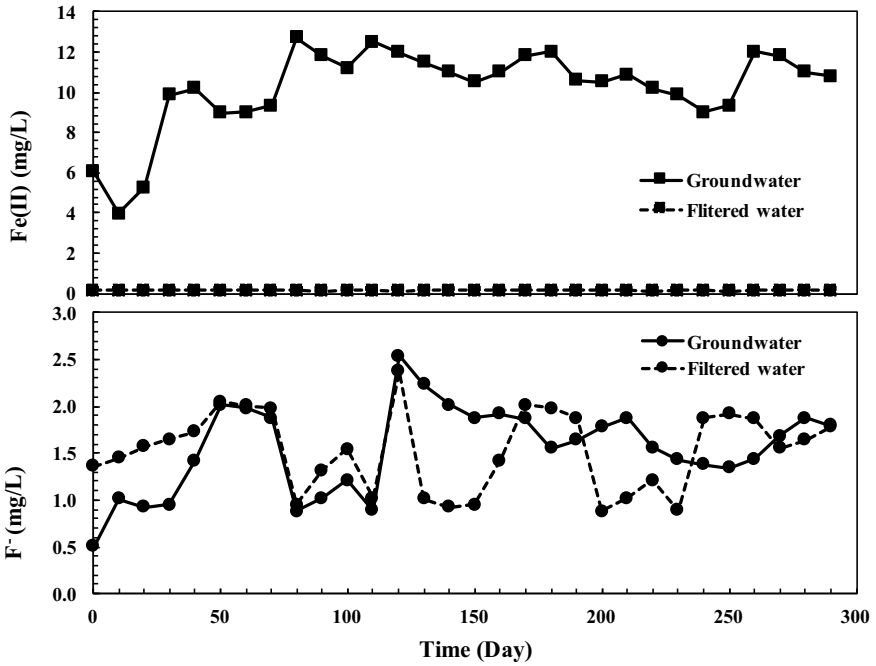

Fig. 13.3 Variation in concentrations of Fe(II) and F^- in groundwater and filtered water

from the groundwater samples. The initial concentrations of Fe(II) and F^- are kept at 3 and 2 mg/L respectively. Since the actual concentration of Fe(II) in groundwater samples is around 12 mg/L, the initial concentration of Fe(II) is reduced to 3 mg/L by diluting the groundwater samples 4 times. It may be noted that F^- removal (or uptake) by PWC is not observed during the studies. The kinetic data obtained are fitted to pseudo-first-order rate kinetic expression of Lagergren (1898)—one of the most widely used rate equations (Cheung et al. 2000; Bhattacharjee et al. 2003) and pseudo-second-order rate kinetic model (Ho and Mckay 2000; Wan Ngah and Koay 2004). The kinetic results yield equilibrium times required (Table 13.2) for carrying out the equilibrium studies. The equilibrium data are analyzed and fitted to Langmuir and Freundlich isotherm models (Langmuir 1918; Freundlich 1926). The best fitted kinetic and equilibrium models are presented in Table 13.3.

13.3.3 Proposed Design Modification of a Field Filter Unit

The field filter unit indicated its inability to reduce F^- concentration to permissible limits for portable use. Hence, efforts are made to re-design the field filter unit for simultaneous removal of dissolved Fe(II) as well as F^- from the groundwater.

Table 13.3 Best fitted kinetic and equilibrium models for Fe(II) and F^- ion uptakes from mono- and binary-ion systems from groundwater samples

Ion system	Studies	Fe(II)		F^-
		PWC	PS	PS
Mono	Kinetic	Pseudo-second order model $q_t = \frac{6.1\times10^{-4}t}{1+1.7\times10^{-3}t}$ for initial conc. of 3 mg/L	Pseudo-second order model $q_t = \frac{2.1\times10^{-4}t}{1+3.6\times10^{-3}t}$ for initial conc. of 3 mg/L	Pseudo-second order model $q_t = \frac{2.9\times10^{-4}t}{1+1.25\times10^{-2}t}$ for initial conc. of 2 mg/L
	Equilibrium	Freundlich isotherm $q_e = 0.13 \times C_e^{0.3649}$	Freundlich isotherm $q_e = 0.0275 \times C_e^{0.0578}$	Freundlich isotherm $q_e = 0.0169 \times C_e^{0.0555}$
Binary	Kinetic	Pseudo-second order model $q_t = \frac{5.7\times10^{-4}t}{1+1.45\times10^{-3}t}$ for initial conc. of 3 mg/L	Pseudo-second order model $q_t = \frac{1.98\times10^{-4}t}{1+3.05\times10^{-3}t}$ for initial conc. of 3 mg/L	Pseudo-second order model $q_t = \frac{2.7\times10^{-4}t}{1+1.2\times10^{-3}t}$ for initial conc. of 2 mg/L
	Equilibrium	Freundlich isotherm $q_e = 0.12 \times C_e^{0.3585}$	Freundlich isotherm $q_e = 0.0258 \times C_e^{0.0386}$	Freundlich isotherm $q_e = 0.01 \times C_e^{0.5396}$

Note In the models, q_e and q_t are expressed in mg/g, C_e in mg/L and t in min

13.3.3.1 Design Approach

The batch studies carried out with mono-ion systems comprising of Fe(II) and F^- indicate ability of PWC to adsorb Fe(II) from the aqueous phase but it fails to adsorb any amount of F^-. Whereas PS is able to adsorb both Fe(II) and F^- from the aqueous phase but to a lower extent for Fe(II) as compared to PWC. The batch studies with binary-ion system [comprising of Fe(II) + F^-] indicate Fe(II) adsorption by PWC and Fe(II) as well as F^- adsorption by PS. Based upon the results obtained from the batch studies, the logical design approach for simultaneous removal of Fe(II) and F^- from groundwater is to use first PWC bed followed by PS bed (instead of PS bed followed by PWC as is the case for the monitored field filter unit). Since, PWC has shown relatively much higher adsorptive capacities for Fe(II) and is not able to adsorb any amount of F^-, application of PS bed followed by PWC may not be a feasible option. If PS adsorb both Fe(II) and F^-, then PWC bed only removes Fe(II) alone. It gives a situation where F^- still remains above the permissible limit in the filtered water. Therefore, the filter is needed to be redesigned as PWC bed followed by PS so that the subsequent PS bed in the arrangement of PWC bed followed by PS bed will only receive un-adsorbed F^- ions from the PWC bed while PWC bed ensures complete removal of Fe(II). If the PWC bed reaches a point where it is not able to adsorb Fe(II) ion any further, the subsequent PS bed will not only remove un-adsorbed F^- ions coming out of the PWC bed but it will be able to remove a part of Fe(II) coming out of the PWC bed as well. Therefore, this combination, i.e. PWC

bed followed by PS bed arrangement is expected to produce treated water quality meeting the regulatory limits in respect of both the ions. Hence, the PWC and PS beds are being designed based on design parameters obtained for binary-ion system.

13.3.3.2 Design Considerations

In the rural and semi-urban area, approximately 5 L of water per capita per day is required for drinking and cooking purposes (Ahamad 2010). Therefore, the field filter unit is designed to produce 5 L of treated water every day per person assuming a family size of five persons and the filter is to be operated for a period of 30 days continuously without changing PWC and PS beds. The maximum initial concentrations of Fe(II) and F^- are 12 and 2.5 mg/L, respectively, in the groundwater. The groundwater with high level of Fe(II) has to be aerated before passing it through the filter unit. It is expected that up to 75% of Fe(II) of 12 mg/L concentration might be precipitated out after aeration (Ahamad 2010). Therefore, the filter bed may only receive Fe(II) concentration of 3 mg/L or lower value. The amount of PWC and PS required to bring down concentrations of Fe(II) and F^- in the treated water equal to or less than 0.3 mg/L for Fe(II) and 1 mg/L for F^- from the respective initial concentrations are estimated using batch adsorption equilibrium data. As discussed above, the amount of PWC and PS required for the treatment of Fe(II) and F^-, respectively, is estimated using binary-ion system data. The detailed design calculations for PWC and PS beds are presented in Table 13.4. The estimated redesigned thickness of PWC and PS beds are 0.31 m and 0.24 m, respectively. The modified traditional filter unit based upon the new designed values is shown in Fig. 13.4. However, the designed filter needs to be fabricated and tested for its efficiency using actual groundwater in the field conditions.

13.4 Summary

The filtered water Fe(II) concentration from the traditional filter unit varies in the range of 0.11–0.15 mg/L which is well below the permissible limit of 0.3 mg/L for Fe(II) in drinking water even though the groundwater Fe(II) concentration varies in the range of 4.0–12.7 mg/L. However, the filtered water F^- concentrations exceed the permissible limit of 1.5 mg/L on a number of days of monitoring. The variation in F^- concentrations in the groundwater is in the range of 0.5–2.5 mg/L while the variation for filtered water is in the range of 0.8–2.4 mg/L. It is clear that the filter unit is not effective in reducing the concentration of F^- from the groundwater. The batch studies with binary-ion system [comprising of Fe(II) + F^-] indicate Fe(II) adsorption by PWC and Fe(II) as well as F^- adsorption by PS but to a lesser extend compared to PWC uptake of Fe(II). Based upon the results obtained from the batch studies, the logical design approach for simultaneous removal of Fe(II) and F^- from groundwater is to use first PWC bed followed by PS bed instead of PS bed followed

Table 13.4 Design calculations for PWC and PS beds for field filter unit

General: Water to be treated every day = 5 L per person; Treatment period adopted = 30 days; Assuming family size of the household = 5 persons, Volume of treated water required = 750 L

PWC Bed	PS Bed
1. Given: Inlet groundwater Fe(II) conc. = 3 mg/L (after aeration and precipitation); Filtered water Fe(II) conc. = 0.3 mg/L; Adsorption equilibrium model used = Freundlich isotherm 2. Estimating PWC usage rate $q_e = \frac{(C_o - C_e)V}{m} = k_f C_e^{\frac{1}{n}}$ $= \frac{\left(3\frac{\text{mg}}{\text{L}} - 0.3\frac{\text{mg}}{\text{L}}\right)\text{V}}{\text{m}} = 0.12\,(0.3)^{0.3585}\frac{\text{mg}}{\text{g}}$ 3. $\frac{\text{m}}{\text{V}} = 34$ g PWC/L 4. Estimating mass of PWC required to treat 750 L of water $\text{Volume of water treated} = \frac{\text{mass of PWC}}{\text{PWC usage rate}}$ $\text{Mass of PWC} = \text{Volume of water treated} \times \text{PWC usage rate}$ $= 750\,\text{L} \times 34\frac{\text{g PWC}}{\text{L}}$ $= 25500\text{ g PWC} = 25.5\text{ kg PWC}$ 5. $\text{Volume of PWC} = \frac{\text{mass of PWC}}{\text{density of PWC}} = \frac{25.5\text{ kg}}{290\,\frac{\text{kg}}{\text{m}^3}} = 0.088\text{ m}^3$ 6. Thickness of PWC bed $= \frac{\text{Volume of PWC}}{\pi\,\text{r}^2} = \frac{0.088}{\pi\left(\frac{0.6}{2}\right)^2} = 0.31$ m	1. Given: Inlet groundwater F^- conc. = 2.5 mg/L; Filtered water F^- conc. = 1 mg/L; Adsorption equilibrium model used = Freundlich isotherm 2. Estimating PS usage rate $q_e = \frac{(C_o - C_e)V}{m} = k_f C_e^{\frac{1}{n}}$ $= \frac{\left(2.5\frac{\text{mg}}{\text{L}} - 1.0\frac{\text{mg}}{\text{L}}\right)\text{V}}{\text{m}} = 0.10\,(1.0)^{0.5396}\ \frac{\text{mg}}{\text{g}}$ 3. $\frac{\text{m}}{\text{V}} = 150$ g PS/L 4. Estimating mass of PS required to treat 750 L of water $\text{Volume of water treated} = \frac{\text{mass of PS}}{\text{PS usage rate}}$ $\text{Mass of PS} = \text{Volume of water treated} \times \text{PS usage rate}$ $= 750\,\text{L} \times 150\frac{\text{g PS}}{\text{L}}$ $= 112500\text{ g PS} = 112.5\text{ kg PS}$ 5. $\text{Volume of PS} = \frac{\text{mass of PS}}{\text{density of PS}} = \frac{112.5\text{ kg}}{1706\,\frac{\text{kg}}{\text{m}^3}} = 0.066\text{ m}^3$ 6. Thickness of PWC bed $= \frac{\text{Volume of PS}}{\pi\,\text{r}^2} = \frac{0.066}{\pi\left(\frac{0.6}{2}\right)^2} = 0.24$ m

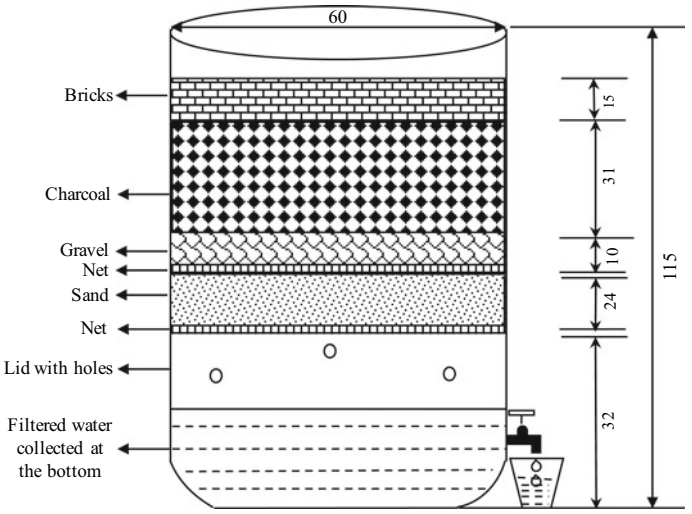

Fig. 13.4 Schematic diagram of re-designed traditional filter unit (All dimensions in cm)

by PWC as is the case for the monitored field filter unit. The estimated redesigned thickness of PWC and PS beds are 0.31 m and 0.24 m respectively, considering 5 L of water required per person per day with a family size of five adults and considering the filter run of 30 days. However, the re-designed filter unit needs to be fabricated and tested for its efficiency using groundwater in the field conditions.

References

Ahamad KU (2005) Iron (II) adsorptive capacity evaluation of wooden charcoal and sand media used in indigenous household iron filtration units of rural and semi-urban Assam. Masters thesis, Department of Civil Engineering, Indian Institute of Technology Guwahati, Guwahati, India

Ahamad KU (2010) Batch and column adsorption studies for simultaneous removal of iron, arsenic and fluoride by wooden charcoal and river sand used as filter media in indigenous household iron filter units of rural and semi-urban Assam (India). Doctoral thesis, Department of Civil Engineering, Indian Institute of Technology Guwahati, Guwahati, India

Ahamad KU, Jawed M (2007) Role of wooden charcoal in indigenous household iron filters used in Assam (India). Asian J Water Environ Poll 5(3):23–28

Ahamad KU, Jawed M (2010) Kinetics, equilibrium and breakthrough studies for Fe (II) removal by wooden charcoal: a low-cost adsorbent. Desal 251(1–3):137–145

APHA (2005) Standard methods for the examination of water and wastewater. American Public Health Association, American Water Works Association, Water Environment Federation, 21th edn, Washington, DC, USA

Bhattacharjee S, Chakravarty S, Maity S, Kar S, Thakur P, Bhattacharyya G (2003) Removal of lead from contaminated water bodies using sea nodule as an adsorbent. Wat Res 37(16):3954–3966

Cheung CW, Porter JF, McKay G (2000) Sorption kinetics for the removal of copper and zinc from effluents using bone char. Sep Puri Tech 19:55–64

Das B, Talukdar J, Sarma S, Gohain B, Dutta RK, Das HB, Das AC (2003) Fluoride and other inorganic constituents in groundwater of Guwahati, Assam, India. Curr Sci 85:657–661

Das B, Hazarika P, Saikia G, Kalita H, Goswami DC, Das HB, Dube SN, Dutta RK (2007) Removal of iron from groundwater by ash: a systematic study of a traditional method. J Hazar Mat 141(3):834–841

Freundlich H (1926) Colloid and capillary chemistry. Methuen and Co., Ltd., London (cited from Ahamad, 2010)

Garaga RL (2015) Evaluation of filter media of traditional filter units of Assam and performance monitoring of a filter unit under field conditions. Masters thesis, Department of Civil Engineering, Indian Institute of Technology Guwahati, Guwahati, India

Ho YS, Mckay G (2000) The kinetics of sorption of divalent metal ions onto sphagnum moss peat. Wat Res 34:735–742

IS 2720 (1975) Bureau of Indian standards. Specification, Indian Standards for Method of Test for Soils, New Delhi

IS 10500 (2012) Bureau of Indian standards. Specification, Indian Standard Drinking Water, New Delhi

Lagergren S (1898) About the theory of so-called adsorption of soluble substances. K Sven Vetenskapsakad Handl 24(4):1–39

Langmuir I (1918) The adsorption of gases on plane surfaces of glass, mica and platinum. J Am Chem Soc 40:1362–1403

Suhag R (2016) Overview of ground water in India. http://www.prsindia.org/administrator/uploads/general/1455682937~~Overview%20of%20Ground%20Water%20in%20India.pdf. Website accessed 16 Sept 2018

Wan Ngah WS, Koay YJ (2004) Equilibrium and kinetics studies of adsorption of copper (II) on chitosan and chitosan/PVA beads. Int J Bio Macr 34:155–161

WHO (1993) Guidelines for drinking water quality, 2nd edn, vol I: Health criteria and supporting information. Recommendations, Geneva, Switzerland, pp 41–42

Chapter 14
Applications of Cascade Feed Forward Neural Network for Modelling of Coagulant Dose in a Drinking Water Treatment Plant: Comparative Study

D. V. Wadkar and A. S. Kote

Abstract Coagulation process is complex and nonlinear and its control plays a crucial role in a water treatment plant (WTP). Traditionally, aluminum sulphate (alum) is used as a coagulant in the coagulation process and the optimum coagulant dose is determined using a jar test. The jar test is quite time-consuming and expensive too. Jar tests are conducted periodically, which means they are reactive rather than proactive. The development of predictive models for coagulant dose in a WTP is needed. The aim of this study was to use an artificial neural network (ANN) to predict coagulant dose. For ANN modelling, the plant laboratory provided data for 48 months of daily water monitoring in terms of inlet and outlet water turbidity and coagulant dosage. By applying various training functions and evaluating the coefficient of regression (R) and mean square error (MSE), the appropriate architecture of the cascade feed forward neural network (CFNN) and feed forward neural network (FFNN) coagulant models were developed. Additionally, the best performing Levenberg–Marquardt (LM) and Bayesian regularization (BR) training functions among resilient back propagation (RBP), one step secant (OSS), conjugate gradient (CG), and variants of gradient descent (GD) were used to build four ANN models of FFNN and CFNN for predicting coagulant dose at WTP. With 40 hidden nodes, a cascade feed forward neural network with BR training function produced very accurate estimates for coagulant dose with architecture (2-40-1) with the highest values of R = 0.952 during training, R = 0.922 during testing, and overall R = 0.947 and MSE = 99.28 mg/lit. As a result, plant operators and decision-makers may benefit from using ANN as a performance assessment tool, as well as an important diagnosing tool for understanding the nonlinear behaviour of the coagulation process.

Keywords Artificial neural network · Water treatment plant · Coagulant dose

D. V. Wadkar · A. S. Kote (✉)
DIT, Savitribai Phule Pune University, Pimpri, Pune 411018, India
e-mail: alkakote26@gmail.com

R. Jha et al. (eds.), *Groundwater and Water Quality*, Water Science and Technology Library 119, https://doi.org/10.1007/978-3-031-09551-1_14

14.1 Introduction

Coagulation is a physio-chemical and nonlinear process, where coagulants are added to raw water under the swiftly mingling condition to promote aggregation of suspended and dissolved particles to produce flocs. These flocs are removed as part of the purification process in water treatment plants. The addition of coagulants need to be optimized to produce water that meets the desired quality. Traditionally, aluminum sulphate (alum) is used as a coagulant in the coagulation process and the optimum coagulant dose is determined using a jar test. The jar test is quite time-consuming and expensive too. Jar tests are conducted periodically, which means they are reactive rather than proactive. In India, generally in a WTP coagulant dose is kept constant for a specific period due to a time delay of jar test. This sometimes results in under dose or overdose of the coagulant.

Several studies have been carried out to apply different control strategies to the coagulation process. Larmrini et al. (2005) developed a multilayer perceptron neural networks with soft sensor for online calculation of the ideal coagulant dose for the Rocade WTP, Marrakech, Morocco. Chen and Hou (2006) developed a controlled coagulant dose strategy with a rational feed forward control system with fuzzy feedback trim of the Changhsing water-purification plant of the Taipei Water Department. Robenson et al. (2009) established a coagulant dose model with inverse ANN in the Segama WTP, Datu, Malaysia.

Similarly, Heddam Salim et al. (2011) developed an ANN model for approximating coagulant dose in water treatment plants in Algeria. The radial basis function neural network (RBNN) and generalized regression neural network (GRNN) were both used to test this hypothesis. On the same ground, Swetland et al. (2013) investigated a gravity-powered chemical dose controller for accurate chemical dosing in water treatment plants is imperative to ensure optimal efficiency of flocculation and disinfection. The combined system adjusts the chemical flow rate automatically in response to changes in the plant flow rate to maintain the target chemical dose.

Furthermore, Bello et al. (2015) proposed a multiple model predictive control based on a fuzzy switching approach for coagulant dose. Kennedy et al. (2015) developed ANN models for the prediction of dissolved organic matter and turbidity at the Akron Water Treatment Plant (Ohio, USA). Gao Larry et al. (2017) developed a real-time coagulant dose approach for both seawater and brackish water Ultra Filtration (UF) treatment. Wu et al., evaluated a neural fuzzy model for the prediction of coagulant dose. Bello et al. (2014, 2017) developed multiple predictive models with a fuzzy weighing system. The motivation of this study is the application of the ANN approach for effective optimization of the coagulation process in WTP. Therefore, this paper presents coagulant dose modelling using the most popular and widely used CFNN and FFNN for a WTP in Pimpri Chinchwad Municipal Corporation (PCMC), Maharashtra, India.

14.2 Material and Methods

14.2.1 Study Area

The WTP under investigation is in PCMC, Maharashtra, India, and is located at 18° 37′ 33.87″ N latitude and 73° 48′ 43.76″ E longitude. With 59 elevated storage reservoirs and 1, 17,936 water connections, this city has an average water supply of 170 L per capita per day. This WTP provides 428 million liters of water per day to a 177-square-kilometer area.

14.2.2 Methodology

Input parameters such as inlet & outlet water turbidity and an output parameter as coagulant dose were identified for ANN modelling. Daily data of input and output parameters spanning 4 years namely years 2012, 2013, 2014 and 2015, were acquired from the site laboratory. There are 11,688 data points in the database of input and target parameters available for ANN modelling. ANN models were developed using MATLAB software with defined codes and modifications such as the number of the epoch, number of hidden nodes and number of hidden layers in the training parameters.

Preliminary investigation of feed forward neural network and cascade feed forward neural network architectures using various training functions such as LM, RBP, BR, OSS, and variants of GD and CG was carried out.

For the highest regression coefficient, the best association of training function, set of neurons, and epoch was calculated. The trained neural network with the lowest validation error was chosen as the coagulant dose model, which was then evaluated using a test dataset to compute the final network error.

14.3 Results and Analysis

This part of the study aims to tackle the problem of predicting alum dose at the treatment plant, which is highly nonlinear and complex. Total of 44 ANN models for alum dose using feed forward neural networks (FFNN) and cascade feed forward neural networks (CFNN) were developed. FFNN consist of a series of layers such as input, hidden and an output layer with weighted connections. Each subsequent layer has a connection from the previous layer. The final layer produces the network's output. FFNN can be used for any kind of input to output mapping. A feed forward network with one hidden layer and enough neurons in the hidden layers can fit any finite input–output mapping problem.

Similarly, cascade feeds forward neural networks (CFNN) are similar to feed forward networks but include a weight connection from the input to each layer, and from each layer to the successive layers. For example, a three-layer network has connections from layer 1 to layer 2, layer 2 to layer 3, and layer 1 to layer 3. The three-layer network also has connections from the input to all three layers. The additional connections might improve the speed and accuracy at which the network learns the desired relationship.

As discussed in the previous section, the development of ANN models consists of many steps of training and testing with training functions. Training and testing data were varied 75:30 and 80:20 during model building Fig. 14.1 depicts a summary of training function results. It was discovered that many training functions performed poorly and that some models had negative correlations, implying that in-capabilities in modelling except BR and LM training functions. In Fig. 14.2, seven combinations of LM training function and six combinations of BR training function were analyzed. Where it was observed that the numbers of Epoch and computation time required for BR training function are more as compared to LM training function. Similarly, it was found BR training function produced higher prediction efficiency.

For the development of FFNN and CFFNN models, the best performing LM and BR training functions were used. The hidden node was diverse from 15 to 60 during the development of these models, and the respective coefficient of regression was found to be between 0.936 and 0.947. The best results were obtained using the cascade feed forward neural network alum dose (CFNNAD2) model with hidden node 40

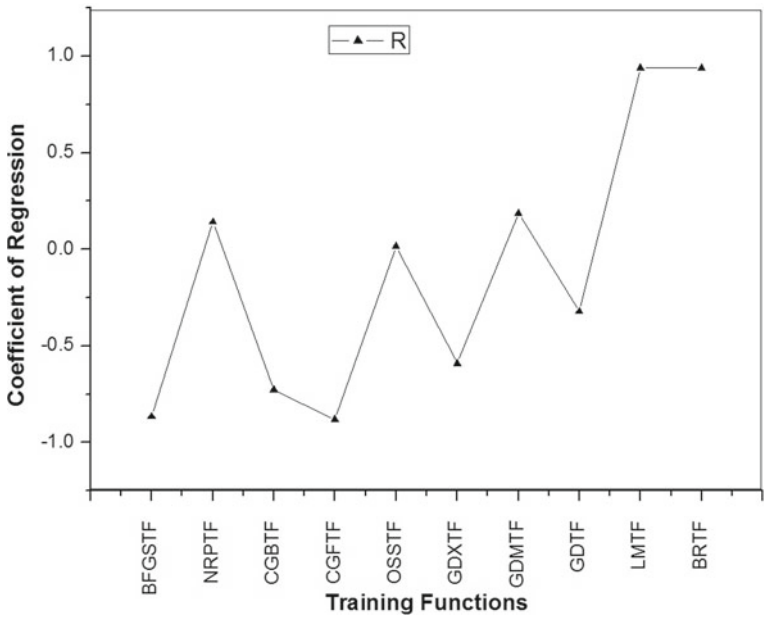

Fig. 14.1 Performance of various types of training functions

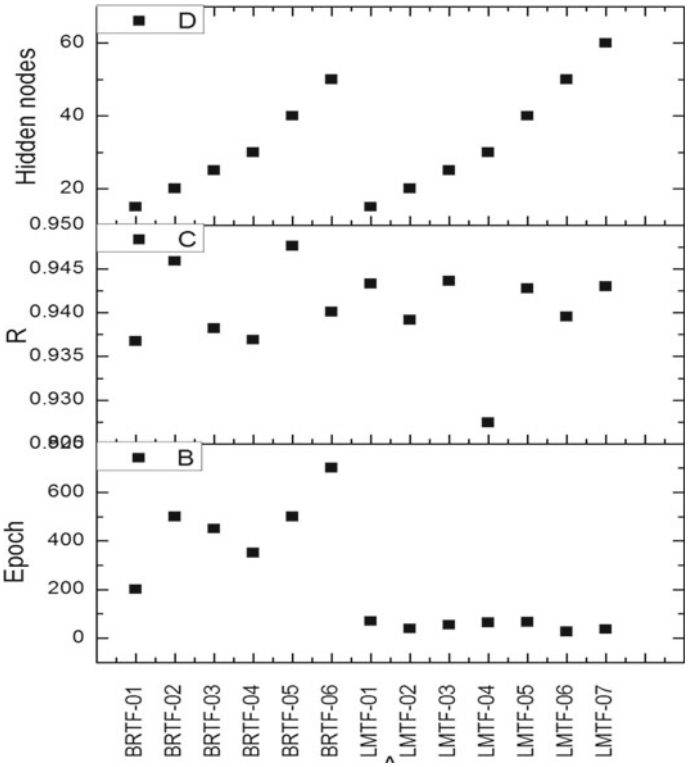

Fig. 14.2 Performance of BR and LM training functions

and the BR training feature, where R stands for training (0.952), testing (0.922), and overall (0.922). A comparison of the performance of the best ANN models is shown in Table 14.1

Table 14.1 shows that in the test stage, the values of the CFNN model prediction accomplished a better surmise than FFNN. The results of the CFNN model also showed better agreement than those of the FFNN analysis. In the test stage, the CFNN model performed with a reduction in MSE of proximately 46.85%. In addition, the forecast results of the CFNN model regarding the coagulant dose value during the test stage showed an improvement of approximately 1% over the FFNN model. The

Table 14.1 Output of the best ANN models

ANN Models	Training function	Epochs	Hidden nodes	R	MSE (mg/lit)
FNNAD1	LM	26	60	0.944	185.09
FNNAD2	BR	500	50	0.945	113.13
CFNNAD1	LM	36	60	0.943	59.22
CFNNAD2	BR	500	40	0.947	99.28

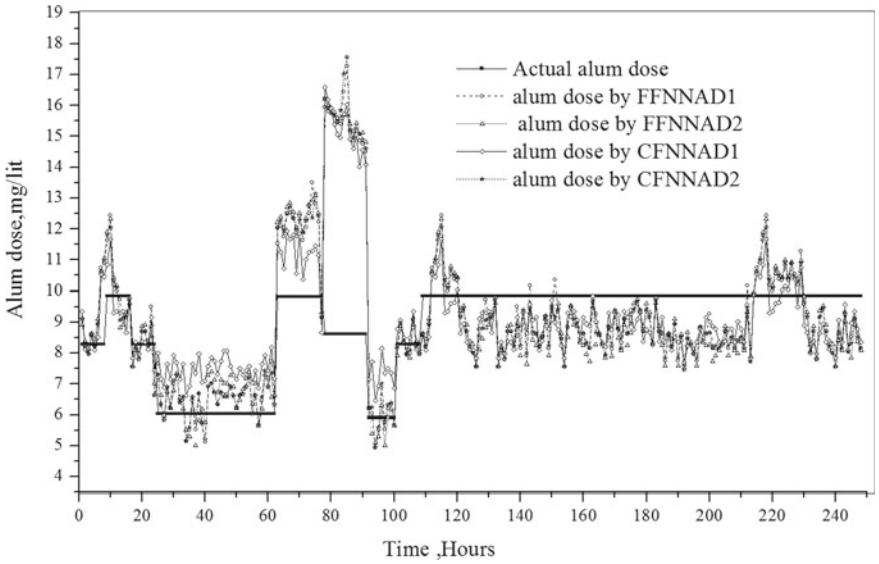

Fig. 14.3 Prediction of alum dose by best ANN Models during testing period

CFNN model produced results that were close to the observed values, signifying that modelling was effective and accurate.

During the testing phase, 248 data points were used to predict alum dose using the built ANN models. Mostly Actual alum dose given at the water treatment plant is nearly the same for a particular period, which is indicated by the straight line in Fig. 14.3 whereas the predicted alum dose is shown by an undulating line. Figure 14.3 shows that the expected alum dose values do not meet the trend of real alum dose from sixty to ninety data points in 2015. These alterations were attained due to a large range of values of inlet water turbidity and coagulant dose during the training of neural networks. The average actual coagulant and predicted coagulant dose were close in spite of the large variations.

Amongst all the models, the CFNNAD2 model gave the best performance with $R = 0.947$ and $MSE = 99.28$ mg/lit. Figure 14.4 shows the scatter plot of the actual and predicted coagulant dose of the CFNNAD2 model during the testing phase.

14.4 Conclusions

Four best ANN models were developed: FFNNAD1, FFNNAD2, CFNNAD1, and CFNNAD2. All the models performed well, especially for lower values of alum dose. However, the higher values showed under prediction. In comparison to FFNNAD1, FFNNAD2, and CFNNAD1 models, the best prediction for coagulant dose was found in the CFNNAD2 model with BR training function. As a result, ANN can be useful

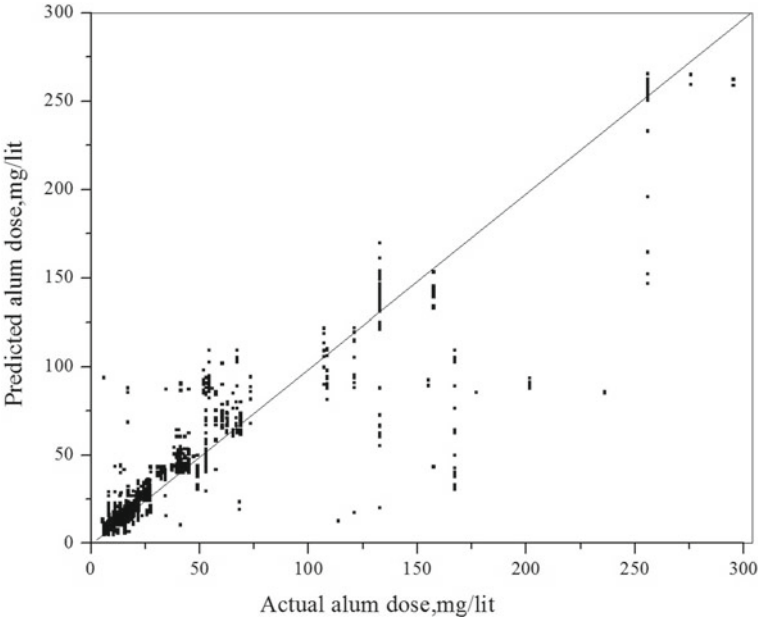

Fig. 14.4 Scatter plot of CFFNNAD2 model during testing phase

for plant operators and decision-makers as a valuable assessment method, as well as an important diagnosing tool for understanding the nonlinear behaviour of the coagulation process. The plant operators would be able to predict the turbidity of the outgoing water based on the turbidity of inlet water.

References

Bello O, Yskandar H, Karim D (2014) Coagulation process control in WTPs using multiple model predictive control. Alexandria Eng J 53(4):959–948

Bello O, Yskandar H, Karim D (2015) Multiple model predictive control based on fuzzy switching scheme of a coagulation chemical dosing unit for WTP. IFAC-Papers On Line 48(11):180–185

Chen CL, Hou PL (2006) Fuzzy model identification and control system design for coagulation chemical dosing of potable water. Water Sci Technol Water Supply 6(3):97–104

Gao Larry X, Gu H, Rahardianto A (2017) Self-adaptive cycle-to-cycle control of in-line coagulant dosing in ultrafiltration for pre-treatment of reverse osmosis feed water. Desalination 401:22–31

Kennedy MJ, Gandomia AH, Miller CM (2015) Coagulation modelling using artificial neural networks to predict both turbidity and DOM-PARAFAC component removal. J Environ Chem Eng 3(4)A:2829–2838

Larmrini B, Benhammou A, Le Lann M, Karama A (2005) A neural software sensor for on-line prediction of coagulant dosage in a drinking water treatment plant. Trans Inst Meas Control 27(3):195–213

Robenson A, Shukor SR, Az A, Araiz N (2009) Development of process inverse neural network model to determine the required alum dosage at Segama water treatment plant Sabah, Malaysia. Comput Aided Chem Eng 27:525–530

Salim H, Bermad A, Dechemi N (2011) Applications of RBF and GRNN for modelling of coagulant dosage in a drinking water-treatment plant comparative study. J Environ Eng 137:1209–1214

Swetland KA, Weber-Shirk ML, Lion LW (2013) Gravity-powered chemical dose controller for sustainable, municipal-scale drinking water treatment. J Environ Eng 139:1023–1034

Wu G, Lo SL (2008) Predicting real-time coagulant dosage in water treatment by artificial neural networks and adaptive network-based fuzzy inference system. Eng Appl Artif Intell 21:1189–1195

Chapter 15
A Conceptual Understanding of Groundwater Levels Using Data-Driven Model—A Case Study in Hyderabad, India

Lakshmi Elangovan, Riddhi Singh, and B. V. N. P. Kambhammettu

Abstract Groundwater is an essential source of water supply to Hyderabad city, meeting about 25% of total demand. Rapid growth in urbanization is likely to lead to extensive exploitation of groundwater in and around Hyderabad. Groundwater recharge dynamics are challenging to model due to the complexity of characterizing the heterogeneous aquifer system. A comprehensive understanding of the relationship between climatic and other drivers of recharge dynamics can help in effective utilization and conservation. In this research, we developed a geographic information system (GIS)-based parsimonious data-driven model for estimating recharge flux and simulating groundwater levels on a monthly scale. The model is based on the conceptual water balance that relates recharge with rainfall as inflow and abstraction rate as outflow, contributing to the change in groundwater level. The data required for the model include monthly rainfall, groundwater level observations, aquifer parameters (Specific yield and Transmissivity), and pumping rate. This study uses the multi-objective optimization method (NSGA-II) application, and a Pareto optimal solution set was achieved for the calibration period. Model calibration was performed during 2004–2007 by matching simulated groundwater levels with the observations. The best optimal solution from the calibrated model is then used to predict groundwater levels for 2008. The ability of the model to capture the intra-annual dynamic of groundwater level variation was analyzed during the validation period using the statistical indicators (RMSE of 0.7 MAE of 0.5 and NSE of 0.9).

Keywords Groundwater levels · Rainfall recharge · Data-driven model · Water balance equation · Hyderabad

L. Elangovan (✉) · B. V. N. P. Kambhammettu
Department of Civil Engineering, Indian Institute of Technology Hyderabad, Kandi 502205, Telangana, India
e-mail: ce15resch11013@iith.ac.in

R. Singh
Department of Civil Engineering, Indian Institute of Technology Bombay, Powai, Mumbai 400076, Maharashtra, India

Interdisciplinary Programme (IDP) in Climate Studies, Indian Institute of Technology Bombay, Powai, Mumbai 400076, Maharashtra, India

R. Jha et al. (eds.), *Groundwater and Water Quality*, Water Science and Technology Library 119, https://doi.org/10.1007/978-3-031-09551-1_15

15.1 Introduction

Groundwater plays a substantial role in water supply, which affects the economic and social well-being of a region, especially in developing countries. In India, over 71 cities and towns depend on groundwater, contributing to nearly 48% of the urban water supply (Narain 2012). Groundwater is generally identified in the weathered, and fractured layer that extends from unconfined to confined conditions with heterogeneous aquifer properties. Several groundwater models exist in the literature that attempt to understand groundwater behavior under different conditions to guide better management policies. A range of groundwater models exists varying from simple conceptualizations to fully physically based approaches (such as MODFLOW) (Baalousha 2005; Massuel et al. 2007). The estimation of groundwater levels in a distributed or semi-distributed model requires many uncertain parameters for simulation that depend upon hydrogeological properties, land use, and soil types (Baalousha 2005). Thus, physically based groundwater models' calibration is challenging, particularly in the regions with heterogeneous subsurface (Sekhar et al. 2013). The simple lumped models for estimating the groundwater budget in heterogeneous areas such as those underlain by hard rocks, mountainous regions, and karst aquifer groundwater systems are discussed by (Majumdar et al. 2009; Sekhar et al. 2013; Xu and Tonder 2001).

This research work focuses on using a conceptual model to predict groundwater levels in a rapidly growing urban center in South Asia, Hyderabad. Hyderabad is currently ranked as the fourth largest Indian city by population and the sixth most populous urban agglomeration in India (Census of India 2011). Major water-related issues such as increasing population growth rate, declining surface water resources, overexploitation of groundwater, and deterioration of groundwater quality lead to the increasing gap between demand and supply of water. It is necessary to properly manage the sustainable development of the water environment. The objectives of this paper are (a) to understand groundwater flow within the city boundary using geographic information systems (GIS), (b) to develop a simple data-driven model of groundwater for the city and simulate the groundwater levels for three scenarios of recharge factor during calibration (2004–2007) and validation periods (2008), (c) to use as multi-objective optimization algorithm (NSGA-II) to identify the recharge rates in different months.

15.2 Study Area

Hyderabad Metropolitan Area (HMA) is located in Telangana state, with a total area of 7200 km^2, and the area considered for the present study is 5500 km^2 (Fig. 15.1). The population of HMA is rapidly growing. According to the population census released by Directorate of Census Operations, the population in 2011 is reported approximately 9.4 million in HMA. The climate in Hyderabad is semi-arid tropical

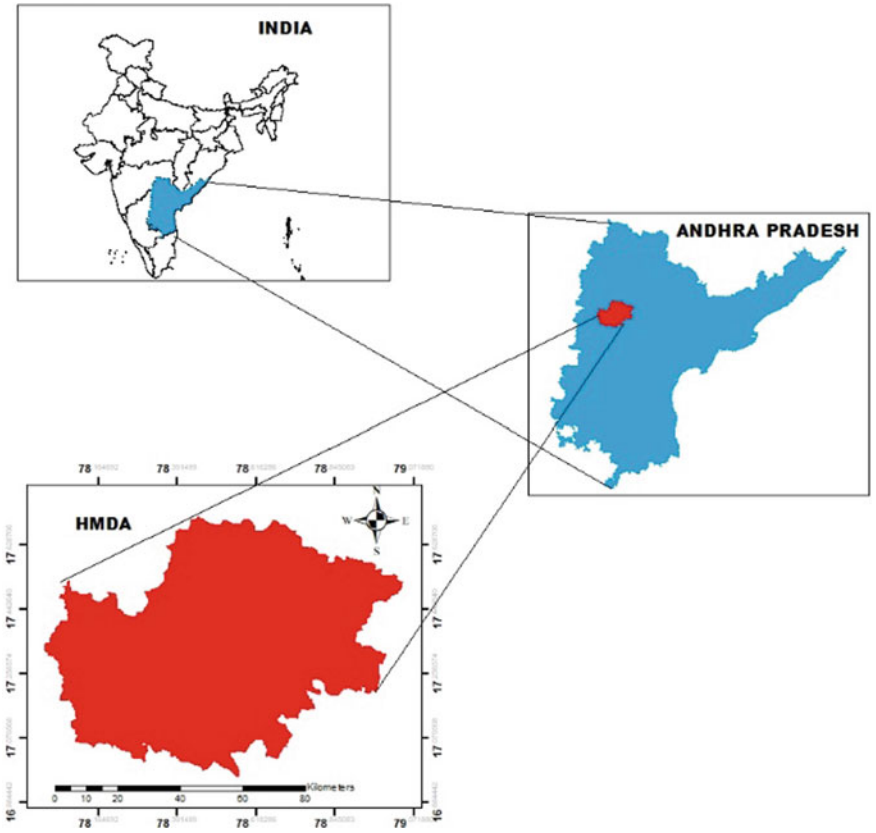

Fig. 15.1 Location of the study area, Hyderabad Metropolitan Development Authority

weather. The average annual rainfall is 810 mm. The monsoon starts in July till early October, with the contribution of southwest and northeast monsoons. The temperature during summer touches 45 °C, and with the onset of monsoons during June, the temperature drops and varies from 26 to 38 °C. Major part of Hyderabad comprises Pre-Cambrian peninsular shield and is underlain with granites intruded by dolerite dykes. Fractures, joints, faults, and fissures are the common structural features of granites found in Hyderabad. The study area covers more than 97% of the area that is underlain by the granites, and the remaining 3% of the area is underlain by the Alluvium, which occurs in the Musi River. Common type soils such as red lateritic, yellow sandy-clay loams and alluvial, and black soils are found in this area with thickness varying from 0.5 to 2.0 m. The land use pattern indicates the changing pattern of land use over the years. It shows an increase in residential and commercial at the expense of vacant and agricultural land.

According to the Hyderabad Metro Water Supply and Sewerage Board, 340 million gallons per day (MGD) of piped water supply is provided from surface

water resources which include Krishna river as a source by covering MCH, ten adjoining municipalities, Osmania University, Secunderabad Cantonment, and ten enroute villages along NH-9 up to Sanga Reddy (793 km^2). It is also reported that 25 MGD is being supplied from groundwater resources other than surface water resources (Gumma et al. 2011).

15.3 Data and Methods

15.3.1 Data Used

Groundwater level data is collected from the Central Ground Water Board, Hyderabad, and Precipitation data with 0.5° resolution is collected from India Metrological Department, Pune (Table 15.1). A total of 178 observation well data was available at a resolution of roughly one measurement per month spanning the time period 1996–2016. Data analysis of 178 observation wells was done, and it was found that 21 wells had continuous monthly time series data for the study area during 2004–2008. Land use land cover (LULC) classification was carried out for the study area for the period 2004–2008 using Landsat 4–5, Thematic Mapper (TM) with 30 m spatial resolution (Fig. 15.2). We find that urban areas' distribution does not vary much, but there is a significant shrinkage of water bodies in the 5 years, 2004–2008. Since the analysis we consider is a single representative time series of groundwater levels, we use the Thiessen method to weigh each well according to its representative area. This procedure is carried out using ArcGIS.

15.3.2 Methodology

The methodology used for simulating the groundwater levels using lumped groundwater model is given in the following sections in detail. The overview of the method is explained in the flowchart, as shown in Fig. 15.3. We first develop a conceptual groundwater model that can simulate groundwater heads as a function of climatic

Table 15.1 Details of the datasets used in the model

S. No.	Data	Temporal scale	Source
1	Groundwater level (m)	Monthly (2004–2008)	CGWD, Hyderabad
2	Rainfall (mm)		IMD, Pune
4	Specific storage, transmissivity	Constant	Varalakshmi et al. (2014)
5	Pumping rate (MCM)	Constant	Van Rooijen et al. (2005)

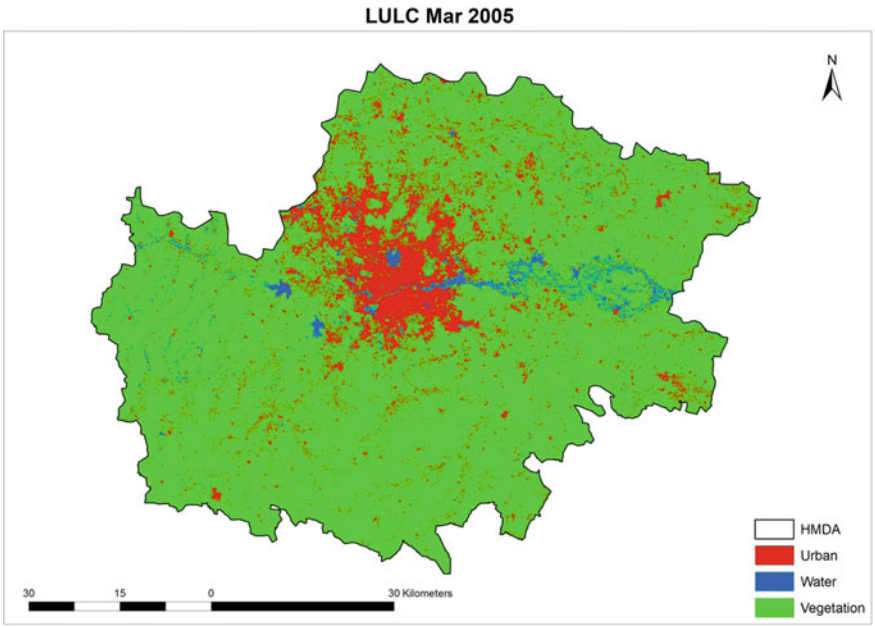

Fig. 15.2 LULC map for the study area developed using Landsat 4–5 TM

and pumping conditions in an area (Sect. 15.3.2.1). We develop three variants of the model that differ in the manner in which they simulate recharge in the area as a function of rainfall. Besides rainfall and pumping data, the model requires lateral flow estimation, further discussed in Sect. 15.3.2.2. Finally, we calibrate the groundwater model parameters using an evolutionary algorithm as explained in Sect. 15.3.2.3.

15.3.2.1 Conceptual Groundwater Model

The conceptual groundwater model used in this analysis is the simple groundwater balance with storage, inflows, and outflows within the study area boundary (Fig. 15.4). The model is based on the method proposed by (Bredenkamp et al. 1995), where recharge is considered here as a function of precipitation. The model is a simple water balance model that simulates groundwater head changes as a function of the inflow and outflow of the groundwater basin. The inflow of the groundwater system is recharged due to precipitation and lateral inflow. The outflow from the groundwater system is groundwater abstraction by pumping and lateral outflow.

The groundwater balance equation for this model is shown in Eq. (15.1).

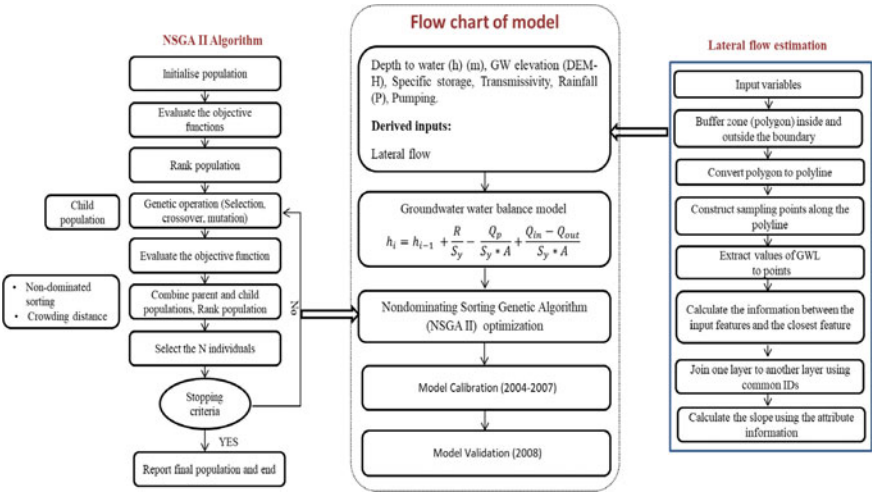

Fig. 15.3 Flowchart of the groundwater model methodology

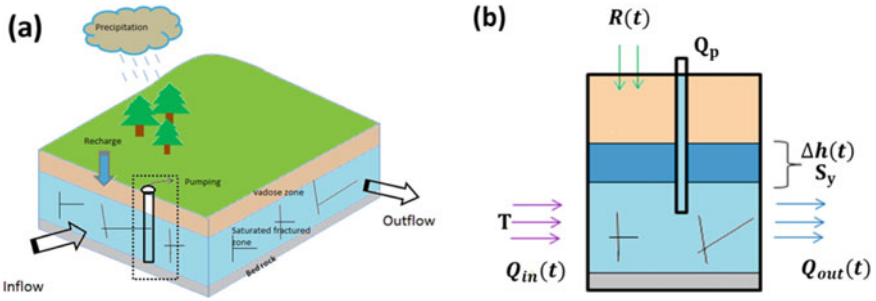

Fig. 15.4 Conceptual groundwater model **a** spatial view of various groundwater fluxes **b** subsection of the lumped model

$$\Delta h_i * A * S_y = R + Q_{in} - Q_{out} - Q_p \tag{15.1}$$

where

R the total recharge to the aquifer [m^3/month],
Q_p the discharge from pumping [m^3/month],
Q_{out} the lateral outflow [m^3/month],
Q_{in} the lateral inflow [m^3/month],
Δh_i the change in groundwater level in a time period i [m^3/month],
A the area of study [m^2], and
S_y the specific yield.

The groundwater level is thus estimated within the model as a function of the inputs such as lateral flow, precipitation, specific yield, and abstraction rate. The recharge factor, specific yield, and maximum pumping rate are assumed to be parameters of the groundwater model, and their optimal values are obtained by optimization as discussed in Sect. 15.3.2.3.

15.3.2.2 Lateral Inflow and Outflow

Lateral flow is one of the variables in the groundwater balance model. Various methods can be used to estimate the lateral flow, such as the difference between two contours, numerical methods, and ArcGIS Darcy's method (Baalousha 2005; Schnaar et al. 2016; Singhal and Goyal 2011). Here, we developed a simple method (Fig. 15.5) with the help of ArcGIS tools to calculate the average lateral flow across the boundary based on the available groundwater head data. The input for the method in the study area boundary file and groundwater elevation raster. A buffer of 1 km is constructed inside and outside of the boundary. Following this, 1000 sample points are selected along the three boundaries: boundary, buffer inside, and outside. Finally, the groundwater elevation value for the sampled points is extracted using the interpolated groundwater elevation raster. Using the ArcGIS Near tool, the attribute table of the buffer line is joined with the study area boundary, and the slope for all the points

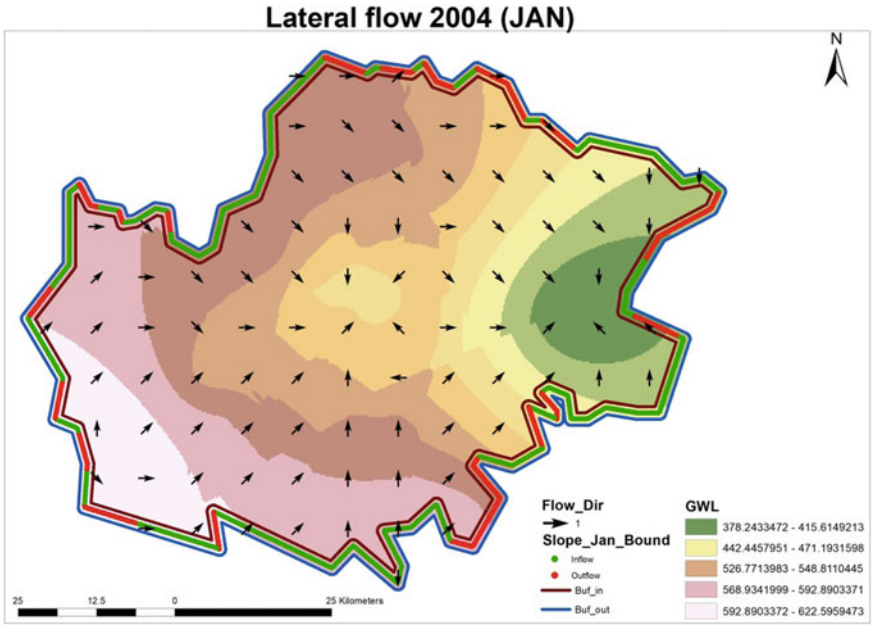

Fig. 15.5 Average slope across the boundary. Red color in the boundary represents a negative slope, i.e. outflow; green color represents a positive slope, i.e. inflow to the system

along the boundary is calculated. The estimated slope points are averaged and used in Darcy's equation (15.2) to find the lateral inflow and outflow across the boundary,

$$Q_{in/out} = T * i * L \tag{15.2}$$

where

$Q_{in/out}$ Lateral inflow [m^3/month],
T Transmissivity of the aquifer [m^2/month],
i hydraulic gradient, and
L length of the boundary [m].

15.3.2.3 Calibration of Groundwater Model

We employ an evolutionary algorithm to calibrate the parameters of the groundwater model. We preferred to use evolutionary algorithms instead of gradient-based methods for calibration as they enable calibration in cases when the response function is not smooth and can have local minima. The non-dominated sorting genetic algorithm (NSGA-II) chosen here is a fast and elitist multi-objective evolutionary algorithm that works with the elitist search method to preserve the best solution in the next iteration (Deb et al. 2002). The main advantages of NSGA-II are less computational complexity, diversity preserving, elitism, and real-valued representation. The flowchart of the NSGA-II algorithm is shown in Fig. 15.6. It starts with the random generation of the initial population and evaluates the fitness based on the non-dominated sorting. Genetic algorithm is used to create the child population using binary tournament selection, recombination, and mutation. Different Pareto

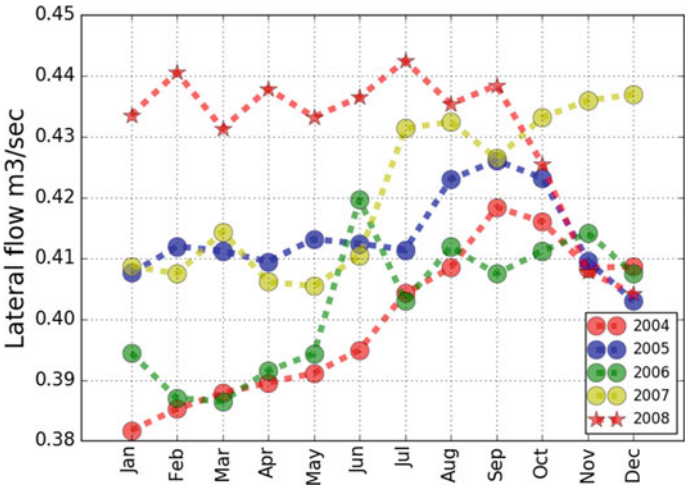

Fig. 15.6 Lateral flow across the boundary for five years (2004–2008)

fronts are identified using non-dominated sorting by combining the child and parent population. The elitism algorithm generates a new population with better solutions for the combined population. Crowding distance sorting is performed in a combined population to ensure that the solutions selected are well spread on the Pareto front. If the crowding distance value is larger, then the solutions are widely distributed and have a chance of diversity. Repeat the procedure until it meets the stopping criteria.

15.3.2.4 Objective Functions

The objective functions used for optimization are root mean squared error (RMSE), mean absolute error (MAE), and Nash–Sutcliffe model efficiency (NSE). RMSE and MAE are minimized while NSE has to be maximized. RMSE, MAE, and NSE are defined as

$$\text{Min. RMSE} = \sqrt{\frac{\sum_{n=1}^{i} \left(h_{sim,i} - h_{obs,i}\right)^2}{N}} \tag{15.3}$$

$$\text{Min. MAE} = \frac{\sum_{n=1}^{i} abs(h_{sim,i} - h_{obs,i})}{N} \tag{15.4}$$

$$\text{Max. NSE} = 1 - \frac{\sum_{n=1}^{i} \left(h_{sim,i} - h_{obs,i}\right)^2}{\sum_{n=1}^{i} \left(h_{obs,i} - \overline{h_{obs}}\right)^2} \tag{15.5}$$

where n is the number of months, $h_{sim,i}$ is the simulated groundwater level at month i, and $h_{obs,i}$ is the observed groundwater level at month i and $\overline{h_{obs}}$ is the average observed depth to groundwater across the time period. The best values for RMSE and MAE are 0, while for NSE it is 1.

15.4 Results and Discussions

15.4.1 Lateral Flow Estimation

Lateral inflow and outflow are obtained from the groundwater elevation across the boundary, as shown in Fig. 15.5. The aquifer's transmissivity varies from 7 to 290 m^2/day (Varalakshmi et al. 2014), and we considered an average value for further analysis to estimate lateral flow in Darcy's equation. It is identified that the direction of flow is moving toward two depressions within the study area. Hence, the flow that enters the system (study area boundary) is more than the flow that exits the system. The estimated mean and standard deviation of lateral flows across all years are 0.41 m^3/s and 0.016 m^3/s, respectively. We find inter-annual variations of lateral

flow varying from 0.38 to 0.44 m^3/s. Besides, we find that intra-annual variations of lateral flow are of the same order of magnitude as the inter-annual variations. For four out of five years, lateral flow peaks post monsoon in the months of July–Oct. The year 2008 showed a significantly different trend than other years as the lateral flow in this year remained higher with a different monthly pattern (Fig. 15.6).

15.4.2 Calibration and Validation of the Model

The NSGA-II optimization method is used to run 100 iterations during the calibration period (2004–2007) and results in the best Pareto optimal front. Three objective functions such as RMSE, MAE, and NSE are considered in this study to check the performance of the model. Recharge factor (r), specific yield (S_y), and maximum pumping rate ($Q_{p,max}$) are the decision variables of the model. Here, the pumping rate attains the maximum pumping rate in non-monsoon season and 50% less $Q_{p,max}$ in monsoon season.

We also considered three recharge scenarios, (i) constant recharge factor, r_1, or all the months; (ii) two sets of recharge factors, r_1 for monsoon season, and r_2 for non-monsoon season; (iii) three sets of recharge factors, r_1 for winter season, r_2 for summer season, and r_3 for monsoon season. The objective functions are not strictly conflicting with each other, but the optimization results with the set of optimal solutions that account for the trade-off between the objectives for three cases are shown in Fig. 15.7. It is observed that the dynamic variation of the recharge rate over the months gives better results and than the constant recharge rate during the calibration period (2004–2007).

The best optimal solution with the lowest RMSE, MAE, and highest NSE is selected from the final Pareto front, which is further used for simulation of the model during the calibration and validation period. Hyderabad is mainly covered with granitic terrain and has hard rock aquifers, which implies the natural recharge can be only 7–8% of precipitation, according to studies conducted for natural recharge

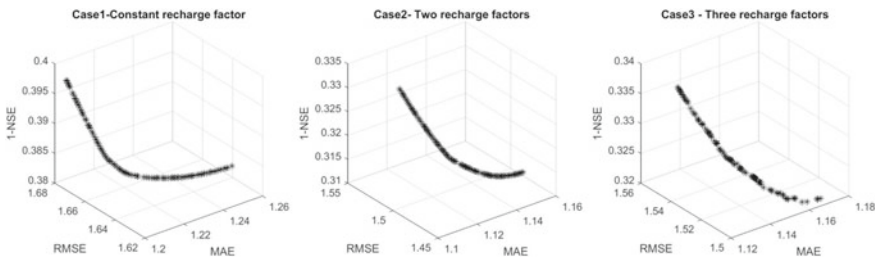

Fig. 15.7 Non-dominated Pareto front between the three objective functions. Case1: constant recharge rate for all the months; case2: two recharge rates for monsoon and non-monsoon season; case3: three recharge rates for cold, hot, and monsoon seasons

measurements in hard rock areas (Van Rooijen et al. 2005). Another study has also estimated recharge to be 9.2% of total rainfall for the Musi catchment using a numerical model (Massuel et al. 2007). We find that dynamic recharge occurs with 25% of rainfall in monsoon and 0, 7.7% of rainfall in the summer and winter seasons as a recharge rate from the rainfall in the calibration period.

It is observed that the simulated groundwater level fits better with the observed data for dynamic variation of recharge sets than the constant recharge factor as shown in Fig. 15.8. We also find that the model overestimates during the monsoon season of the year 2005 for all the cases. The performance of the model is identified with the help of statistical metrics such as RMSE, MAE, and NSE for the three cases as detailed in Table 15.2. The best solution set obtained during the calibration is simulated for the validation period (year 2008) as shown in Fig. 15.9. Here, we find that the constant recharge factor fits better with RMSE as 0.71, NSE as 0.9, and MAE as 0.53 than the other dynamic variation in case2 with RMSE as 1.22, NSE as 0.71, and MAE as 0.99, and case3 with RMSE as 1.08, NSE as 0.77, and MAE as 0.85. It is also observed that groundwater level is overestimated during the non-monsoon season.

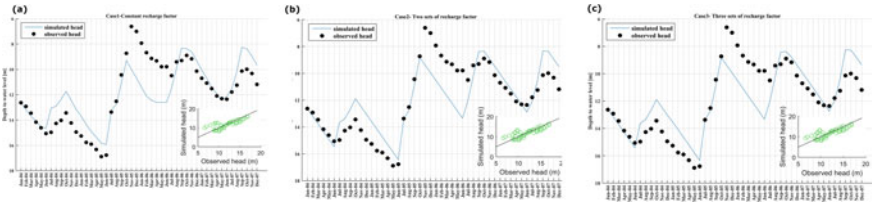

Fig. 15.8 Observed versus simulated head for three cases during calibration period (2004–2007): **a** constant recharge factor. **b** Two sets of recharge factors. **c** Three sets of recharge factors

Table 15.2 Best solution of the decision variables and its objective functions from the Pareto optimal set for the three cases

Cases	S_y	r_1	r_2	r_3	$Q_{p,max}$	RMSE	MAE	1-NSE
1	0.01411	0.125	–	–	56.13	1.64	1.25	0.38
2	0.02588	2.01E-05	0.25	–	81.57	1.48	1.15	0.31
3	0.02654	0.078	0.0008	0.254	83.78	1.5	1.17	0.32

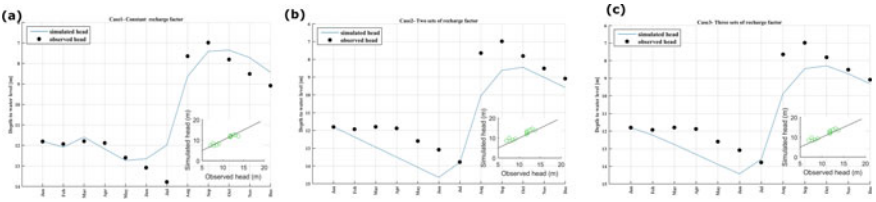

Fig. 15.9 Observed versus simulated head for three cases during 2008: **a** constant recharge factor. **b** Two sets of recharge factors. **c** Three sets of recharge factors

15.5 Conclusions

The study understands the conceptual framework of the groundwater model and calibrates the model with the application of NSGA-II. A data-driven model is a good, efficient tool with less uncertain data that is used for the groundwater level investigation. Based on the above results, it is clear that lumped groundwater balance model can be easily applied based on the inflow (rainfall, lateral inflow) and outflow (lateral outflow, abstraction rate) of the system. The study finds that lumped model is able to capture the trend and remains stable across the calibration period (2004–2007) and is observed with the variation of groundwater level for different recharge scenarios. The best set of solutions is identified from the Pareto optimal solution during the simulation of 4 years using NSGA-II. We identified the simulated groundwater level fits better for dynamic recharge variation conditions (case2, case3) than the constant recharge factor for all the months. It was also observed that the simulated groundwater level shows a better fit with the observed data for constant recharge with RMSE as 0.7, MAE as 0.5, and NSE as 0.9 during the validation period (2008). Hence, this paper illustrates the lumped groundwater modeling with the optimization method in a hard rock semi-arid region, which can be a well-suited tool for estimating available groundwater resources and building the future management scenarios for framework analysis.

Acknowledgements The authors are thankful to CGWC and IMD for providing data for this research work.

References

Baalousha H (2005) Using CRD method for quantification of groundwater recharge in the Gaza Strip, Palestine. Environ Geol 48:889–900. https://doi.org/10.1007/s00254-005-0027-x

Bredenkamp DB, Botha LJ, Van Tonder GJ, Van Rensburg HJ (1995) Manual on quantitative estimation of groundwater recharge and aquifer storativity: based on practical hydro-logical methods. Water Research Commission

Census of India (2011) http://www.census2011.co.in/census/metropolitan/342-hyderabad.html. Accessed 13 Oct 2018

Deb K, Pratap A, Agarwal S, Meyarivan T (2002) A fast and elitist multiobjective genetic algorithm: NSGA-II. IEEE Trans Evol Comput 6:182–197. https://doi.org/10.1109/4235.996017

Gumma RK, Rao PN, Varadaraj N, Kumar GP (2011) GW-senarioin cities-May 2011

Majumdar PK, Ram S, Rao PR (2009) Artificial recharge in multiaquifers of a mountainous watershed. J Hydrol Eng 14:215–222. https://doi.org/10.1061/(ASCE)1084-0699

Massuel S, George B, Gaur A, Nune R (2007) Groundwater modeling for sustainable management in the Musi catchment, India resource. In: International congress on modelling and simulation, pp 1429–1435

Narain S (2012) Excreta matters, vol 1. Center for Science and Environment, New Delhi

Schnaar G, Dodge JJ, Cullen SJ (2016) Comprehensive groundwater balance development to characterize selenium loading to surface water channels in Orange County, California. J Contemp Water Res Educ 5–23

Sekhar M, Shindekar M, Tomer SK, Goswami P (2013) Modeling the vulnerability of an urban groundwater system due to the combined impacts of climate change and management scenarios. Earth Interact 17. https://doi.org/10.1175/2012EI000499.1

Singhal V, Goyal R (2011) GIS based methodology for groundwater flow estimation across the boundary of the study area in groundwater flow modeling. J Water Resour Prot 3:824–831. https://doi.org/10.4236/jwarp.2011.311092

Van Rooijen DJ, Turral H, Biggs TW (2005) Sponge city: water balance of mega-city water use and wastewater use in Hyderabad, India. Irrig Drain 54:S81–S91. https://doi.org/10.1002/ird.188

Varalakshmi V, Rao BV, SuriNaidu L, Tejaswini M (2014) Groundwater flow modeling of a hard rock aquifer: case study. J Hydrol Eng 19:877–886. https://doi.org/10.1061/(ASCE)HE.1943-5584.0000627

Xu Y, Tonder GJV (2001) Estimation of recharge using a revised CRD method. Water SA 27:341–344

Chapter 16
Assessment of Groundwater Quality of the Aquifer Adjacent to River Bharalu in Guwahati City, Assam, India

Mamata Das, Jayashree Sarma, Bhrigumani Sharma, and Rajib Kumar Bhattacharjya

Abstract In this study, the groundwater quality adjacent to river Bharalu is monitored for three years to understand its seasonal and spatial variation. The physiochemical analysis of water samples such as Turbidity (NTU), Total Dissolved Solids (mg/L), pH, Alkalinity (mg/L), Hardness (mg/L), Dissolved Oxygen (mg/L), Biochemical Oxygen Demand (mg/L), Chemical Oxygen Demand (mg/L), Iron (mg/L), Fluoride (mg/L), Chloride (mg/L), Potassium (mg/L), Calcium (mg/L), and Magnesium (mg/L) are analyzed as per standard methods prescribed by APHA (Standard methods for the examination of water and wastewater. American Public Health Association, 1989). From the investigation, it is observed that the groundwater is extremely turbid with different inorganic and organic waste, metals, and ions. The concentration of different pollutants present in the groundwater increases sufficiently towards the downstream site of the Bharalu river basin with some variation in the middle course. This variation may be due to the presence of point source contamination (domestic and municipal wastewater), non-point source contamination (runoff from refineries, construction sites), as well as natural processes (weathering of soil and rock), or surface water-groundwater interaction.

Keywords Concentration · Groundwater · Water quality · Bharalu River · Pollutants

M. Das · J. Sarma · B. Sharma · R. K. Bhattacharjya (✉)
Department of Civil Engineering, Indian Institute of Technology Guwahati, Guwahati 781039, India
e-mail: rkbc@iitg.ernet.in

J. Sarma
e-mail: jayashreesarma@iitg.ernet.in

B. Sharma
e-mail: bhrigumani@iitg.ernet.in

R. Jha et al. (eds.), *Groundwater and Water Quality*, Water Science and Technology Library 119, https://doi.org/10.1007/978-3-031-09551-1_16

16.1 Introduction

Guwahati is one of the fastest-growing cities in India. The city is considered as the gateway of Northeast India. The population of the city is increasing at an alarming rate, and thus the people of the city are more concerned over the quality and quantity of water resources that are present on both surface and under the ground. Though the river Brahmaputra is flowing through the heart of the city, the major source of water for the people of Guwahati city is still groundwater, extracted from confined and unconfined aquifers. The water supply system is not yet developed fully, and as such, only a few percentage of the city population are getting the municipal water supply. Therefore most people are still dependent on open wells and tube wells to meet their daily water requirements.

A small tributary of the river Brahmaputra, known as river Bharalu, is flowing through the city. In the early days, people residing on the bank of the river Bharalu use it as a portable source of drinking water. Nowadays, due to a lack of proper management, the untreated sewage, effluent, municipal solid wastes, and domestic wastes of Guwahati city are disposed of directly to river Bharalu. Hence, converting the river as the main drainage channel of Guwahati city. The river Bharalu carries the pollutants from the entire city and is disposed it into the Brahmaputra at Bharalumukh. This has also polluted the river Brahmaputra. Due to the presence of such a polluted river, there is a high chance of groundwater contamination as a result of surface water-groundwater interaction (SWGWI). SWGWI is one of the major issues of contamination of groundwater aquifers. However, as it is difficult to observe and measure the contamination, it has been ignored in many water management policies. As such, there is a need to evaluate the groundwater quality of the aquifers adjacent to the river.

In this study, a water quality assessment is carried out on the groundwater aquifers adjacent to the river Bharalu within Guwahati city.

16.2 Study Area

The study is carried out adjacent to the longitudinal section of the river Bharalu in the greater Guwahati city of Kamrup Metro district, Assam, India. Guwahati is the premier city of North-East India that lies in between the Brahmaputra River and the Shillong Plateau. The city connects the valley of river Bharalu, which is a small tributary of the Brahmaputra. The city extends latitudinally from 26° 5′ N to 26° 12′ N and longitudinally from 91° 24′ E to 91° 51′ E. The climate of Guwahati is a humid subtropical type. The average annual temperature is 24.2 °C with extremes ranging from 40.6 °C recorded on April 24, 2014, to 3.0 °C recorded in January 1964. The population of the city is growing at an alarming rate. As per the census of 2001, the population of the city was 808,021. It has been recorded that the population

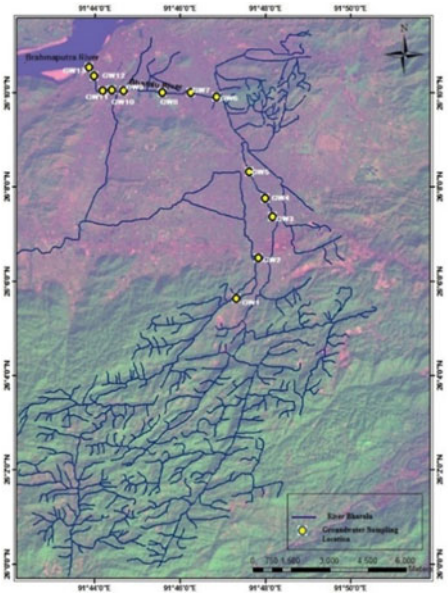

Fig. 16.1 Map showing the groundwater sampling sites on the river Bharalu basin

is growing rapidly in the metropolitan area and had risen to 1.5 million by 2012. Figure 16.1 shows the groundwater sampling locations adjacent to river Bharalu.

16.3 Methodology

Monitoring Sites

In the present study, a total of thirteen sampling locations were selected for monitoring the groundwater quality. The sampling locations shown in Fig. 16.1 are starting from Basistha Mandir to Bharalumukh. Table 16.1 listed the sampling locations. The sampling location is designed to cover the entire Bharalu River within Guwahati city. This will reasonably able to represent the water quality of groundwater adjacent to the river basin.

The first four sampling locations (GW1–GW4) are located at the upstream site of the river, and the area is less populated relative to other areas. The other locations (GW5–GW9) are located in the heart of the city adjacent to the river Bharalu, where the river is interconnected with different drains and industrial, and municipal waste disposal sites. The remaining four locations (GW10–GW13) are present at the downstream region of the River Bharalu, which is thickly populated.

Collection of Samples

The groundwater samples were collected for 13 locations, as stated above. Water samples are collected within a time interval of three months from 2014 to 2016.

Table 16.1 Sampling location along the river Bharalu

Sampling point	Locations
GW1	Basistha Mandir
GW2	Natun Bazar, Basistha
GW3	Bhetapara
GW4	Beltola
GW5	Rukminigaon
GW6	Jonali
GW7	Anilnagar
GW8	Ulubari
GW9	Chabipool
GW10	Athgaon
GW11	Fatasil
GW12	Sluicegate
GW13	Bharalumukh

Water samples are collected in pre-cleaned plastic bottles of 2.5 L capacity. Plastic bottles are rinsed a number of times with distilled water and dried thoroughly before the collection of the sample. After that, the collected water samples are stored for further analysis.

Laboratory Analysis of Water Samples

The experimental study is carried out as per standard methods prescribed by APHA (1989). The parameters that were examined are given in Table 16.2. Among them, Dissolved oxygen (mg/L), Electrical Conductivity (μmhos/cm) and pH were measured on the sampling spot by using the YSI Multi-parameter water testing probe. The concentration of the analyzed parameters is compared with the standard permissible limit as given by IS: 10500-2012 for drinking water (Table 16.3). The maximum acceptable limit of COD is considered as 10 ppm as set by W.H.O., I.S.I., I.C.M.R., Govt. of India for drinking water standard. The maximum value of BOD for fresh river water should be below 1 mg/L (Connor 2016).

16.4 Results and Discussion

The physicochemical analysis of the groundwater samples adjacent to river Bharalu is carried out with seasonal and spatial variation. A total of three samples were collected in the dry season and four samples in the wet season. The concentration obtained after the analysis is presented graphically to understand its spatial variation.

Dry season: In the dry season, three samples were collected from all thirteen locations. Among the three, the samples having the maximum concentration of the parameters are considered to compare the longitudinal variation.

Table 16.2 The water quality parameters considered in this study

Parameters	Symbols	Units
Turbidity	~	NTU
Total dissolved solids	TDS	mg/L
pH	pH	mg/L
Alkalinity	~	mg/L
Total hardness	TH	mg/L
Dissolved oxygen	DO	mg/L
Biochemical oxygen demand	BOD	mg/L
Chemical oxygen demand	COD	mg/L
Iron	Fe^{+2}	mg/L
Fluoride	F^{-}	mg/L
Chloride	Cl^{-}	mg/L
Potassium	K^{+}	mg/L
Calcium	Ca^{+2}	mg/L
Magnesium	Mg^{+2}	mg/L

Table 16.3 Standard value of the water quality parameters for drinking water as per IS: 10500: 2012

Water quality parameters	Requirement (acceptable limit)	Permissible limit in the absence of alternate sources
pH	6.5–8.5	No relaxation
TDS (mg/l)	500	2000
Total hardness (mg/l)	200	600
Alkalinity (mg/l)	200	600
Iron	**0.3**	**No relaxation**
Chloride (mg/l)	250	1000
Fluoride (mg/l)	1	1.5
Calcium (mg/l)	75	200
Magnesium (mg/l)	30	100
Turbidity (NTU)	1	5

Wet season: In the wet season, four samples were collected from all thirteen locations. Among the four, the samples having the maximum concentration of the parameters are considered to compare the longitudinal variation.

pH: The pH range is measured to know the presence of hydrogen ion concentration in drinking water. In our investigation, groundwater's pH value ranged from 6.0 to 7.9, as shown in Figs. 16.2 and 16.5. This indicates that water is slightly acidic in the same sampling locations, and it is slightly alkaline also in some other locations. Both in the dry and wet seasons, the pH value in the Beltola location is high compared to the

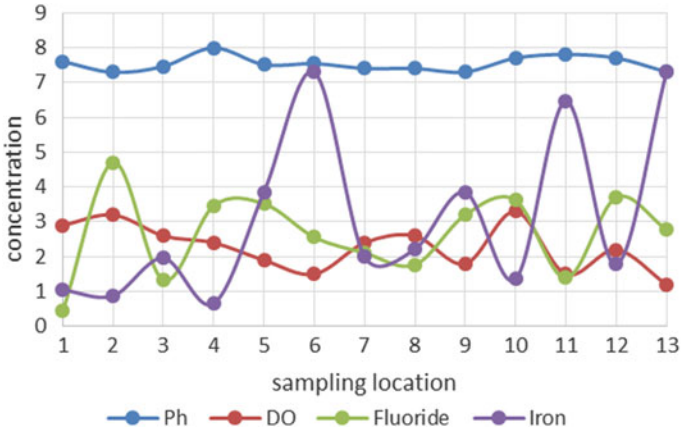

Fig. 16.2 Variation of pH, DO (mg/L), fluoride (mg/L), and iron (mg/L) concentration of groundwater at different sampling locations during the dry season

other locations. The pH values are well within their permissible limit as prescribed by IS: 10500: 2012 in almost all the sampling locations.

Total Dissolved Solids: The dissolved solids that are present in natural water are mainly due to the dissolution and weathering of rock and soil. Water having high total dissolved solids (TDS) is harmful to human health. This study has shown that the TDS present in groundwater is high in the wet season than in the dry season. The TDS value ranges from 237 to 500 mg/l, with the maximum value recorded in Chabipool and Fatasil locations. Figures 16.3 and 16.6 show that the TDS value increases from the upstream site to the downstream site of the river with some fluctuation in the middle sampling locations.

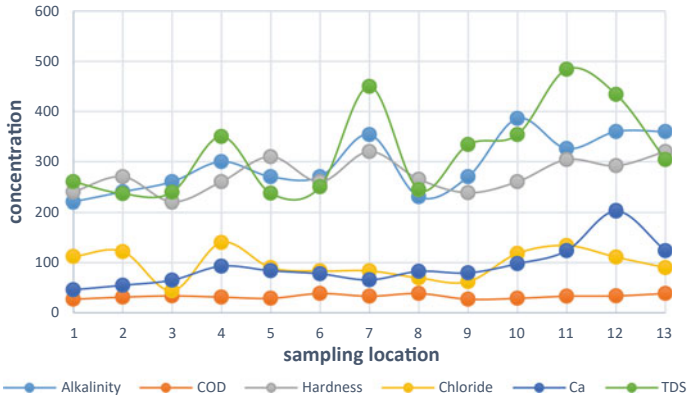

Fig. 16.3 Variation of alkalinity (mg/L), TDS, hardness (mg/L), COD (mg/L), chloride and calcium concentration of groundwater at different sampling locations during dry season

Turbidity: The turbidity of the water is mainly influenced by the presence of different organic and inorganic matters and the suspended solids present in the water. The turbidity of water varies seasonally. The chemical analysis shows that the turbidity value ranges from 8.8 to 28.2 NTU, which is not acceptable as per the drinking water standard. The maximum value is recorded in the downstream site with some variation within the middle region. The average value of turbidity found in groundwater is 19 NTU. Based on the average value of turbidity, the groundwater adjacent to river Bharalu can be termed as highly turbid.

Alkalinity: Alkalinity can be termed as the ability to neutralize acids and is expressed as mg/l. Water with high alkalinity is indigestible, which may cause gastrointestinal discomfort to the human being. From the investigation, it is noted that during the dry season, the observed mean value of alkalinity is 295.84 mg/l and ranges from 220 to 386 mg/l (Fig. 16.3). In the wet season, the alkalinity value ranges from 186 to 292 mg/l with a mean value of 243 mg/l (Fig. 16.6). From these figures, it is found that the alkalinity content near Basistha Mandir is within the permissible limit.

Hardness: In natural water, the hardness of water is influenced by the presence of dissolved calcium and magnesium salts. In the case of surface water, seasonal variations of water hardness often occur. Whereas on the other hand, Groundwater hardness is less variable. From Figs. 16.3 and 16.6, it can be noted that the average mean value of hardness observed in the groundwater sample is 227.017 mg/l. The highest value (272 mg/l) was recorded in the Jonali location, which is located in the middle region of the basin. The lowest value (190 mg/l) was recorded during the wet season near Athgaon, which is located downstream region of the basin. Thus, no clear trend of variation of hardness from season to season or from point to point has been seen.

Dissolved Oxygen: For healthy water quality, an adequate amount of dissolved oxygen is necessary. From Figs. 16.2 and 16.5, it is observed that the DO value ranges from 1.2 to 3.5 mg/l. The high value of DO was recorded in Natun Bazar, Basistha, and low value in Bharalumukh location. The graphical representation shows a decreasing trend of DO from the upstream section of the river Bharalu towards the downstream section in both the season (Figs. 16.2 and 16.5).

Organic Matters: Both BOD (Biochemical Oxygen Demand) and COD (Chemical Oxygen Demand) are considered as the main parameters to evaluate the degree of pollution in the river (Sawyer and McCarty 1978). When the BOD values exceed 8 ppm, then the water is severely polluted (Connor 2016). The BOD below 1 mg/l is considered to be freshwater. In this investigation, it is observed that the BOD concentration ranges from 1.5 to 7 mg/l. The BOD level in the dry season is less compared to the wet season, as shown in Figs. 16.4 and 16.7. In the case of COD, the value ranges from 17 to 38.4 mg/l, which is not acceptable for drinking purposes. The high COD value is noticed at the river basin's downstream site and low in the upstream section. In comparison to the seasonal variation, the COD value is less in the wet season than in the dry season. Thus, this may result in a decrease in dissolved oxygen in groundwater.

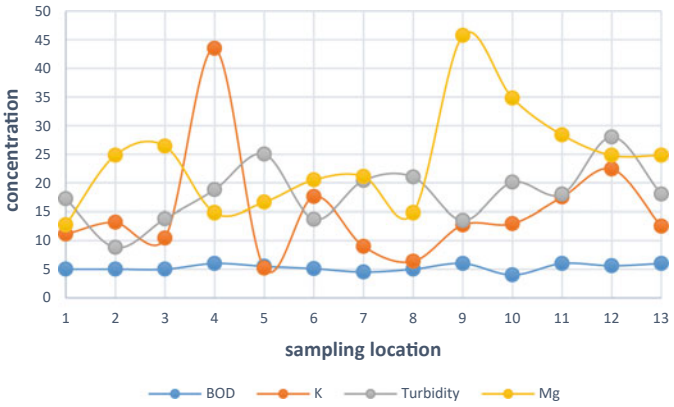

Fig. 16.4 Variation of BOD, potassium (K), magnesium (Mg), and turbidity (NTU) concentration of groundwater at different sampling locations during the dry season

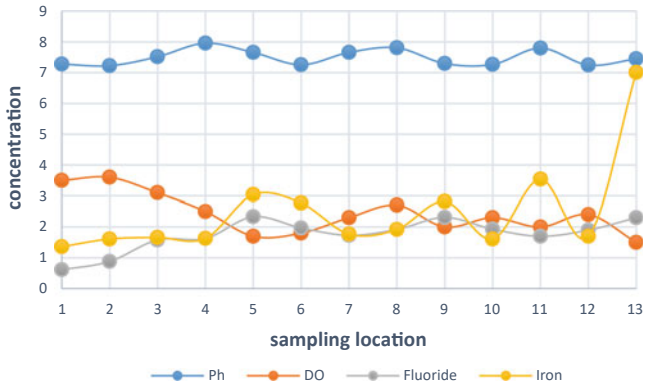

Fig. 16.5 Variation of pH, DO (mg/L), fluoride (mg/L), and iron (mg/L) concentration of groundwater at different sampling locations during the wet season

Basic Ions: Chloride (Cl^-), Potassium (K^+), Calcium (Ca^{+2}), and Magnesium (Mg^{+2}) are the ions that are examined in the groundwater samples. The high chloride content in drinking water is unhealthy for human or livestock watering. In this present study, the chloride concentration was found to range from 59.66 to 119.3 mg/l (Figs. 16.3 and 16.6). The value is within the permissible limit of the drinking water standard. Potassium is a highly soluble salt that is found in the form of ions in water. It is observed from Figs. 16.4 and 16.7 that the value of potassium concentration ranges from 12.4 to 48 mg/l. The high potassium content is observed in Beltola both during the dry and the wet season. Magnesium, along with the calcium content, is the main contributor to water hardness. Magnesium is usually less abundant in water than calcium. For calcium the average concentration recorded is 91 mg/l (range 45–202 mg/l). In both dry and wet seasons, the minimum Calcium content is observed

near Basistha Mandir (upstream site), and the maximum is found in the Sluice gate location (downstream site). In the upstream site of the river basin, the calcium content in groundwater is within its permissible limit (Figs. 16.3 and 16.6). In the case of Magnesium, the average mean value of concentration is noted as 26 mg/l. The low Magnesium value is recorded at the upstream sampling point, i.e., near Basistha Mandir, and the water quality of this region is better due to the presence of natural vegetation. Both in the dry and the wet season, the magnesium content in Bharalumukh, Sluice gate, Chabipool, and Athgaon locations is more than its permissible limit.

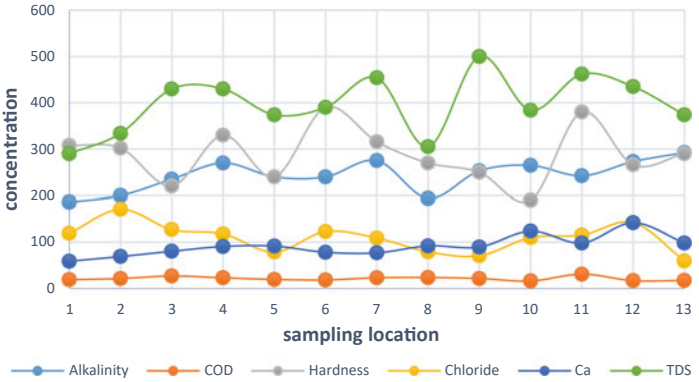

Fig. 16.6 Variation of alkalinity (mg/L), TDS, hardness (mg/L), COD (mg/L), chloride, and calcium concentration of groundwater at different sampling locations during the dry season

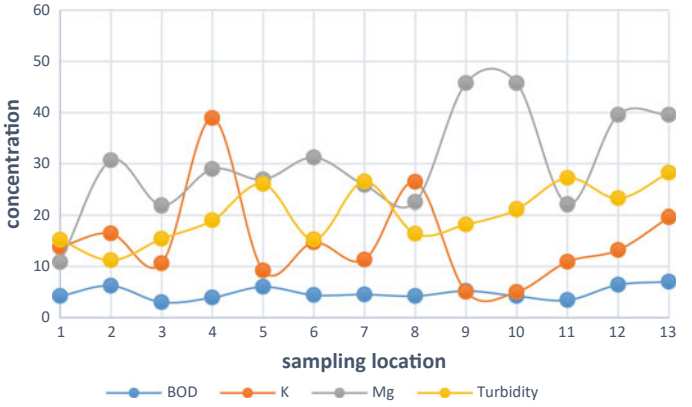

Fig. 16.7 Variation of BOD, potassium (K), magnesium (Mg) and turbidity (NTU) concentration of groundwater at different sampling locations during the dry season

Other Inorganic Variables and Metals: In this study, Fluoride and Iron content in groundwater is also investigated. The major inorganic contaminant found in groundwater is Fluoride (Maheshwari 2006; Das and Bhattacharjya 2020). This contamination takes place due to the fluoride-bearing rocks that get break down naturally. Thus, the Fluoride level is often higher in groundwater than the surface water. Climatic conditions may also influence the rate and degree of fluoride dissolution in water from rocks and soil. The analysis of data shows that the Fluoride of groundwater ranged from 0.03 to 3.98 mg/l with an average value of 1.52 mg/l (Figs. 16.2 and 16.5). The low Fluoride values are recorded at the sampling points near Basistha Mandir for all the seasons. At the downstream side of river Bharalu, the fluoride content of groundwater is found to exceed the permissible limit. The investigation shows that Fluoride concentration in many places is higher than the allowable limit and not safe for drinking. Iron is a common metallic element that is found in nature. When water percolates through soil and rock, it dissolves iron, and this mineral subsequently enters groundwater supplies. The average value of 1.46 mg/l with the highest value (7.29 mg/l) was recorded during the dry season in Bharalumukh and Jonali locations. The lowest value (0.13 mg/l) was recorded near the Basistha Mandir location.

16.5 Conclusions

The investigation shows that the groundwater adjacent to river Bharalu is thickly polluted with different inorganic and organic waste, metals, and ions. Though the pH value is within the permissible limits, the other parameters are not acceptable as per the drinking water standard. The groundwater near the river basin can be termed as "very hard" based on the average value. Magnesium and calcium contain also show high concentration. The groundwater is also rich in Fluoride and Iron concentration. The BOD and COD concentration is high at the downstream site of the river than the upstream site. This may produce high organic contamination and growth of algae. The low value of dissolved oxygen has been recorded at the downstream site of the river Bharalu. In summary, the quality of the groundwater adjacent to river Bharalu is inferior, and proper treatment should be done before using it for different domestic purposes.

Acknowledgements This work was carried out with the research grant received from the NRDMS division of the Department of Science and Technology, Govt. of India.

References

American Public Health Association, & American Water Works Association (1989) Standard methods for the examination of water and wastewater. American Public Health Association

Bureau of Indian Standards, Indian Standards (IS:10500:2012) Drinking Water Specification: New Delhi (2004)

Connor R (2016) The United Nations world water development report 2016: water and jobs. Chapter 2: The global perspective on water. UNESCO, Paris, p 26. ISBN 978-92-3-100155-0

Das M, Bhattacharjya RK (2020) A regression-based analysis to assess the impact of Fluoride Reach River water on the groundwater aquifer adjacent to the river: a case study in Bharalu River Basin of Guwahati, India. Pollution 6(3):637–665

Maheshwari RC (2006) Fluoride in drinking water and its removal. J Hazard Mater 137(1):456–463

Sawyer CN, McCarty PL (1978) Chemistry for environmental engineers. McGraw-Hill Book Company, New York

Chapter 17
Groundwater Modelling Using Coupled Model SWAT-MODFLOW in the Hiranyakeshi Sub-Watershed

H. T. Veena and Nagraj S. Patil

Abstract Groundwater modeling is a tool for estimating and solving several groundwater problems. There is an occurrence of proper quantification of the scarce water resources that are under the threats of growing population and changing climate, especially, in a country like India because of its low capacity to adapt. In an attempt to quantification of water resources, this study focuses on modeling the hydrologic process and groundwater flow process respectively. The coupled SWAT-MODFLOW model is used for groundwater modeling which was released recently in the year 2016. This model is fully coupled with surface water and subsurface water. The study area is the Hiranyakeshi sub-watershed in the Gataprabha sub-basin, this area is fully covered by hard rock and this watershed faces many groundwater problems, this is due to more industrial and agricultural activity. And this model is fully linked with sub-basin, HRU (Hydrological response unit), and river cells from SWAT are assigned to MODFLOW. Groundwater flow exchange rate between the aquifer and stream MODFLOW return to SWAT. Not many works have been done in the modeling of groundwater and this paper contributes to developing a proper understanding of the assessment of groundwater availability using coupled model SWAT-MODFLOW.

Keywords Groundwater modelling · Hydrologic process · Groundwater flow process · Hiranyakeshi watershed · SWAT-MODFLOW

17.1 Introduction

With the expanding populace and globalization, there is an expansion in water interest. (Bharath A et al., 2020). Both surface water and groundwater are significant assets to support human existence. As people have direct admittance to the surface water, it has been broadly misused, corrupting its quality and amount, making it a scant source. Nonetheless, headway in the innovation made it simple to extract water from the subsurface. In the new year, the utilization of water assets is reliant on

H. T. Veena · N. S. Patil (✉)
Department of Civil Engineering, Centre for PG Studies, VTU, Belagavi, Karnataka, India
e-mail: nagrajspatil@yahoo.com

R. Jha et al. (eds.), *Groundwater and Water Quality*, Water Science and Technology Library 119, https://doi.org/10.1007/978-3-031-09551-1_17

the ruling source accessibility, either groundwater or surface water. Groundwater is affected by natural processes and also by human activities. So they require a focused on and progressing administration to keep up the groundwater assets inside as far as possible. Groundwater administration and the strategy choices must be taken on the basis of past and present scenarios and a response should be made for future changes and to understand the uncertainties in those reactions. These groundwater models also provided an insight into the complex system behavior and when they are properly designed they are also an asset in developing conceptual understandings. Further, they can also forecast the outcome of the future, they can also conjecture the result of future groundwater behavior that helps in decision making and also assist in developing alternative management approaches. (Patil and Chetan, 2017). SWAT-MODFLOW model is based on the existing SWAT (version 2012) model that has been created with the Arc-SWAT interface. And a finite difference grid for a MODFLOW model, which is then linked with the HRUs and sub-basins of the SWAT model through geo-reprocessing routines.

17.2 Study Area

Hiranyakeshi Watershed was selected as the study area, which will come within the Ghataprabha sub-basin in Krishna basin, India and is one of the most essential areas of farming in the north Karnataka. Therefore, for the most part, the rural population in the catchment is flourishing aggressively, which results in raising requirements for the natural water resource. Basin catchment is generally semi-dry represented by its natural water resources shortage, low per capita water stipend and conflicting demands, and in addition, shared water resources. The basin area of the Hiranyakeshi Watershed lies in the region between the northern Lat 15° 56' N to 16° 21' N and eastern Long 74° 00' E to 74° 35'E. It covers a territory of 1233.33 sq. km. The climate is moderate subtropical with an average precipitation of 1500 mm physically. The Hiranyakeshi River begins in the Kaldagi gathering of Sahayadri extent, which comprises quartzite, sandstones, minor conglomerated, shales, and limestone. Ghataprabha River having the major tributaries namely Hiranyakeshi and Markandeya forms the main drainage for the area. The major part of the Hukkeri taluk is covered by black to red soils. These black soils are from the trap basement. The thickness of the soil varies from 0.5 m to 1.5 m in some parts of the Hukkeri. The major part of the Hukkeri taluk is covered by black to red soils. These black soils are from the trap basement. The thickness of the soil varies from 0.5 m to 1.5 m in some parts of the Hukkeri. The mean maximum varies between 35°c and 37.5°c and the mean minimum varies to about 10.7°c. South-west monsoon season starts from May and may exist till October. The irrigation tanks do not exist in the area, but a few percolating tanks are constructed at the initial catchment zones near Nerli, Shirahatti, Kudur, etc. Agriculture is the main occupation of Hukkeri taluk. Out of the total irrigated area, 60% of water is used by the surface water resources and the

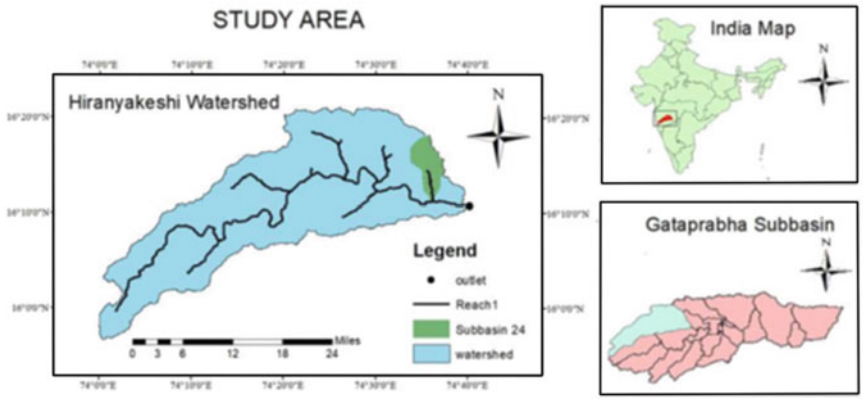

Fig. 17.1 Hiranyakeshi sub-watershed study map

rest 40% is groundwater. As per the Central Groundwater Board (CGWB) report the groundwater has been over-exploited in recent years (Fig. 17.1).

17.3 Methods and Methodology's

The methodology is the major/vital part of the modeling. The methodology adopted here, in this modeling depends on the objectives defined. Here SWAT-MODFLOW has been used for the groundwater modeling.

17.3.1 Data Required for SWAT and SWAT-MODFLOW Model

SWAT model requires data to physically represent the watershed, where the data used are DEM of topography, land use map, soil map, slope, and meteorological data (daily or monthly). The model accuracy depends on the quality of data and quantity of data available for the watersheds. SWAT-MODFLOW model requires data used are SWAT output shape files of HRU, sub-basin, river cell, MODFLOW parameters like aquifer thickness, hydraulic conductivity, specific storage, and specific yield. DEM of topography, and Observation wells.

17.3.2 SWAT Model

SWAT is a stream basin scale display created to evaluate the effect of land administration observes on water, residue, and farming invention yields an extensive complex watershed with differing soils, land utilization, and administration conditions over significant lots of time. The principle parts of SWAT incorporate climate, surface spill over, return stream, permeation, evapotranspiration, transmission misfortunes, lake and supply stockpiling plant development and water system, groundwater stream, reach routing, nutrient & pesticide loading and water exchange (Neitsch et al. 2011).

17.3.3 Description of SWAT Model

The initial phase in setting up of SWAT model is the watershed delineation utilizing DEM. An interface Arc-SWAT was utilized for this situation to prepare necessary input files to run the SWAT model. Arc-SWAT measures the Digital Elevation Model (DEM) and automatically delineates the watershed and sub-watersheds (Fig. 17.2).

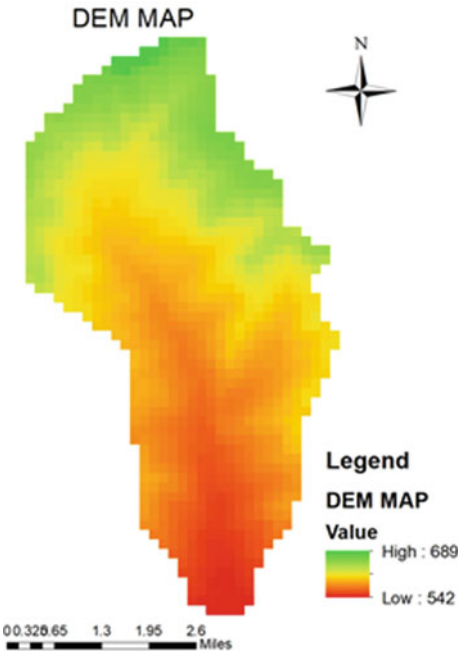

Fig. 17.2 Figure showing Digital Elevation Map

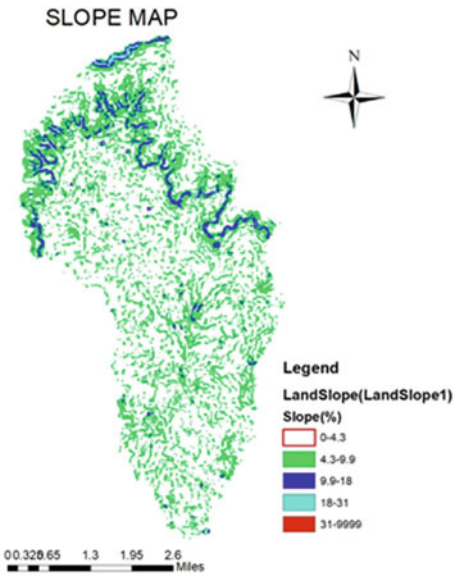

Fig. 17.3 Figure showing Slope map

17.3.4 HRU Analysis

Land use/ land cover map and soil map slope map were then overlaid. Based on the overlaying, basic units of modelling (Hydrologic Response Unit, HRUs) were extracted and create HRU feature class. In the current study, HRUs were defined by taking all land uses, soil type and slope occupying Zero threshold area into account. The maps of land slope (Fig. 17.6.) are shown below (Fig. 17.3).

17.3.5 Weather Stations Data

Precipitation and temperature information obtained from IMD, Pune was fed into the model as user-defined data for the weather parameters. A climate generator was utilized to produce and compose meteorological boundaries documents. After every one of these strategies, SWAT was run for the time of a long time from the year 1991 to 2005 with a warm-up time of 3 years.

17.4 Calibration and Validation of SWAT Model

The calibration and validation technique employed in SWAT to work out the sensitive parameter that influence the flow, sediment etc., and therefore the adjustment of sensitive parameters ought to be thoroughly done, the sensitive parameters area unit to be rigorously understood by the user before dynamic the values. Validation procedure involves comparing the calibrated value for the next set of your time series of discharge data with observed data to visualize how well the graph of simulated and observed flows fits once calibration. The activity is also done either manually or auto calibration also best matches the simulated and observed graph. Calibration and validation of area unit performed by mistreatment of observed discharge information could either be daily, monthly or yearly (Table 17.1).

17.4.1 SWAT-MODFLOW Model

SWAT-MODFLOW model is based on the existing SWAT (version 2012) model that has been created with the Arc-SWAT interface. And a finite difference grid for a MODFLOW model, which is then linked with the HRUs and sub-basins of the SWAT model through geo-reprocessing routines (Fig. 17.4).

SWAT demonstrates a MODFLOW model to give a coupled surface–subsurface hydrologic display. SWAT-MODFLOW is a combined hydrologic model that couples SWAT arrive surface procedures with spatially-express groundwater stream practices. SWAT-MODFLOW is the procedure for connecting SWAT highlights (HRUs, sub-basins) with MODFLOW framework cells. Recharge rates are passed from SWAT

Table 17.1 Showing parameters adjusted during calibration and Validation period

Parameters	Range	Initial value	Final value
CN_2	35–98	87	90
CH_N_2	0.01–0.3	0.014	0.3
CH_K_2	0–500	0	50
ALPHA_BF	0–1	0.048	0.2
GW_DELAY	0–500	31	50
RCHRG_DP	0–1	0.05	0.2
GWQMIN	0–5000	1000	1500
GW_REVAP	0.02–0.2	0.02	0.2
REVAP_MN	0–1000	750	900
SOL_AWC	0–1	0.104	0.2
SOL_K	0–2000	8.36	1000
SOL_Z	0–3500	300	500

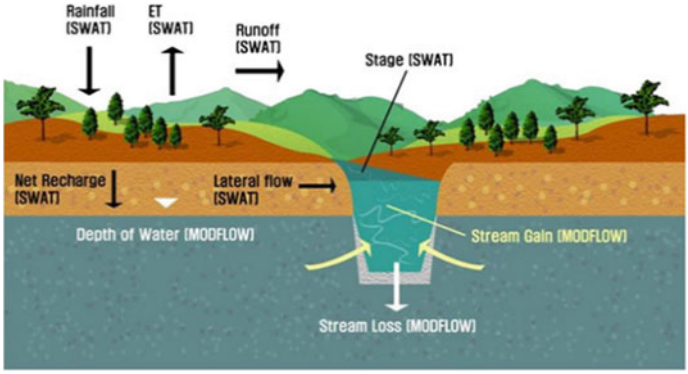

Fig. 17.4 Schematic diagram of integrated SWAT-MODFLOW (Kim et al., 2008)

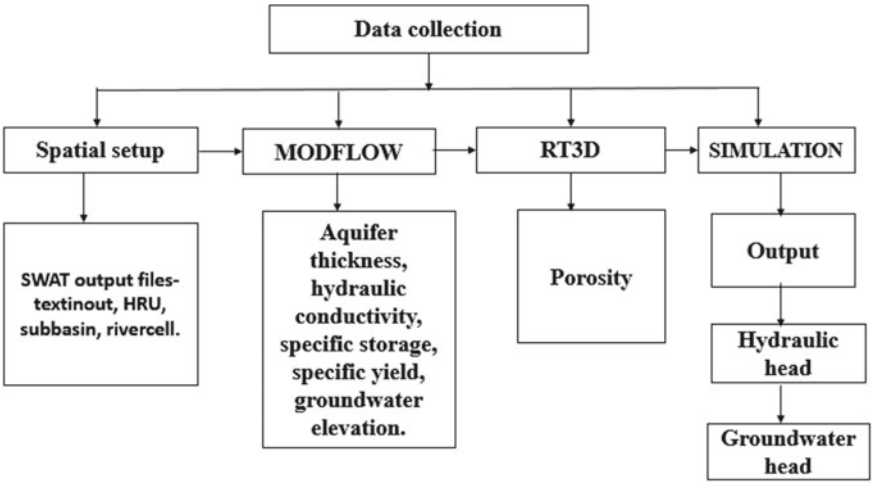

Fig. 17.5 Workflow process of Swat-Modflow

HRUs to the MODFLOW framework, and groundwater to surface product cooperation reproduced by MODFLOW is passed to SWAT sub-basin channels for directing (Fig. 17.5, Table 17.2).

17.4.2 SWAT-MODFLOW Model Set-Up & Execution

The first step of the interface provides the basic linkage between the existing SWAT model and a new MODFLOW model. Define the SWAT-MODFLOW project folder by specifying the path to the SWAT TxtInOut folder associated with the existing

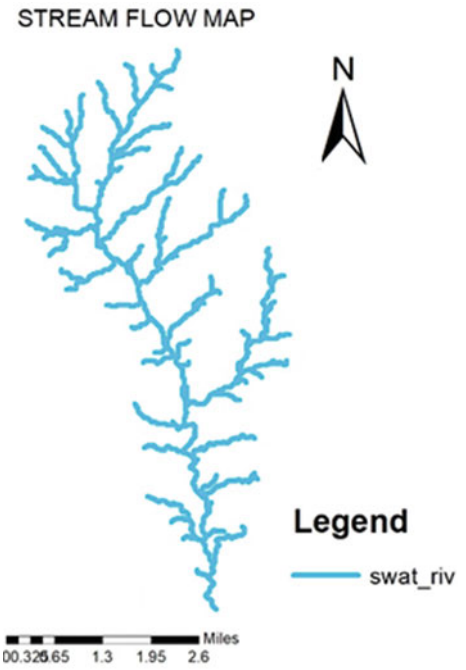

Fig. 17.6 Stream flow map

Table 17.2 Showing MODFLOW parameters

	Parameters	Values
1	Aquifer thickness	3 m
2	Hydraulic conductivity	0.01 m/day
3	Specific storage	0.001 1/m
4	Specific yield	0.2

SWAT model. Specify the paths to the sub-basin, HRU (no thresholds) and river network shape files that were created by Arc-SWAT. The Arc-SWAT shape files need to be converted to a raster format. Grid Cell Dimension for conversion of the raster is 30 m and it is strongly recommended to choose a MODFLOW resolution that is a multiple of the grid cell dimension selected for rasterizing the Arc-SWAT shape files. The MODFLOW grid cell dimension is 210 m. The Modflow tab required data to construct a MODFLOW model include aquifer characteristics, streambed conductivity, and initial values of groundwater hydraulic head. Most parameters can be provided as a single value, which then is copied to each grid cell, or else as spatially distributed values. SWAT-MODFLOW includes an optional linkage to RT3D (Reactive Transport in 3 Dimensions), which simulates the reactive transport of solutes through the aquifer system. Currently, only nitrate is included in the transport module. General SWAT-MODFLOW simulation settings such as simulation period and output specifications can be defined in the Simulation.

17.5 Result and Discussion

17.5.1 SWAT Model Results

The figure shows below stream flow, hydrological response unit, sub-basin and the shape files of SWAT model output. And these shape maps are the input files of the SWAT-MODFLOW model. As SWAT HRUs don't have an assigned geographic area, HRUs are disaggregated in pre-preparing GIS schedules. Disaggregation parts separated an HRU into singular polygons that have a particular geographic area. These disaggregated HRUs (DHRUs) are then converged with MODFLOW framework cells to pass factors among SWAT and MODFLOW likewise, MODFLOW River Cells, for which volumetric stream trade rates between the aquifers and the stream are assessed, are intersected with SWAT sub-basins for moving groundwater turn stream rates to the right sub-basin stream (Figs. 17.7 and 17.8).

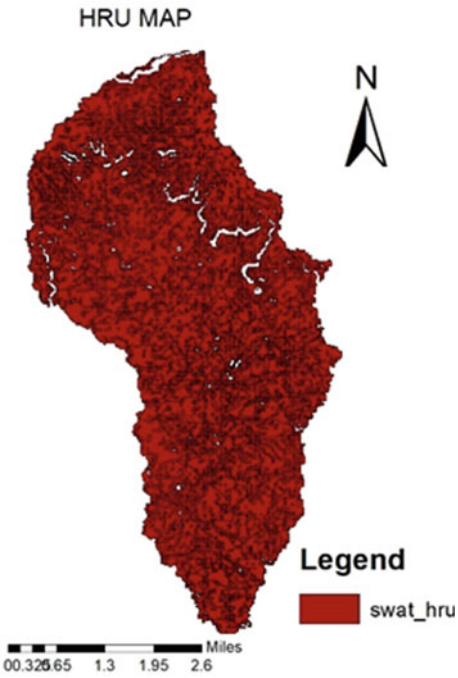

Fig. 17.7 HRU map

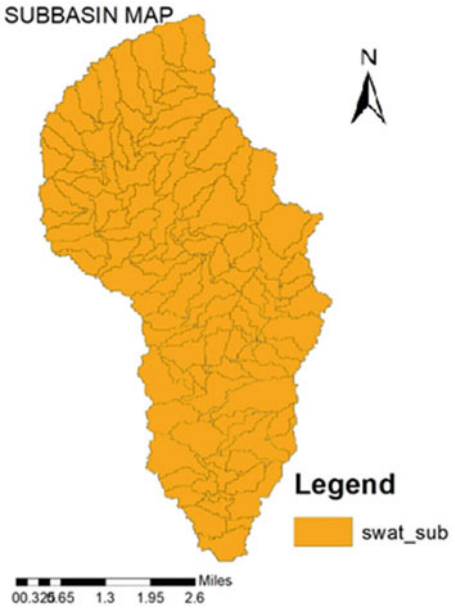

Fig. 17.8 Sub-basin map

17.5.2 Results of SWAT Calibration and Validation

In this calibration, the most sensitive parameters are CH_N_2, REVAP_MN, and SOL_K. The CH_N_2 is the Manning's co-efficient for the main channels. The threshold depth in the shallow aquifer for the re-evaporation (REVAP_MN) is 900 mm, which the land is capable of releasing less water for the evaporation in the shallow aquifer. The Flow graphs and R^2 values of the Goturu station are given below after the calibration process. The calibration is carried out for 10 years (1991–2000). And validated for 5 years (2001–2005).

After Calibration, next step taken was the validation of the model, again the model results and the simulated results were made a comparison with the next set of observed data from 2001 to 2005. Examination between the simulated and observed during the time of validation is shown in Figs. 17.9 and 17.10 shows the scattered plot of observed versus simulated discharge (Figs. 17.11 and 17.12).

The model performance is checked by R^2 and NSE values. The results are satisfied with the model. The values of R^2 and NSE values are shown below (Table 17.3).

The figure shown below is disaggregated hydrological response unit to determine each value of the MODFLOW grid (Fig. 17.13).

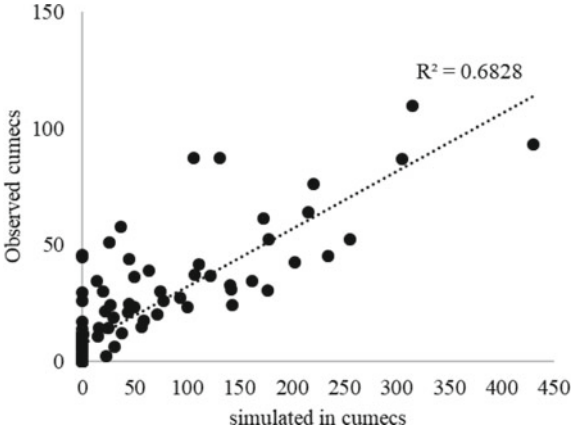

Fig. 17.9 Comparison of simulated and observed data after calibration

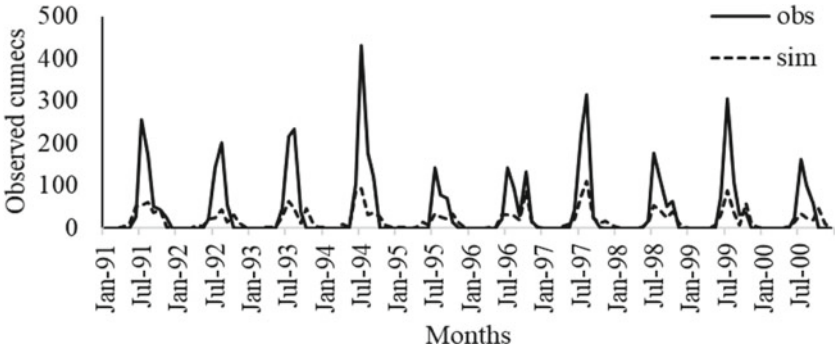

Fig. 17.10 Scattered graph of simulated and observed discharge after calibration

Fig. 17.11 Comparison of simulated and observed data for validation period

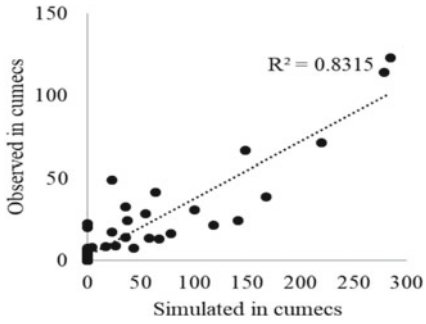

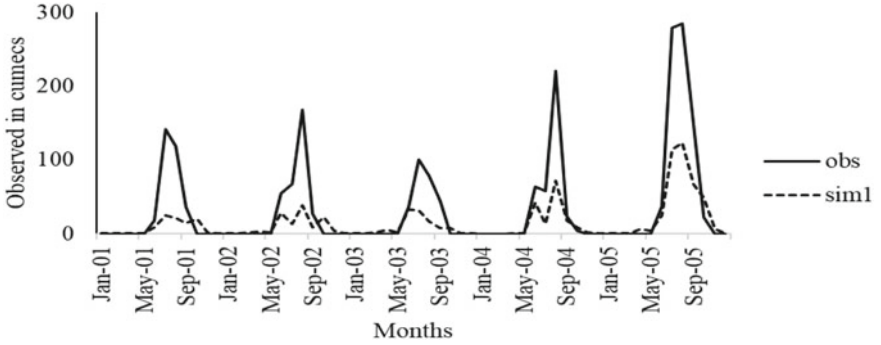

Fig. 17.12 Scattered graph of Simulated and Observed Data for Validation Period

Table 17.3 Showing results of R^2 and NSE for calibration and validation

Objective function	Calibration results	Validation results
R^2	0.68	0.83
NSE	0.72	0.73

Fig. 17.13 Figure showing Disaggregated HRU map

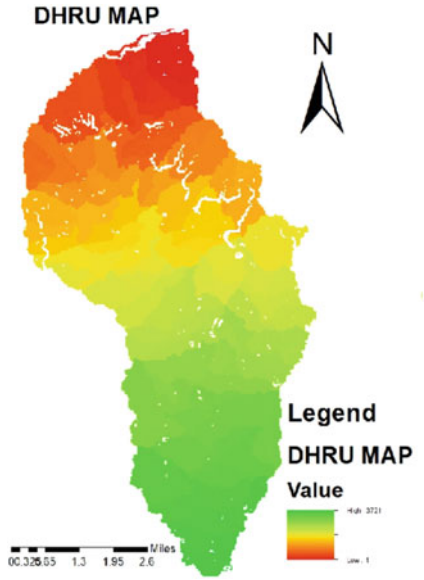

17.5.3 Modflow Head

Modflow head contains values, to find the groundwater table head for every single MODFLOW matrix cell, for each and every time period of the simulation. For each yield time, there is a header line followed by the hydraulic head values written by

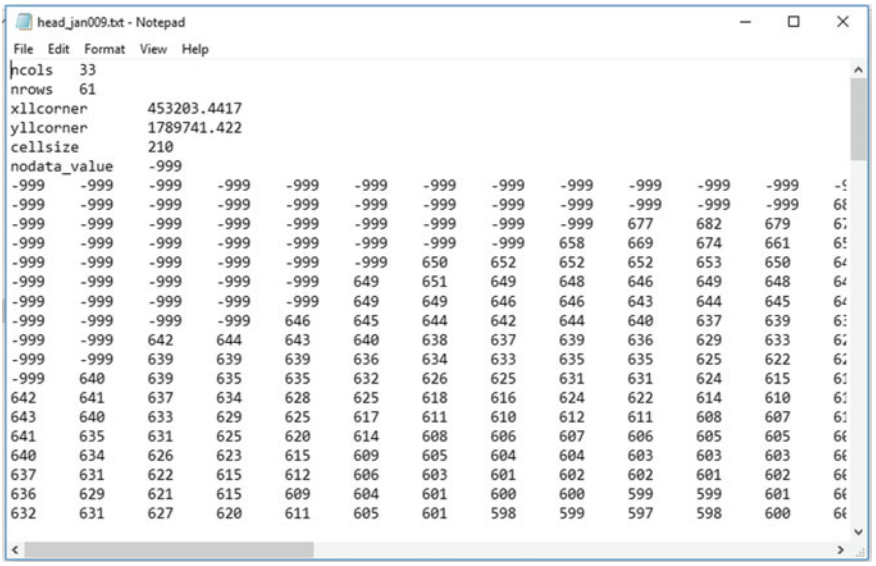

Fig. 17.14 Figure showing Groundwater head values

row and column. No-data values (i.e. cells outside of the basin area) are represented by "-999.0". Modflow. head values are converted to raster. Finally, groundwater head is obtained (Figs. 17.14 and 17.15).

17.6 Conclusion

Groundwater modelling is a tool that can help to analyze many groundwater problems. It is necessary to protect the water resource from the scarcity of water under the growing population and changing environmental conditions, especially, in a country like India. The study is carried out to quantify the water resource by modelling of the hydrological process. The groundwater head is determined by the SWAT-MODFLOW with the help of the SWAT model. The Hiranyakeshi watershed is facing groundwater problems due to the hard rock region. The groundwater head in this region is varying due to the changes in the Hydrological Response Units (HRU's) of the watershed. The results from the SWAT model are satisfied for the input of the SWAT_MODFLOW, and the calibration and validation are carried out to check the model performance. The R^2 and NSE are carried out and are satisfactory. The SWAT_MODFLOW is simulated to get the groundwater head. The model experiment is carried out to check the SWAT_MODFLOW out. The results show the groundwater head is very deep in the hard rock region. The proper surface water protections are to be carried out in this watershed. The proper groundwater recharge methods are adopted to increase the groundwater head.

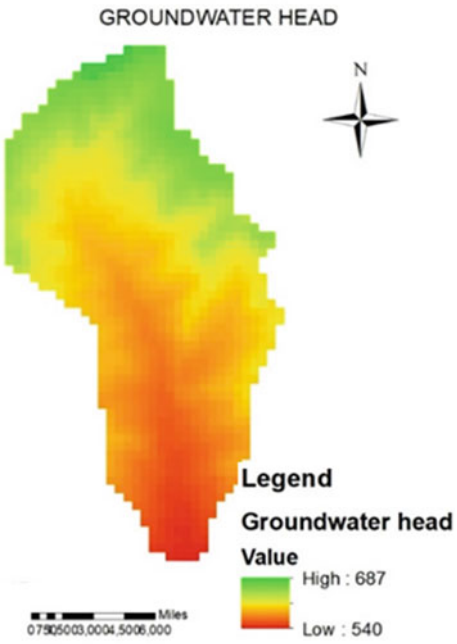

Fig. 17.15 Figure showing Groundwater head

Acknowledgements The authors would like to take this opportunity to recognize the efforts and assistance from every individual on all aspects in the preparation of this paper.

References

Arnold JG, Moriasi DN, Gassman PW, Abbaspour KC, White MJ, Srinivasan R, Kannan N (2012). SWAT: model use, calibration, and validation. Trans ASABE, 55(4), 1491-1508

Bailey RT, Wible TC, Arabi M, Records RM, Ditty J (2016) Assessing regional-scale spatio-temporal patterns of groundwater–surface water interactions using a coupled SWAT-MODFLOW model. Hydrol Process 30(23):4420–4433

Bharath A, Preethi S, Manjunatha M, Tangadagi RB (2020) Predict temp data ghataprabha sub-basin 26:140–144

Chu J, Zhang C, Zhou H (2010) Study on interface and frame structure of SWAT and MODFLOW models coupling. In: Egu General Assembly Conference Abstracts (vol 12, p 4559)

Chung IM, Kim NW, Lee J, Sophocleous M (2010) Assessing distributed groundwater recharge rate using integrated surface water-groundwater modelling: application to Mihocheon watershed, South Korea. Hydrogeol J, 18(5), 1253-1264

Kim NW, Chung IM, Won YS, Arnold JG (2008) Development and application of the integrated SWAT–MODFLOW model. J Hydrol 356(1–2):1–16

Lenz BN, Saad DA, Fitzpatrick FA (2003) Simulation of ground-water flow and rainfall runoff with emphasis on the effects of land cover, Whittlesey Creek, Bayfield County, Wisconsin, 1999–2001 (No. 3). US Department of the Interior, US Geological Survey

Neitsch SL, Arnold JG, Kiniry JR, Williams JR (2011) Soil and water assessment tool theoretical documentation version in 2009. Texas Water Resources Institute, College Station

Patil NS, Chetan NL (2017) Groundwater modeling of Hiranyakeshi watershed of Ghataprabha sub-basin. J Geol Soc India 90(3):357–361

Poojari M, Jayaraj GK (2017) Runoff modeling using SWAT hydrological model for ghataprabha Basin. Int J 2(1)

Priyanka NS (2016) Runoff modelling for Malaprabha sub-basin using SWAT hydrological model. Int J Res Eng Technol e-ISSN, 2319-1163

Saba N, Umar R, Ahmed S (2016) Assessment of groundwater quality of major industrial city of Central Ganga plain, Western Uttar Pradesh, India through mass transport modeling using chloride as contaminant. Groundw Sustain Dev 2:154–168

Sophocleous M, Perkins SP (2000) Methodology and application of combined watershed and ground-water models in Kansas. J Hydrol 236(3–4):185–201

Yi L, Sophocleous M (2011) Two-Way coupling of unsaturated-saturated flow by integrating the SWAT and MODFLOW models with application in an irrigation district in arid region of West China. 3(3):164–173

Chapter 18
Effect of Rainfall on Groundwater Levels in Sina Basin, Maharashtra

Thendiyath Roshni, Kumar Suraj, Madan K. Jha, and Ram Pravesh Sah

Abstract The groundwater is a major source of water supply for both industrial and domestic purposes. Groundwater level is regularly declining at a faster rate due to its continuous withdrawal. The Indian state of Maharashtra has been in a constant state of drought due to the lower monsoon rainfall. Therefore the study has been done to assess the impact of rainfall and consequent change on the groundwater regime and surface water storage in the Sina Basin, Maharashtra using GIS and statistical analysis. Correlation methods were applied to investigate groundwater level response to rainfall, as well as its seasonal variations in the alluvial aquifer Sina basin. Data were collected from IMD for the year (1985–2009) of 9 stations. Trend analysis of rainfall was done using the Mann–Kendall test and a correlation was established between water level residual and moving average of rainfall. Results obtained by correlation analysis showed that the overall trend of rainfall in the Sina basin is increasing. Also, the results exhibited that the 2–year moving average of the annual rainfall of different stations was showing the best correlation with groundwater level in the study area.

Keywords Groundwater · Correlation · Mann–Kendall test

18.1 Introduction

Groundwater is an invaluable and vital natural resource for the reliable and economic provision of water supply in the world. “Groundwater is the most important water resource on earth. It comprises of the major and the preferred source of drinking water in rural as well as urban areas and caters to 80% of the total drinking water requirement and 50% of the agricultural requirement in rural India”. It plays a very important role

T. Roshni · K. Suraj (✉) · R. P. Sah
Department of Civil Engineering, National Institute of Technology Patna, Patna, Bihar 800005, India
e-mail: suraj244263@gmail.com

M. K. Jha
Department of Agricultural and Food Engineering, Indian Institute of Technology Kharagpur, Kharagpur, West Bengal 72130, India

R. Jha et al. (eds.), *Groundwater and Water Quality*, Water Science and Technology Library 119, https://doi.org/10.1007/978-3-031-09551-1_18

in the environment and supply of water. Groundwater is supplied to a third part of the population of the world. The groundwater provides water for different purposes that are human consumption, agriculture purpose different industries and other work. Due to its good quality and taste, groundwater is mostly preferred for drinking purposes. Groundwater represents the biggest new water asset on the planet (Nyakundi et al. 2015). Groundwater is most useful in areas where surface water is contaminant in volume. Groundwater is the most precious and economic source of freshwater, but it is a limited natural resource. Due to the withdrawal of groundwater, the level of groundwater is continuously degrading. But less attention is given to groundwater than surface water mostly in developing countries. In India, groundwater contributes about 24% of total water. Groundwater is regularly withdrawn due to its various uses. The result is groundwater level is continuously degrading at a faster rate. Sina basin is one of the basins in Maharashtra, India which experience decreasing groundwater levels in the last few years. Fresh water demand in this region is very high due to the increase in industries and population. So, Groundwater plays a very important role in water supply for the future in the Sina basin region due to the scarcity of surface water resources. Overview of Sina basin shows that Groundwater level is declining continuously day by day. This problem is highlighted therefore forecasting Groundwater level becomes essential which helps to develop and implement more accurate and sustainable groundwater management strategies. Rainfall is the major source of groundwater. Various investigations have been done to understand the effect of precipitation on the alluvial aquifer and water table (Jan et al. 2007; Mandal and Singh 2010; Dyer 2008). The aim of this study is highly accurate forecasting of groundwater0level that can be used to help water management in every manner. In a watershed, where data are limited and for obtaining more accurate groundwater level forecasting a data-based model is more suitable than for statistical simulation and forecasting. The "monitoring of groundwater for good management and provision of all the solutions to its problems has to be done with trend analysis (Hamilton et al. 2001; Burn and Hag Elnur 2002; Yue et al. 2002). Non-parametric analysis is a good method for trend identification. This study was designed to gauge the consequences of variations in rainfall on groundwater levels in deposit aquifers from the Sina basin. A secondary objective was to create inferences regarding the basin and geological formation characteristics that manage natural (climate driven) water-level variation and our ability to resolve this variation in areas wherever water-level amendment is dominantly controlled by anthropogenesis influences (pumping and irrigation)". Water-level and precipitation information were compared across basins and hydro-geologic settings.

.

18.2 Study Area

This study is carried out in a small river basin of Maharashtra, India popularly known as the Sina basin. This area receives very less rainfall and therefore is semiarid. The

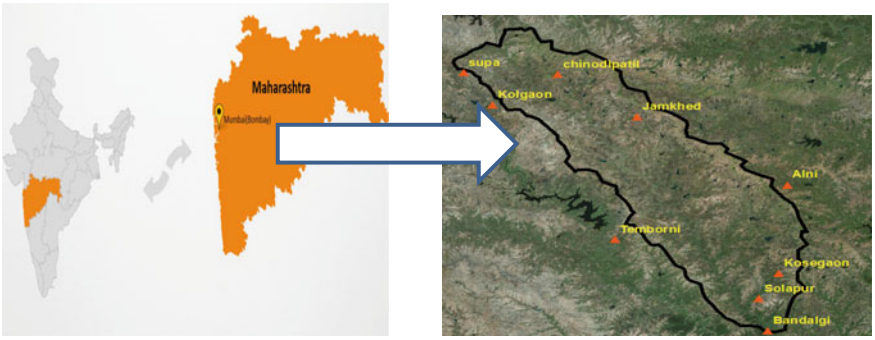

Fig. 18.1 Location of study area, selected wells and rainfall station in Sina basin, Maharashtra (1985–2009)

study area along with the positions of data collection sites are shown in Fig. 18.1. The study area witnessed dry spells during the year 2001–2004. The rainfall is mostly in the months from June to October end. The study area experiences three different seasons namely summer, winter and the rainy season. The daily data of rainfall of 9 rain-gauge stations were obtained from IMD (Indian Meteorological Department), Pune for the period 1990–2009. Seasonal groundwater level data of 132 shallow observations well and 15 deep wells have been obtained from the Groundwater survey and development agency, Pune, India for the same period.

18.3 Methodology

Time varying information on rainfall and level of groundwater are utilized for assessing the impacts of rainfall on the level of groundwater. The techniques utilized in this investigation use information obtained from different agencies. The rainfall stations are known by their name and 9 digit number has been assigned for every well. The water level data of 9 stations for 19 years period were obtained from Central Ground Water Board (CGWB). Rainfall data of 24 years (1985–2009) for similar stations were obtained from the Indian meteorological station (IMD). The months of January, May, August and November were investigated for water level variance. Curve fitting was done for the missing information. The system stream outline appeared. The groundwater information and the precipitation information were arranged on a monthly premise and designed for the long term. Then they were translated graphically to comprehend precipitation and level of groundwater. The normal water level and rainfall data for 19 and 24 years were utilized to show their interdependence. The outcomes were utilized to make the spatial maps of water level and changes from the groundwater information. Maps of precipitation were also developed in the GIS atmosphere.

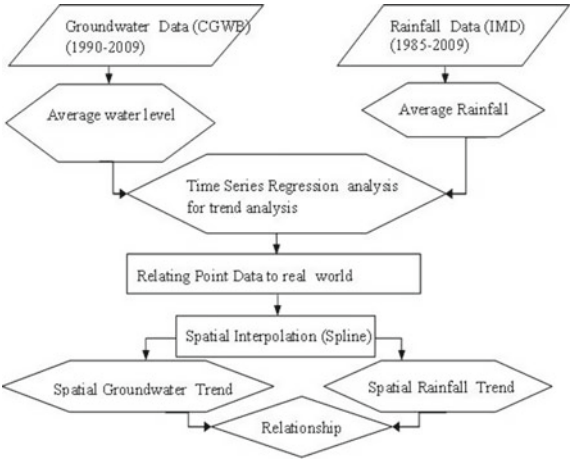

Fig. 18.2 Flowchart of steps involved

18.3.1 Steps Involved in the Analysis

- The spatial data of 9 stations were utilized to make the thiessen polygon of the study area in ArcGIS 10.3.
- By using the groundwater data and the spatial data of the study area contour map of groundwater depth was made in ArcGIS 10.3.
- The moving average was calculated based on monthly observed rainfall data.
- The trends of varying groundwater levels were found using the Mann–Kendall test.
- The average groundwater level data was used to calculate the water level residual.
- Finally, the correlation analysis was done using the moving average of rainfall data and water level residual (Fig. 18.2).

18.3.2 Trend Analysis

The "Mann–Kendall test is a non-parametric test for distinguishing patterns in time arrangement information. The test looks at the relative sizes of test information instead of the information esteems themselves. One advantage of this test is that the information requires does not fit in with a specific appropriation. In addition, the information detailed as non-identifies can be incorporated by doling out them a typical esteem that is littler than the littlest estimated incentive in the informational index. The technique that will be depicted in the ensuing passages expects that there exists just a single information esteem for every day and age. At the point when different information focuses exist for a solitary day and age, the middle esteem is" utilized.

Mann–Kendall test: It is commonly employed to detect monotonic trends, trends in a series of environmental data, climate data or hydrological data. The null Hypothesis, H0 symbolizes that the data came from a population with independent realizations" and are identically distributed.

Equation.

Let $x_1, x_2, \ldots x_n$ represent n data values where x_j signifies the data point at time j. Then the statistic (S) given by Mann–Kendall

$$S = \sum_{k=1}^{n-1} \sum_{j=k+1}^{n} sign(x_j - x_k) \tag{18.1}$$

$sign(x_j - x_k) = 1,$
if $x_j - x_k > 0.$
if $x_j - x_k = 0$
if $x_j - x_k = 0$
Where,

High positive1value of (S) indicates an increasing trend, and a low negative value signifies a decreasing tendency. However, it is important to calculate the probability linked with S and the magnitude of sample, n, to statistically evaluate the significance of the tendency.

18.3.3 ArcGIS 10.3

ArcGIS stands for a geographic information system for working with maps and geographic information. It provides better results than many methods and also it saves time with fewer efforts.

ArcGIS developed by ESRI is the most versatile and comprehensive GIS package used by the water resources group of researchers, academicians, engineers and many hydrologists. Several modules like the application user guide, user manual etc. of ArcGIS are specially developed for this type of user. Thiessen polygon and the contour map have been made with the use of input data of the sub-basin layer and gauge point layer in ArcGIS 10.3.

18.3.4 Moving Average

18.3.4.1 Calculation of moving average: A moving average is a fast method to get an overall idea of the patterns in a set of data and the average of any subgroup of numbers. It is extremely useful for the prediction of long-term patterns. It can be calculated for any spell of time. For example, if one has data of rainfall for a period

of twenty years, one can calculate the moving average of five years, four years, three years and so on.

18.3.5 Water Level Residual

Residual analysis approaches

The tides introduce two difficulties to the investigation of non-tidal procedures in north-west European rack oceans. Initially, the semi-diurnal tides are overwhelming—the change credited to the tides in the rise or momentum estimations, for the most part, surpasses 90% of the aggregate difference and can surpass 99%. Besides since the time scales for residuals, for example, because of tempests running from hourly to maybe a couple of days, cover with diurnal, semi-diurnal and higher consonant tidal periodicities, the refinement amongst tidal and non-tidal can end up obscured. Two methodologies have been taken to assessing residuals—right off the bat computing the tides and subtracting them from the perceptions and besides low-pass separating.

Calculation of water-level residual:

The difference between the observed value of the dependent variable (y) and the predicted value ($\hat{y}$) is called the residual (e). Each data point has one residual.

Residual = Observed value − Predicted value.

$$e = y - \hat{y} \tag{18.2}$$

Both the sum and the mean of the residuals are equal to zero.

A residual plot is a graph that shows the independent variable on the horizontal axis i.e. on x-axis and residuals on the vertical i.e. y-axis. If the points on a residual plot are dispersed haphazardly around the horizontal axis a linear regression model is suitable for the data otherwise a non-linear model is more suitable.

Residuals of Water-Level and Patterns of rainfall:

Time series residuals of the level of water were analyzed with respect to moving averages of yearly rain from designated rainfall stations so as to look at the impacts precipitation causes on the level of water and storage. Moving averages for 2–5-year time periods of rainfall were calculated. Matching of the water-level residual time sequence for each well with the 2–5-year moving average was done with which it was best correlated.

18.4 Data Used

See Table 18.1.

Table 18.1 Data available and location of different stations

	Stations								
	Solapur	Supa	Temborni	Chinodipati	Koregoan	Jhamkhed	Kolgoan	Bandalgi	Alni
Latitude (E)	75.906	74.52	75.22	74.96	75.97	75.32	74.66	75.92	76.01
Longitude (N)	17.6	18.9	18	18.9	18.9	17.8	18.7	18.8	18.3
Monthly rainfall	1985–2009								
Ground water level	133 Observation well in Sina basin								

Fig. 18.3 Location of rainfall in thiessen polygon of Sina basin (1985–2009)

18.5 Results and Discussions

18.5.1 Thiessen Polygon of Study Area

By using the ArcGIS 10.3 and position of the station, the thiessen polygon of study area was made. Figure 18.3 shows the thiessen polygon of the study area.

18.5.2 Contours of Ground-Water Level

By using ArcGIS 10.3 the contours showing the groundwater level of the study area during pre-monsoon and post-monsoon were made (Fig. 18.4). If the groundwater level has a higher value that means the groundwater level is at a lesser depth from the surface which suggests that the area has high rainfall.

18.5.3 Trend Detection

Trend analysis has been done using the Mann–Kendall trend test. Vivid results were obtained as shown in Table 18.2 for post-monsoon and Table 18.3 for pre-monsoon. For post-monsoon 2 stations were showing an increasing trend and decreasing trend was showed by seven stations. For pre-monsoon 8 stations depicted an increasing trend and a decreasing trend was depicted at station.

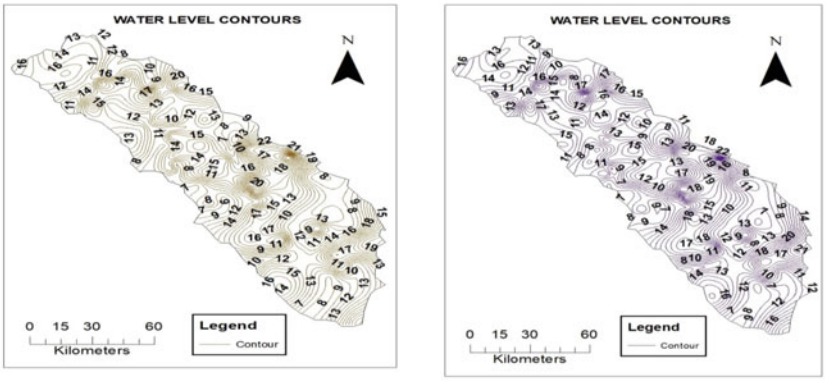

Pre-monsoon Post-monsoon

Fig. 18.4 Contours of groundwater level in polygon of Sina basin Maharashtra (1985–2009)

Table 18.2 Results of Mann–Kendall trend test on water-level for wells in Sina basin for Post-Monsoon

Basin	Well name	p-value	Mann–Kendall test	Trend-direction	Statistically significant
Sina basin	Solapur	0.165	0.232	Increasing	Yes
	Supa	0.086	−0.282	Decreasing	Yes
	Temborni	0.209	−0.211	Decreasing	Yes
	Chinodipati	0.319	−0.168	Decreasing	Yes
	Kasegaon	0.233	−0.200	Decreasing	Yes
	Jamkhed	0.128	−0.253	Decreasing	Yes
	Kolgaon	0.165	0.232	Increasing	Yes
	Bandalgi	0.186	−0.228	Decreasing	No
	Alni	0.209	−0.211	Decreasing	Yes

18.5.4 Groundwater Water Level Residuals and Rainfall Patterns

Time arrangement of the residuals of level of water was contrasted with moving average of yearly rainfall of chosen rainfall stations. Residuals of the level of water were compared with 2–5-year moving average of yearly rainfall of delegate stations. The level of water of remaining time arrangement for each of the wells was coordinated with the 2–5-year moving average normal of yearly rainfall with which it was well corresponded. Tables 18.4 and 18.5 show the correlation between the level of water residual and the moving average of post-monsoon and pre-monsoon.

Table 18.3 Results of Mann–Kendall trend test on water-level for wells in Sina basin for Pre-Monsoon

Basin	Well name	p-value	Mann–Kendall test	Trend direction	Statistically significant
Sina basin	Solapur	0.165	0.221	Increasing	Yes
	Supa	0.002	0.504	Increasing	Yes
	Temborni	0.319	0.168	Increasing	Yes
	Chinodipati	0.064	0.305	Increasing	Yes
	Kasegaon	0.823	0.042	Increasing	Yes
	Jamkhed	0.165	0.232	Increasing	Yes
	Kolgaon	0.631	0.084	Increasing	Yes
	Bandalgi	0.850	-0.037	Decreasing	No
	Alni	0.542	0.105	Increasing	Yes

18.6 Conclusions

In this study, an attempt has been done to evaluate the effect of precipitation on groundwater table. Due to the uneven rainfall, it has been found that the groundwater level increases at some stations and decreases at other stations. From the results obtained from the Mann–Kendall test, with shows the trend, it has been found that there will be an increase at some stations and a decrease at other stations for pre-monsoon and post-monsoon. The correlation between water level residual and rainfall was best correlated with a 2-year moving average of annual precipitation. Climate change is0predicted to effect sources0of recharge as well as aquifers as the0demand for ground water0increases in the Sina basin, Maharashtra. Despite the limitations of existing data, the results of this study should aid in the future examination of water-level records in other basins of Maharashtra.

Table 18.4 Coefficients of correlation between water-level residual and moving average of precipitation for wells in Sina basin

Post-Monsoon

Correlation coefficients of moving average and water level residual		Solapur	Supa	Temborni	Chinodipati	Koregoan	Jhamkhed	Koalgoan	Bandalgi	Alni
	2-year	−0.1294	−0.25	−0.28639	−0.40631	−0.10471	−0.15493	−0.37456	0.2333	−0.395
	3-year	0.0214	−0.25	−0.34199	0.065898	0.005971	−0.04257	−0.07392	0.0473	−0.267
	4-year	−0.0674	−0.28	−0.51967	−0.23716	0.03830	−0.26295	−0.29882	−0.0210	−0.291
	5-year	−0.0987	−0.23	−0.15536	0.396553	0.057057	0.030736	0.158695	−0.008	0.143

Pre-Monsoon

Correlation coefficients of moving average and water level residual		Solapur	Supa	Temborni	Chinodipati	Koregoan	Jhamkhed	Koalgoan	Bandalgi	Alni
	2-year	0.0719	−0.29	−0.233	−0.3534	−0.0282	−0.5003	−0.506	0.2333	0.59
	3-year	0.092	0.026	0.0345	−0.3033	0.0899	−0.4577	−0.5782	0.0473	−0.46
	4-year	0.2027	0.123	0.0732	−0.1664	0.149358	−0.43334	−0.5920	−0.021	−0.541
	5-year	0.2242	−0.57	0.0564	−0.01727	0.270199	−0.52289	−0.6925	−0.008	−0.502

Table 18.5 Strength of correlation of water level residual and moving average

Strength of correlation
-1 to -0.5 - correlation good
-0.49 to -0.3 - correlation fair
-0.29 to -0.1 - correlation poor
-0.1 to 0 – correlation of no significance

References

Burn DH, Hag Elnur MA (2002) Detection of hydrological trends and variability. J Hydrol 255(1–4):107–122

Dyer JL (2008) Basin-scale precipitation analysis for southeast US watersheds using high-resolution radar precipitation estimates. Phys Geogr 29:320–340

Hamilton JP, Whitelaw GS, Fenech A (2001) Mean annual temperature and annual precipitation trends at Canadian biosphere reserves. Environ Monit Assess 67:239–275

Jan CD, Chen TH, Lo WC (2007) Effect of rainfall intensity and distribution on groundwater level fluctuations. J Hydrol 332:348–360

Mandal NC, Singh VP (2010) Entropy-based approach for estimation of natural recharge in Kodaganar River Basin, Tamil Nadu, India. Curr Sci 99:1560–1569

Nyakundi RM, Makokha M, Mwangi JK, Obiero C (2015) Impact of rainfall variability on groundwater levels in Ruiru municipality, Kenya. Afr J Sci Technol Innov Dev 7(5):329–335

Yue S, Pilon P, Cavadias G (2002) Power of the Mann-Kendall and Spearman's rho tests for detecting monotonic trends in hydrological series. J Hydrol 259(1–4):254–271

Chapter 19
Management of Arsenic Sludge Using Solidification

Saurabh Kumar, Virender Singh, and A. R. Quaff

Abstract In this paper, the management of arsenic sludge residue, which was produced during the treatment of arsenic contaminated water by the coagulation flocculation process, is presented. The arsenic sludge (As-FC) was generated in the laboratory by using ferric chloride as a coagulant. The management was done by solidification and fixation of the arsenic residue using binding materials. The binding materials like cement, lime and polyvinyl chloride (PVC) in different combinations and proportions were used for the preparation of three forms of solid matrices of the arsenic sludge. To check the proper fixation of arsenic sludge with binding materials, the semi-dynamic leachability test was performed. This test gives the amount of arsenic leached from solid matrices at different leaching times (0, 2, 6, 24, 72, and 120 h), and the leachability period of arsenic from all forms of matrices of solid residue. The results are reported in terms of diffusion coefficients (D_e) and Leachability Index (L). Both parameters were determined by penetration theory. A smaller diffusion coefficient and a larger leachability index are desired for good solidification. The amount of arsenic leached through the As-FC solid matrices varies from 8.0% to 18.6%. The leachability period of arsenic through solid matrices was found to be more than 8.0, showing the low mobility of the solid matrices. Further, the addition of lime and PVC improved the diffusion coefficient. Polyvinyl chloride also resulted in a reduction of arsenic leachability. The lowest leaching of arsenic was observed for the matrix having cement, lime, and PVC which shows that this matrix is fit for arsenic waste stabilization.

Keywords As-Fc sludge · Diffusion coefficient · Leachability index · Solidification · Matrices

S. Kumar
Assistant Professor, PEC Chandigarh, Chandigarh, India

Formerly, Research Scholar, NIT Patna, Patna, India

V. Singh
Formerly M.Tech Student, NIT Patna, Patna, India

A. R. Quaff (✉)
Associate Professor, Department of Civil Engineering, NIT Patna, Patna, India
e-mail: arquaff@nitp.ac.in

R. Jha et al. (eds.), *Groundwater and Water Quality*, Water Science and Technology Library 119, https://doi.org/10.1007/978-3-031-09551-1_19

19.1 Introduction

At present, heavy metal concentration in the environment is increasing daily due to weathering action, anthropogenic activities, metal mining, smelting, fossil fuel combustion, and pesticide use in agriculture (Song and Garcia 2014). These metals have serious effects on human health and the environment. Arsenic is the 20th most abundant (Sarkar and Paul 2016) toxic and carcinogenic metalloid (Lest et al. 2000) present in the environment. Chronic exposure to inorganic arsenic can cause several problems such as digestive, respiratory, cardiovascular, endocrine, renal, neurological, and reproductive system disorders, which ultimately lead to cancer. The global problem of arsenic contamination in water has been reported in many countries including Italy (Guan et al. 2008), New Zealand (Roddick-Lanzilotta et al. 2002), India, Chile, and Taiwan, (Sharma and Sohn 2009). In arsenic-enriched environments, a major concern is a potential for mobilization and transport of this toxic element to groundwater and drinking water supplies.

Various treatment technologies, such as coagulation/flocculation, precipitation, ion exchange, adsorption, membrane filtration, and reverse osmosis have been conventionally used for arsenic removal from water. Most of these methods impose a sludge burden and produce toxic solids rich in arsenic (Singh and Pant 2006). Disposal of the sludge generated with high levels of arsenic directly into the landfill should be abandoned due to the risk of leaching waste into groundwater. Therefore a pre-treatment of arsenic sludge is required before disposal to a land-fill (Mandal et al. 2016).

Some researchers adopted solidification/stabilization (S/S) treatment for the removal of arsenic from arsenic-containing sludge i.e. blast furnace slag based solidification (Dutre and Vandecasteele 1995), fly ash based stabilization (Akhter et. al,1997), lime based solidification(De villers, 1995; Camacho et al. 2009) and cement based solidification (Singh and Pant 2006; Clancy et al. 2015) and found satisfactory control on leaching of arsenic from arsenic-containing sludge.

The main objective of this study is to manage the arsenic sludge/residue (As-FC) by solidification and fixation using cement, lime and PVC as binding materials, and to find out better combinations of binding materials which result in minimal leaching in terms of the leachability index and diffusion coefficients.

19.2 Materials and Methods

19.2.1 Preparation of Arsenic Residual Sludge

Arsenic residual sludge was generally settled sludge obtained during treatment of synthetic arsenic-contaminated water sample using coagulation/flocculation process in the Environmental Engineering Laboratory at NIT Patna, Bihar and was obtained by using ferric chloride as a coagulant. The synthetic arsenic-contaminated water

Fig. 19.1 Picture of dried As-FC sludge

sample was prepared by dissolving appropriate amounts of arsenic trioxide (As_2O_3) in tap water as per the standard method. Figure 19.1 presents the picture of dried As-FC residue.

19.2.2 Preparation of Solidified Matrices

The binder materials (cement, lime, and polyvinyl chloride) were mixed with arsenic residual sludge in a specific ratio to prepare three different solidified matrices(W_1,W_2,W_3) and details of the composition of these matrices including matrix nomenclature, matrix composition, notations of binding materials, and quantity of binding materials used are given in Table 19.1. Water was added so that the paste could be molded in a disc of defined size. After preparation of solidified matrices, these were kept for setting at room temperature for 24 h. After the passage of setting time, these were cured for the next 10 days to strengthen the matrices. The amount of sludge was such that the initial loading of arsenic in all three matrices was 2.000 mg/g.

Table 19.1 Composition of solidified matrices

Matrix	Matrices composition	Notations	Quantity (gm)
W_1	Cement + Lime + As-FC sludge	C + CH + FS	3: 1: 4
W_2	Cement + PVC powder + As-FC sludge	C + PVC + FS	4: 0.5: 4.5
W_3	Cement + Lime + PVC powder + As-FC sludge	C + CH + PVC + FS	3: 1: 0.5: 4.5

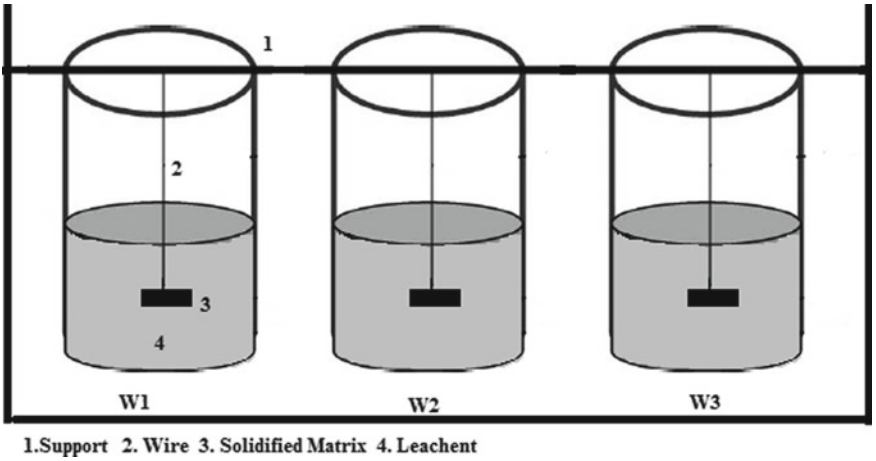

Fig. 19.2 Schematic diagram of an experimental setup for leachability studies from solidified matrices W1, W2 and W3 for safe disposal of arsenic

19.2.3 Semi Dynamic Leachability Test

For determining the leachability of solidified matrices (W_1, W_2, W_3) a semi-dynamic leachability test (in which the leachate is replaced periodically after intervals of static leaching) was performed to measure the leaching amount of arsenic from solidified matrices. In this test, the ratio of the solid matrix to the water was fixed as 100 mL water per gm. of the solid matrix. The leachate was collected after fixed time intervals of 0, 2, 6, 24, 48, 72, and 120 h etc. and analyzed for arsenic concentration. The schematic diagram of the experimental setup for performing this test is shown in Fig. 19.2.

19.2.4 Diffusion Coefficient (D_e) and Leachability Index as Per Penetration Theory

According to penetration theory, the slope of the curve of CFR versus $\sqrt{t}$ is used for the determination of the effective diffusion coefficient (D_e). The Cumulative Fraction of a substance (CFR) is the ratio of the amount of arsenic in a solidified matrix (mg) at any time (t) of leaching (M_t) to the total initial amount (mg) of arsenic in the solidified matrix (M).

In 1995, Dutre and Vandecasteele derived the equation for determination of the total amount of arsenic leached that has diffused out of the medium surface at time t, M_t by performing integration over time and surface area, and is given by:

$$M_t = 2M\frac{S}{V}\sqrt{\frac{D_e t}{\pi}} \tag{19.1}$$

where

M = The total initial amount of arsenic in the solidified matrix (mg).

S = Surface area of matrix (cm^2).

V = Volume of matrix (cm^3).

D_e = Effective diffusion coefficient.

The Leaching of arsenic from solidified matrices is mainly due to diffusion, so a constant diffusion coefficient for each of the solidified matrices may be assumed. The cumulative fraction of a substance (CFR) or ratio of M_t/M is given by.

$$\text{CFR} = \frac{-2}{\sqrt{\pi}}\frac{S}{V}\sqrt{D_e \text{t}} \tag{19.2}$$

where

CFR = Cumulative Fraction of a substance (CFR).

t = Time of leaching.

Leachability index (L) as per Penetration theory.

The Leachability index is used for determining the applicability of solidified waste matrices and specific changes in matrices. The leachability index equation in terms of diffusion coefficient also shows the characteristics of the matrices.

$$L = \left(\frac{1}{m}\right)\sum_{n=1}^{m}(-\log(D_e))_n \tag{19.3}$$

where

n = Leaching period index.

m = Total number of individual leaching periods.

D_e = Coefficient of diffusion.

Arsenic-containing solidified matrices are also categorized according to the leachability index (L) and is given in Table 19.2 below (Dutre and Vandecasteele 1996).

Table 19.2 Category of solidified matrix according to leachability index (L)

Leachability index (L)	Category of solidified matrix
L < 6.5	Very mobile
6.5 < L < 8.0	Moderate
L > 8.0	Low mobility

19.2.5 Analytical Method

Arsenic concentration in solution was analyzed as per the standard method by using the atomic absorption spectrophotometer(AAS) equipped with a VGA at 193.7 nm wavelength. For the determination of arsenic concentration in an unknown solution, the calibration curve was prepared with a known arsenic concentration solution with a range between 0 and 100 ppb. The amount of arsenic present in the residue/sludge was determined as per the standard method (Clesceri et al. 1989). Digestion of 1 gm sludge was done with the nitric acid method before measuring arsenic concentration. Solution pH was measured with a pH meter (Oaklton 700).

19.3 Results and Discussion

19.3.1 Characterization of Solidified Matrices

Before starting the leachability test, the physical and geometric characteristics of all solid matrices were calculated. The dry weight of all matrices after solidification, geometric surface area, and volume are tabulated in Table 19.3.

19.3.2 Leaching of Arsenic from Solidified Matrices

The leaching of arsenic from solidified matrices was examined by subjecting the matrices to a semi-dynamic leachability test. The resultant leachate was analysed on AAS for the amount of arsenic leached. Arsenic concentration (ppb) and Cumulative arsenic concentration (ppb) in the leachate of solidified matrices at different leaching

Table 19.3 Characteristics of solidified matrices

Matrix	Weight (gm.)	Surface area (cm^2)	Volume (cm^3)
W_1	8.4	34.38	6
W_2	7.8	29.29	4
W_3	9.3	35.86	7

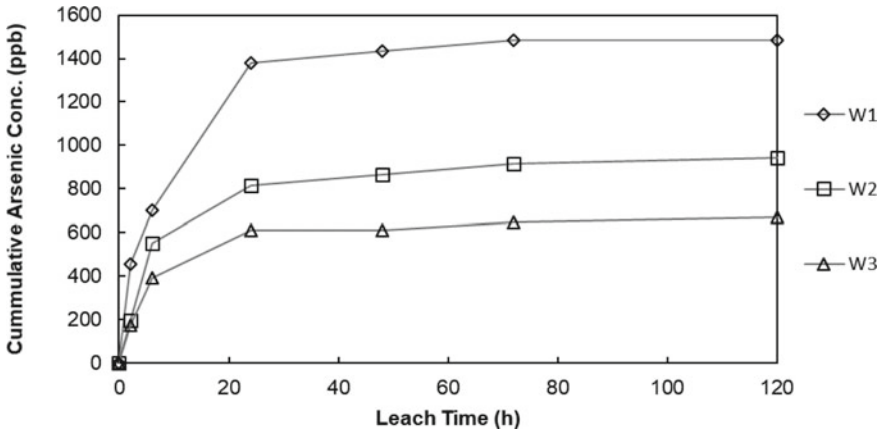

Fig. 19.3 Cumulative concentration of arsenic leached out from all solidified matrix (W_1-W_3) as a function of leach time for the semi-dynamic leach test

times (0, 2, 6, 24, 72, and 120 h) are presented in Fig. 19.3. These experiments indicate that after a period of 48 h., the leaching of arsenic in all matrices is minimal.

Initially, the amount of arsenic leached in these matrices was high, indicating that the arsenic may be easily released from the outer surface of the matrix. The mass balance shows that a total of 18.56%, 10.47% and 8.0% of arsenic leached out from W_1, W_2 and W_3 respectively in 120 h. of leaching time. The lowest leaching of arsenic was observed for the matrix having cement, lime and PVC with As-FC sludge which shows that this matrix is the best fit for arsenic waste stabilization.

19.3.3 Diffusion Coefficient and Leachability Index as Per Penetration Theory

The value of D_e and L calculated as per Eqs. (19.1) and (19.2) is presented in Table 19.4. Based on D_e values, it can be concluded that the diffusion is minimum in W_3 matrix. The best arrangement for the solidification of arsenic can be a matrix composed of cement, lime, PVC and As-FC sludge (W_3 matrix). The mechanism of solidification is that there is the formation of calcite which blocks the pores of the solidified sample. The precipitation and conversion into a non-soluble form (calcium arsenite) in the cement also adds to the mechanism for low leaching in the solidified sample (Bothe et al., 1999). From these leaching amounts, it is clear that the addition of lime and PVC improves the diffusion coefficient. PVC also resulted in a reduction of arsenic leachability. Leach tests indicated that all the matrices had leachability indices better than the target $L > 6$ for arsenic showing immobile.

Table 19.4 Effective diffusion coefficient and leachability index (L) of all matrices (W_1-W_3) according to penetration theory

Matrix	Matrix composition	Penetration theory		Amount of leaching (%)
		$D_e(10^{-10}Cm^2/s)$	L	
W_1	C:L:As-FC	59.2	8.27	18.6
W_2	C:PVC:As-FC	4.68	9.33	10.5
W_3	C:L:PVC:As-FC	6.27	9.2	8.0

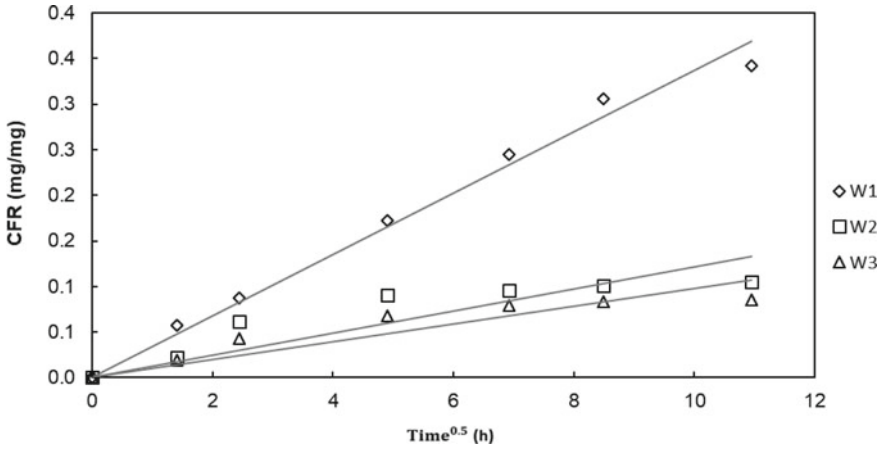

Fig. 19.4 Cumulative Fraction of arsenic released from the all solidified matrix (W_1-W_3) as a function of the square root of leach time for the semi dynamic leach test

Figure 19.4 shows the relationship between CFR value and the square root of leaching time. A linear relationship between CFR and the square root of leaching time suggests that diffusion is the responsible mechanism for arsenic leaching.

19.4 Conclusions

From the results obtained in the above studies, the following conclusions may be drawn:

- The results obtained from the leaching test as per penetration theory are consistent and logically matching with the value of L and the percentage of arsenic leached. Therefore, it may be concluded that a good agreement between diffusion coefficient and leachability indices is obtained from penetration theory.
- The addition of lime and PVC improves the diffusion coefficient. PVC also resulted in a reduction of arsenic leachability. The lowest leaching of arsenic

was observed for the matrix having cement, lime and PVC which shows that this matrix (W_3) is fit for arsenic waste stabilization.

Acknowledgements The authors would like to thank the Department of Civil Engineering, National Institute of Technology Patna, for all facilities and support provided.

References

Akhter H, Cartledge FC, Roy, Tittleba A, ME (1997) Solidification/stabilization of arsenic salts: Effects of long cure times. J Hazard Mater, 247–264

APHA (1995) Standard methods for the examination of water and wastewater, Standard Methods. https://doi.org/10.2105/AJPH.51.6.940-a

Bothe JV, Brown PW (1999) Arsenic immobilization by calcium arsenate formation. Environ Sci Technol 33(21):3806–3811

Camacho J, Wee HY, Kramer TA, Autenrieth R (2009) Arsenic stabilization on water treatment residuals by calcium addition. J Hazard Mater 165(1–3):599–603

Clancy TM, Snyder KV (2015) Evaluating the cement stabilization of arsenic-bearing iron wastes from drinking water treatment. J Hazard Mater 300:522–529

Clesceri LS, Greenberg AE, Trussell RH (1989) Standard Method for the examination of water and wastewater. APHA, NW, Washington DC

De Villiers (1995) Arsenic stabilization on water treatment residuals by calcium addition. J Hazard Mater, 165(1–3), 599–603

Dutré V, Vandecasteele C (1995) Solidification/Stabilisation of hazardous arsenic containing waste from a copper refining process. J Hazard Mater 40(1):55–68

Guan XH, Jianmin W, Charles CC (2008) Removal of arsenic from water using granular ferric hydroxide: macroscopic and microscopic studies. J Hazard Mater 156(1–3):178–185

Leist M, Casey RJ, Caridi D (2000) The management of arsenic wastes: problems and prospects. J Hazard Mater 76(1):125–138

Mandal P, Debbarma SR, Saha A, Ruj B (2016) Disposal problem of arsenic sludge generated during arsenic removal from drinking water. Procedia Environ Sci 35:943–949

Roddick-Lanzilottaa JA, McQuillana AJ, Craw D (2002) Infrared spectroscopic characterisation of arsenate (V) ion adsorption from mine waters, Macraes mine, New Zealand. Appl Geochem 17:445–454

Sarkar A, Paul B (2016) The global menace of arsenic and its conventional remediation—a critical review. Chemosphere 158:37–49

Singh TS, Pant KK (2006) Solidification/Stabilization of arsenic containing solid wastes using portland cement, fly ash and polymeric materials. J Hazard Mater 131(1–3):29–36

Song, Shaoxian, and Marisol Gallegos-Garcia (2014) The role of colloidal systems in environmental protection Chapter 11—Arsenic removal from water by the coagulation

Chapter 20
Assessment of Water Quality Index of Tapi River: A Case Study of Surat City

Maitri H. Surati, Keyur J. Prajapati, Urvi K. Parmar, and Darshan J. Mehta

Abstract Deteriorating the water quality of river is a major concern in India. This is especially true for river being used as drinking water sources. The water quality of river changes with time and development in the surrounding and upstream area. Therefore, it is necessary to determine the various water quality parameters of river as its presence and amount reflect in water treatment plants and in the surrounding areas which are dependent on river water only. One such river considered in the study is the Tapi river near Surat, Gujarat. The aim of the study is to determine the status of water quality in the Tapi river throughout the year. Surat city is dependent on the Tapi river for its drinking water needs. There are several intake structures constructed to take-off the raw river water. Our study area contains five intake structures from Valak to Rander on Tapi river from where water samples were collected. For assessment of WQI of Tapi river twelve physico-chemical parameters of river water were used. WQI is determined for monsoon, post-monsoon and pre-monsoon from the assessed water quality parameters of the Tapi river. The overall trend of results shows that the river water quality is very poor at stations Valak, Mota Varachha and Rander, while the water quality is poor at stations Sarthana and Katargam. The study indicates that water quality is continuously degrading from monsoon to post-monsoon and from post-monsoon to pre-monsoon which makes it unsuitable for drinking and fish culture.

Keywords Water quality index · Physico-chemical parameters · Drinking water · Surat city · Tapi river

M. H. Surati · U. K. Parmar
Civil Engineering Department, UG Student, Shree Swami Atmanand Saraswati Institute of Technology, Surat, Gujarat 395006, India

K. J. Prajapati (✉)
Civil Engineering Department, Shree Swami Atmanand Saraswati Institute of Technology, Surat, Gujarat 395006, India
e-mail: keyurprajapati34@gmail.com

D. J. Mehta
Research Scholar, Department of Civil Engineering, Sardar Vallabhbhai National Institute of Technology, Surat, Gujarat 395010, India

R. Jha et al. (eds.), *Groundwater and Water Quality*, Water Science and Technology Library 119, https://doi.org/10.1007/978-3-031-09551-1_20

20.1 Introduction

Urbanization, industrial development, various agriculture and other activities of humans have increased the pollution of surface water & groundwater. In India, 70% of water quality has been infected due to contaminants. As safe & potable drinking water is needed, various treatment methods are adopted to raise the quality of drinking water. It ought to be free from different contamination viz. pollutants, dense metals and pesticides etc. And also, the entirety of its parameters like pH, electrical conductivity, calcium, magnesium, total dissolved solids, alkalinity water, sodium, potassium, nitrate, BOD and sulphate do ought to be within the allowable limit. The water quality of river changes with time and development in the surrounding and upstream area. Therefore, it is necessary to determine the various water quality parameters of river as its presence and amount reflect in treatment plants and in the surrounding areas which are dependent on river water only. Due to pollution in the air, water and land, less amount of rainfall is observed in the last few years. In May 2015, water level in the Ukai dam was 95 m & in May 2016, it degraded to 90 m while in 2017 it is observed at 88.26 m. In 2018 March it is lowest at 85 m. Only 12% of water is there in the Ukai dam to total water storage capacity. So due to less amount of water we should worry about existing water quality. If the quality of raw water is degraded it affects human health. Surat is the eighth largest and fourth cleanest city of India. Water source of Surat city is the Tapi river. Most people use water from Tapi river only. The study objective is to determine the WQI by assessing various physio-chemical parameters of Tapi river water in Surat city.

20.2 Study Area

Tapti river is a river in central India between the Godavari and Narmada rivers. Tapi covers a zone of approximately (79% Maharashtra, 15% Madhya Pradesh and 6% Gujarat) states having tributaries on both the banks. Tapi river is divided into fourteen major tributaries. Four on the right bank namely Vanki, Gomai, Arunavati and aner and ten on the left bank. The Tapi basin extends to a total area of 65, 145 sq. km, which is approximately 2.0% of the total geographical area of India. The main tributaries of the Tapi river are Purna and the Girna as shown in Fig. 20.1 respectively.

Second largest stream flows westward over a length of 724 km before draining through the Gulf of Khambhat into the Arabian sea. Large area covers the state of Maharashtra. The river starts from the Betul district of Madhya Pradesh in the Saputara range at an elevation of 752 m above sea level. The Tapi basin is the basin of the Deccan hill and is located amongst 200 n to 220 n approximately. On the west part, the basin finds its channel in the Arabian sea. It is surrounded on all three sides by hill ranges. The Tapi river drains an area of 65,145 sq. Out of which nearly 80 percentile in Maharashtra.

Fig. 20.1 Tapi river path in Surat. *Source* www.mapofindia.com

The city Surat is located in the southern part of Gujarat $21^{0}10^{"}$ and latitude and $72^{0}50^{'}$ longitude on the southern bank of river Tapi presently spread over 334.23 km areas Surat head population of 5,877,241 as per census 2010 Surat has been blessed with a flow of river Tapi which fulfils most its water requirement.It flows throw the city and the Arabian sea at about 16 km from Surat. Big water resources projects like Ukai dam, Kakrapar weir Mindhola in the south of it. As mentioned earlier Surat has been blessed by the flow of Tapi however, it has also suffered a lot because of floods in the Tapi since historic times.

Surat city is located on the banks of river Tapi. Obstructing of Tapi made the original port facilities to close the nearest port and is presently in the region of Hazira and Magdala. 13 m is the average elevation of Surat city. The climate is tropical and monsoon rainfall is abundant (about 2500 mm per year).

In the present study 5 stations are selected as these are the location of river water intake for Surat city. The sampling locations are Valak, Mota Varachha, Sarthana, Katargam, and Rander as shown in Fig. 20.2 respectively.

20.3 Methodology & Data Collection

The river water was collected near the location of river intake from Valak, Mota Varachha, Sarthana, Katargam & Rander. The overall analysis is done for the year 2017–18 and water samples are taken considering the monsoon, post-monsoon and pre-monsoon. For monsoon season samples were collected in August and September, for post-monsoon season the samples were collected in the month of December and January. While the water samples were collected in March for pre-monsoon analysis. The water samples were taken by bottle sampler and kept in glass bottles away from sunlight to reduce the chances of the change in water quality. The taken

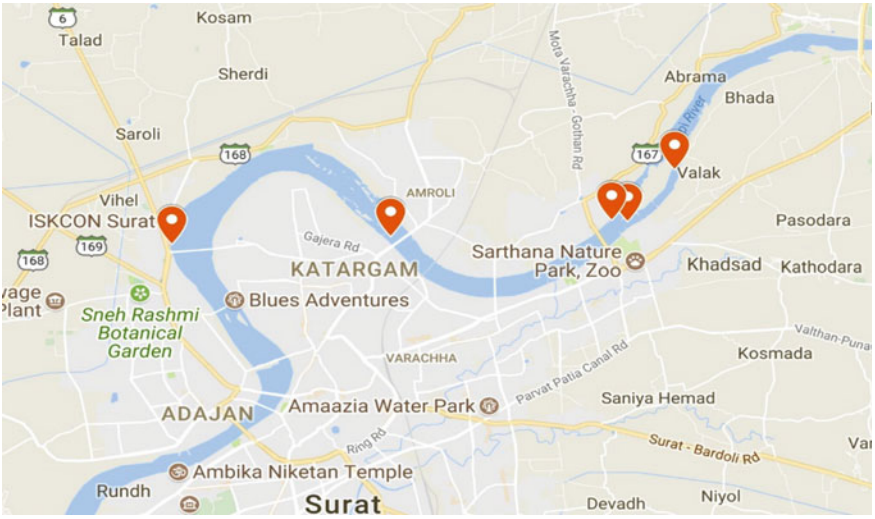

Fig. 20.2 Location of sample station

water samples were then tested for 12 different physico-chemical parameters with the methods which are shown in Table 20.1.

Thus, tested parameters were then used to determine the water quality index of the Tapi river.

WQI is a tremendous organization and general managerial tool in imparting water quality information. In order to calculate the water quality index, the list of data has been verified and useful from a number of different geographical areas all over the

Table 20.1 Test methods for Physio-chemical parameters

Sr. No	Parameters	Test name/equipment	Unit
1	pH	Electo metric method	-
2	Conductivity	Multi-meter	Mohs/cm
3	TDS	Multi-meter	Mg/l
4	Do	Wrinkler method and azide modification	Mg/l
5	BOD	Titrimetric & resriometric method	Mg/l
6	Alkalinity	Standard process	Mg/l
7	Hardness	IS: 3025(p−21): 2009	Mg/l
8	Chloride (cl^{-})	IS: 3025(p−32): 1988	Mg/l
9	Nitrate ($no_3{}^{-2}$)	Apha & awwa.22nd ed.4500 -$no_3{}^{-2}$−b (4–122)	Mg/l
10	Sulphate ($so_4{}^{-2}$)	Apha & awwa.22nd ed.4500 $so_4{}^{-2}$−e (4–190)	Mg/l
11	Magnesium (mg^{+})	Apha & awwa.22nd ed.3500 mg−b (3–84)	Mg/l
12	Calcium (ca^{+2})	Apha & awwa.22nd ed.3500 ca−b (3–67)	Mg/l

world of various water bodies critical pollution parameters were considered. Using Delphi techniques or the weighted arithmetic index method WQI has been calculated. With the help of five water quality, the quality rating scale for each parameter [qi] would be calculated.

There are mainly four types of water quality index:

(a) Nsf-WQI (National sanitation foundation water quality index)
(b) CCME WQI (Canadian council of ministry of environment water quality index)
(c) OWQI (organ water quality index)
(d) WaWQI (weighted arithmetic water quality index).

Using the WaWQI method, the current study deals with the determination of quality using because it has an edge over further approaches for example: in this method numerous water quality parameters are combined into a scientific equation that rates the health of water body through a number called water quality index as well as it describes the suitability of surface and groundwater quality source for human consumption.

Methodology to Calculate Water Quality Index:

Various physio-chemical data with water quality parameters then calculate proportionality constant k value using Eq. 20.1.

$$K = 1/(1/\int si) \tag{20.1}$$

where, si = standard permissible for parameter.

For calculating quantity rating for a parameter using Eq. 20.2.

$$Qn = 100((vn - vio)/(sn - vio)) \tag{20.2}$$

where, vn = estimated value of the nth parameter in pure water.

sn = standard permissible value of the n parameter.

The value of sn is taken from the various agencies for given physio-chemical parameters are shown in below mentioned Table 20.2.

Using Eq. 20.3, Calculate the unit weight for nth parameters:

$$Wn = (k/sn) \tag{20.3}$$

Using Eq. 20.4, now Calculate the WQI

$$WQI = ((\int wnqn)/\int wn) \tag{20.4}$$

Thus, the calculated water quality index represents the corresponding grade of quality and status of water quality (Brown et al. 1972) as shown in Table 20.3.

Table 20.2 Recommended standard from various agencies

Sr. No	Parameters	Recommended standard (sn)	Agencies
1	pH	7.5	Icmr/bis
2	Electrical conductivity	300 mohs/cm	Icmr
3	TDS	500 mg/l	Icmr/bis
4	Do	5 mg/l	Who
5	BOD	5 mg/l	Icmr/bis
6	Alkalinity	120 mg/l	Icmr
7	Hardness	300 mg/l	Icmr
8	Chloride (cl^-)	250 mg/l	Icmr
9	Nitrate (no_3^-)	45 mg/l	Icmr/bis
10	Sulphate (so_4^{-2})	150 mg/l	Icmr/bis
11	Magnesium (mg^{+2})	30 mg/l	Icmr/bis
12	Calcium (ca^{+2})	75 mg/l	Icmr/bis

Table 20.3 Water quality index, status & grading of water quality

WQI level	Water quality status	Grading
0–25	Excellent water quality	A
26–50	Good water quality	B
51–75	Poor water quality	C
76–100	Very poor quality	D
100	Unsuitable for drinking and fish culture	E

20.4 Result & Result Analysis

The water samples taken from different locations of Tapi river in Surat city were tested in the laboratory to evaluate 12 physio-chemical parameters. These results were compared with the standard values given by various agencies for assessing the quality index of the Tapi river.

20.4.1 For Monsoon Season

Various samples were collected in August & September month for the monsoon season. The results for 12 physio-chemical parameters as shown in Table 20.4 for August and in Table 20.5 for September.

Table 20.4 Results for August month

Sr. No	Parameters	Unit	Valak	Mota Varachha	Sarthana	Katargam	Rander
1	pH	–	7.53	7.52	7.65	7.57	7.65
2	Electrical conductivity	Mohs/cm	0.627	0.581	0.617	0.573	0.621
3	TDS	Mg/l	0.409	0.389	0.406	0.362	0.423
4	Do	Mg/l	7.5	4.1	7.6	4.8	7.9
5	BOD	Mg/l	4.1	2.6	2.3	1.2	2.7
6	Alkalinity	Mg/l	8.8	8.8	8.7	8.9	11.6
7	Hardness	Mg/l	150.6	152.6	156.62	160.64	204.81
8	Chloride (cl^{-})	Mg/l	30.49	27.99	29.49	29.49	38.98
9	Nitrate ($no_3{}^{-2}$)	Mg/l	0	0.97	0.86	0.98	0.57
10	Sulphate ($so_4{}^{-2}$)	Mg/l	19.65	17.24	23.26	21.12	17.37
11	Magnesium (mg^{+2})	Mg/l	15.61	15.61	16.58	17.07	25.86
12	Calcium (ca^{+2})	Mg/l	34.46	35.27	35.27	36.07	39.27

Table 20.5 Results for September month

Sr. No	Parameters	Unit	Valak	Mota Varachha	Sarthana	Katargam	Rander
1	pH	–	7.5	7.54	7.55	7.5	7.43
2	Electrical conductivity	Mohs/cm	0.58	0.5893	0.621	0.672	0.603
3	TDS	Mg/l	0.396	0.385	0.41	0.446	0.398
4	Do	Mg/l	5.8	5.1	6	2.5	4.1
5	BOD	Mg/l	4.9	3	3.3	0.9	3.2
6	Alkalinity	Mg/l	7.6	15.5	6.6	6.8	8.3
7	Hardness	Mg/l	149.1	147.1	143.1	155.2	145.1
8	Chloride (cl^{-})	Mg/l	35.15	73.87	32.77	32.26	56.2
9	Nitrate ($no_3{}^{-}$)	Mg/l	1.35	0.31	0.71	0	0.38
10	Sulphate ($so_4{}^{-2}$)	Mg/l	6.41	13.36	8.55	15.5	8.82
11	Magnesium (mg^{+2})	Mg/l	18.1	13.7	12.72	14.68	14.68
12	Calcium (ca^{+2})	Mg/l	29.84	36.36	36.36	37.97	33.93

Table 20.6 Water quality index for Valak station for August month

Sr. No	Parameters	Observed values	Qn	Standard values (sn)	(1/sn)	Wn	Qnwn	WQI
1	pH	7.53	106.00	7.5	0.1333	0.2117	22.438	76.26
2	Electrical conductivity	0.627	0.21	300	0.0033	0.0053	0.001	
3	TDS	0.409	0.08	500	0.0020	0.0032	0.000	
4	Do	7.5	73.96	5	0.2000	0.3175	23.483	
5	BOD	4.1	82.00	5	0.2000	0.3175	26.037	
6	Alkalinity	8.8	7.33	120	0.0083	0.0132	0.097	
7	Hardness	150.6	50.20	300	0.0033	0.0053	0.266	
8	Chloride (cl^{-})	30.49	12.20	250	0.0040	0.0064	0.077	
9	Nitrate (no_3^{-})	0	0.00	45	0.0222	0.0353	0.000	
10	Sulphate (so_4^{-2})	19.65	13.10	150	0.0067	0.0106	0.139	
11	Magnesium (mg^{+2})	15.61	52.03	30	0.0333	0.0529	2.754	
12	Calcium (ca^{+2})	34.46	45.95	75	0.0133	0.0212	0.973	
					0.6299	1.0000	76.264	
				K = (1/(e(1/sn))	1.5876			

The water quality index is determined from the above results for the monsoon season for each station and the average value of the water quality index represents the quality of river water of Tapi. The water quality index calculated by WaWQI for the Valak station is shown in Table 20.6.

The water quality index is calculated for each station for samples taken in August and September month, the results of the water quality index for the monsoon season are shown in below mentioned Table 20.7.

The result shows that water quality index is higher in September compared to August while the station wise comparison shows that the station on the upstream (u/s) side gives a higher value of WQI and the values are decreasing for the locations in the downstream (d/s) side area.

Table 20.7 Water quality index for Monsoon season

Station	August	September	Average	Grade
Valak	76.26	86.01	81.14	D
Mota Varachha	77.64	77.51	77.58	D
Sarthana	69.88	76.48	73.18	C
Katargam	68.88	71.11	69.99	C
Rander	73.25	77.38	75.32	C
Average	73.18	77.70		
Grade	C	D		

20.4.2 For Post-Monsoon Season

Similarly, various samples were collected in December & January months for post-monsoon season. The result for 12 physio-chemical parameters as shown in Table 20.8 for December and in Table 20.9 for January.

The water quality index is determined from the above results for post-monsoon season for each station and the average value of the water quality index represents the quality of river water of Tapi. The water quality index calculated by WaWQI for the Valak station is shown in Table 20.10.

Table 20.8 Results for December month

Sr. No	Parameters	Unit	Valak	Mota Varachha	Sarthana	Katargam	Rander
1	pH	–	7.6	7.8	7.65	7.51	7.5
2	Electrical conductivity	Mohs/cm	0.58	0.5893	0.621	0.672	0.603
3	TDS	Mg/l	0.396	0.385	0.41	0.446	0.398
4	Do	Mg/l	5.8	5.1	6	2.5	4.1
5	BOD	Mg/l	4.9	3	3.3	0.9	3.2
6	Alkalinity	Mg/l	7.6	15.5	6.6	6.8	8.3
7	Hardness	Mg/l	149.1	147.1	143.1	155.2	145.1
8	Chloride (cl^-)	Mg/l	35.15	73.87	32.77	32.26	56.2
9	Nitrate (no_3^-)	Mg/l	1.35	0.31	0.71	0	0.38
10	Sulphate (so_4^{-2})	Mg/l	6.41	13.36	8.55	15.5	8.82
11	Magnesium (mg^{+2})	Mg/l	18.1	13.7	12.72	14.68	14.68
12	Calcium (ca^{+2})	Mg/l	29.84	36.36	36.36	37.97	33.93

Table 20.9 Results for January month

Sr. No	Parameters	Unit	Valak	Mota Varachha	Sarthana	Katargam	Rander
1	pH	–	8.06	8.35	8.6	7.4	8
2	Electrical conductivity	Mohs/cm	599	641	614	727	761
3	TDS	Mg/l	0	0	0	0	0
4	Do	Mg/l	5	3.8	3.8	0	3.6
5	BOD	Mg/l	4	0	0	0	2.5
6	Alkalinity	Mg/l	4.4	5.5	6.5	7	6
7	Hardness	Mg/l	176	168	160	194	200
8	Chloride (cl^{-})	Mg/l	40.98	38.98	40.48	48.48	57.48
9	Nitrate (no_3^{-})	Mg/l	0.75	0.58	0.33	0.28	0.39
10	Sulphate (so_4^{-2})	Mg/l	15.5	17.27	15.77	27.13	27.67
11	Magnesium (mg^{+2})	Mg/l	23.32	19.92	18.46	23.81	25.27
12	Calcium (ca^{+2})	Mg/l	32.06	34.46	33.66	38.47	38.47

The water quality index is calculated for each station for samples taken in December and January and the results of the water quality index for post-monsoon season are shown in below mentioned Table 20.11.

The result shows that the water quality index is higher in January compared to December while the station wise comparison shows that the station on the upstream (u/s) side gives a higher value of WQI and the values are decreasing for the locations in the downstream (d/s) side area. As the monsoon recedes the water quality in the river starts degrading.

20.4.3 For Pre-Monsoon

Similarly, the samples were collected in March month for Pre-monsoon season. The result for 12 physio-chemical parameters is shown in Table 20.12.

The water quality index is determined from the above results for Pre-monsoon season for each station and the average value of water quality index represents the quality of river water of Tapi. The water quality index calculated by WaWQI for the Valak station is shown in Table 20.13.

The water quality index is calculated for each station for samples taken in March. The results of the water quality index for Pre-monsoon season are shown in below mentioned Table 20.14.

Table 20.10 Water quality index for Valak station for December month

Sr. No	Parameters	Observed values	Qn	Standard values (sn)	(1/sn)	Wn	Qnwn	WQI
1	pH	7.6	120.00	7.5	0.1333	0.2110	25.322	90.24
2	Electrical conductivity	0.58	0.19	300	0.0033	0.0053	0.001	
3	TDS	0.396	0.08	500	0.0020	0.0032	0.000	
4	Do	5.8	91.67	5	0.2000	0.3165	29.014	
5	BOD	4.9	98.00	5	0.2000	0.3165	31.019	
6	Alkalinity	7.6	6.33	120	0.0083	0.0132	0.084	
7	Hardness	149.1	49.70	300	0.0033	0.0053	0.262	
8	Chloride (cl^-)	35.15	14.06	250	0.0040	0.0063	0.089	
9	Nitrate ($no_3{}^-$)	1.35	3.00	45	0.0222	0.0352	0.106	
10	Sulphate ($so_4{}^{-2}$)	6.41	4.27	150	0.0067	0.0106	0.045	
11	Magnesium (mg^{+2})	18.1	60.33	30	0.0333	0.0528	3.183	
12	Calcium (ca^{+2})	29.84	39.79	75	0.0133	0.0211	0.840	
					0.6299	0.9969	89.964	
				K = (1/(e(1/sn))	1.5876			

Table 20.11 Water quality index for Post-Monsoon season

Station	December	January	Average	Grade
Valak	90.25	108.73	99.49	D
Mota Varachha	88.52	99.11	93.82	D
Sarthana	80.71	109.34	95.03	D
Katargam	71.53	72.54	72.04	C
Rander	80.34	102.27	91.31	D
Average	82.27	98.40		
Grade	D	D		

The result shows that the water quality index is higher in March compared to other seasons while the station wise comparison shows that in Pre-monsoon all stations had a higher value of water quality index but the overall trend of variation in value remain same.

Table 20.12 Results for March month

Sr. No	Parameters	Unit	Valak	Mota Varachha	Sarthana	Katargam	Rander
1	pH	–	8.7	8.06	8.35	8.6	7.4
2	Electrical conductivity	Mohs/cm	4.83	599	641	614	727
3	TDS	Mg/l	0	0	0	0	0
4	Do	Mg/l	10.1	5	3.8	3.8	0
5	BOD	Mg/l	8	4	0	0	0
6	Alkalinity	Mg/l	6.5	4.4	5.5	6.5	7
7	Hardness	Mg/l	214	176	168	160	194
8	Chloride (cl^{-})	Mg/l	29.49	40.98	38.98	40.48	48.48
9	Nitrate (no_3^{-})	Mg/l	0.18	0.75	0.58	0.33	0.28
10	Sulphate (so_4^{-2})	Mg/l	14.7	15.5	17.27	15.77	27.13
11	Magnesium (mg^{+2})	Mg/l	32.56	23.32	19.92	18.46	23.81
12	Calcium (ca^{+2})	Mg/l	32.06	32.06	34.46	33.66	38.47

20.4.4 Comparison of Water Quality Index (WQI)

By comparing the values of the WQI for the year 2017–18, it is observed that the quality of water is fairly good in the monsoon season but as the monsoon recedes the quality also gradually starts decreasing and in Pre-monsoon season it is not suitable for human consumption without treatment. The overall comparison of WQI is shown in below mentioned Table 20.15.

The WQI in the Tapi river shows the same trend for all the seasons in which WQI is higher in station Valak and Mota Varachha, while it decreases at Sarthana and gives the minimum value at Katargam & again increases at Rander. The graphical representation for the same WQI for the Tapi river for the years 2017–18 is shown in Fig. 20.3.

20.5 Conclusion

- Water quality index of Tapi river from Valak to Rander during monsoon is 75.44 (grade c) which falls under the poor river water quality.
- Water quality index of Tapi river from Valak to Rander during post-monsoon is 85.11 (grade d) which falls under the very poor river water quality.

Table 20.13 Water quality index for Valak station for March month

Sr. No	Parameters	Observed values	Qn	Standard values (sn)	(1/sn)	Wn	Qnwn	WQI
1	Ph	8.29	258.00	7.5	0.1333	0.2110	54.441	95.74
2	Electrical conductivity	0.00499	0.00	300	0.0033	0.0053	0.000	
3	TDS	290	58.00	500	0.0020	0.0032	0.184	
4	Do	6.75	81.77	5	0.2000	0.3165	25.882	
5	BOD	1	20.00	5	0.2000	0.3165	6.330	
6	Alkalinity	157.5	131.25	120	0.0083	0.0132	1.731	
7	Hardness	165.3 31.81	55.10	300	0.0033	0.0053	0.291	
8	Chloride (cl^-)		12.72	250	0.0040	0.0063	0.081	
9	Nitrate (no_3^-)	0.01	0.02	45	0.0222	0.0352	0.001	
10	Sulphate (so_4^{-2})	33.65	22.43	150	0.0067	0.0106	0.237	
11	Magnesium (mg^{+2})	30.7	102.33	30	0.0333	0.0528	5.398	
12	Calcium (ca^{+2})	30.7	40.93	75	0.0133	0.0211	0.864	
					0.6299	0.9969	95.439	
				K = (1/(e(1/sn))	1.5876			

Table 20.14 Water quality index for monsoon season

Station	March	Grade
Valak	162.89	D
Mota Varachha	153.57	D
Sarthana	145.97	D
Katargam	124.01	D
Rander	149.69	D
Average	147.23	
Grade	D	

- The overall trend of results shows that the river water quality is very poor at stations Valak, Mota Varachha and Rander, while the very quality is poor at stations Sarthana and Katargam.
- Decrease in BOD, do, nitrate, sulphate and magnesium content in water evident to aquatic plant growth in water.

Table 20.15 Comparison of WQI of Tapi river for year 2017–18

Station	August	September	December	January	March	Average	Grade
Valak	76.26	86.01	90.25	108.73	162.89	81.14	D
Mota Varachha	77.64	77.51	88.52	99.11	153.56	77.58	D
Sarthana	69.88	76.48	80.71	109.34	145.97	73.18	C
Katargam	68.88	71.11	71.53	72.54	124.01	69.99	C
Rander	73.25	77.38	80.34	102.27	149.69	75.32	C
Average	75.44		85.11				
Grade	C		D				

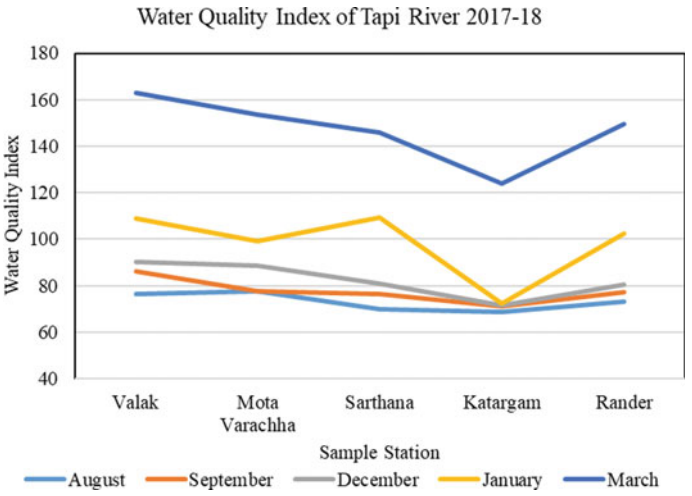

Fig. 20.3 WQI of Tapi river for the year 2017

- Unknown sources of untreated water released in the river water may lead to an increase in the water quality index between Valak, Sarthana and Mota Varachha at which the WQI score is above 100 (grade e).
- Water quality is continuously degrading from monsoon to post-monsoon season which makes it unsuitable for drinking and fish culture.

References

Bhalme SP, Nagarnaik PB (2012) Analysis of drinking water of different places: A review. Int J Eng Res Appl 2(3):3155–3158

Cristina R, Ioana P, carmen R, Ozunu A (2014) "Water quality index for assessment of drinking water sources from medias town, sibiu county." Aerul si apa. Componente ale mediului, 24

Dubey M, Ujjania NC. (2015) Assessment of water quality and sources of pollution in downstream of Ukai, tapi river (Gujarat). Curr World Environ 10(1):350

Effendi, H, Wardiatno Y (2015) Water quality status of ciambulawung river, banten province, based on pollution index and nsf-WQI. Procedia Environ Sci 24, 228–237

Gor A, Shah A (2014) Water quality index of mahi river, vadodara, Gujarat. J. Engg. Devel. Res 2(3):3214–3219

Gupta N, Pandey P, Hussain J (2017) Effect of physicochemical and biological parameters on the quality of river water of Narmada, Madhya Pradesh, India. Water Sci 31(1):11–23

Pathak SK, Prasad S, Pathak T (2015) Determination of water quality index river Bhagirathi in Uttarkashi, Uttarakhand, India. Int J Res Granthaalayah 3(9):1–7

Shrivastava A, Tandon SA, Kumar R (2015) Water quality management plan for patalganga river for drinking purpose and human health safety. Int J Sci Res Environ Sci 3(2):71

Tyagi S, Singh P, Sharma B, Singh R (2014) Assessment of water quality for drinking purpose in district pauri of Uttarakhand, India. Appl Ecol Environ Sci 2(4):94–99

Ankit N Chaudhari, Darshan J Mehta, Dr. Neeraj D Sharma (2021) An assessment of groundwater quality in South-West zone of Surat city. Water Supply, ws2021083. https://doi.org/10.2166/ws.2021.083

Chapter 21
Spatial Variability of Groundwater Quality Parameters of East Godavari District, Andhra Pradesh, India

Nathi Ajay Chandra and Sanat Nalini Sahoo

Abstract The nature of groundwater is vital for the protected utilization of water. The purposes of this investigation were. (1) To outline the present groundwater quality of the study area. (2) To develop the spatial distribution map of groundwater quality parameters (viz; Chloride (Cl), Sodium (Na), Calcium (Ca), potential Hydrogen (pH), Potassium (K), Sulfate (SO_4), Magnesium (Mg), Bicarbonate (HCO_3), and Thorium (Th)). The ordinary kriging technique was used to analyze the spatial variability of groundwater quality parameters. To develop the study area's groundwater quality parameters map, the spatial analyst tool and geostatistical analysis tool in ArcGIS 10.2.1 version was used.

Keywords Geostatistical wizard · Semivariogram · Drinking water quality standards · Spatial analyst tool

21.1 Introduction

Groundwater is a significant source in India for all purposes, and it plays a vital role in India for economic development and food security. 66% of the freshwater assets of the world are in groundwater. For drinking water, more rural population than the urban population depends on groundwater. In the coastal areas of Andhra Pradesh, the majority of the people rely on groundwater sources for their domestic usage, agricultural water, and aquacultural purposes. Groundwater contains various concentrations of dangerous organic chemicals and minerals and many dissolved constituents. The most common dissolved mineral substances are Chloride (Cl), Sodium (Na), Calcium (Ca), potential Hydrogen (pH), Potassium (K), Sulfate (SO_4), Magnesium (Mg), Bicarbonate (HCO_3), and Thorium (Th). If they are within the permissible limits, they are not harmful. Groundwater is less prone to bacterial pollution than surface water because of the soil and rocks through which groundwater flows screen out most bacteria. Significant factors that affect groundwater quality

N. A. Chandra · S. N. Sahoo (✉)
Civil Engineering Department, NIT Rourkela, Rourkela 769008, India
e-mail: sahoosanat@nitrkl.ac.in

R. Jha et al. (eds.), *Groundwater and Water Quality*, Water Science and Technology Library 119, https://doi.org/10.1007/978-3-031-09551-1_21

are depth from the ground surface, chemical composition of the sediments, permeability through which groundwater moves, and variation in climate. Depth of soil and subsurface geological formations through which groundwater passes were mainly influenced by the natural chemical composition of groundwater. Nas and Berktay (2010) stated that contribution from the atmosphere, surface water bodies, and anthropogenic factors also influence groundwater quality; the groundwater quality map in Konya City was developed using the ordinary kriging interpolation technique. Chatterjee et al. (2010) used the spline contouring method to generate the contours needed for creating a triangulated network for each thematic layer. Dash et al. (2010) used the Water Quality Index(WQI) to assess water quality; the best-fitted semivariogram was found using RMS value and adopted best-fitted interpolation techniques and generated spatial variability and quality information maps. Srinivasamoorthy et al. (2010) estimated the water quality in affected areas. A total of 148 groundwater samples were collected and analyzed for major cations and anions. Overall, a water quality index rating obtains water quality for human consumption. Oliver and Webster (2014) explained that Kriging is a generic term for a range of least square methods to provide the best linear unbiased predictions (BLUP). The best-fitting model may have a more considerable nugget variance than other reasonable models. Benthungo Murry (2013) used the semivariogram to analysis of geostatistical data, and variograms expressed the created mathematical models of spatial correlation structures, their study also showed the estimation of base flow by using VIC (variable infiltration capacity) model.

21.2 Materials and Methods

21.2.1 Study Area

The examination zone East Godavari District shown in Fig. 21.1 is in Andhra Pradesh-India, with latitude 17.3213° N and longitude 82.0407° E. Climate of this area is mild and generally warm; the average temperature of this area is 16.4-degree Centigrade. The annual average rainfall is 1201.1 mm. According to statistics 2011, the region has a population of 5,151,549, with a density of 477/Km^2 and the urban population is 25.52%. Andhra Pradesh is one of the largest rice producers in India only because of the East Godavari district.

21.2.2 Data Collection

Data from 119 groundwater sampling points was collected from the groundwater board Kakinada-Andhra Pradesh. Collected samples were tested to measure the quality parameters consolidation (GWB KKD 2017). The water samples

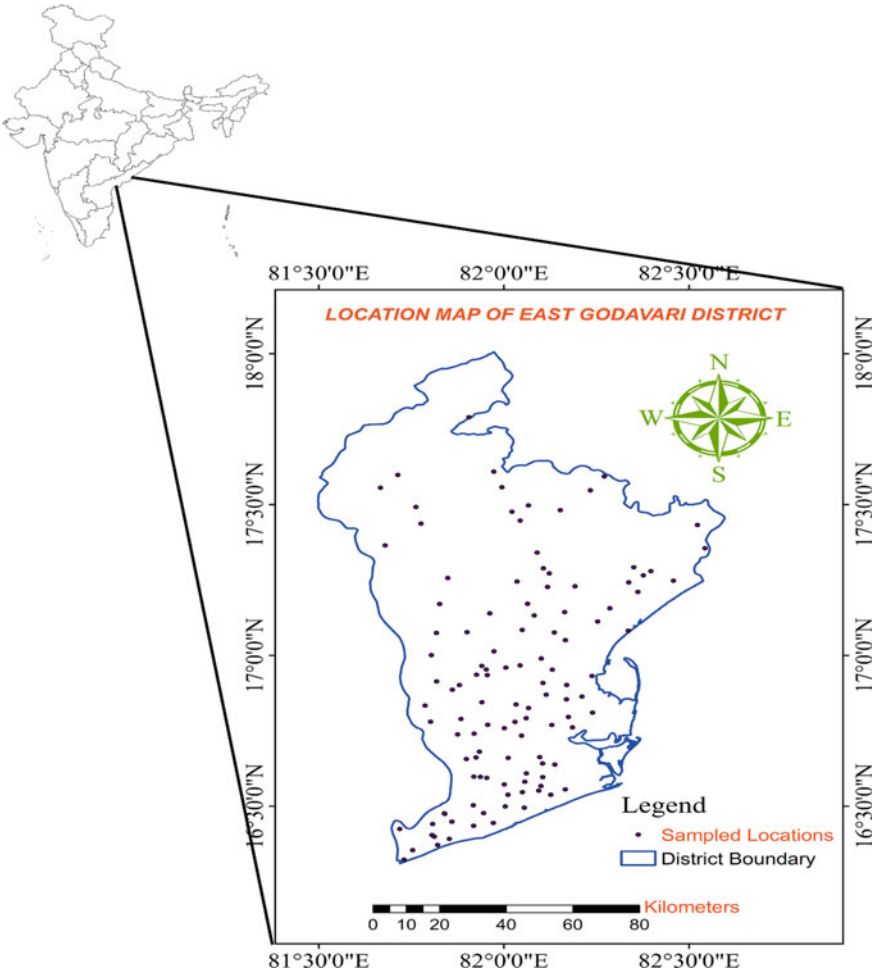

Fig. 21.1 Location map of the study area

were collected from general observation wells, APERP OB Wells, open wells, piezometers, and aquaculture nearest bore wells.

21.2.3 Semivariogram Modeling

Spatial dependence between two observations is measured in semi-variance and observations as a function of the distance between them. Semivariogram: The change of semi-variance distance between observations in a graph. The degree of dissimilarity between observations is measured using a semivariogram, which is a function

of distance. Things close together are more similar than things apart; if two locations are close to each other generally, the semi-variance is low, and all these are based on the "first rule of Geography."

21.2.4 Spatial Structure of Quality Parameters

Sill, Range, and Nugget are the measures of a variogram. The distance between the observations cannot explain variability in the field data refereed by the nugget. The magnitude of the nugget is affected by imprecision in sampling methods, basic variability of the property is estimated and the minimum spacing between observations makes it impossible to estimate "close-range" spatial dependence when there are no observations close to each other. The maximum noticed the sill refers to uncertainty in the data. Generally, in theory, the sill corresponding variance of the data is usually estimated in statistics. The sill and the nugget difference represent the observed variables that the distance between observations can explain. If semi-variance stops increasing, this point is called Range. The Range represents the distance at which two observations are unrelated. The spatial design is quantified utilizing a semivariogram. The exploratory semivariograms can be fitted to various hypothetical models like circular and spherical, linear, gaussian, and exponential. Semivariograms can be determined in different ways to perceive any anisotropy of spatial uncertainty.

21.2.5 Kriging

Kriging is a kind of spatial interpolation that utilizes numerical formulei to assess values at new points dependent on the values at known points. There are various kriging methods, i.e. Indicator kriging, Universal kriging, Ordinary kriging, and Co Kriging. Kriging is a geostatistical interpolation method, and it is helpful in many fields. Ordinary Kriging doesn't assume overriding trends (or) directional drift, but it takes spatial autocorrelation. The overarching trend exhibits only when you are particular with your data. The ordinary kriging strategy gives the best direct fair gauge of a regionalized variable at an unsampled extent, known as the best straight unprejudiced assessor. This is because the presented values are dealt with from conditions that limit the qualification of the evaluation error. Further, the ordinary kriging technique expects to have a mean error of almost similar to zero. The supposition in standard Kriging depends on the mean of the cycle is consistent and inside the spatial area is invariant. The assumption in ordinary Kriging is based on the mean of the process being constant and within the spatial domain is invariant.

21.2.6 Model Selection and Cross Validation

Log-normal and square root transformations were used to distribute the data normally. Various semivariogram parameters, such as exponential, Gaussian, and spherical, were generated. The selection of the most suited model depended on the statistical metrics such as R2 ≅ 1(Max) and Regression Sum of Squares (RSS) Should be minimum. The relating nugget, range, and sill values of the most suited hypothetical model were noticed. By choosing the appropriate theoritical model and the corresponding semivariogram parameters, and using the ordinary kriging technique, the spatial variability maps of groundwater quality parameters were generated.

21.2.7 Groundwater Quality Parameters

Different organizations have set acceptable water quality parameters for drinking, and these quality exceedance would cause human well-being threat. For instance, the desirable limit of chloride in water is 250 mg/l. Sulphate 200.00 mg/l. The permissible limit for pH is 8.5 by Bureau of Indian standrads (BIS) for drinking water quality IS:10500. Mg values vary from 12 to 125 mg/l with an average of 50 mg/l, Ca desirable limit is 250 mg/l. Bicarbonates minimum is 196 mg/l, and the maximum is 855 mg/l.

21.3 Results and Discussion

As shown in Fig. 21.2a, almost 79% of the area contains desirable limits of chloride in the area and a 5% area is more than the permissible limits. Chloride can cause a salty taste in drinking water. Groundwater contains natural chloride. Electro dialysis, reverse osmosis (RO), and distillation are important methods to remove chloride content in drinking water. The sodium (Fig. 21.2b) content is more on the eastern side of the study area. Near the ocean regions, calcium content is more (Fig. 21.2c). For drinking purposes, the study area has 99.96% area within desirable limits. The term pH stands for "potential for hydrogen." The study area has 62.22% area in tolerance limits i.e. 6.5–8.5 on the logarithmic scale (Fig. 21.2d). As shown in Fig. 21.2e and Fig. 21.2f, the eastern part of the study area (coastal region) has more potassium and sulfate content. Hardness is caused by calcium and magnesium. Low magnesium status has been implicated in hypertension, coronary heart disease, diabetes, and metabolic syndrome. For drinking purposes, the study area has 44.20% area (Fig. 21.2g) within desirable limits. Figure 21.2h shows bicarbonate content is more in the southwest and northern region of the basin. Significant thorium values were observed along the coastal region (Fig. 21.2i).

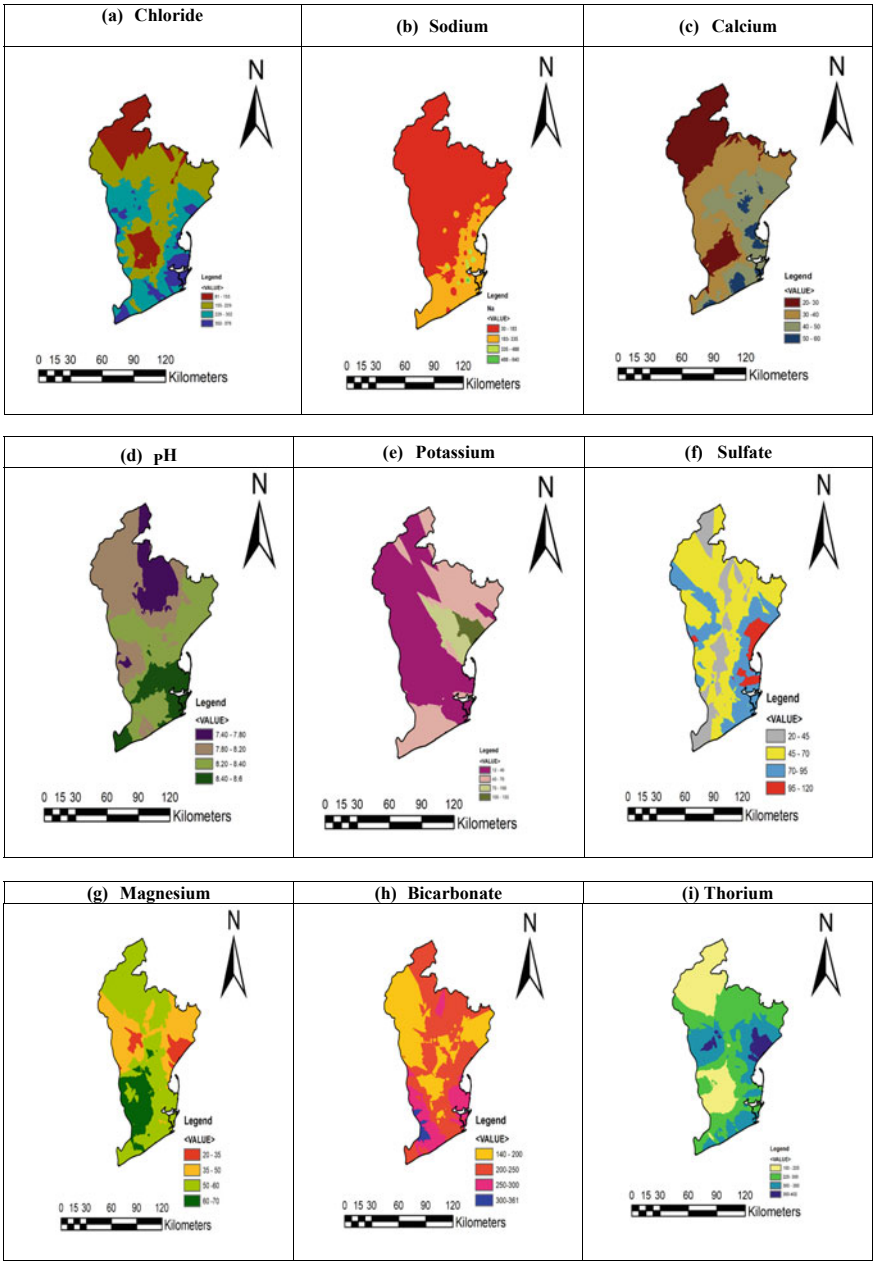

Fig. 21.2 Spatial variability maps of (a) Chloride (b) Sodium (c) Calcium (d) pH (e) Potassium (f) Sulfate (g) Magnesium (h) Bicarbonate and (i) Thorium

21.4 Conclusions

The water quality parameters were normally distributed using logarithm distribution method to guarantee the ordinariness of the information pattern for analysis. The spatial variability maps produced utilizing the ordinary kriging strategy demonstrated that the sodium concentration was more than the standard drinking level. The magnesium concentration more than the standard drinking level in the Polam cheruvu and Korukonda region. In Pedapudi, Vidyuth Nagar, the pH level is below the tolerance limit. Papampeta and Batsaluru region, the pH level is more than the tolerance limit for drinking purposes. The information in these spatial variability maps will assist the researchers and the hydrological community in outlining guidelines for effective management of groundwater resources.

Acknowledgements The authors would like to acknowledge Department of Civil Engineering, NIT Rourkela, for providing the necessary facility to carry out the research work.

References

Benthungo Murry Y (2013) Geospatial modeling for assessing ground water resources: a study in Dimapur Area, NE India

Chatterjee R, Tarafder G, Paul S (2010) Groundwater quality assessment of Dhanbad district, Jharkhand, India. Bull Eng Geol Env 69(1):137–141

Dash JP, Sarangi A, Singh DK (2010) Spatial variability of groundwater depth and quality parameters in the national capital territory of Delhi. Environ Manag 45(3):640–650

Nas B, Berktay A (2010) Groundwater quality mapping in urban groundwater using GIS. Environ Monit Assess 160(1–4):215–227

Oliver MA, Webster R (2014) A tutorial guide to geostatistics: computing and modelling variograms and kriging. Catena, Elsevier B.V. 113:56–69

Srinivasamoorthy MVK, Rajiv KVR, Anandhan SCP, Vasudevan RMS (2010) Application of water quality index for groundwater quality assessment: Thirumanimuttar sub-basin, Tamilnadu, India, pp 595–609

Chapter 22
Pumping Optimization for Saltwater Intrusion Management in a Coastal Aquifer with Combined Use of Sharp Interface and Density Dependent Models

Subhajit Dey and Om Prakash

Abstract Coastal areas are densely populated due to socioeconomic benefits and in turn also have a greater demand for fresh water. This ever-increasing demand for fresh water can be met by coastal aquifers, which act as large reservoirs of freshwater. Excessive and unmanaged pumping from coastal aquifer allows the salt water to flow inward encroaching on the voids created by the pumping of freshwater. This phenomenon is called saltwater intrusion. To stop the saltwater intrusion, an optimal pumping strategy needs to be adopted. Simulation models are generally linked with an optimization algorithm to develop an optimal pumping strategy for management of saltwater intrusion. Sharp interface based simulation models are often used which are computationally inexpensive but lacks in prediction accuracy, as it does not incorporate the effects of dispersion and diffusion. Density dependent simulation models include the effect of dispersion and diffusion, but have a very high computational budget in evaluating an optimal pumping strategy. To overcome above-mentioned limitation a new methodology is developed, where a density dependent model is used in conjunction with a sharp interface model to derive an optimal density ratio, such that interface obtained using this density ratio implicitly accommodated the effect of dispersion and diffusion in a sharp interface model. The performance of the developed methodology is evaluated for three hypothetical scenarios of saltwater intrusion. The performance evaluation results show the applicability of the methodology for management of saltwater intrusion while maximizing fresh water pumping in coastal aquifers.

Keywords Groundwater modelling · Coastal aquifer management · Pumping optimization · Saltwater intrusion · Density dependent model · Sharp interface model

Subhajit Dey · O. Prakash (✉)
Department of Civil and Environmental Engineering, Indian Institute of Technology Patna, Patna 801106, India
e-mail: om.prakash@iitp.ac.in

Subhajit Dey
e-mail: sri.pce15@iitp.ac.in

R. Jha et al. (eds.), *Groundwater and Water Quality*, Water Science and Technology Library 119, https://doi.org/10.1007/978-3-031-09551-1_22

22.1 Introduction

Ever increasing demand for fresh water has resulted in the excessive pumping of ground water aquifers (Chakraborty and Prakash 2020). Aquifers that are hydraulically connected to the sea are referred to as coastal aquifers when subjected to excessive pumping result in saltwater intrusion. Excessive unmanaged pumping causes a reversal of groundwater head gradient allowing the saline water to flow towards the land and fill the voids created by pumping of fresh water. This phenomenon is called saltwater intrusion. Therefore, the main challenge in the management of coastal aquifers is to maximize the pumping of fresh water without causing saltwater intrusion.

Several pumping based management alternative can be designed to meet this challenge. Sequentially evaluating all possible pumping alternatives to find an optimal pumping strategy is not possible or practical, as an infinite combination of pumping strategies can exist (Dhar and Datta 2009; Sreekanth and Datta 2015). Therefore, simulation models are linked with optimization algorithms to evaluate various pumping based management alternatives in order to find the optimal pumping strategy that maximizes the production of fresh water without causing saltwater intrusion (Chakraborty and Prakash 2021; Dey and Prakash 2019).

Among various simulation models available, density dependent numerical simulation models incorporate effects of dispersion and diffusion, which makes the models more realistic (Abarca et al. 2007; Dausman et al. 2010; Dokou and Karatzas 2012). To incorporate effects of dispersion and diffusion, flow equation and transport equations are solved sequentially which increases the computational budget (Werner et al. 2013). As pumping optimization problems in coastal aquifers are non-convex in nature, heuristic optimization techniques are found to be most suitable (Singh 2014; Sreekanth and Datta 2015) for finding the optimal pumping. Use of a heuristic optimization algorithm with density dependent simulation model increases the computational budget significantly (Dhar and Datta 2009).

Surrogate models have been used with heuristic optimization algorithms to reduce computational effort generally faced by numerical simulation models like density dependent model. Surrogate models are pattern recognizing algorithm like Artificial Neural Network (ANN) which maps the relationship between production well pumping and location of the saltwater-freshwater front (Datta et al. 2014; Sreekanth and Datta 2015). ANN was first applied as surrogate model (Banerjee et al. 2011; Bhattacharjya and Datta 2009; Kourakos and Mantoglou 2006; Rao et al. 2004; Rao et al. 2003), but in recent times Modular Neural Network (Ataie-Ashtiani et al. 2013; Kourakos and Mantoglou 2009), Genetic Algorithm (Sreekanth and Datta 2011a, b), Fuzzy Inference System (Roy and Datta 2017) and Multivariate Adaptive Regression Spline (Roy and Datta 2018) are also used as surrogates. Surrogates models need large comprehensive data sets to train the model. In addition, changes in hydrogeological conditions also affect the performance of surrogate models (Werner et al. 2013).

Another numerical simulation model is sharp interface model, which is a tradeoff between the accuracy of prediction and computational efficiency. In case of Sharp interface model saltwater and freshwater are considered as two immiscible fluids, therefore a sharp interface is present in between saltwater and freshwater. In reality, there is a mixing zone present between freshwater and saltwater due to dispersion and diffusion. In the sharp interface, effects of dispersion and diffusion are not considered which leads to inaccuracy in prediction (Christelis and Mantoglou 2013; Dausman et al. 2010; Llopis-Albert and Pulido-Velazquez 2014; Pool and Carrera 2011). Sharp interface model based on Starck's potential (1976) is widely used in pumping optimization study (Mantoglou 2003; Mantoglou and Kourakos 2013; Mantoglou and Papantoniou 2008; Mantoglou et al. 2004).

It is evident from the above discussion that realistic representation of coastal aquifers is performed by density dependent model, but requires a large computational budget. Sharp interface model requires less computational budget but lacks in prediction accuracy. Therefore, it is required to develop a methodology that reduces computational effort and still predicts the saltwater-freshwater front accurately. Christelis and Mantoglou (2016), Pool and Carrera (2011) and Dey and Prakash (2020) had showed that the outcome of the sharp interface model can be more realistic if effects of dispersion and diffusion can be incorporate in the model. On the basis of above hypothesis, a new methodology is presented in this paper where optimal pumping values derived using a sharp interface model is further adjusted with help of density dependent model to achieve greater accuracy in prediction of the saltwater-freshwater front. In pumping optimization problem first a sharp interface model is called within an optimization algorithm and optimal pumping value is estimated. This optimal pumping value is used in a density dependent numerical simulation model within an optimization algorithm to update the density ratio. The adjusted density ratio is again passed on to the sharp interface model to improve the optimal pumping value with the new density ration. This iterative procedure is repeated until there is no improvement in the density ratio value obtained from the density dependent model. Particle Swarm Optimization (PSO) based optimization algorithm is used for solving the pumping maximization.

22.2 Methodology

A methodology is developed to maximize the freshwater pumping in coastal aquifer such that it meets the freshwater demand without causing saltwater intrusion. The developed methodology reduces the computational time without compromising on the accuracy of the prediction of the saltwater-freshwater front. The goal is met by modifying the density ratio in the sharp interface model such that freshwater-saltwater interface predicted using this modified density ratio represents the actual freshwater-saltwater interface as would have been predicted by a density dependent model which incorporates the effect of dispersion and diffusion in the process.

22.2.1 Sharp Interface Model

The developed sharp interface model is based on the principals of Ghyben-Herzberg relation and Dupuit approximation. In this case, saltwater and freshwater are considered as two immiscible fluids assuming a sharp interface is present separating the two fluids. A typical cross-section of sharp interface model for an unconfined coastal aquifer is shown in Fig. 22.1. As shown in Fig. 22.1, there are two distinct zones present in the aquifer; Zone 1, where only freshwater is present and Zone 2, where both freshwater and saltwater are present. In the zone 2, freshwater and saltwater are separated by a sharp interface. The head of the water from datum is h, depth of freshwater below the water table is b, and d is the height of mean sea level (MSL) from the datum. In addition, let ρ_f is the density of the freshwater and ρ_s is the density of saltwater. Density ratio ε defined as:

$$\varepsilon = \frac{\rho_s - \rho_f}{\rho_f} \tag{22.1}$$

From, Ghyben-Herzberg observation, the relation between the height of freshwater above MSL (h_f) and depth of freshwater below MSL (h_s) for zone 2 is given by Eqs. 22.2.1 and 22.2.2.

$$h_s = \varepsilon \times h_f \tag{22.2.1}$$

$$h - d = \varepsilon \times h_f \tag{22.2.2}$$

Strack (1976) and Mantoglou et al. (2004) developed a differential equation based on a single potential which applies to both the zones for the unconfined aquifer, given by Eq. 22.3.

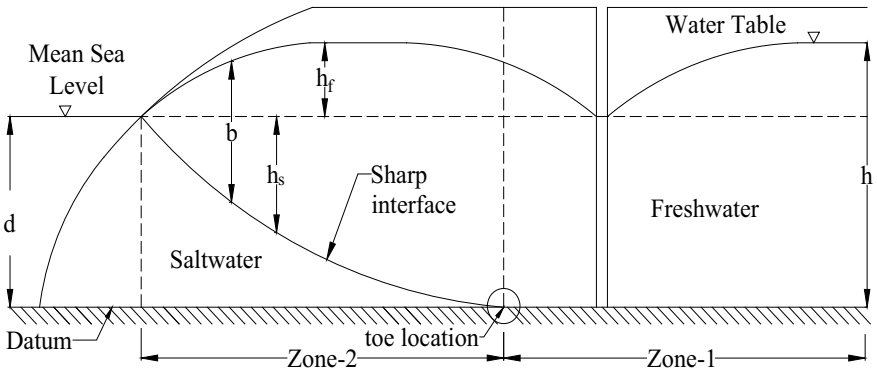

Fig. 22.1 Schematic cross section of an unconfined coastal aquifer based on sharp-interface flow

$$\frac{\partial}{\partial x}\left(K\frac{\partial \phi}{\partial x}\right)+\frac{\partial}{\partial y}\left(K\frac{\partial \phi}{\partial y}\right)+Q(x,y)=0 \tag{22.3}$$

The potential for each zone-1(ϕ_1) and for zone-2(ϕ_2) is expresses as follows:

$$\phi_1=\frac{1}{2}\left[h^2-(1+\varepsilon)d^2\right] \tag{22.4a}$$

$$\phi_2=\frac{1+\varepsilon}{\varepsilon}(h-d)^2 \tag{22.4b}$$

The potential at the location of the toe of interface (ϕ_τ) is defined by Eq. 22.5 (Cheng et al. 2000; Mantoglou et al. 2004):

$$\phi_\tau=\left[\frac{\varepsilon(\varepsilon+1)}{2}\right]d^2 \tag{22.5}$$

MODFLOW-2000 (Harbaugh et al. 2000) is used to solve Eq. 22.3 and a Lagrangian interpolation (Eq. 22.6) method is used to calculate the toe location of interface with help of Eq. 22.5.

$$\delta(x_0,x_1,\ldots x_k)=\prod_{j=0}^{n}(x-x_j)\sum_{i=0}^{n}\frac{f(x_i)}{(x-x_i)\prod_{j=0,j\neq i}^{n}(x_i-x_j)} \tag{22.6}$$

22.2.2 Density Dependent Model

In an undisturbed coastal aquifer, a mixing zone is present between freshwater and saltwater. In this zone density of water gradually decreases from the density of saltwater to the density of the freshwater. This zone is created due to hydrodynamic dispersion. This coupled flow (advection and hydrodynamic dispersion) is expressed mathematically in form of a partial differential equation given in Eq. 22.7 (Guo and Langevin 2002):

$$-\nabla\cdot\left(\rho\vec{q}\right)+\overline{\rho}q_s=\rho S_p\frac{\partial P}{\partial t}+\theta\frac{\partial \rho}{\partial C}\frac{\partial C}{\partial t} \tag{22.7}$$

where ρ is the fluid density, $\vec{q}$ is the specific discharge vector, $\overline{q}$ is the fluid density entering or leaving the medium, q_s is the volumetric flow rate at source or sink, θ is the porosity, t is the time, P is the fluid pore pressure, C is the concentration of the solute. Equation 22.7 is a combination of flow and transport equation linked by density term. There are various finite difference and finite element based methods to

solve this equation. In this study finite difference based model SEAWAT (Guo and Langevin 2002) is used to solve the Eq. 22.7. SEWAT uses flow model MODFLOW (Harbaugh et al. 2000) and transport model MT3DMS (Zheng and Wang 1999) together to solve the above equation.

22.2.3 Formulation of Pumping Optimization Problem

The main objective is to maximize pumping without causing saltwater intrusion to the pumping wells. To achieve this objective, it is required to combine optimization algorithm with a simulation model. Here sharp-interface model as discussed in Sect. 2 is used as a simulation model.

$$\text{Maximize } Q_t = \sum_{i=1}^{n} Q_i \tag{22.8a}$$

$$\text{Subjected to : } x_{wi} \geq x_{\tau i} \tag{22.8b}$$

$$Q_i^{min} \geq Q_i \geq Q_i^{max} \tag{22.8c}$$

where, Q_i is the pumping from *i*th pumping well, n is the total number of pumping well, x_{wi} is the distance of the *i*th well location from the shoreline, $x_{\tau i}$ is the distance of the location of the toe from the shoreline of the saltwater-freshwater interface corresponding to the *i*th well, Q_i^{min} is the minimum allowable pumping from *i*th well, Q_i^{max} is the maximum allowable pumping from *i*th well. The freshwater pumping from the production well is maximized subject to the constraint set given by Eqs. 22.8b and 22.8.3. Equation 22.8b essentially constrains the location of the saltwater-freshwater front in such a way that it never crosses the pumping well location. This ensures that the salt water never reaches the production well, thus preventing saltwater intrusion.

22.2.4 Particle Swarm Optimization

In this study heuristic optimization, PSO is chosen for solving the optimization problem. The working principle of PSO is derived from the movement of a flock of bird or a school of fish. It is observed that a flock of bird or a school of fish behaves like an intelligently to find food but each bird or fish is not that much intelligent. This concept is used in PSO to find an optimal pumping. PSO is introduced in 1995 by Eberhart and Kennedy (1995). In this study, a modified version of PSO as proposed by Shi and Eberhart (1998) is used as an optimizer. In the used PSO, m number of particles are arbitrarily selected in the search space. In the second step, the particles

Table 22.1 PSO parameters

Parameters	Value
Constant inertia weight	0.8
Cognitive constant	2
Social constant	2
Number of swarm particles (m)	30
Max number of iterations	1000
Tolerance limit	10^{-3}
Number of iterations of same global optima require to terminate optimization	60

are evaluated for the objective function. In the final step, the particles modified there location based on historical best location and current best location (Poli et al. 2007). Used parameters for PSO is listed in Table 22.1.

22.2.5 Linking of Sharp Interface Model with Density Dependent Model

Pool and Carrera (2011) proposed a correction factor for density ratio to incorporate effects of dispersion and diffusion in sharp interface model. This idea was further extended by Christelis and Mantoglou (2016), where density ratio is modified with help of density dependent model within an optimization framework. On basis of the above, a methodology is developed where optimal pumping achieved by sharp interface model is adjusted by use of density dependent model. The idea is to modify the density ratio of sharp interface model in an optimization framework such that outcomes of the sharp interface model matches with the outcome of the density dependent model. As pumping is varied, the hydraulic head also changes. Since the estimates by the sharp interface model is a function of the hydraulic head and density ratio (Eqs. 22.4a, 4b and 22.5), the density ratio can be adjusted to accommodate for the change of hydraulic head in order to match the outcome from the density dependent model. Therefore, an optimal pumping and density ratio can be designed such that location of sharp interface and isosalinity contour (calculated by density depend model) at each well locations will match (Fig. 22.2). As optimization of density ratio is constrained by density dependent model, simultaneous optimization of pumping and density ratio needs to call density dependent model along with sharp interface model, which increases the computational budget. To overcome this problem, an iterative process is designed where, first pumping is optimized and then, the optimized pumping value is used with density dependent model to find an optimal density ratio. This eliminated the need to run the density dependent model with every iteration of the pumping optimization and therefore reduces the computational budget.

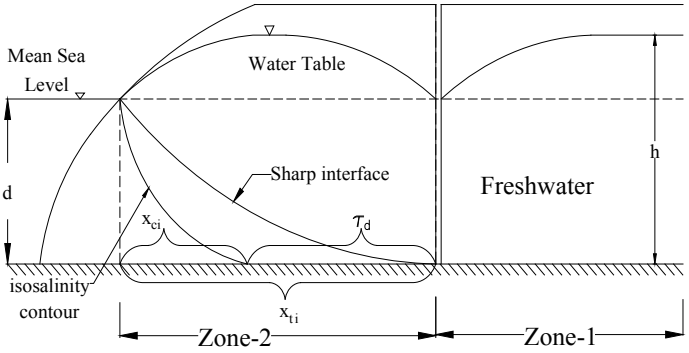

Fig. 22.2 Cross-section showing sharp interface and Isosalinity contour

The Optimization of density ratio performs based on the idea that at the optimal density ratio, location of the toe of sharp interface and location of the toe of isosalinity contour closely match at well locations (Fig. 22.2). To optimize density ratio, the following optimization problem is developed in Eq. 22.9.1 subjected to constrain given by Eq. 22.9.2.

$$\text{Minimize } \tau_d = \sum_{i=1}^{n} |x_{\tau i} - x_{ci}| \tag{22.9.1}$$

$$\text{Subjected to : } 0 \leq \varepsilon \leq 0.035 \tag{22.9.2}$$

where $x_{\tau i}$ is the distance of the toe location of sharp interface from the coast at *i*th well location, x_{ci} is the distance of the toe location of isosalinity contour from the coast at *i*th well location.

The iterative process has two parts. First part is the optimization of the pumping with help of sharp interface model linked with PSO algorithm. To calculate the sharp interface, head values and density ratio are required. The optimization is initialized with a density ratio value as proposed by Pool and Carrera (2011) and Christelis and Mantoglou (2016). In the second step, the density ratio is optimized. The optimized pumping value from the pumping optimization by sharp interface model is used to run the density dependent model (SEAWAT). Then, the outcome of the SEAWAT is used to locate toe of isosalinity contour with help of Lagrangian interpolation (Eq. 22.6). The optimization algorithm in the second case minimizes the difference between the toe location obtained using the density dependent model and sharp interface model. The density ratio corresponding to the optimal value of this minimization problem (Eq. 22.9.1) is used to update the density ratio in the sharp interface model. This process is continued until there is no significant change in the density ratio value. This process is shown through a schematic chart (Fig. 22.3).

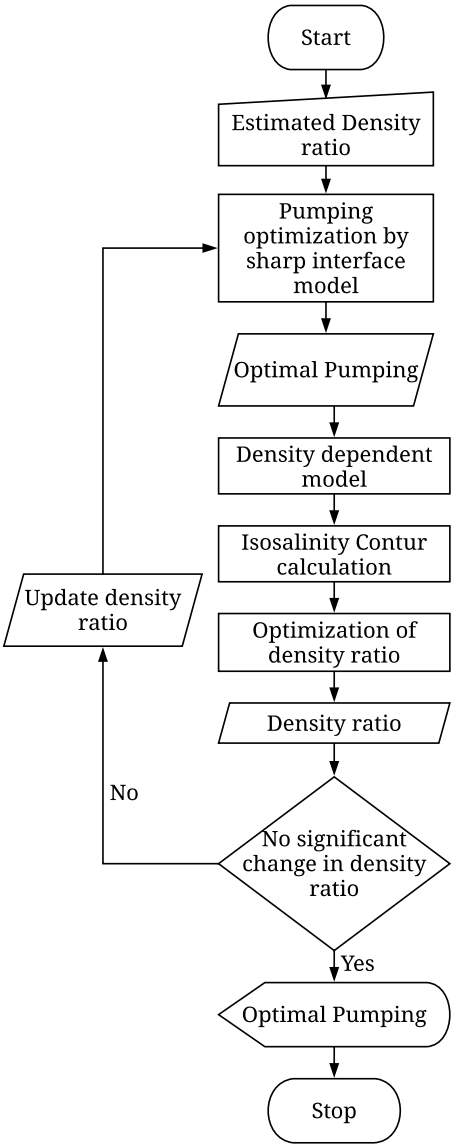

Fig. 22.3 Schematic chart of the developed methodology

22.3 Results and Discussion

22.3.1 Development of Hypothetical Study Area

To test the hypothesis three scenarios of pumping from a costal aquifer is considered (Dey and Prakash 2020). A hypothetical study area (Fig. 22.4) comprises of a

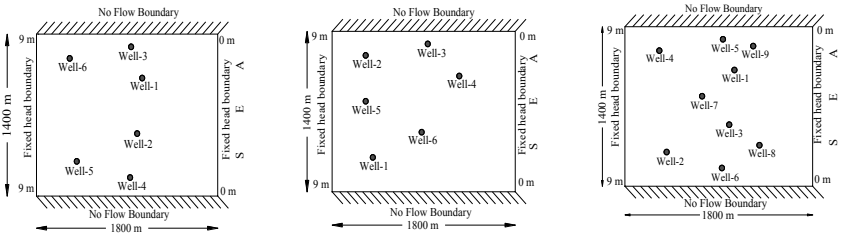

(a) Scenario 1 (b) Scenario 2 (c) Scenario 3

Fig. 22.4 Plan view of the study areas

homogeneous, isotropic three dimensional unconfined costal aquifer having an area of $25.2 \times 10^5 m^2$ (1800 m × 1400 m × 100 m). The study areas are discretized into finite difference grids (10 m × 10 m × 10 m). The left side boundary is considered as the sea. The different aquifer parameters used in this study area is given in Table 22.2. It is assumed that the aquifer is pumped uniformly throughout the depth of the aquifer at the well locations. The remaining three boundaries were considers as no-flow boundary. Therefore two flow boundaries are taken i.e. the left and right side which are taken as a Dirichlet condition. At the start the head is considered lineally varying from land surface at 9 m to the seaside at 0 m. Initially, the salt concentration in the aquifer is assumed to be zero. Dirichlet boundary condition is assigned at seaside and landside with concentration 0 kg/m^3 and 35 kg/m^3. The aquifer is studied for a period duration of 10 years. The other parameters used in the model are presented in Table 22.2.

In scenario one and two the coastal aquifer are pumped using six pumping wells each, and for scenario three the number of pumping wells are nine. The wells are

Table 22.2 Hydrogeological parameters of the study are

Parameter	Value
Dimension of area	1800 m × 1400 m × 100 m
Grid dimension	10 m × 10 m × 10 m
Hydraulic conductivity	15 m/day
Vertical anisotropy	1
Horizontal anisotropy	1
Specific storage	0.00001524
Specific yield	0.22
Recharge rate	0.001 m/day
Salt concentration in seawater	35 kg/m^3
Longitudinal dispersivity (αt)	2 m
αh/αt and αv/αt	1
Stress period length and number	10 years and 1

uniformly pumped throughout the stress period. The upper and lower limit of the pumping is considered as 15000–300 m^3/day respectively, for every well.

22.3.2 *Performance Evaluation of the Developed Model*

The iterative process of pumping optimization followed by density ratio optimization is run 31 times for study area-1, and 15 times on study area-2 and 3 respectively, to find the optimal pumping value. Corresponding density ratio is also calculated that would reflect the effect of dispersion and diffusion in a sharp interface simulation model, thereby giving a more realistic estimate of the actual scenario without causing saltwater intrusion. The performance evaluation results of the optimal pumping value and the corresponding density ratio is presented in Fig. 22.5.

It was noted that total optimal pumping achieved is 35375 m^3/day after 7 iterations for scenario-1, 35,648 m^3/day after 9 iterations for scenario-2 and 30,036 m^3/day after 8 iterations for scenario-3. In addition, corresponding optimal density ratio is found to be 0.010854 after 7 iterations in scenario-1, 0.012406 after 9 iterations for scenario-2 and 0.012036 after 8 iterations for scenario-3. No significant change in pumping and density ratio is observed after 7th iteration in scenario-1, 9th iteration in scenario-2 and 8th iteration in scenario-3 till end of the iteration.

The locations of the toe of interface and toe isosalinity contour are presented in Fig. 22.6. It was found that for test scenario-1 (Fig. 22.6) sharp interface crosses at the well locations 2, 3 and 4 by less than 5 m. Since the grid size taken in this study is 10 m, these violations can be easily neglected. Figure 22.6 shows a significant gap between the isosalinity contour and location of the interface in all the three scenarios. This is due to difference in the head values estimated using SEAWAT and MODFLOW. The calculated head by density dependent model (SEAWAT) is not same as calculated by MODFLOW because density dependent model calculates

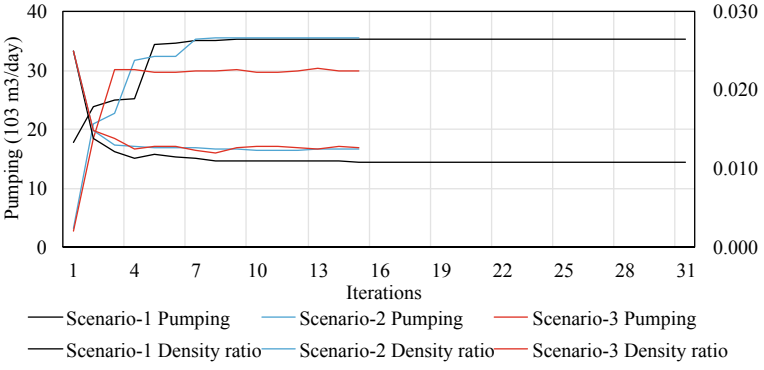

Fig. 22.5 Plot of total pumping and density ratio for study areas

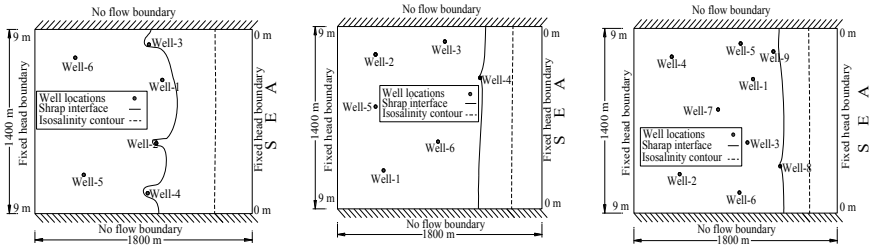

(a) Scenario 1 (b) Scenario 2 (c) Scenario 3

Fig. 22.6 Estimated locations of toe by isosalinity contour and sharp interface in study area

equivalent freshwater head (Guo and Langevin 2002) instead of the total head as incase of MODFLOW.

In addition to optimal pumping, total CPU runtime of sharp interface model, density dependent model and the iterative process is recorded. It was found that average CPU runtime for the sharp model was 8.698 s on an i7 3.6 GHz CPU. The maximum-recorded CPU runtime for the sharp interface model was 30.696 s and minimum-recorded CPU runtime recorded was 3.569 s. The Density dependent model i.e. SEAWAT is also run for the same data sets to compare the runtime of two models. The average CPU runtime for SEAWAT was recorded as 150 min. It is found that minimum CPU runtime for SEAWAT is 95 min and maximum runtime is 310 min. In addition, it was also noted that average CPU runtime for single iteration of pumping optimization followed by density ratio optimization was about 420 min. The maximum-recorded runtime for single iteration of pumping optimization followed by density ratio optimization was 896.58 min and the minimum runtime was 350.17 min. In addition, it was also noted that average 70 iterations are required for PSO with 30 particles to produce an optimal pumping. The previous discussion indicates that an average of 8 iterations is required for the sharp interface model to produce an optimal pumping. Therefore, total time require to produce an optimal solution by the iterative method of pumping optimization followed by optimization sharp interface model is 8×420 min. $= 3360$ min. With the same analogy and the same problem scenario when solved using density dependent model the estimated time taken by a density dependent model would be $30 \times 70 \times 150$ min. $= 315{,}000$ min. It is to be noted that optimization using density dependent model would not require multiple iterative optimizations as in case of sharp interface (8 iterations). It can be seen that there is a reduction of the computational time by a 98.93% while using the developed methodology.

22.4 Conclusions

This new methodology utilized in this study performs satisfactorily in optimizing the freshwater pumping from the coastal aquifer without causing saltwater intrusion. The developed methodology needs to test against more realistic scenarios. In addition developed model is found computationally inexpensive. The develop model have potential to reduce computational budget by 98.93%. The computational time can be further reduced by application of parallel processing. Thus it can be concluded that the new methodology is require tiny amount of computational budget compared to used of density dependent model in coastal aquifer pumping optimization problem. Therefore, the developed methodology can be a viable option in managing coastal aquifer with greater accuracy with limited computational budget.

References

Abarca E, Carrera J, Sánchez-Vila X, Dentz M (2007) Anisotropic dispersive Henry problem. Adv Water Resour 30(4):913–926

Ataie-Ashtiani B, Ketabchi H, Rajabi MM (2013) Optimal management of a freshwater lens in a small island using surrogate models and evolutionary algorithms. J Hydrol Eng 19(2):339–354

Banerjee P, Singh V, Chatttopadhyay K, Chandra P, Singh B (2011) Artificial neural network model as a potential alternative for groundwater salinity forecasting. J Hydrol 398(3–4):212–220

Bhattacharjya RK, Datta B (2009) ANN-GA-based model for multiple objective management of coastal aquifers. J Water Resour Plan Manag 135(5):314–322

Chakraborty A, Prakash O (2020) Identification of clandestine groundwater pollution sources using heuristics optimization algorithms: a comparison between simulated annealing and particle swarm optimization. Environ Monit Assess 192(12):1–19

Chakraborty A, Prakash O (2021) Characterization of groundwater pollution sources by kriging based linked simulation optimization. Int J 20(81):79–85

Cheng AD, Halhal D, Naji A, Ouazar D (2000) Pumping optimization in saltwater-intruded coastal aquifers. Water Resour Res 36(8):2155–2165

Christelis V, Mantoglou A (2013) Improved sharp interface models in coastal aquifers of finite dimensions. In: Proceedings of EGU general assembly conference abstracts

Christelis V, Mantoglou A (2016) Coastal aquifer management based on the joint use of density-dependent and sharp interface models. Water Resour Manage 30(2):861–876

Datta B, Prakash O, Sreekanth J (2014) Application of genetic programming models incorporated in optimization models for contaminated groundwater systems management. In: EVOLVE-A bridge between probability, set oriented numerics, and evolutionary computation V. Springer, pp 183–199

Dausman AM, Langevin C, Bakker M, Schaars F (2010) A comparison between SWI and SEAWAT—the importance of dispersion, inversion and vertical anisotropy. Proceed SWIM 21:271–274

Dey S, Prakash O (2019) Management of saltwater intrusion in coastal aquifers: an overview of recent advances. In: Raj Mohan Singh PS, Shukla P (ed) Environmental processes and management. Springer Nature

Dey S, Prakash O (2020) Managing saltwater intrusion using conjugate sharp interface and density dependent models linked with pumping optimization. Groundwater Sustain Dev 100446

Dhar A, Datta B (2009) Saltwater intrusion management of coastal aquifers. I: linked simulation-optimization. J Hydrol Eng 14(12):1263–1272

Dokou Z, Karatzas GP (2012) Saltwater intrusion estimation in a karstified coastal system using density-dependent modelling and comparison with the sharp-interface approach. Hydrol Sci J 57(5):985–999

Eberhart R, Kennedy J (1995) A new optimizer using particle swarm theory In: Proceedings of the sixth international symposium on micro machine and human science, MHS'95. IEEE, pp 39–43

Guo W, Langevin CD (2002) User's guide to SEAWAT; a computer program for simulation of three-dimensional variable-density ground-water flow

Harbaugh AW, Banta ER, Hill MC, McDonald MG (2000) MODFLOW-2000, the U.S. geological survey modular ground-water model-user guide to modularization concepts and the ground-water flow process. Open-file Rep U. S. Geol Surv (92), 134

Kourakos G, Mantoglou (2006) A pumping optimization of coastal aquifers using 3-d density models and approximations with neural networks. In: Proceedings of XVI international conference on computational methods in water resources, Copenhagen

Kourakos G, Mantoglou A (2009) Pumping optimization of coastal aquifers based on evolutionary algorithms and surrogate modular neural network models. Adv Water Resour 32(4):507–521

Llopis-Albert C, Pulido-Velazquez D (2014) Discussion about the validity of sharp-interface models to deal with seawater intrusion in coastal aquifers. Hydrol Process 28(10):3642–3654

Mantoglou A (2003) Pumping management of coastal aquifers using analytical models of saltwater intrusion. Water Resour Res 39(12)

Mantoglou A, Kourakos G (2013) An efficient simulation-optimization coupling for management of coastal aquifers. In: Proceedings of AGU fall meeting abstracts

Mantoglou A, Papantoniou M (2008) Optimal design of pumping networks in coastal aquifers using sharp interface models. J Hydrol 361(1–2):52–63

Mantoglou A, Papantoniou M, Giannoulopoulos P (2004) Management of coastal aquifers based on nonlinear optimization and evolutionary algorithms. J Hydrol 297(1–4):209–228

Poli R, Kennedy J, Blackwell T (2007) Particle swarm optimization. Swarm Intell 1(1):33–57

Pool M, Carrera J (2011) A correction factor to account for mixing in Ghyben-Herzberg and critical pumping rate approximations of seawater intrusion in coastal aquifers. Water Resour Res 47(5)

Rao S, Sreenivasulu V, Bhallamudi SM, Thandaveswara B, Sudheer K (2004) Planning groundwater development in coastal aquifers/Planification du développement de la ressource en eau souterraine des aquifères côtiers. Hydrol Sci J 49(1):155–170

Rao S, Thandaveswara B, Bhallamudi SM, Srinivasulu V (2003) Optimal groundwater management in deltaic regions using simulated annealing and neural networks. Water Resour Manage 17(6):409–428

Roy DK, Datta B (2017) Fuzzy c-mean clustering based inference system for saltwater intrusion processes prediction in coastal aquifers. Water Resour Manage 31(1):355–376

Roy DK, Datta B (2018) A surrogate based multi-objective management model to control saltwater intrusion in multi-layered coastal aquifer systems. Civ Eng Environ Syst 1–26

Shi Y, Eberhart R (1998) A modified particle swarm optimizer. In: The 1998 IEEE international conference on evolutionary computation proceedings. IEEE world congress on computational intelligence. IEEE, pp 69–73

Singh A (2014) Optimization modelling for seawater intrusion management. J Hydrol 508:43–52

Sreekanth J, Datta B (2011a) Comparative evaluation of genetic programming and neural network as potential surrogate models for coastal aquifer management. Water Resour Manage 25(13):3201–3218

Sreekanth J, Datta B (2011b) Coupled simulation-optimization model for coastal aquifer management using genetic programming-based ensemble surrogate models and multiple-realization optimization. Water Resour Res 47(4)

Sreekanth J, Datta B (2015) Review: simulation-optimization models for the management and monitoring of coastal aquifers. Hydrogeol J 23(6):1155–1166

Strack O (1976) A single-potential solution for regional interface problems in coastal aquifers. Water Resour Res 12(6):1165–1174

Werner AD, Bakker M, Post VE, Vandenbohede A, Lu C, Ataie-Ashtiani B, Simmons CT, Barry DA (2013) Seawater intrusion processes, investigation and management: recent advances and future challenges. Adv Water Resour 51:3–26

Zheng C, Wang PP (1999) MT3DMS: a modular three-dimensional multispecies transport model for simulation of advection, dispersion, and chemical reactions of contaminants in groundwater systems; documentation and user's guide. Alabama Univ University

Chapter 23
Two-Dimensional Laboratory-Scale Experiments on Saltwater Intrusion Dynamics

Chitaranjan Dalai and Anirban Dhar

Abstract Saltwater intrusion (SWI) is one of the challenging problems for coastal aquifers. SWI occurs due to the higher density difference between the denser seawater and inland freshwater aquifer. In this regard, groundwater flux plays an important role in saltwater Intrusion dynamics. In the present work, experiments in a laboratory sandbox tank with automated measurement equipment have been performed. Preferential flow patterns were determined by using a dye tracer in porous media. Moreover, the diffusive toe location of the saltwater interface was determined from the experimental observations. A set of four experiments were conducted under the same boundary conditions, material, and operating conditions to ascertain the correctness. The experimental results were validated using the numerical codes FEFLOW and SEAWAT. The model and experimental results show the changes in the saltwater interface under the same operating conditions. These results provide evidence of SWI dynamics under the influence of freshwater flux and constant head boundary conditions.

Keywords Saltwater intrusion · Coastal aquifer · Image analysis · SEAWAT · FEFLOW

C. Dalai (✉)
School of Water Resource, Indian Institute of Technology Kharagpur, Kharagpur, West Bengal 721302, India
e-mail: cdchittaranjan1@gmail.com

A. Dhar
Department of Civil Engineering, Indian Institute of Technology Kharagpur, Kharagpur, West Bengal 721302, India
e-mail: anirban@civil.iitkgp.ac.in

Present Address:
C. Dalai
Department of Civil Engineering, Odisha University of Technology and Researh, Bhubaneswar 751003, India

R. Jha et al. (eds.), *Groundwater and Water Quality*, Water Science and Technology Library 119, https://doi.org/10.1007/978-3-031-09551-1_23

23.1 Introduction

Saltwater intrusion is the movement of saltwater from the ocean into coastal aquifers (Freeze and Cherry 1979; Fang 1997; Todd and Mays 2005). In the last century, saltwater intrusion is one of the most challenging environmental problems. This global issue is aggravated by increasing demands for freshwater in coastal aquifers. It is considered as the outcome of the density-dependent interaction between freshwater and seawater. Typically, when saltwater and freshwater are in contact with each other, the heavier fluid such as saltwater overlies relatively freshwater.

Past studies on laboratory scale saltwater intrusion experiments are available in Goswami and Clement (2007), Lu et al. (2013), Abdoulhalik and Ahmed (2018). However, most of the studies have neglected the effects of sloping beach faces. Moreover, numerical studies were considering variable-density flow on sloping beaches (Sulis et al. 2010; Han et al. 2018). Werner (2013) and Robinson et al. (2015) have performed experiments and quantitative analysis of saltwater intrusion. Physically based models remain essential tools to gain information about SWI in porous media. In this context, previous studies did not include the effect of shoreline (beach face) on saltwater intrusion.

This research is an effort of laboratory experiment for realistically describing the saltwater intrusion dynamics in the porous media. The two-dimensional flow simulations include the dynamic equilibrium between saltwater and freshwater. The objective of the present study is to validate laboratory scale experiments with numerical results (both finite difference and finite element based). Additionally, the image analysis technique is used to understand the flow dynamics of the saltwater interface.

23.2 Methodology

The saltwater intrusion dynamics is assessed in this study using experimental and numerical approaches. In the laboratory, two-dimensional sandbox experiments were used to develop a physical basis for assessing the SWI process in a coastal aquifer. Such laboratory scale experiments allowed for better identification of the saltwater interface in the porous media system. In particular, to determine the density-dependent flow within the sandbox experiments, toe location was measured by varying hydraulic gradients and image analysis. In the second step, validation of the experimental data with a numerical study was performed.

23.2.1 Laboratory Experimental Setup

Experiments were performed in a sandbox of 3.3 m length, 1.0 m height and 0.20 m width. Visual data was acquired during the test through an 80 mm thick transparent

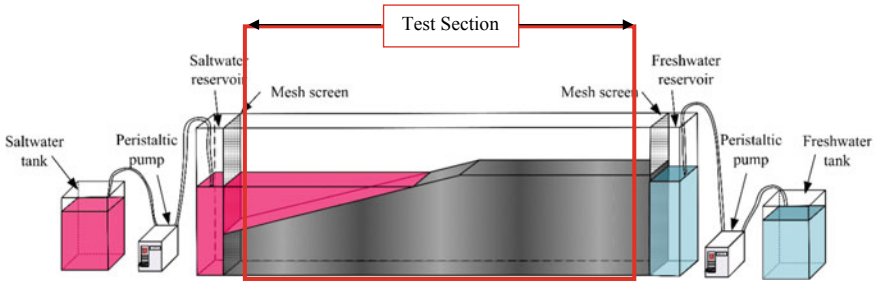

Fig. 23.1 A schematic diagram of the physical model setup

Table 23.1 Transport and hydraulic parameters'

Hydraulic conductivity	$40 * 10^{-4}$ m/s
Porosity	0.37
Saltwater density	1025 kg/m^3
Freshwater density	1000 kg/m^3
Longitudinal dispersivity	0.01 m
Transverse dispersivity	0.001 m

glass plate supported by a rectangular steel frame. All gaps and connections were made water tight with adhesive silicone gel. Figure 23.1 shows a schematic diagram of the experimental setup.

Boundaries on both sides were maintained as constant head by using two peristaltic pumps (PP-50vx from Electro lab). Freshwater was supplied through the right-side boundary, while the saltwater head was maintained in the right-side boundary. The CTD Driver [D127x (DI272 50 m) from Schlumberger] was used to monitor the density at saltwater side.

Clean coarse sand ($d_{50} = 1.02$ mm and $d_{60} = 1.4$) was used as aquifer material. The shoreline with a slope face angle of 15° was maintained. The hydraulic flow and transport parameters are summarized in Table 23.1. The average porosity was measured by both the volumetric and gravitational methods.

Rhodamine B (lobachemie) with a concentration of 0.00125 kg/L was chosen to trace the saltwater. It irradiates at a longer wavelength ($\lambda = 554$ nm). The luminosity at each point of the sandbox was recorded by a digital camera (DSLR, Nikon d5300) for imaging analysis.

23.2.2 Experimental Methods

The natural condition was simulated under head differences $\Delta h = 0.05$ m. Freshwater flows towards the left side through the sand aquifer in the middle chamber. The head differences were maintained as constant to obtain a pseudo steady state flow. The

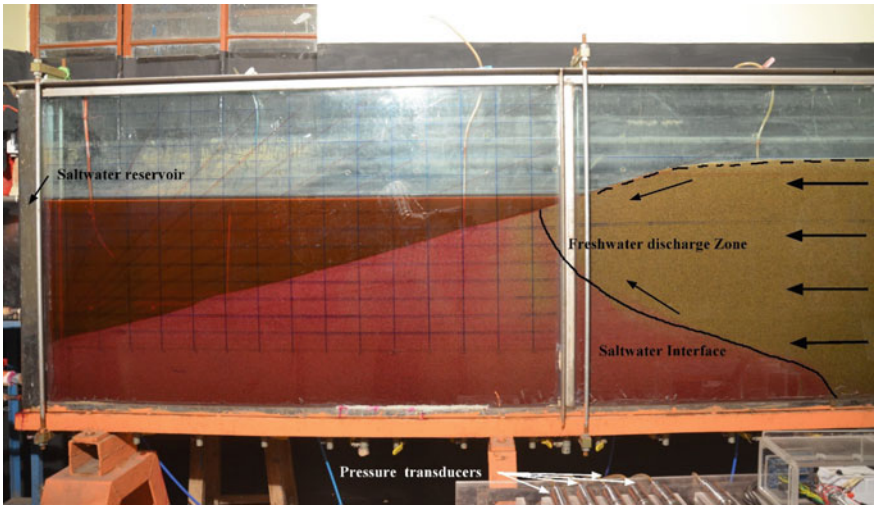

Fig. 23.2 This image shows the experimental setup

profile of the freshwater-saltwater interface was determined from the image analysis (Fig. 23.2).

23.3 Physical Model Simulations

A Series of steady state flow simulations were performed to validate seawater intrusion characteristics. These include the freshwater-saltwater flow balance in the unconfined aquifer under natural conditions.

23.3.1 SEAWAT Model Settings

Variable density models consider freshwater and saltwater mixing due to the hydrodynamic dispersion mechanism. SEAWAT code (Langevin et al. 2008) was simulated based on the integration of MODFLOW (groundwater flow equation model), MT3DMS (multi-species contaminant transport model), and VDF package (variable-density Flow). The aquifer was assumed to be homogenous and isotropic. A two-dimensional uniform grid of dimension 0.1 m (cells in the X and Z direction are 31 and 10 respectively) was used to discretize the sandbox model. The lateral model cell thickness was assumed to be 0.02 m, which represents the thickness of the experimental setup. Top condition was specified in the lines of Goswami and Clement (2007). The model was simulated for a long time to attain the steady state condition.

23.3.2 FEFLOW Model Settings

Finite Element Subsurface Flow and Transport Simulation model (FEFLOW 6.2) was used (Diersch 2005) for the simulation of two-dimensional sandbox setups with a set of standard parameters. A triangular meshing with 29,022 elements and 14,762 nodes was used. To avoid numerical dispersion, the grid was refined at all boundaries. The left side boundary was defined as the Dirichlet boundary (constant head) with the saltwater head of 0.65 m. The right-side boundary was assigned as a Neumann (constant flux) boundary condition, allowing freshwater to enter into the setup.

23.4 Results

SEAWAT is based on the finite difference method (FDM), whereas FEFLOW works on the finite element method (FEM). FDM is simple and very effective. However, FDM do not offer a better description of the complex geometry. The numerical model accuracy depends upon the model input parameters, the size of space and time steps and also the numerical technique used to solve equations. The compared simulation results indicate that FEFLOW results are better compared to the SEAWAT simulation for the SWI problem (Fig. 23.3).

The images were acquired with a digital single-lens reflex camera (DSLR, Nikon d5300) with a 18–55 mm zoom lens, fixed tripod was placed in front of the experimental setup at a distance of 1.8 m. The image analysis was performed with a pixel by pixel approach covering a range of RGB values with the help of Matlab® (Mathworks 2017). Color tracer concentration equivalent pixel value (combination of RBG value) was calculated from the following equation:

$$\overline{C}_{i,j} = D^{R}_{i,j} + \left(255 - D^{G}_{i,j}\right)$$

where $\overline{C}_{i,j}$ is the converted value applied original image of the pixel located in the i, j positions of the image. $D^{R}_{i,j}$ is the depurated Red values located in the i, j positions is the image. $D^{G}_{i,j}$ is the depurated Green values located in the i, j positions in the image. Figure 23.4 shows the concentration equivalent pixel value contours.

Experimental data were compared against model predicted results to validate the performance of the saltwater intrusion model. Four different time periods were utilized to identify the variation of interface movement over time. Figure 23.5 compares the experimental interface location for four time periods against the FEFLOW and SEAWAT generated results. The discrepancies between the experimental and predicted extent of saltwater interface shapes are approximately within 0.1 m. The results indicate that unstable flow patterns and salt-fingering flow influenced numerical conditions. Salt fingering is likely to occur under realistic conditions. The numerical models simulated under perfect homogenized conditions and Grain

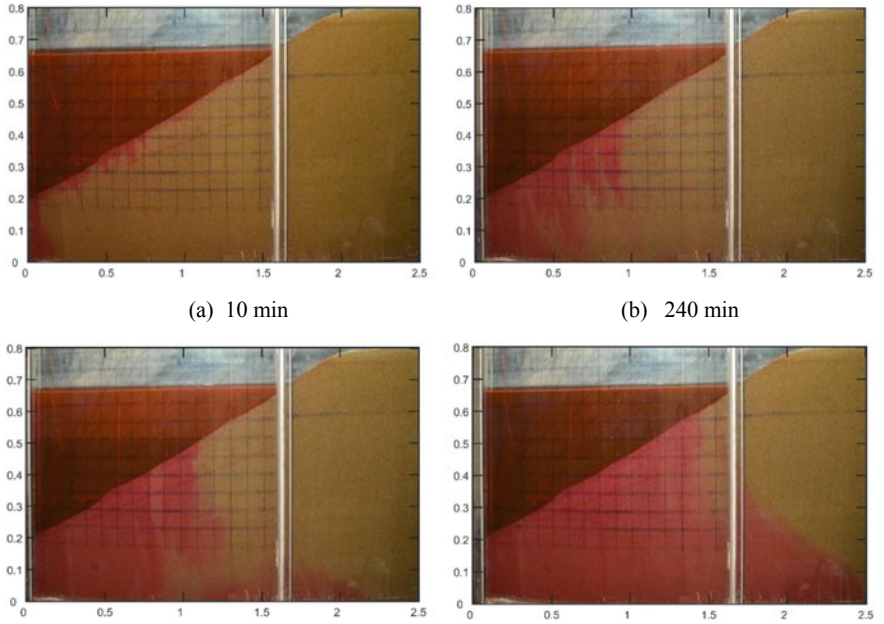

(a) 10 min (b) 240 min

(c) 400 min (d) 520min

Fig. 23.3 Observed SWI profiles at various time periods in experimental conditions

size deviations around the average diameter or minor heterogeneities introduced during packing are not taken into consideration. These effects are clearly visible in the experiment results. Deviation observed in Fig. 23.5b is due to the viscous fingering effect and variations in grain arrangement.

23.5 Conclusions

In the present study, the most important aspects related to modeling of Saltwater intrusion dynamics has discussed. The dynamics of saltwater intrusions were studied using a set of laboratory experiments. The experimental framework can be effectively utilized to understand the two-dimensional flow in unconfined aquifers. The results obtained from the simplified conditions are very useful for the qualitative assessment of saltwater intrusion.

The experimental setup represented during this study provides a novel approach for simulating the sloping sea face boundary condition in a laboratory. The results demonstrate that image processing is a useful method for interface tracking. The image processing was based on pixel level RGB value analysis. It is evident that the difference is higher for both numerical simulations compared to experimental

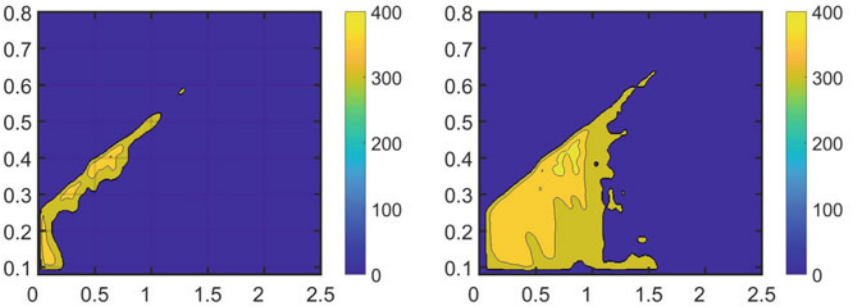

(a) 10 min

(b) 240 min

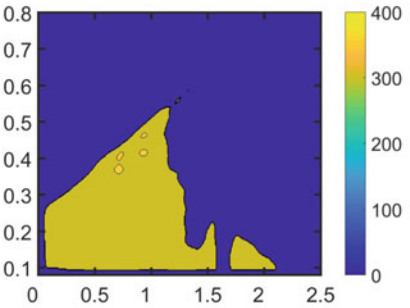

(c) 400 min

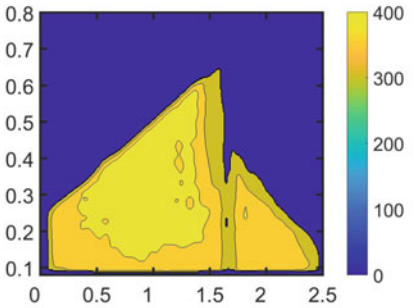

(d) 520min

Fig. 23.4 Observed Salt-wedge profiles in terms of concentration equivalent pixel value contours at various time periods

data. Differences are due to variations in permeability, dispersivity and density concentration.

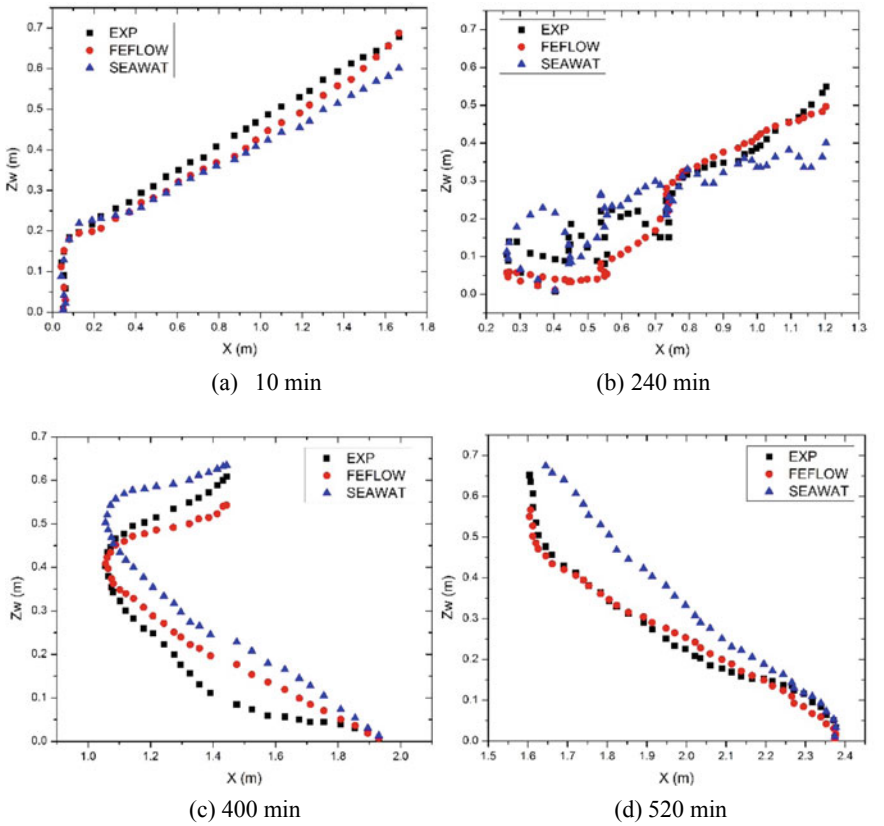

Fig. 23.5 Comparison of experimental data with both models predicted saltwater interface at different time periods

References

Abdoulhalik A, Ahmed AA (2018) Transience of seawater intrusion and retreat in response to incremental water-level variations. Hydrol Process 32(17):2721–2733

Diersch HJG (2005) FEFLOW finite element subsurface flow and transport simulation system. Inst. for Water Resources Planning and System Res, Berlin

Fang HY (1997) Introduction to environmental geotechnology. CRC Press LLC, New York

Freeze RA, Cherry JA (1979) Groundwater. Prentice Hall, New York

Goswami RR, Clement TP (2007) Laboratory-scale investigation of saltwater intrusion dynamics. Water Resour Res 43(4)

Han Q, Chen D, Guo Y, Hu W (2018) Saltwater-freshwater mixing fluctuation in shallow beach aquifers. Estuar Coast Shelf Sci 207:93–103

Langevin CD, Thorne Jr DT, Dausman AM, Sukop MC, Guo W (2008) SEAWAT version 4: a computer program for simulation of multi-species solute and heat transport (No. 6-A22). Geological Survey (US)

Lu C, Chen Y, Zhang C, Luo J (2013) Steady-state freshwater–seawater mixing zone in stratified coastal aquifers. J Hydrol 505:24–34

MATLAB. Version 7.10.0 (R2017a) The MathWorks Inc., Natick, Massachusetts

Robinson G, Hamill GA, Ahmed AA (2015) Automated image analysis for experimental investigations of salt water intrusion in coastal aquifers. J Hydrol 530:350–360

Sulis M, Meyerhoff SB, Paniconi C, Maxwell RM, Putti M, Kollet SJ (2010) A comparison of two physics-based numerical models for simulating surface water–groundwater interactions. Adv Water Resour 33(4):456–467

Todd DK, Mays LW (2005) Groundwater hydrology. Wiley, New York, Hoboken, p 656

Werner AD, Bakker M, Post VE, Vandenbohede A, Lu C, Ataie-Ashtiani B, Barry DA (2013) Seawater intrusion processes, investigation and management: recent advances and future challenges. Adv Water Res 51:3–26

Chapter 24
GIS Based Groundwater Potential Zone Identification Using AHP for Ponnaniyaru Watershed, Tamil Nadu, India

Devanantham Abijith, Subbarayan Saravanan, Jesudasan Jacinth Jennifer, Leelambar Singh, Thiyagarajan Saranya, Ramanarayan Sankriti, Ayyakkannu Selvaraj, and K. S. S. Parthasarathy

Abstract Groundwater is a vital source of water among the other sources due to its quality. An increase in urbanization and population creates tremendous pressure on its quality and quantity. The judicial utilization of Groundwater resources is essential. Though the world is covered by 70% of water, only 2.5% is potable water, so it is necessary to safeguard them for potential use without the water demand. In this study, the Ponnaniyaru river watershed, the sub-basin of the Cauvery River, has an area of 817 sq. km and is located at 12° 47′ 6″ N, 80° 17′ 1″ E, and 13° 15′ 22″ N, 79° 55′ E, as shown in Fig. 24.1. It origins from Kaduvur hills and joins with the Cauvery in West Trichy. The basin is comprised of hard rock terrain, which in turn results in low infiltration and a dry river basin. Water demand is high as the region is semi-arid, and the average temperature is 28 °C. The red loamy soil is predominant in the basin, which has excellent water holding capacity. In recent periods agricultural activities and urbanization have increased drastically in this watershed. GIS and remote sensing are important techniques that could be adopted to analyse the potential groundwater zones and predict possible artificial recharge locations. The artificial recharge system enhances the groundwater potential in the region, but the necessary study has to be carried out to spot the promising areas to set up recharge wells. The geology and geomorphology of the region with a detailed description of the aquifers beneath has to be well understood. The study adopts Saaty's Analytical Hierarchy Process (AHP),

D. Abijith · S. Saravanan · J. J. Jennifer · L. Singh (✉) · T. Saranya · R. Sankriti · A. Selvaraj
Department of Civil Engineering, National Institute of Technology, Tiruchirappalli, Tamil Nadu, India
e-mail: leeli.singh@gmail.com

D. Abijith
e-mail: abijith9007@gmail.com

S. Saravanan
e-mail: ssaravanan@nitt.edu

K. S. S. Parthasarathy
Department of Water Resources and Ocean Engineering, National Institute of Technology, Mangalore, Karnataka, India

R. Jha et al. (eds.), *Groundwater and Water Quality*, Water Science and Technology Library 119, https://doi.org/10.1007/978-3-031-09551-1_24

a multi-criteria decision-making approach to determine the weights of the factors. The crucial parameters considered in the study include geomorphology, geology, soil, slope, lineament density, drainage density, land use/land cover, and rainfall. The thematic maps of the parameters are prepared using the ArcGIS tool and are assigned with weights using the AHP technique to determine the potential groundwater zone. After overlaying the factors, the resultant map portrays the potential groundwater zones, which are classified into very poor, poor, moderate, good, and very good zones, and the result is validated with well yield data. With the obtained result, suitable sites for artificial recharge for sustainable groundwater management were identified.

Keywords Analytical hierarchy process · Artificial recharge · GIS · Groundwater potential zone · Ponnaniyaru river watershed

24.1 Introduction

Nature is facing climate change problems at the micro-level which is evident while experiencing water scarcity, which is a major threat. Freshwater is the only source for drinking, irrigation, and industrialization, which has a steady increase in demand and a decrease in groundwater level. Overall, India experiences good rainfall of 1100 mm due to the uneven distribution of rainfall and sometimes no rain in the regular rainy season cause water scarcity (Garg and Hassan 2007). Water Security is expected to be the biggest challenge in the twenty-first century (Jha et al. 2014). Groundwater utilization reduces the demand, and contamination of water is also very much (Arkoprovo et al. 2012). Groundwater contributes 62% in irrigation, 85% in the rural water supply, and 45% in the urban water supply (MoWR, RD and GR) (2013). For sustainable development, it is necessary to identify the potential zone for groundwater recharge. Using Geospatial technology, the groundwater prospects can be identified by studying, slope, soil, lithology, drainage, geomorphology, and annual average rainfall which reduces the time and cost (Jha et al. 2014). Furthermore, GIS is used for processing the remote sensing data more efficiently and in integration. Multi-criteria decision technique is a widely used technique for groundwater management and the Analytic hierarchy process (AHP) is one of them which is proposed by Saaty; the prepared layers are derived by the pair wise comparison of thematic layer for decision making using the AHP technique (Shekhar and Pandey 2015: Siva et al. 2017). Expert's opinion or own weights can be assigned to the features based on the priority. Researchers Satyanarayan Shashtri et al. (2010), Mayilvaganan and Naidu (2011), Nag and Anindita (2011), Bhupal and Reddy (2013), Manjare et al. (2014), Hachem et al. (2015), Bera and Ahmad (2016), Sharma et al. (2016), Reddy et al. (2018) and Bhunia et al. (2012) delineated groundwater potential zone using RS and GIS techniques.

24.2 Study Area and Materials Used

Ponnaniyaru watershed of Tiruchirappalli district, Tamil Nadu, is selected for the present study which is 819.2 sq. km in area. Tiruchirappalli is the fourth major city in Tamil Nadu with a dense population. They are geographically located at 10° 34′ 48.17″ N, 78° 15′ 23.37″ E. The average temperature is 28.8 °C, and the average rainfall is 816 mm. Ponnaiayar watershed commences from Kaduvur hills and flows until KeelaChenthamani of 60 km and confluence in the Cauvery river. More than 110 villages use the watershed as a source for agriculture purposes. Using ArcSWAT, an ArcGIS extension, the boundary of the watershed and stream has been delineated. Landuse and land cover, geomorphology, and Lineament map were prepared using Landsat-8 OLI (Path 143 Row 53). The soil map was obtained from the National Bureau of Soil Survey and Land Utilisation Planning (NBSS and LUP) and the Geology map from the Geological Survey of India (GSI). Using the Saaty scale based on the priority, the weights were assigned to each factor. Then the layers are integrated using GIS to find the potential zone for groundwater and classified as very high, high, moderate, low, and very low zones.

24.3 Methodology

The Maps from different sources were digitized, and remote sensing data is processed using Arc GIS. Eight thematic layers, Geomorphology, lineament density, Landuse and Landcover, Geology, slope, soil drainage density, and rainfall, are the influencing factors which were chosen for assessing the groundwater potential Fig. 24.1. All the maps were in Universal Transverse Mercator (UTM) coordinate system and WGS84 spatial reference (WGS84-UTMZone44N). From the published Survey of India (SOI) toposheet (58 J, 1:250,000) the watershed was delineated, and the drainage pattern was digitized using ArcGIS 10.4 software. The geology map was prepared by digitizing the district resource map of the Geological Survey of India (GSI) and the geomorphology map has been prepared from the visual and digital interpretation of satellite imagery Landsat-8 OLI (Path 143 Row 53) and cross-verified with published district resources map. The soil data were obtained and digitized from the National Bureau of Soil Survey and Land Use Planning (NBSS and LUP). Landsat-8OLI (Path 143 Row 53) satellite data were used to generate Land-use and Land-cover maps. Using Shuttle Radar Topography Mission (SRTM) Version 3.0 Global 1 arc sec data slope map was prepared. False colour composite in spatial analysis tool in ArcGIS 10.4 was used to extract the lineaments, and their density has been calculated. Layers extracted through the digitization process were transformed into raster data using the feature to raster tool in ArcGIS. Rainfall data were obtained from the Indian Meteorological Department (IMD) and spatial distribution was generated by using Inverse

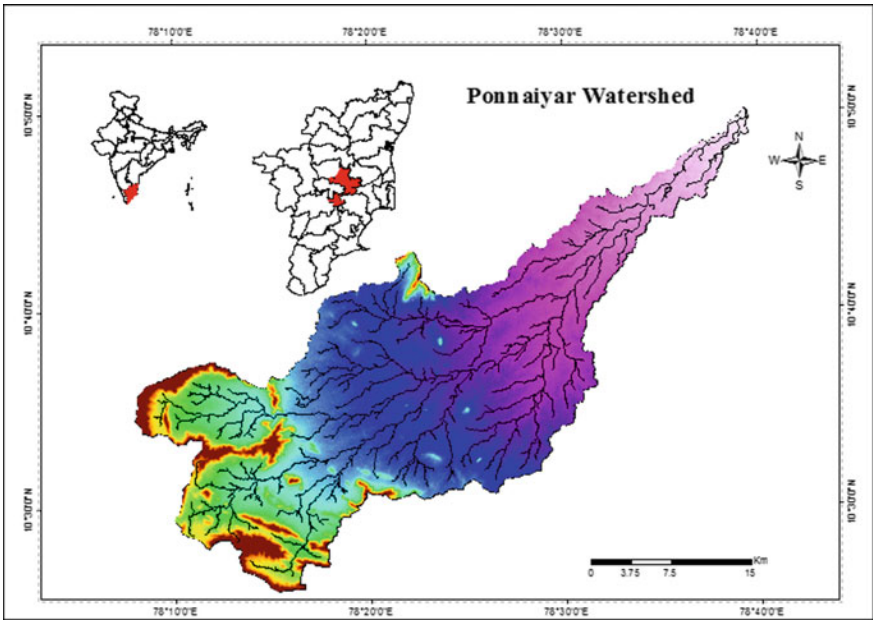

Fig. 24.1. Study area map

Distance Weightage (IDW) tool in ArcGIS 10.4. All the layers, including the delineated watershed, were resampled using the nearest neighbourhood technique and converted into 30 m * 30 m cell size (Abijith et al. 2020) (Fig. 24.2).

24.3.1 Geomorphology

Figure 24.3a shows the mapping of various landforms using image interpretation techniques, which helps identify groundwater prospects. The present study area has Structural hills in the northern part, where it has more runoff and poor groundwater potential. Denudational hills have a gradient slope with medium vegetation cover and infiltration as it has some fissures. Widely in the present study area is covered by Pediplains which has gentle steepness with rich plantation and rich potential. Bazada zones are deposition along the stream channel, which is very rich in potential.

24.3.2 Lineament

The fractured zones are called lineaments formed due to deformations with porosity and permeability potential for groundwater. Lineament map Fig. 24.3b is prepared

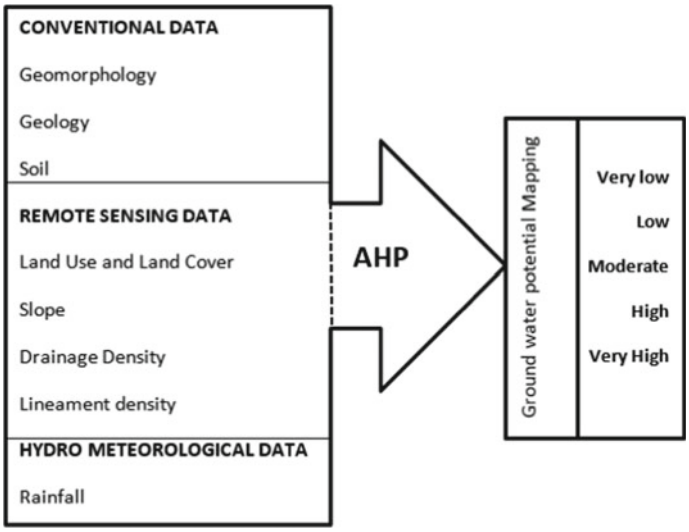

Fig. 24.2 Methodology flow chart

from satellite data visual interpretation and density is calculated. The density scale of high to low directly implies the groundwater potential.

24.3.3 Landuse and Landcover

Using supervised classification Barren Rocky, cropland, forest, Gullied land, land with scrub, land without scrub, plantation, river, and settlements are interpreted using Satellite data Landsat-8. Barren rocky and settlement areas are poor in groundwater potential whereas cropland, and plantations are very good in groundwater potential Fig. 24.3c.

24.3.4 Geology

Gneiss, Granite, Syenite, Conglomerate, Sandstone, and Shale, Shales with bands of limestone and Quartz Vein are the lithological forms found in the study area Fig. 24.3d, which control the infiltration of groundwater; therefore, ranks were assigned. Conglomerate, Sandstone, and shales are good aquifer and aquitard as it is highly weathered and fractured.

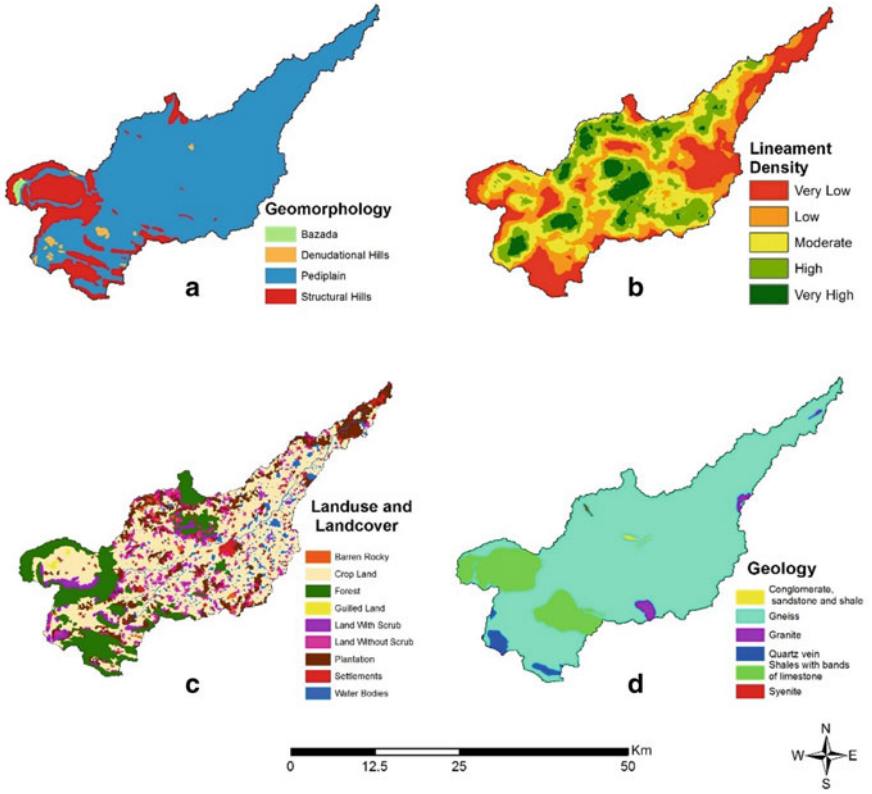

Fig. 24.3 **a** Geomorphology **b** Lineament density **c** Landuse and landcover **d** Geology

24.3.5 Slope

The slope Fig. 24.4a controls the runoff, which in turn controls the infiltration. Groundwater potentiality is expected to be more significant in flat and gently sloping areas (Subba Rao 2006). The slope ranges from 0° to 60°. Only the hilly region shows a high slope and the overall area has a gentle slope, and the prospects for groundwater are more.

24.3.6 Soil

Soil Fig. 24.4b characteristics are significant prospects in delineating groundwater potential as it controls the water holding capacity. Soil classified according to the drainage classes implies the duration of wetness and imperfectly drained, moderately

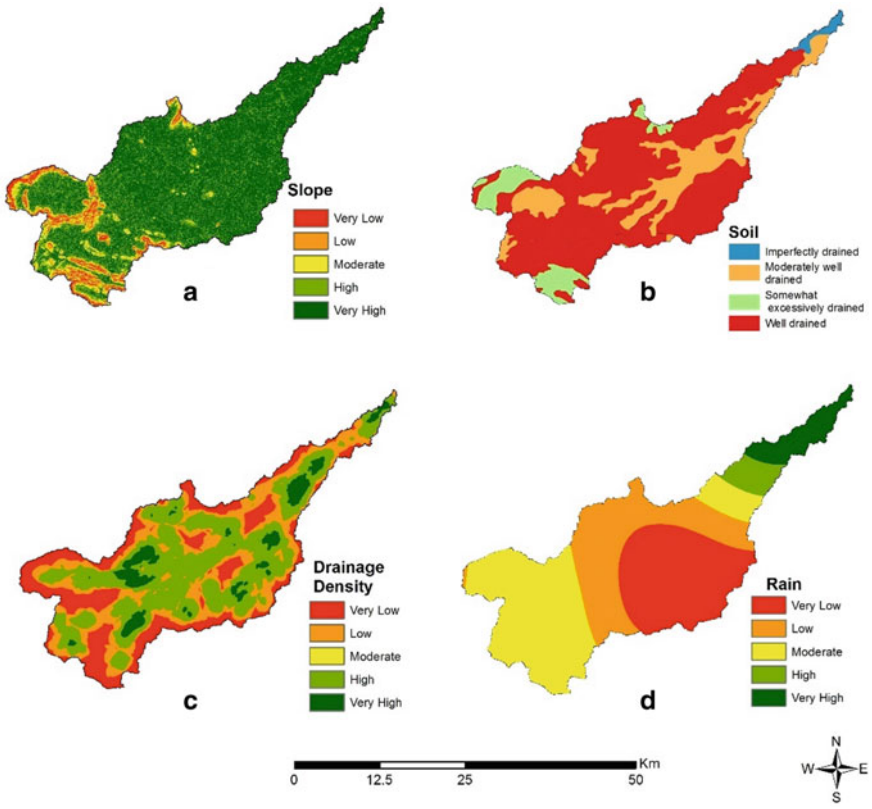

Fig. 24.4 **a** Slope **b** Soil **c** Drainage density **d** Rain

well-drained, well-drained, and somewhat excessively drained found in the study area. Mostly the area is covered by well-drained soil, and those are cropland regions.

24.3.7 Drainage Density

Drainage Fig. 24.4c network helps in the evaluation of recharge levels. The high-density regions have high percolation levels, which means low runoff. The number of streams is more in low elevated areas, and drainage density can directly indicate the groundwater potential.

24.3.8 Rainfall

Rainfall Fig. 24.4d is the only groundwater recharge source (Adiat et al. 2012). The annual rainfall of the study area is 956 mm. Overall, the maximum area is moderate, whereas there is maximum rainfall towards the northeast regions.

24.4 Analytic Hierarchy Process (AHP)

The multi-criteria evolution technique is used in this study to analyze the Groundwater potential mapping. Based on the hierarchy, the decision-makers evaluate the factors with co-factors based on the influence level through pairwise comparison. Using Saaty's scale, weights are assigned based on influencing factors and expert opinion. The consistency index is calculated using Eq. (24.1), and the Consistency ratio is checked, which should be less than 0.1, which is considered consistent in pairwise comparison.

$$CI = \frac{\lambda \max - n}{n} \tag{24.1}$$

$$CR = \frac{CI}{CR} \tag{24.2}$$

CI is consistency index, *CR* is consistency ratio, and *RI* is the random index, *n* is the number of conditioning factors, and λmax is the matrix's principle eigenvalue. RI value is directly taken from the (Saaty 1980) research paper, which depends upon the number of components.

24.5 Results and Discussion

In this study, AHP is used, and thematic layers were assigned weights to identify potential groundwater zone. Table 24.1 denotes each parameter weight in AHP, and those weights are multiplied by each sub-feature inside the parameter. The groundwater potential is evaluated by integrating all layers in ArcGIS. The results were classified into five classes: very good, good, moderate, low, and very low groundwater potential. Expect gneiss in geology: The most prominent groundwater prospects identified are pediplain in geomorphology, cropland in Landuse and Landcover, and well-drained soil found across the study area. High groundwater potential is seen in the central watershed region, where the slope of 2–8% is gentle, and proportionally, it has a high drainage density. The northwest of the watershed comprises structural hills, and there, the Lineament density is low, and those areas are under the category low and very low. As rain is the only source of this watershed, rainfall is a critical

Table 24.1 AHP pairwise comparison matrix

	GM	LD	LULC	G	SL	S	DD	R	AHP weight
Geomorphology (GM)	1	2	2	4	3	3	2	3	0.24
Lineament density (LD)	0.5	1	2	2	3	2	3	4	0.19
Land use and land cover (LULC)	0.5	0.5	1	3	4	4	3	3	0.18
Geology (G)	0.25	0.5	0.3	1	2	3	2	3	0.14
Slope (SL)	0.33	0.33	0.25	0.5	1	3	4	2	0.1
Soil (S)	0.33	0.5	0.25	0.33	0.33	1	2	2	0.07
Drainage density (DD)	0.5	0.33	0.33	0.5	0.25	0.5	1	3	0.07
Rainfall (R)	0.33	0.25	0.33	0.33	0.5	0.5	0.33	1	0.04

role; low rainfall is identified across the watershed; therefore, south-east regions are at a moderate level for groundwater potential. Thus finding the groundwater potential helps in accurate zones for exploration for agricultural, industrialization, and urban uses.

24.6 Conclusion

This study aims to examine the capability of AHP, GIS, and RS techniques for groundwater potential mapping. This study's morphological character features are geomorphology, lineament density, land use, land cover, geology, slope, soil, drainage density, and rainfall. The hard-rock terrain in the northern part of the study area led to the generally low groundwater potential due to the subsurface hydrogeological conditions. Assessing the groundwater potential will help the decision-makers in groundwater management and identify suitable locations for drilling production wells. The results indicate 9.9% very low, 12.9% Low, 27.3% moderate, 29.5% high, and 20.10% very high. This research would encourage the effective production and protection of groundwater supplies in the field of research. This groundwater potential map can be utilized for groundwater resources management in the Ponnaniyaru watershed and can help policymakers to formulate better planning. The potential groundwater assessment would support decision-makers in groundwater management and select appropriate drilling wells based on demand. Furthermore, augmentation of available water resources can be done to maintain the sustainability of aquifer management.

References

Abijith D, Saravanan S, Singh L, Jennifer JJ, Saranya T, Parthasarathy KSS (2020) GIS-based multi-criteria analysis for identification of potential groundwater recharge zones-a case study from Ponnaniyaru watershed, Tamil Nadu, India. HydroResearch 3:1–14

Al-Abadi A, Al-Shamma A (2014) Groundwater potential mapping of the major aquifer in Northeastern Missan Governorate, South of Iraq by using analytical hierarchy process and GIS. J Environ Earth Sci 4(10):125–150. Retrieved from https://d1wqtxts1xzle7.cloudfront.net/34228764/Factors_Affecting_Some_Hematology_and_Serum_Biochemicalwith-cover-page-v2.pdf?Expires=1658992887&Signature=HOJRBfeu~~gs7hAaMiF6exGObVK8QEUD72NHVHVzNv8avI5aK0b6saaUF~brkl-AsYAV9yIHbvkQOYbMiwrGfZGf5u02TGn5daQO8R0FsNLAmWdlgRsQVfRiXd4UndGP0qyb90NmSjhzyItdKmrFXinxgvLzRlTsDJuidCnAUn868Sbo7KZ-tIFPMqh-w28z7ZyqmcR6Ti8-hUPhGccuxPM9PuHmrqiv9aWhBuA5hUs9NIRbnJeH1tM0gaDgbfftX3-NJzOrlvMWg~Ztvvw62ygotuUh9TPFIN0sBarveAOu5bJT2Lu7lgAJdFVSdYG4IN-H14UVwf-LqDm0oSew__&Key-Pair-Id=APKAJLOHF5GGSLRBV4ZA

Arkoprovo B, Adarsa J, Prakash SS (2012) Delineation of groundwater potential zones using satellite remote sensing and geographic information system techniques: a case study from Ganjam district, Orissa, India. Res J Recent Sci 1(9):59–66

Bera S, Ahmad M (2016) Delineation of ground water potential zones in Dhanbad district, Jharkhand, using remote sensing and GIS techniques. Int Res J Eng Technol 3(7):1607–1615

Bhunia GS, Samanta S, Pal DK, Pal B (2012) Assessment of groundwater potential zone in Paschim Medinipur District, West Bengal—a meso-scale study using GIS and remote sensing approach. 2(5):41–59

Bhupal K, Reddi BRM (2013) Analysis of ground water potential in Chandragiri mandal, Chittoor district, Andhra Pradesh. Adv Appl Sci Res 4(4):255–265

Brindha K, Elango L (2011) Hydrochemical characteristics of groundwater for domestic and irrigation purposes in Madhuranthakam, Tamil Nadu, India. Earth Sci Res J 15(2):101–108. https://doi.org/10.4236/ajcc.2012.14019

Description L (n.d.) Soil drainage class (April 2010), 1–4. https://doi.org/10.1016/B978-0-444-41828-9.50011-9

Hachem AM, Ali E, Abdelhadi EO, Abdellah EH, Said K (2015) Using remote sensing and GIS-multicriteria decision analysis for groundwater potential mapping in the middle atlas plateaus. Morocco 4(7):33–41

Jha MK, Chowdary VM, Kulkarni Y, Mal BC (2014) Rainwater harvesting planning using geospatial techniques and multi-criteria decision analysis. Resour Conserv Recycl 83:96–111. https://doi.org/10.1016/j.resconrec.2013.12.003

Kumar GNP, Srinivas P, Chandra KJ, Sujatha P (2010) Delineation of groundwater potential zones using remote sensing and GIS techniques: a case study of KurmapalliVagu Basin in Andhra Pradesh, India. Environ Eng 2(May):70–78

Machiwal D, Jha MK, Mal BC (2011) Assessment of groundwater potential in a semi-arid region of India using remote sensing, GIS and MCDM techniques. Water Resour Manage 25(5):1359–1386. https://doi.org/10.1007/s11269-010-9749-y

Manjare BS (2014) Identification of groundwater prospecting zones using Remote Sensing and GIS techniques in upper Vena river watersheds Nagpur district, Maharashtra, India. Abstract, pp 1–14

Mayilvaganan MK, Naidu KB (2011) Application of artificial neural network for the prediction of groundwater level in hard rock region, vol 204. Springer, Berlin, Heidelberg, pp 673–682

Nag SK, Anindita L (2011) Integrated approach using remote sensing and GIS techniques for delineating groundwater potential zones in Dwarakeswarwatershed, Bankura district, West Bengal. Int J Geomat Geosci 2(2):430–442

Reddy YVK, Student U, Sciences T (2018) Identification of groundwater potential zones using GIS and remote sensing. 119(17):3195–3210

Siva G, Nasir N, Selvakumar R (2017) Delineation of groundwater potential zone in Sengipatti for Thanjavur district using analytical hierarchy process. In: IOP conference series: Earth and environmental science. IOP Publishing Vol 80, No. 1, p 012063

Sharma RS (2016) Identification of groundwater recharge potential zones in Thiruverumbur block, Trichy district using GIS and remote sensing. SSRG Int J Geo Inform Geol Sci 3(2):8–14. Retrieved from www.internationaljournalssrg.org

Shekhar S, Pandey AC (2015) Delineation of groundwater potential zone in hard rock terrain of India using remote sensing, geographical information system (GIS) and analytic hierarchy process (AHP) techniques. Geocarto Int 30(4):402–421. https://doi.org/10.1080/10106049.2014.894584

Singh P, Thakur JK, Kumar S (2013) Délimitation des zonesde prospection d'eauxsouterrainesen zone de socleàl'aided'outils. Hydrol Sci J 58(1):213–223. https://doi.org/10.1080/02626667.2012.745644

Chapter 25
Development of Groundwater Recharge Relationship with Rainfall for Thane District

Kushal Singh and V. D. Loliyana

Abstract In coastal areas, salinity intrusion and dry wells, water level declination, etc., are some of the substantial unplanned groundwater development. For a developing country like India, an accurate estimation technique is needed for better planning, management, and development of the groundwater. In the present study, groundwater recharge is estimated using the groundwater budget model for Thane District, India. Rainfall data, well, draft, crops, groundwater levels data and other corresponding data for the period of 1997–2016, were used for deriving the relationship between rainfall and groundwater recharge. The developed relationship is verified using different statistical indices and found reasonably good results. The AARE (average absolute relative error) is found to be reduced by 14.51% using a developed relationship compared to recharge calculated by the rainfall infiltration factor method. The developed relationship evaluates the rationally fit quantity of available groundwater recharge in the Thane district.

25.1 Introduction

Dry wells, Salinity intrusion in coastal areas, water level declination, etc., are some of the out-turns of un-planned groundwater development. For a developing country like India, an accurate estimation technique is needed for better planning, management, and development of the groundwater. India is accountable for 25% of total groundwater extracted around the globe annually. A better practice of groundwater management can result-in better irrigation techniques and proper urban planning and development. There are various methods to estimate groundwater recharge such as Rainfall Infiltration Factor (RIF), Water Table Fluctuation, One-dimensional soil water flow model, Remote Sensing (RS) and Geographic Information Systems (GIS), Water budget method, Zero flux plane method, Chloride mass balance methods, Inverse modelling techniques, Soil moisture method, Isotope and Solute Techniques.

K. Singh · V. D. Loliyana (✉)
Department of Civil and Construction Engineering, University of Wolverhampton, Rustomjee Academy for Global Careers, Dahanu Road (East), Dahanu, Maharashtra 401602, India
e-mail: viraj.nishi@gmail.com; virajloliyana88@gmail.com

R. Jha et al. (eds.), *Groundwater and Water Quality*, Water Science and Technology Library 119, https://doi.org/10.1007/978-3-031-09551-1_25

Ground-water Resource Estimation Committee (GEC-15, India) endorses to use rainfall infiltration method to estimate the recharge of groundwater. Recent studies show that there is no empirical relationship between to use rainfall infiltration method for computation and generation of recharge and the empirical formula for the coastal areas. It was also found by the study that the rainfall infiltration method overestimates the recharge. In this study, an empirical equation is established for the development of the recharge. As the ground-water budget model is useful for the estimation of groundwater recharge to provide a solution for rising groundwater levels and as all the data other than recharge are available. Natural recharge usually depends on rainfall, type of soil, slope, vegetation characteristics, etc. There is a great influence of draft and recharge on groundwater resources. The natural recharge obtained from the developed formula can be useful to assess the stage of groundwater development. Knowledge of accurate values of groundwater resources can ultimately help to achieve better management and irrigation practices in un-planned groundwater zones. Therefore, the established formula would be used to estimate the groundwater recharge in the Thane district of Maharashtra, western India. The present study may be useful to the local authorities for planning and management of groundwater resources within the study region. Similar methodology can be applied for estimating groundwater recharge intended for another region also.

Keeping in view of the aforesaid need, the following objectives are undertaken for the present study for Thane district, Maharashtra, India:

(i) To Collect required hydrological, meteorological, geological, soil and groundwater data of the study area.
(ii) To estimate the groundwater recharge by using water balance studies and rainfall infiltration method for coastal rural Thane district, Maharashtra, India.
(iii) To develop of groundwater recharge equation for the study area.
(iv) To learn the required software. (ANOVA test, *t*-test, linear regression in Excel, and GIS).

25.2 Study Area

The Thane district of Maharashtra is situated in the western part of India which falls within the boundaries of 18° 25″ N and 20° 12″ N latitudes and 72° 27″ E and 73° 29″ E longitude. The geographical area of the district is about 9337 km^2, see Fig. 25.1. Vaitarna and Ulhas are the main rivers flowing through the district. Vaitarna river rises in the Tryambak Hills of Nashik district and enters the Arabian Sea. Vaitarna has many tributaries viz., barvi, pinjal, surya, daherja, Tansa and bhatsa. (Pagdhare 2015). Ulhas is also the main river which originates from Rajmachi Hills of Raigad district and then enters the Arabian Sea. The important tributaries of the Ulhas River are Salpe, Pej, Kalu, Bhivapuri, Barvi, Poshir, Murbari, Shari, Shilarr and Bhatsa. Thane district is divided into 15 Talukas viz., Ambarnath, Bhivandi, Dahanu, Jawahar, Kalyan, Mokhada, Murbad, Palghar, Shahapur, Talasari, Thane, Ulhasnagar, Vasai, Vikramgad, and Wada. The climate of the Thane district is wet

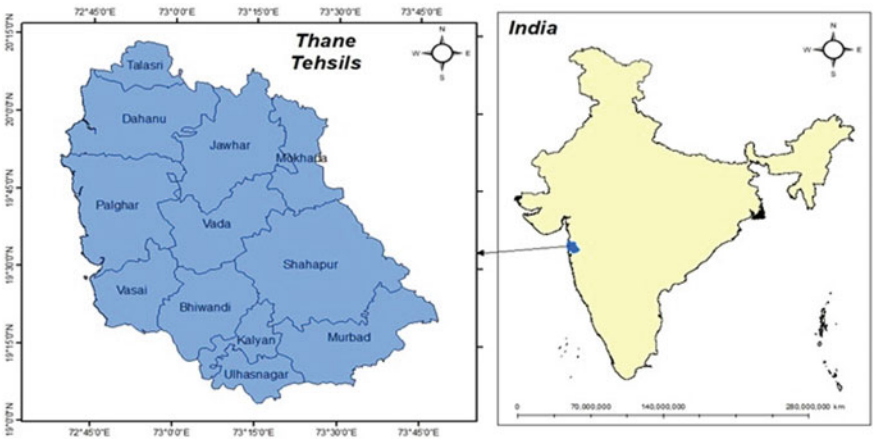

Fig. 25.1 Study area

in the south-west monsoon season. The mean annual rainfall of the Thane district is about 2504 mm, whereas the average annual temperature is 26.9 °C.

The groundwater budget method is adopted for the computation of groundwater recharge, where rainfall data, ground-water level, cropping pattern, sown area, canal and the population data of the past 20 years are collected and derived to develop an empirical formula for the study area.

25.3 Methodology

The developed equation is tested on four statistical parameters viz., Coefficient of determination (R^2), Root-mean squared error (RMSE), Average absolute relative error (AARE), and Nash coefficient of efficiency (CE), where the results are found to be acceptable. Adopted methodology is depicted in Fig. 25.2.

25.4 Results and Discussion

By comparing the recharge obtained by the developed equation, groundwater budget study and rainfall infiltration method. It was found that the values calculated from the groundwater budget and developed formula are close and different from the recharge calculated from the rainfall infiltration factor. Where the average absolute error between the groundwater budget and the developed formula is reduced by 14.51%. The developed equation is a good replacement to the rainfall infiltration method and groundwater budget method, where the developed empirical equation

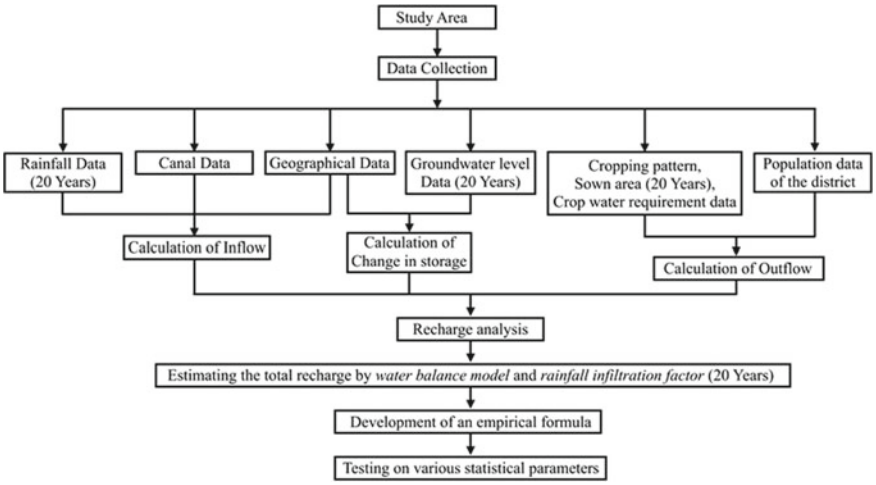

Fig. 25.2 Adopted methodology

triumphs over the limitations of both methods and estimates the precise amount of recharge. The proposed formula is capable to quantify the natural recharge for the coastal areas accurately.

It was found by the study that the average value of specific yield for the study area is about 1%. Specific yield is beneficial to find the capacity of the aquifer storage. Table 25.1 shows the final recharge obtained by ground-water budget studies by deducting the discharge from natural discharges i.e. via base flow and evapotranspiration. In this study, an empirical equation is developed for the study area by using the linear regression method. Table 25.1 shows the average absolute error between the recharge calculated by the rainfall infiltration method and by the developed equation. Similarity was seen between the increase and decrease of the relationship between recharge and rainfall, where the recharge increases as the rainfall increases. The result from these four tests concluded that the established formula is capable to give satisfactory results within tolerable limits. By using R^2 the value was found to be 0.9781 (see Fig. 25.3). Coefficient of determination is helpful to provide a proportion of variance of one variable which is foreseeable from the other variable. The variable indicates the dominance of the linear relationship between the two variables. RMSE is used to calculate the difference between the predicted and sample values. The result from RMSE indicates that the average absolute relative error between the recharge obtained from rainfall infiltration and the developed equation is 14.51%.

The recharge calculated from groundwater budget model and from the developed equation is close to each other. Comparison of the recharge by various methods is shown in Fig. 25.4. The main objective of this research was to find an alternative method to estimate the recharge and to develop an empirical formula is completed. The other available empirical equations overestimate the recharge as they are more capable for different hydrogeological conditions.

Table 25.1 Recharge from rainfall

Sr. No.	Year	Σ Δhw * Area m km^2	Sy	Σ Δhw * Area * Sy (ΔS)	Draft for wet season in MCM	Return flow from irrigation field in wet season in MCM	Recharge by other sources in MCM	Provision for natural discharges	Recharge from rainfall MCM
1	1997	25,571.39	0.028217	721.54	459.47	101.40	75.09	50.23	1004.53
2	1998	17,820.93	0.047414	844.96	470.29	103.54	75.09	56.83	1136.63
3	1999	13,633.18	0.046723	636.99	470.36	102.99	75.09	46.46	929.28
4	2000	18,405.98	0.036797	677.29	468.03	101.84	75.09	48.42	968.40
5	2001	18,388.53	0.042088	773.93	467.09	101.04	75.09	53.25	1064.90
6	2002	16,338.56	0.049013	800.79	467.44	100.56	75.09	54.63	1092.59
7	2003	20,741.80	0.046524	964.99	468.04	100.14	75.09	62.89	1257.81
8	2004	25,128.31	0.039320	988.04	468.75	99.75	75.09	64.10	1281.96
9	2005	28,325.99	0.041813	1184.39	466.89	98.72	75.09	73.87	1477.47
10	2006	32,417.00	0.037694	1221.92	470.58	99.08	75.09	75.92	1518.33
11	2007	25,858.73	0.036343	939.79	474.68	99.54	75.09	61.99	1239.85
12	2008	55,705.66	0.018181	1012.77	474.18	98.84	75.09	65.65	1313.02
13	2009	20,409.63	0.032575	664.84	451.80	92.68	75.09	47.44	948.88
14	2010	21,035.35	0.042394	891.78	462.30	94.74	75.09	59.21	1184.25
15	2011	20,873.58	0.041656	869.51	466.18	95.14	75.09	58.27	1165.46
16	2012	29,105.88	0.024288	706.91	453.13	91.31	75.09	49.68	993.64
17	2013	16,836.67	0.061362	1033.14	472.95	95.70	75.09	66.76	1335.30
18	2014	27,262.80	0.030106	820.78	453.29	90.22	75.09	55.44	1108.77
19	2015	11,347.65	0.054070	613.57	473.70	94.76	75.09	45.87	917.43
20	2016	19,955.19	0.049583	989.43	466.12	92.30	75.09	64.41	1288.17

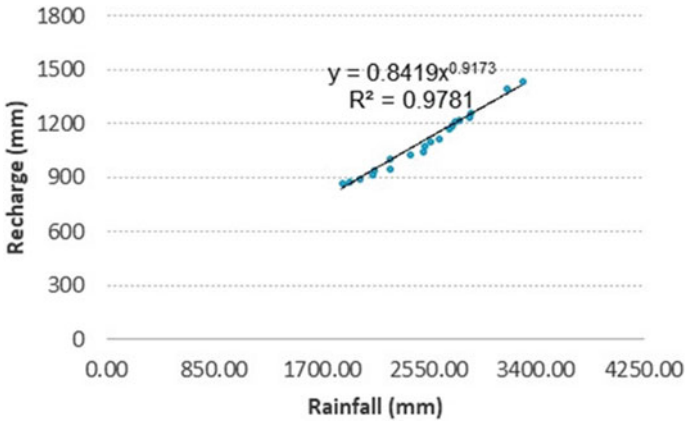

Fig. 25.3 Proposed relationship between rainfall and runoff

$$R = 0.8410\ P^{0.9173} \tag{25.1}$$

where R = Recharge; and P = Rainfall.

It was found by the study that the average value of specific yield for the study area is about 1%. Specific yield is beneficial to find the capacity of the aquifer storage. In this study, Table 25.1 shows the calculation of specific yield. Table 25.2 shows the recharge from rainfall during the year 1996–2016 by using groundwater balance studies. The final recharge is obtained by groundwater budget studies deducting the discharge from natural discharges i.e. base flow and evapotranspiration. In this study, an empirical equation is developed for the study area by using the linear regression method. Table 25.3 shows the average absolute error between the recharge calculated by the rainfall infiltration method and by the developed equation. Similarity was

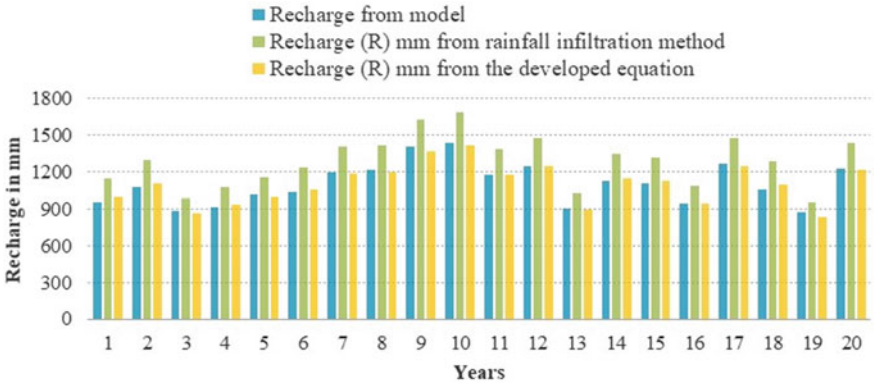

Fig. 25.4 Comparison of recharge by various methods

seen between the increase and decrease of the relationship between recharge and rainfall. Where the recharge increases as the rainfall increases. The equation was tested on four statistical parameters viz., Coefficient of determination (R^2), Root-mean squared error (RMSE), Average absolute relative error (AARE), and Nash coefficient of efficiency (CE). The result from these four tests concluded that the established formula is capable to give satisfactory results within tolerable limits. By using R^2 (Coefficient of determination) the value was found to be 0.9781. Coefficient of determination is helpful to provide a proportion of variance of one variable which is foreseeable from the other variable. The variable indicates the dominance of the linear relationship between the two variables. RMSE is used to calculate the difference between the predicted and sample values. The result from RMSE indicates that the average absolute relative error between the recharge obtained from rainfall infiltration and the developed equation is 14.51%. CE, (Nash coefficient of efficiency) is used to determine the relative magnitude of the residual variance as compared to the measured data variance.

Table 25.2 Average absolute error with RIF method

Sr. No.	Year	Recharge from proposed equation	Recharge from rainfall infiltration factor	Relative error in %
1	1997	991.73	1150.20	13.78
2	1998	1106.04	1295.45	14.62
3	1999	862.38	987.66	12.68
4	2000	935.82	1079.69	13.33
5	2001	994.15	1153.26	13.80
6	2002	1057.92	1234.14	14.28
7	2003	1190.83	1404.09	15.19
8	2004	1201.12	1417.32	15.25
9	2005	1365.68	1630.27	16.23
10	2006	1413.41	1692.47	16.49
11	2007	1181.13	1391.63	15.13
12	2008	1247.78	1477.44	15.54
13	2009	894.14	1027.38	12.97
14	2010	1149.36	1350.86	14.92
15	2011	1122.58	1316.59	14.74
16	2012	941.15	1086.40	13.37
17	2013	1251.29	1481.98	15.57
18	2014	1100.34	1288.18	14.58
19	2015	836.56	955.47	12.44
20	2016	1215.41	1435.71	15.34
			AARE (%)	14.51

Table 25.3 Statical parameters for proposed equation

Sr. No.	Statical parameter	Value
1	RMSE	0.23
2	R^2	0.9781
3	CE	0.98
4	AARE	0.20

Table 25.4 Results obtained from ANOVA test

Summary						
Groups	Count	Sum	Average	Variance		
Recharge (R) mm from model	20	22,065.33	1103.27	28,173.51		
Recharge (R) mm from the developed equation	20	22,058.83	1102.94	26,308.17		
ANOVA						
Source of variation	SS	df	MS	F	*P*-value	F crit
Between groups	1.06	1	1.06	0.00	1.00	4.10
Within groups	1,035,151.84	38	27,240.84			
Total	1,035,152.90	39				

ANOVA test and *t*-test are performed. The results from the ANOVA and *T*-test are listed in Tables 25.4 and 25.5 respectively. The results from both the test show that the means of both groups i.e. Recharge (R) mm from model and Recharge (R) mm from the developed equation are almost equal. Whereas, the variance of both groups is within the tolerable limits, which means that the null hypothesis will not be rejected.

Table 25.5 Results obtained from *t*-test

	Variable 1	Variable 2
Mean	1103.267	1102.941
Variance	28,173.508	26,308.167
Observations	20	20
Pearson correlation	0.9902	
Hypothesized mean difference	0.0000	
df	19.0000	
t Stat	0.0611	
P(T ≤ t) one-tail	0.4759	
t Critical one-tail	1.7291	
P(T ≤ t) two-tail	0.9519	
t Critical two-tail	2.0930	

25.5 Conclusions

(i) The study developed an empirical formula to estimate the natural recharge of the groundwater. The developed formula is tested on various statistical parameters, such as Coefficient of determination (R^2), Root-mean squared error (RMSE), Average absolute relative error (AARE), and Nash coefficient of efficiency (CE) and are found to be within the tolerable limits.

(ii) The proposed formula is capable to quantify the recharge accurately. The developed formula is suitable for coastal areas. By comparing the recharge obtained by the developed equation, groundwater budget study and rainfall infiltration method. It was found that the values calculated from groundwater budget and the developed formula are close and different from the recharge calculated from the rainfall infiltration factor.

(iii) Whereas, the developed empirical equation (Eq. 25.1) triumphs over the limitations of both methods and estimates the precise amount of recharge. The formula requires P value or rainfall data to estimate the total groundwater recharge. The natural recharge obtained from the developed formula can be useful to assess the stage of groundwater development, which can be helpful for planning the artificial recharge across the study area.

(iv) The present study may be useful to the local authorities for planning and management of groundwater resources within the study region. Similar methodology can be applied for estimating groundwater recharge intended for another region also.

Reference

Pagdhare MDL (2015) Sch Res J Interdiscip Stud 3/21. http://www.srjis.com/pages/pdfFiles/14671929205%20PROF.%20DARSHAN%20L.%20PAGDHARE.pdf. Accessed Nov–Dec, 2015

Chapter 26
Changes in Water Quality of River Ganga Passing Through Urban Cities with Remote Sensing and GIS Support

Kamakshi Singh and Ramakar Jha

Abstract In the present work, water quality samples of river Ganga at Kanpur, Prayagraj, Varanasi, Patna and Bhagalpur were collected and analyzed for the years 2017–2018 to assess the change in water quality of the river at inlet and outlets of different cities. The change in spectral reflectance of water along the river in the visible region has been analyzed using the Landsat-8 MSS data. The results obtained show that the total suspended sediment, turbidity, DO and BOD are varying significantly at different locations due to variation in flow in river Ganga, effluent disposal and sediment transport. The satellite based remote sensing approach can be effectively used to make qualitative and quantitative estimates of suspended sediment and turbidity. However, assessment of locations discharging effluent and increasing BOD is found possible using satellite data.

26.1 Introduction

Urbanization states a course in which a growing proportion of a complete population lives in cities and the suburbs of cities. Such a process of urbanization is obstinate for many decades due to population growth, reclassification of the rural localities into urban centres and migration of people from rural areas towards cities (UN 2009).

A case study of the influence of urbanization on the water resources of Guangzhou, China, showed that urban growth has affected the water resources both qualitatively and quantitatively (Baier et al. 2009; Strohschön et al. 2009, 2012; Wiethoff et al. 2011; Baier and Strohschön 2012).

Every year, the human population increases, but the amount of natural resources required to sustain this population, improve the quality of human lives and eliminate mass poverty remains fixed (United Nations World Commission on Environment and Development 1987). This builds stress on the authorities to use natural resources to deliver basic facilities such as water, sanitation, transportation, etc. to the residents. Such stress on water resources can be observed in many major cities in developing

K. Singh (✉) · R. Jha
National Institute of Technology Patna, Patna, India
e-mail: kamakshi.1991@gmail.com

R. Jha et al. (eds.), *Groundwater and Water Quality*, Water Science and Technology Library 119, https://doi.org/10.1007/978-3-031-09551-1_26

and newly industrialized Asian countries, which are dealing with problems of water scarcity (Uitto and Biswas 2000; Mohr et al. 2012; Rahman 2007).

Remote sensing and GIS techniques provide a powerful tool to measure inland water quality data (Klemas et al. 1971; Kritikos et al. 1974; Johnson 1975; Ritchie et al. 1976; Doxaran et al. 2002; Garg et al. 2017; Sebastiá-Frasquet et al. 2019; Ritchie et al. 1976; Garg et al. 2017; Quang et al. 2017). Satellite time series data offer great potential for a quantitative assessment of inland water in rivers and urban sprawl and for monitoring land use changes and soil consumption (Ritchie et al. 1976; Moore 1980; Doxaran et al. 2002; Pavelsky and Smith 2009; Gholizadeh et al. 2016; Garg et al. 2017; IOCCG 2000; Toming et al. 2016; Caballero et al. 2019; Sebastiá-Frasquet et al. 2019; Nolè et al. 2012; Youssef et al. 2010; Jha et al. 2008a, b).

In the present work, water quality data have been collected from cities and analyzed for total suspended solids, turbidity, BOD and DO. An attempt has been made to use a satellite based remote sensing approach effectively to make qualitative and quantitative estimates of water quality variables.

26.2 The Study Area and Data Collection

The longitudes 73° 30′ to 89° 0′ east and latitudes 22° 30′ to 31° 30′ north is the location between which the catchment area of the River Ganga falls in four countries, namely India, Bangladesh, Nepal and Tibet (China) with a major part in India. The Ganga basin extends over an area of 1,086,000 km^2. Almost 26.2% of the total geographical area of the country is the drainage area of the Ganga in India, which is 862,769 km^2. The entire length of the River Ganga is 2,525 km and the steerable length is 631 km. The study area includes the Ganga river basin extending from Kanpur to Bhagalpur (Fig. 26.1), which includes the cities of Prayagraj (Allahabad), Varanasi and Patna. The sampling in Kanpur is done at Balu ghat and Gola ghat. In Prayagraj (Allahabad) the sampling is done at the Sangam mela ground having three points; i.e. Ganga river, Yamuna river and Sangam. At the holy city of Varanasi, two points of sampling were selected, one being the downstream (Dashashwamedh Ghat) and the second being the upstream (Assi Ghat). In Patna, twelve points around Gandhi Ghat were selected. For Bhagalpur, two points were selected for sampling i.e. at Kuppa Ghat and Barrari Ghat.

26.3 Methodology

26.3.1 Water Quality Data Collection and Analysis Procedure

The sampling was done on monthly basis on the dates coinciding with the satellite pass dates (±5 days) of LANDSAT-8 from Kanpur, Prayagraj, Varanasi, Patna & Bhagalpur. The grab sampling method was applied for collecting the samples.

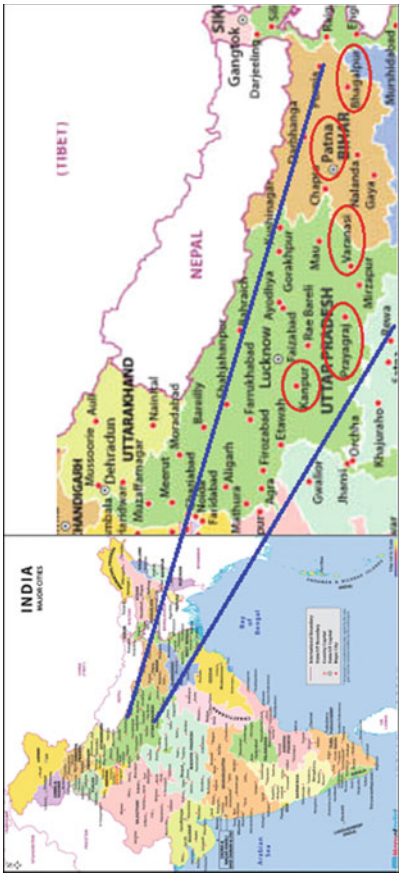

Fig. 26.1 The location map of the study area

Samples were collected within 5 m from the river bank at a depth of ~0.5 m in Teflon bottles of 2 L. The samples were transported and stored at 4 °C until analysis. The water quality parameters, Total suspended solids, turbidity, BOD and DO were measured in the laboratory by the standard method (APHA, 2017).

26.3.2 Satellite Data Collection and Analysis Procedure

In the present work, Landsat-8 satellite data was collected from the USGS website and were used of estimating total suspended solids, turbidity and effluent inlet locations. For this normalized difference water index (NDWI), normalized difference turbidity index (NDTI) and land use land cover (LULC) maps were developed and used for the analysis.

26.3.2.1 NDWI

The NDWI, defined by McFeeters (1996) was obtained using Eq. (26.1):

$$\text{NDWI} = (\text{Band } 3 - \text{Band } 5)/(\text{Band } 3 + \text{Band } 5) \tag{26.1}$$

In NDWI the values range between −1 and 1, where the positive value indicates the presence of water.

26.3.2.2 NDTI

The NDTI is obtained using Eq. (26.2)

$$\text{NDTI} = (\text{Band } 4 - \text{Band } 3)/(\text{Band } 4 + \text{Band } 3) \tag{26.2}$$

The higher value of turbidity provides a high value of NDTI and vice versa.

26.3.2.3 LULC Map

Using Landsat-8 data, land use maps have been developed with special emphasis on water bodies and its depth by studying the spectral signature and their variations.

26.4 Results and Discussion

The water quality variables, total suspended solids, turbidity, BOD and DO have been analyzed to verify the change in the quality of Ganga River water at all five cities under consideration.

The results indicate that BOD values are increasing significantly in all the cities except Prayagraj (Fig. 26.2). However, the values are found to be less than 10 mg/l and can be managed using bioremediation, reaeration and chemical dosing.

The DO values are found to decrease at the outlet of each city (Fig. 26.3). However, the maximum variations are observed at Kanpur and Patna. At Prayagraj the variation is found to be very less.

The NDWI, NDTI and LULC maps developed using remote sensing indicate synoptic view, qualitative as well as quantitative estimates of total suspended solids, turbidity and source of pollution in terms of water quality (Figs. 26.4, 26.5 and 26.6,

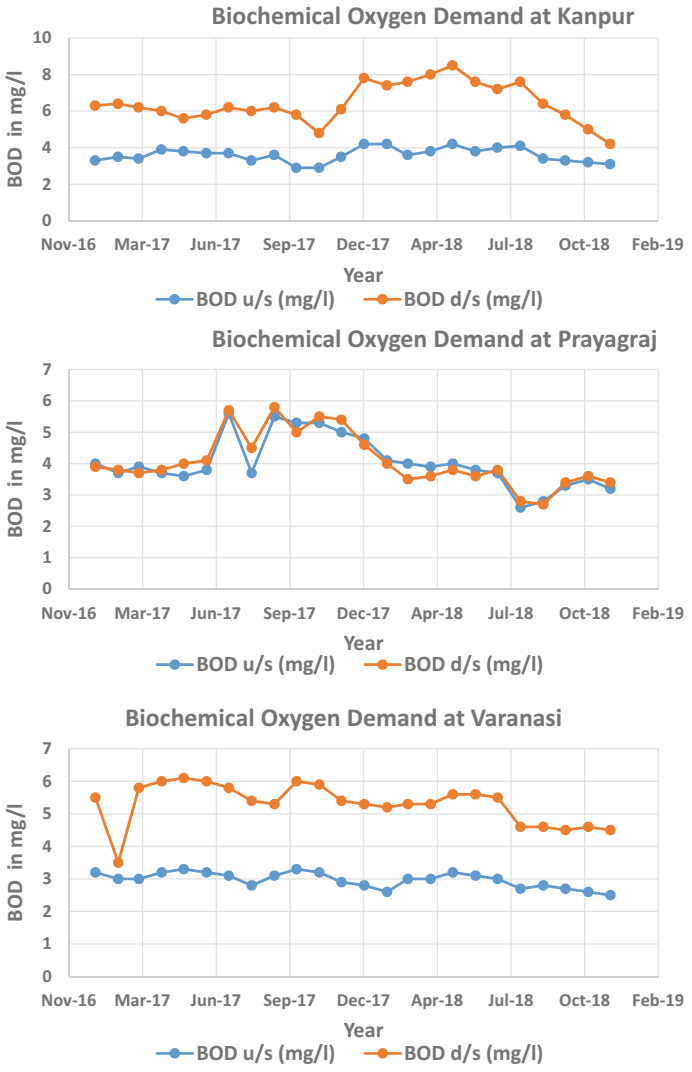

Fig. 26.2 Biochemical oxygen demand at inlet and outlet of all cities

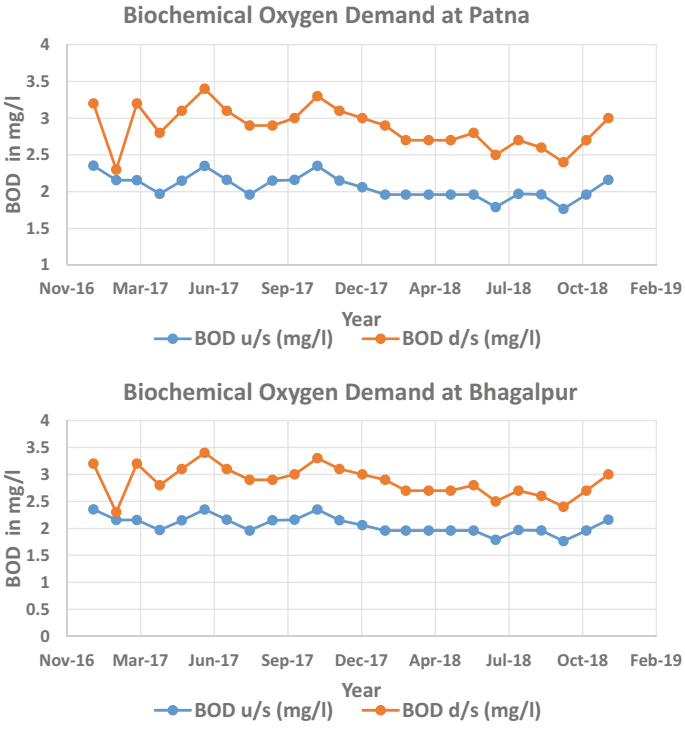

Fig. 26.2 (continued)

respectively). The suspended solids and turbidity are found to be maximum in Patna followed by Bhagalpur, which may be due to suspended sediment movement. The land use map indicates the location of the influx of pollutants.

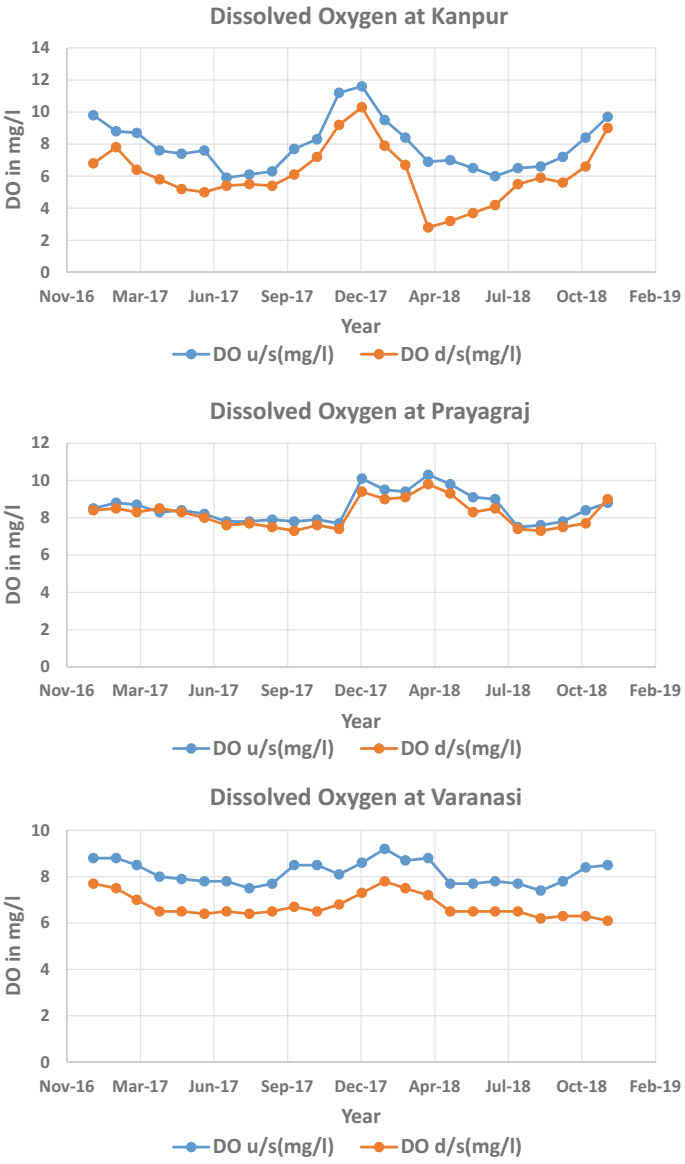

Fig. 26.3 Dissolved oxygen demand at inlet and outlet of all cities

26.5 Conclusions

The water quality samples of river Ganga at Kanpur, Prayagraj, Varanasi, Patna and Bhagalpur were collected and analyzed for the years 2017–2018 and indicate significant changes in water quality of the river at inlet and outlets of different cities.

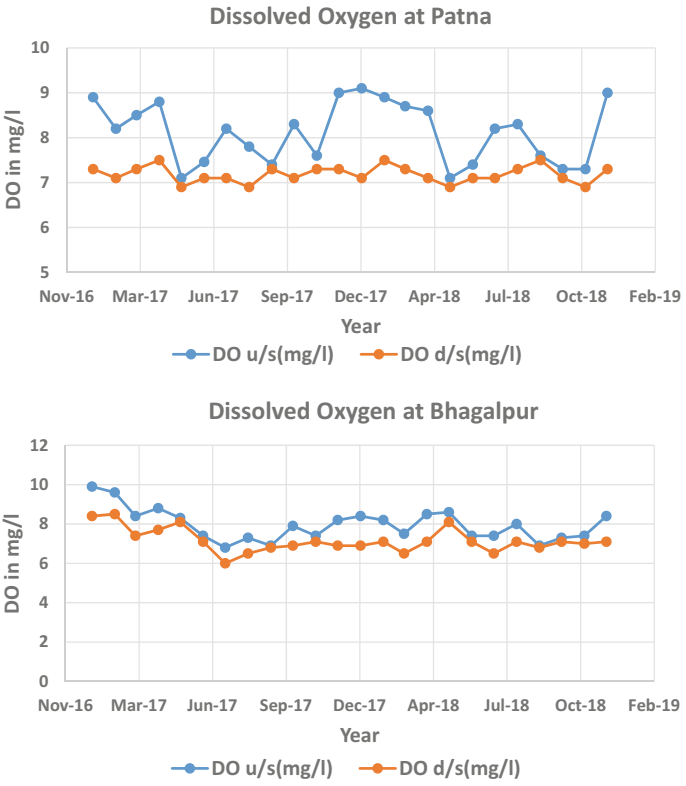

Fig. 26.3 (continued)

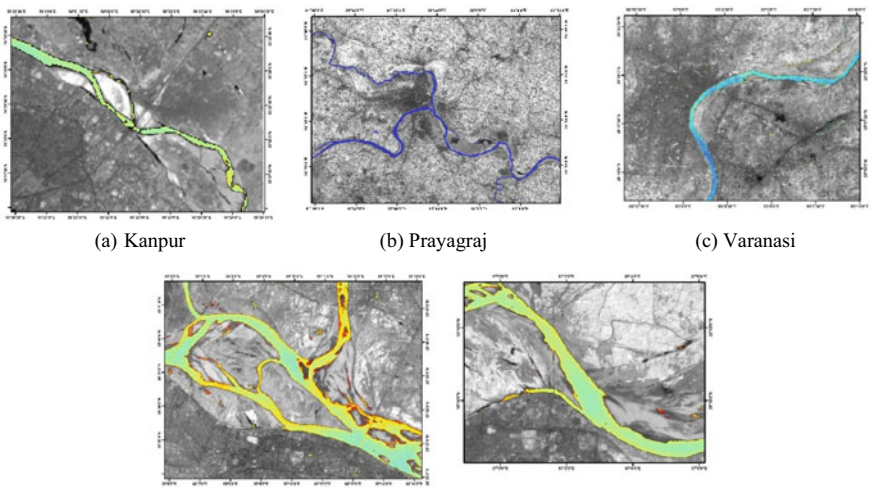

Fig. 26.4 NDWI of study area in cities along river Ganga

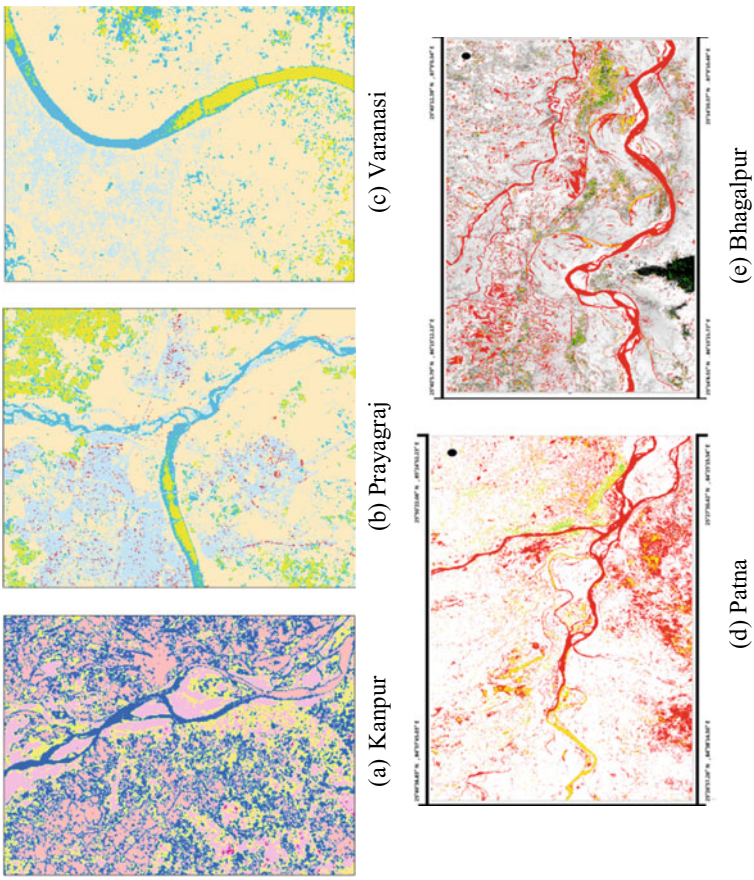

Fig. 26.5 NDTI of study area in cities along river Ganga

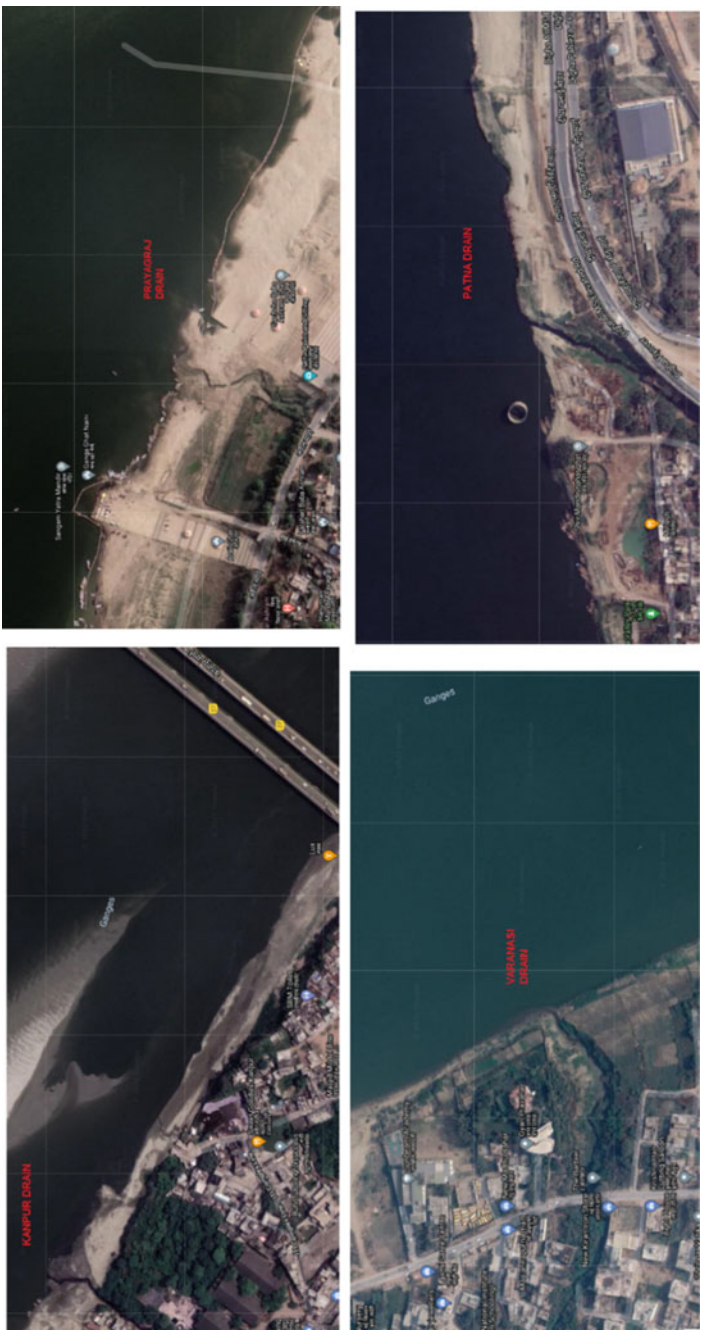

Fig. 26.6 LULC of study area in cities along river Ganga

The results obtained using the Landsat-8 MSS data shows that the total suspended sediment, turbidity, DO and BOD are varying significantly at different locations due to variation in flow in river Ganga, effluent disposal and sediment transport.

The satellite based remote sensing approach can be effectively used to make qualitative and quantitative estimates of suspended sediment and turbidity.

References

Baier K, Strohschön R (2012) Die Grundwassersituation der südchinesischen Megastadt Guangzhou. DVGW Energie Wasserpraxis 4(2012):18–23

Baier K, Real A, Strohschön R, Azzam R (2009) Ansätze eines alternativen Wassermanagementkonzepts für mega urbane Räume am Beispiel der südchinesischen Megastadt Guangzhou. Umw WirtschaftsForum 17(3):281–289

Caballero I, Stumpf RP, Meredith A (2019) Preliminary assessment of turbidity and chlorophyll impact on bathymetry derived from Landsat-8A and Sentinel-3A satellites in South Florida. Remote Sens 11(6):645. https://doi.org/10.3390/rs11060645

Doxaran D, Froidefond JM, Lavender S, Castaing P (2002) Spectral signature of highly turbid waters application with SPOT data to quantify suspended particulate matter concentrations. Remote Sens Environ 81(1):149–161

Garg V, Senthil Kumar A, Aggarwal SP, Kumar V, Dhote PR, Thakur PK, Nikam BR, Sambare RS, Siddiqui A, Muduli PR (2017) Spectral similarity approach for mapping turbidity of an inland waterbody. J Hydrol 550:527–537. https://doi.org/10.1016/j.jhydrol.2017.05.039

Geuttler FN, Niculescu S, Gohin F (2013) Turbidity retrieval and monitoring of Danube Delta waters using multi-sensor optical remote sensing data: an integrated view from the delta plain lakes to the western–northwestern Black Sea coastal zone. Remote Sens Environ 132:86–101. https://doi.org/10.1016/j.rse.2013.01.009

Gholizadeh MH, Melesse AM, Reddi L (2016) A comprehensive review on water quality parameters estimation using remote sensing techniques. Sensors 16(8):1298

IOCCG (2000) Remote sensing of ocean colour in coastal, and other optically-complex, waters. In: Sathyendranath S (ed) Reports of the International Ocean-Colour Coordinating Group, No. 3. Dartmouth, NS, Canada, IOCCG

Jha R, Singh VP (2008a) Analytical water quality model for biochemical oxygen demand simulation in river Gomti of Ganga basin, India. KSCE J Civil Eng 12(2):141–147. https://doi.org/10.1007/s12205-008-0141-x

Jha R, Singh VP (2008b). Evaluation of river water quality by entropy. KSCE J Civil Eng 12(1):61–69. https://doi.org/10.1007/s12205-008-8061-3

Jha R, Singh VP, Vatsa V (2008a) Analysis of urban development of Haridwar, India using entropy approach. KSCE J Civ Engineering 12(4):281–288

Jha R, Sharma KD, Singh VP (2008b) Critical appraisal of methods for the assessment of environmental flows and their application in two river systems of India. KSCE J Civ Eng 12(3):213–219. https://doi.org/10.1007/s12205-008-0213-y

Johnson RW (1975) Quantitative sediment mapping from remotely sensed multispectral data. In: Shahrokhi F (ed) Remote sensing of earth resources, vol IV. The University of Tennessee Space Institute, Tullahoma (TN), pp 565–576

Klemas V, Borchardt JF, Treasure WM (1971) Suspended sediment observations from ERTS1. Remote Sens Environ 2:205–221

Kritikos H, Yorinks L, Smith H (1974) Suspended solids analyses using ERT-A data. Remote Sens Environ 3(1):69–78

Mohr J, Baier K, Jha R, Azzam R (2012) Urbanization and the social impact on water resources in India. In: Fourth international conference on water resources and renewable energy development in Asia. Chiang Mai, Thailand

Moore GK (1980) Satellite remote sensing of water turbidity. Hydrol Sci J 25(4):407–421

Nolè G, Danese M, Murgante B, Lasaponara R, Lanorte A (2012) Using spatial autocorrelation techniques and multi-temporal satellite data for analyzing urban sprawl. In: Computational science and its applications–ICCSA, pp 512–527

Pavelsky TM, Smith LC (2009) Remote sensing of suspended sediment concentration, flow velocity, and lake recharge in the Peace-Athabasca Delta, Canada. Water Resour Res 45(11):W11417. https://doi.org/10.1029/2008WR007424

Quang NH, Sasaki J, Higa H, Huan NH (2017) Spatiotemporal variation of turbidity based on Landsat 8 OLI in Cam Ranh Bay and Thuy Trieu Lagoon, Vietnam. Water 9(8):570. https://doi.org/10.3390/w9080570

Rahman A (2007) Application of remote sensing and GIS technique for urban environmental management and sustainable development of Delhi, India. In: Applied remote sensing for urban planning, governance and sustainability. Springer, Berlin, pp 165–197

Ritchie JC, McHenry JR, Schiebe FR, Wilson RB (1974) The relationship of reflected solar radiation and the concentration of sediment in surface water of reservoirs. In: Shahrokhi F, Garg et al (eds) Remote sensing of earth resources, vol III. The University of Tennessee Space Institute, Tullahoma (TN), pp 52–72

Ritchie J, Schiebe FR, McHenry JR (1976) Remote sensing of suspended sediments in surface waters. Photogramm Eng Remote Sens 42(12):1539–1545

Sahoo BB, Jha R, Singh A, Kumar D (2019) Application of support vector regression for modeling low flow time series. KSCE J Civ Eng 23(2):923–934. https://doi.org/10.1007/s12205-018-0128-1

Sebastiá-Frasquet M-T, Aguilar-Maldonado JA, Santamaría-Del-Ángel E, Estornell J (2019) Sentinel 2 analysis of turbidity patterns in a coastal lagoon. Remote Sens 11(24):2926. https://doi.org/10.3390/rs11242926

Singh K, Jha R (2018) Assessment of water quality in River Ganga at Patna, India. In: Jha R, Singh VP, Singh V, Roy LB, Thendiyath R (eds) Hydraulics, water resources and coastal engineering: groundwater and water quality, vol 5. Springer USA Book, pp 40–48

Singh K, Jha R (2020) Water quality of river Ganga using remote sensing and GIS techniques—a review. In: ASCE Conference, Kolkata India, 2–4 March 2020

Strohschön R, Romich M, Baier K (eds) (2009) Strukturen, Prozesse und Dynamiken der Mega-Urbanisierung in China—Landnutzung und Wasserressourcen. Aachener Studien zur Sozial-Ökonomischen Entwicklungsforschung, Band 11, Schriftenreihe des Internationalen Zentrums für Vergleichende Sozial-Ökonomische Entwicklungsforschung, 95

Strohschön R, Wiethoff K, Baier K, Lu L, Bercht AL, Wehrhahn R, Azzam R (2012) Land-use and water quality in Guangzhou, China: a survey of ecological and social vulnerability in four urban units of the rapidly developing megacity. Int Environ Res (Accepted)

Toming K, Kutser T, Laas A, Sepp M, Paavel B, Noges T (2016) First experiences in mapping lake water quality parameters with Landsat-8 MSI imagery. Remote Sens 8(8):640. https://doi.org/10.3390/rs8080640

Uitto JI, Biswas AK (2000) Water for urban areas: challenges and perspectives. United Nations University Press, Tokyo

United Nations World Commission on Environment and Development (1987) Our common future, The Brundtland Report. Oxford University Press, Oxford

Chapter 27
A Review on the Various Cost Effective Water Filtration Techniques

Nekita Boraah, Abhijit Mondal, and Mrinmoy Majumder

Abstract The development of low cost projects for the treatment of water is not a new concern. The population of India is mainly dependent on surface and groundwater for different purposes including drinking. Statistics reveal that about 76 million people in India lack access to safe drinking water. Many projects related to the filtration of water have been proposed so far. But in most cases, the filters either had drawbacks or were limited to a certain region. The improved water purifiers developed so far are not affordable for each and every household in India. So the necessity of developing such a filter which can serve every corner of our country is in utmost demand. The major contamination in water is now a days because of two main reasons: increasing pollution and increasing population which leads to an increase in demand, both being interrelated. Major contaminants reported so far are iron (Fe), arsenic (As) and fluoride (F^-) that are so harmful as to have led to many diseases. So, a technology which is able to overcome the present contamination and also serve the people of the country should be developed. In this context, a number of researchers have developed different types of filters owing to the problems faced by people of the specific region. Treatment options for the removal of emerging contaminants from drinking as well as wastewater have been reported as adsorption, Advanced Oxidation Processes (AOPs), Nano-filtration (NF) and Reverse Osmosis (RO) membranes by the use of nanoparticles. Also, natural adsorbents like rice husk ash, bagasse ash, tulsi, neem and also bamboo charcoal have been used to remove contaminants from water. A review of such developments is the discussion of this paper.

Keywords Safe drinking water · Low cost projects · Nano-filtration · Natural adsorbents

N. Boraah · M. Majumder (✉)
School of Hydro-Informatics, Civil Engineering Department, NIT Agartala, Agartala, India
e-mail: mmajumder15@gmail.com

A. Mondal
Chemical Engineering Department, NIT Agartala, Agartala, India

R. Jha et al. (eds.), *Groundwater and Water Quality*, Water Science and Technology Library 119, https://doi.org/10.1007/978-3-031-09551-1_27

27.1 Introduction

Water, being the most important resource of the world, has become a cause of concern now-a-days. About one-fifth of the population on earth lacks access to safe drinking water, a condition that resulted in the death of 2 million people in 2004, as per the records of the United Nations. Access to safe drinking water has been a grave problem for India, especially in rural areas where lack of usable water has resulted in decades old sanitation and health problems. Government records show that in 1980, just 1% of India's rural areas had access to safe, usable water. By 2013, that had increased to 30%, but the majority of rural India continues to live without proper access to safe drinking water. In 2016, an estimate reported that 76 million people have no access to safe water supply and with passing of time, the problem is only getting more serious.

The current status reveals the unavailability of safe drinking water, especially from natural sources. An important cause is the alarming rate of increase of contamination of natural sources. This can be related to the increasing demand for water due to the increasing population. The vital sources of accessible water include rain water, surface water and groundwater. But an increasing rate of pollution has led to tremendous contamination of the available water sources. Rain water, once considered as the purest form of water, now falls as acid rain with the contamination of sulphides and nitrates. It can be estimated as to how much harmful it is in today's world. Even the surface water has fallen prey to mainly organic wastes and groundwater has been found to be tainted with heavy metals. The harmful effects of water contamination can be seen in the diseases that living organisms are facing now-a-days. Not only human beings but also plants and animals are being affected by diseases. At the present time, all types of water require proper treatment before bringing it to any use.

The conventional water treatment includes coagulation/flocculation followed by sedimentation/clarification which is then treated biologically with the help of filtration, aeration and disinfection. The present day filtration techniques talk of reverse osmosis technique, ultraviolet water treatment, activated carbon or a mixture of all of these techniques into one. It is to be noted that the common filters available in the market i.e., AquaGuard, PureIt, Kent etc. have been able to safely purify water but the main concern is the cost. The people living in the rural areas cannot afford such innovations. There have been situations in which people have used just sand and pebbles as filtration media to purify water. The simple rural people have very little knowledge about the heavy metals contamination which is a growing cause of concern in the present day world. They are not aware of the terms contamination or disinfection and as such, they are getting affected day by day.

Many low cost projects have been proposed so far and some of them implemented in some areas. This paper reviews the cost effective projects anticipated so far along with their advantages and demerits.

27.2 Review of Different Cost-Effective Technologies

Various treatment processes have been reported in the past which have been effective in the removal of various types of contaminants. Ultraviolet (UV) water treatment process has been found to be efficient in disinfection of micro-organisms such as harmful bacteria, viruses, molds and parasites, but the inactive micro-organisms do not get removed from the water. This process also cannot be used to treat raw wastewater. A combination of pre or post filtration devices may be useful for producing safe and potable water (Chan et al. 2009). Reverse osmosis technique, one of the most excellent water filtration methods is known to diminish approximately every bit of organic and inorganic chemicals, micro-organisms, salt, metals and particulates, present in tainted water. It also recovers tastes, odour and appearance. RO technique is a very effective technique yet very expensive and, requires skilled maintenance (Chan et al. 2009). Activated carbons are common filters generally found in water treatment systems. The main functionality of this system is the improvement of tastes and odours, and it also, effectively removes organic compounds including VOCs, radon, and chlorine. It also works as a pre-treatment technique for other water purification systems, such as reverse osmosis and ultraviolet water filters. The major disadvantage of this technique is that the reuse of activated carbon bits is not likely and hence, replacement is required after filtering about 150 L of water (Chan et al. 2009; Dalai 2014). Ceramic filter is one of the most economical filtration methods. Ceramic filtration technique is best known in the household systems as it does not allow the passing of molecules larger than a water molecule through its pores. These filters are very useful as it offers a highly effective barrier against particles and harmful micro-organisms. They are known to possess a long life, have self-sterilising properties and minerals are also maintained in water. The reaction of ceramic water filter with colloidal silver proves to completely eradicate bacteria and the development of molds and algae inside the body of the filter. The main drawback of these filtration systems is that they are fragile and require high maintenance as compared to other filters. Since sediments fill up the pores on the filter surface, they need to be cleaned regularly (Chan et al. 2009).

Treatment options recently considered for the removal of emerging contaminants from drinking water as well as wastewater are adsorption, Advanced Oxidation Processes (AOPs), Nano-filtration (NF), and Reverse Osmosis (RO) membranes. A report on water purification indicated the use of noble metal nanoparticles, by the process of adsorption. Nanomaterials include metals, oxides, clays, dendrimers etc. (Pradeep 2009). A project developed at IIT Madras made a nanoparticle water filtration system that could produce potable water for the poorest communities in India and could be very useful in future too. The setup is said to have microbe-killing capacity along with the removal of harmful contaminants like lead and arsenic. The microbe filter relies on silver nanoparticles embedded in a cage made of aluminium and chitosan, a carbohydrate derived from the chitin in crustacean shells. The cage blocks macroscale water contaminants as well as protects the nanoparticles from sediments that would otherwise accumulate on their surfaces, thereby preventing

them from releasing microbe-zapping ions. The team used nanoparticles that release iron- and arsenic-trapping ions to make its chemical filter (Gravotta 2013).

Purification of water is done by adsorption, focusing in a better way on iron removal using two economic adsorbents, rice husk ash and bagasse ash (Dalai 2014). In Sri Lanka, researchers have developed a technique to remove iron and manganese using laterite which had great efficiency. Also, they developed a defluoridator for removing fluoride, which had a filter made of burnt clay or bricks. Also, laterite has been used as filter media for defluoridator (Attanayake et al. 1995). A low cost purification system design for the removal of arsenic has also been reported. The study was conducted in tubewell water in Bangladesh and some parts of India, mainly West Bengal. The design has two components: the physical design of a water treatment tank that can be constructed next to a tube well, and the chemical design of an adsorbent bed of harmless low-cost chemicals which can trap and remove arsenic species from the water. The design allows 750 L volumes of water to be treated each day, sufficient for several families, who could share the costs of construction and maintenance (Crisp and Chowdhury 2001). The design idea was indeed innovative but lacked experimental assessment. In an attempt to remove arsenic, iron oxide adsorbers have also been utilised. Nanoscale iron oxide particles were synthesized and deposited on porous alumina tubes to develop tubular ceramic adsorbers for the removal of arsenic (Sabbatini et al. 2009). Also, a technique was developed to evaluate a cost-effective biosand filter, modified with the addition of zeolites (clinoptilolite). Filtration was done for 3 h to mimic water filtration in private homes. Results indicated removal of up to 80 calcium, 89 magnesium, 99 iron, 56 arsenic, 54 fluorides, 96 turbidities, 37 nitrates and 41% total organic carbon. The study was exclusively carried out in South Africa and the whole setup was cost-effective and could be afforded by rural people. The filter could efficiently produce water that could be used for drinking and cooking purposes. The filter could be used for the removal of calcium and magnesium hardness and also iron but its use is not recommended for the removal of arsenic, carbon, nitrates and fluorides in highly contaminated water. Filtration of highly turbid water is not recommended as it may clog the filter media (Mahlangu et al. 2011).

Another filter which was introduced is the terafil water filter. Terafil is a low cost burnt red clay porous media, used for filtration and treatment of turbid raw water into clean drinking water for domestic or community applications. It has been proved to remove suspended particles, sediment, iron and many heavy metals, micro-organisms, colour and odour effectively. during filtration, without clogging the core of the terafil. It has also been proposed by CSIR-IMMT as a highly efficient low cost device. Nearly 99% of turbidity, 95–100% of micro-organisms, 90–95% of soluble iron, colour, bad odour etc. are effectively removed from the raw water by filtration through the terafil disc. Pathogen free product water can be obtained from groundwater by filtration through terafil disc, while mild chlorination (0.01 g/L water) is necessary for surface water.

In an attempt to construct low-cost water purification system, a team of students and faculty from IIT proposed a low-ceramic water filter as a means to remove turbidity and eliminate harmful micro-organisms. With improved efficiency, decreased energy and less equipment necessary, the proposed filter was named

"KlarAqua" with the aim that it can effectively eliminate micro-organisms and other pollutants, people find it easier to use, can be easily constructed, and flow rate is acceptable, very cost-effective, inspires users to practice good hygiene and also, its production causes economic growth by creating new jobs. The design has achieved efficiency of upto 98% in removing harmful micro-organisms, also a good flow rate and no leaks have been identified in the design. However, minimisation of the need for colloidal needs to be reduced without affecting the present efficiency (Act 2006–2007).

Construction of low-cost water purifiers has also been implicated in using natural herbs. The process was mainly suggested for the removal of fluoride. Materials such as tulsi and neem have been used to remove fluoride mainly from well water and bore well water. The efficiency of these filters has been shown to be around 50% (Yevate and Mane 2017). A study performed in Assam indicated the use of bamboo charcoal for the removal of iron. Four different varieties of bamboos were charcoaled into four samples to prepare the filtration bed and their efficiencies compared to obtain the best species (Baruah et al. 2011).

27.3 Conclusion

Many projects have been proposed so far, regarding different filtration techniques which can be provided at a considerable cost. Some techniques have been developed under governmental research and their implementation has provided good results. Though so many techniques have been developed, yet people not only in India but also, in the world, are facing a potable water crisis. This can possibly be because a technology not only needs to be developed but also it should reach the people so that it can be used for their benefit. Today, the ones available in the market are made of high technologies but cannot be afforded by every section of people. A look at the review suggests many cost-efficient technologies but yet it fails to reach people around the corner. A feasible solution might be to popularise the most efficient cost-effective techniques amidst every possible area so that all the sections of people can have access to safe and healthy water.

References

Panda AK, Acharya PS, Srivastava A, Keshari U, Suna SN, Paul S, Subba SH, Mahajan PB (2019) Improving access to safe drinking water requires leadership at different levels: a photo-essay from a rural area in eastern India (Tangi-Odisha). Int J 3:1

Act, U. S. E. P. (2006–2007) Low-cost water purification system: developing an effective water purification system for local production which offers sustainable economic stimulus. SU833176, Illinois Institute of Technology

Attanayake M, Padmasiri JP, Fernando W (1995) Laterite for water treatment. In: WEDC conference. Water, Engineering and Development Centre, pp 253–255

Baruah BK, Das B, Haque A, Misra K, Misra AK (2011) Iron removal efficiency of different bamboo charcoals: a study on modified indigenous water filtration technique in rural areas of Assam. J Chem Pharm Res 3(2):454–459

Chan L, Chan M, Wang J (2009) Design of water filter for third world countries

Crisp PT, Chowdhury AH (2001) Design of a low-cost purification system for the removal of arsenic from tubewell water in Bangladesh and India. In: BUET-UNU international workshop on technologies for arsenic removal from drinking water, Bangladesh, May

Dalai C (2014) Water quality improvement using different filter materials. M Tech, National Institute of Technology, Rourkela, Odisha

Pradeep T (2009) Affordable clean water using nanotechnology. In: OECD. Indian Institute of Technology, Chennai

Gravotta L (2013) Cheap nanotech filter clears hazardous microbes and chemicals from drinking water. Sci Am 10

Mahlangu TO, Mpenyana-Monyatsi L, Momba MNB, Mamba BB (2011) A simplified cost-effective biosand filter (BSFZ) for removal of chemical contaminants from water. J Chem Eng Mater Sci 2(10):156–167

Sabbatini P, Rossi F, Thern G, Marajofsky A, de Cortalezzi MMF (2009) Iron oxide adsorbers for arsenic removal: a low cost treatment for rural areas and mobile applications. Desalination 248(1–3):184–192

Yevate A, Mane S (2017) Low cost water purifier by using natural herbs. IJSART 3(9):112–115

Chapter 28
Analysis of Location of Oil Spills and Use of Marine Tar in Bituminous Road Construction Collected Near Alibaug Beaches (Maharashtra)

Priyanka S. Bhatkar, Raju Narwade, and Kartik Nagarajan

Abstract Tar residue deposition could also be a seasonal phenomenon because it's ascertained throughout the monsoon season. It's vital to review impact of oil spills and tar ball pollution because this problem produces awfully results on the ecosystem of the beaches. This paper reports a widespread prevalence of tar balls on the beaches of the Alibaug region within the Arabian sea of India. Additionally, causes of the formation of tar balls and the use of remote sensing in oil spill response were also analyzed. Tar Balls are an indicator of oil spillage at the sea shore. Tar balls are found in the slightest degree over the globe. In addition, this study includes, the use of marine tar balls in bituminous road construction which help to reduce marine pollution caused due to presence of tar balls as well as to achieve economy in road construction.

Keywords Tar balls · Marine pollution · Oil Spill · Use of Tar Ball

28.1 Introduction

India has a long coastline approximately 8110 km. We studied the coastline of Alibaug beach (Raigad District) which is in Maharashtra State. In previous couple of years, Alibaug becomes one of the major tourist destination places. Hence, it is necessary to study marine pollution at Alibaug beach. Figure 28.1 shows a map of the Coastal Districts of India. Alibaug is the District Headquarter of Raigad. The Latitude and the line of Longitude of Alibaug are 18.39 N and 72.55 E. The total population of Alibaug is 20,752 (As per 2001 Census). The problem of oil spillage

P. S. Bhatkar · R. Narwade · K. Nagarajan (✉)
Department of Civil Engineering, Pillai HOC College of Engineering and Technology, University of Mumbai, Rasayani Raigad, Khalapur Maharashtra, India
e-mail: knagarajan@mes.ac

P. S. Bhatkar
e-mail: bhatkarpriyanka10@gmail.com

R. Narwade
e-mail: narwaderajp@mes.ac.in

R. Jha et al. (eds.), *Groundwater and Water Quality*, Water Science and Technology Library 119, https://doi.org/10.1007/978-3-031-09551-1_28

was first time observed at Alibaug in August 2010, after a collision between MSC Chitra and MV Khalijia 3 ships close to Mumbai coast in August 2010.

The location of Raigad District is in Konkan Region that is in Maharashtra State shown in Fig. 28.2. From last few years Raigad District becomes the main destination place for tourists, as a result of it includes totally different beaches with or so 720 km long coastline and 50–60 km in broad.

In recent years, some activities like routine ship maintenance, underwater drilling operations and harmful fishing operations produces more than thousands liters of oil

Fig. 28.1 Coastal districts of India

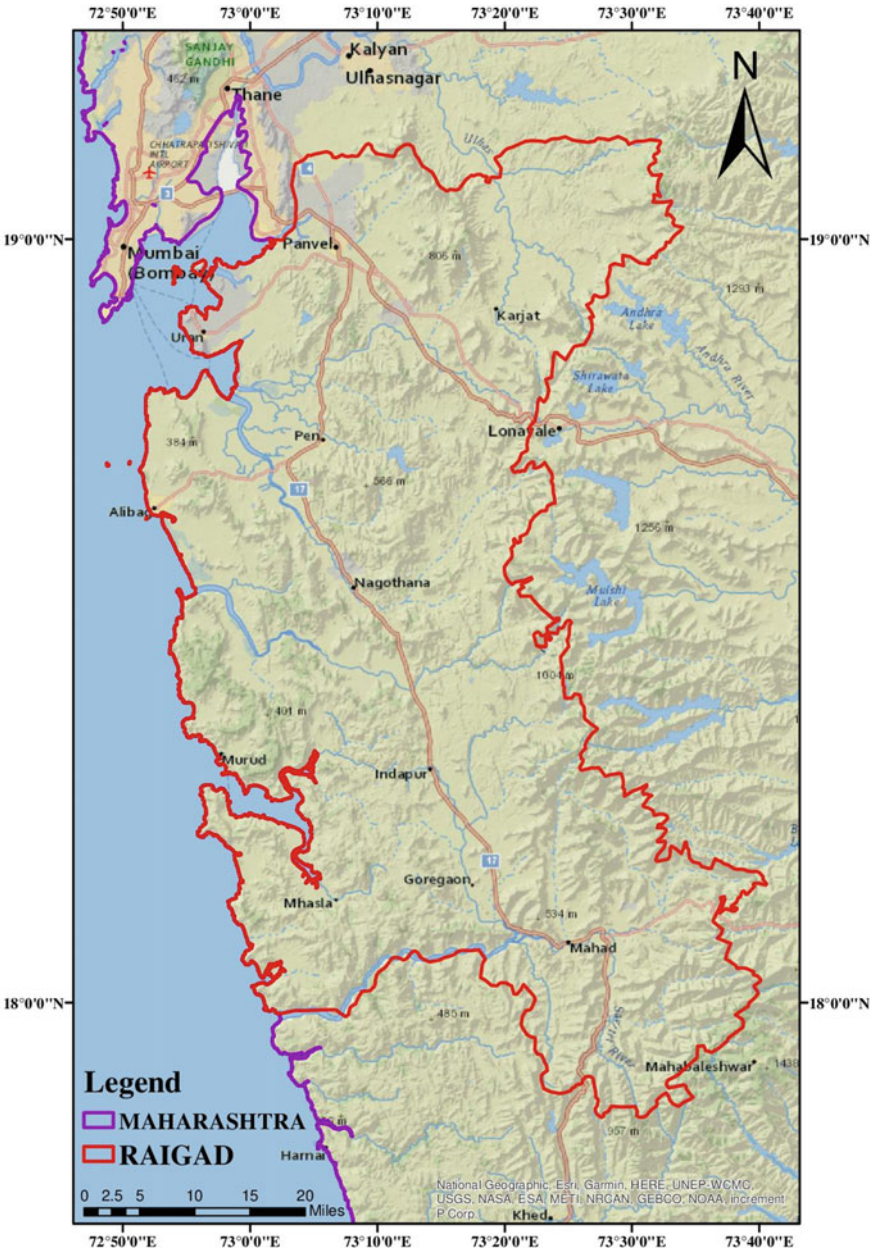

Fig. 28.2 Location of Raigad district in Maharashtra State

spill issues discovered, which is the main reason of the degradation of the marine ecosystem. The main reason of the effect on the coastal biodiversity of Alibaug is uncontrolled drilling activities which pollute the beaches. Because of this reason, a negative impact is discovered on the economy of Raigad district by reducing in the progress of the tourism industry. The government decided to take the necessary management actions to revive Alibaug beaches and also the surrounding areas. In the present paper, some beaches in the Alibaug region were selected for identifying the effects and causes of the formation of tar-ball. The locations of different studies areas are shown in Fig. 28.3. To gather information regarding marine pollution different field surveys were conducted during the first phase of assessment on respective beaches. The tar balls and oil spills reduces the coastal water quality.

28.2 Objectives of Study

1. To recognize the source of marine pollution in the Arabian Sea.
2. To study the causes of tar ball pollution.
3. To find the use of marine tar in Bituminous Road Construction.

28.3 Causes of Formation of Tar Balls

Marine tar balls are formed from natural and artificial sources of an oil spill. Natural sources include seepage of oil on the seafloor while artificial sources include oil transportation from the ships, drilling operations, emissions from oil exploration, ship accidents etc. Oil released from a natural or artificial source comes in contact with the atmosphere. Then, beneath weathering process tar balls are formed. Their size varies from a few millimeters up to tens of centimeters. They become soft when heated by sunlight. There is a large variation in the internal structure of tar ball, some tar ball have shell like structure with liquid inside whereas some includes small debris with a particular grain size.

28.4 Methodology Used

In this study, beaches in the Alibaug region such as Kihim, Nagaon, Aakshi and Revdanda were selected for investigating the impact of oil spills pollution on their respective marine ecosystems. First phase assessment includes gathering general information regarding oil spill points and tar balls by conducting a field survey. In the first phase of the assessment, we collected information at Kihim and Revdanda beaches. After the collection of samples, certain chemical testing's conducted on tar ball samples to check their chemical composition. Then, the next step includes

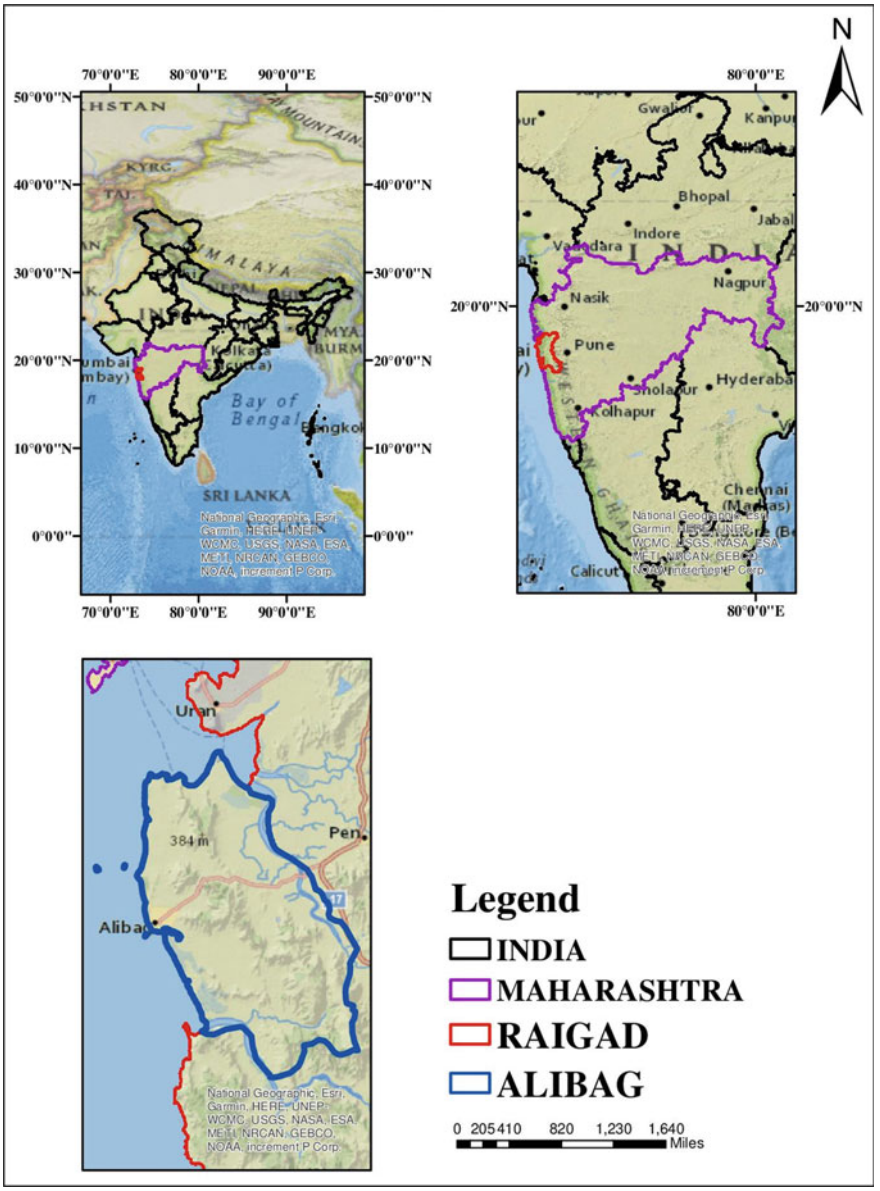

Fig. 28.3 Map of the studied area

analysis of the location of tar residue by using Remote Sensing Software's and use of marine tar residue in bituminous road construction by conducting bituminous material testing's. We know different forms of bituminous materials like Asphalt, Cutback Bitumen, Bitumen Emulsion, Tar are available to use in construction activities. Hence, by studying the properties of different bituminous materials and identifying compatibility with marine tar we ensure that will find a solution to avoid the effects of marine tar pollution.

28.4.1 Kihim Beach

It is located in the north of Alibaug city. Figure 28.4 shows the location of Kihim beach. The latitude of Kihim village is 18.72 N and the longitude 72.86 E. It is located approximately 11 km from Alibaug city.

We implemented our first step of methodology that is the first phase assessment in the second week of February 2018 at Kihim Beach. We observed huge numbers of tar balls at this beach in the summer season also. But even in February month, we observed many numbers of tar balls in at the coastline of Kihim beach. Figure 28.5 shows observed tar balls at this beach during the first assessment phase. The colour of the observed tar balls is black. They are very hard and ranges in average size from 3 to 7 cm. Tar balls are mostly spherical in shape but most of them are ellipsoid in nature. Tar balls observed at this beach are benthic in nature, which means they are observed at the sea shore. The density of tar balls increases in the monsoon season. The main reason behind the formation of tar balls is oil leakage from ships and oil tankers, accidents of ships and seepage from the bottom of the sea.

28.4.2 Revdanda Beach

Revdanda beach is also known as Revati region beach, because Revati is the old name of Revdanda village. The colour of sand observed at this beach is black which gives it a unique look. It is located at 17 km distance from Alibaug city and 125 km from Mumbai City. The location of Revdanda Village is shown in Fig. 28.6. The latitude and longitude of this beach are 18° 33′ N and 72° 56′ E respectively. We conducted our first phase assessment stage at Revdanda Beach in March 2018. We observed a huge numbers of tar balls and oil spills even in the summer season. Figure 28.7 shows the observed oil spill at Revdanda Beach.

The following techniques are essential to consider for the protection of the marine ecosystem of the beaches:

1. Tar balls having a size greater than 15 cm should be removed manually.
2. Tar balls containing hydrocarbon materials should be removed by using microorganism techniques.

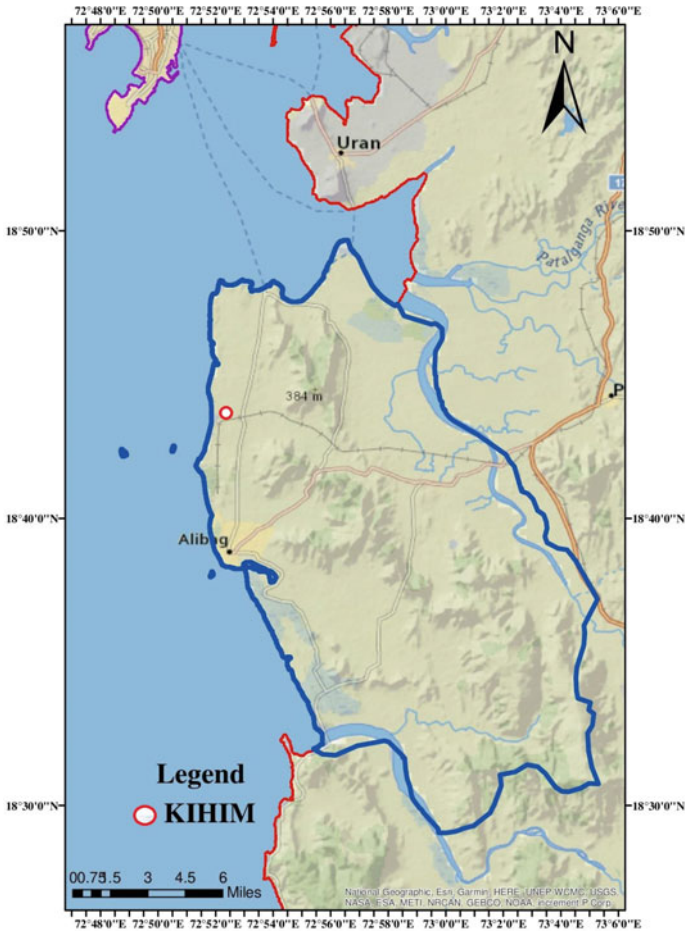

Fig. 28.4 Map shows location of Kihim Beach

3. The State Government should create strict regulations for activities like washing ships at designated ports and harbours.

28.5 Effects of Tar Balls

A very simple effect observed at the beach because of tar residue is, that tar balls stick to our feet which gives unpleasant looks and skin becomes oily. If we have to minimize this effect, we need to wash the affected body part with Sailor soap immediately. It also creates a damaging effect on marine organisms. Another effect is, that tar balls contain "Vibro Vulnificus" bacteria. This bacteria is mostly found in beached tar balls. This bacteria produces illness in the human body.

Fig. 28.5 Image of tar ball observed at Kihim Beach

28.6 Use of Remote Sensing in Detection of Location of Oil Spill

Remote Sensing is a necessary part of oil spill response. It is precious to locate the extent of the oil spill. We can monitor oil spills even in an open area by using newly developed remote sensing instruments. Sometimes, oil spill surveillance is done by using simple video photography. The most common method of an oil spill location is by using unnamed aerial vehicles (UAV'S) like drones. Radar technique and Micro wave technique are commonly used in Remote Sensing for the detection of the oil spill.

Figure 28.8 shows an image taken from RADARSAT-1 Satellite on 3rd November 2011 at Alibaug beach. The biggest problem in detection of the location of the oil spill is to differentiate between oil slicks and look likes spots because oil slicks may include all oil related surface films consisting of oil rigs whereas look alike contains natural films of grease ice. In Fig. 28.8, oil slicks are indicated by dark blue spots. Table 28.1 shows some SAR equipped satellite based sensors used for oil spill detection.

As per observation, 38% of oil pollution in the sea is because of the fuels and 28% of petroleum oil. Remaining is because of tanker accidents and operative discharges from ships. For capturing two dimensional images active microwave sensors like SAR are used. RADARSAT-1 and ENVISAT are the most commonly used providers for satellite images oil spill monitoring. Oil spills dampen the Bragg waves on the ocean surface because of this reason dark spots are observed in satellite images which indicates the location of an oil spill. Different processes like evaporation,

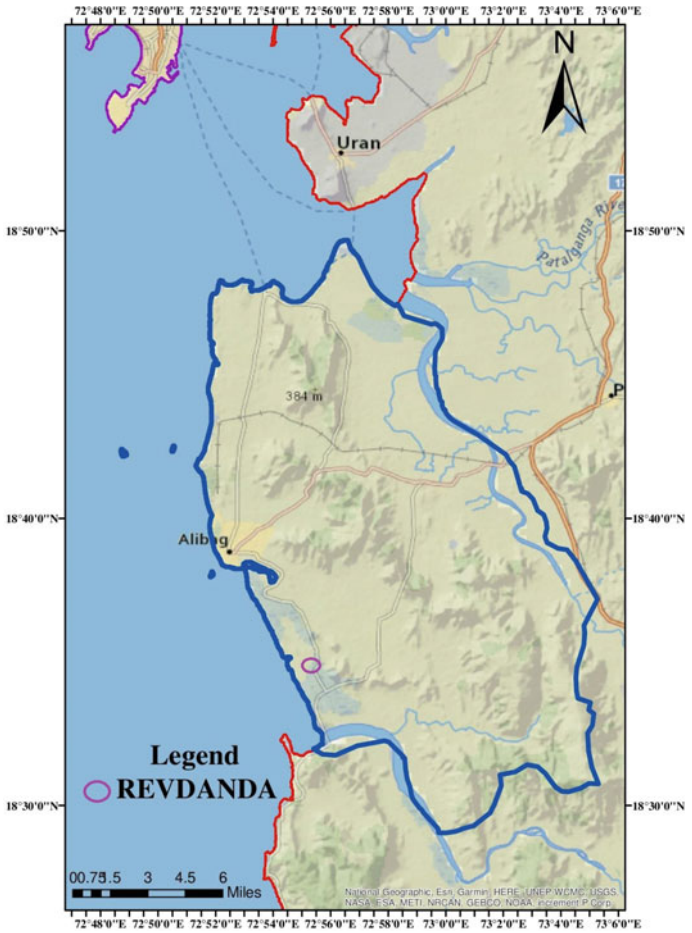

Fig. 28.6 Location of revdanda beach

emulsification and dispersion plays important role in oil spill detection technology. The component of oil having light in weight will evaporate to the atmosphere. The factors affecting on the rate of evaporation include the type of slick, thickness of slick, speed of the wind, sea water temperature etc.

28.7 Use of Marine Tar Balls in Bituminous Road Construction

Disposal of marine tar balls is a little more complicated process. The disadvantage of the disposal method is that it produces a harmful effect on the marine ecosystem.

Fig. 28.7 Observed oil spill at revdanda beach

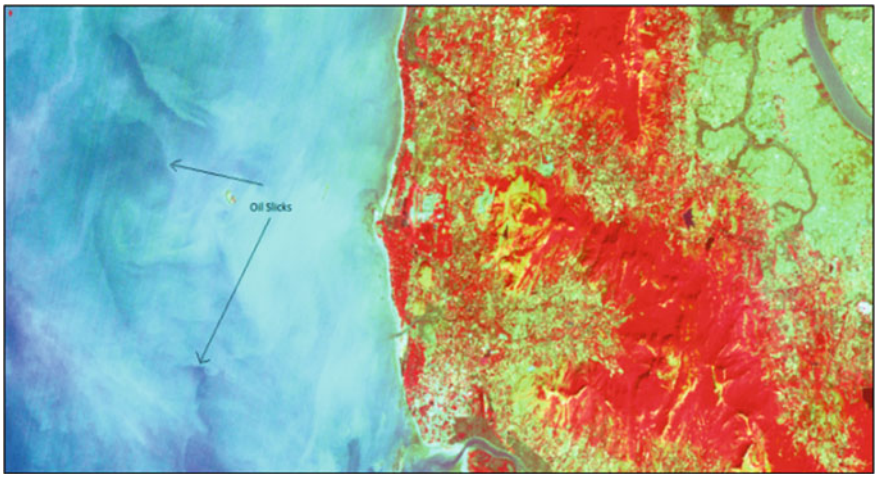

Fig. 28.8 Satellite Image shows oil spill. (*Source* www.bhuvan.com)

Table 28.1 SAR equipped satellite used for oil spill detection

Satellite	Year of operation	Owner	Properties
SEASAT	1978	NASA	L-band, HH-pol
ALMAZ-I	1991–1992	Russian space	S-band, HH-pol
ERS-1	1991–1996	Agency	C-band, VV-pol
ERS-2	1995-Till	ESA	C-band, VV-pol
RADARSAT-1	1995-Till	ESA	C-band, HH-pol
ENVISAT	2002-Till	CSA	C-band, HH and VV pol

Source Merv Fingus & Carl Brown (2014)

Hence, to avoid this harmful effect we decided to use marine tar residue in bituminous road construction. Marine tar residue i.e. marine tar balls contains naphthalene hence, it shows the same properties as bituminous material. We conducted certain tests like Penetration test, softening point test, ductility test and flash and fire test on a mixture of marine tar residue and bitumen. For testing, we used a mixture of 100 gm bitumen and 50 gm marine tar. We prepared the mixture by heating bitumen and marine tar at about 75–100 °C Temperature.

Penetration values mean a measure of viscosity. Different types of bitumen used in road construction having penetration values ranging between 20 and 25. 30/40 and 80/100 grade bitumen are most common for road construction depending upon the type of construction and climate conditions. Ductility value of the specimen indicates its elasticity and ability to return to its original shape after removal of the applied load. Ductility value is measured by ductility machine; its value should be a minimum of 50 as per Indian Standard. Another test is softening test, which determines the temperature at which a specimen pass through a disc contained in a ring by using the "Ring and ball test". For road construction, the softening point of bitumen varies from 30 to 45 °C. From obtained test result we concluded that, the use of marine tar ball sample in bituminous road construction is suitable by mixing it with bitumen because its help to achieve economy in road construction and it also reduces marine pollution. Further study includes some other testing's like softening point test, flash and fire point test, and ductility test so that we can reach towards a final solution that will be used for minimizing marine tar pollution.

28.8 Conclusion

As we studied, beaches in Alibaug are one of the tourist attracted beaches around the whole Raigad region. This region was not highly impacted compared to other shorelines. But, in today's age because of problems like oil spillage from ship accidents, there is a decrease in the biodiversity of Alibaug beach. Instead of using the disposal method, we used tar residue in road construction because the mixture of tar residue and bitumen gives the somewhat same result as required for road construction. Marine tar pollution produces a very damaging effect on the ecological system as well as on human beings. This project gives general information about tar ball pollution. So from this, we can minimize the effect of marine pollution on the ecosystem of Alibaug Beach.

Acknowledgements I express my gratitude to Dr. Chelpa Lingam, Principal and Prof. Dr. Tejaswini D.N., Head of Civil Engineering Department, Pillai HOC College of Engineering and Technology, Rasayani, for their constant encouragement, co-operation and support. I also thankful to Mr. Raju P. Narwade, Associate Professor in Civil Engineering Department, for his support and constant encouragement throughout this work. I am thankful to my family members for providing the moral support, without which this work would not have been completed.

Bibliography

Andrady AL (2011) Microplastics in the marine environment. Mar Pollut Bull 62:1596–1605
Asuquo FE (1991) Tar balls on Ibeno-Okposo Beach of Southeast Nigeria. Mar Pollut Bull 22(3):150–151
Bacosaa HP, Kristen M et al (2016) The tar balls on Texas beaches following the 2014 Texas City "Y" spill: modeling, chemical, and microbiological studies. Mar Pollut Bull 109:236–244
Brekke C, Solberg AHS (2005) Oil spill detection by satellite remote sensing. Remote Sens Environ 95(2005):1–13
Corbin CJ, Singh JG, Ibiebele DD (1993) Tar ball survey of 6 Eastern Caribbean countries. Mar Pollut Bull 26(9):482–486
Derraik JGB (2002) The pollution of the marine environment by plastic debris. Mar Pollut Bull 44:842–852
Fingus M, Brown C (2014) Review of oil spill remote sensing. Mar Pollut Bull
Goodman R (2003) Tar balls: the end state. Spill Sci Technol Bull 8(2):117–121
Hu G, Xiao X (2013) Edge detection of oil spill using SAR image. Cross Strait Quad-Regional Radio Science and Wireless
Kankara RS, Arockiaraj S, Prabhu K (2016) Environmental sensitivity mapping and risk assessment for oil spill along the Chennai Coast in India. Elsevier, MPB-0756
Klemas V (2012) Remote sensing of coastal and ocean currents: an overview. J Coast Res 28(3):576–586
Krishan JG (2013) The present situation and ecological restoration methods of marine pollution in China. Geol Geosci
Maitieg AS (2017) Final thesis on, "Oil Spill assessment and coastal zone management planning for the Misratah coastline, Libya", by ARAN-Access to Research at NUI Galway
Mc Carthy J, Thomas M (2017) International and national principles and area based local application for sustainable coastal development. OMICS Int Coast Zone Manag 20:2
Misra A, Balaji R (2017) Simple approaches to oil spill detection using sentinel application platform (SNAP)-ocean application tools and texture analysis: a comparative study. J Indian Soc Remote Sens
Nambi IN, Rajasekhar B et al (2017) An assessment of subsurface contamination of an urban coastal aquifer due to an oil spill. Environ Monit Assess 189:148. https://doi.org/10.1007/s10661-017-5833-6
Payne JR (1982) The chemistry and formation of water-in-oil emulsions and tar balls from the release of petroleum in the marine environment. National Academy of Sciences, Washington
Rekadwad BN, Khobragade CN (2015) A case study on effects of oil spills and tar-ball pollution on beaches of Goa (India). MPB-07125:4
Solberg AHS (2012) Remote sensing of ocean oil-spill. IEEE Trans 100(10)
Suneel V et al (2015) Identifying the source of tar balls deposited along the beaches of Goa in 2013 and comparing with historical data collected along the West Coast of India. Sci Total Environ 527–528, 313–321
Varkey MJ (1999) Pollution of coastal seas. General Article, Resonance
Warnock AM, Hagen SC, Passeri DL (2015) Marine tar residues: a review. Water Air Soil Polluter 226:68. https://doi.org/10.1007/s11270-015-2298-5
Wate SR, Kumar A et al (2013) The final report, "Environmental Assessment of Mumbai Oil Spill from MV RAK Carrier", by MPCB & NEERI in April 2013
Wong CS, Green DR, Cretney WJ (1976) Distribution and source of tar on the pacific ocean. Mar Pollut Bull 7(6)
Zakaria MP, Okuda T, Takada H (2001) Polycyclic aromatic hydrocarbon (PAHs) and hopanes in stranded tar-balls on the coasts of Peninsular Malaysia: applications of biomarkers for identifying sources of oil pollution. Mar Pollut Bull 42(12):1357–1366

Chapter 29
A Study on Assessment of Groundwater Resources in a Basin by Water Table Fluctuation Method

D. Gouse Peera and R. Bhavani

Abstract In India assessment of groundwater is based on guidelines of the Groundwater Estimation Committee. Groundwater assessment is to be carried out with the current gross ground water draft, recharge from other sources, recharge from rainfall, net annual groundwater availability, current stage of groundwater development, water table trend, categorisation for future groundwater development, groundwater allocation for domestic and industrial water supply, net annual groundwater availability for future use. The study area considered for assessment of groundwater resources is Handri river basin, a tributary of the Tungabadra river in the Kurnool district of Andhra Pradesh.

Keywords Groundwater · Assessment · Recharge · Draft · River

29.1 Introduction

Groundwater resources estimations are very difficult. There are various methods for the computation of groundwater resources. The assessment of groundwater in India is based on the guidelines of the Groundwater Estimation Committee (GEC). Assessment of groundwater resources involves estimation of current gross groundwater draft, recharge from other sources i.e. other than rainfall, recharge from rainfall, net annual groundwater availability, current stage of groundwater development, water table trend, categorisation for future groundwater development, groundwater allocation for domestic and industrial water supply, net annual groundwater availability for future use. Water table data as recorded from a number of observation wells will be made use of in the assessment of groundwater.

D. G. Peera (✉)
AITS Rajampet, Rajampet, Andhra Pradesh, India
e-mail: gouse_mgr@yahoo.in

R. Bhavani
JNTUA Ananthapuramu, Anantapur, Andhra Pradesh, India

R. Jha et al. (eds.), *Groundwater and Water Quality*, Water Science and Technology Library 119, https://doi.org/10.1007/978-3-031-09551-1_29

Fig. 29.1 Study area Map

29.2 Study Area

The study area considered for assessment of groundwater resources is the Handri river basin, a tributary of the Tungabadra river in Kurnool district, which is in Andhra Pradesh state (India) lies between a latitude of 140 35′ 35″–160 09′ 36″ N and longitude of 750 58′ 42″–780 56′ 06″ of E (Fig. 29.1). The origin of sub-basin is between Pattikonda and Aspari and mingle in river Tungabhadra which is one of the major tributaries of river Krishna. The study area receives an average rainfall of 665 mm per annum. The geological formation consists of shales, limestones, granite gneisses and quartzites.

29.3 Data Used

Water table data as recorded from a number of observation wells will be made use of in the assessment of groundwater. Rainfall data was taken from 1995 to the present year. In the present study, data is taken for the command area only.

29.4 Methodology

In the present study groundwater assessment was carried out based on the guidelines of the Groundwater Estimation Committee (GEC). This assessment focused on the estimation of rainfall recharge. Out of the two methods namely Water Table Fluctuation Method and Rainfall Infiltration Factor Method which is guided by GEC former method is adopted. Rainfall recharge is estimated as follows

$$\text{Rainfall recharge during monsoon} = \left[\frac{\text{Normal monsoon rainfall}}{\text{Monsoon rainfall for years of assessment}}\right] * \text{Rainfall recharge} \quad (29.1)$$

$$\text{Rainfall recharge} = \text{Change GW storage} + \text{Gross GW draft for All uses} - \text{Recharge of other} \quad (29.2)$$

$$\text{Change in GW storage} = \text{Area} * \text{Water table fluctuation} * \text{Specific yield} \quad (29.3)$$

$$\text{Watertablefluctuation} = \text{Premonsoonwaterlevel} - \text{Postmonsoonwaterlevel} \quad (29.4)$$

29.5 Results and Discussions

In the present study, only the command area is studied. Three mandals fall under the command area namely Adoni-A, Adoni-C and Kodumur-A.

The water table trend has to be computed in each groundwater assessment unit for pre-monsoon and post-monsoon intervals in the command area, and pre-monsoon and post-monsoon intervals in the non-command area. In the present study water table trends are estimated for the command area only for both pre-monsoon and post-monsoon (Figs. 29.2 and 29.3). Rainfall recharge is estimated using Eqs. (29.1), (29.2), (29.3) and (29.4). Rainfall recharge is estimated for Mandal Adoni-A at 46 Ha.m, for Mandal Adoni-C at 170 Ha.m and for Mandal Kodumur-A at 47 Ha.m. (Fig. 29.4). Rainfall recharge values are also shown in Table 29.1.

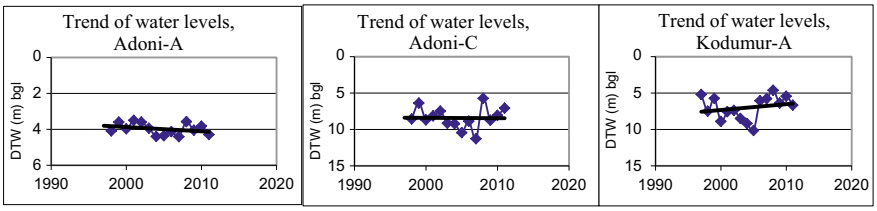

Fig. 29.2 Water table trends shown for pre-monsoon season for 3 Mandals

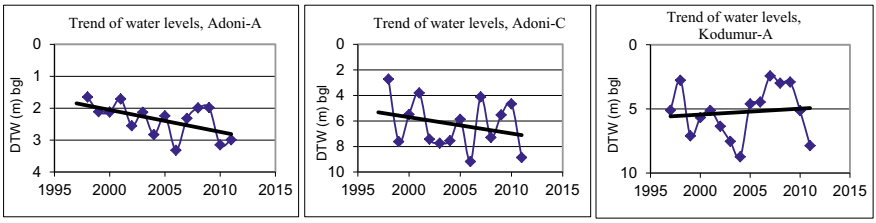

Fig. 29.3 Water table trends shown for post-monsoon season for 3 Mandals

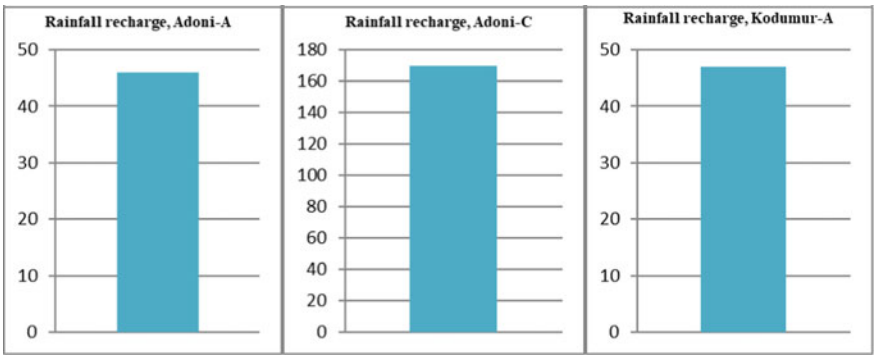

Fig. 29.4 Rainfall recharge values shown for 3 Mandals

Table 29.1 Rainfall recharge values for 3 Mandals

S. No	Mandal	Rainfall recharge Ha.m
1	Adoni-A	46
2	Adoni-C	170
3	Kodumur-A	47

29.6 Conclusions

Groundwater assessment is carried out based on recommendations of the Groundwater Estimation Committee (GEC). But rainfall recharge is only estimated using the water table fluctuation method. Rainfall recharge values are estimated for the command area only. For groundwater assessment, more data is required for a long duration. Present study was carried out with limited available data. Estimation of water table trends was also carried out in this study.

Bibliography

Batelaan O, De Smedt F (2001) WetSpass: a flexible, GIS based, distributed recharge methodology for regional groundwater modeling. Impact Human Activity on Groundwater Dynamics. IAHS Publ. no. 269, pp 11–17

Bhavani R (2015) Computation of yield based on weighted normal monsoon rainfall for Kundu sub-basin of Pennar basin. Int J Adv Sci Tech Res 7(5):25–31. ISSN 2249-9954

Central Ground Water Board (1987a) Hydrogeology and groundwater balance of the Vedavathi river basin in parts of Karnataka and Andhra Pradesh. An interim report

Central Ground Water Board (1987b) Water balance studies in upper Yamuna basin. Terminal report

Chatterjee R (2011) Groundwater resource estimation. J Geol Soc 77

Chavent G (1983) Local stability of the output least square parameter estimation technique. Math Appl Comput 2:3–22

Gousepeera D (2000) Estimation of specific yield and rainfall recharge factor in a regional groundwater system. M.Tech thesis., NITK, Surathkal, Karnataka

Ground Water Resource Estimation Methodology (2009) Report of the ground water resource estimation Committee, Ministry of water resources, Government of India

Groundwater Brochure, Kurnool District, Andhra Pradesh, Central Ground Water Board, Southern Region Hyderabad, September 2013, Ministry of Water Resources, Government of India

Karanth KR (1994) Groundwater assessment development and management. Tata McGraw Hill publishing Co., Ltd

Nagaraj MK (1999) Parameter estimation of regional ground water system. Ph.D thesis., IIsc., Bangalore

Nagaraj MK (2012) Estimation of aquifer parameters using inverse modeling by incorporating prior information about rainfall recharge factor as constraints. Int Sci J Earth Sci Eng 1001–1003

National Conference on Emerging Trends in the Development of Sustainable Groundwater Resources (1997) JNTU, Hyderabad p 361

Nowel Njamnsi Y (2009) Estimation for groundwater balance based on recharge and discharge: a tool for sustainable groundwater management, Zhongmu county alluvial plain aquifer, Henna province, China. J Am Sci 83–90

Pandian M, Rajasimman UAB (2014) Identification of groundwater potential recharge zones using WETPASS model in parts of Coimbatore & Tirupur districts in Tamilnadu, India. Int J Water Res 2(1):27–32

Pradeepkumar GN, Srinivas P (2009) Estimation of groundwater resources in a basin: a case study. IGC, Guntur, India, pp 590–594

Raghunath HM (1992) Groundwater. Willy Eastern Ltd, p 563

Sophocleous M. Groundwater recharge. Encyclopedia of life support systems

Umamaheswarrao B, Sankara Pitchaiah P (2015) Estimation of groundwater recharge of Yadalavagu sub-basin using rainfall infiltration factor method, and GIS, Prakasam district, Andhra Pradesh, India. Indian J Appl Res 5(9):685–687. ISSN: 2249–555X

Yashoda L, Meenambal T, Ranganna C (1990) Comparative analysis of for estimation of groundwater potential—a case study for Hosur block, Krishnagiri district, Tamilnadu. Int J Innov Res Technol Sci 1:4–8. ISSN:2321–1156

Chapter 30
Simulation of Soil Moisture Movement and Solute Transport Characteristics in Parts of Malaprabha Sub Basin

B. K. Purandara, N. Varadarajan, Sudhir Kumar, B. Venkatesh, and J. V. Tyagi

Abstract In recent years, the advancement in agriculture with special emphasis on crop yield has encouraged farmers to apply large quantities of fertilizers and pesticides. As the top soils are enriched with high organic matter and clay, particularly in black soils, promotes sorption, biological degradation and transformation of contaminants. During the process, some of the chemicals applied to farmland, move down with the deep percolating water from the root zone and pollute the underlying groundwater. Therefore, the present study was carried out to understand the effects of different soil texture configurations on water movement and solute transport to provide a reliable scientific basis for the application of negative-pressure irrigation (NPI) technology. Two agricultural plots (Sugarcane and banana plantation) located in parts of the Malaprabha sub-basin covering parts of (Belagavi district) were identified, and the transport process was modelled using a HYDRUS-1D model. Hydraulic properties such as infiltration, hydraulic conductivity and soil textures were determined using field and laboratory methods. It is observed that in the layered soils, when a coarse texture of loamy soil is present below the fine textured soils such as silty loam or clayey loam, irrigation water accumulated in the top soil, and this led to an increase in evaporation compared with the homogeneous loam profile. However, fine texture silty loam or clay loam layers beneath the loamy soil was more conducive to water infiltration into the lower layer, and this increased the amount of water infiltration and simultaneously reduced the surface evaporation effectively. It is also noticed that the layered soils have obvious effects on solute transport under NPI, and salt accumulation readily occurs in the clay-rich soil layer at the interface. The average salt accumulation observed in the study area within the soil profile is 19.87 g/kg. The maximum salt accumulation that occurred in the top layer is 24.54 g/kg in the sugarcane plots and 17.85 g/kg in the banana plantation. The study also indicated that interlayered soils showed remarkable changes in the water infiltration characteristics and salt-leaching intensities under NPI, and also indicated that the properties

B. K. Purandara · N. Varadarajan · B. Venkatesh (✉)
National Institute of Hydrology, Hard Rock Regional Center, Visvesvarayanagar, Belagavi, Karnataka 590019, India
e-mail: bvenki30@gmail.com

S. Kumar · J. V. Tyagi
Scientist 'G', NIH, Jal Vigyan Bhavan, Roorkee, Uttarakhand 2447267, India

R. Jha et al. (eds.), *Groundwater and Water Quality*, Water Science and Technology Library 119, https://doi.org/10.1007/978-3-031-09551-1_30

of the soil profile with a silty loam interlayer are better than with a silty clay loam interlayer.

Keywords Infiltration · Soil moisture · Solute transport · HYDRUS-1D and negative pressure irrigation

30.1 Introduction

Soil moisture movement and solute transport processes are mutually dependent and play a significant role, particularly in arid and semi-arid regions where the imbalance between incoming and outgoing salt occurs which ultimately resulted in the accumulation of salts in the irrigated soils. Therefore. It is very important to understand the extent of salinity hazards in areas where the water intensive crops are grown. The transport of reactive chemicals accumulated in the root zone moves through the porous media and undergoes various kinds of chemical transformation due to processes such as advection, diffusion and dispersion. In addition, it involves other mechanisms like rate-limited sorption and desorption, biodegradation, and chemical reaction. The downward movement of a chemical in an agriculture field can be measured by applying a known amount of the chemical at the surface and then measuring solute concentration one or more times later. The increase in the amount of the chemical may be found at different depths in all or part of the unsaturated zone. Alternatively, the downward movement may be represented more simply by the increase in the amount of the chemical below some arbitrary depth, such as the root zone. In most instances, the chemical forms added in fertilizers are the same as those naturally present in soils and absorbed by plants, but in some instances, the forms added are transformed after addition to the forms naturally present in soils. Researchers have different opinions on the effects of initial SWC on the degree of preferential flow and transport (Shipitalo et al. 1990; Edwards et al. 1992; Hanson et al. 1998; Kung et al. 2000; Katterer et al. 2001; Hardie et al. 2011). The higher the application rate was, the more preferential flow was observed (Quisenberry et al. 1994; Hawke et al. 2006). Elango and Sivakumar (2007) carried out groundwater modeling studies in Tamilnadu for understanding the movement of contaminant in the Kalpakkam area. Varalakshmi et al. (2014) carried out, modeling studies with particular reference to hard rock areas. Though there are limited studies available with reference to solute Water Quality monitoring and Modeling studies were carried out in Ghataprabha command by a number of researchers viz. Purandara et al. (2002), Hebsur (2005) and Varadarajan (2013). Groundwater modeling study was carried out by Anju et al. (2015) for Malaprabha command and successfully simulated the groundwater levels of both open and bore wells using a mathematical model viz. MODFLOW. The study reported here combines both field measurements and model predictions that are based on the Richards equation. HYDRUS-1D model was applied to two sections of Malaprabha sub-basin (one in headwater catchment

with sandy and loamy soil and the other downstream region dominated by black and clayey soils).

30.2 Study Area

Malaprabha River originates in the Western Ghats at an altitude of 792 m at Kanakumbi village, Khanapur taluka, Belagavi District, Karnataka state. Malaprabha sub-basin lies between latitude 15° 28′ 27.75″ N to 16° 5′ 43.62″ N and longitude 74° 12′ 34.5″ E to 75° 17′ 9′ E. The catchment area of the sub-basin is about 3000 km^2. The study area covers parts of Belagavi, Khanapur, Bailahongal, Savadatti and Ramadurga Taluks of the Belagavi district. It flows North–East and North–West and joins the river Krishna at Kudalasangam in the Bagalkot district of Karnataka (Fig. 3.2). The approximate length of the river is 306 km (point of confluence at Kudal sangam). The Bennihalla and the Hirehalla are the principal tributaries of the river Malaprabha. To harness the water of the Malaprabha river, a dam is constructed at Naviluteerth village, Savadatti taluk of Belagavi District to impound 1377 MCM (37.7 TMC) of water. The location of the Malaprabha is shown in Fig. 30.1. The climate of the Malaprabha basin is influenced by the south-west monsoon (June–September), which accounts for 91% of the total rainfall. The average annual rainfall of the catchment is 2259 mm. The temperature varies between 19.2 °C and 29.5 °C and the mean evaporation is 1496.9 mm. The average annual discharge at the Khanapur gauge site is 8953.6 cumecs.

The catchment can be topographically divided into three units. The first unit between altitudes 662–1038 m, forming the uppermost reaches, is a narrow and deep valley bounded by the high hills. The slope in this region varies from 30 to 50%. The streams in this region are located in this valley and are characterized by rocky beds and wide streams, with large discharges. The second unit is comparatively less undulating and the slope varies from 10 to 30%. Most of this region is covered by forests and small isolated villages and agricultural fields in between. This area is identified between the hills and the valley plains. The streams are narrow and gently sloped, with low discharges. The third unit comprises plain lands with gentle slopes of less than 5% in the plains and increasing to 10% towards the hilly regions. Streams in this region are wide with rocky bottoms and low velocity.

Geologically, the area comprises of tertiary basalt over 96% of the area and sedimentary formations of the Pre-Cambrian age. There are two types of soils found within the basin; red loamy soil, which covers about 80% of the basin and medium black soil. About 63% of the total area is covered by forests, 17% by agricultural lands and the rest by shrubs and fallow land. According to the reports from Central Ground Water Board (CGWB), Ramdurg, Saundatti and Nargund taluks had a yearly rainfall varying between 221–836 mm, 224–894 mm and 181–1166 mm respectively. Wheat, cotton, jowar, and groundnut were a few of the agricultural crops cultivated in the Malaprabha sub-basin. Canal water is used during the Rabi season and the water was available only for 3–4 months which was utilized for agricultural requirements. Less

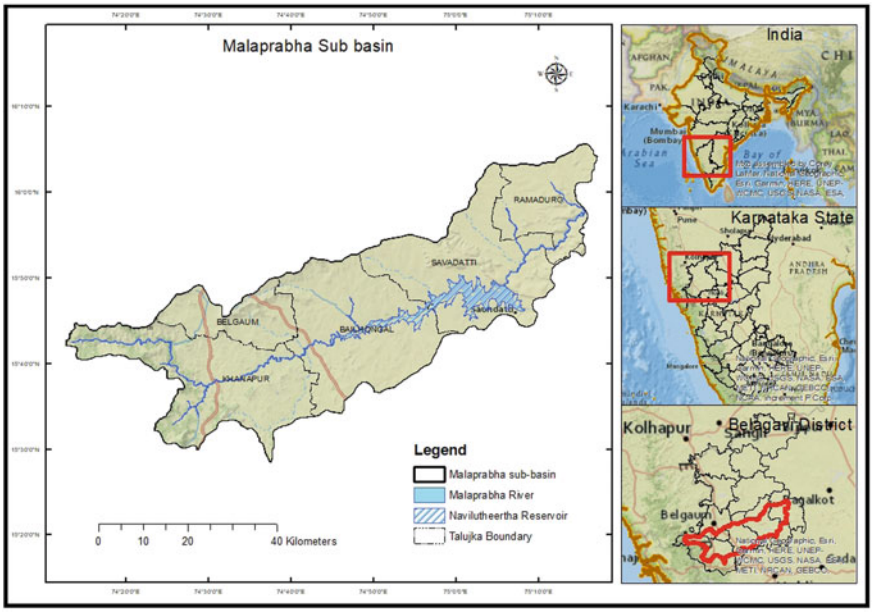

Fig. 30.1 Location map of study area

precipitation and high temperature made the entire command area dry. As a result, residents were compelled to take water from the dug wells and bore wells to fulfill their domestic requirements. Over exploitation of wells to fulfill human needs has caused the present conditions of scarcity of water. According to the present scenario, drilling of new bore wells or dug wells has been banned in the area.

30.3 Modelling Using HYDRUS-1D

HYDRUS-1D is a public domain computer software package that simulates the one-dimensional movement of water, heat and multiple solutes in variably saturated media. It numerically solves Richards's equation for variably-saturated water flow and advection–dispersion type equations for heat and solute transport. The governing partial differential equation (Richards' equation) applicable for one-dimensional flow in the unsaturated zone can be written as.

$$\frac{\partial \theta}{\partial t} = \frac{\partial}{\partial x} K \left[\frac{\partial \psi}{\partial x} + \frac{dz}{dx} \right] + S$$

where, θ = volumetric water content [cm^3/cm^3]; t = time [h]; x = distance into the soil [cm soil]; K = hydraulic conductivity [cm^2 water/cm soil/h]; ψ = matric potential

[cm water]; z = gravitational potential [cm]; S = sink strength [cm^3 water/cm^3 soil/h].

30.4 Simulation of Water and Solute Movement Using HYDRUS-1D Model

30.4.1 Input Data

1. Precipitation: Rainfall of study area were given as input for time variable boundary conditions in HYDRUS-1D model. The average rainfall of the area varies from 221.3 to 2259 mm/yr.
2. Soil hydraulic properties: Saturated hydraulic conductivity was measured in the study area by using disc permeameter apparatus for different depths. Collected soil samples from locations were analyzed in the laboratory to know the soil's hydraulic properties. The results were used as input to the model. Table 30.1 shows the soil and lithological characteristics of the study area.
3. Geometry information: As an input to the HYDRUS-1D model, the geometry of the study area based on the number of soil types, total depth of the soil profile and cell size of each unit can be defined as per the local hydrological conditions.
4. Time information: Under this section, time units, time discretization, and time-variable boundary conditions need to be included. In the present case, the unit of time was in hours and initial time is 0 and the final time is 24 days.

Table 30.1 Model parameters based on soil and lithology

Catchment zones	Soil type	Saturated hydraulic conductivity (mm/hr)	Saturated moisture content (θs)	Residual moisture content (θr)	Van Genuchten parameters	
					α	n
Headwater catchment	Red sandy	30	0.372	0.09	0.00085	1.378
	Clayey skeletal	18	0.44	0.19	0.00185	1.265
	Loamy	24	0.38	0.15	0.00029	1.447
Downstream part of Malaprabha sub basin	Black	9	0.46	0.22	0.00168	1.276
	Mixed	12	0.39	0.18	0.00171	1.432

30.5 Simulation Results

Modeling was done in two parts (i) headwater zone between Kankumbi and Khanapur dominated sandy and loamy with sugarcane and jowar as major crops, (ii) Khanapur downstream to Naviluteerth dam and adjoining parts of command area. Experiments were carried out in plot level based on the dominant crops grown in the area, i.e. sugarcane and jowar in upstream and sugarcane and grams in the downstream region. During the investigations and from the laboratory study, it is observed that there is a significant variation in the moisture content in the sugarcane plot as compared to the adjoining jowar plot. Figure 30.2 explains the variation of moisture with depth in the sugarcane plot located in the upstream part (Khanapur taluk). It is noticed that the wetting and drying processes depend on the hydrological behaviour of soils. The relative percentage of moisture is lower in the top soil and below few cms, there is a significant increase in moisture contents which could be attributed to the presence of fine clay materials in various pockets of Khanapur taluk. Further, it is presumed that the variations could be due to the irrigation scheduling of crops without adopting scientific procedures. Further, sugar cane consumes more water resulting in early drying of soils in deeper layers and therefore, farmers apply water randomly due to which there is a probability of wider variation in water content.

In Fig. 30.3, the solute concentration of nitrate is considered for the simulation. Top layers have shown significant movement of solutes due to the high surface permeability and drainage characteristics of red soil. However, an accumulation of nitrate content is observed at a depth between 0.6 and 1 m, below which there is a decline in the concentration with depth. The distinct trend observed in the two soil layers could be attributed to the variation in soil texture where the top soil is predominantly loamy in nature which is underlain by medium to heavy loam. Therefore, the trend of solute movement indicates the absence of higher nitrate content in the bottom layers and also in the groundwater of the study area.

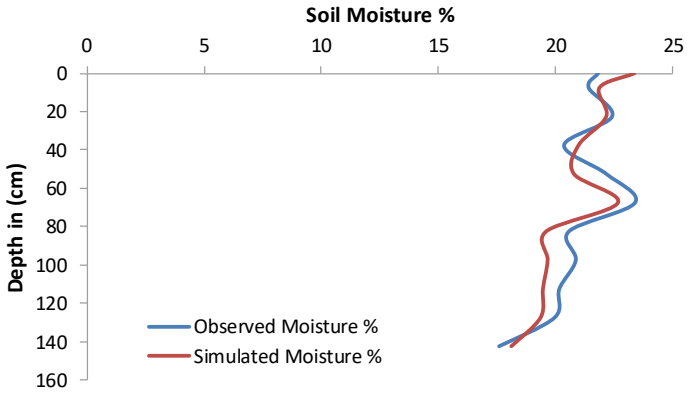

Fig. 30.2 Simulated and observed soil moisture by HYDRUS-1D model in parts of Khanapur taluk

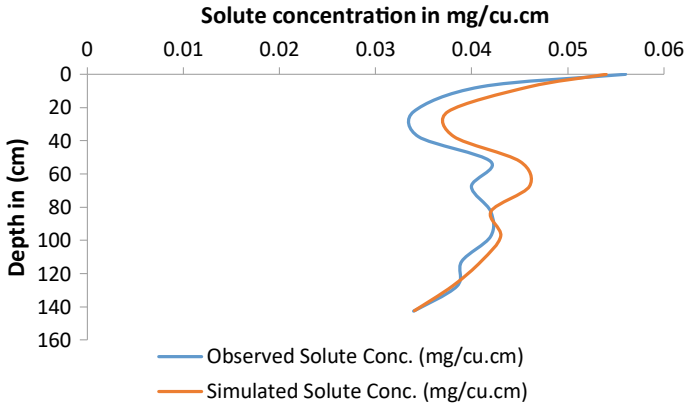

Fig. 30.3 Simulated and observed Solute concentration by HYDRUS-1D model in parts of Khanapur taluk

Figures 30.4 and 30.5 shows the observed and simulated soil moisture distribution and nitrate distribution at varying depth in parts of the command area dominated by black soils. The observed and simulated moisture profiles ($r = 0.76$) showed a reasonably good match except between 15 and 30 cm depth. This is attributed to high temperature conditions existed in the downstream where the top soil dries out fast and shows wide cracks in the soil providing means for preferential flow of both water and solute. However, in the case of solute movement, the results showed a significantly higher correlation ($r = 0.92$) between observed and simulated profiles. In both cases, the solute concentration for the simulation was the observed concentration at an identified site before and after the irrigation (24 days from the date of first irrigation).

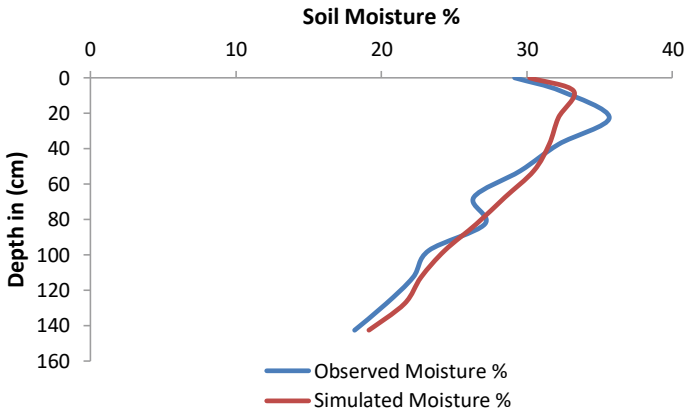

Fig. 30.4 Simulated and observed soil moisture by HYDRUS-1D in downstream parts of Malaprabha sub basin

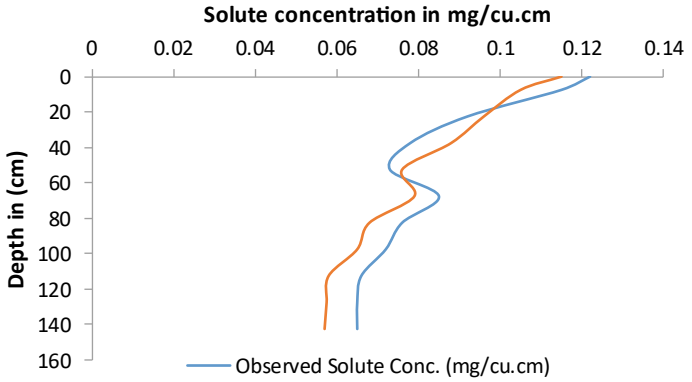

Fig. 30.5 Simulated and observed solute conc. by HYDRUS-1D in downstream parts of Malaprabha sub-basin

30.6 Conclusion

The modeling of water and solute movement using the HYDRUS-1D model may be highly useful for soil moisture and solute movement prediction. Soils in the region are dominated by loamy to fine textured on the top followed by medium to heavy loam which significantly restricts the downward movement of soil under negative pressure irrigation. It is further noticed that there is an accumulation of solute between the interface of loamy and clayey layers. In the headwater catchment (Khanapur). However, in the downstream part of the Malaprabha sub-basin covering parts of the command area, soil moisture showed significant variation which could be attributed to irrigation scheduling and also due to the occurrence of preferential flow paths. This is further supported by relatively lower solute accumulation (18.7 g/kg) at the interface (clay rich and organic rich) in headwater catchment dominated by loamy soils, whereas, in the downstream (dominated by fine clayey black soils) salt accumulation was higher with 27.8 g/kg in the sugarcane plot. Soils found in the interlayers showed remarkable changes in the water infiltration characteristics and salt-leaching intensities under NPI. At the outset, the results demonstrated that soil texture configurations have a significant influence on water movement and solute transport under NPI. Therefore, careful consideration should be given to the use of NPI to achieve target soil water and solution conditions and reduce water loss.

Acknowledgements Authors are highly grateful to Dr. S. K. Jain, Director, NIH, Roorkee for his constant encouragement and support for carrying out the study and to bring out the publication.

References

Elango L, Sivakumar C (2007) Groundwater modelling to predict the migration of solutes in subsurface environment. In: Puranik VD et al (eds) Mitigation of pollutants for clean environment. Macmillan Publications, pp 102–108

Hanson JD, Ahuja LR, Shaffer MD, Rojas KW, DeCoursey DG, Farahani H, Johnson K (1998). Agric Syst (Elsevier) 57(2):161–195

Hardie MA, Cotching WE, Doyle RB, Holz G, Lisson S, Mattern K et al (2011) Effect of antecedent soil moisture on preferential flow in a texture-contrast soil. J Hydrol 398:191–201. https://doi.org/10.1016/j.jhydrol.2010.12.008

Hawke RM, Price AG, Bryan RB et al (2006) The effect of initial soil water content and rainfall intensity on near-surface soil hydrologic conductivity, a laboratory investigation. Catena 65:237–246. https://doi.org/10.1016/j.catena.2005.11.013

Hebsur NS (2005) Groundwater quality appraisal of Malaprabha and Ghataprabha command areas and its impact on crop production and soil health. PhD thesis, University of Agricultural Sciences, Dharwad

Katterer T, Schmied B, Abbaspour KC, Schulin R (2001) Single- and dual-porosity modelling of multiple tracer transport through soil columns: effects of initial moisture and mode of application. Eur J Soil Sci 2001(52):25–36. https://doi.org/10.1046/j.1365-2389.2001.00355.x

Kung KJS, Steenhuis TS, Kladivko EJ, Gish TJ, Bubenzer G, Helling CS (2000) Impact of preferential flow on the transport of adsorbing and non-adsorbing tracers. Soil Sci Soc Am J 2000(64):1290–1296. https://doi.org/10.2136/sssaj2000.6441290x

Purandara BK, Varadarajan N, Kumar CP (2002) Simulation of solute transport in parts of Ghataprabha command of Bagalkot and Biligi Taluks. NIH Technical Report (Unpublished), Karnataka

Quisenberry VL, Phillips RE, Zeleznik JM (1994) Spatial distribution of water and chloride macropore flow in a well-structured soil. Soil Sci Soc Am J 58(5):1294–1300. https://doi.org/10.2136/sssaj1994.03615995005800050003x

Shipitalo MJ, Edwards WM, Dick WA, Owens LB et al (1990) Initial storm effects on macropore transport of surface-applied chemicals in no-till soil. Soil Sci Soc Am J 54:1530–1536. https://doi.org/10.2136/sssaj1990.03615995005400060004x

Varadarajan N (2013) Ground water quality assessment in the salinity affected areas of Ghataprabha command, Karnataka (India). PhD thesis, National Institute of Hydrology, Belagavi

Varalakshmi V, Venkateswara Rao B, Suri Naidu L, Tejaswini M (2014) Groundwater flow modeling of a hard rock aquifer: case study. J Hydrol Eng 19(5):877–886

Varghese AA, Raikar RV, Purandara BK (2015) Simulation of groundwater levels in Malaprabha command area using visual MODFLOW FLEX. Int Res J Eng Technol (IRJET) 434–440

Chapter 31
Oxygenation in Turbulent Flows Over Block Ramps

Thendiyath Roshni, Stefano Pagliara, and Vishal Singh Rawat

Abstract A significant oxygenation is associated with flows over most of the hydraulic structures due to the entrainment of air into the flow. Block ramps (BR) are low-head hydraulic structures which contribute to considerable oxygenation and act as natural aerators in riverine flows. BR uniquely serves an essential paradigm in riverine management, to encounter deliveries in an ecologically sound manner. It permits safe fish passage, stabilizes stream banks and bed profiles and creates habitat diversity. The present experimental study investigates the oxygenation process in turbulent flows over BR. Air concentrations were measured using an air concentration probe for three different discharges ($Q = 9$, 15 and 21 L/s) in the uniform flow region. Oxygen concentration is determined from the air concentration as ambient air is entrained in the flows over BR. Longitudinal variations of the average oxygen concentration have been studied using air concentration profiles and oxygen profiles and plotted in the uniform region for the tested range of discharges and slopes. An empirical expression is also developed to estimate the average oxygen concentration (O_m) for $S = 27.5\%$ in the uniform flow region. The results show that in the tested range of discharge and slope there is a reduction of oxygen concentration in the uniform flow region.

Keywords Aeration · Block ramps · Oxygenation · Turbulent flows

T. Roshni · V. S. Rawat (✉)
Department of Civil Engineering, National Institute of Technology Patna, Bihar 800005, India
e-mail: vishaalssr@gmail.com

T. Roshni
e-mail: roshni@nitp.ac.in

S. Pagliara
DESTEC-Department of Energy, Systems, Territory and Construction Engineering, 56122 Pisa, Italy
e-mail: s.pagliara@ing.unipi.it

R. Jha et al. (eds.), *Groundwater and Water Quality*, Water Science and Technology Library 119, https://doi.org/10.1007/978-3-031-09551-1_31

31.1 Introduction

Flow over block ramps occurs in nature as flow in rocky rivers, flow over gravel beds etc. The flow over the block ramp develops two-phase flows and the flow is very dynamic in nature. In the case of Mountain Rivers, the presence of large rocks and boulders with steep slopes results in a complex velocity and thereby the flow appears to be highly turbulent. Due to the turbulent nature of the flow, ambient air entrains and leads to a complex two-phase flow. Only a very few literature (Pagliara et al. 2010a, b, 2011a, b, 2015) can be seen in studies related to air–water flow. This air-entrained flow is a complex two-phase flow, where water resources engineers have to be more focused.

In rocky rivers, the boulders found lie in the range of 0.60 m < D_{50} < 0.80 m and the slope of the rocky rivers vary from 10–40% with a height of 2–3 m (Baturst 1985). These boulder pathways enact as a natural stream restoration structure that ensures the morphological continuity of the river and it also guarantees the biotic continuity of the watercourse. As the rocks or boulders are freely available in the premises of the rock- riverbed and arrangement of the rocks/boulders in a regular, fashion leads to an eco-friendly less environmental impact hydraulic structure. The water flow over the rocky beds arises several wake and fall effects, which in turn leads to more energy dissipation (Pagliara et al. 2015). The energy dissipation is because of the variation of stream slope and due to different roughness conditions formed by the bed material (Boes 2000; Boes and Minor 2000). A few studies happened on the stability of the ramps and found that the stability can be improved by incorporating boulders in different configurations over the base ramps (Boes 2000; Boes and Minor 2000; Boes and Hager 2003a, b). This ramp flow allows fish migration, reduces solid transport, and problems with landscape insertion (Bezzola 2002). These ramps can be used as an alternative structure for drop structures and can be placed in the downstream of hydraulic structures for the smooth transition of flow to the river (Bindo et al. 1993).

The study of aerated flows over ramps is very limited and has received little attention among the Hydraulic engineer's society. In ramp flow, many researchers have concentrated in the flows over uniform flow region. In this paper, authors have tried to develop an expression for finding the oxygen content for discharge varying from 9 to 21 L/s for a slope of 27.5%. Also, the oxygen concentration profiles in the uniform flow region for the tested range of discharges are also studied.

31.2 Experimental Setup and Data Collection

Experimental data were collected from Pagliara et al. (2010a, b) for a slope of 27.5%. The ramp properties and D_{84} of the material used are detailed in Pagliara et al. (2010a, b). The experiments were conducted on a tilting flume in which the recirculation of flow is ensured (Fig. 31.1). The length of the flume is 7 m long and 30 cm wide. The discharge varies from 9 to 21 L/s. The air concentration was measured using a

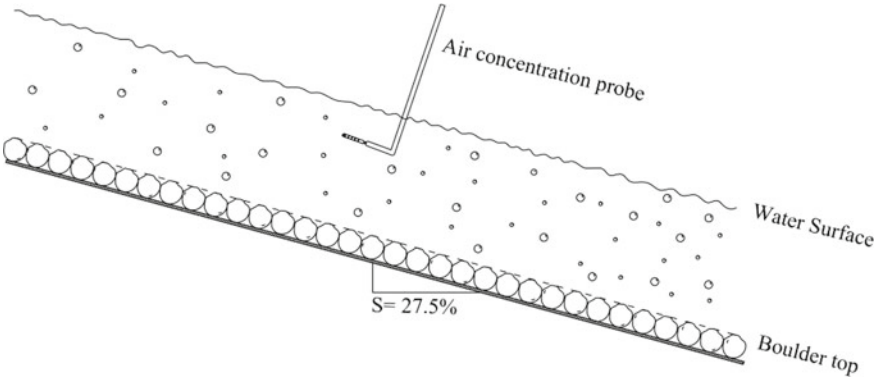

Fig. 31.1 Flow profile in aerated flows over a ramp at a slope of 27.5%

double tip conductivity probe. The flow meter ensures the discharge into the flume. Data have been collected for different cross-sections from 3.0 to 6.2 m. At each longitudinal section, 5 cross-sectional data have been taken for data analysis from the physical top to the y_{90} depth. Where y_{90} is the depth of flow corresponding to 90% of air concentration. In each cross-section, from the physical top, air concentration measurements were taken at a 3 mm step.

31.3 Data Analysis

Considering that the same ambient air is entrapping in the aerated flows (Pagliara et al. 2011a), it is well known that approximately 20% of ambient air contains oxygen (https://en.wikipedia.org/wiki/Atmosphere_of_Earth). At each longitudinal section, representative cross-sectional data from physical top to y_{90} is calculated. Each depth data is calculated by taking an average of 5 sectional data at that particular depth and so on. The longitudinal profile for each discharge is analysed using MATLAB 2015 tool. The equivalent depth of flow denoted as d_e (Pagliara et al. 2010a, b) has been established as:

$$d_e = 0.2D_{65} + \int_{y=0}^{y=y_{90}} (1 - C)dy = 0.2D_{65} + y_{90}(1 - C_m) \tag{31.1}$$

where, C is the air concentration at different depths, D_{65} is the particle size and C_m is the average air concentration.

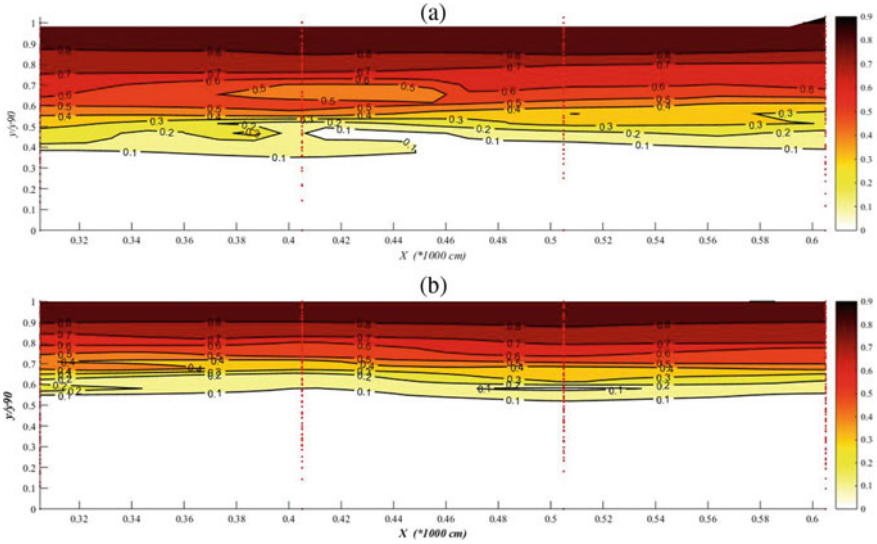

Fig. 31.2 Air concentration profile at different longitudinal distances for **a** 9 L/s and **b** 21 L/s

31.4 Results

31.4.1 Uniform Flow Properties

Flow properties like depth of flow and air concentration were measured for a longitudinal length of 3 m from the inlet of the flume to the end of the flume. Figure 31.2a, b show the longitudinal air concentration profile for a discharge of 9 and 21 L/s. As it is observed from Fig. 31.2a that except for a few disturbances in the aeration profile at different depths, the rest of the aeration data is uniform in the longitudinal direction. The disturbance is due to lesser discharge and the protruding ramp material. This is very clear from Fig. 31.2b that air concentrations at different depths follow same parallel line at different longitudinal distance. As it is evident from Fig. 31.2a, b that the flow region from 3 m till 6.2 m lies in the uniform flow region.

31.4.2 Average Oxygen Concentration (O_m)

The oxygen concentration is computed by considering 20% of ambient entrapped air as oxygen. Oxygen concentration is then averaged in the uniform flow region resulting in average oxygen concentration (O_m). O_m is calculated for 9, 15 and 21 L/s. The d_e/D_{84} for all the different discharges are calculated as per the Eq. (31.1). A plot of average oxygen concentration (O_m) for various equivalent depths is depicted

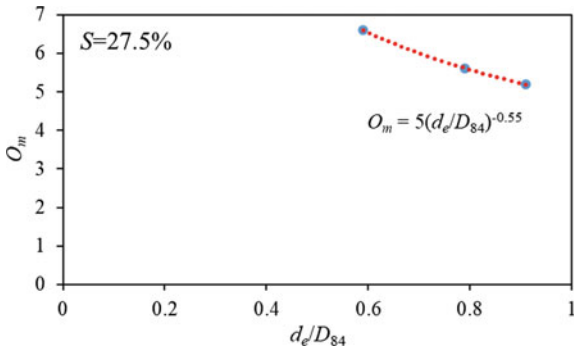

Fig. 31.3 A plot of O_m for different equivalent depth at slope 27.5%

in Fig. 31.3. It is seen in the figure that with the increase in the equivalent depth, the average oxygen concentration decreases. With the experimental data, an expression is developed for finding oxygen concentration for a slope of 27.5%. It is given as

$$O_m = 5.\left(\frac{d_e}{D_{84}}\right)^{-0.55} \tag{31.2}$$

31.5 Conclusions

The studies of aeration property over block ramps/rock chutes are very limited. The flow properties are measured in the uniform flow region for all experimental studies. However, the uniform flow region is demarcated by visual comparison from the non-uniform flow region. Hence, in this study, the main two objectives set were: (1) to validate the flow properties in the uniform flow region with that of visual flow and (2) to develop an expression for finding the average oxygen concentration in the uniform flow region for a slope of 27.5%.

The results reveal that the flow properties measured from a longitudinal distance of 3–6.2 m lie in the uniform flow region for all the discharges lying between 9–21 L/s. An empirical expression is developed for finding the average oxygen concentration for 27.5% slopes against different equivalent depths.

References

Baturst JC (1985) Flow resistance estimation in Mountain Rivers. J Hydraul Eng 111(12):625–643

Bezzola GR (2002) Fliesswiderstand und Sohlenstabilität natürlicher Gerinne unter besonderer Berücksichtigung des Einflusses der relativen überdeckung. Mitt. ETH-VAW, 173, Zurich, Switzerland

Bindo M, Gautier J, çacroix F (1993) The stepped spillway of M'Bali Dam. Int Water Power Dam Constr 45(1):35–36

Boes RM (2000) Scale effects in modelling two-phase stepped spillway flow. In: Minor HE, Hager WH (eds) Proceedings of hydraulics of stepped spillways. Balkema, Rotterdam, pp 53–60

Boes RM, Hager WH (2003a) Hydraulic design of stepped spillways. J Hydraul Eng 129(9):671–679

Boes RM, Hager WH (2003b) Two-phase flow characteristics of stepped spillways. J Hydraul Eng 129(9):661–670

Boes RM, Minor H-E (2000) Guidelines for the hydraulic design of stepped spillways. In: Minor H-E, Hager WH (eds) Proceedings of hydraulics of stepped spillways. Balkema, Rotterdam, pp 163–170

https://en.wikipedia.org/wiki/Atmosphere_of_Earth

Pagliara S, Carnacina I, Roshni T (2010a) Air-water flows in presence of staggered and row boulders under macro-roughness conditions. Water Resour Res 46(8):11

Pagliara S, Carnacina I, Roshni T (2010b) Self-aeration and friction over rock chutes in uniform flow conditions. J Hydraul Eng 136(11):959–964

Pagliara S, Carnacina I, Roshni T (2011a) Inception point and air entrainment on flows under macro-roughness conditions. J Environ Eng 137(7):629–638

Pagliara S, Roshni T, Carnacina I (2011b) Turbulence, aeration and bubble features of air-water flows over macro- and intermediate roughness. Water Sci Eng 4(2):170–184

Pagliara S, Roshni T, Michele P (2015) Energy dissipation over large-scale roughness for both transition and uniform flow conditions. Int J Civ Eng 13(3); Trans A: Civ Eng 341–346

Chapter 32
Seasonal Variations of Major Ion Chemistry and Solute Fluxes of Meltwater of River Bhagirathi, a Himalayan Tributary, India

M. K. Sharma, Renoj J. Thayyen, C. K. Jain, Manohar Arora, and Shyamlal

Abstract River Ganga originates from the portals of the Gangotri glacier which is the largest glacier in the Ganga basin. Meltwaters of the Himalayan tributaries and streams originating from the glaciers and snow in the basin are characterised by its low ionic concentrations which dilute the solute and pollutant load in the river. Hence, any change in the quality and quantity of the Himalayan tributaries under the climate change regime will affect the quality parameters of the River Ganga as well. The stream runoff in the Himalayas tributaries has significant seasonal variations forced by the melting of the winter snow preceded by the summer monsoon rains and intervening dry periods forcing lean flows. In the present paper, seasonal variations of major ion chemistry and solute fluxes of meltwater of River Bhagirathi (River Ganga originating from glacier) have been discussed covering three consecutive melt seasons from 2014 to 2016. The results revealed that the anions for all sampling seasons in decreasing order were observed to be $SO_4^{-2} > HCO_3^- > Cl^- > NO_3^-$. Sulphate was the dominant anion accounting for 75.4% during rising limb of hydrograph, 75.2% during peak flow and 77.9% during falling limb of hydrograph of total anions (TZ^-). Bicarbonate was the next dominant anion after sulphate accounting for 21% during rising limb of hydrograph, 22% during peak flow and 20% during falling limb of hydrograph of total anions. First possibility of acquiring SO_4^{-2} content in the Gangotri glacier meltwater is the dissolution of sulphate minerals (gypsum and anhydrite), whereas the second possibility is sulphide oxidation. The cations for all sampling seasons in decreasing order were observed to be $Ca^{2+} > Mg^{2+} > K^+ > Na^+$. Calcium was the dominant cation accounting for 64.9% during rising limb of hydrograph, 69.1% during peak flow and 59.8% during falling limb of hydrograph of total cations (TZ^+). Magnesium was the next dominant cation after calcium accounting for 19.8% during both rising limb of hydrograph and peak flow and 22% during falling limb of hydrograph of total cations. The seasonal variation of the dissolved ions in the Gangotri glacier meltwater indicates that generally dissolved ions concentration was low during the peak flow period and high during rising and falling limb period of hydrograph. Such dissolved ion concentration variations are

M. K. Sharma (✉) · R. J. Thayyen · C. K. Jain · M. Arora · Shyamlal
National Institute of Hydrology, Roorkee 247667, Uttrakhand, India
e-mail: sharmamk.1967@gmail.com; mks.nihr@gov.in

R. Jha et al. (eds.), *Groundwater and Water Quality*, Water Science and Technology Library 119, https://doi.org/10.1007/978-3-031-09551-1_32

indicative of climatic control on the intensity of different processes operating in the study area. Solute fluxes in glacial meltwaters usually increase with discharge in an aquatic system. The largest solute fluxes are transported by the most dilute meltwater as solute concentration is usually inversely related to discharge. Fluxes of all major dominating cations (Ca^{+2} and Mg^{+2}) and major dominating anions (HCO_3^- and SO_4^{-2}) follow the same trend as that of discharge. Suspended sediment concentration and load are low during the low discharge period (falling limb) and high during the high discharge period (monsoon + Glacier melt). These seasonal variations in suspended sediment concentration during the study period may be attributed to the progression of subglacial drainage network development. The distributed channel system in the subglacial zone is dormant during the winter season with less water availability and high overburden pressure of glacier ice. As melt season progresses, more and more snow and glacier melt routed to the subglacial zone and the distribution channel spread to the higher elevations of the glacier. Higher sediment flux from the glacier is also indicative of good integration of the distributed system. These processes are also linked with the solute acquisition in the meltwater, which could be distinctly different for Alpine and Himalayan glacier systems.

32.1 Introduction

Most of the large river systems of the world originate from mountains where a significant quantity of fresh water is stored in the form of snow and glaciers. The Himalayas is the youngest and tallest mountain system which includes the world's most erosion prone regions (Pandey et al. 1999). The glacier distribution in the Himalayas is uneven with higher concentrations in northwest as compared to northeast Himalayas (Vohra 1981; GSI 1999). Seven great Asian rivers: Ganga, Indus, Brahmaputra, Yangtze, Huang He or Yellow River, Salween and Mekong are fed by Himalayan glaciers. Total number of glaciers in the Indus, Ganga and Brahmaputra basins are 16,049, 6237 and 10,106 covering total glaciated areas of 32,246.43, 18,392.90 and 20,542.75 km^2, respectively (SAC 2011) and have substantial contribution of annual runoff from the melting of snow and glaciers. River Ganga originates from the portals of the Gangotri glacier which is the largest glacier in the Ganga basin.

The stream runoff in the Uttarakhand Himalaya has significant seasonal variations forced by the melting of the winter snow preceded by the summer monsoon rains and intervening dry periods forcing lean flows. The runoff from the glacierized valleys of the Ganga river basin is first fed by snowmelt as the transient snowline recedes, which results in discharge from snow melt peaks by the end of June. Further, the southwest monsoon between July and August over the Garhwal Himalaya facilitates the annual discharge peaks in these months. Of particular importance is the monsoon which bursts over the eastern part of the Himalayas in the first week of June and contributes a large proportion of the annual runoff in a few months (Sharma 1993). The monsoon is deflected by mountains and moves westward, extending throughout the region by the end of July, where it persists till mid-September (Mani 1981). The

percentage of the monsoon runoff component varies across the elevations in the basin as higher elevations receive relatively lower precipitation than lower elevations. The form of precipitation is also critical for the glacier melt component with rainfall over glacier enhancing the melting and snow deceleration. As glaciers also melt fast during the same time of monsoon leading to a complex system at work. Meltwaters of the Himalayan tributaries and streams originating from the glaciers and snow in the basin are characterised by its low ionic concentrations which dilute the solute and pollutant load in the river. Hence, any change in the quality and quantity of the Himalayan tributaries under the climate change regime will affect the quality parameters of the River Ganga as well. In the present paper, seasonal variations of major ion chemistry and solute fluxes of meltwater of River Bhagirathi (Name of River Ganga while originating from the glacier) have been discussed covering three consecutive melt seasons of 2014–2016.

32.2 Study Area

Gangotri glacier exists in district Uttarkashi of Uttarakhand state in the central Himalaya. Geographical location of this glacier lies between 30° 43′ 22″–30° 55′ 49″ N and 79° 4′ 41″–79° 16′ 34″ E (Fig. 32.1). The snout of the Gangotri glacier, known as Gomukh is situated at about 4000 m a.s.l. (Arora 2008). The Gangotri glacier valley comprises of a number of small and big glaciers. Gangotri glacier covers an area of 286 km^2 and an extent of 30.2 km in length. The glacier has three major tributary glaciers called Raktavarn glacier, Kirti glacier and Chaturangi glacier (Singh et al. 2006, 2011; Naithani et al. 2001). Some of these tributary glaciers are detached from the trunk glacier but its meltwater feeds into the main glacier system. The total basin area of the Gangotri glacier up to the snout at Gomukh is 513 km^2 which increased to 556 km^2 at Bhojwasa and 691 km^2 up to Gangotri. Correspondingly, glacier cover in the basin vary from 60% at the snout to 51.4% at Bhojwasa (Arora 2008) and 53.52% at Gangotri.

Geology of the Gangotri glacier system consists of quartzite, phyllite, tourmaline granite, mica schist, sericite schist, sulphide minerals like arsenopyrites, pyrite, chalcopyrite and fine grained limestone (Bhatt 1963). Generally, sulphate minerals are adhered with carbonate rocks (Srivastava et al. 2004). National Institute of Hydrology (NIH), Roorkee is studying the Gangotri glacier system since 1995 and the studies are helped in understanding the Gangotri glacier system better (Fig. 32.1) (Arora 2008; Arora et al. 2008, 2009, 2010; Haritashya et al. 2006, 2010; Kumar et al. 2007, 2009; Rai et al. 2009; Singh et al. 2005, 2006, 2011).

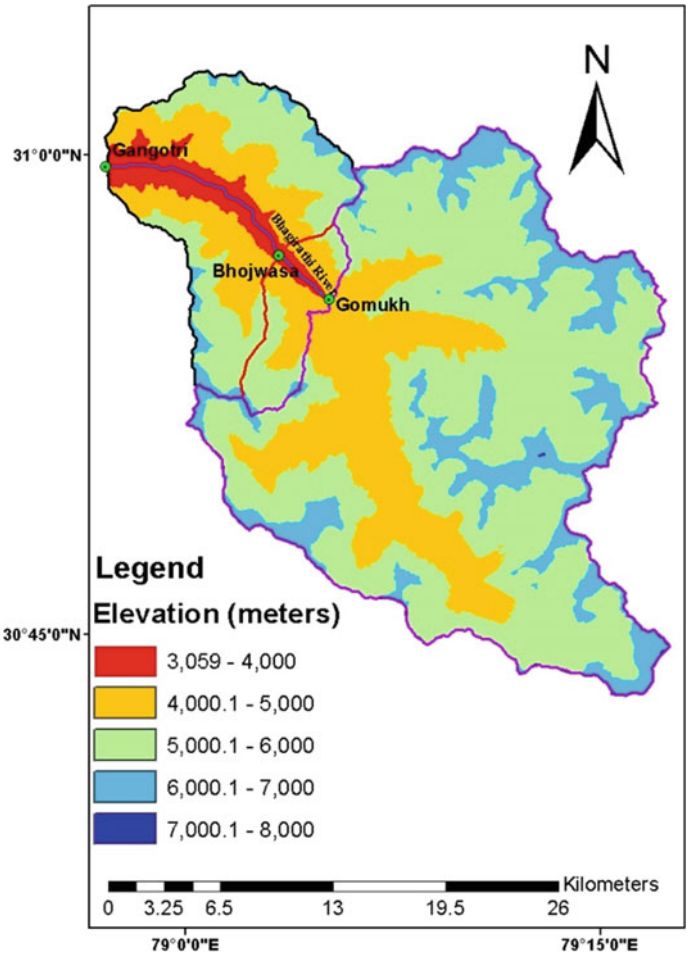

Fig. 32.1 Digital elevation map of the study area

32.3 Sampling and Methodology

Meltwater samples were collected using the grab sampling method from River Bhagirathi at Bhojwasa during the period of May–October of the year 2014, 2015 and 2016 and immediately filtered the samples for suspended sediment concentration through 0.45 μm membrane Whatman filter paper by using hand operated vacuum pump (Tarson make) and filtration apparatus. Discharge was observed and calculated by establishing a rating curve for the gauging site at Bhojwasa. pH, electrical conductivity and temperature of meltwater samples were measured using a pH meter (Model: HQ11d, Make: Hach, USA) and EC meter (Model: HQ14d, Make: Hach, USA).

Hydro-chemical analysis of filtered meltwater samples collected from river Bhagirathi was carried out using Ion Chromatograph with Auto Titrator (Metrohm, Switzerland) in Water Quality laboratory, NIH, Roorkee. The charge balance errors were < 5% for each analysis determined by the formula $[\{(TZ^+ TZ^-)/(TZ^+ + TZ^-)\} \times 100]$ confirming the reliability and quality of the analytical results.

32.4 Results and Discussions

Daily average meltwater discharge of River Bhagirathi at Bhojwasa for the rising limb of the hydrograph (May–June), peak flow (July–August) and falling limb of the hydrograph (September–mid October) during the years 2014, 2015 and 2016 was observed to be 43.4, 107.7 and 42.2 m^3/s respectively. The pH of was slightly acidic to alkaline during the rising limb of the hydrograph (6.26–7.65), peak flow (6.05–7.97) and falling limb of the hydrograph (6.43–7.62). The EC varied from 43.8 to 113 μS/cm with an average value of 72.3 ± 16.5 μS/cm during the rising limb of the hydrograph, from 43.4 to 102 μS/cm with an average value of 69.7 ± 12.8 μS/cm during peak flow and from 50.5 to 116 μS/cm with an average value of 79.1 ± 17.5 μS/cm during falling limb of hydrograph. TDS of meltwater samples varied from 22.1 to 80.0 mg/L with an average value of 51.5 ± 14.7 mg/L during the rising limb of the hydrograph, from 20.1 to 77.5 mg/L with an average value of 42.2 ± 11.6 mg/L during peak flow and from 24.1 to 79.5 mg/L with an average value of 47.6 ± 13.4 mg/L during falling limb of hydrograph during the year 2014, 2015 and 2016. Same trend was observed by Singh et al. (2014).

The anions for all sampling seasons were observed to be in decreasing order $SO_4^{-2} > HCO_3^- > Cl^- > NO_3^-$. Sulphate was the dominant anion accounting for 75.4% during the rising limb of the hydrograph, 75.2% during peak flow and 77.9% during falling limb of the hydrograph of total anions (TZ^-). Bicarbonate was the next dominant anion after sulphate accounting for 21% during the rising limb of the hydrograph, 22% during peak flow and 20% during the falling limb of the hydrograph of total anions. First possibility of acquiring SO_4^{-2} content in the Gangotri glacier meltwater is from the dissolution of sulphate minerals (gypsum and anhydrite), whereas the second possibility is from the sulphide oxidation (Srivastava et al. 2004). Gangotri glacier is a tourist spot. Due to trekking and its religious importance, many tourists and pilgrims arrive during the study period. Relatively very low concentration of NO_3^- was reported from Gangotri glacier meltwater, indicating palatability of meltwater. The possible source of NO_3^- may be anthropogenic activities taking place in the study area. Whereas other possible sources of NO_3^- may be the influence of atmospheric deposition associated with the acidic NO_3^- aerosol (Tranter et al. 1993).

The cations for all sampling seasons in decreasing order were observed to be $Ca^{2+} > Mg^{2+} > K^+ > Na^+$. Calcium was the dominant cation accounting for 64.9% during the rising limb of the hydrograph, 69.1% during peak flow and 59.8% during the

falling limb of the hydrograph of total cations (TZ^+). Magnesium was the next dominant cation after calcium accounting for 19.8% during both rising limb of hydrograph and peak flow and 22% during falling limb of hydrograph of total cations.

The seasonal variation of the dissolved ions in the Gangotri glacier meltwater is given in Fig. 32.2, which indicates that generally dissolved ions concentration was low during the peak flow period and high during the rising and falling limb period of the hydrograph. Such dissolved ion concentration variations are indicative of a climatic control on the intensity of different processes operating in the study area (Singh and Hasnain 1998). Due to the availability of high incoming solar radiation and the larger extent of the exposed glacier ice during peak flow season (July–August) intense melting takes place in the study area (Singh et al. 2006). This is responsible for increasing the discharge and dilution of the dissolved ions, resulting in depressed dissolved ion concentration. Whereas during rising and falling limb of hydrograph season, due to reduced incoming solar radiation, the melting is also low, which decreases discharge in falling limb of hydrograph period (Singh et al. 2006; 2012; Singh and Hasnain 1998), resulting in enhanced dissolved ion concentration in meltwater draining from Gangotri glacier.

The relative importance of two major proton producing reactions—sulphide oxidation and carbonation can be calculated on the basis of the ($HCO_3/HCO_3 + SO_4$) ratio, called the C-ratio (Brown et al. 1996). A ratio of 1 would signify weathering by carbonation reactions (Reynolds and Johnson 1972); and dissolution and dissociation of the atmospheric CO_2 are exclusively deriving protons. Conversely, if the C-ratio is 0.5, it signifies a coupled reaction involving carbonate dissolution and sulphide oxidation and protons derived from the pyrite oxidation. The average C-ratio for meltwater of River Bhagirathi at Bhojwasa is 0.24 ± 0.08 during the rising limb period of the hydrograph, 0.22 ± 0.09 during peak flow and 0.20 ± 0.05 during the falling limb period of the hydrograph, which indicates that the major proton producing reaction is the oxidation of sulphide (Fig. 32.3). The coupled reaction involving carbonate and CO_2 dissolution and oxidation of sulphide minerals derived

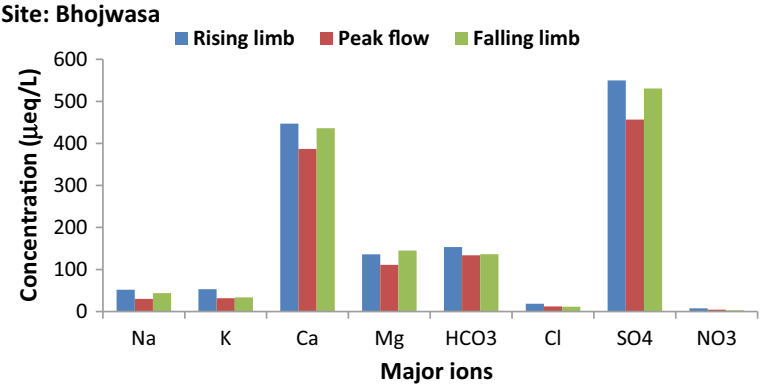

Fig. 32.2 Seasonal variations of dissolved ions at Bhojwasa

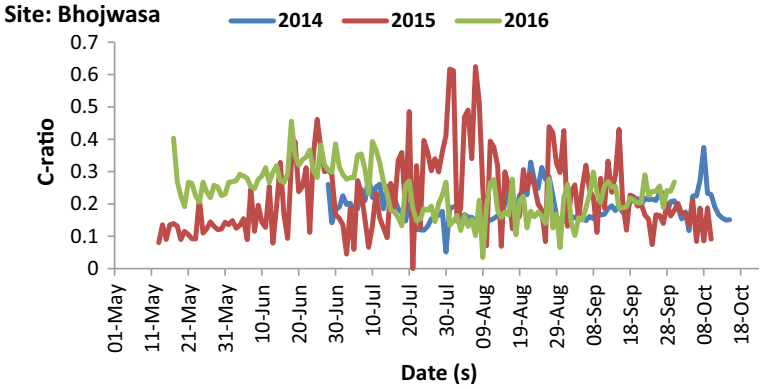

Fig. 32.3 Variation of C-ratio in the meltwater of River Bhagirathi at Bhojwasa

protons largely control the chemistry of meltwater draining from Gangotri glacier (Ahmad and Hasnain 2001).

Solute fluxes in glacial meltwaters usually increase with discharge in an aquatic system. The largest solute fluxes are transported by the most dilute meltwater as solute concentration is usually inversely related to discharge (Sharp et al. 1995). Daily variation of fluxes of TSS, Ca, Mg, HCO_3, SO_4 and TDS in the meltwater of River Bhagirathi at Bhojwasa during the period 2014–2016 is shown in Fig. 32.4. Fluxes of all major dominating cations (Ca^{+2} and Mg^{+2}) and major dominating anions (HCO_3^- and SO_4^{-2}) follow the same trend as that of discharge. Daily average meltwater discharge for the rising limb of the annual hydrograph (May and June), crest (July and August) and falling limb of the annual hydrograph (September to Mid-October) from 2014 to 2016 were observed to be 43.4, 107.7 and 42.2 m^3/s respectively.

Bedrock system (glacier bottom ice and bedrock), glacier system (sedimentation from different parts of the glacier such as snout, ablation zone, accumulation zone and lateral moraines) and channel system are the main sources of production of sediment from the glacier fed channels (Singh et al. 2003). Daily mean suspended sediment concentrations were observed to be 1.569, 1.932 and 0.514 g/L during the rising limb of the annual hydrograph, peak flow and falling limb of hydrograph respectively showing the highest suspended sediment concentration during the peak flow period, which coincides with the period of high glacial melt in the "Himalayan catchments" (Thayyen and Gergan 2010). This is followed by the rising and falling limb period respectively. Daily mean suspended sediment load was calculated to be 5885, 17,982 and 1874 t/day for rising limb, peak flow and falling limb of hydrograph period respectively during the study period. Suspended sediment concentration and load are low during the low discharge period (falling limb) and high during the high discharge period (monsoon + Glacier melt). These seasonal variations in suspended sediment concentration during the study period may be attributed to the progression of subglacial drainage network development. The distributed channel system in the subglacial zone is dormant during the winter season with less water availability and

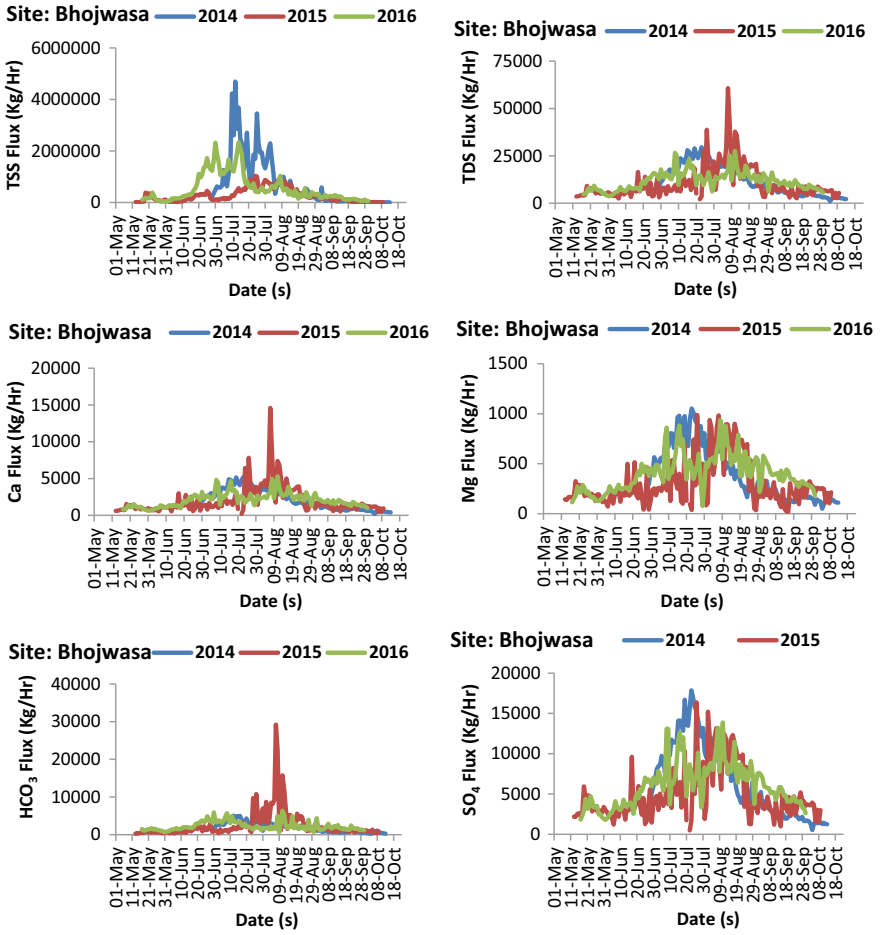

Fig. 32.4 Variations of daily mean fluxes of TSS, Ca, Mg, HCO_3, SO_4 and TDS in meltwater at Bhojwasa during the period 2014–2016

high overburden pressure of glacier ice. As melt season progresses, more and more snow and glacier melt routed to the subglacial zone and the distributed channel spread to the higher elevations of the glacier. Higher sediment flux from the glacier is also indicative of good integration of distributed system (Thayyen et al. 1999, 2003). These processes are also linked with the solute acquisition in the meltwater, which could be distinctly different for Alpine and Himalayan glacier systems (Hasnain and Thayyen 1999). Along with the subglacial channel development, intensive melting (high discharge), increased stream area cross section and higher availability of glacier debris are the factors responsible for high suspended sediment concentration and load in the seasonal high flow period (Singh and Hasnain 1998; Haritashya et al. 2006) whereas in the recession limb of the glacial hydrograph, suspended sediment

concentration is reduced significantly. This trend may be attributed to flush out of sediment by the meltwater in the preceding months (Ostrem 1975; Collins 1990). The average ratio of TSS/TDS was observed to be 30.9 in the rising limb of the hydrograph, 46.2 during peak flow and 10.9 in the recession limb of the annual hydrograph indicating varying degrees of the dominance of physical weathering over chemical weathering with increasing discharge in the Gangotri glacier basin. The suspended sediment load of Gangotri glacier meltwater is much higher than that of other Himalayan glaciers, which may be due to high discharge, a large quantity of rock debris and geology of the study area.

Daily mean HCO_3 flux for rising limb, peak flow and recession limb of the annual hydrograph was calculated to be 35.1, 76.0 and 30.4 t/day respectively whereas daily mean SO_4 flux for rising limb, peak flow and recession limb of the annual hydrograph was calculated to be 99.0, 204.0 and 92.9 t/day respectively. Although the concentrations of HCO_3 and SO_4 of meltwater of River Bhagirathi at Bhojwasa draining from Gangotri glacier were minimum in monsoon season but the fluxes of $HCO_3$and SO_4 were maximum due to high discharge during monsoon season. This supports our contention that the weathering of supra glacial moraines initiated by monsoonal rainfall enhances the sulphate concentration at high discharges.

TDS flux is calculated with the help of discharge and TDS of meltwater. TDS was calculated by summation of the masses of all the major dissolved constituents (HCO_3^-, Cl^-, SO_4^{-2}, NO_3^-, Na^+, K^+, Ca^{+2} and Mg^{+2}). Daily mean TDS flux for rising limb, peak flow and recession limb of the annual hydrograph was calculated to be 190.3, 389.1 and 172.2 t/day respectively. Although TDS of meltwater of river Bhagirathi at Bhojwasa draining from Gangotri glacier was minimum during peak flow period but TDS flux was maximum due to high discharge during the same period.

32.5 Conclusion

Melt waters of the Himalayan tributaries and streams originating from the glaciers and snow in the basin are characterised by its low ionic concentrations which dilute the solute and pollutant load in the river. These ionic concentrations were low during the peak flow period and high during the rising and falling limb period of the hydrograph. Such dissolved ion concentration variations are indicative of a climatic control on the intensity of different processes operating in the study area. Suspended sediment concentration and load are low during the low discharge period (falling limb) and high during the high discharge period (monsoon + Glacier melt). These seasonal variations in suspended sediment concentration during the study period may be attributed to the progression of subglacial drainage network development. Higher sediment flux from the glacier is also indicative of good integration of the distributed system. The dominance of physical weathering over chemical weathering with the increasing discharge was observed in the Gangotri glacier basin. The suspended sediment load of Gangotri glacier meltwater is much higher than that of other Himalayan glaciers,

which may be due to high discharge, a large quantity of rock debris and the geology of the study area.

Acknowledgements This work is a part of the project sponsored by SERB, Department of Science & Technology, Gov. of India, New Delhi (DST-SERB No. SB/DGH-49/2013) and hereby acknowledged. The authors are highly grateful to Director, National Institute of Hydrology, Roorkee for providing the required analytical facilities and support and encouragement for carrying this work. Assistance of Miss Parul Prajapati and Miss Prerna in analysis work is also acknowledged.

References

Ahmad S, Hasnain SI (2001) Chemical characteristics of stream draining from Dudu glacier: an Alpine meltwater stream in Ganga Headwater, Garhwal Himalaya. J China Univ Geosci 12(1):75–83

Arora M (2008) Seasonal characterization of ablation, storage and drainage of melt runoff and simulation of streamflow for the Gangotri glacier. Project report-1/2008, National Institute of Hydrology, Roorkee, Uttarakhand

Arora M, Singh RD, Kumar A (2008) Applications of snow cover estimation in snow melt runoff modeling: a case study of Gangotri glacier basin Himalayas. In: Proceedings international workshop on snow, ice, glacier and avalanches, January 7–9, 2008, IIT Bombay, Mumbai, pp 26–33

Arora M, Singh RD, Kumar A, Singh P (2009) Melt runoff delaying characteristics of Gangotri glacier. In: International conference "Water, Environment, Energy and Society" WEES 2009, New Delhi, 12–16 January 2009, pp 359–365

Arora M, Kumar R, Kumar N (2010) Temperature index modelling of Gangotri glacier melt stream. In: National workshop on "Case studies on real time hydrological modelling for Ganga Brahmaputra Basin", NIT Rourkela, 23–25 September 2010, p 20

Bhatt BK (1963) Preliminary study of the Bhagirathi basin between Uttarkashi and Gomukh. In: Proceeding of national symposium on Himalayan Geology, Calcutta, Geological Society of India. Miscellaneous Publication Number 15, pp 1–8

Brown GH, Sharp M, Tranter M (1996) Subglacial chemical erosion—seasonal variations in solute provenance, Haut Glacier d'Arolla, Switzerland. Ann Glaciol 22:25–31

Collins DN (1990) Seasonal and annual variations of suspended sediment transport in meltwaters draining from an Alpine glacier. In: Proceeding of two Lausanne symposium. IAHS Publication Number 193, pp 439–446

GSI (1999) Inventory of the Himalayan glaciers—a contribution to the international hydrological programme. In: Kaul MK (ed). Special Publication 34, 165 pp

Haritashya UK, Singh P, Kumar N, Gupta RP (2006) Suspended sediment from the Gangotri glacier: quantification, variability and associations with discharge and air temperature. J Hydrol 321:116–130

Haritashya UK, Kumar A, Singh P (2010) Particle size characteristics of suspended sediment transported in meltwater from the Gangotri glacier, central Himalaya—an indicator of subglacial sediment evacuation. Geomorphology 122(1–2):140–152

Hasnain SI, Thayyen RJ (1999) Controls on the major-ion chemistry of the Dokriani glacier meltwaters, Ganga basin, Garhwal Himalaya, India. J Glaciol 45(149):87–92

Kumar B, Rai SP, Jain SK, Senthil Kumar AK, Verma SK, Garg P, Rawat YS (2007) Streamflow modelling of Bhagirathi River: hydrograph separation using isotopic and geochemical techniques. Technical report, CS/AR-2/2006-07, National Institute of Hydrology, Roorkee

Kumar K, Miral MS, Joshi S, Pant N, Joshi V, Joshi LM (2009) Solute dynamics of meltwater of Gangotri glacier, Garhwal Himalaya, India. Environ Geol 58:1151–1159

Mani A (1981) The climate of the Himalaya. In: Lal JS, Moddie AD (eds) The Himalaya: the aspects of change. Oxford University Press, Oxford, pp 3–15

Naithani AK, Nainwal HC, Sati KK, Prasad C (2001) Geomorphological evidences of retreating of Gangotri glacier and its characteristics. Curr Sci 80(1):87–94

Ostrem G (1975) Sediment transport in glacial meltwater stream. In: Jopling AV, McDonald BC (eds) Glacio-fluvial and Glacio-lacustrine sedimentation. Society of Economic Palaeontologists and Mineralogists, Special Publication Number 23, pp 101–122

Pandey SK, Singh AK, Hasnain SI (1999) Weathering and geochemical processes controlling solute acquisition in Ganga Headwater-Bhagirathi River, Garhwal Himalaya, India. Aquatic Geochem 5(4):357–379

Rai SP, Kumar B, Singh P (2009) Estimation of contribution of South West-monsoon rain in Bhagirathi River near Gomukh, Western Himalayas, India, using stable isotope ($\delta^{18}O$). Curr Sci 97(2):240–245

Reynolds RC, Johnson NM (1972) Chemical weathering in the temperate glacial environment of the Northern Cascade Mountains. Geochim Cosmochim Acta 36(5):537–554

SAC (2011) Technical report snow and glaciers of the Himalayas. Space Application Centre (ISRO), Ahmedabad, India, p 258

Sharma KP (1993) Role of meltwater in major river systems of Nepal. International Association of Hydrological Sciences Publication 218 (Symposium at Kathmandu 1992—snow and glarier hydrology), pp 113–122

Sharp M, Tranter M, Brown GH, Skidmore M (1995) Rates of chemical denudation and CO_2 drawdown in a glacier-covered alpine catchment. Geology 23:61–64

Singh AK, Hasnain SI (1998) Major ion chemistry and weathering control in a high altitude basin: Alaknanda River, Garhwal Himalaya, India. Hydrol Process 43(6):825–843

Singh P, Haritashya UK, Kumar N (2006) Hydrological characteristics of the Gangotri glacier, Central Himalayas, India. Hydrol Process 327:56–67

Singh P, Haritashya UK, Ramasastri KS, Kumar N (2005) Diurnal variations in discharge and suspended sediment concentration, including runoff-delaying characteristics, of the Gangotri glacier in the Garhwal Himalayas. Hydrol Process 19:1445–1457

Singh P, Kumar A, Kishore N (2011) Melt water storage and delaying characteristics of Gangotri glacier (Indian Himalayas) during ablation season. Hydrol Process 25:159–166

Singh P, Ramasastri KS, Kumar N, Bhatnagar NK (2003) Suspended sediment transport from the Dokriani glacier in the Garhwal Himalayas. Nord Hydrol 34(3):221–244

Singh VB, Ramanathan AL, Pottakkal JG, Sharma P, Linda A, Azam MF, Chatterjee C (2012) Chemical characterisation of meltwater draining from Gangotri glacier, Garhwal Himalaya, India. J Earth Syst Sci 121(3):625–636

Singh VB, Ramanathan AL, Pottakkal JG, Kumar M (2014) Seasonal variation of the solute and suspended sediment load in Gangotri glacier meltwater, Central Himalaya, India. J Asian Earth Sci 79:224–234

Srivastava D, Absar A, Sangewar CV, Pandey SN, Oberoi LK, Siddiqui MA (2004) Chemical signatures of lithology on Gangotri glacier meltwater and Gaumukh–Tehri dam section of Bhagirathi River. In: Proceeding of workshop on Gangotri glacier. Geological Survey of India Special Publication Number 80, pp 223–226

Thayyen RJ, Gergan JT (2010) Role of glaciers in watershed hydrology: a preliminary study of a Himalayan catchment. Cryosphere 4:115–128

Thayyen RJ, Gergan JT, Dobhal DP (1999) Particle size characteristics of suspended sediments and subglacial hydrology of Dokriani glacier, Garhwal Himalaya, India. Hydrol Sci J 44(1):47–61

Thayyen, RJ, Gergan, JT, Dobhal, DP (2003) Glacier drainage evolution and control on suspended sediment concentration in meltwater, Dokriani Glacier, Garhwal Himalaya, India. J Geol Soc India 62:237–242

Tranter M, Brown G, Raiswell R, Sharp M, Gurnell A (1993) A conceptual model of solute acquisition by Alpine glacier meltwaters. J Glaciol 39(133):573–581
Vohra CP (1981) Himalayan glaciers. In: Lall JS, Moddie AD (eds) The Himalaya. Oxford University Press, pp 138–151

Chapter 33
Gis Approach to Identify the Influence of Rock Water Interaction and Land Use Land Cover on Groundwater Quality Degradation

Uday Kumar Devalla, Vikash Kumar, and Y. B. Katpatal

Abstract Groundwater is an important source of water available at any desired location with the requirement of less treatment. Its quality has been declining, which may be ascribed to both anthropogenic activities and gigantic natural processes. Maintaining groundwater quality is a significant issue as still many people depend on it for agricultural and even drinking purposes. The present study pertains to spatial analysis of the groundwater resources of 23 Mandals of Sri Potti Sreeramulu Nellore district located in Andhra Pradesh, a region which has been reported to have fast quality decline. Geological classes belonging to Toposheets numbered 57 M, 57 N, and 57O are used to develop the geology map. More than 90% of the area is underlain by quartzite, gneisses, hornblende schists and mica schists. LISS-III images of IRS P6 Resources at II are used for land use classification. Chemical data of 57 groundwater observation wells evenly distributed in the area has been obtained from Groundwater and Groundwater audit department Nellore, for the year 2016. Spatial distribution maps are developed for each quality parameter of available data for both pre-monsoon and post-monsoon seasons by inverse distance weighted interpolation method using ArcGIS. Even though the wells of pre-monsoon are showing maximum concentrations, its spatial distribution is more in post-monsoon (more than acceptable and permissible limits). It is observed that rock-water interaction is one cause in reducing water quality in some areas. This indicates the source of the groundwater pollution to be geogenic. The study also attempts to tie up the land use classes present in the area to the groundwater quality distribution in the region. So in this study, satellite data from the LISS-III sensor along with the collateral information derived from the field and other sources have been used to identify the sources of pollution behind the quality degradation of groundwater.

Keywords Groundwater quality · Geogenic natural processes · Land use classification · ArcGIS · Pearson correlation

U. K. Devalla (✉) · V. Kumar · Y. B. Katpatal
Visvesvaraya National Institute of Technology (VNIT), Nagpur 440010, India
e-mail: udaykumardevalla@gmail.com

R. Jha et al. (eds.), *Groundwater and Water Quality*, Water Science and Technology Library 119, https://doi.org/10.1007/978-3-031-09551-1_33

33.1 Introduction

Nellore is one of the fastest developing cities in Andhra Pradesh. The present study aims at identifying the causes for the quality reduction of groundwater with respect to the drinking aspect, using the Geographic Information System (GIS) approach with help of the Pearson correlation coefficients. Groundwater Quality Data of pre and post-monsoon was collected for the year 2016 from various observation wells from Groundwater and Groundwater Audit Department, Nellore. The following parameters like chloride, pH, total hardness, calcium, sodium, potassium, magnesium, TDS, and HCO_3^-, were considered for the water quality estimation. The study reveals that the level of some toxicants is much more than the permissible limits. The possible reason for this may be ascribed to increased Geogenic contaminants due to over-extraction of groundwater, and anthropogenic activities.

33.2 Location and Geomorphology

The study area is situated in SPSR Nellore district, Andhra Pradesh, in the southern part of India, between 79°5′20”E and 80°0′57”E Longitude to 13°59′27”N and 15°6′28″ N latitude having an area of 7488.23 Km^2 (Fig. 33.1).

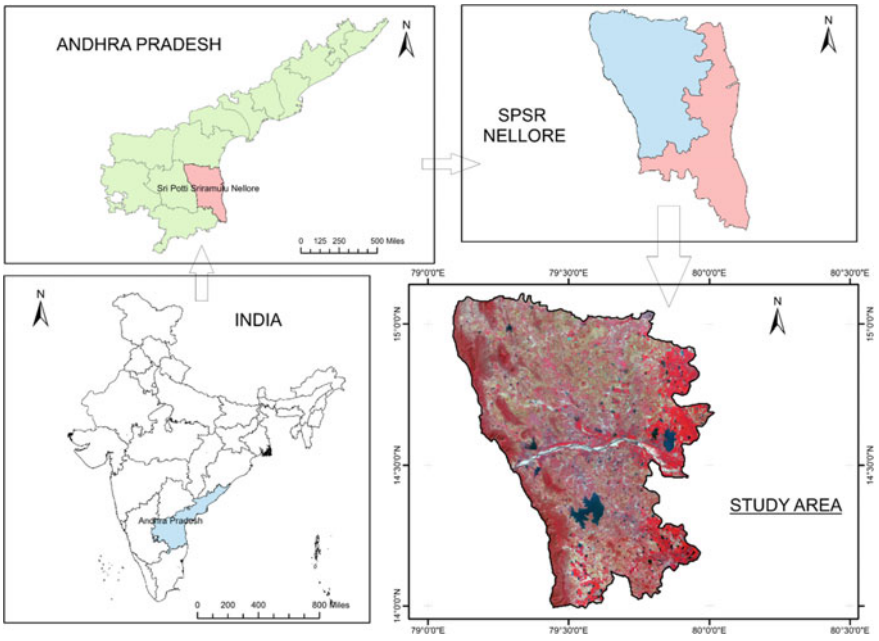

Fig. 33.1 Location of study area

Nellore district is generally classified into three parts; central pediplains, western hills and coastal and eastern deltaic plains. Hill ranges of the Eastern Ghats are represented as higher relief, on the western side border of this district. These are widely known as Veligonda hills, which run in a north-west direction having the highest elevation of 1,105 m above mean sea level at Penchalakonda. In the central part, the pediplain area of this district extends in the direction of north–south. The altitude of this unit ranges from 36 to 170 m above mean sea level with separated hillocks. The major slope of this area lies from the west to east closer to the Bay of Bengal. Figure 33.2 depicts the distribution of all the observation wells spatially.

Soils

Black cotton, alluvial soils, red loam, and lateritic sandy are the predominant soils in this district. Over 70% of the area is covered by red loamy soils except for the deltaic area. Nearly 10% of the district has black cotton soils and can be found in patches near the southern part of the Pennar river. Red laterite soil can be found along the east of this district. Most of the alluvial soil is found along the Swarnamukhi and Pennar rivers, and alongside the eastern margin of the district in the north of Pennar.

Hydrogeology

The study area contains a no. of geological formations ranging from Archaeans to the Alluvium (Fig. 33.3). Geological formations here can be generally categorized into 3 categories unconsolidated (Soft) formations, semi-consolidated (Soft) and consolidated (Hard). The migmatised high-graded metamorphic (pelitic schist and garnetiferous amphibolites), low-grade metamorphic (politic schists and amphibolites) of schist belt of Nellore, Cuddapahs (Shales and Quartzites) and granitic gneiss are the consolidated formation. A high-graded mica in the world occurs in the pegmatites is being mined near Gudur. Of the all consolidated formations, the major area of the district is covered by gneisses and schists (pelitic schists and amphibolites) and, whereas the western margin of this district consists of Cuddapah shales quartzites.

The semi-consolidated formations are represented by Gondwana sandstones occurring as discrete patches and Cuddalore sandstone, and Quaternary periods, Tertiary and laterites of Triassic respectively. The Gondwana sandstone usually occurs as a patch in the north part of this district. Laterite and Cuddalore sandstone occur in different patches along the eastern margin of this district whereas, windblown sand deposits, Laterite, and river alluvium, comprises the unconsolidated formations.

Even though groundwater occurs in almost all the geological formations, but its potential depends on, the incidence of rainfall, recharge, the geographical setup, the type of geological formations, and other hydrogeological aquifer characterstics. Gneisses are relatively better aquifers among the consolidated formations. The well tapping contact zone with intrusive schistose formations also forms potential aquifers. Since shales of Cuddapah and the quartzites are generally restricted to the hilly terrain in the western margin of the district, and these have less significance from the groundwater view point.

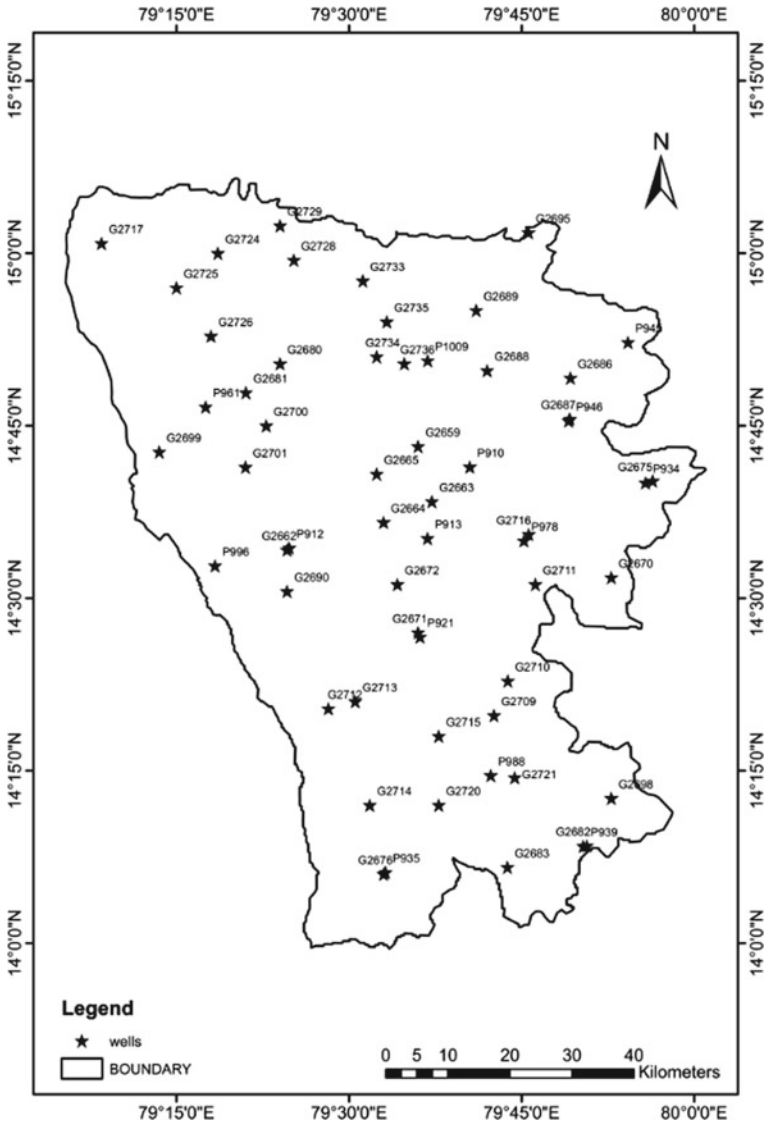

Fig. 33.2 Location of wells

In this consolidated formations, groundwater generally occurs under semi-confined to unconfined conditions. Groundwater is extracted by bore wells, dug wells and dug cum bore wells tapping weathered and fractured zones. Wells in this region yield from 15 to 35 m^3/day which reduces significantly for the period of the peak summer time. Fractures occurring in these formations lie between 40 to 60 m below ground level and sometimes it extends even more than 70 to 80 m. In

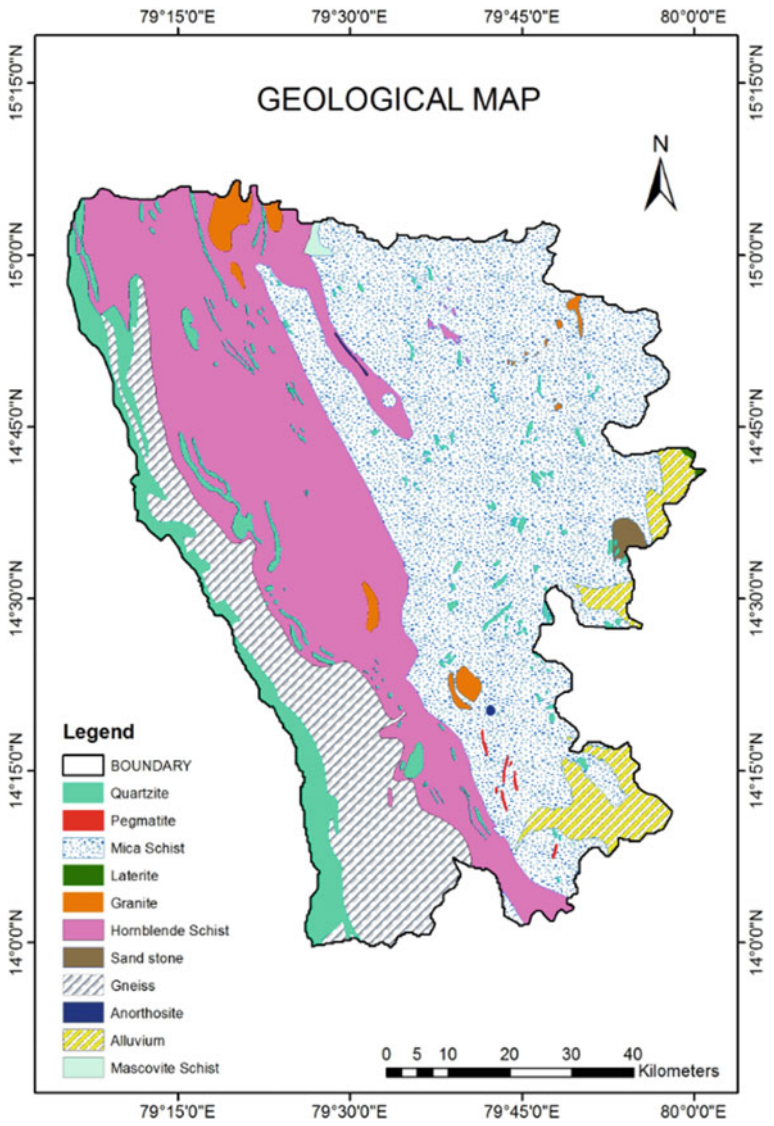

Fig. 33.3 Geology

these formations, the bore wells generally tap the fractured and weathered zones. Generally, the bore well's yield ranges between 80 to 350 m^3/day. The thickness of fractured zones limits the higher yields.

Climate and Rainfall

The study area lies in a zone of precarious and uncertain rainfall. As such, the climate of the district is mostly salubrious and dry. Generally, the maximum temperature is recorded in April, May, and June, whereas the lowest temperature is recorded in the months of November, December and January where the maximum temperature recorded was 41.2 °C In May and minimum temperature recorded was 21.9 °C in January in the year 2013–2014. The district receives an annual rainfall of 1080.5 mm. For the year 2013–2014, the actual quantum of rainfall received was 758.9 mm and during 2015–2016 it was 1358 mm. The major chunk of the rainfall was received in the North East Monsoon period of about 369.6 mm.

33.3 Datasets and Methodology

In this study, data on water quality, geology, soil and satellite images are used. Digitization and interpolation maps of various parameters are developed in ArcGIS software. IBM SPSS is used to develop Pearson correlation coefficients. Parameters are used, like land use in the study area, groundwater flow directions, and interaction of water with the soils and rocks affects the groundwater quality. In the study, in place of groundwater flow modeling, buffers are created around the affected wells to visualize the flow of water.

Correlation analysis is useful in understanding the chemical reactions occurring in groundwater systems (Wu et al. 2015). The statistical results obtained by IBM SPSS software for pre and post-monsoon are correlated and compared with the conclusions obtained by overlay analysis in GIS software. Methodology is shown in Fig. 33.4 in a simplified manner.

33.4 Results and Discussions

All parameters are showing a negative correlation with pH value, in both pre and post-monsoon data (Tables 33.1, 33.2 and 33.3). Its correlation is significant with potassium and sodium in post-monsoon. So it may be inferred that, because the geology is constant, if pH decreases, H^+ ions increases. Interpolation maps of potassium, developed in GIS software are showing concentrations more than permissible limits for drinking water (Fig. 33.5). The weathering of feldspar present in schists, is leading to an increase in potassium content in post-monsoon season, due to the decrease of pH in groundwater. So it can be concluded that the geological actions are the main causes of reduced water quality.

$$2KAlSi_3O8 + 2H^+ + 9H_2O \Leftrightarrow Al_2Si_2O_5(OH)_4 + 4H_4SiO_4 + 2K^+$$

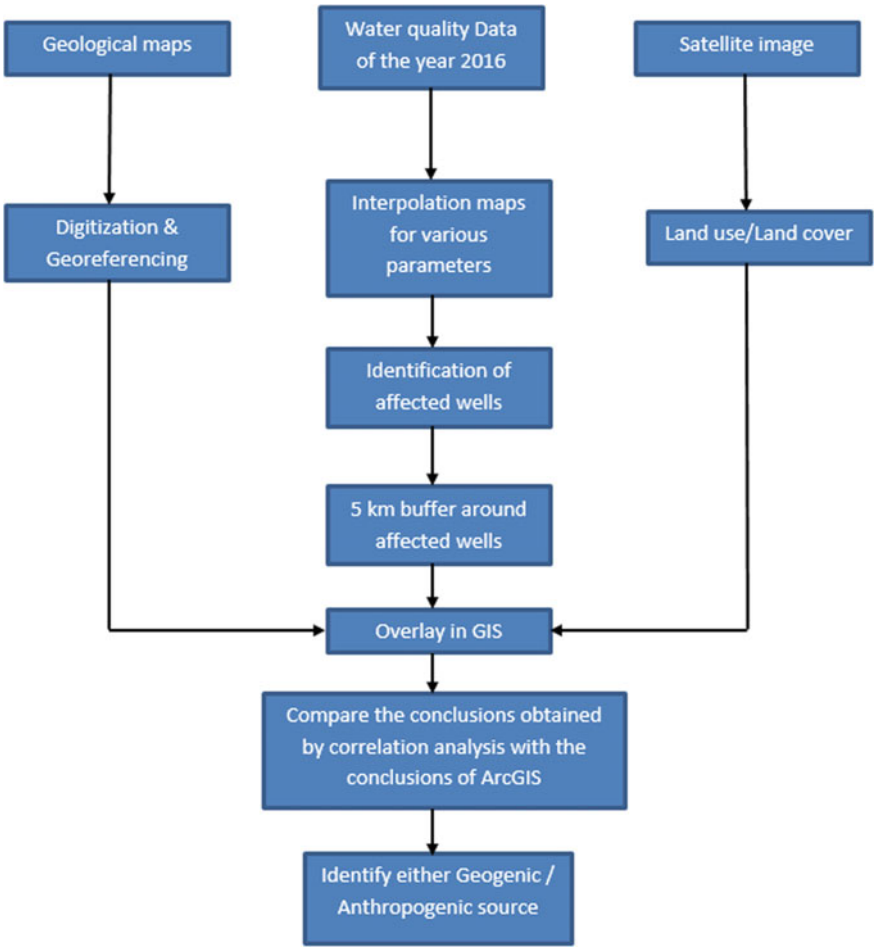

Fig. 33.4 Flow chart of methodology

There is a significant correlation between calcium and magnesium (Table 33.2). As pH in the wells is reduced from pre to post-monsoon, the area surrounding these wells are showing a rise in calcium and magnesium contents (Figs. 33.6 and 33.7) having the same trend of increase. The soil type of these area which is clay is supporting the statistical results. Thus, an increment in calcium content occurred in the post-monsoon season probably because of the incoming rain and its interaction with clay layers. Hence, strengthening the claims of geological traces for the increased calcium content in the post-monsoon period. Hence it indicates that the source for quality degradation of water is, clay minerals present in that area.

Total hardness is showing a high correlation coefficient with calcium and magnesium ions because hardness is an approximate measure of Ca^{2+} & Mg^{2+} (Li et al. 2013). It can be observed that the interpolation maps of total hardness (Fig. 33.8)

Table 33.1 Summary statistics (quantitative data)

Variable (mg/l)	Minimum		Maximum		Mean		Std. deviation	
	Pre	Post	Pre	Post	Pre	Post	Pre	Post
pH[a]	7.76	7.61	9.08	8.30	8.134	7.971	0.250	0.140
TDS	262.40	263.68	4515.20	3262.08	891.857	1044.720	705.657	668.632
HCO3	60.00	120.00	800.00	600.00	201.754	246.786	112.077	88.763
Chloride	50.00	40.00	1500.00	1100.00	257.719	316.250	267.849	250.018
Sulphate	15.00	24.00	550.00	476.00	96.368	107.589	90.578	80.296
Sodium	5.00	51.00	740.00	220.00	128.123	138.054	127.079	50.392
Potassium	1.00	1.00	50.00	31.00	6.860	10.393	8.169	8.622
Calcium	16.00	16.00	400.00	320.00	44.351	62.857	51.048	58.171
Magnesium	19.00	19.00	490.00	340.00	74.421	90.714	74.574	73.995
Total hardness	118.189	118.189	3016.461	2199.177	417.137	530.453	416.980	446.734

[a]Unit (mg/l) not applicable for pH

and Ca^{2+} & Mg^{2+} (Figs. 33.6 and 33.7) are showing approximately the same trend in increase.

The pH measurements of all observation wells are ranging from 7.76 to 9.08 in pre-monsoon and 7.61 to 8.30 in post-monsoon, with standard deviations 0.25 and 0.14 respectively (Table 33.1). There is no evidence of industrial mixing with groundwater because the fluctuations in pH is less. So decrease in pH value of groundwater from pre to post-monsoon may be due to the decomposition of organic matter.

TDS has a positive correlation with Ca, Mg, K, Na, HCO_3, Cl, and the mean value is increased from 891 mg/l in pre-monsoon to 1045 mg/l in post-monsoon. Sulphate concentrations are within permissible limits in both the seasons.

33.5 Conclusions

This study using the spatial analyses in GIS has shown that the source of the groundwater pollution in the Nellore District of Andhra Pradesh is geogenic. The results of Pearson correlation analysis when correlated with the lithologic classes within the area and the land use land cover classes very well indicate towards the source of pollution more to be geogenic. Except for a few villages like Karatampadu, Marripadu, Varikuntapadu, Bata, where wells show GW quality parameters more than permissible limits, groundwater is acceptable for drinking.

Table 33.2 Pearson correlation coefficients of water quality data for Pre-Monsoon with confidence intervals (95%)/Lower bound

	pH	TDS	HCO_3^-	Cl^-	SO_4^{2-}	Na^+	K^+	Ca^{2+}	Mg^{2+}	Total hardness
pH	1	−0.392	−0.389	−0.375	−0.406	−0.306	−0.350	−0.318	−0.445	−0.414
TDS		1	0.425	0.926	0.974	0.662	0.968	0.637	0.690	0.724
HCO_3^-			1	0.215	0.440	0.171	0.408	0.661	0.325	0.453
Cl^-				1	0.891	0.555	0.903	0.542	0.746	0.735
SO_4^{2-}					1	0.624	0.946	0.632	0.684	0.718
Na^+						1	0.625	0.130	0.050	0.088
K^+							1	0.662	0.676	0.722
Ca^{2+}								1	0.696	0.838
Mg^{2+}									1	0.972
Total hardness										1

Table 33.3 Pearson correlation coefficients of water quality data for Post-Monsoon with confidence intervals (95%)/Lower bound

	pH	TDS	HCO_3^-	Cl^-	SO_4^{2-}	Na^+	K^+	Ca^{2+}	Mg^{2+}	Total hardness
pH	1	−0.585	−0.332	−0.625	−0.362	−0.700	−0.649	−0.495	−0.537	−0.525
TDS		1	0.757	0.986	0.122	0.586	0.897	0.914	0.978	0.969
HCO_3^-			1	0.656	0.079	0.223	0.579	0.817	0.791	0.810
Cl^-				1	0.126	0.623	0.906	0.880	0.953	0.941
SO_4^{2-}					1	0.092	0.103	0.101	0.104	0.106
Na^+						1	0.688	0.290	0.437	0.394
K^+							1	0.701	0.852	0.812
Ca^{2+}								1	0.945	0.975
Mg^{2+}									1	0.994
Total hardness										1

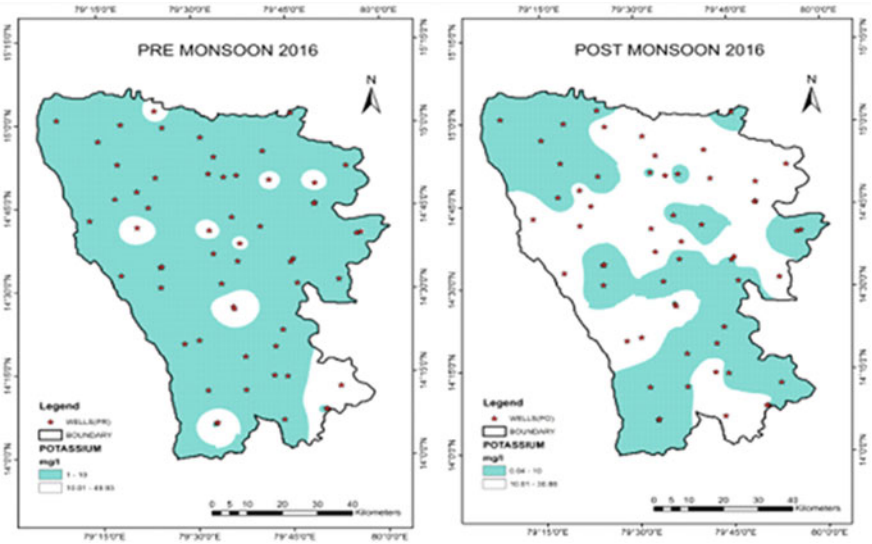

Fig. 33.5 Spatial distribution of potassium

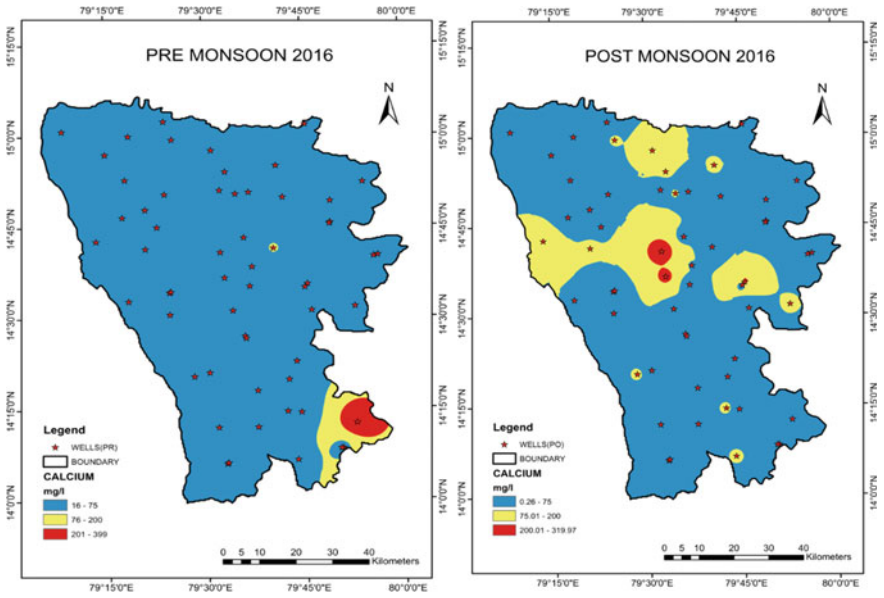

Fig. 33.6 Spatial distribution of calcium

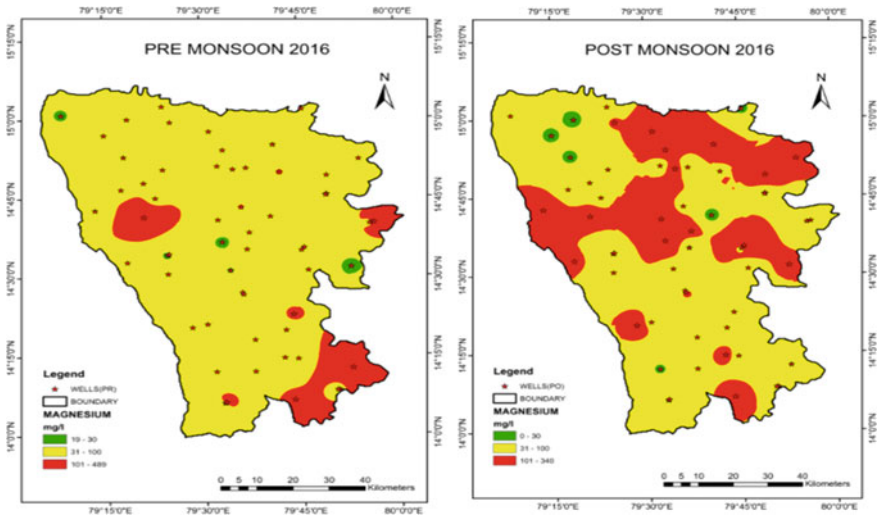

Fig. 33.7 Spatial distribution of magnesium

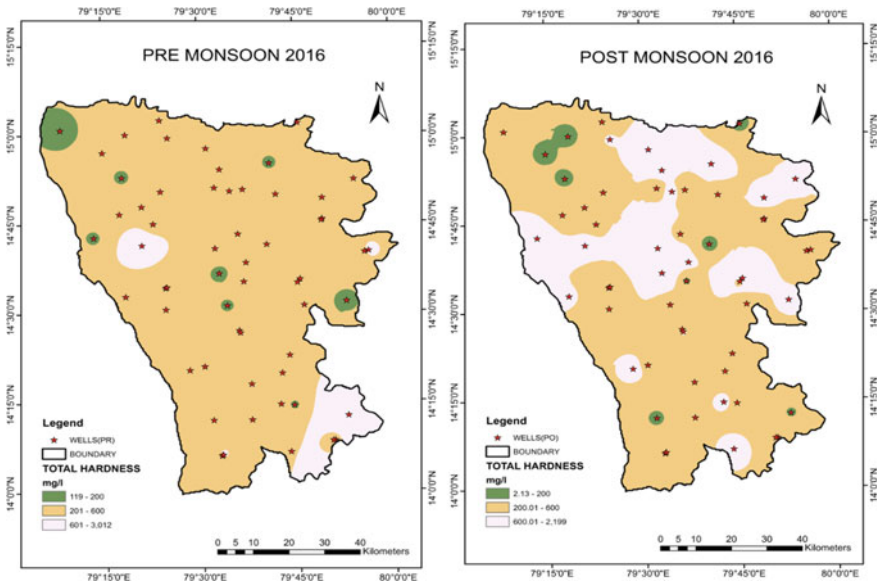

Fig. 33.8 Spatial distribution of total hardness

Acknowledgements The authors would like to thank our Director Dr. P M Padole, Dean (R & C) Dr. V.B. Borghate, Head CED Dr. Rajesh Gupta, Mr. Mukesh M S, PhD Scholar, Mr. Digambar Sambhaji Londhe, PhD Scholar, Department of Civil Engineering, for their support.

References

A.V.S.S. Anand Scientist-C (2013) Groundwater brochure Nellore district, Andhra Pradesh, Central Groundwater Board, Ministry of Human Resources, Government of India

Li P, Qian H, Wu J, Zhang Y, Zhang H (2013) Major ion chemistry of shallow groundwater in the Dongsheng coalfield, Ordos Basin, China. Mine Water Environ 32:195–206. https://doi.org/10.1007/s10230-013-0234-8

Nagaraju A, Thejaswi A, Sreedhar Y (2016) Assessment of groundwater quality of Udayagiri area, Nellore District, Andhra Pradesh, South India using multivariate statistical techniques. Earth Sci Res J. https://doi.org/10.15446/esrj.v20n4.54555

Sudhakar P, Scientist-D (2017) Ground water year book 2016–2017 Andhra Pradesh State, Central Ground Water Board, Ministry of Water Resources, River Development & Ganga Rejuvenation Govt. of India

Tashtoush SM, Al-Subh SA (2015) Interpretation of groundwater quality parameters for springs in Tafileh area in South of Jordan using principal components analysis. Environ Sci 3(1):31–44. https://doi.org/10.12988/es.2015.523

Todd DK, Mays LW (2005) Groundwater hydrology, 3rd edn. Wiley, New York

Wu J, Li P, Qian H (2015) Hydrochemical characterization of drinking groundwater with special reference to fluoride in an arid area of China and the control of aquifer leakage on its concentrations. Environ Earth Sci 73:8575